# WP 4 – Tectonic control on fluid flow

# Task 4.3 – Final Report on geochemical characterization and origin of cold and thermal fluids

- Deliverable D4.3 -

# WP 4 – Tectonic control on fluid flow

# Task 4.3 – Final Report on geochemical characterization and origin of cold and thermal fluids

## - Deliverable D4.3 -

Version 1.2

Matteo Lelli and Ruth Alfaro Cuevas Villanueva

Contact: Matteo Lelli (m.lelli@igg.cnr.it)

Work package WP4

29/03/2019

Website: http://www.gemex-h2020.eu

The GEMex project is supported by the European Union's Horizon 2020 programme for Research and Innovation under grant agreement No 727550

# AUTHORS

**Part 1 – Los Humeros geothermal system**

**Chapter 1:** Domenico Liotta (UNIBari), Matteo Lelli (IGG-CNR), Andrea Brogi (UniBari), Jacopo Cabassi (IGG-CNR), Thomas Kretzschmar (CICESE-Ensenada BC), Ruth Alfaro Cuevas Villanueva (UMSNH)

**Chapter 2:** Matteo Lelli (IGG-CNR), Thomas Kretzschmar (CICESE-Ensenada BC), Juan Sanchez-Avila (CICESE-Ensenada BC), Yan Rene Ramos (Guanajuato University), Roberto Gomez (Guanajuato University), Marco Doveri (IGG-CNR), Jacopo Cabassi (IGG-CNR), Francesco Norelli (IGG-CNR), Fabrizio Gherardi (IGG-CNR), Gabriella Magro (IGG-CNR), Eleonora Braschi (IGG-CNR), Guia Morelli (IGG-CNR), Pedro Alfaro Cuevas Vilanueva (UMSNH), David Maldonado (Puebla University), Ruth Alfaro Cuevas Villanueva (UMSNH)

**Chapter 3:** Bernard Sanjuan (BRGM), Frederik Gal (BRGM), Ruth Alfaro Cuevas Villanueva (UMSNH)

**Chapter 4:** Egbert Jolie (GFZ, Potsdam), Anna Jenstch (GFZ, Potsdam), Chris Rochelle (BGS-NERC), Helen Taylor-Curran (BGS-NERC), Bob Lister (BGS-NERC)

**Chapter 5:** Andrea Orlando (IGG-CNR), Giovanni Ruggeri (IGG-CNR), Daniele Borrini (UniFi)

**Chapter 6:** Giordano Montegrossi (IGG-CNR), Maren Brehme (GFZ, Potsdam), Patricia Pinkowski (GFZ, Potsdam)

**Chapter 7:** Jiri Miller (IFE)

**Part 2– Acoculco geothermal system**

**Chapter 1:** Domenico Liotta (UNIBari), Jacopo Cabassi (IGG-CNR), Andrea Brogi (UniBari), Thomas Kretzschmar (CICESE-Ensenada BC), Ruth Alfaro Cuevas Villanueva (UMSNH)

**Chapter 2:** Matteo Lelli (IGG-CNR), Thomas Kretzschmar (CICESE-Ensenada BC), Jacopo Cabassi (IGG-CNR), Juan Sanchez-Avila (CICESE-Ensenada BC), Orlando Vaselli (UniFi-IGG-CNR), Franco Tassi (UniFi-IGG-CNR), Barbara Nisi (IGG-CNR), Belinda Sandoval Rangel (Cicese-Ensenada BC), Romel Gonzales Hernandez (UMSNH), Carlos Ramirez Gaytan (UMSNH), Ruth Alfaro Cuevas Villanueva (UMSNH).

**Chapter 3:** Matteo Lelli (IGG-CNR), Ruth Alfaro Cuevas (UMSNH) and WP4.3 research group

**Task coordinators:** Matteo Lelli (Europe, IGG-CNR) – Ruth Alfaro Cuevas Villanueva (Mexico, UMSNH)

## TABLE OF CONTENTS[1]

### PART 1 – LOS HUMEROS GEOTHERMAL SYSTEM



[1] The content of this report reflects only the authors' view. The Innovation and Networks Executive Agency (INEA) is not responsible for any use that may be made of the information it contains.

## PART 2– ACOCULCO GEOTHERMAL SYSTEM

## OBJECTIVE AND RESULTS

This report regard the activities and results of two years of fieldwork and laboratory analyses performed in Los Humeros (LHGF) and Acoculco (AGF) geothermal fields, in the framework of the WP4.3 of the GeMex project. The report is organized in two parts, the first for Los Humeros and the second for Acoculco. Each part summarize and illustrates the scientific activities and approaches used to fulfil the aim of the Task 4.3. This task is included in the Workpackage 4 (Tectonic control on fluid flow) and it is aimed to the *Geochemical characterization and origin of cold and thermal fluids*. It involve *the sampling and analysis of fluids from boreholes and surface (natural cold and thermal springs, gas manifestations, rivers, etc.) and quantification of degassing processes at the surface (in particular diffuse emissions in selected areas), and HT tracer tests.* In order to emphasise the links between the objectives of the project and results obtained, the task description (copied by the contract and highlighted in bold) is presented here as bullet list, providing a brief description of the scientific activities performed.

- **Fluid flow-path: – field maps of natural manifestations (waters and gases) and productive wells (Los Humeros) and comparison with main structure lineaments.**

Various research groups involved in the task 4.3 performed sampling trip aimed to collect water and gas samples from natural manifestations, water wells and geothermal wells. Before sampling trips, each partner involved carried out an accurate review of the previous literature, in particular for what concern the geology, tectonics and fluid geochemistry in general. Field maps of sampling points and location of geothermal surface manifestations are included and discussed in Chapters 2, 3 and 4 (part 1 for Los Humeros) and in Chapter 2-part2 for Acoculco. In Chapter 2 (parts 1 and 2) the correlation between the geographical distribution of high values for temperature and dissolved $CO_2$ measured in some water wells located in Perote plain is discussed and compared with the main structure lineaments. In Chapter 4 the correlation between high values for $CO_2$ flux diffused from soil (and also radon and thoron concentration) and alignment of main known faults/structure is underlined.

- **Hydrology: sampling of selected cold springs located around “target” areas in Los Humeros and Acoculco geothermal sites; isotopic analysis (in particular for 18O, D and Tritium) to provide information regarding the origin of fluids (cold and thermal) and the relationship between cold surface waters and hydrothermal/geothermal water rising from depth.**
- **Fluid geochemistry: sampling and analysis (chemical and isotope) of cold and thermal springs, fumaroles and soil gases, as well as wells/boreholes in order to identify the origin (stable, radiogenic and radioactive isotope systematics) and**

**physical-chemical characteristics of reservoir fluids, steam separation/condensation and/or mixing processes and estimate the thermodynamic conditions (P and T) of the equilibration zone present at depth. For example, geothermometric estimations of the reservoir fluids will be done using classical and new auxiliary chemical and isotopic geothermometers**

In Chapter 2 (parts 1 and 2), chemical and isotope (stable, radiogenic and radioactive) data for water samples collected from cold and thermal springs, wells and maar lakes located in target areas in Los Humeros and Acoculco, properly selected to provide information regarding the origin of fluids and feeding zones, are discussed. In Chapter 2 (parts 1 and 2) chemical and isotope data regarding fumaroles and dry gas samples are included and discussed. Chemical and isotope analysis for water samples from some cold and thermal springs, cold wells and geothermal wells are included and discussed also in Chapter 3. Geothermometric estimations performed using classical and new auxiliary chemical and isotope geothermometers are discussed in Chapter 3 (part 1), both for Los Humeros and Acoculco geothermal systems. Literature data of Los Humeros geothermal wells are also included and discussed in suitable diagrams in order to obtain information regarding the relationships between cold surface waters and hydrothermal/geothermal fluids.

- **Measurements of $CO_2$, $H_2S$ and $CH_4$ fluxes diffused from soil using the accumulation chamber and static chamber methods, aimed to the elaboration of isoflux maps. In addition, radon ($^{222}Rn$) and thoron ($^{220}Rn$) measurements will be performed. The analysis of further parameters, such as helium and gamma-spectroscopic measurements, will be considered.**

These issues regard the Chapter 4 in which isoflux maps for $CO_2$ fluxes diffused from soil are inserted and discussed, in particular for what concern the relationships between high flux values and alignments of main faults/fractures. The estimation of total output of $CO_2$ emitted from soil and data regarding radon and thoron concentrations measured in Los Humeros geothermal field are also provided. In Chapter 2 (part 2) the results for measurements of $CO_2$ fluxes diffused from soil in Acoculco geothermal field are discussed and reported as maps and tables. Estimations of total output are also provided. The results obtained by mobile $CO_2$ laser detection are also included and discussed.

- **Geochemical modelling: Study of water saturation respect to “relevant” mineral phases and modelling of gas-waterrock interaction processes as well as relevant physical processes (e.g. boiling or phase segregation) at depth.**

Chapter 6 (part 1) regard the geochemical modelling. Data and results for some Los Humeros geothermal wells are discussed in terms of saturation of several mineral phases, trying to obtain information regarding their scaling potential.

- **Development, qualifying and application of high temperature tracers adapted to conditions in Los Humeros and Acoculco (IFE)**

Research activities regarding the development of high temperature tracers are part of the Chapter 7 (part 1). The behaviour of the different tracers tested at different temperature conditions and in presence of rock particles are illustrated and discussed.

- **Laboratory experiments for the study of fluid/rock interaction processes at high-temperature.**

In Chapter 5, the results of fluid–rock interaction experiments performed at different temperature (200-300°C), using two andesitic rocks from Los Humeros and local meteoric fluids, are discussed. Description of mineral assemblages obtained from the experiments is reported, together with the comparison with some phases typically encountered in Los Humeros alteration products.

## EXECUTIVE SUMMARY

In order to reach the goals of the task, detailed studies regarding fluid geochemistry were performed, together with laboratory experiments and geochemical modelling on fluid/rock interaction processes at high-temperature and high-T tracer tests. This study represent a novelty for LHGF and AGF, since detailed investigation at regional scale has not been done before. One of the most important novelty regard the role played by the meteoric recharge as a source component of the Los Humeros geothermal fluids (Chapter 2, part 1). Stable isotopes data of geothermal fluids are compatible with physico-chemical process commonly identified in several geothermal wells worldwide (e.g. oxygen-shift due to interaction of meteoric water with reservoir rocks). Mean values of $\delta^2H$ and $\delta^{18}O$ for cold water collected in the AGF (excluding the acid waters) are similar to those for LHGF and this feature point out to the regionalization of the meteoric component. Regional recharge cannot be ruled out for LHGF and it could represent an important percentage of the total amount. In Perote plain and toward the south side of the Los Humeros study area, a cluster of “warm” water wells (T up to ≈33°C) aligned in NE-SW direction were identified for the first time. New details regarding chemical and isotopic properties of circulating waters from springs and wells were also acquired in AGF (Chapter 2, part 2), with better understanding of the characterization and evolution of meteoric component at regional scale.

Several kinds of classical and auxiliary geothermometers are applied and developed for thermal/geothermal fluids of both geothermal systems (Chapter 3, part 1). The Na-Li and Na-Cs auxiliary geothermometers, recently defined, give concordant temperature values (320 ± 30°C) with those estimated using the classical Silica-quartz, Na-K and Ca-K geothermometers, and the isotopic $\delta^{18}O_{H2O-SO4}$ geothermometer, for the Los Humeros deep dilute geothermal waters, depleted in Ca, Mg and Sr, and enriched in $SiO_2$, B and Li, after interaction with andesitic rocks in the reservoir. For numerous thermal waters from both geothermal areas, which are mainly constituted of shallow waters rich in Ca, Mg and Sr, interacting with Mesozoic limestone at temperatures estimated from 60 to 100°C, the Na/K and Na/Li ratios similar to those of the Los Humeros geothermal waters and the relatively high B concentrations suggest small inflows of high-temperature deep waters (close to 300°C), despite the low permeability of these areas.

Detailed study of soil degassing was performed inside the LHGF producing zone and also in AGF (Chapter 2, part 2). In LHFG some areas are characterized by good correlation between known faults and the increasing in $CO_2$ flux rate and elevated radon and thoron concentrations (Chapter 4, part 1). The presence of very high degassing areas ($CO_2$ efflux > 300 g $m^{-2}d^{-1}$) at the surface can only be explained by convection along permeable faults/ fractures. In some areas of interest, more detail regarding soil degassing was obtained by mobile laser survey. By carbon isotopic analysis of $CO_2$ and helium isotopic analysis $^3He/^4He$ determined in gases released by the soil, it is indicated that faults and fractures in the subsurface have a link to the deep geothermal reservoir and favor the upflow of hydrothermal fluids. The results of soil degassing study suggest that the most permeable zone in the Los Humeros geothermal field is located in SW area and extends towards the north and northeast. In Acoculco, gas flux was very low and no significant correlations with alignment of regional faults/fracture were evidenced (Chapter 2, part 2). Just in a few sites, evidences for enhanced gas flow associated to the location of natural gas emissions, drilled boreholes and/or with a few specific tectonic features seems to be present.

Several fluid-rock interaction experiments at different temperatures (T) and pressure (P) have been carried out to constrain the physical-chemical processes occurring in the upper reservoir of the LHGF (Chapter 5, part 1). The obtained results indicate that silicification is the most important alteration process. Analytical methods used suggest that in LHGF high mineralized waters likely reacted with andesitic reservoir. In particular, the presence of wairakite in some experimental products could corroborate the hypothesis that infiltrating waters extensively reacted with crossed rocks before reaching the reservoir.

Geochemical modeling was used in several fluid from Los Humeros geothermal wells, investigating the possible mineral phases and their behavior as function of temperature. Possible hydrothermal/methamorphic high temperature secondary minerals were identified, together with a group of secondary minerals with scaling potential. Also, some information regarding the origin of chemicals present in the fluids of Los Humeros geothermal field are obtained.

Seven tracer candidates were first tested for thermal stability in closed quarts vials at temperatures from 150 to 250$^{o}$C (Chapter 7, part 1). Of the seven compounds tested, one tracer candidate (Tracer C) showed satisfactory properties as geothermal tracer and is expected to be suitable at temperatures up to at least 375$^{o}$C.

Concluding, the task 4.3 aims were completely reached, with important novelties representing an improvement of our knowledge for: i) identification of feeding zones of geothermal fluids, ii) physico-chemical evolution of hot fluids, iii) characterization of flow-paths linked with geological structures in fractured media. All the milestones were also reached on time.

# Chapter 1

## STATE OF THE ART ON LOS HUMEROS GEOTHERMAL SYSTEM BEFORE GeMex

### 1.1 Geological and geothermal settings

Los Humeros geothermal field is located ca. 200 km SE of Mexico City, on the eastern portion of the Plio-Pleistocene Trans-Mexican Volcanic Belt, near the border of this province with the Sierra Madre Oriental province. This geothermal field lies within a wide caldera complex constituted by the Potreros caldera (9-10 km in diameter), where all geothermal wells were drilled, nested within the larger Los Humeros caldera (15 x 21 km). The evolution of the caldera complex was proposed to begin at 460 ky by Ferriz and Mahood (1984), with ignimbrite eruptions, when a highly differentiated magmatic chamber was emplaced beneath the Mezozoic calcareous sequences, interrupted by the construction of several rhyolitic domes and basaltic-andesite volcanoes. However, recent studies suggest that the onset of the caldera activity occurred last at 164 ky (Carrasco-Nuñez et al., 2018). The basement rocks of this field are granites and schists of Paleozoic age, covered by a thick series of Jurassic and Cretaceous limestones, metamorphosed during the Laramide orogeny and by Oligocene magmatic intrusions (De la Cruz, 1983). Fissural volcanic activity in the area started in the Miocene (≈ 10 Ma), producing the Alseseca andesites that outcrop in the north-eastern part of the Los Humeros caldera. Further volcanic activity did not take place until the Pliocene, when the volcanism associated with the Mexican volcanic belt started, producing the Teziutlan andesites in the area (3.3-1.9 Ma ago; Yañez García and Casique Vásquez, 1980). The LHGF is located 200 km SE of Mexico city, within a complex caldera system active from 0.46 Ma, when ignimbrite eruptions began. The activity ends 20ka ago, reaching the final hydrothermal stage (Ferriz and Mahood, 1984). LHGF represents one of the most important Mexican geothermal system used for electric power generation (about 65MW). Maximum temperature close to 400°C was measured in geothermal wells located in the northern part of the producing area. Excess enthalpy condition (>2400 KJ/Kg; (Gutierrez-Negrin and Izquierdo-Montalvo, 2010) characterize the LHGF since the first stage of fluid extraction (started in 1982: Arellano et al., 2015) and it was enhanced by twenty-nine years of exploitation (started in 1990; Arellano et al., 2003), causing aquifer boiling, phase separation and steam condensation (Barragan et al., 2008; Arellano et al., 2015). Since 1982 to December 2012, about 123 Mt of fluid was extracted (Arellano et al., 2015), including ca. 104 Mt of steam (84.3%) and ca. 19 Mt of liquid (15.7%). Re-injection started in 1995 and in the same period (up to December 2012) about 6.3 Mt of extracted fluid was re-injected in the reservoir (Arellano et al., 2015). This represents a small fraction of the total extracted fluid (5.1%) and the effect of re-injection in LHGF is still debated: for Arellano et al. (2015) it is not clear, whereas Pinti et al. (2017), based on noble gas elemental ratios, suggest the presence of some geothermal wells producing a high fraction of re-injected fluids (62 to 100% of the production fluid). Geothermal fluids are exploited by producing levels, consisting of sequence of fractured blocks characterized by low permeability. Chemical and isotopic composition of geothermal fluids highly depend on depth, enthalpy and flow rate of the wells. For LHGF many geochemical data regard the characterization of geothermal fluids from producing wells and the identification of their important chemical and isotopic temporal evolution due to exploitation (Barragan et al., 1988, 1989, 1991; Truesdell, 1991a,b; Prol-Ledesma 1998; Arellano et al., 2003, 2015). Conversely, very few geochemical data on cold water from springs and wells are used or no data are available for the identification of feeding zones and mean altitude of recharge areas, and to link the meteoric component with geothermal fluid evolution in terms of water-rock interaction and phase separation. Before GeMex, the recharge mechanism of LHGF was still unclear and no detailed study regarding the meteoric component was performed. Therefore, this issue represent one of the most important question that has to be clear in order to fulfil specifics goals of the Task 4.3.

**References**

Arellano Gomez V.M., García A., Barragán Reyes R.M., Izquierdo G., Aragón A., Nieva D. (2003) - An updated conceptual model of the Los Humeros geotermal reservoir (México). Journal of Volcanology and Geothermal Research, 124, 67-88.

Arellano Gomez V.M., Barragán R.M., Ramírez M., Lopez S., Paredes A., Aragón A., Tovar R. (2015) - The response to exploitation of the Los Humeros (México) geothermal reservoir. Proceedings World Geothermal Congress 2015, Melbourne, Australia, 19-25 April 2015, 7 p.

Barragan, R.M., Santoyo, E., Nieva, D., Portugal, E., Verma, M.P., 1988. Caracterizacio¤n de yacimientos geotermicos mediante la determinacion de parametros fisico-quimicos. Internal Report IIE/11/2386/I 01/F, Instituto de Investigaciones Electricas, Temixco, Mor., 250 pp.

Barragan, R.M., Cervantes, M., Diaz, R., Garduno, V., Gonzalez, E., Holguin, S., Meza, F., Nieva, D., Oliver, R., Rosas, N., Sampedro, J., 1989. Caracterizacion del fenomeno de corrosion y obturacion en pozos de Los Humeros. Report IIE/11/3753/I for the Comision Federal de Electricidad, Instituto de Investigaciones Electricas, Temixco, Mor., 83 pp.

Barragan, R.M., Nieva, D., Santoyo, E., Gonza¤lez, E., Verma, M., Lo¤pez, J., 1991. Geoquimica de fuidos del campo geotermico de Los Humeros (Me¤xico). Geotermia Rev. Mex. Geoenerg. 7, 23-47.

Barragán-Reyes R.M., Arellano Gomez V.M., Flores Armenta M., Tovar Aguado R. (2008) - Cambios químicos en fluidos de pozos del campo geotérmico de Los Humeros: evidencia de recarga profunda. Geotermia, 21, n°2, 11-20.

Carrasco-Núñez G., Bernal J.P., Dávila P., Jicha B., Giordano G., Hernández J., Navarro M. (2018) - Reapraisal of Los Humeros volcanic complex by new U/Th zircon and 40Ar/39Ar dating: implications for greater geothermal potential. Geochem.Geophys. Geosyst., 19. https://doi.org/10.1002/2017GC007044.

De la Cruz V. (1983) - Estudio geológico a detalle de la zona geotérmica de Los Humeros, Pue. Internal report 10/83, CFE, 51 p.

Ferriz H. and Mahood G. (1984) - Eruption rates and compositional trends at Los Humeros volcanic center. Puebla, México. J. Geophys. Res., 89 (B10), 8511-8524.

Gutiérrez-Negrín L.C.A., Izquierdo-Montalvo G. (2010) - Review and update of the main features of the Los Humeros geothermal field, Mexico. Proceedings World Geothermal Congress 2010, Bali, Indonesia, 25-29 April 2010, 7 p.

Pinti D.L., Castro M.C., Lopez-Hernández A., Han G., Shouakar-Stash O., Hall Ch.M., Ramírez-Montes M. (2017) - Fluid circulation and reservoir conditions of the Los Humeros Geotermal Field (LHCF), México, as revealed by a noble gas survey. Journal of Volcanology and Geothermal Research, 333-334, 104-115.

Prol-Ledesma R.M. (1998) - Pre- and post-exploration variations in hydrothermal activity in Los Humeros geothermal field, Mexico. Journal of Volcanology and Geothermal Research, 83, 313-333.

Truesdell, A.H., 1991a. The origin of high-temperature zones in vapor-dominated geothermal systems. Proc. Sixteenth Workshop on Geotherm. Res. Eng., Stanford Univ., Stanford, CA, pp. 15-20.

Truesdell, A.H., 1991b. Origins of acid £uids in geothermal reservoirs. Geotherm. Res. Counc. Trans. 15, 289-296.

Yáñez García C, Casique Vázquez J. (1980) - Informe geológico del Proyecto geotérmico Los Humeros-Las Derrumbadas, Estados de Puebla y Veracruz, México. Internal CFE report (unpublished).

# Chapter 2

# WATER AND GAS GEOCHEMISTRY

## 2.1 Introduction

Specifics tasks of the hydro-geochemical study are related to define chemical and isotopic characteristics of cold and thermal waters and geothermal gases, in order to: i) identify “feeding zones” of geothermal fluids; ii) constrain the equilibrium temperature reached by the fluid at depth; iii) identify the secondary processes (i.e. phase separation, precipitation of mineral phases), which take a part during the evolution of geothermal fluids from reservoir conditions to surface levels.

Before sampling, an accurate study of available hydro-geochemical data, geological and structural maps and also 3D morphological model was performed. This phase allowed to select suitable sampling points for the study in the framework of the task 4.3. In addition, some other important information about sampling points was obtained during various teleconference with CFE’s personnel. Once in the field, many new sampling points were discovered and identified, also thanks to CFE support. Two sampling campaigns were performed in LHGF, in particular in June 05$^{th}$-14$^{th}$, 2017 and March 16$^{th}$-28$^{th}$, 2019. A total of 57 and 87 water samples from cold springs, cold water wells, maar lakes, thermal springs and reinjection wells were collected in June 2017 and March 2018, respectively (see table A1 in appendix). Both sampling trips are performed in collaboration with CICESE (Ensenada, BC), University of Guanajuato, (Guanajuato) and University of Michoacán, Morelia (UMSNH). On March 2018, also BRGM took part in the field trip.

## 2.2 Waters: Sampling, field measurements and laboratory analyses

Sampling points are shown in the location map of figure 2.2.1, in which waters samples collected in the GeMex project (in green) are reported together with water samples collected during previous works (in red). As showed by the map, the distribution of samples collected during the GeMex project cover an area bigger than the previous investigated surface, and also include different kind of lithology. Particular attention was focused on the selection of “target” areas in which to perform sampling of cold springs, providing information regarding the origin of fluids and relationship between cold surface waters and hydrothermal/geothermal fluids. In particular, springs located on limestone outcrops of the Sierra Madre Oriental and at higher altitude (>3500 m.a.s.l on the Cofre de Perote.) were sampled for the first time. Since no thermal springs are present close to the Los Humeros producing area, during the first field trip samples from Chignahuapan and El Carrizal thermal springs were also collected, in order to obtain significant indication regarding physico-chemical characteristics of hot fluids circulating in different lithology.

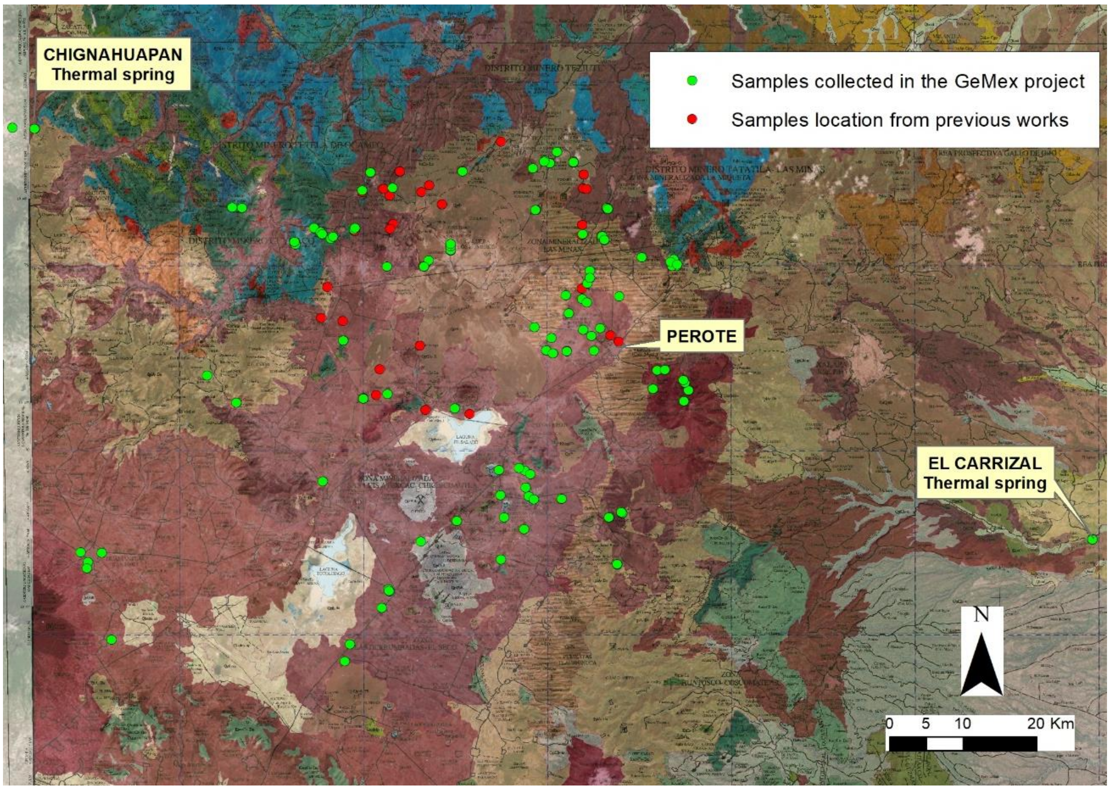


Figure 2.2.1 - Location map of water samples collected in LHGF during the GeMex project. Samples collected during previous work are also shown (blue points). Geological map 1:250000 is also reported (Veracruz E14-3, SGM, 2002).

During field trips, Temperature, pH, Electrical Conductivity, Redox Potential, Dissolved Oxygen and in situ determination of total alkalinity were performed using suitable portable instruments (figure 2.2.2a and 2.2.2b). Total alkalinity was measured by acid-base titration, using a micro-dosimeter containing HCl 0.1N and methyl-orange as pH-indicator (figure 2.2.2b). When possible, the flow rate was measured by means of flow-meter or estimated by visual observation or suitable vessel (figure 2.2.3). Each sampling point was documented by photos and sampling cards indicating GPS coordinates, altitude, presence of rock alteration and/or mineral deposition, measured flow rate and results about field determinations/measurements. All parameters measured in the field are inserted in table A1 in appendix. Waters from wells were collected using the installed pumping system and suggested (2x well volume) waiting time to avoid the presence of stagnant water in the pipes (figure 2.2.4).

Figure 2.2.2a – Portable instruments used in the field

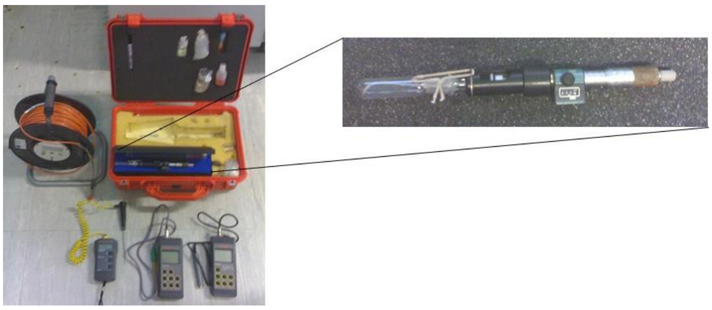

Figure 2.2.2b – Micro-dosimeter used for total alkalinity determinations

Figure 2.2.3 – Flow rate measurement

Figure 2.2.4 – Temperature measurement from water well with installed pumping system

Different kind of aliquots were collected, each of one characterized by specific treatment in order to preserve chemicals parameters up to laboratory analysis. In particular:

- n°1 of 125ml Polyethylene (PE) bottle of filtered water (0.45 µm membranes of cellulose acetate) for analysis of Cl, $NO_3$, $SO_4$, F, Br;
- n°1 of 50ml PE bottle of un-filtered water for stable water-isotopes analysis (δD‰, $\delta^{18}$O‰, $^{87}Sr/^{86}Sr$);
- n°1 of 50ml PE bottle of filtered (0.45 µm membranes of cellulose acetate) and acidified ($HNO_3$ 1:1 superpure) for analysis of Na, K, Ca, Mg, B, Li, Sr, $SiO_2$;
- n°1 of 100ml PE or glass bottles of acidified (HCl 1:1) for $NH_3$ analysis;
- n°1 of 250/500 ml PE bottle of un-filtered water for Tritium analysis.

Chemical and isotopic analyses of water samples were carried out in IGG-CNR labs, applying the following analytical techniques:

- $Li^+$, $Na^+$, $K^+$, $Mg^{2+}$, $Ca^{2+}$, B in the filtered-acidified aliquot by Inductively Coupled Plasma-Optical Emission Spectroscopy (ICP-OES);
- $Cl^-$, $SO_4^{2-}$, $NO_3^-$ and Br in the filtered aliquot by ion chromatography (IC);
- $F^-$ in the filtered aliquot by ion-selective electrodes (ISE);
- dissolved $SiO_2$ in the filtered-acidified aliquot by visible spectrophotometry (UV-VIS);
- the isotope ratios $^{18}O/^{16}O$ $D/^1H$ and $^{87}Sr/^{86}Sr$ of water in the filtered aliquot respectively by Mass Spectrometry (LGR) and MC-ICP-MS.
- Tritium was determined through measurement of β- decay events in a liquid scintillation counter.

Short-term analytical precision (repeatability) is better than 2% for ICP-OES analyses, 3-5% for IC and ISE determinations, and close to 5 % for visible spectrophotometry. The uncertainties on the $\delta^{18}$O and δD values are ±0.05‰ and ±1‰, respectively.

Results of water analyses are given in appendix (table A2). Charge balance is also reported, and it is lower than 3% for all samples.

### 2.2.1 Hydrogeochemical classification and binary plots

Chemical classification is one of the most important phases of data elaboration in which significant information regarding water-rock interaction and others physico-chemical processes (e.g. ion-exchange, dilution, mixing, precipitation of mineral phases) can be obtained.

Water chemistry is initially analysed in terms of the relative concentrations of major anions ($HCO_3$, $SO_4$, and Cl) and major cations (Na, K, Ca, and Mg), by means of the conventional Langelier-Ludwig (LL) compositional pyramid and relevant cross-section (Langelier and Ludwig, 1942). In the LL compositional diagrams the samples are displayed using a suitable coefficients $R_i$, calculated starting from the concentrations ($C_i$) expressed in eq/L:

$$R(Na+K) = 50 * \frac{(C_{Na}+C_K)}{(C_{Na}+C_K+C_{Ca}+C_{Mg})}$$

$$R(Ca+Mg) = 50 * \frac{(C_{Ca}+C_{Mg})}{(C_{Na}+C_K+C_{Ca}+C_{Mg})}$$

$$R(HCO3) = 50 * \frac{(C_{HCO3})}{(C_{HCO3}+C_{Cl}+C_{SO4})}$$

$$R(HCO3+SO4) = 50 * \frac{(C_{HCO3}+C_{SO4})}{(C_{HCO3}+C_{Cl}+C_{SO4})}$$

$$R(HCO3+Cl) = 50 * \frac{(C_{HCO3}+C_{Cl})}{(C_{HCO3}+C_{Cl}+C_{SO4})}$$

Data of geothermal fluids collected from geothermal wells (previous public data and new data from CFE) are included in the elaboration processes, both as for reference and also to identify possible correlation between surface and deep fluids.

LL diagrams (figures 2.2.5a, b and c) show that most collected waters have $HCO_3$ and Na or Ca as dominant anion or cations dissolved species, respectively. The distributions of points in the LL classification diagrams allow to identify three main “hydrochemical type”: 1) Na-$HCO_3$, 2) Ca-$HCO_3$ and 3) Ca-$SO_4$($HCO_3$) waters. The first one is represented by spring waters located at high altitude in the Cofre de Perote volcano (PER13 and PER14) or close to Zaragoza country, in which outcrops of lava rocks (i.e. andesites, trachyandesites, dacites) are extensively present. This hydrochemical type represents the first stage of water-rock interaction between meteoric water and andesites. Calcium bicarbonate waters (Ca-$HCO_3$) is the most abundant hydrochemical type in the study area and is composed by waters from cold springs and wells located at different altitude. It represents different evolution stage of interaction between meteoric waters and carbonate rocks (i.e. limestone). The third hydrochemical type ($Ca-SO_4-HCO_3$) characterize some wells (LH17, LH17bis and PER43) located in the south part of the studied area close to “Laguna de Totolcingo”, in which higher $SO_4$ concentrations are shown. The arid climate conditions characterizing this sector of the study area result in intense evapotranspiration/evaporation. In fact, around the “Laguna de Totolcingo” a widespread mineral salt deposit is present, known as *“Tequesquite”*, which is mainly composed by sodium-carbonate and sodium-chloride with associated potassium-carbonate, sodium-sulfate and clay (Alcocer and Hammer, 1998). The $Ca-SO_4-HCO_3$ hydrochemical type waters can reflect the interaction at surface levels of meteoric water with Tequesquite salt incrustation. This process probably involve others samples from wells located close to maar lakes (i.e. LH20, PER38 and PER48), in which Total Ionic Salinity increase (T.I.S.) and Cl concentration is higher than in other samples (see figure 2.2.5b). Chloride concentration is particular high for sample PER51, which is water from local wells characterized by the higher T.I.S. value (c.a. 115 meq/L). $Ca-SO_4$ chemical composition is showed by sample PER85, a water collected at an altitude close to 3000 m.a.s.l. in the south-west side of the study area: taking into account that no salt incrustations or evaporite formations are present, the interpretation of its physico-chemical characteristic is ambiguous. Water from Alchichica maar (LH18) is characterized by very high T.I.S. value and Na-Cl composition. Of course, its characteristics can be interpreted in terms of interaction with salt deposits/incrustations and/or intense evaporation. Same chemical composition and evolution characterize a sample from a shallow well close to the Pizarro volcano (PER78), even if higher $HCO_3$ concentration is also present.

In the Perote plain, some wells show temperature ranging from 20°C to 33.1°C (LH50, LH50bis, LH54, LH55, LH61, PER27, PER31, PER54, PER55, PER56, PER57 and PER59). These wells are exploited by farms and have depth ranging from 120 to 180m and flow rate of about 60-70 L/sec. Productive levels are located in rock formations, probably represented by andesites and dacites lavas located at shallow level close to Perote (see stratigraphic section in Carrasco et al., 2017). Their composition is $HCO_3$-Na-Ca. The thermal spring of Cignahuapan (50.4°C) shows $Ca-HCO_3(Cl)$ chemical composition, suggesting an origin probably due to interaction with limestone, but also with volcanic rocks (Na is the second most abundant dissolved cation).

As well known from literature (Barragan et al., 1988, 1989, 1991; Truesdell, 1991a,b; Prol-Ledesma 1998; Arellano et al., 1998, 2003, 2015), fluids from geothermal wells show variable chemical composition from $Na-HCO_3$ to Na-Cl. Some geothermal wells (H12, H23, H43, H58) show different Na(+K)/Ca(+Mg) ratio, approaching the line (Na+K) =25 %eq in LL diagrams. Some samples collected in different time from few productive wells (H7, H16, H17, H19, H34, H43) show temporary spike toward higher $SO_4$ concentrations: it is could be due to partial condensation of excess steam with dissolution of $H_2S$ and subsequently oxidation to sulfate. As for reference, re-injected fluids show $Na-SO_4(HCO_3)$ chemical composition.

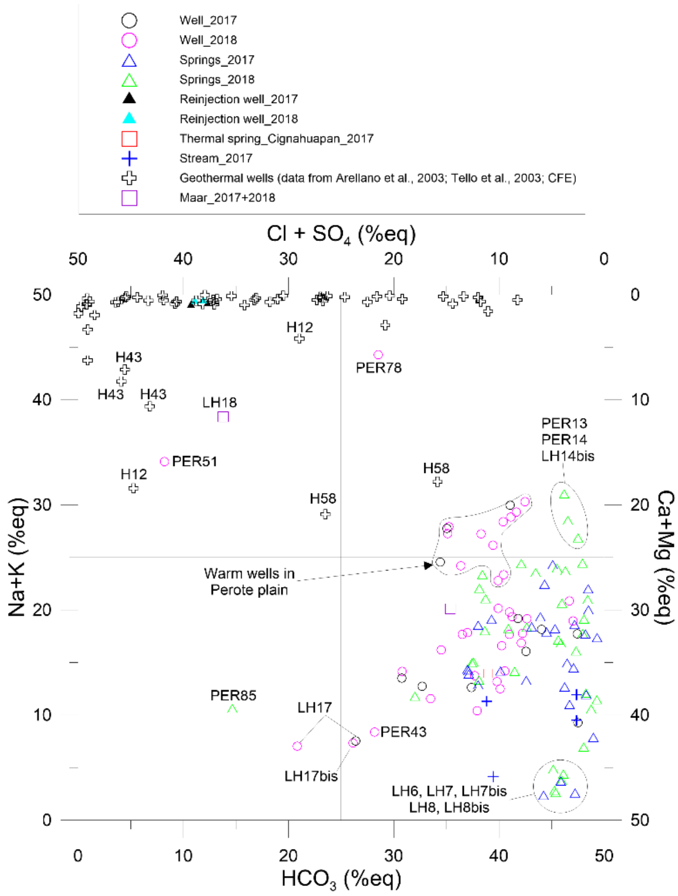


Figure 2.2.5a – LLHCO$_3$ classification diagram

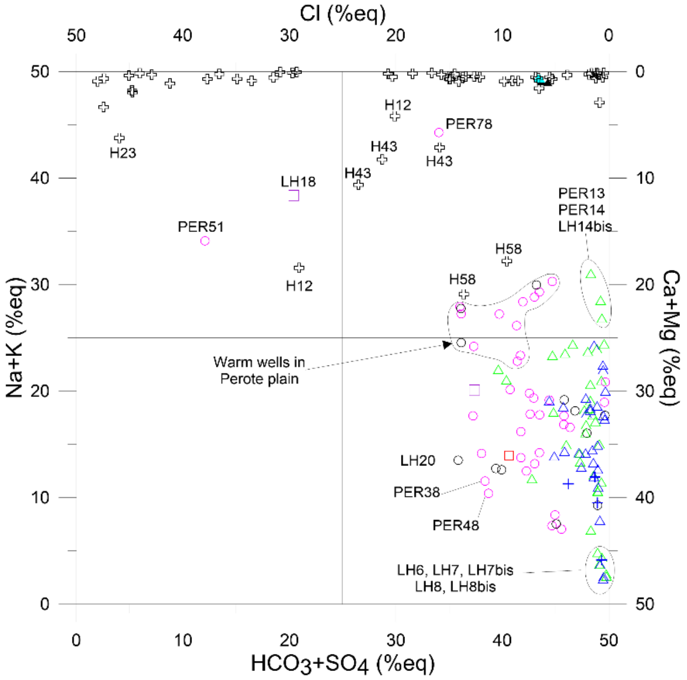


Figure 2.2.5b – LLCl classification diagram

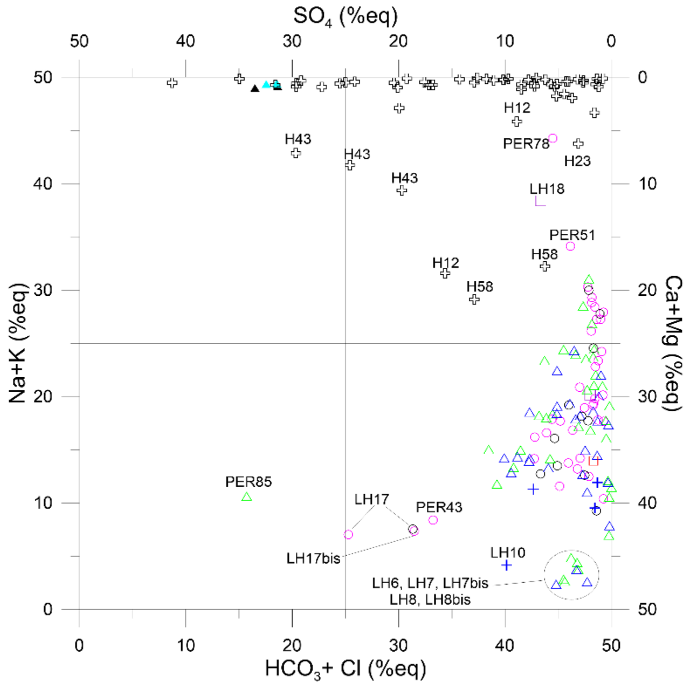


Figure 2.2.5c – LLSO$_4$ classification diagram

Since the LL plots of major anions and major cations do not deliver any information on the T.I.S. of the waters of interest, it is advisable to inspect suitable cross-section of LL plots. In fact, the T.I.S. of water samples can be appreciated in these diagrams, by comparing their position with respect to the lines of slope -1, which are iso-T.I.S. lines (see Tonani et al., 1998 for further details). In figures 2.2.6 and 2.2.7, correlation plots $HCO_3$ vs. $Cl+SO_4$ and Na vs. Ca+Mg+K are presented, respectively. The two correlation plots show that water from the Alchichica maar lake has the highest T.I.S. (c.a. 320 meq/L), followed by PER51 (114 meq/L) and PER55 (96 meq/L). Among samples collected during this work, T.I.S. varies from 0.7 to 3.4 meq/L for cold spring waters, 0.5 to 114 meq/L for well waters and 5.2 to 9.8 meq/L for surface water of creeks. The salinity of Cignahuapan's thermal spring is c.a. 33 meq/L. Langelier-Ludwig cross sections allow the identification of samples affected by different extent of salt dissolution (e.g. LH17, LH17bis, LH20, PER38, PER43, PER48 and PER78). Although PER51 and PER55 show similar high T.I.S. and temperature values, their chemical compositions are very different. PER51 is Na-Cl water and is located close to the *Tequesquite* deposits/incrustations, whereas PER55 is $Na-HCO_3$ water and is characterized by very high $HCO_3$ concentration (2028 mg/L). Waters from warm wells in Perote plain show a different alignment compared to wells located in the south part of the study area.

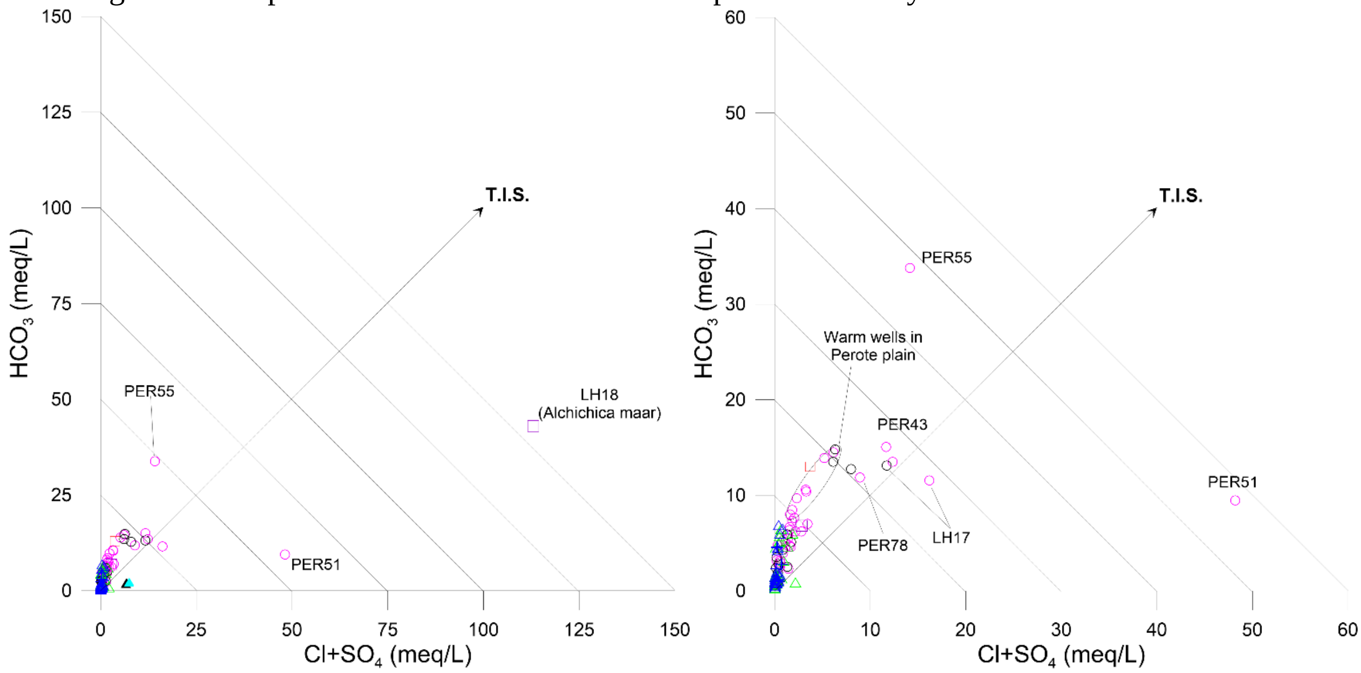


Figure 2.2.6 – Correlation plot $HCO_3$ vs. $SO_4$+Cl (left) and its magnification for TIS value <120 meq/L. Symbols as in figure2.2.5a

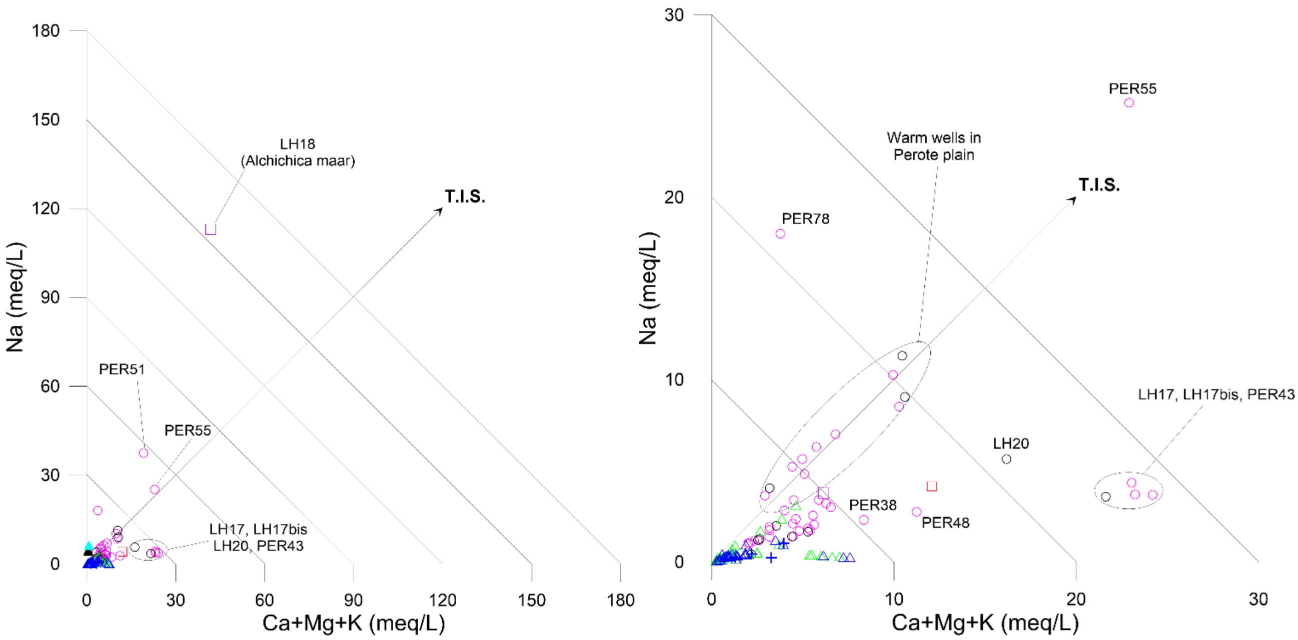


Figure 2.2.7 – Correlation plot Na vs. Ca+Mg+K (left) and its magnification for TIS value <60 meq/L. Symbols as in figure 2.2.5a.

Correlation plots contrasting each solute with chloride, which is the mobile (conservative) constituent of reference, are used to investigate (a) mixing effects and (b) the differences/similarities among warm waters from central sector of the Perote plain or area close to Totolcingo lagoon.

The chloride plots of boron (Figure 2.2.8) and lithium (Figure 2.2.9) show that samples from wells located close to Totolcingo lagoon and La Derrumbadas volcano (i.e. LH17, LH17bis, LH20, PER43, PER48, PER51 and PER78) are affected by salt dissolution. Also some warm waters from wells in Perote plain seem to be influenced by the same process (LH54, LH55 and PER55). Boron and lithium contents respectively higher than 1 mg/L and 0.1 mg/L determined in some spring and well waters can be interpreted in terms of interaction with volcanic rock formations and/or deposits composed by their debris. Also in the chloride diagrams of deuterium and oxygen-18 (Figure 2.2.10), samples LH17, LH17bis, PER38, PER43, PER48, LH20, LH54, LH55, PER51, PER55 seem to be influenced by salt dissolution. For these samples, same correlations are obtained also using $HCO_3$ and $SO_4$ contents (which represent others two major chemical component of local salt incrustations). In both diagrams, water samples from maar lakes (Alchichica and Quecholac) and shallow well close to Pizarro volcano (PER78) are distributed toward enriched values of stable isotopic composition, owing to the isotopic fractionation during evaporation process. In terms of stable isotopic compositions it is interesting to note the low values for springs located close to the top of the Cofre de Perote volcano (LH35, LH36, LH37, PER13, PER14, PER15 included in group 1 in figures 2.2.10). This is associated to the high altitude of infiltration (close to 4000 m.a.s.l.) and it is in agreement with stable isotopic values for samples collected from wells located at the foothill of the Cofre de Perote volcano (samples in group 2): in fact, lower altitude means less altitude of infiltration or mixing between waters infiltrated at different altitude. Wells located in the south part of the studied area, as PER36, PER37, PER47, PER49, PER53 (group 3 in figures 2.2.10) show similar stable isotopic composition as for group 2, but higher values of chloride. Other wells as LH17, LH17bis, PER38, PER43 and PER48 (also located in the south part), show chloride concentration even greater. For all these samples, a mean altitude of infiltration close to 3000 m.a.s.l. can be hypothesized.

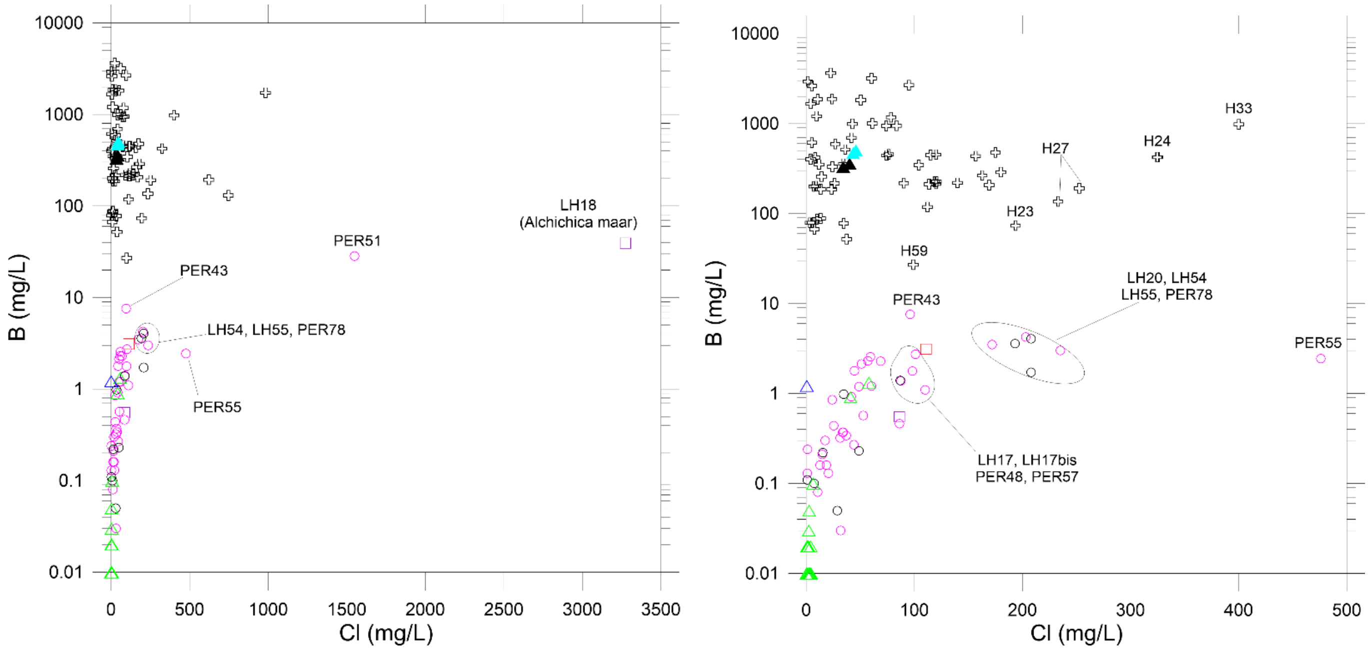


Figure 2.2.8 – Correlation plot B vs. Cl (left) and its magnification (right) for Cl value <500 mg/L. Symbols as in figure 2.2.5a.

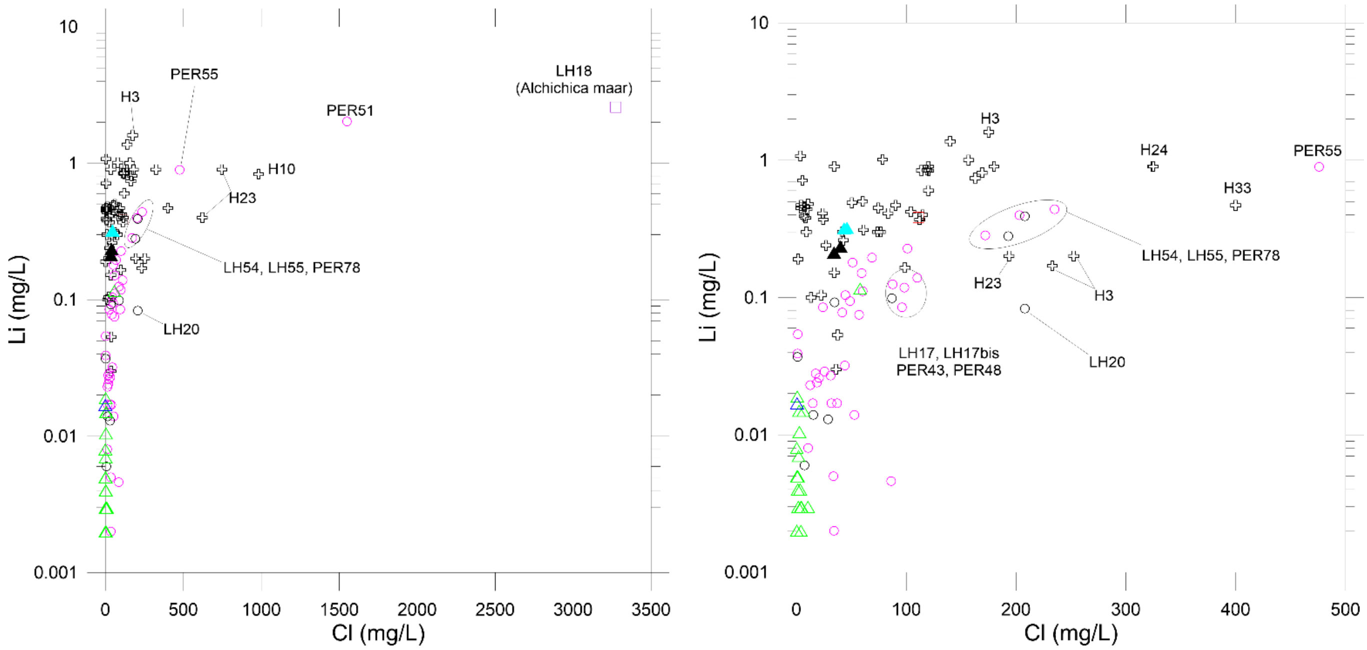


Figure 2.2.9 – Correlation plot Li vs. Cl (left) and its magnification (right) for Cl value <500 mg/L. Symbols as in figure 2.2.5a.

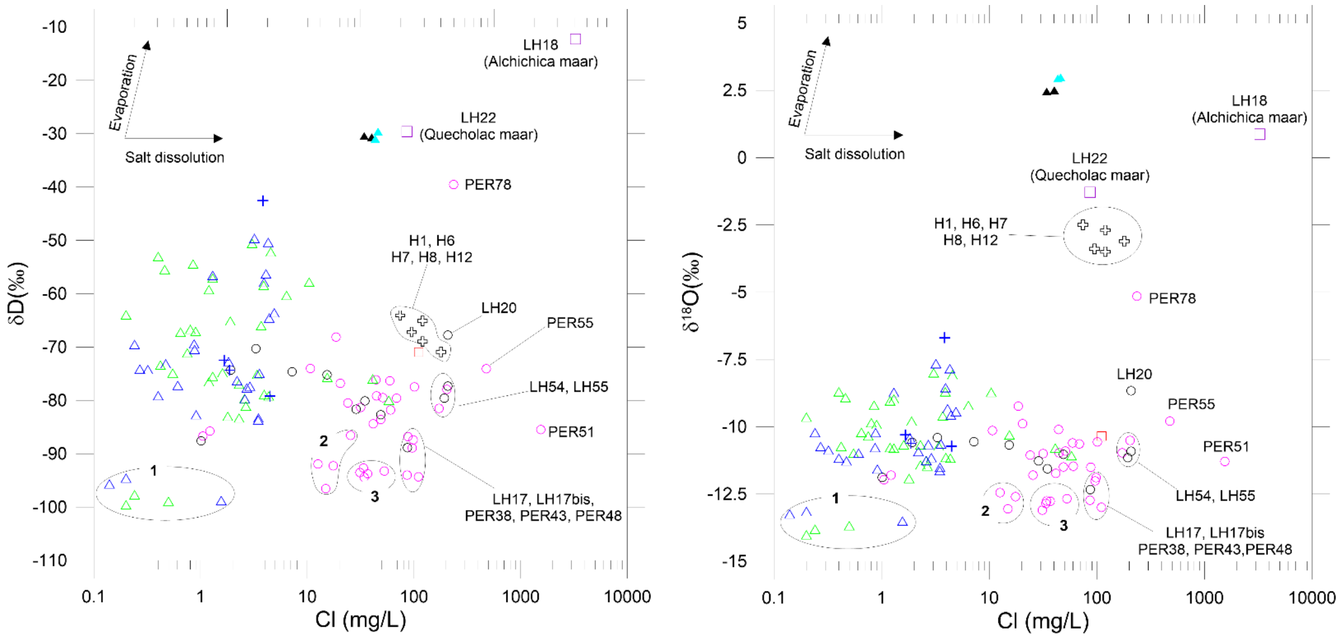


Figure 2.2.10 – Correlation plots Cl vs. δD (left) and Cl vs. $\delta^{18}O$ (right). Black arrows are inserted to easily identify the evolution of points due to dissolution of salt and evaporation. Symbols as in figure 2.2.5a.

### 2.2.2 Saturation Index

The dissolution of generic solid phases can takes place only if the aqueous solution is in under saturation state. Of course, if aqueous solutions are over-saturated with respect to specific solid phase, this latter cannot precipitate. Therefore, in order to acquire information regarding water-rock interaction process and, more in general, secondary processes (e.g. precipitation of mineral phases), it is very important to evaluate the equilibrium degree (i.e. the Saturation Index – SI) of aqueous solution with respect to the mineral phases of interest. This evaluation can be performed by the calculation of SI:

$$S.I. = log\left(\frac{Q_j}{K_j}\right)$$

where $Q_j$ is the ion activity product and $K_j$ is the solubility product.

The aqueous solution is saturated when S.I. = 0. For negative values (S.I.<0) the aqueous solution is under-saturated, whereas positive values (S.I.>0) mean over-saturation.

For samples collected in the framework of the GeMex project, the Solveq numerical code with Soltherm_98 database was used (Spycher and Reed, 1998). The results obtained are showed in correlation diagrams between the S.I. values and the pH. The choice is dictated by the strong dependence on the pH of the S.I., for different groups of minerals of interest. In fact, the dissolution reactions of mineral phases are governed, to a large extent, by the activity of the H + ion. Gypsum and Anhydrite are an exception since their S.I. is not correlated by the pH: in these cases, S.I. is plotted versus $SO_4$ concentration. To take into account the uncertainties inherent in the calculation, we consider under-saturated the waters with SI <-0.2, saturate those with -0.2 <SI <+0.2 and over-saturated those with SI> +0.2.

Correlation plots Calcite Vs  pH and Calcite Vs Temperature (Figures 2.2.11) show that saturation to over-saturation conditions on calcite characterize water from springs located close to limestone outcrops (e.g. LH6, LH7, LH7bis, LH8, LH8bis, LH12) or from wells characterized by higher salinity and/or temperature (e.g. LH54, LH55, LH61, PER51, PER56, PER78). Of course, waters from maar lakes are in over-saturation conditions. The other samples are distributed between S.I. values close to 0 towards negative values (S.I. ≈ -3). Cignahuapan's thermal spring show saturation with calcite (S.I. = 0.059). Same considerations can be performed for correlation plots Dolomite Vs pH and Dolomite Vs Temperature (Figures 2.2.12). In general, S.I. values respect to main carbonates (i.e. calcite and dolomite) suggest the significant role played by limestones, in areas close to their outcrops or in areas in which carbonate-rich debris can be accumulated.

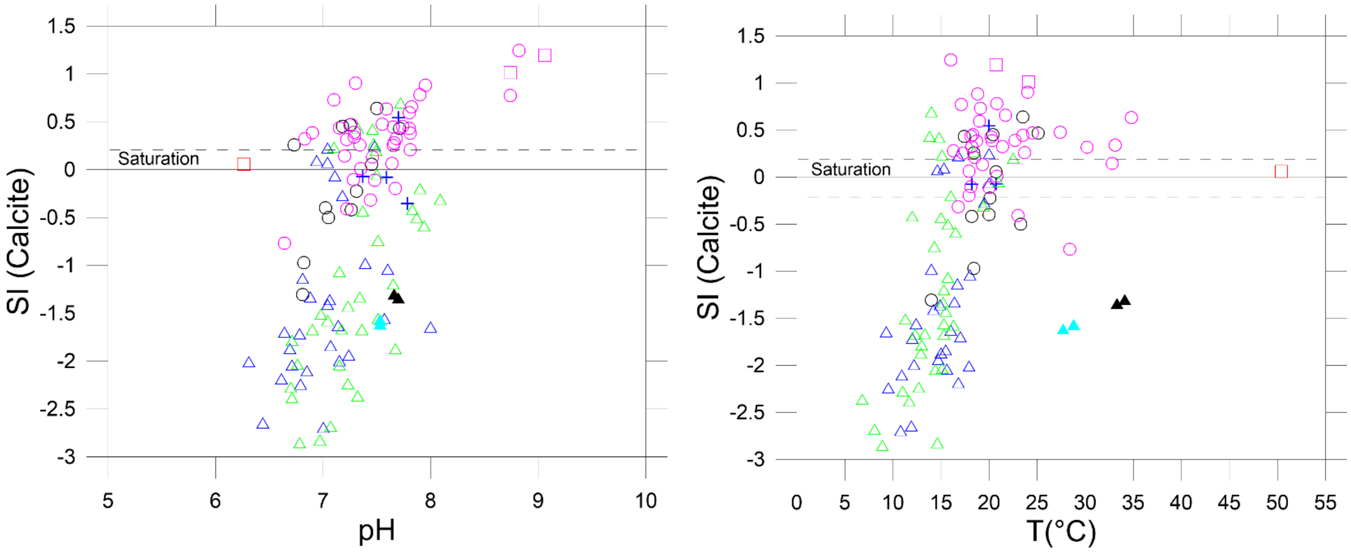


Figure 2.2.11 – Correlation plots S.I.$_{calcite}$ vs. pH (left) and S.I.$_{calcite}$ vs. T (right) for collected water samples. Dashed lines (for values -0.2<S.I.<+0.2) define conditions of saturation respect to mineral phases considered. Symbols as in figure 2.2.5a.

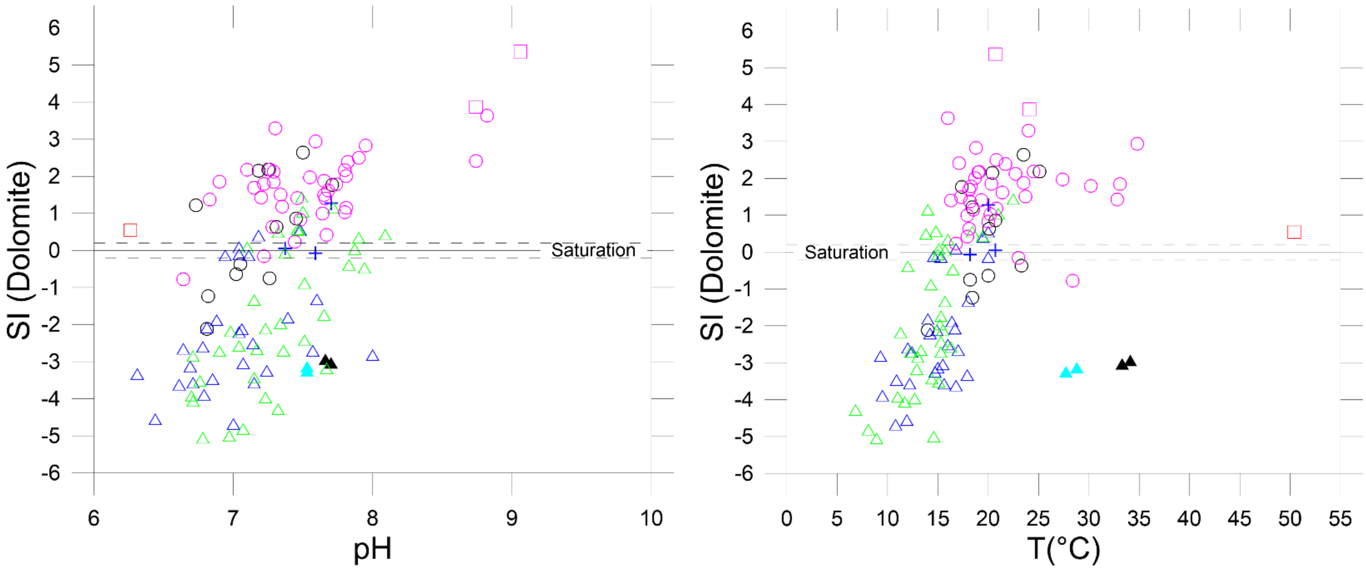


Figure 2.2.12 – Correlation plots S.I.$_{dolomite}$ vs. pH (left) and S.I.$_{dolomite}$ vs. T (right) for collected water samples. Dashed lines (for values -0.2<S.I.<+0.2) define conditions of saturation respect to mineral phases considered. Symbols as in figure 2.2.5a.

Collected samples are under-saturated respect to Gypsum and Anhydrite. Just samples from some wells located close to Totolcingo lagoon (LH17, LH17bis and PER43) show $SO_4$ concentration >400mg/L, approaching S.I. values close to -1. Samples from re-injection wells are shifted from the alignment defined by other samples, since their sulphates contents probably depend from other sources (i.e. oxidation of deep $H_2S$). Also the $SO_4$ content for the Alchichica maar lake depend from other process and not from interaction with gypsum(anhydrite-)-rich formations. The observation of figures 2.2.13 suggest the minor role played by $SO_4$-rich formation, as a source of dissolved sulphate in collected water samples. In fact, evaporite formation are not reported in the study area (see geological maps of Los Humeros, from Carrasco et al., 2017).

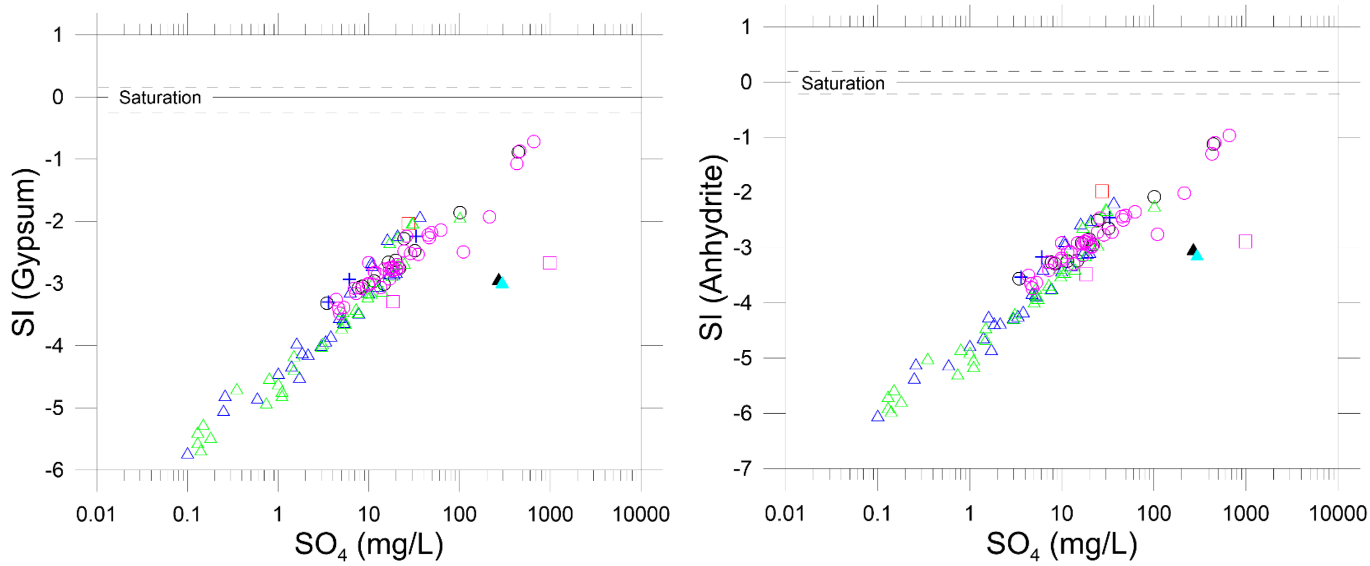


Figure 2.2.13 – Correlation plots S.I.$_{gypsum}$ vs. $SO_4$ (left) and S.I.$_{anhidrite}$ vs. $SO_4$ (right) for collected water samples. Dashed lines (for values -0.2<S.I.<+0.2) define conditions of saturation respect to mineral phases considered. Symbols as in figure 2.2.5a.

Correlation plots amorphous silica vs temperature and chalcedony vs temperature (Figures 2.2.14) show conditions close to saturation respect to $SiO_{2(am)}$ and over-saturation for chalcedony, suggesting that amorphous silica is the most probable $SiO_2$ polymorph in equilibrium with collected waters. Samples from maar lakes (LH18 and LH22) show lowest values of S.I. for both mineral phases, probably due to joining effect of their high pH values (8.74 and 9.06 respectively for LH22-Quecholac and LH18-Alchichica) and water temperature. The Cignahuapan thermal spring (T = 51°C) show S.I. values among the lowest, since higher temperatures favour the solubility.

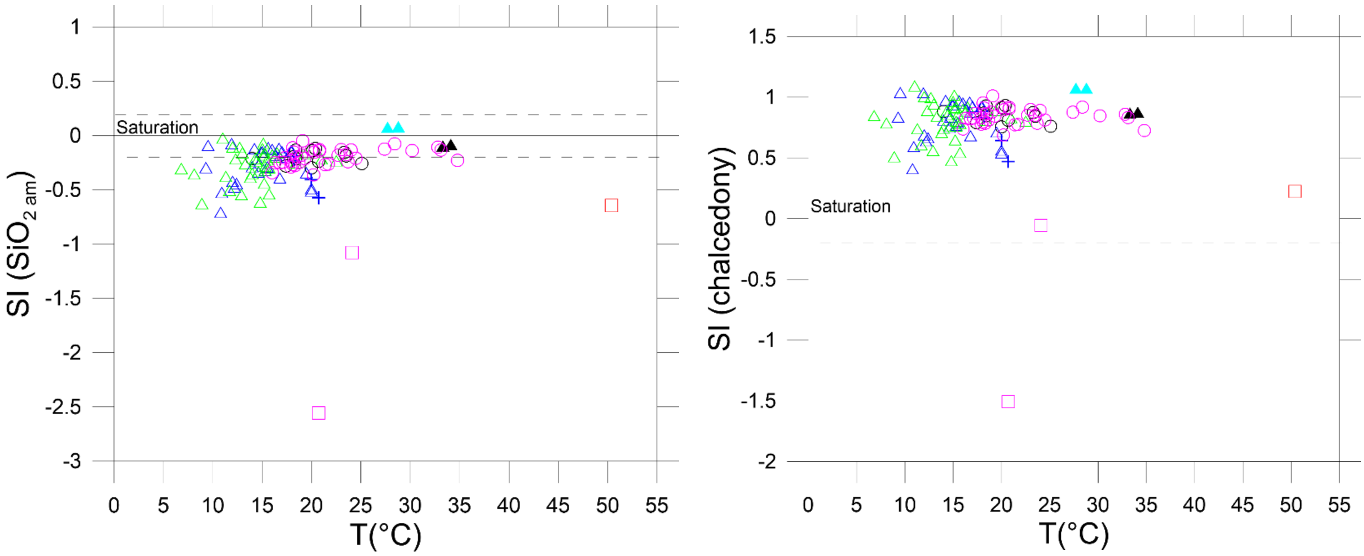

Figure 2.2.14 – Correlation plots S.I.$_{gypsum}$ vs. $SO_4$ (left) and S.I.$_{anhidrite}$ vs. $SO_4$ (right) for collected water samples. Dashed lines (for values -0.2<S.I.<+0.2) define conditions of saturation respect to mineral phases considered. Symbols as in figure 2.2.5a.

### 2.2.3 **Strontium isotopes**

Taking into account the presence of different reservoir rocks, which can be involved in water-rock interaction processes, eighteen water samples were selected for Sr isotope ($^{87}Sr/^{86}Sr$) analyses. Data are shown in table A3 in appendix. Collected waters show an intermediate ratio between the range of variation determined in andesite and limestone samples collected during the GeMex in outcropping areas. These values correlate well with values for local andesite-ryolite rocks (0.70407±0.00001, Verma, 2000) and carbonates (0.70885±0.00001, Veizer et al., 1997), even if the last range is higher than that of limestone collected in the GeMex. Only two cold springs (LH39, LH44) show the lowest signature ratio, in agreement with that of the andesite inside the caldera. In general, we distinguish at least three different groups of waters on the basis of their Sr isotope signatures. In the first group Sr-isotopic ratio ranges from 0.70528 to 0.70553 in the well waters (LH1, LH46, LH50) and in two cold springs (LH32, LH36). In the second group, the Sr isotopes ratio ranges between 0.70599 and 0.7064 in three well waters (LH3, LH54, LH55) and three cold springs (LH6, LH8, LH12). In the third group two well samples (LH17 and LH20) have the highest ratio between 0.70698 and 0.70712. Also, two thermal hot springs sampled outside the caldera have different isotopic ratios. The hot thermal spring (LH28) from El Carrizal, representing the water collected at the lowest altitude, has the highest Sr-isotope ratio reflecting the limestone signature of the geology of the area. The Cignahuapan thermal spring (LH51) shows an intermediate isotopic ratio: in fact it is located in the Sierra Madre Oriental in which limestone, but also andesite rocks outcrop.

In order to understand the origin of dissolved strontium and its evolution, Sr isotope signatures are plotted against concentration of Sr and Cl measured in the same samples. In the correlation plot $^{87}Sr/^{86}Sr$ vs Sr (Figure 2.2.15), starting from typical value of local andesite (LH39, LH44 and LH51), a rapid increase in strontium isotopic ratio is reported for Sr concentrations up to

≈300 mg/L. For higher strontium concentration, the gradient of the increment become less and buffering effect appear close to the typical value of local limestone (LH28 – El Carrizal thermal spring). These features characterize also the distribution of points in the correlation plot $^{87}Sr/^{86}Sr$ vs Cl (Figure 2.2.16), in which water from cold springs span in a wide range of strontium isotopic ratio. Water from wells are scattered, probably owing to the different origin of chloride. It is worth to mention that strontium isotopic signature for some geothermal wells (H12, H19 and H45) is in the range 0.70853-0.70885 (Pinti et al., 2017), in agreement with the value for carbonates suggested by Veizer et al. (1997).

The distribution of points in figures 2.2.15 and 2.2.16 suggest that: i) sources of strontium in analysed waters are identified in andesite and limestone rocks; ii) water from wells located around LHGF (e.g. in Perote plain) represent mixed terms.

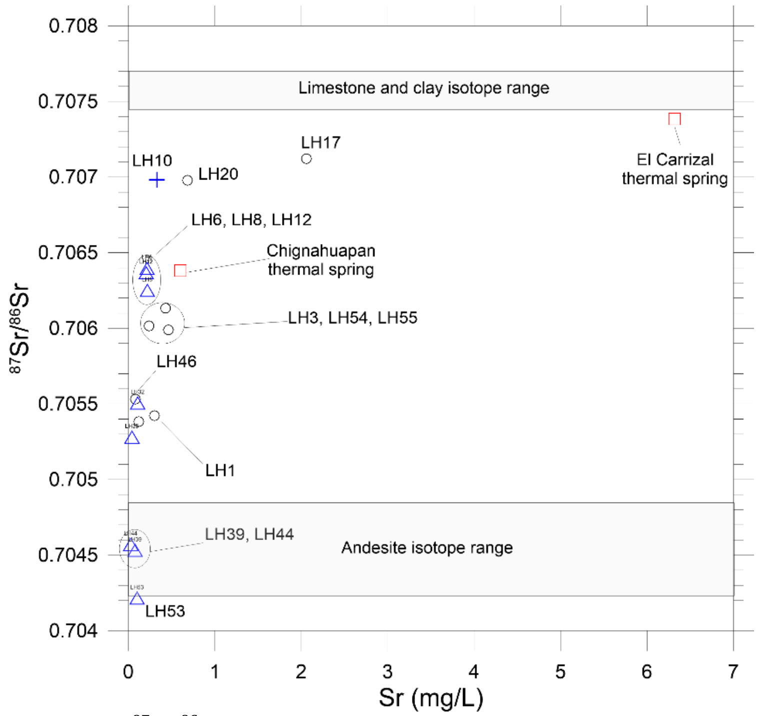


Figure 2.2.15 – Correlation plot $^{87}Sr/^{86}Sr$ vs Sr for collected water samples in Los Humeros. Isotope range for andesite and limestone and clay samples collected at Los Humeros during the GeMex project are also reported.

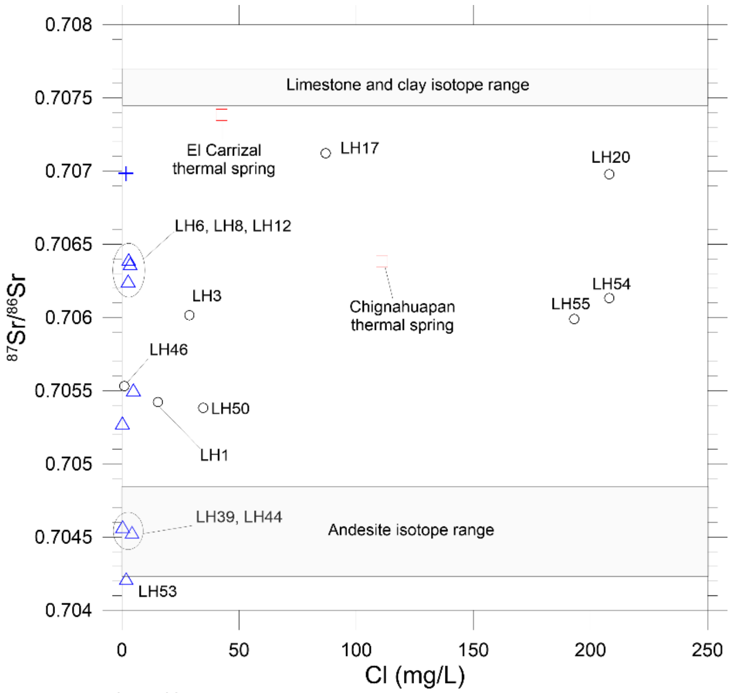

Figure 2.2.16 - Correlation plot $^{87}Sr/^{86}Sr$ vs Cl for collected water samples in Los Humeros. Isotope range for andesite and limestone and clay samples collected at Los Humeros during the GeMex project are also reported.

### 2.2.4 Dissolved carbon dioxide

LHGF are characterized by the presence of high $CO_2$ concentrations in fluids from geothermal wells (in general $CO_2$ > 85%, as Total Discharge). The exploitation in Los Humeros enhanced the enthalpy excess conditions for most of geothermal wells, raising the vapour fraction (generally expressed as y coefficient) and favouring the presence of $CO_2$ in the steam-gas mix extracted. Taking into account these considerations and also the presence of warm wells in Perote plain, first measurements of $CO_2$ fluxes diffused from soil were performed in selected sites inside the Los Potreros caldera and in Perote plain (Figure 2.2.17). In particular, four areas were investigated: 1) an area corresponding to a crossover of fractures connected to the Maxtaloya master-fault, near the village of Maxtaloya; 2) Xalapazco Crater, characterized by an area with evident hydrothermal alteration; 3) north of Xalapazco, in the prospects of a CFE (Comisión Federal de Electricidad) geothermal plant and of the continuation of the Maxtaloya master-fault; 4) in Perote plain, close to water well PER 55, which is characterized by high water temperature. Grid of points is shown in figure 2.2.17 together with the alignments of main faults/fractures systems. The $\phi CO_2$ values were measured at 160 sites inside and outside the Los Humeros Caldera by using the Accumulation Chamber (AC) method (Chiodini et al, 1996). Flux data ($\phi CO_2$) are reported in table A3 (in appendix), together with soil temperature, atmospheric pressure and maximum, minimum, average, median and standard deviation values for $\phi CO_2$. The results indicate that higher values for $CO_2$ flux (up to 3151 g $m^{-2}$ $day^{-1}$) were only observed near and inside the Xalapazco hydrothermalized area, already known for its gaseous emissions (Peiffer et al., 2018). In other areas, correlation between distribution of high values of $CO_2$ flux and alignment of faults/fractures lines were not clearly observed, and low $CO_2$ fluxes were measured (up to 12 $g \cdot m^{-2} day^{-1}$). Total $CO_2$ output calculated in each selected areas inside the Los Humeros Caldera, i.e. “Xalapaxco” (~5700 $m^2$), “Maxtaloya” (~230000 $m^2$) and “CFE plant” (~253000 $m^2$), was ~0.09, 0.1 and 1.1 t $day^{-1}$, respectively.

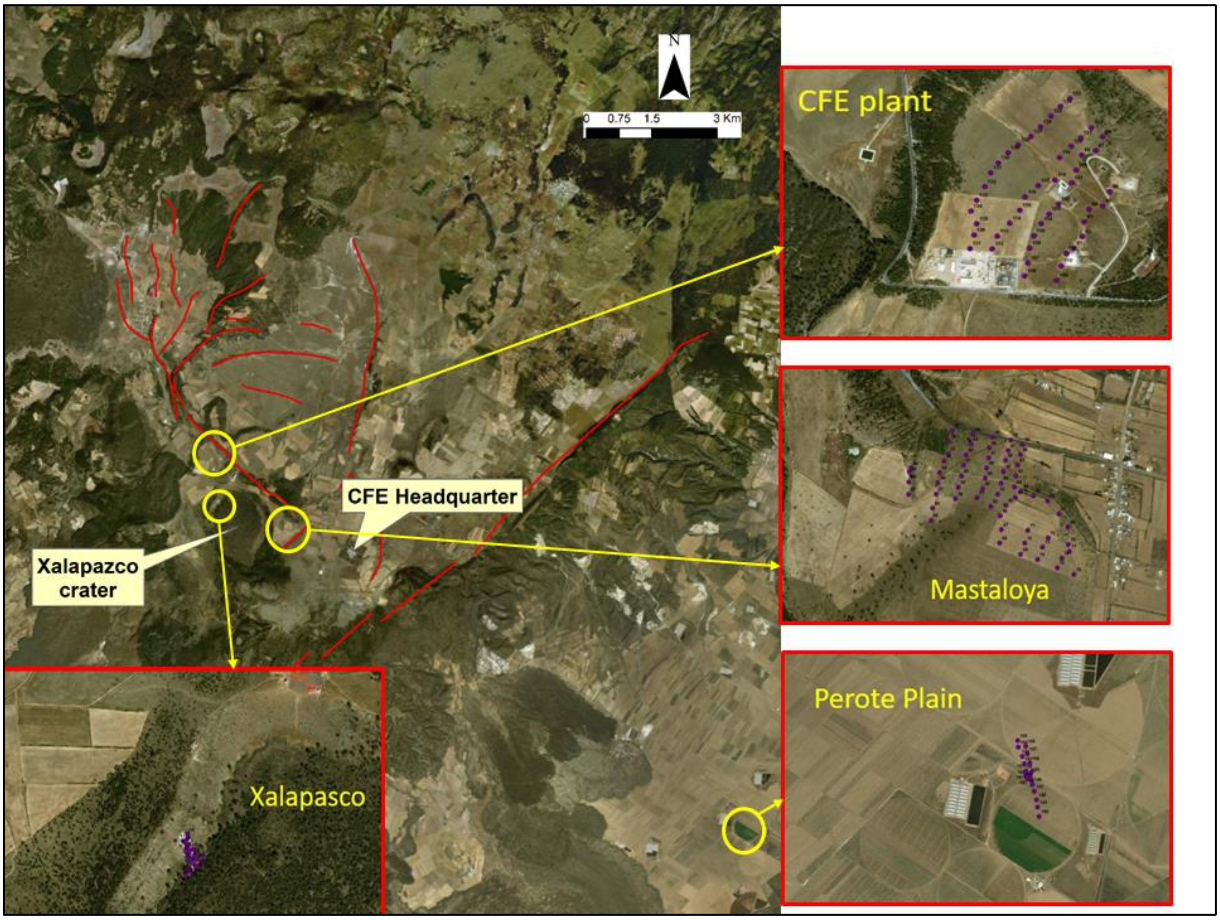


Figure 2.2.17 – Location map of $CO_2$ flux measurements performed in LHGF. Alignments of main faults/fractures systems are also shown.

$CO_2$ fluxes measured in Perote plain were very low and of the same order of magnitude of fluxes measured in soil with grass cover (more or less, up to 0.05 $mol/m^2day$). Considering the presence of some wells characterized by warm water, dissolved $CO_2$ was also calculated in collected waters samples. Numerical code Solveq with the Soltherm_98 database was used for computation (Spycher and Reed, 1998). Data on dissolved $CO_2$ is shown in table A4, both as partial pressure (bars) and concentration (in mmol/L and $\log F_{CO2}$). These data are used in a GIS project and it is shown in map of figure 2.2.18.

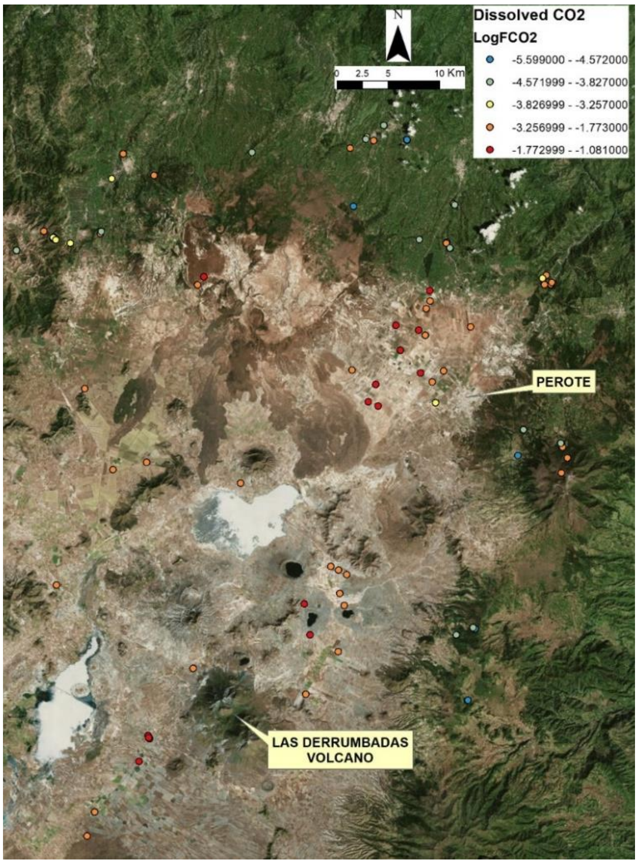

Figure 2.2.18 – Distribution map of dissolved $CO_2$ displayed as Log $CO_2$ fugacity ($LogF_{CO2}$).

This map shows an alignment NE-SW defined by water wells in which dissolved $CO_2$ reach higher values (red point), but anyway less than 0.1bar. This value is typical for soils, in which the $P_{CO2}$ is direct connected to decomposition of organic substances and soil respiration. Some of these wells include warm wells identified in Perote plain, but also few wells located in the south part of the study area, around Las Derrumbadas Volcano. In Las Derrumbadas, fumarolic activity is reported in literature and associated altered rocks indicates an active geothermal system (Siebe C., 1988). Therefore, local temperature anomaly can be hypothesized and it could explain the rather high temperature (up to 34.8°C for sample PER51) of some water wells located to the southern site. For water wells close to Perote, temperature values higher than 22°C are widely present with maximum value of 33.1°C (PER56).

### 2.2.5 Stable isotopes

The $\delta^2H$ and $\delta^{18}O$ values of $H_2O$ for the water samples collected in the LHGF and its surrounding are shown in the correlation diagram of Figure 2.2.19, together with the worldwide meteoric water line (WMWL - $\delta^2H = 8\cdot\delta^{18}O+10$, Craig, 1961). As for reference, a meteoric water line (MWL) defined by Perez Quezadas et al. (2015) is also reported, even if it was defined using precipitation samples collected along a transect from the Port of Veracruz to Cofre de Perote. Therefore, it represent a local meteoric water line for the upwind Sierra Madre Oriental area but it is not specific for Los Humeros area. A detailed study regarding the isotopic composition of $\delta^2H$ and $\delta^{18}O$ values of $H_2O$ from springs and wells located around the LHGF was performed for a first time, during the GeMex project. All samples plot preferentially along the WMWL, even if some of them are slightly shifted on the right. This scatter of isotope values could be due to the occurrence of evaporation processes, in particular for wells located in the south part of the study area (e.g. around Pizarro volcano and Totolcingo lagoon). Collected samples span in a wide range of stable isotopic composition, mainly owing to different altitude of infiltration. Samples collected from cold springs and wells located in different areas and at different distance from the LHGF producing area show similar isotopic composition. In addition, $\delta^{2}H$ and $\delta^{18}O$ values of geothermal fluids span in a wide range of variation. In figure 2.2.19, geothermal wells plot on the right of the W.M.W.L., showing an enrichment in $\delta^{18}O$ values. Conversely, mean value for $\delta^{2}H$ of geothermal fluids is similar to that for collected cold springs. These characteristics, commonly observed in several geothermal fields worldwide, are compatible with oxygen-shift process due to the interaction of meteoric water with reservoir rocks. Other physical processes such as boiling and phase separation (especially after several years of exploitation) contribute to the spreading of the points in the $\delta^{2}H$ vs $\delta^{18}O$ plot. Stable isotopes data obtained in this study are in agreement with the hypothesis of regional meteoric component as source of geothermal fluids. Therefore, a regional recharge cannot be excluded for LHGF.

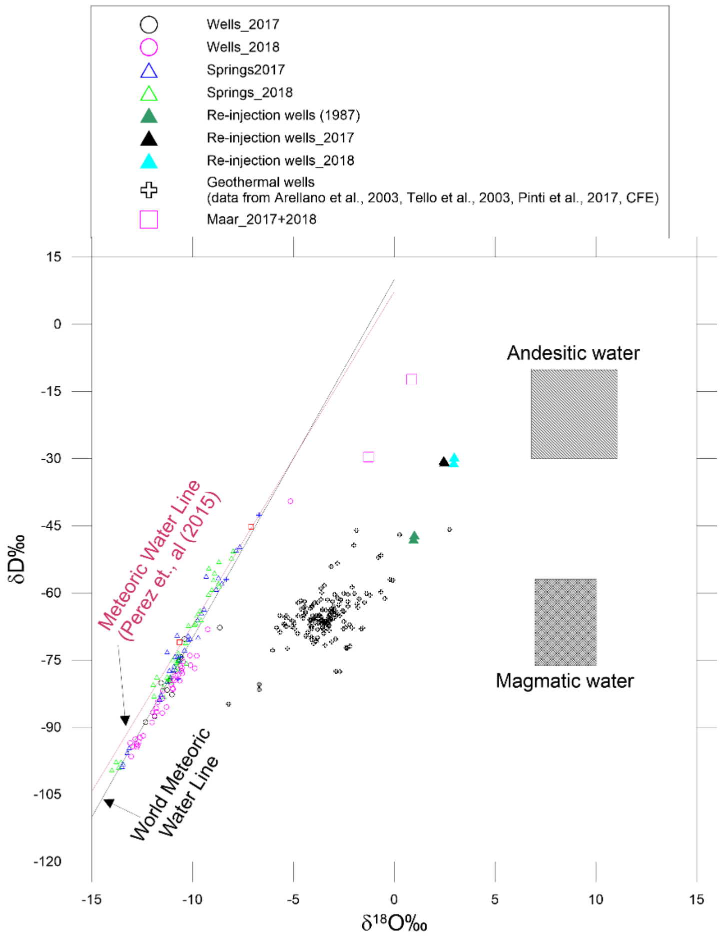


Figure 2.2.19 - Correlation diagram of $\delta^{2}H$-$H_2O$ vs. $\delta^{18}O$-$H_2O$ for the water samples collected in the LHGF and its surroundings. The World Meteoric Water Line (WMWL – Craig, 1961) and Meteoric Water Line (MWL) by Perez et al. (2015) are also shown.

### 2.3 Natural gas emissions

Gas manifestations are reported in literature just in very limited zone inside the producing area of the LHGF and in particular in: Cueva Ahumada (50°C) in Xalapazco crater, Los Humeros (70°C) and Loma Blanca (80°C) (Casique et al., 1982). During sampling trip performed in March 2018, two sites having suitable fumaroles were identified and samples were collected: two aliquots in Loma Blanca (LB1 and LB2) and one in Xalapazco (XA1) (see map in figure 2.3.1). First gas manifestation is located in Loma Blanca at 200-300m north to the Los Humeros country, whereas the second is inside the Xalapazco crater. Loma Blanca is a small altered area in which some weak fumarolic emissions are present with maximum temperature of 92.8°C (boiling temperature at the local altitude ≈ 2800 m.a.s.l.). In Xalapazco some gas emissions and steaming ground with maximum temperature of 64.5°C characterize small area of the inner north side of the crater.


Figure 2.3.1 – Location map of natural gas manifestation sample in March 2018. Some geothermal wells are also shown.

### 2.3.1 Sampling and laboratory analyses

In Loma Blanca, gas sampling was performed, using Giggenbach bottles partially filled with sodium hydroxide solution (≈4.5N) and then evacuated to remove atmospheric air (Giggenbach W.F., 1975). With this sampling, steam and gas reactive species (as $CO_2$ and $H_2S$) dissolve in NaOH aqueous solution, whereas the others incondensable gases (such as Ar, $H_2$, $O_2$, $N_2$, $CH_4$, He) can be accumulated in the headspace of the Giggenbach's bottles. However, since this method is not suitable to analyze carbon monoxide content, other aliquots were collected. In particular, a suitable quartz sampling line was used to perform condensation of the steam, thus separating the condensable fraction from the incondensable ones (Cioni et al., 1988). Incondensable gases can be stored in suitable dry gas bottles, whereas plastic bottles with double cap can be used for condensed steam (Figure 2.3.2).

Figure 2.3.2 - Sampling of Loma Blanca fumaroles, using method by Cioni et al., 1988.

All analyses were performed in IGG-CNR laboratories in Pisa. Incondensable inorganic gases were determined in the headspace of Giggenbach's bottles and in dry gas bottles, using a gas-chromatograph (Perkin Elmer Clarus 500), equipped with a 30 m long 5Å molecular sieve capillary column (I.D. 0.53 mm) and a Thermal Conductivity Detector (TCD). This column is able to separate Ar from $O_2$ at room temperature. Low $CH_4$ contents (<10 ppmv) were measured using the same gas-chromatograph and capillary column, but employing a Flame Ionization Detector (FID). Carbon dioxide and $H_2S$ in dry gas bottles were determined by means of a gas-chromatograph (Carlo Erba 5300) equipped with a packed Chromosorb column and a Thermal Conductivity Detector (TCD). Carbon monoxide in dry gas bottles was determined by means of a gas-chromatograph equipped with a packed molecular sieve (5 Å, 80/100 mesh) column (3 m long, using He as carrier gas) and a high-sensitivity reduced gas detector (HgO; detection limit 0.05 ppmv). The alkaline solution of the Giggenbach's bottles was analyzed for $H_2S$ and $CO_2$. To measure $H_2S$, sulfur species were converted to sulfate through oxidation with hydrogen peroxide and sulfate concentration was measured by ion-chromatography. Carbon dioxide was measured on the alkaline solution by titration against HCl 0.1N, using an automatic titrator. Analyses of $^{13}C$–$CO_2$ were performed via GC-combustion (GcTrace Thermo Fisher) interface with a Mass Spectrometer (Delta XP plus Thermo-Finnigan) for isotopes ratio. Noble gases were analyzed in the IGG Rare Gas Lab for He, Ne, Kr, Xe abundances, and for their isotopic composition. The samples for Noble Gases analysis were processed on a stainless steel high-vacuum line to separate noble gases from reactive gases (Magro et al., 2003). Noble gases are then cryogenically separated each other at selected temperatures. The extraction line is connected to both a magnetic mass spectrometer (MAP 215-50) and a quadrupole mass spectrometer (Spectralab 200, VG-Micromass). Resolution for $^3He$ was close to 600 AMU for HD-$^3He$ at 5% of the peak.

All obtained chemical data have analytical uncertainties ≤5% for the main gas components and ≤10% for minor and trace gas species. The uncertainties for carbon isotopes is ±0.1‰, whereas isotopes analyses for noble gases report a reproducibility better than 10% over the analysis period. Chemical data are shown in table A7 (appendix).

### 2.3.2 Chemical classification

$CO_2$ and $N_2$ are the most abundant gas components in collected gas samples from the LHGF, with concentration of about >81% and 0.6-9%, respectively. Sample LB2 is an exception, since it suffers of air contamination. The triangular diagram of $CO_2$-$N_2$-Ar (Figure 2.3.3, left) shows that all samples plot inside the compositional triangle mantle-air-air saturated water (asw), suggesting mixing processes between this three components. The LB2 sample seems to derive their atmospheric components by mixing between air and asw (not from simple addition of air), whereas sample XA1 is shifted towards $CO_2$-rich component. Same path is also showed for most of the gas phases collected from geothermal wells (data from literature, see table A5 in appendix) and no relation with geographical location seems to be evident. In the triangular diagram $CH_4$-$CO_2$-$N_2$ gas samples from Loma Blanca are positioned along the $CO_2$-$N_2$ axis, whereas Xalapazco sample (XA1) plots close to the $CH_4$ vertex. Geothermal wells are in general distributed along the $CH_4$-$CO_2$ axis, even if some geothermal wells characterized by less deepest permeable horizons (<2000 m.a.s.l.) are shifted toward the $N_2$ vertex. More in general, diagrams in figure 2.3.3 show that fumarole samples LB1 and LB2 have similar chemical composition of geothermal wells (H43 and H59) located in the northern sector of the production area, close to these natural manifestations. Sample XA1 is more similar to geothermal wells H12 and H41, which are located in the south sector of LHGF.

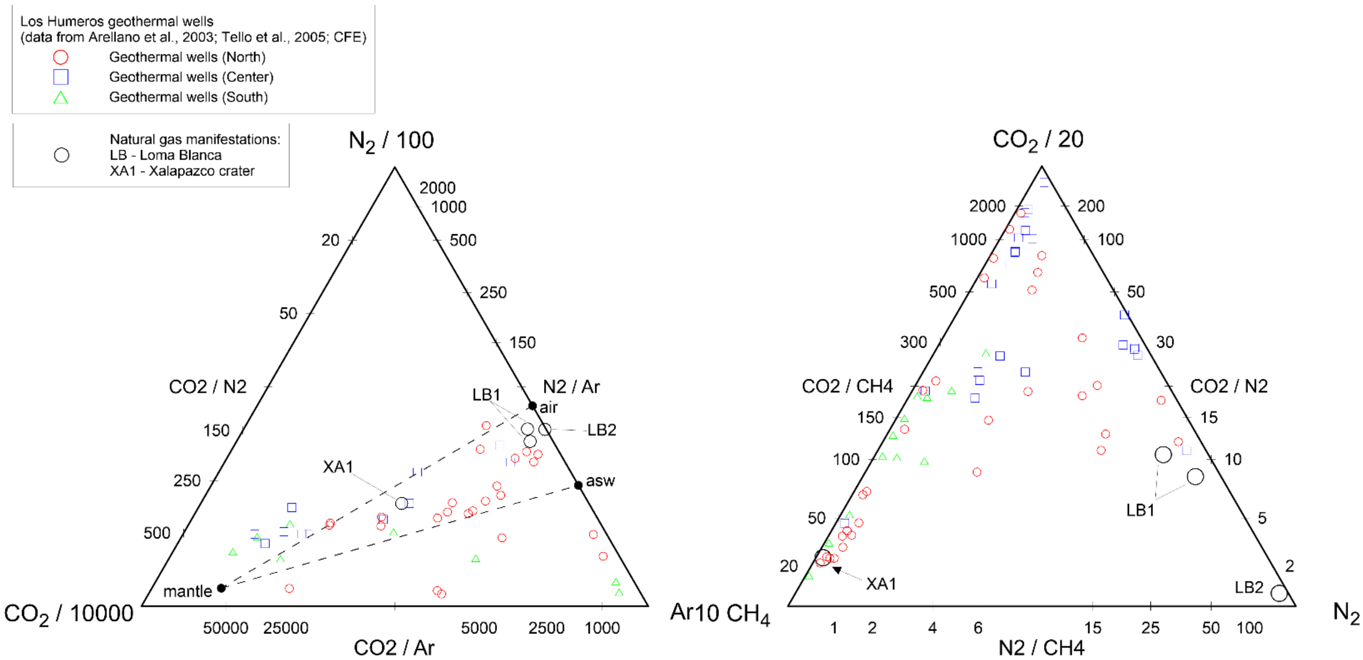


Figure 2.3.3 – Triangular diagrams of $CO_2$-$N_2$-Ar (left) and $CH_4$-$CO_2$-$N_2$ (right) for the gas samples collected in LHGF. Data for geothermal wells are referred to previous works.

## 2.4 Conclusions

Two sampling campaigns were performed in the LHGF, in particular in June 05$^{th}$-14$^{th}$, 2017 and March 16$^{th}$-28$^{th}$, 2019. A total of 57 and 87 water samples from cold springs, cold water wells, maar lakes, thermal springs and reinjection wells were collected in June 2017 and March 2018, respectively. Moreover, three gas samples were collected from natural manifestations inside the LHGF producing area. Both sampling trips are performed in collaboration with CICESE (Ensenada, BC), University of Guanajuato, (Guanajuato) and University of Michoacán, Morelia (UMSNH). On March 2018, also BRGM took part in the field trip. Particular attention was focused on the selection of “target” areas in which to perform sampling of cold springs, providing information regarding the origin of fluids and relationship between cold surface waters and hydrothermal/geothermal fluids. In particular, springs located on limestone outcrops of the Sierra Madre Oriental and at higher altitude (>3500 m.a.s.l on the Cofre de Perote.) were sampled for the first time.

Chemical and isotopic characteristics of samples collected from cold springs and wells suggest an origin from meteoric water. Depending on the kind of interacting rocks/formations/deposits, the chemistry of waters can evolve in Na-$HCO_3$ type, for andesite-rhyolites rocks, to Ca-$HCO_3$ for limestone. Ca-$SO_4$($HCO_3$) type waters can be attributed to the interaction of meteoric water with salt deposits/incrustations present in particular in the southern part of the study area (around the Pizarro volcano and the Totolcingo lagoon). The effects of salts deposits were also evidenced for water samples collected from wells located more close to the Perote country. The study of saturation index and radiogenic isotopes (i.e. $^{87}Sr/^{86}Sr$) confirm the pivotal role played by limestone and volcanic rocks as the main sources of dissolved Ca, $HCO_3$ and Na ions. Data on the dissolved $CO_2$ calculated for some water wells show a distribution of higher values associated to NE-SW direction, according to one of the main alignment of regional faults/fractures. However, calculated $P_{CO2}$ values are less than 0.1 bar, which represent a typical value for the decomposition of organic substances and soil respiration.

Stable isotopic composition of cold waters from springs and wells shows a wide range of variation, mainly owing to different altitude of infiltration. It is interesting to note that samples collected from cold springs and wells located in different areas and at different distance from the LHGF producing area show similar isotopic signature. It suggest that meteoric component is very important at regional scale. Also $\delta^2H$ and $\delta^{18}O$ values of the geothermal fluids from producing wells span in a wide range of variation. In general, their mean values for $\delta^{18}O$ and $\delta^2H$ are respectively enriched and similar to the mean values for collected cold waters. These characteristics, commonly observed in several geothermal fields worldwide, are compatible with various processes, such as oxygen-shift due to the interaction of meteoric water with reservoir rocks, boiling and phase separation (especially after several years of exploitation). Stable isotopes data obtained in this study support the hypothesis of regional meteoric component, as source of geothermal fluids. Therefore, a regional recharge cannot be excluded for LHGF. Natural gas emissions located inside the LHGF producing area were sampled for the first time and it represent a mixing between deep and surface components. The latter seems to suggest two component, atmospheric air and air saturated water.

**Acknowledgements**

We want to thank the CFE staffs from Los Humeros and from Morelia for their collaboration, effort and helpful discussions before and during field trips. Also, special thanks to CFE for permission and access to the Los Humeros geothermal producing area. We also are particularly grateful to Rafael Alfaro Garcia and Marcela Sanchez from CFE for their help in collecting fluid samples in the field and to Oscar Lopez Romero and Jesus Hipolito Guzman Sanchez from CFE for their help in the preparation of “Giggenbach bottles” for gas sampling. The Authors also thank Chiara Boschi and Ilaria Baneschi for stable isotope analysis of carbon in Los Humeros fumaroles and Samuele Agostini for strontium isotope analysis. Finally, we are very grateful to Aída López Hernández, scientific coordinator of the GEMEX project, for her support during all phases of scientific activities.

**Reference**


Alcocer J., Hammer U.T. (1998). Saline lake ecosystems of Mexico. Aquatic Ecosystem Health and Management 1, pp. 291-315.

Arellano, V.M., Garc|¤a, A., Barraga¤n, R.M., Izquierdo, G., Arago¤ n, A., Nieva, D., Portugal, E., Torres, I., 1998. Desarrollo de un modelo ba¤sico actualizado del yacimiento de Los Humeros, Puebla. Report IIE/11/11459/I01/F for the Comisio¤n Federal de Electricidad, Instituto de Investigaciones Ele¤ctricas, Temixco, Mor., 450 pp.

Arellano Gomez V.M., García A., Barragán Reyes R.M., Izquierdo G., Aragón A., Nieva D. (2003). An updated conceptual model of the Los Humeros geotermal reservoir (México). Journal of Volcanology and Geothermal Research, 124, 67-88. Arellano et al., 2015

Barraga¤n, R.M., Santoyo, E., Nieva, D., Portugal, E., Verma, M.P., (1988). Caracterizacioin de yacimientos geotermicos mediante la determinacio¤n de para¤metros fisico-quimicos. Internal Report IIE/11/2386/I 01/F, Instituto de Investigaciones Electricas, Temixco, Mor., 250 pp.

Barragan, R.M., Cervantes, M., Diaz, R., Garduno, V., Gonzalez, E., Holgu|¤n, S., Meza, F., Nieva, D., Oliver, R., Rosas, N., Sampedro, J., (1989). Caracterizacioin del fenomeno de corrosion-obturacion en pozos de Los Humeros. Report IIE/11/3753/I for the Comision Federal de Electricidad, Instituto de Investigaciones Electricas, Temixco, Mor., 83 pp.

Barragan, R.M., Nieva, D., Santoyo, E., Gonzalez, E., Verma, M., Lopez, J., 1991. Geoquimica de fuidos del campo geotermico de Los Humeros (Mexico). Geotermia Rev. Mex. Geoenerg. 7, 23-47.

Barragan R.M., Arellano V.M., Armenta M.F., Aguado R.T., (2008). Cambios quimicos en fluidos de pozos del campo geotermico de Los Humeros: Evidencia de recarga profunda. Geotermia, Vol.21, n°2.

Barragán-Reyes R.M., Arellano Gomez V.M., Ramírez Montes M., Tovar Aguado R. (2010) - Geoquimica isotópica (d18O, dD) inicial de fluidos de pozos del campo geotérmico de Los Humeros, Pue. Geotermia, 23, n°1, 16-25. Casique et al., 1982

Carrasco-Núñez G., Hernández J., De León L., Dávila P., Norini G., Bernal J.P., Jicha B., Navarro M., López P. (2017b) - Geologic map of Los Humeros volcanic complex and geothermal field, eastern Trans-Mexican Volcanic Belt. Terra Digitalis, 1(2), 1-11.Cioni R., Corazza E., Magro G., Guidi M., Marini L. (1988). Reactive and inert gases in low temperature fumaroles (Aeolian Islands, Italy). Rend. Soc. Ita. Min. Petr., vol43: 1003-1011

Ferriz H. and Mahood G. (1984) - Eruption rates and compositional trends at Los Humeros volcanic center. Puebla, México. J. Geophys. Res., 89 (B10), 8511-8524.Giggenbach W.F., 1975.

Giggenbach W.F., (1992). Isotopic shifts in waters from geothermal and volcanic systems along convergent plate boundaries and their origin. Earth and planetary Science Letters, 113: 495-510.

Gutiérrez-Negrín L.C.A., Izquierdo-Montalvo G. (2010) - Review and update of the main features of the Los Humeros geothermal field, Mexico. Proceedings World Geothermal Congress 2010, Bali, Indonesia, 25-29 April 2010, 7 p. Langelier and Ludwig, 1942

Langmuir, C.H., Vocke Jr., R.D., Hanson, G.N., Hart, S.R., 1978. A general mixing equation with applications to Icelandic basalts. Earth Planet. Sci. Lett. 37, 380–392.

Magro G., Ruggieri G., Gianelli G., Bellani S., Scandiffio G., (2003). Helium isotopes in paleofluids and present-day fluids of the §Larderello geothermal field: Constraints on the heat source. J. Geophy. Res., vol.108(B1). doi:10.1029/2001JB001590, 2003.

Perez J.Q., Silva A.C., Inguaggiato S., Ortega M., Perez J.C., Heilweil V.M. (2015). Meteoric isotopic gradient on the windward side of the Sierra Madre Oriental area, Veracruz-Mexico. Geofisica International, 54(3): 267-276.

Pinti, D.L., Marty, B., 1998. The origin of helium in deep sedimentary aquifers and the problem of dating very old groundwaters. Geol. Soc. Lond. Spec. Publ. 144, 53–68.

Pinti, D.L., Castro, M.C., Shouakar-Stash, O., Tremblay, A., Garduño, V.H., Hall, C.M., Hélie, J.-F., Ghaleb, B., (2013). Evolution of the geothermal fluids at Los Azufres, Mexico, as traced by noble gas isotopes, $\delta^{18}O$, $\delta D$, $\delta^{13}C$ and $^{87}Sr/^{86}Sr$. J. Volcanol. Geotherm. Res. 249, 1–11.

Pinti D.L., Castro M.C., Lopez-Hernández A., Han G., Shouakar-Stash O., Hall Ch.M., Ramírez-Montes M. (2017). Fluid circulation and reservoir conditions of the Los Humeros Geotermal Field (LHCF), México, as revealed by a noble gas survey. Journal of Volcanology and Geothermal Research, 333-334, 104-115. Pinti et al., 2019

Prol-Ledesma R.M. (1998). Pre- and post-exploration variations in hydrothermal activity in Los Humeros geothermal field, Mexico. Journal of Volcanology and Geothermal Research, 83, 313-333.Quijano et al., 1991

Sano, Y., Marty, B., 1995. Origin of carbon in fumarolic gas from island arcs. Chem. Geol. 119, 265–274.

SGM (2002). Carta Geologico-Minera, Veracruz E14-3 (Veracruz, Puebla y Tlaxcala).

Siebe C., 1988. Major element Geochemistry and tectonic setting of Las Derrumbadas rhyolitic domes, Puebla, Mexico. Chemie der Erde – Geochemistry, vol.48(1): 177-185

Spycher N, Reed M.H. (1998). SOLVEQ: A Computer Program for Computing Aqueous Mineral Gas Equilibria. Department of Geological Sciences, University of Oregon, Eugene, OR., 28 pp.

Tello H.E., Verma M.P., Tovar R.A. (2000). Origin of acidity in the Los Humeros, Mexico, geothermal reservoir. Proceedings World Geothermal Congress, Japan, May 28-June 10.

Tonani F., Nagao K., Moore J., Natale G., Sperry T. (1998) Water and gas geochemistry of the Cove-Fort Sulphurdale geothermal system. Proceedings, Twenty-Third Workshop on Geothermal Reservoir Engineering. Stanford University, Stanford, California, January 26-28, 1998.

Truesdell, A.H., 1991a. The origin of high-temperature zones in vapor-dominated geothermal systems. Proc. Sixteenth Workshop on Geotherm. Res. Eng., Stanford Univ., Stanford, CA, pp. 15-20.

Truesdell, A.H., 1991b. Origins of acid £uids in geothermal reservoirs. Geotherm. Res. Counc. Trans. 15, 289^296.Veizer, J., Buhl, D., Diener, A., Ebneth, S., Podlaha, O.G., Bruckschen, P., Jasper, T., Korte, C., Schaaf, M., Ala, D., Azmy, K., 1997. Strontium isotope stratigraphy: potential resolution and event correlation. Palaeogeogr. Palaeoclimatol. Palaeoecol. 132, 65–77.

Verma, S.P., 2000. Geochemical evidence for a lithospheric source for magmas from Los Humeros caldera, Puebla, Mexico. Chem. Geol. 164, 35–60.

# APPENDIX

Table A1 – Main physico-chemical parameters measured in the field for collected water samples (Los Humeros). Total alkalinity was determined on the field by acid-base titration

| Code | Name | Date (dd/mm/yy) | Type | X (m) | Y (m) | Alt. (m.a.s.l.) | Depth (m) | Flow rate (L/min.) | T (°C) | pH | O2 diss. (mg/L) | E.C. (µS/cm) |
|---|---|---|---|---|---|---|---|---|---|---|---|---|
| | | | | | | Sampling 2017 | | | | | | |
| LH1 | hualco - Sar | 05/06/2107 | Well | 653278 | 2157817 | 2385 | 80 | ≈1200 | 20.7 | 7.45 | 5.24 | 555 |
| LH2 | iguel - Barr | 05/06/2107 | Well | 650030 | 2157135 | 2355 | n.k. | ? | 18.4 | 6.82 | 6.35 | 356 |
| LH3 | Puchintoc | 05/06/2107 | Well | 647263 | 2165018 | 2416 | n.k. | ? | 20 | 7.02 | 2.18 | 561 |
| LH4 | uitzitzilapa | 06/06/2017 | Well | 648787 | 2180106 | 2506 | n.k. | ? | 14 | 6.81 | 5.54 | 250 |
| LH15 | ıgoza-El Sal | 07/07/2017 | Well | 651017 | 2187878 | 2220 | n.k. | 300 | 18.2 | 7.26 | 6.1 | 263 |
| LH17 | la del Carm | 08/06/2017 | Well | 653493 | 2131005 | 2363 | 70 | 900 | 18.4 | 6.73 | 1.66 | 1871 |
| LH20 | hichicuautl | 08/06/2017 | Well | 668638 | 2144050 | 2351 | 68 | 18 | 20.4 | 7.18 | 1.3 | 1698 |
| LH21 | Xaltepec | 08/06/2017 | Well | 672506 | 2143906 | 2350 | 80 | 65 | 17.4 | 7.71 | 5.39 | 564 |
| LH46 | l4-Los Hume | 13/06/2017 | Well | 658264 | 2175116 | 2761 | 350 | 285 | 23.3 | 7.05 | 3.07 | 317 |
| LH50 | cho Los Sau | 13/06/2017 | Well | 680858 | 2173556 | 2400 | 180 | 3000 | 20.1 | 7.31 | 3.57 | 593 |
| LH54 | ardin Dorac | 14/06/2017 | Well | 674864 | 2163728 | 2379 | 120 | ≈4000 | 23.5 | 7.5 | n.m. | 1755 |
| LH55 | ardin Dorac | 14/06/2017 | Well | 675821 | 2163313 | 2371 | 150 | ≈4000 | 25.1 | 7.25 | n.m. | 1871 |
| LH5 | uitzitzilapa | 06/06/2017 | Spring | 648880 | 2180326 | 2509 | - | 8.2 | 14.2 | 7.04 | 5.81 | 148 |
| LH6 | pan - San M | 06/06/2017 | Spring | 645867 | 2179182 | 2433 | - | 9.5 | 16.8 | 7.04 | 6 | 602 |
| LH7 | La Olimpica | 06/06/2017 | Spring | 644203 | 2179731 | 2365 | - | 10 | 14.6 | 7.04 | 4.45 | 503 |
| LH7 bis | La Olimpica | 06/06/2017 | Spring | 644234 | 2179774 | 2360 | - | - | - | - | - | - |
| LH8 | La Olimpica | 06/06/2017 | Spring | 644459 | 2179515 | 2437 | - | not measurable | 15.3 | 6.94 | 1.56 | 554 |
| LH9 | Buena Vista | 06/06/2017 | Spring | 633513 | 2183084 | 2392 | - | 0.9 | 17.9 | 6.31 | 2.08 | 201 |
| LH12 | Sesder | 07/06/2017 | Spring | 640647 | 2178480 | 2205 | - | 3.6 | 20 | 7.11 | 3.1 | 603 |
| LH13 | Sesder | 07/06/2017 | Spring | 640643 | 2178488 | 2205 | - | 0.15 | 20 | 7.48 | 4.26 | 412 |
| LH14 | Acuaco | 07/07/2017 | Spring | 649898 | 2185463 | 2286 | - | 12 | 16.7 | 6.81 | 8.02 | 192.3 |
| LH19 | n Luis Atexc | 08/06/2017 | Spring | 662709 | 2140536 | 2438 | - | not measurable | - | - | - | - |
| LH23 | ı del Nacimi | 09/06/2017 | Spring | 685242 | 2141605 | 2998 | - | 0.5? | 10.8 | 7 | 10.0? | 29 |
| LH24 | ı del Nacimi | 09/06/2017 | Spring | 685059 | 2141722 | 2977 | - | 1.8 | 10.9 | 6.85 | 6.42 | 59.1 |
| LH25 | Oczotla | 09/06/2017 | Spring | 683402 | 2141025 | 2770 | - | not measurable | 12 | 6.78 | 7 | 119.5 |
| LH26 | issima Trin | 09/06/2017 | Spring | 684493 | 2134626 | 2907 | - | 0.3 | 12.4 | 7.57 | 8.91 | 43.2 |
| LH27 | issima Trin | 09/06/2017 | Spring | 684558 | 2134658 | 2906 | - | ≈200_estimated | 12.2 | 7.15 | 8.9 | 63 |
| LH30 | Mazapa | 10/06/2017 | Spring | 682513 | 2179254 | 2239 | - | 7.5 | 20 | 7.23 | 3.4 | 96.1 |
| LH31 | Mazapa2 | 10/06/2017 | Spring | 682812 | 2178692 | 2280 | - | 1.4 | 14.9 | 7.06 | 5.59 | 154.5 |
| Code | Name | Date (dd/mm/yy) | Type | X (m) | Y (m) | Alt. (m.a.s.l.) | Depth (m) | Flow rate (L/min.) | T (°C) | pH | O2 diss. (mg/L) | E.C. (µS/cm) |
| LH32 | Mazapa3 | 10/06/2017 | Spring | 682801 | 2178708 | 2280 | - | 30 | 15 | 6.69 | 7.38 | 144.5 |
| LH33 | tzingo-El Tes | 10/06/2017 | Spring | 683257 | 2182923 | 2095 | - | 55 | 15.6 | 6.71 | 5.48 | 104.1 |
| LH34 | Escobillo | 11/06/2017 | Spring | 689388 | 2158492 | 3075 | - | 190 | 9.3 | 8 | 6.8 | 27.2 |
| LH35 | o-Rancho N | 11/06/2017 | Spring | 689961 | 2160999 | 3020 | - | 80 | 11.9 | 6.44 | 6.6 | 84.1 |
| LH36 | El Conejo | 11/06/2017 | Spring | 693563 | 2159689 | 3406 | - | 5 | 9.5 | 6.79 | 9.34 | 63.8 |
| LH37 | Dos Aguas | 11/06/2017 | Spring | 691046 | 2161084 | 3098 | - | 80-100 | 11.7 | 6.53 | 6.6 | 98 |
| LH38 | icaco-Ahuc | 11/06/2017 | Spring | 678612 | 2189214 | 1950 | - | 6.5 | 16 | 7.14 | 6.37 | 113 |
| LH39 | icaco-Ahuc | 11/06/2017 | Spring | 678606 | 2189267 | 1937 | - | 18 | 18 | 7.6 | 6.92 | 122 |
| LH40 | Xiutetelco | 11/06/2017 | Spring | 675386 | 2189176 | 1933 | - | ≈1000 | 15.9 | 7.85 | 6.5 | 81.2 |
| LH41 | anta Rosali | 11/06/2017 | Spring | 676367 | 2190668 | 1876 | - | - | 15.5 | 7.07 | 8.31 | 83.7 |
| LH42 | La Quinta | 12/06/2017 | Spring | 674704 | 2189494 | 1939 | - | 90 | 17 | 6.64 | 6.75 | 205 |
| LH43 | El Progreso | 12/06/2017 | Spring | 674627 | 2189327 | 1965 | - | 12 | 16.4 | 6.88 | 6.18 | 187 |
| LH44 | Guaje-A Tol | 12/06/2017 | Spring | 673429 | 2182780 | 2516 | - | 32 | 14.7 | 7.24 | 7.99 | 54.2 |
| LH44bis | Guaje-A Tol | 12/06/2017 | Spring | 673429 | 2182765 | 2520 | - | n.m. (very low) | - | n.m. | n.m. | n.m. |
| LH45 | Mixquiapar | 12/06/2017 | Spring | 679821 | 2179539 | 2292 | - | 12 | 16.8 | 6.61 | 4.4 | 96.8 |
| LH49 | Chagchar | 13/06/2017 | Spring | 663532 | 2188048 | 2389 | - | ≈1000 | 14 | 7.39 | 6.56 | 106.3 |
| LH53 | Cignahuapa | 14/06/2017 | Spring | 602311 | 2193963 | 2263 | - | >10000 | 19.5 | 7.18 | n.m. | 177 |
| LH10 | Buena Vista | 06/06/2017 | Creek | 632199 | 2183156 | 2136 | - | 12 | 20.7 | 7.37 | 8.51 | 322 |
| LH11 | Sesder | 07/06/2017 | Creek | 640766 | 2178104 | 2165 | - | 0.2 | 20 | 7.7 | 6 | 436 |
| LH16 | ıgoza-El Sal | 07/07/2017 | Creek | 651010 | 2187877 | 2219 | - | 6 | 18.2 | 7.59 | 5.76 | 224 |
| LH29 | El Carrizal | 10/06/2017 | Stream | 749109 | 2138017 | 204 | - | 30000? | | 7.78 | 4.91 | 155 |
| LH52 | Cignahuapa | 14/06/2017 | Creek | 605336 | 2193833 | 2250 | - | vari m3 | 18.4 | 7.47 | n.m. | 190 |
| LH18 | Alchichica | 08/06/2017 | Maar | 668436 | 2147447 | 2326 | - | - | 20.7 | 9.06 | 7.59 | 12150 |
| LH22 | Quecholac | 08/06/2017 | Maar | 673240 | 2143473 | 2342 | - | - | 24.1 | 8.74 | 8.51 | 846 |
| LH28 | El Carrizal | 10/06/2017 | ıermal sprir | 749122 | 2138022 | 204 | - | ≈1200 | 39.1 | 6.77 | 0 | 1670 |
| LH51 | Cignahuapa | 14/06/2017 | ıermal sprir | 605354 | 2193816 | 2260 | - | n.k. | 50.4 | 6.26 | n.m. | 1600 |
| LH47 | Pozo 29 | 13/06/2017 | injection w | 661884 | 2177843 | 2809 | 2817 | - | 33.3 | 7.7 | 5.56 | 1028 |
| LH48 | Pozo 38 | 13/06/2017 | injection w | 661899 | 2178151 | 2794 | 2202 | - | 34.1 | 7.66 | 4.43 | 1069 |
| | | | | | | Sampling 2018 | | | | | | |
| LH2 | Miguel Barri | 23/03/2018 | well | 650030 | 2157135 | 2355 | n.k. | n.k. | 18.5 | 7.81 | n.m. | 441 |
| LH3 | Pochintol | 23/03/2018 | well | 647263 | 2165018 | 2416 | 95 | n.k. | 20.2 | 7.8 | n.m. | 610 |

| Code | Name | Date (dd/mm/yy) | Type | X (m) | Y (m) | Alt. (m.a.s.l.) | Depth (m) | Flow rate (L/min.) | T (°C) | pH | O2 diss. (mg/L) | E.C. (µS/cm) |
|---|---|---|---|---|---|---|---|---|---|---|---|---|
| LH17 | Zacatepec | 23/03/2018 | well | 653448 | 2131216 | 2363 | 55 | 22 | 18.2 | 6.83 | 4.68 | 2372 |
| LH17bis | la del Carm | 23/03/2018 | well | 653583 | 2130937 | 2365 | 70 | 15 | 19.1 | 7.1 | n.m. | 2080 |
| LH46 | 4_Los_Hum | 21/03/2018 | well | 658269 | 2175133 | 2753 | 350 | n.k. | 23 | 7.22 | 4.56 | 349.4 |
| LH46_bis | verancia_Lc | 21/03/2018 | well | 658859 | 2175920 | 2755 | 320 | n.k. | 28.4 | 6.64 | 6.64 | 499.5 |
| LH50 | cho_Los_Sa | 19/03/2018 | well | 680858 | 2173556 | 2400 | 180 | 50 | 20 | 7.48 | 4.91 | 570 |
| LH50_bis | cho_Los_Ol | 19/03/2018 | well | 680475 | 2172813 | 2396 | 200 | n.k. | 21.4 | 7.68 | 6.75 | 610 |
| LH54 | ardin_Dora | 17/03/2018 | well | 674864 | 2163728 | 2379 | 120 | 67 | 22.7 | 7.29 | 4.16 | 1569 |
| LH55 | ardin_Dora | 17/03/2018 | well | 675821 | 2163313 | 2371 | 150 | n.k. | 24.5 | 7.26 | 3.27 | 1445 |
| LH61 | ijol_Colora | 20/03/2018 | well | 673285 | 2166838 | 2397 | 136 | n.k. | 27.4 | 7.55 | 5.51 | 994.9 |
| LH77 | evo_Horizor | 16/03/2018 | well | 611575 | 2136286 | 2531 | 170 | 25 | 17.6 | 6.39 | 3.59 | 531.6 |
| LH78 | os_San_Ant | 16/03/2018 | well | 612596 | 2134938 | 2532 | 250 | 30 | 21.9 | 6.42 | 3.96 | 606.3 |
| LH79 | ozos_San_Lu | 16/03/2018 | well | 612459 | 2134071 | 2580 | 300 | 22 | 20 | 6.32 | 3.43 | 674.3 |
| LH80 | o_Lienzo_Ch | 16/03/2018 | well | 614467 | 2136187 | 2469 | 150 | 24 | 21.8 | 6.75 | 5.66 | 660.6 |
| LH81 | n_Paolo_Zit | 16/03/2018 | well | 615761 | 2124399 | 2517 | 210 | 22 | 20.5 | 7.47 | 5.52 | 654 |
| PER27 | ncho_Lome | 20/03/2018 | well | 680844 | 2174565 | 2378 | 180 | 35 | 20.8 | 7.35 | 3.58 | 959 |
| PER30 | /PH1_Perot | 21/03/2018 | well | 677699 | 2163587 | 2358 | 200 | n.k. | 18.1 | 7.28 | 5.99 | 916.2 |
| PER31 | quiapan_P | 21/03/2018 | well | 679749 | 2170703 | 2379 | 200 | 45 | 32.8 | 7.2 | 3.66 | 1158 |
| PER36 | Alchichico1 | 22/03/2018 | well | 671945 | 2147350 | 2344 | 100 | 50 | 19.3 | 7.46 | 5.43 | 606 |
| PER37 | Xaltepa1 | 22/03/2018 | well | 672734 | 2146889 | 2341 | 100 | 50 | 18.7 | 7.81 | 6.01 | 590 |
| PER38 | Alchichico2 | 22/03/2018 | well | 671211 | 2147703 | 2347 | 100 | 50 | 18.8 | 7.95 | 6.27 | 855 |
| PER39 | ncho_El_Pre | 22/03/2018 | well | 681398 | 2163652 | 2377 | 200 | 75 | 17.1 | 8.74 | 7.83 | 283 |
| PER40 | Animas1 | 23/03/2018 | well | 681064 | 2165652 | 2372 | 200 | 100 | 16.8 | 7.44 | 6.87 | 379.6 |
| PER42 | ncho San Ia | 23/03/2018 | well | 648232 | 2123760 | 2372 | n.k. | n.k. | 19 | 7.8 | 4.24 | 748.7 |
| PER43 | cho San Abr | 23/03/2018 | well | 652557 | 2128714 | 2363 | 60 | n.k. | 20.3 | 6.9 | 2.83 | 2315 |
| PER44 | | 23/03/2018 | well | 647497 | 2121426 | 2355 | n.k. | n.k. | 17.3 | 7.65 | 2.72 | 652.6 |
| PER47 | | 26/03/2018 | well | 671917 | 2139383 | 2360 | 145 | 20 | 18.3 | 7.74 | 5.93 | 700.9 |
| PER48 | | 26/03/2018 | well | 669183 | 2141039 | 2351 | n.k. | n.k. | 18.1 | 7.15 | 2.18 | 948.5 |
| PER49 | | 26/03/2018 | well | 668760 | 2135259 | 2361 | n.k. | n.k. | 16.3 | 7.66 | 5.22 | 572.3 |
| PER51 | | 26/03/2018 | well | 657833 | 2137770 | 2406 | 140 | 25 | 34.8 | 7.59 | 4.56 | 6083 |
| PER52 | | 26/03/2018 | well | 644520 | 2145892 | 2333 | 56 | 74 | 20.8 | 7.9 | 6.58 | 915.3 |
| PER53 | | 27/03/2018 | well | 672068 | 2145060 | 2336 | 18 | 15 | 21.7 | 7.82 | 5074 | 1003 |
| Code | Name | Date (dd/mm/yy) | Type | X (m) | Y (m) | Alt. (m.a.s.l.) | Depth (m) | Flow rate (L/min.) | T (°C) | pH | O2 diss. (mg/L) | E.C. (µS/cm) |
| PER54 | | 27/03/2018 | well | 679934 | 2166525 | 2380 | 127 | 26 | 23.7 | 7.34 | 5.14 | 1465 |
| PER55 | | 27/03/2018 | well | 675570 | 2165414 | 2383 | 137 | 24 | 24 | 7.3 | 5.35 | 4351 |
| PER56 | | 27/03/2018 | well | 677541 | 2171184 | 2394 | 150 | 40 | 33.1 | 7.29 | 4.04 | 1309 |
| PER57 | | 27/03/2018 | well | 677973 | 2168749 | 2377 | 127 | n.k. | 30.2 | 7.22 | 4.57 | 1686 |
| PER58 | | 27/03/2018 | well | 682191 | 2166730 | 2381 | 130 | 26 | 17.9 | 7.67 | 7.43 | 471.1 |
| PER59 | | 27/03/2018 | well | 680414 | 2170213 | 2365 | 130 | 26 | 23.5 | 7.65 | 6.45 | 991.2 |
| PER60 | | 27/03/2018 | well | 684817 | 2171039 | 2368 | 116 | 18 | 17.9 | 7.64 | 6.7 | 709.5 |
| PER71 | La Soledad | 28/03/2018 | well | 637092 | 2140786 | 2391 | n.k. | n.k. | 24.3 | 8 | 6.31 | 591 |
| PER72 | nguito CNA T | 28/03/2018 | well | 634758 | 2141050 | 2394 | n.k. | n.k. | 20.8 | 8.2 | 7.01 | 431.3 |
| PER73 | a José Ma. N | 28/03/2018 | well | 636376 | 2140801 | 2389 | n.k. | n.k. | 21.5 | 8.03 | 6.66 | 504.5 |
| PER74 | ría Las Cuev | 28/03/2018 | well | 632711 | 2141047 | 2404 | n.k. | n.k. | 21.4 | 7.67 | 6.65 | 344.8 |
| PER78 | uevo Pizarr | 23/03/2018 | well | 662435 | 2155825 | 2340 | n.k. | n.k. | 16 | 8.82 | n.m. | 2090 |
| LH5 | uitzitzilapa | 22/03/2018 | spring | 648888 | 2180329 | 2473 | - | 0.22 | 14.3 | 7.51 | 7.53 | 544.5 |
| LH6 | apan(lavad | 22/03/2018 | spring | 645866 | 2179181 | 2436 | - | 0.17 | 15.1 | 7.1 | 6.77 | 706 |
| LH6bis | Tihuapan | 22/03/2018 | spring | 645586 | 2178908 | 2476 | - | not_measuarable | 13.8 | 7.32 | 6.1 | 954.3 |
| LH7 | La Olimpica | 22/03/2018 | spring | 644236 | 2179782 | 2345 | - | 0.36 | 13.3 | 7.8 | 6.81 | 493.2 |
| LH7* | La Olimpica | 22/03/2018 | spring | 644174 | 2179649 | 2379 | - | not_measuarable | 14.8 | 7.46 | 6.58 | 671 |
| LH8 | La Olimpica | 22/03/2018 | spring | 644457 | 2179520 | 2435 | - | dripping | 14.1 | 7.1 | 4.78 | 686.5 |
| LH8bis | | 27/03/2018 | spring | 643291 | 2180338 | 2232 | - | not_measuarable | 14 | 7.72 | 8.43 | 559.5 |
| LH9 | Buena vista | 27/03/2018 | spring | 633513 | 2183084 | 2392 | - | very low | 13 | 6.71 | 8.47 | 559.5 |
| LH12 | sender | 27/03/2018 | spring | 640647 | 2178480 | 2205 | - | n.m. | 18.4 | 7.47 | 4.07 | 869.3 |
| LH14bis | ntloiuquitep | 27/03/2018 | spring | 654015 | 2185782 | 2405 | - | 2 | 12.7 | 7.23 | 7.33 | 61.95 |
| LH23 | Nacimiento | 26/03/2018 | spring | 685242 | 2141605 | 2998 | - | 0.042 | 8.9 | 6.78 | 7.5 | 188 |
| LH24 | Nacimiento : | 26/03/2018 | spring | 685059 | 2141722 | 2977 | - | 0.57 | 11.7 | 6.71 | 7.25 | 210 |
| LH25 | Oczotla | 26/03/2018 | spring | 683402 | 2141025 | 2770 | - | 2 | 11.3 | 6.98 | 7.34 | 114.4 |
| LH26 | issima Trin | 26/03/2018 | spring | 684493 | 2134626 | 2907 | - | n.m. | n.s. | n.s. | n.s. | n.s. |
| LH27 | issima Trin | 26/03/2018 | spring | 684558 | 2134658 | 2906 | - | n.m. | n.s. | n.s. | n.s. | n.s. |
| LH30 | Mazapa | 19/03/2018 | spring | 682518 | 2179263 | 2221 | - | 0.003 | 13.3 | 7.17 | 7 | 122 |
| LH30_bis | Mazapa2_bi | 19/03/2018 | spring | 682456 | 2179186 | 2255 | - | 1.5 | 15.2 | 7.34 | 6.52 | 126 |
| LH32 | Mazapa3 | 19/03/2018 | spring | 682802 | 2178721 | 2280 | - | 1.5 | 15.3 | 6.9 | 6.92 | 172 |
| LH33 | zingo-El_Te | 19/03/2018 | spring | 683257 | 2182923 | 2095 | - | 0.75 | 15.1 | 6.76 | 6.97 | 123 |

| Code | Name | Date (dd/mm/yy) | Type | X (m) | Y (m) | Alt. (m.a.s.l.) | Depth (m) | Flow rate (L/min.) | T (°C) | pH | O2 diss. (mg/L) | E.C. (µS/cm) |
|---|---|---|---|---|---|---|---|---|---|---|---|---|
| LH33bis | zingo-El _Te | 23/03/2018 | spring | 683140 | 2183042 | 2055 | - | not_measuarable | 22.5 | 7.49 | n.m. | 787 |
| LH33* | zingo-El _Te | 23/03/2018 | spring | 683146 | 2183042 | 2055 | - | n.m | 21 | 7.5 | n.m. | 610 |
| LH36 | Conejo | 18/03/2018 | spring | 693563 | 2159689 | 3406 | - | 0.71 | 9.6 | 6.98 | 7.43 | 84 |
| LH38 | icaco-Ahuac | 19/03/2018 | spring | 678612 | 2189214 | 1950 | - | 0.23 | 15.5 | 7.23 | 6.7 | 137 |
| LH39 | icaco-Ahuac | 19/03/2018 | spring | 678592 | 2189267 | 1905 | - | not_measuarable | 16.5 | 7.94 | 7.23 | 166 |
| LH40 | etelca Las P | 25/03/2018 | spring | 675386 | 2189176 | 1933 | - | 123 | 15.3 | 7.65 | 6.46 | 106.4 |
| LH42 | La Quinta | 25/03/2018 | spring | 674704 | 2189494 | 1939 | - | 2.12 | 16 | 7.9 | 6.8 | 250.7 |
| LH43 | El Progreso | 25/03/2018 | spring | 674627 | 2189327 | 1965 | - | 0.26 | 15.7 | 7.15 | 6.5 | 252.2 |
| LH44bis | Agua Je | 25/03/2018 | spring | 673429 | 2182765 | 2518 | - | 0.01 | 12.3 | 7.36 | 7.64 | 82.13 |
| PER13 | _Perote_Na | 18/03/2018 | spring | 694218 | 2158259 | 3645 | - | 0.85 | 8.1 | 7.07 | 7.56 | 3227 |
| PER14 | e_Perote_El | 18/03/2018 | spring | 693642 | 2156814 | 3873 | - | 0.7 | 6.8 | 7.32 | 7.59 | 56 |
| PER15 | _Perote_El_ | 18/03/2018 | spring | 693740 | 2159327 | 3490 | - | 3 | 11 | 6.7 | 7.61 | 108 |
| PER65 | La libertad1 | 27/03/2018 | spring | 687870 | 2176388 | 2413 | - | 0.49 | 16.3 | 7.04 | 6.28 | 133.7 |
| PER66 | Descarga | 27/03/2018 | spring | 692623 | 2175190 | 1936 | - | high, not measurable | 19.4 | 8.09 | 7.13 | 186.4 |
| PER67 | Ell Llano | 27/03/2018 | spring | 691984 | 2175163 | 2305 | - | 0.19 | 14.6 | 6.97 | 7.38 | 31.4 |
| PER68 | Las Minas2 | 27/03/2018 | spring | 692180 | 2176055 | 2101 | - | n.m | 15.3 | 7.51 | 7.52 | 75.79 |
| PER69 | Las Minas3 | 27/03/2018 | spring | 691789 | 2175770 | 2278 | - | n.m | 12.9 | 7.67 | 7.67 | 40.74 |
| PER70 | linas1 - Las | 27/03/2018 | spring | 692700 | 2175366 | 1850 | - | n.m | 15.7 | 7.87 | 8.15 | 224 |
| PER83 | Panaloya | 25/03/2018 | spring | 673096 | 2188450 | 2128 | - | high, not measurable | 14.4 | 7.15 | 6.94 | 74.38 |
| PER84 | Canada | 28/03/2018 | spring | 632731 | 2156590 | 2553 | - | 0.06 | 15 | 7.37 | 5.64 | 592.5 |
| PER85 | bellavista | 28/03/2018 | spring | 628747 | 2160290 | 2935 | - | 0.05 | 12 | 7.83 | 6.49 | 338.9 |
| PER45 | una San Mig | 23/03/2018 | lagoon | 653201 | 2175087 | 2341 | - | not_measurable | 24.3 | 9.83 | 0.6 | 7869 |
| LH47 | o29_reinjec | 20/03/2018 | _well_pozo | 661884 | 2177843 | 2809 | 2807 | - | 27.7 | 7.53 | 4 | 1262 |
| LH48 | o38_reinjec | 20/03/2018 | _well_pozo | 661899 | 2178151 | 2794 | 2202 | - | 28.8 | 7.53 | 2.56 | 1253 |

n.m. = not measured

n.k. = not known

n.a. = not analysed or sample collected just for isotopes analysis

n.s. = not sampled

Table A2 – Concentration of chemical species determined in collected water samples (Los Humeros). Data are expressed in mg/L. Charge balance is also included.

| Code | Na | K | Ca | Mg | Sr | Li | Cl | $HCO_3$ | $SO_4$ | B | F | Br | $NO_3$ | $SiO_2$ | Charge balance (%) |
|---|---|---|---|---|---|---|---|---|---|---|---|---|---|---|---|
| **Sampling 2017** | | | | | | | | | | | | | | | |
| LH1 | 45.8 | 5.12 | 39.8 | 17.3 | 0.3 | 1.40E-02 | 15.3 | 262 | 19.8 | 0.22 | 0.57 | <0.05 | 19.6 | 60.1 | 0.41 |
| LH2 | 29.2 | 5.8 | 29.7 | 12.2 | 0.19 | 6.00E-03 | 7.2 | 171 | 8.47 | 0.1 | 0.54 | <0.05 | 36.1 | 59.7 | 1.56 |
| LH3 | 32 | 3.22 | 72.8 | 8.3 | 0.24 | 1.30E-02 | 28.8 | 153 | 24.5 | 0.05 | 0.27 | <0.05 | 127 | 51.4 | -0.76 |
| LH4 | 9.7 | 14.2 | 23 | 6.26 | 0.13 | <5.00E-03 | 3.29 | 116 | 11.5 | <0.01 | <0.02 | <0.05 | 8.99 | 54.1 | 1.5 |
| LH15 | 9.6 | 2.43 | 36.3 | 3.6 | 0.1 | <5.00E-03 | 1.92 | 146 | 3.44 | <0.01 | 0.33 | <0.05 | 6.6 | 62.3 | -1.13 |
| LH17 | 82.5 | 8.1 | 264 | 99.9 | 2.06 | 9.90E-02 | 87 | 799 | 445 | 1.4 | 0.75 | <0.05 | 0.41 | 71.2 | 0.7 |
| LH20 | 130 | 9.26 | 101 | 132 | 0.68 | 8.30E-02 | 208 | 778 | 101 | 1.72 | 1 | 0.52 | <0.05 | 77.9 | 2.46 |
| LH21 | 38.4 | 3.2 | 50.5 | 32.5 | 0.3 | <5.00E-03 | 48.8 | 311 | 16.5 | 0.23 | 0.27 | <0.05 | 5.6 | 50.5 | 0.2 |
| LH46 | 28 | 4.4 | 31.5 | 10.3 | 0.08 | 3.70E-02 | 1 | 214 | 7.72 | 0.11 | 0.75 | <0.05 | <0.05 | 76.8 | 0.35 |
| LH50 | 93 | 11 | 22.9 | 21.2 | 0.12 | 9.20E-02 | 34.7 | 360 | 14.7 | 0.98 | 0.5 | <0.05 | 0.3 | 74 | 0.02 |
| LH54 | 260 | 30 | 52.6 | 85.6 | 0.43 | 3.90E-01 | 208 | 903 | 21.8 | 4.05 | 0.94 | 0.47 | <0.05 | 71.7 | 1.37 |
| LH55 | 208 | 23.2 | 66.3 | 81.2 | 0.46 | 2.80E-01 | 193 | 824 | 32.1 | 3.58 | 0.74 | 0.38 | <0.05 | 63.1 | -0.03 |
| LH5 | 11 | 3.73 | 13 | 4.63 | 0.06 | <5.00E-03 | 2.2 | 79.3 | 4.73 | <0.01 | <0.02 | <0.05 | 5.07 | 67.7 | 1.93 |
| LH6 | 6.36 | 3.73 | 142 | 4.93 | 0.22 | <5.00E-03 | 2.9 | 397 | 36.7 | <0.01 | 0.3 | <0.05 | <0.05 | 38.3 | 3.26 |
| LH7 | 8.5 | 4.57 | 112 | 5.22 | 0.24 | <5.00E-03 | 3.88 | 365 | 20.7 | <0.01 | <0.02 | <0.05 | <0.05 | 41.2 | -0.27 |
| LH7 bis | n.a. | n.a. | n.a. | n.a. | n.a. | n.a. | n.a. | n.a. | n.a. | n.a. | n.a. | n.a. | n.a. | n.a. | n.c. |
| LH8 | 6.6 | 4 | 134 | 5.27 | 0.22 | 5.00E-03 | 2.6 | 421 | 16 | <0.01 | <0.02 | <0.05 | <0.05 | 44 | 1.43 |
| LH9 | 12 | 5.82 | 20.5 | 8.16 | 0.12 | <5.00E-03 | 3.57 | 113 | 17 | <0.01 | <0.02 | <0.05 | 0.48 | 69.8 | 1.21 |
| LH12 | 22.7 | 3.76 | 68 | 5.3 | 0.21 | 8.00E-03 | 3.48 | 278 | 10.7 | <0.01 | 0.86 | <0.05 | 0.88 | 33.2 | -0.14 |
| LH13 | 27.8 | 7.8 | 57.7 | 5.12 | 0.2 | 9.00E-03 | 3.46 | 261 | 10.9 | <0.01 | 0.91 | <0.05 | <0.05 | 31.7 | 0.66 |
| LH14 | 22.1 | 2.77 | 29.7 | 3.84 | 0.07 | <5.00E-03 | 2.72 | 122 | 6.24 | <0.01 | 0.37 | <0.05 | 13.8 | 72.2 | 7.27 |
| LH19 | n.a. | n.a. | n.a. | n.a. | n.a. | n.a. | n.a. | n.a. | n.a. | n.a. | n.a. | n.a. | n.a. | n.a. | n.c. |
| LH23 | 1.54 | 0.78 | 3.14 | 1.46 | 0.03 | <5.00E-03 | 0.32 | 18.9 | 0.1 | <0.01 | <0.02 | <0.05 | <0.05 | 16 | 6.31 |
| LH24 | 6 | 2.7 | 6.8 | 3.41 | 0.1 | <5.00E-03 | 0.27 | 55.5 | 0.25 | <0.01 | <0.02 | <0.05 | <0.05 | 24.5 | 1.54 |
| LH25 | 4.55 | 1.75 | 13 | 7.87 | 0.08 | <5.00E-03 | 0.91 | 89.1 | 0.26 | <0.01 | <0.02 | <0.05 | <0.05 | 31.9 | 1.64 |
| LH26 | 2.64 | 0.94 | 5.92 | 1.37 | 0.06 | <5.00E-03 | 0.4 | 30.5 | 1.41 | <0.01 | 0.1 | <0.05 | 0.6 | 30.8 | -0.68 |
| LH27 | 3.13 | 0.96 | 6.4 | 1.5 | 0.09 | <5.00E-03 | 0.61 | 30.5 | 3.35 | <0.01 | 0.1 | <0.05 | 0.24 | 28.6 | 0.73 |
| LH30 | n.a. | n.a. | n.a. | n.a. | n.a. | n.a. | n.a. | n.a. | n.a. | n.a. | n.a. | n.a. | n.a. | n.a. | n.c. |
| LH31 | 8.5 | 5.5 | 16.3 | 5.5 | 0.08 | <5.00E-03 | 4.4 | 67.1 | 12.6 | <0.01 | <0.02 | <0.05 | 15.1 | 63.7 | 1.43 |
| LH32 | 7.8 | 5.5 | 15.8 | 5.54 | 0.11 | <5.00E-03 | 4.9 | 61 | 10 | <0.01 | 0.16 | <0.05 | 18.3 | 64.2 | 2.25 |
| Code | Na | K | Ca | Mg | Sr | Li | Cl | $HCO_3$ | $SO_4$ | B | F | Br | $NO_3$ | $SiO_2$ | Charge balance (%) |
| LH33 | 7.1 | 5.24 | 10.4 | 2.9 | 0.05 | <5.00E-03 | 1.3 | 54.9 | 5.15 | <0.01 | <0.02 | <0.05 | 11.8 | 71.1 | -1.25 |
| LH34 | 2.34 | 2.97 | 3 | 0.83 | 0.02 | <5.00E-03 | 0.14 | 18.9 | 1.72 | <0.01 | 0.13 | <0.05 | 0.3 | 40.2 | 4.6 |
| LH35 | 7.02 | 4.06 | 7.16 | 3.53 | 0.04 | <5.00E-03 | 1.56 | 54.3 | 3.8 | <0.01 | <0.02 | <0.05 | 3.25 | 70.9 | -0.36 |
| LH36 | 5.7 | 4.1 | 6.62 | 2.41 | 0.04 | <5.00E-03 | 0.2 | 51.9 | 1 | <0.01 | <0.02 | <0.05 | <0.05 | 64 | 0.34 |
| LH37 | n.a. | n.a. | n.a. | n.a. | n.a. | n.a. | n.a. | 57.9 | n.a. | n.a. | n.a. | n.a. | n.a. | n.a. | n.c. |
| LH38 | 7.4 | 5.7 | 8.9 | 4.24 | 0.07 | <5.00E-03 | 3.2 | 48.8 | 7.77 | <0.01 | <0.02 | <0.05 | 12.7 | 69.3 | 0.21 |
| LH39 | 8.24 | 6.41 | 9.5 | 4.5 | 0.08 | <5.00E-03 | 4.3 | 51.9 | 5.3 | <0.01 | <0.02 | <0.05 | 14.2 | 70.4 | 2.16 |
| LH40 | n.a. | n.a. | n.a. | n.a. | n.a. | n.a. | n.a. | 57.9 | n.a. | n.a. | n.a. | n.a. | n.a. | n.a. | n.c. |
| LH41 | 10.4 | 1.8 | 6.55 | 2.42 | 0.03 | 1.68E-02 | 0.88 | 48.8 | 2.98 | <0.01 | 0.27 | <0.05 | 2.8 | 47.1 | 4.76 |
| LH42 | 10.3 | 7.67 | 18.4 | 8.5 | 0.11 | <5.00E-03 | 3.92 | 88.5 | 18.9 | <0.01 | <0.02 | <0.05 | 13.5 | 67.6 | 2.07 |
| LH43 | 9.7 | 6.4 | 18.5 | 9.3 | 0.13 | 6.65E-03 | 4.1 | 104 | 20.2 | <0.01 | <0.02 | <0.05 | 14.5 | 61.2 | -4.07 |
| LH44 | 4.56 | 2.97 | 4.35 | 1.6 | 0.03 | <5.00E-03 | 0.24 | 36.6 | 0.59 | <0.01 | <0.02 | <0.05 | <0.05 | 50.1 | 0.38 |
| LH44bis | n.a. | n.a. | n.a. | n.a. | n.a. | n.a. | n.a. | 57.9 | n.a. | n.a. | n.a. | n.a. | n.a. | n.a. | n.c. |
| LH45 | 8.5 | 2.7 | 8.32 | 3.93 | 0.04 | 6.70E-03 | 0.87 | 64.1 | 1.85 | <0.01 | <0.02 | <0.05 | 2.83 | 60.1 | 0.84 |
| LH49 | 9.73 | 1.9 | 14.3 | 1.75 | 0.03 | 1.70E-02 | 0.47 | 76.3 | 1.6 | 1.22 | 0.46 | <0.05 | 1.93 | 46 | -0.74 |
| LH53 | 9.44 | 3.56 | 11.8 | 7.8 | 0.1 | <5.00E-03 | 1.83 | 952 | 2.15 | <0.01 | <0.02 | <0.05 | 1.43 | 45.8 | 1.55 |
| LH10 | 5.39 | 2.13 | 53.3 | 6.5 | 0.33 | <5.00E-03 | 1.67 | 168 | 33 | <0.01 | <0.02 | <0.05 | <0.05 | 27.6 | 0.08 |
| LH11 | 23.6 | 6.28 | 63.2 | 7.7 | 0.26 | <5.00E-03 | 4.47 | 278 | 6.1 | <0.01 | 0.78 | <0.05 | <0.05 | 40 | 1.4 |
| LH16 | 10 | 2.5 | 36.6 | 3.6 | 0.1 | <5.00E-03 | 1.87 | 140 | 3.6 | <0.01 | 0.19 | <0.05 | 6.8 | 57.6 | 1.5 |
| LH29 | 5.6 | 3.89 | 19.1 | 2.7 | 0.21 | <5.00E-03 | 3.84 | 67.1 | 10 | <0.01 | <0.02 | <0.05 | 10.6 | 31.5 | -2.11 |
| LH52 | n.a. | n.a. | n.a. | n.a. | n.a. | n.a. | n.a. | 57.9 | n.a. | n.a. | n.a. | n.a. | n.a. | n.a. | n.c. |
| LH18 | 2597 | 227 | 8.15 | 432 | 0.04 | 2.59E+00 | 3273 | 2623 | 993 | 39.3 | 0.07 | 9.8 | <0.05 | 0.41 | -0.41 |
| LH22 | 87 | 7.8 | 13.3 | 63.9 | 0.06 | <5.00E-03 | 86.1 | 415 | 18.5 | 0.55 | 0.51 | <0.05 | <0.05 | 10.3 | 1.37 |
| LH28 | 34.6 | 12.3 | 216 | 58.3 | 6.32 | 1.06E-01 | 42.6 | 238 | 635 | 0.23 | 1.68 | <0.05 | <0.05 | 41.9 | -2.64 |
| LH51 | 95.5 | 14.7 | 191 | 26.5 | 0.6 | 3.82E-01 | 111 | 793 | 27.3 | 3.1 | 0.75 | 0.7 | <0.05 | 42.4 | -1.51 |
| LH47 | 95 | 13 | 1.77 | 0.05 | 0.03 | 2.13E-01 | 34.2 | 110 | 270 | 330 | 1.94 | <0.05 | <0.05 | 110 | n.c. |
| LH48 | 107 | 14.5 | 1.73 | 0.05 | 0.03 | 2.36E-01 | 40.1 | 134 | 269 | 360 | 2.2 | <0.05 | <0.05 | 115 | n.c. |
| **Sampling 2018** | | | | | | | | | | | | | | | |
| LH2 | 31.8 | 5.7 | 35 | 15.3 | 0.22 | 8.00E-03 | 10.7 | 180 | 12.5 | 0.08 | 0.46 | n.a. | 49.5 | 63.3 | 1.73 |
| LH3 | 39.3 | 5.2 | 78.5 | 9.07 | 0.26 | 1.70E-02 | 31.7 | 138 | 26 | 0.03 | 0.27 | n.a. | 183 | 44.8 | -1.42 |
| LH17 | 84.6 | 9.18 | 290 | 115 | 2.47 | 1.25E-01 | 87.7 | 693 | 658 | 1.38 | 0.41 | n.a. | 4.2 | 67.9 | 0.13 |
| LH17bis | 85 | 10.2 | 280 | 109 | 2.36 | 1.18E-01 | 98.1 | 810 | 460 | 1.77 | 0.38 | n.a. | 3.4 | 88.4 | 1.92 |

| Code | Na | K | Ca | Mg | Sr | Li | Cl | $HCO_3$ | $SO_4$ | B | F | Br | $NO_3$ | $SiO_2$ | Charge balance (%) |
|---|---|---|---|---|---|---|---|---|---|---|---|---|---|---|---|
| LH46 | 27 | 6.01 | 27.8 | 9.6 | 0.07 | 3.90E-02 | 1.05 | 192 | 8.3 | 0.13 | 0.7 | n.a. | 0.53 | 80.7 | 0.87 |
| LH46_bis | 44.1 | 8.14 | 35.9 | 14.3 | 0.1 | 5.40E-02 | 1.22 | 288 | 14.8 | 0.24 | 0.68 | n.a. | 0.37 | 103 | -0.84 |
| LH50 | 83.9 | 13 | 21.2 | 18.6 | 0.11 | 8.50E-02 | 24 | 324 | 13.5 | 0.85 | 0.45 | n.a. | 5.5 | 75.1 | 0.79 |
| LH50_bis | 65.1 | 10.9 | 34.6 | 24.1 | 0.18 | 7.80E-02 | 41.6 | 327 | 9.9 | 0.92 | 0.38 | n.a. | 9.37 | 57 | -1.27 |
| LH54 | 236 | 29.1 | 51.7 | 80.3 | 0.49 | 3.98E-01 | 203 | 870 | 20.1 | 4.24 | 0.59 | n.a. | 6 | 71 | -1.38 |
| LH55 | 196 | 22.5 | 64.5 | 78.7 | 0.53 | 2.84E-01 | 172 | 834 | 17 | 3.48 | 0.35 | n.a. | 2.7 | 69.5 | -0.95 |
| LH61 | 111 | 14.1 | 43.2 | 31.3 | 0.25 | 1.51E-01 | 59.4 | 458 | 17.7 | 2.56 | 0.63 | n.a. | 5.1 | 90.5 | 0.72 |
| PER27 | 120 | 16.7 | 28.09 | 31.4 | 0.18 | 1.04E-01 | 44.5 | 480 | 16.9 | 1.79 | 0.6 | n.a. | <0.05 | 75 | n.c. |
| PER30 | 48.5 | 8.15 | 44.7 | 24.4 | 0.25 | 7.50E-02 | 57 | 276 | 4.35 | 2.3 | 0.16 | n.a. | 2 | 52.7 | n.c. |
| PER31 | 130 | 18.4 | 36.6 | 32.4 | 0.19 | 1.80E-01 | 51.1 | 508 | 18.5 | 2.13 | <0.02 | n.a. | 7.6 | 105 | n.c. |
| PER36 | 47 | 5.2 | 39 | 43 | 0.39 | 5.00E-03 | 33.6 | 354 | 20.5 | 0.37 | 0.16 | n.a. | 8.5 | 61.6 | n.c. |
| PER37 | 40.3 | 5.07 | 32.6 | 44.1 | 0.33 | 2.00E-03 | 34.2 | 330 | 21.3 | 0.37 | 0.15 | n.a. | 9.79 | 56.2 | n.c. |
| PER38 | 53.1 | 6.02 | 65.9 | 59.5 | 0.67 | 4.60E-03 | 86.2 | 420 | 48.9 | 0.46 | 0.2 | n.a. | 7.3 | n.a. | -0.01 |
| PER39 | 24 | 5.2 | 18.9 | 11.2 | 0.11 | 1.70E-02 | 14.9 | 147 | 4.8 | 0.21 | 0.25 | n.a. | 2.9 | 58.1 | 1.73 |
| PER40 | 27.5 | 6.1 | 24.7 | 14.8 | 0.13 | 2.80E-02 | 17.5 | 192 | 4.62 | 0.3 | 0.16 | n.a. | 1.93 | 53.1 | 0.97 |
| PER42 | 58.8 | 5.11 | 48.8 | 36.2 | 0.36 | 2.60E-02 | 20.4 | 381 | 46.2 | 0.13 | 0.38 | n.a. | 6.9 | 66 | 1.65 |
| PER43 | 100 | 9.5 | 186 | 164 | 1.43 | 8.50E-02 | 96 | 903 | 430 | 7.58 | 0.33 | n.a. | 4.5 | 71.7 | 0.5 |
| PER44 | 54.3 | 4.19 | 39.1 | 31.1 | 0.32 | 2.40E-02 | 18.6 | 306 | 28.7 | 0.16 | 0.71 | n.a. | 31.6 | 60.1 | 0.39 |
| PER47 | 42.9 | 4 | 52.1 | 31.4 | 0.32 | 1.70E-02 | 36.9 | 285 | 24.5 | 0.34 | 0.32 | n.a. | 39.6 | 51.9 | 0.23 |
| PER48 | 63.3 | 6.11 | 120 | 61.8 | 0.95 | 1.39E-01 | 110 | 624 | 9.99 | 1.1 | 0.35 | n.a. | <0.05 | 74.9 | -0.31 |
| PER49 | 32.4 | 2.4 | 45.2 | 26.2 | 0.26 | 2.70E-02 | 31.2 | 273 | 11.6 | 0.32 | 0.35 | n.a. | 12.4 | 52.7 | 0.56 |
| PER51 | 861 | 47 | 67 | 178 | 2.1 | 2.02E+00 | 1550 | 567 | 214 | 28.3 | 0.25 | n.a. | 3 | 82.2 | 1.09 |
| PER52 | 74 | 6.5 | 59 | 38.3 | 0.62 | 3.20E-02 | 44 | 372 | 45 | 0.27 | 0.77 | n.a. | 54 | 77.5 | 1.57 |
| PER53 | 69 | 3.35 | 52.6 | 46.4 | 0.39 | 1.40E-02 | 52.7 | 372 | 62.2 | 0.57 | 0.41 | n.a. | 20 | 58.2 | 1.43 |
| PER54 | 78.2 | 12.9 | 50.8 | 36.4 | 0.24 | 1.11E-01 | 60.2 | 438 | 6.96 | 1.21 | 0.44 | n.a. | 2.54 | 63.8 | 0.98 |
| PER55 | 579 | 64.9 | 97.2 | 199 | 0.78 | 8.94E-01 | 476 | 2028 | 34.9 | 2.44 | 0.73 | n.a. | 2.3 | 81.3 | -0.02 |
| PER56 | 145 | 20.9 | 41.4 | 38.1 | 0.28 | 1.95E-01 | 68.7 | 582 | 17.8 | 2.29 | 0.6 | n.a. | 5.54 | 99.5 | -0.89 |
| PER57 | 161 | 20.1 | 48.9 | 46.6 | 0.31 | 2.27E-01 | 101 | 636 | 18.6 | 2.72 | 0.59 | n.a. | 5.67 | 92.8 | 1.07 |
| PER58 | 23.5 | 6.5 | 20.5 | 10.8 | 0.1 | 2.30E-02 | 12.6 | 162 | 5.3 | 0.16 | 0.28 | n.a. | 7.5 | 50.2 | 1.12 |
| PER59 | 78.1 | 11.5 | 39 | 27.5 | 0.21 | 9.40E-02 | 48.8 | 402 | 9.9 | 1.19 | 0.32 | n.a. | 4.1 | 73.9 | 0.33 |
| PER60 | 40.2 | 7.6 | 29.9 | 17.9 | 0.17 | 2.90E-02 | 25.5 | 237 | 7.22 | 0.44 | 0.2 | n.a. | 2.81 | 56.8 | 0.06 |
| PER71 | n.a. | n.a. | n.a. | n.a. | n.a. | n.a. | n.a. | n.a. | n.a. | n.a. | n.a. | n.a. | n.a. | n.a. | -0.33 |

| Code | Na | K | Ca | Mg | Sr | Li | Cl | $HCO_3$ | $SO_4$ | B | F | Br | $NO_3$ | $SiO_2$ | Charge balance (%) |
|---|---|---|---|---|---|---|---|---|---|---|---|---|---|---|---|
| PER72 | n.a. | n.a. | n.a. | n.a. | n.a. | n.a. | n.a. | n.a. | n.a. | n.a. | n.a. | n.a. | n.a. | n.a. | n.c. |
| PER73 | n.a. | n.a. | n.a. | n.a. | n.a. | n.a. | n.a. | n.a. | n.a. | n.a. | n.a. | n.a. | n.a. | n.a. | n.c. |
| PER74 | n.a. | n.a. | n.a. | n.a. | n.a. | n.a. | n.a. | n.a. | n.a. | n.a. | n.a. | n.a. | n.a. | n.a. | n.c. |
| PER78 | 414 | 49.7 | 18.6 | 19 | 0.2 | 4.39E-01 | 235 | 711 | 110 | 3 | 1.1 | n.a. | 51.2 | 46.6 | 0.28 |
| LH5 | 11.6 | 4.53 | 15.2 | 5.2 | 0.07 | 3.00E-03 | 1.6 | 96 | 5.2 | 0.01 | 0.33 | n.a. | 6.2 | 54.7 | -1.69 |
| LH6 | 6.62 | 3.8 | 131 | 4.5 | 0.21 | 5.00E-03 | 1.2 | 390 | 30.1 | 0.02 | 0.41 | n.a. | 0.15 | 60 | 0.81 |
| LH6bis | 6.72 | 3.9 | 123 | 4.4 | 0.21 | 4.00E-03 | 1.3 | 387 | 30.7 | 0.02 | 0.2 | n.a. | <0.05 | 36.2 | -1.68 |
| LH7 | 8.36 | 4.46 | 110 | 4.69 | 0.26 | 2.00E-03 | 3.94 | 342 | 18.6 | 0.02 | 0.23 | n.a. | 0.5 | 34.2 | 1.13 |
| LH7* | 9.26 | 4.1 | 98 | 4.41 | 0.21 | <5.00E-03 | 2.59 | 303 | 16.9 | 0.01 | 0.16 | n.a. | <0.05 | 22.1 | 2.53 |
| LH8 | n.a. | n.a. | n.a. | n.a. | n.a. | n.a. | n.a. | 57.9 | n.a. | n.a. | n.a. | n.a. | n.a. | n.a. | n.c. |
| LH8bis | 9.72 | 5.93 | 99 | 4.8 | 0.23 | <5.00E-03 | 4.35 | 312 | 21 | 0.01 | 0.16 | n.a. | <0.05 | 39.7 | 1.27 |
| LH9 | 8.78 | 3.87 | 13.8 | 6.41 | 0.08 | 4.00E-03 | 3.39 | 87 | 9.7 | 0.01 | 0.15 | n.a. | <0.05 | 60 | -1.64 |
| LH12 | 22 | 4.18 | 63 | 5.18 | 0.21 | 1.50E-02 | 2.3 | 270 | n.a. | 0.03 | 0.62 | n.a. | 2.2 | 55 | 0.07 |
| LH14bis | 5.5 | 4.3 | 2.9 | 0.83 | 0.02 | 5.00E-03 | 0.65 | 30 | 1.1 | <0.01 | 0.08 | n.a. | 0.7 | 67 | 0.55 |
| LH23 | 1.6 | 1 | 3.5 | 1.5 | 0.03 | <5.00E-03 | 0.42 | 24 | 0.13 | <0.01 | 0.02 | n.a. | <0.05 | 18.5 | -2.68 |
| LH24 | 2.9 | 1.1 | 6.6 | 3 | 0.1 | <5.00E-03 | 0.55 | 43.8 | 0.15 | <0.01 | 0.03 | n.a. | <0.05 | 26.2 | -1.22 |
| LH25 | 3.63 | 1.79 | 12.4 | 7.75 | 0.08 | <5.00E-03 | 1.8 | 85.8 | 0.35 | <0.01 | 0.07 | n.a. | 1.3 | 34.8 | -1.71 |
| LH26 | n.a. | n.a. | n.a. | n.a. | n.a. | n.a. | n.a. | n.a. | n.a. | n.a. | n.a. | n.a. | n.a. | n.a. | n.c. |
| LH27 | n.a. | n.a. | n.a. | n.a. | n.a. | n.a. | n.a. | n.a. | n.a. | n.a. | n.a. | n.a. | n.a. | n.a. | n.c. |
| LH30 | 6.5 | 4 | 9.07 | 3.71 | 0.04 | <5.00E-03 | 1.2 | 43.5 | 1.5 | <0.01 | 0.08 | n.a. | 24.4 | 48 | -1.88 |
| LH30_bis | 8 | 4 | 9.22 | 3.94 | 0.05 | 7.00E-03 | 1.9 | 57 | 7.6 | 0.02 | 0.1 | n.a. | 9.1 | 33.3 | -3.06 |
| LH32 | 7.8 | 5.044 | 13.8 | 4.94 | 0.08 | <5.00E-03 | 3.7 | 58.5 | 10.7 | 0.01 | 0.1 | n.a. | 17.3 | 61.7 | -0.69 |
| LH33 | 7.02 | 5 | 10 | 3 | 0.05 | <5.00E-03 | 1.3 | 51 | 5.3 | <0.01 | 0.06 | n.a. | 13 | 77 | -1.23 |
| LH33bis | 72 | 11.22 | 37.3 | 30 | 0.22 | 1.16E-01 | 58 | 360 | 11.2 | 1.32 | 0.41 | n.a. | 8 | 63.4 | -1.68 |
| LH33* | 55 | 9 | 26 | 28 | <0.01 | <5.00E-03 | 41 | 279 | 9.5 | 0.91 | 0.34 | n.a. | 8 | 63.9 | 0.61 |
| LH36 | n.a. | n.a. | n.a. | n.a. | n.a. | n.a. | n.a. | n.a. | n.a. | n.a. | n.a. | n.a. | n.a. | n.a. | n.c. |
| LH38 | 11.6 | 9.32 | 8.74 | 4.16 | 0.07 | <5.00E-03 | 3.1 | 64.2 | 5.5 | 0.01 | 0.05 | n.a. | 15.9 | 54.9 | -0.21 |
| LH39 | 9.02 | 6.52 | 11.7 | 4.95 | 0.09 | 3.00E-03 | 4.54 | 57 | 7.23 | 0.01 | 0.04 | n.a. | 21.3 | 65.7 | -0.7 |
| LH40 | 10 | 1.7 | 6.32 | 2.47 | 0.02 | 1.90E-02 | 0.75 | 51 | 3.02 | 0.02 | 0.25 | n.a. | 5.13 | 43.5 | -1.59 |
| LH42 | 11.5 | 8 | 26 | 12 | 0.17 | 3.00E-03 | 10.4 | 78 | 21 | <0.01 | 0.05 | n.a. | 59 | 62 | 0.14 |
| LH43 | 10.4 | 6.8 | 18.4 | 9.72 | 0.14 | 3.00E-03 | 3.9 | 93 | 18 | <0.01 | 0.05 | n.a. | 15.6 | 26.7 | 1.27 |
| LH44bis | 4.93 | 2.93 | 5.73 | 2.2 | 0.03 | <5.00E-03 | 0.9 | 42 | 0.13 | <0.01 | 0.22 | n.a. | 3.1 | 51.6 | -2.1 |

| Code | Na | K | Ca | Mg | Sr | Li | Cl | $HCO_3$ | $SO_4$ | B | F | Br | $NO_3$ | $SiO_2$ | Charge balance (%) |
|---|---|---|---|---|---|---|---|---|---|---|---|---|---|---|---|
| PER13 | 3.6 | 3.23 | 2.32 | 0.78 | 0.01 | 2.00E-03 | 0.24 | 24 | 1.1 | 0.01 | 0.08 | n.a. | 0.25 | 33.7 | -2.14 |
| PER14 | 3 | 3.4 | 2.6 | 0.7 | 0.02 | 2.00E-03 | 0.2 | 24 | 0.74 | 0.01 | 0.06 | n.a. | 0.2 | 36.7 | -2.66 |
| PER15 | 6.7 | 4.8 | 7 | 2.7 | 0.05 | 5.00E-03 | 0.5 | 57 | 0.8 | 0.01 | 0.11 | n.a. | 0.3 | 77.7 | -0.23 |
| PER65 | 6.2 | 4.01 | 11.4 | 3.6 | 0.06 | <5.00E-03 | 0.8 | 57 | 14 | 0.01 | 0.06 | n.a. | <0.05 | 59.3 | -1.14 |
| PER66 | 16.8 | 5.8 | 7.99 | 6.98 | 0.04 | 1.05E-02 | 2.66 | 105 | 3.1 | 0.05 | 0.3 | n.a. | 0.64 | 69.8 | -1.65 |
| PER67 | 1.65 | 0.9 | 2.45 | 0.94 | 0.02 | <5.00E-03 | 0.46 | 16.8 | 0.14 | <0.01 | 0.04 | n.a. | <0.05 | 41.9 | -0.54 |
| PER68 | 5.6 | 2.3 | 5.1 | 2.13 | 0.03 | <5.00E-03 | 0.85 | 37.8 | 1.5 | <0.01 | 0.1 | n.a. | 4.9 | 47.7 | -2.44 |
| PER69 | 2.31 | 1.2 | 3.1 | 1.01 | 0.03 | <5.00E-03 | 0.4 | 21 | 0.18 | <0.01 | 0.17 | n.a. | 1 | 24.8 | -2.71 |
| PER70 | 21.1 | 4.5 | 9.2 | 8.5 | 0.05 | 1.50E-02 | 6.4 | 114 | 5.02 | 0.1 | 0.32 | n.a. | 4.3 | 46.8 | -1.76 |
| PER83 | 6.12 | 3.08 | 4.4 | 1.71 | 0.02 | 8.00E-03 | 0.2 | 36.6 | 1 | 0.01 | 0.18 | n.a. | 4 | 51.6 | -0.32 |
| PER84 | 40 | 12.8 | 25.2 | 13.3 | 0.22 | <5.00E-03 | 15.4 | 189 | 24.7 | 0.02 | <0.02 | n.a. | 33 | 68.3 | -2.29 |
| PER85 | 12.2 | 4.34 | 34 | 8.3 | 0.36 | <5.00E-03 | 2.3 | 54 | 101 | 0.03 | <0.02 | n.a. | <0.05 | 66.4 | -0.65 |
| PER45 | 1839 | 192 | 4.42 | 7.7 | 0.09 | 2.80E-02 | 1707 | 2040 | 296 | <0.01 | <0.02 | n.a. | <0.05 | 34.5 | -1.46 |
| LH47 | 138 | 20 | 1.53 | 0.1 | 0.03 | 3.19E-01 | 43.3 | 126 | 295 | 468 | 1.97 | n.a. | <0.05 | 144 | n.c. |
| LH48 | 150 | 23.4 | 1.5 | 0.1 | 0.03 | 3.22E-01 | 460 | 140 | 295 | 505 | 1.94 | n.a. | <0.05 | 150 | n.c. |

n.m. = not measured

n.k. = not known

n.a. = not analysed or sample collected just for isotopes analysis

n.s. = not sampled

n.c. =not calculated

Table A3 – $CO_2$ flux measurements performed in selected site of the LHGF study area. Data on soil T and atmospheric pressure are also reported, together with maximum, minimum, average, median and standard deviation values of $CO_2$ fluxes.

| ID # | Date | X(m) | Y(m) | T (°C) soil | P (mbar) | $CO_2$ flux (g $m^{-2}$ $day^{-1}$) |
|---|---|---|---|---|---|---|
| 1 | 22/03/2018 | 663475 | 2172509 | 22.6 | 722 | 2.5 |
| 2 | 22/03/2018 | 663467 | 2172512 | 12.8 | 722 | 68.57 |
| 3 | 22/03/2018 | 663472 | 2172515 | 21.5 | 722 | 47.87 |
| 4 | 22/03/2018 | 663478 | 2172516 | 18.4 | 722 | 10.62 |
| 5 | 22/03/2018 | 663487 | 2172533 | 14.5 | 722 | 24.64 |
| 6 | 22/03/2018 | 663480 | 2172541 | 17.3 | 722 | 59.22 |
| 7 | 22/03/2018 | 663472 | 2172538 | 18.1 | 722 | 89.77 |
| 8 | 22/03/2018 | 663469 | 2172551 | 19.7 | 722 | 105.72 |
| 9 | 22/03/2018 | 663462 | 2172544 | 22.4 | 722 | 238.61 |
| 10 | 22/03/2018 | 663467 | 2172552 | 19.9 | 722 | 140.86 |
| 11 | 22/03/2018 | 663458 | 2172558 | 26.9 | 721 | 121.36 |
| 12 | 22/03/2018 | 663464 | 2172567 | 22 | 721 | 130.36 |
| 13 | 22/03/2018 | 663452 | 2172562 | 21.3 | 721 | 84 |
| 14 | 22/03/2018 | 663465 | 2172572 | 17.7 | 721 | 55.51 |
| 15 | 22/03/2018 | 663465 | 2172578 | 19.9 | 720 | 35.12 |
| 16 | 22/03/2018 | 663460 | 2172558 | 53.5 | 720 | 3150 |
| 17 | 22/03/2018 | 663465 | 2172539 | 15.4 | 722 | 59.61 |
| 18 | 22/03/2018 | 663485 | 2172524 | 23.9 | 722 | 22 |
| 19 | 22/03/2018 | 663491 | 2172514 | 20.1 | 722 | 1.88 |
| 20 | 22/03/2018 | 663508 | 2172509 | 26.5 | 722 | 6.89 |
| 21 | 22/03/2018 | 663511 | 2172523 | 21.3 | 722 | 3.86 |
| 22 | 22/03/2018 | 663467 | 2172527 | 22 | 722 | 67.6 |
| 23 | 22/03/2018 | 663461 | 2172535 | 23.8 | 722 | 98.47 |
| 24 | 22/03/2018 | 663474 | 2172512 | 26.8 | 721 | 17.18 |
| 25 | 22/03/2018 | 663473 | 2172490 | 17.8 | 722 | 3.78 |
| 26 | 22/03/2018 | 663466 | 2172483 | 20.5 | 722 | 6.79 |
| 27 | 22/03/2018 | 663475 | 2172481 | 22.6 | 722 | 2.68 |
| 28 | 22/03/2018 | 663462 | 2172472 | 18.9 | 722 | 7.66 |
| 29 | 22/03/2018 | 663488 | 2172495 | 18.2 | 722 | 4.84 |
| 30 | 22/03/2018 | 663495 | 2172498 | 31.7 | 722 | 2.37 |
| 31 | 22/03/2018 | 665331 | 2172139 | 37.7 | 715 | 3.29 |
| 32 | 22/03/2018 | 665319 | 2172102 | 25.7 | 715 | 4.33 |
| 33 | 22/03/2018 | 665318 | 2172059 | 20.2 | 714 | 2.9 |
| 34 | 22/03/2018 | 665302 | 2172033 | 30.2 | 714 | 3.93 |
| 35 | 22/03/2018 | 665287 | 2171993 | 30.1 | 714 | 2.8 |
| 36 | 22/03/2018 | 665280 | 2171958 | 28.4 | 713 | 3.83 |
| 37 | 22/03/2018 | 665275 | 2171919 | 30.7 | 713 | 4.81 |
| 38 | 22/03/2018 | 665346 | 2171903 | 39.1 | 713 | 1.96 |
| 39 | 22/03/2018 | 665355 | 2171943 | 27.1 | 713 | 3.62 |
| 40 | 22/03/2018 | 665366 | 2171982 | 29.7 | 713 | 3.59 |
| 41 | 22/03/2018 | 665374 | 2172020 | 30.8 | 713 | 6.26 |
| 42 | 22/03/2018 | 665383 | 2172055 | 29.3 | 713 | 4.83 |
| 43 | 22/03/2018 | 665400 | 2172093 | 38.9 | 714 | 4.69 |
| 44 | 22/03/2018 | 665407 | 2172127 | 34.5 | 714 | 2.21 |
| 45 | 22/03/2018 | 665479 | 2172117 | 25.7 | 715 | 6.16 |
| 46 | 22/03/2018 | 665467 | 2172080 | 29.7 | 714 | 4.49 |
| 47 | 22/03/2018 | 665465 | 2172046 | 23.8 | 713 | 5.95 |
| 48 | 22/03/2018 | 665458 | 2172011 | 25.9 | 713 | 3.64 |
| 49 | 22/03/2018 | 665453 | 2171975 | 29.5 | 712 | 2.8 |
| 50 | 22/03/2018 | 665444 | 2171939 | 23.3 | 712 | 3.89 |
| 51 | 22/03/2018 | 665424 | 2171908 | 24.2 | 712 | 3.88 |
| 52 | 22/03/2018 | 665473 | 2171878 | 23 | 712 | 3.44 |
| 53 | 22/03/2018 | 665499 | 2171921 | 15.6 | 711 | 3.52 |
| 54 | 22/03/2018 | 665511 | 2171959 | 17.1 | 712 | 4.21 |
| 55 | 22/03/2018 | 665519 | 2171999 | 19.5 | 712 | 7.65 |
| 56 | 22/03/2018 | 665526 | 2172038 | 18.1 | 712 | 10.34 |
| 57 | 22/03/2018 | 665536 | 2172071 | 20.7 | 713 | 8.09 |
| 58 | 22/03/2018 | 665545 | 2172108 | 15.3 | 714 | 4.36 |
| 59 | 23/03/2018 | 665587 | 2172093 | 48.3 | 713 | 10.57 |
| 60 | 23/03/2018 | 665580 | 2172058 | 19.6 | 713 | 2.32 |
| 61 | 23/03/2018 | 665570 | 2172022 | 24.8 | 712 | 10.02 |
| 62 | 23/03/2018 | 665564 | 2171984 | 36.8 | 711 | 3.93 |
| 63 | 23/03/2018 | 665560 | 2171946 | 35.9 | 711 | 5.26 |
| 64 | 23/03/2018 | 665563 | 2171910 | 35.5 | 710 | 3.29 |
| 65 | 23/03/2018 | 665529 | 2171882 | 35.6 | 710 | 5.04 |
| 66 | 23/03/2018 | 665509 | 2171846 | 38.8 | 709 | 1.73 |
| 67 | 23/03/2018 | 665513 | 2171798 | 34.7 | 709 | 2.19 |
| 68 | 23/03/2018 | 665508 | 2171751 | 33.5 | 709 | 4.41 |
| 69 | 23/03/2018 | 665584 | 2171713 | 32.1 | 709 | 4.43 |
| 70 | 23/03/2018 | 665599 | 2171752 | 35 | 709 | 1.97 |
| 71 | 23/03/2018 | 665610 | 2171796 | 34.6 | 709 | 2.52 |
| 72 | 23/03/2018 | 665684 | 2171771 | 28 | 709 | 2.24 |
| 73 | 23/03/2018 | 665664 | 2171739 | 32 | 709 | 2.44 |
| 74 | 23/03/2018 | 665646 | 2171696 | 31.6 | 709 | 3.33 |
| 75 | 23/03/2018 | 665718 | 2171668 | 33.7 | 709 | 3.3 |
| 76 | 23/03/2018 | 665734 | 2171701 | 34.3 | 709 | 3.52 |
| 77 | 23/03/2018 | 665762 | 2171725 | 31.5 | 709 | 1.89 |
| 78 | 23/03/2018 | 665779 | 2171645 | 36.1 | 709 | 2.4 |
| 79 | 23/03/2018 | 665758 | 2171749 | 28.4 | 709 | 3.81 |
| 80 | 23/03/2018 | 665755 | 2171809 | 28.7 | 709 | 3.92 |
| 81 | 23/03/2018 | 665722 | 2171854 | 29.6 | 710 | 4.47 |
| 82 | 23/03/2018 | 665681 | 2171899 | 28.5 | 710 | 4.04 |
| 83 | 23/03/2018 | 665629 | 2171916 | 32.2 | 710 | 4.43 |
| 84 | 23/03/2018 | 665584 | 2171932 | 24.5 | 710 | 4.21 |
| 85 | 23/03/2018 | 665262 | 2171870 | 21.6 | 711 | 5.29 |
| 86 | 23/03/2018 | 665257 | 2171828 | 23.6 | 711 | 9.13 |
| 87 | 23/03/2018 | 665174 | 2171917 | 25.7 | 711 | 1.13 |
| 88 | 23/03/2018 | 665175 | 2171960 | 25.1 | 712 | 3.64 |
| 89 | 23/03/2018 | 665176 | 2171995 | 20.4 | 712 | 1.62 |

Table A3 – continue

| ID # | Date | X(m) | Y(m) | T (°C) soil | P (mbar) | $CO_2$ flux (g m$^{-2}$ day$^{-1}$) |
|---|---|---|---|---|---|---|
| 90 | 23/03/2018 | 665183 | 2172006 | 23.1 | 712 | 9.62 |
| 91 | 24/03/2018 | 663357 | 2173331 | 31 | 721 | 2.26 |
| 92 | 24/03/2018 | 663383 | 2173369 | 18.6 | 721 | 2.71 |
| 93 | 24/03/2018 | 663388 | 2173417 | 20.9 | 721 | 1.99 |
| 94 | 24/03/2018 | 663402 | 2173457 | 25.2 | 721 | 3.45 |
| 95 | 24/03/2018 | 663443 | 2173468 | 14.8 | 720 | 2.5 |
| 96 | 24/03/2018 | 663464 | 2173515 | 15 | 720 | 2.62 |
| 97 | 24/03/2018 | 663420 | 2173646 | 23 | 720 | 3.13 |
| 98 | 24/03/2018 | 663440 | 2173691 | 30.7 | 720 | 1.81 |
| 99 | 24/03/2018 | 663378 | 2173632 | 20.1 | 719 | 2.69 |
| 100 | 24/03/2018 | 663361 | 2173583 | 24.5 | 720 | 1.5 |
| 101 | 24/03/2018 | 663348 | 2173542 | 26.5 | 720 | 2.63 |
| 102 | 24/03/2018 | 663310 | 2173473 | 13.2 | 720 | 11.98 |
| 103 | 24/03/2018 | 663281 | 2173441 | 15.3 | 720 | 3.33 |
| 104 | 24/03/2018 | 663258 | 2173409 | 18.4 | 720 | 3.29 |
| 105 | 24/03/2018 | 663236 | 2173370 | 14.7 | 720 | 2.03 |
| 106 | 24/03/2018 | 663224 | 2173330 | 16.4 | 720 | 3.55 |
| 107 | 24/03/2018 | 663219 | 2173282 | 22.1 | 720 | 5 |
| 108 | 24/03/2018 | 663210 | 2173240 | 24.7 | 719 | 5.75 |
| 109 | 24/03/2018 | 663306 | 2173227 | 22.5 | 719 | 3.48 |
| 110 | 24/03/2018 | 663319 | 2173274 | 14.4 | 719 | 2.14 |
| 111 | 24/03/2018 | 663335 | 2173314 | 24.8 | 719 | 8.51 |
| 112 | 24/03/2018 | 663111 | 2173327 | 18.1 | 719 | 3.53 |
| 113 | 24/03/2018 | 663126 | 2173368 | 21 | 719 | 4.89 |
| 114 | 24/03/2018 | 663163 | 2173410 | 21.5 | 719 | 2.33 |
| 115 | 24/03/2018 | 663193 | 2173452 | 23.4 | 719 | 1.73 |
| 116 | 24/03/2018 | 663208 | 2173495 | 22.5 | 719 | 6.26 |
| 117 | 24/03/2018 | 663248 | 2173532 | 26.8 | 719 | 3.65 |
| 118 | 24/03/2018 | 663298 | 2173551 | 24.4 | 719 | 10.82 |
| 119 | 24/03/2018 | 663311 | 2173624 | 15.7 | 719 | 7.12 |
| 120 | 24/03/2018 | 663346 | 2173660 | 21.3 | 719 | 5.24 |
| 121 | 24/03/2018 | 663375 | 2173687 | 19.2 | 719 | 10.9 |
| 122 | 24/03/2018 | 663406 | 2173721 | 25.1 | 718 | 1.84 |
| 123 | 24/03/2018 | 663340 | 2173814 | 17.1 | 718 | 2.24 |
| 124 | 24/03/2018 | 663313 | 2173788 | 21.3 | 718 | 6.97 |
| 125 | 24/03/2018 | 663284 | 2173757 | 24.6 | 718 | 5.17 |
| 126 | 24/03/2018 | 663253 | 2173722 | 22.5 | 719 | 8.11 |
| 127 | 24/03/2018 | 663225 | 2173690 | 22.3 | 719 | 3.83 |
| 128 | 24/03/2018 | 663187 | 2173663 | 22.2 | 719 | 4.18 |
| 129 | 24/03/2018 | 663156 | 2173637 | 22.5 | 718 | 1.62 |
| 130 | 24/03/2018 | 663127 | 2173604 | 22.9 | 718 | 4.97 |
| 131 | 24/03/2018 | 663104 | 2173572 | 20 | 718 | 3.97 |
| 132 | 24/03/2018 | 663087 | 2173527 | 23.1 | 718 | 3.23 |
| 133 | 24/03/2018 | 663063 | 2173483 | 20.3 | 718 | 1.4 |
| 134 | 24/03/2018 | 663046 | 2173448 | 20.5 | 718 | 3.15 |
| 135 | 24/03/2018 | 663064 | 2173407 | 23 | 718 | 9.36 |
| 136 | 24/03/2018 | 663056 | 2173371 | 21 | 718 | 5.81 |
| 137 | 24/03/2018 | 663044 | 2173327 | 22.6 | 717 | 10.4 |
| 138 | 28/03/2018 | 675598 | 2165426 | 20 | 763 | 0 |
| 139 | 28/03/2018 | 675576 | 2165427 | 20 | 763 | 0 |
| 140 | 28/03/2018 | 675571 | 2165419 | 20 | 763 | 10.29 |
| 141 | 28/03/2018 | 675566 | 2165421 | 20 | 763 | 1.49 |
| 142 | 28/03/2018 | 675573 | 2165411 | 20 | 763 | 5.9 |
| 143 | 28/03/2018 | 675576 | 2165404 | 20 | 763 | 5.58 |
| 144 | 28/03/2018 | 675581 | 2165418 | 20 | 763 | 5.83 |
| 145 | 28/03/2018 | 675603 | 2165398 | 20 | 763 | 4.19 |
| 146 | 28/03/2018 | 675613 | 2165359 | 20 | 763 | 2.38 |
| 147 | 28/03/2018 | 675628 | 2165312 | 20 | 763 | 1.87 |
| 148 | 28/03/2018 | 675645 | 2165253 | 20 | 763 | 2.26 |
| 149 | 28/03/2018 | 675652 | 2165202 | 20 | 763 | 4.1 |
| 150 | 28/03/2018 | 675665 | 2165138 | 20 | 763 | 1.49 |
| 151 | 28/03/2018 | 675568 | 2165454 | 20 | 763 | 6.7 |
| 152 | 28/03/2018 | 675557 | 2165503 | 20 | 763 | 2.98 |
| 153 | 28/03/2018 | 675540 | 2165553 | 20 | 763 | 6.08 |
| 154 | 28/03/2018 | 675512 | 2165618 | 20 | 763 | 1.86 |
| 155 | 28/03/2018 | 675507 | 2165663 | 20 | 763 | 4.55 |
| 156 | 28/03/2018 | 675565 | 2165625 | 20 | 763 | 3.1 |
| 157 | 28/03/2018 | 675576 | 2165571 | 20 | 763 | 0.91 |
| 158 | 28/03/2018 | 675595 | 2165507 | 20 | 763 | 1.61 |
| 159 | 28/03/2018 | 675610 | 2165450 | 20 | 763 | 4.22 |
| 160 | 28/03/2018 | 675596 | 2165428 | 20 | 763 | 3.6 |

| **XALAPASCO** | | | **MASTALOYA** | | |
|---|---|---|---|---|---|
| N = 30 | | | N = 60 | | |
| | φ$CO_2$ g m$^{-2}$ day$^{-1}$ | Soil temperature °C | | φ$CO_2$ g m$^{-2}$ day$^{-1}$ | Soil temperature °C |
| max | 3151 | 54 | max | 11 | 48 |
| min | 1.9 | 13 | min | 1.1 | 15 |
| average | 156 | 22 | average | 4.3 | 29 |
| median | 41 | 21 | median | 3.9 | 29 |
| st. dev. | 568 | 7.1 | st. dev. | 2.2 | 6.6 |
| **CFE PLANT** | | | **PEROTE PLAIN** | | |
| N = 47 | | | N = 23 | | |
| | φ$CO_2$ g m$^{-2}$ day$^{-1}$ | Soil temperature °C | | φ$CO_2$ g m$^{-2}$ day$^{-1}$ | Soil temperature °C |
| max | 12 | 31 | max | 10 | 20 |
| min | 1.4 | 13 | min | 0 | 20 |
| average | 4.4 | 21 | average | 3.5 | 20 |
| median | 3.5 | 22 | median | 3.1 | 20 |
| st. dev. | 2.8 | 4 | st. dev. | 2.5 | 0 |

Table A4 – Isotopic composition determined in collected water samples (Los Humeros). δD‰ and $\delta^{18}O$‰ are referred to V-SMOW, whereas certified standard NIST SRM 987 was used for $^{87}Sr/^{86}Sr$ analyses. Data for dissolved $CO_2$ are also inserted.

| Code | $\delta^{18}O$‰ | δD‰ | $^{87}Sr/^{86}Sr$ | U.T. | $P_{CO2}$(bars) | $CO_{2(aq)}$ (mmol/L) | $\log F_{CO2}$ |
|---|---|---|---|---|---|---|---|
| **Sampling 2017** | | | | | | | |
| LH1 | -10.68 | -75.2 | 0.705422 | | 0.007796 | 0.322 | -2.11 |
| LH2 | -10.55 | -74.6 | | | 0.01697 | 0.7449 | -1.773 |
| LH3 | -11.27 | -81.6 | 0.706016 | | 0.01064 | 0.4477 | -1.975 |
| LH4 | -10.4 | -70.3 | | | 0.01099 | 0.5437 | -1.962 |
| LH15 | -10.58 | -74.3 | | | 0.006393 | 0.2821 | -2.197 |
| LH17 | -12.34 | -88.9 | 0.707121 | | 0.08346 | 3.66 | -1.081 |
| LH20 | -8.66 | -67.8 | 0.706978 | | 0.0369 | 1.535 | -1.435 |
| LH21 | -11.03 | -82.7 | | | 0.004923 | 0.2219 | -2.31 |
| LH46 | -11.88 | -87.6 | 0.705531 | | 0.01519 | 0.5868 | -1.821 |
| LH50 | -11.56 | -80.1 | 0.705383 | | 0.01417 | 0.5945 | -1.851 |
| LH54 | -10.91 | -77.3 | 0.706132 | | 0.02324 | 0.8927 | -1.636 |
| LH55 | -11.14 | -79.6 | 0.70599 | 0.3±0.5 | 0.03711 | 1.369 | -1.433 |
| LH5 | -10.92 | -76.3 | | | 8.38E-05 | 0.004123 | -4.079 |
| LH6 | -11.15 | -77.3 | 0.706397 | | 0.000409 | 0.01873 | -3.391 |
| LH7 | | | | | 0.000369 | 0.01794 | -3.436 |
| LH7 bis | -11.11 | -78.8 | | | | | |
| LH8 | -11.25 | -79.7 | 0.706251 | | 0.000512 | 0.02442 | -3.294 |
| LH9 | -10.64 | -74.9 | | | 0.000373 | 0.01659 | -3.431 |
| LH12 | -11.51 | -83.3 | 0.706369 | | 0.000271 | 0.01141 | -3.569 |
| LH13 | -11.63 | -83.7 | | | 0.00012 | 0.005033 | -3.925 |
| LH14 | -10.66 | -77.6 | | | 0.000199 | 0.009141 | -3.704 |
| LH19 | -9.73 | -69.9 | | | | | |
| LH23 | -10.87 | -74.2 | | | | | |
| LH24 | -10.74 | -74.1 | | | | | |
| LH25 | -11.57 | -82.7 | | | | | |
| LH26 | -11.17 | -79.1 | | | | | |
| LH27 | -10.97 | -77.2 | | | | | |
| LH30 | -8.83 | -59.2 | | | | | |
| LH31 | -9.56 | -64.5 | | | | | |
| LH32 | -9.43 | -63.6 | 0.705508 | | | | |
| LH33 | -8.72 | -56.6 | | | | | |
| LH34 | -13.24 | -95.6 | | | | | |
| LH35 | -13.5 | -98.8 | | | | | |
| LH36 | -13.15 | -94.6 | 0.705282 | | | | |
| LH37 | -13.46 | -98.1 | | | | | |
| LH38 | -7.66 | -49.6 | | | | | |
| LH39 | -7.84 | -50.4 | 0.704532 | | | | |
| LH40 | -10.12 | -70.3 | | | | | |
| LH41 | -10.22 | -70.4 | | | | | |
| LH42 | -8.55 | -57.9 | | | | | |
| LH43 | -9.33 | -56.2 | 0.704573 | | | | |
| LH44 | -10.22 | -69.5 | | | | | |
| Code | $\delta^{18}O$‰ | δD‰ | $^{87}Sr/^{86}Sr$ | U.T. | $P_{CO2}$(bars) | $CO_{2(aq)}$ (mmol/L) | $\log F_{CO2}$ |
| LH44bis | -9.75 | -66.1 | | | | | |
| LH45 | -10.77 | -69.4 | | | 0.000145 | 0.00664 | -3.841 |
| LH49 | -11.27 | -73.1 | | | 4.03E-05 | 0.001996 | -4.397 |
| LH53 | -10.4 | -72.7 | 0.704216 | | 8.34E-05 | 0.003556 | -4.081 |
| LH10 | -10.3 | -72.5 | 0.706982 | | | | |
| LH11 | -10.72 | -79.2 | | | | | |
| LH16 | -10.62 | -74.4 | | | | | |
| LH29 | -6.7 | -42.5 | | | | | |
| LH52 | -8.33 | -57 | | | | | |
| LH18 | 0.87 | -12.3 | | | | | |
| LH22 | -1.28 | -29.6 | | | | | |
| LH28 | -7.09 | -45.2 | 0.707384 | | 0.000556 | 0.01484 | -3.257 |
| LH51 | -10.35 | -71 | 0.706381 | 0.5±0.4 | 0.004878 | 0.1037 | -2.313 |
| LH47 | 2.46 | -30.5 | | | | | |
| LH48 | 2.5 | -30.7 | | | | | |
| **Sampling 2018** | | | | | | | |
| LH2 | -10.14 | -74 | | | 0.002414 | 0.1057 | -2.62 |
| LH3 | -11 | -81.3 | | | 0.001892 | 0.07915 | -2.725 |
| LH17 | -11.51 | -86.8 | | | 0.06135 | 2.704 | -1.215 |
| LH17bis | -11.89 | -87.4 | | | 0.04383 | 1.887 | -1.361 |
| LH46 | -11.97 | -86.7 | | 0.2±0.7 | 0.009906 | 0.3856 | -2.006 |
| LH46_bis | -11.8 | -85.8 | | | 0.04617 | 1.572 | -1.338 |
| LH50 | -11.05 | -80.5 | | | 0.009088 | 0.3823 | -2.044 |
| LH50_bis | -11.73 | -84.4 | | | 0.006004 | 0.2435 | -2.224 |
| LH54 | -10.51 | -77.9 | | | 0.03538 | 1.387 | -1.454 |
| LH55 | -10.97 | -81.5 | | | 0.03719 | 1.393 | -1.432 |
| LH61 | -10.6 | -76.3 | | | 0.01201 | 0.419 | -1.923 |
| PER27 | -10.97 | -79.2 | | | 0.0176 | 0.7249 | -1.757 |
| PER30 | n.a. | n.a. | | | | | |
| PER31 | -10.9 | -79.5 | | | 0.03056 | 0.9383 | -1.517 |
| Code | $\delta^{18}O$‰ | δD‰ | $^{87}Sr/^{86}Sr$ | U.T. | $P_{CO2}$(bars) | $CO_{2(aq)}$ (mmol/L) | $\log F_{CO2}$ |
| PER36 | -12.85 | -92.7 | | | 0.01007 | 0.4314 | -1.999 |
| PER37 | -12.76 | -94.4 | | | 0.004331 | 0.1885 | -2.366 |
| PER38 | -12.73 | -94 | | | 0.003909 | 0.1697 | -2.41 |
| PER39 | -13.05 | -96.5 | | | | | |
| PER40 | -12.6 | -92.3 | | | 0.005687 | 0.2606 | -2.248 |
| PER42 | -9.89 | -76.8 | | | 0.005102 | 0.2203 | -2.295 |
| PER43 | -12.01 | -88.9 | | | 0.07324 | 3.055 | -1.138 |
| PER44 | -9.24 | -68.1 | | | 0.005635 | 0.2547 | -2.252 |
| PER47 | -12.77 | -93.8 | | | 0.004342 | 0.191 | -2.365 |
| PER48 | -12.99 | -94.3 | | | 0.03174 | 1.404 | -1.501 |
| PER49 | -13.1 | -93.5 | | | 0.004875 | 0.2264 | -2.314 |
| PER51 | -11.29 | -85.5 | | | 0.01326 | 0.3884 | -1.879 |
| PER52 | -10.1 | -76.1 | | | 0.004041 | 0.1664 | -2.396 |
| PER53 | -12.67 | -93.2 | | | 0.004898 | 0.1971 | -2.312 |
| PER54 | -11.47 | -81.8 | | | 0.01704 | 0.6517 | -1.771 |
| PER55 | -9.79 | -74.1 | | | 0.07628 | 2.89 | -1.12 |
| Code | $\delta^{18}O$‰ | δD‰ | $^{87}Sr/^{86}Sr$ | U.T. | $P_{CO2}$(bars) | $CO_{2(aq)}$ (mmol/L) | $\log F_{CO2}$ |
| PER56 | -10.64 | -79.6 | | | 0.02893 | 0.882 | -1.541 |
| PER57 | -10.56 | -77.4 | | | 0.03456 | 1.127 | -1.463 |
| PER58 | -12.45 | -91.9 | | | 0.00299 | 0.133 | -2.527 |
| PER59 | -11.5 | -83.6 | | | 0.008072 | 0.3102 | -2.095 |
| PER60 | -11.8 | -86.6 | | | 0.004584 | 0.2039 | -2.341 |
| PER71 | -10.49 | -75.3 | | | | | |
| PER72 | -10.84 | -78.5 | | | | | |
| PER73 | -10.73 | -78.4 | | | | | |
| PER74 | -10.53 | -76.7 | | | | | |
| PER78 | -5.15 | -39.5 | | | 0.000828 | 0.03875 | -3.084 |
| LH5 | -10.67 | -74.8 | | | 0.00242 | 0.1188 | -2.619 |
| LH6 | -10.77 | -76.5 | | | 0.0216 | 1.036 | -1.668 |
| LH6bis | -10.79 | -75.5 | | | | | |
| LH7 | -11.14 | -78.9 | | | 0.003351 | 0.1691 | -2.477 |
| LH7* | -11.26 | -79.6 | | | 0.00826 | 0.3998 | -2.085 |
| LH8 | -11.26 | -78.8 | | | | | |
| LH8bis | -11.17 | -79.2 | | | 0.004688 | 0.232 | -2.332 |
| LH9 | -10.71 | -75.1 | | | 0.00972 | 0.4947 | -2.015 |
| LH12 | -11.42 | -83.3 | | | | | |
| LH14bis | -10.21 | -67.2 | | | 0.001353 | 0.06945 | -2.871 |
| LH23 | -10.72 | -73.4 | | | | | |
| LH24 | -10.98 | -74.9 | | | | | |
| LH25 | -11.92 | -83 | | | | | |
| LH26 | -11.95 | -80.5 | | | | | |
| LH27 | -11.78 | -78.7 | | | | | |
| LH30 | -9.04 | -59.3 | | | 0.002197 | 0.1109 | -2.661 |
| LH30_bis | -9.79 | -65.1 | | | 0.002101 | 0.1006 | -2.68 |
| LH32 | -9.59 | -66 | | | 0.004996 | 0.2385 | -2.304 |
| LH33 | -8.96 | -57.1 | | | 0.005514 | 0.2647 | -2.261 |
| LH33bis | -11.07 | -79.9 | | | 0.01035 | 0.4081 | -1.987 |
| LH33* | -10.79 | -76 | | | | | |
| LH36 | -13.56 | -97.8 | | | | | |
| LH38 | -7.99 | -50.6 | | | 0.002965 | 0.1408 | -2.53 |
| LH39 | -8.07 | -52.2 | | | 0.000578 | 0.0267 | -3.24 |
| LH40 | -10.34 | -71.1 | | | 0.00098 | 0.04677 | -3.011 |
| LH42 | -8.72 | -57.8 | | | 0.000838 | 0.03926 | -3.079 |
| LH43 | -8.7 | -58.4 | | | 0.004975 | 0.2349 | -2.306 |
| LH44bis | -9.91 | -67.1 | | | 0.001438 | 0.07466 | -2.845 |
| PER13 | -13.8 | -97.7 | | | 0.001373 | 0.08052 | -2.865 |
| PER14 | -14.01 | -99.6 | | 1.5±0.6 | 0.000831 | 0.05063 | -3.083 |
| PER15 | -13.67 | -98.9 | | | 0.006298 | 0.3393 | -2.203 |
| PER65 | -9.85 | -66.7 | | | | | |
| PER66 | -11.46 | -81 | | | 0.000788 | 0.03369 | -3.106 |
| PER67 | -8.92 | -55.5 | | | 0.001285 | 0.06252 | -2.894 |
| PER68 | -9.2 | -54.4 | | | 0.000987 | 0.04714 | -3.008 |
| PER69 | -8.7 | -53 | | 1.4±0.4 | 0.000379 | 0.01935 | -3.424 |
| Code | $\delta^{18}O$‰ | δD‰ | $^{87}Sr/^{86}Sr$ | U.T. | $P_{CO2}$(bars) | $CO_{2(aq)}$ (mmol/L) | $\log F_{CO2}$ |
| PER70 | -9.21 | -60.3 | | | 0.001327 | 0.06267 | -2.879 |
| PER83 | -9.64 | -63.9 | | | 0.001974 | 0.09664 | -2.707 |
| PER84 | -10.3 | -75.7 | | | | | |
| PER85 | -10.67 | -76.9 | | | 0.00064 | 0.0335 | -3.197 |
| PER45 | n.a. | n.a. | | | | | |
| LH47 | 2.94 | -31 | | | | | |
| LH48 | 2.98 | -29.6 | | | | | |

Table A5 – Chemical composition of liquid samples from geothermal wells in Los Humeros. All data are in mg/Kg in Total Discharge (T.D.).

| code | Date | Reference | Na | K | Ca | Mg | Li | Cl | $HCO_3$ | $SO_4$ | B | As | $SiO_2$ |
|---|---|---|---|---|---|---|---|---|---|---|---|---|---|
| H1 | 21/10/1987 | 1 | 269 | 43.8 | 1.2 | 0.012 | 0.9 | 120 | 361 | 114 | 214 | 3.9 | 800 |
| H6 | 22/10/1987 | 1 | 196 | 40.2 | 0.4 | 0.02 | 0.9 | 180 | 203 | 6.5 | 288 | 12.1 | 1000 |
| H7 | 21/10/1987 | 1 | 168 | 27.9 | 0.9 | 0.02 | - | 95 | 241 | 90.5 | 2665 | 26 | 900 |
| H8 | 22/10/1987 | 1 | 239 | 45.7 | 0.6 | 0.03 | 0.6 | 120 | 294 | 94.8 | 452 | 5.1 | 967 |
| H12 | 22/10/1987 | 1 | 108 | 20 | 0.3 | 0.05 | 0.3 | 74 | 196 | 17.2 | 942 | 162 | 600 |
| H-1 | 04/01/1996 | 2 | 267 | 45 | 2.04 | 0.12 | 0.47 | 90.2 | 162 | 233 | 218 | 2.79 | 1005 |
| H-3 | 05/10/1994 | 2 | 420 | 49 | 1.6 | 0.02 | 1.6 | 175 | 334 | 71 | 477 | 4 | 556 |
| H-6 | 04/01/1996 | 2 | 142 | 31 | 1.6 | 0.18 | 0.42 | 104 | 48 | 23 | 345 | 27.41 | 946 |
| H-7 | 04/01/1996 | 2 | 177 | 36 | 2.24 | 0.18 | 0.41 | 83.3 | 34 | 239 | 946 | 8.5 | 915 |
| H-8 | 04/01/1996 | 2 | 243 | 48 | 2.04 | 0.22 | 0.3 | 76.3 | 139 | 213 | 453 | 3.1 | 1120 |
| H-9 | 03/01/1996 | 2 | 250 | 52 | 2.08 | 0.08 | 0.49 | 50.3 | 122 | 89 | 1823 | 73.62 | 838 |
| H-10 | 19/07/1989 | 2 | 142 | 19 | 1.8 | 0.4 | 0.83 | 983 | 28 | 33 | 1716 | n.a. | 909 |
| H-11 | 05/01/1996 | 2 | 207 | 32 | 2.56 | 0.16 | 0.45 | 74.5 | 156 | 113 | 443 | 7.6 | 844 |
| H-12 | 04/01/1996 | 2 | 87 | 19 | 0.22 | 0.12 | 0.3 | 41.6 | 11 | 12 | 695 | 16.35 | 688 |
| H-13 | 05/10/1995 | 2 | 341 | 54 | 3.61 | 0.07 | 1.37 | 140 | 117 | 409 | 219 | n.a. | 1006 |
| H-15 | 03/01/1996 | 2 | 113 | 21 | 1.2 | 0.22 | 0.39 | 6.9 | 61 | 30 | 200 | 0.5 | 797 |
| H-16 | 06/01/1996 | 2 | 549 | 24 | 1.2 | 0.08 | 0.45 | 4.1 | 216 | 408 | 402 | 7.9 | 580 |
| H-17 | 03/01/1996 | 2 | 91 | 19 | 1.4 | 0.16 | 0.37 | 24.3 | 55 | 91 | 333 | 24.41 | 893 |
| H-18 | 13/10/1989 | 2 | 123 | 23 | 0.92 | 0.04 | 0.37 | 112 | 397 | 43 | 118 | n.a. | 229 |
| H-19 | 05/01/1996 | 2 | 140 | 21 | 2.18 | 0.14 | 0.41 | 23.8 | 57 | 112 | 1873 | 21.71 | 486 |
| H-20 | 09/01/1996 | 2 | 160 | 20 | 1.8 | 0.18 | 0.4 | 115 | 20 | 35 | 447 | 5.53 | 838 |
| H-23 | 13/11/1987 | 2 | 290 | 22 | 37 | 0.4 | 0.4 | 622 | 21 | 57 | 194 | n.a. | 114 |
| H-24 | 18/05/1989 | 2 | 285 | 46 | 1.5 | 0.11 | 0.9 | 325 | 58 | 27 | 423 | n.a. | 406 |
| H-27 | 14/02/1989 | 2 | 68 | 3 | 1.8 | 0.4 | 0.17 | 233 | 14 | 26 | 136 | n.a. | 100 |
| H-28 | 05/01/1996 | 2 | 228 | 19 | 0.6 | 0.3 | 0.46 | 7.6 | 267 | 56 | 67 | 1.9 | 424 |
| H-29 | 10/01/1992 | 2 | 220 | 6 | 0.2 | 0.001 | 0.03 | 36 | 17 | 21 | 513 | n.a. | 80 |
| H-30 | 03/01/1996 | 2 | 205 | 29 | 1.74 | 0.16 | 0.44 | 9.7 | 55 | 39 | 1203 | 37.3 | 747 |
| H-31 | 08/01/1996 | 2 | 115 | 21 | 2 | 0.12 | 0.38 | 8.3 | 16 | 16 | 421 | 7.6 | 869 |
| H-32 | 05/01/1996 | 2 | 64 | 12 | 0.22 | 0.24 | 0.24 | 26.8 | 38 | 23 | 592 | 18.71 | 710 |
| H-33 | 03/01/1996 | 2 | 363 | 33 | 2.24 | 0.14 | 0.47 | 400 | 13 | 49 | 978 | 29.51 | 458 |
| H-34 | 05/01/1996 | 2 | 177 | 24 | 1 | 0.08 | 0.3 | 9 | 67 | 91 | 202 | 0.5 | 1130 |
| code | Date | Reference | Na | K | Ca | Mg | Li | Cl | $HCO_3$ | $SO_4$ | B | As | $SiO_2$ |
| H-35 | 09/01/1996 | 2 | 30 | 5 | 1.6 | 0.1 | 0.19 | 1.4 | 80 | 43 | 2930 | 10.6 | 231 |
| H-36 | 08/01/1996 | 2 | 1201 | 52 | 3.16 | 0.52 | 0.5 | 60.4 | 3498 | 1133 | 3169 | 0.5 | 16 |
| H-36 | 08/03/1996 | 2 | 266 | 17 | 2.4 | 0.321 | 0.48 | 10.6 | 347 | 300 | 1864 | 6.44 | 304 |
| H-37 | 11/03/1996 | 2 | 466 | 56 | 4.6 | 0.01 | 0.47 | 4.3 | 102 | 407 | 1660 | 0.96 | 594 |
| H-22 | 04/02/1988 | 5 | 310 | 33 | 2.6 | 0.2 | 0.9 | 34.5 | 443 | 22.2 | 77.9 | n.a. | 879 |
| H-28 | 14/08/2002 | 5 | 180 | 17.4 | 0.38 | 0.09 | 0.71 | 5.4 | 209 | 52.9 | 78.7 | n.a. | 591 |
| H-28 | 03/09/2002 | 5 | 206 | 17 | 0.26 | 0.12 | 1.08 | 3.6 | 160 | 81.8 | 78.7 | n.a. | 520 |
| H-29 | 10/01/1992 | 5 | 6 | 1 | 0.1 | 0 | 0.03 | 36 | 17 | 10.5 | 513 | n.a. | 80 |
| H-43 | 12/01/2016 | 5 | 4 | 42.4 | 4.12 | 0.53 | <0.1 | 26 | 8.66 | 40.7 | 217 | n.a. | 34.9 |
| H-43 | 12/01/2016 | 5 | 4.5 | 31.6 | 4.52 | 0.56 | <0.1 | 23.7 | 11.8 | 26.8 | 186 | n.a. | 34.9 |
| H-43 | 12/01/2016 | 5 | 88 | 10.6 | 11.4 | 1.41 | 0.15 | 34.3 | 16.5 | 86.7 | 356 | n.a. | 88.4 |
| H-58 | 03/02/2017 | 5 | 11.3 | 3.3 | 4.89 | 0.88 | <0.1 | 5.2 | 31.9 | 4.6 | 2638 | n.a. | 57.8 |
| H-58 | 07/02/2017 | 5 | 34.7 | 1.69 | 20.4 | 1.14 | 0.1 | 22.7 | 67.2 | 29 | 3635 | n.a. | 51.4 |
| H-58 | 15/02/2017 | 5 | 54.5 | 0.7 | 8.66 | 0.53 | <0.1 | - | 6.93 | 27.9 | 3349 | n.a. | 18 |
| H-59 | 17/02/2017 | 5 | 172 | 1.88 | <0.1 | <0.1 | 0.16 | 98.9 | 109 | 29.5 | 26.9 | n.a. | 46.1 |
| H-59 | 24/02/2017 | 5 | 22 | 1.93 | 0.44 | <0.1 | <0.1 | 10 | 1.77 | 11.6 | 86.3 | n.a. | 5.6 |
| H-59 | 24/02/2017 | 5 | 103 | 1.4 | 0.53 | <0.1 | 0.05 | 37.5 | 85 | 12.2 | 52 | n.a. | 58.8 |
| H-23 | 02/11/1987 | 5 | 464 | 28.4 | 15.15 | 0.15 | 0.9 | 746 | 1 | 117 | 130 | n.a. | 155 |
| H-23 | 13/11/1987 | 5 | 290 | 22 | 18.5 | 0.2 | 0.4 | 622 | 20.7 | 28.5 | 194 | n.a. | 114 |
| H-23 | 21/01/1988 | 5 | 146 | 10 | 3 | 0.03 | 0.2 | 194 | 2.4 | 53.9 | 73.2 | n.a. | 162 |
| H-27 | 13/04/1989 | 5 | 75 | 6 | 0.85 | 0.04 | 0.2 | 253 | 10.3 | 10.5 | 191 | n.a. | 18.5 |
| H-27 | 19/05/1989 | 5 | 88 | 27 | 0.9 | 0.17 | 0.1 | 13.1 | 130 | 13.8 | 88.4 | n.a. | 51.8 |
| H-27 | 08/06/1989 | 5 | 74 | 8 | 1.9 | 0.2 | 0.1 | 13.1 | 133 | 12 | 187 | n.a. | 777 |
| H-49 | 07/04/2016 | 5 | 266 | 42.5 | 1.94 | <0.1 | 1 | 1570 | 195 | 123 | 434 | n.a. | 334 |
| H-49 | 21/09/2016 | 5 | 245 | 39.9 | 1.95 | <0.1 | 0.85 | 1190 | 118 | 86.4 | 227 | n.a. | 809 |
| H-49 | 06/10/2016 | 5 | 249 | 40.8 | 2.63 | <0.1 | 0.84 | 1200 | 48.5 | 95.3 | 227 | n.a. | 919 |
| H-56 | 25/01/2017 | 5 | 237 | 37.6 | 2.5 | <0.1 | 0.8 | 114 | 235 | 64.6 | 212 | n.a. | 642 |
| H-56 | 10/02/2017 | 5 | 233 | 37.9 | 1.9 | <0.1 | 0.8 | 170 | 236 | 21.2 | 207 | n.a. | 627 |
| H-56 | 17/02/2017 | 5 | 251 | 31.2 | 1.6 | <0.1 | 0.7 | 163 | 277 | 49.8 | 264 | n.a. | 467 |
| H-12 | 01/08/2014 | 5 | 2.51 | 0.63 | 1.46 | n.a. | n.a. | 11.8 | 3.68 | 8.6 | 350 | 91.9 | 84.5 |
| H-12 | 25/03/2015 | 5 | 21.9 | 3 | 1.88 | n.a. | n.a. | 14.2 | 25.5 | 8.5 | 258 | 46.5 | 3 |
| H-12 | 11/01/2017 | 5 | 5.49 | 3.71 | n.a. | n.a. | n.a. | 5.11 | 6.99 | 10.7 | 614 | n.a. | 72.76 |
| code | Date | * Reference | Na | K | Ca | Mg | Li | Cl | HCO3 | SO4 | B | As | SiO2 |
| H-24 | 18/05/1989 | 5 | 285 | 46 | 0.75 | 0.05 | 0.9 | 325 | 58.2 | 13.6 | 4230 | n.a. | 406 |
| H-41 | 21/01/2013 | 5 | 351 | 59.05 | 5.65 | 0.14 | 1.01 | 78.5 | 530.37 | 62.6 | 1176 | n.a. | 1284 |
| H-41 | 22/01/2015 | 5 | 87.4 | 25.5 | 0.08 | 0 | 0.31 | 60.9 | 40.9 | 18.9 | 1005 | 17.63 | 1022 |
| H-41 | 25/01/2016 | 5 | 82.7 | 5.25 | 0.63 | 0.13 | 0.26 | 42.6 | 26.11 | 13.3 | 992 | n.a. | 210 |

* 1 – Arellano et al., 2003

2- Tello et al., 2005

5 - CFE

Table A6 – Chemical composition of gas samples from geothermal wells in Los Humeros, as Total Discharge (T.D.). $CO_2$, $CH_4$, $H_2$, $H_2S$, $N_2$ and $NH_3$ are expressed in %. Ar, He, HCl and HF are in ppm.

| POZO | FECHA | Gas Total (% weight) | Ar | $CH_4$ | $CO_2$ | $H_2$ | $H_2S$ | He | $N_2$ | $NH_3$ | HCl | HF | * Reference |
|---|---|---|---|---|---|---|---|---|---|---|---|---|---|
| H-28 | 14/08/2002 | 3.8 | 39 | 0.12 | 97.8 | 0.02 | 1.61 | n.a. | 0.06 | 0.38 | n.m. | n.m. | 5 |
| H-29 | 03/09/2002 | 4.5 | 140 | 0.16 | 98.2 | 0.03 | 1.5 | n.a. | 0.09 | 0.02 | n.m. | n.m. | 5 |
| H-30 | 07/11/2002 | 2.56 | 139 | 0.05 | 94.8 | 0.02 | 5 | n.a. | 0.07 | 0.05 | n.m. | n.m. | 5 |
| H-29 | 06/09/1989 | 8.23 | n.a. | 0.4 | 86.6 | 0.12 | 10.94 | n.a. | 1.88 | 0.07 | n.m. | n.m. | 5 |
| H-29 | 13/10/1989 | 7.67 | n.a. | 8 | 88.5 | 0.11 | 9.08 | n.a. | 1.99 | 0.28 | n.m. | n.m. | 5 |
| H-29 | 22/08/1991 | 0.81 | 331 | 0.62 | 79.6 | 0.1 | 16.74 | n.a. | 2.87 | n.d. | n.m. | n.m. | 5 |
| H-43 | 19/07/2014 | 9.46 | 2383 | 0.12 | 88.9 | 0.35 | 7.16 | n.a. | 3.18 | 0.002 | n.m. | n.m. | 5 |
| H-43 | 15/08/2014 | 25.8 | 2690 | 0.25 | 87.4 | 0.58 | 6.09 | n.a. | 5.42 | 0.002 | n.m. | n.m. | 5 |
| H-43 | 29/09/2014 | 9.38 | 544 | 0.17 | 90.2 | 0.39 | 5.96 | n.a. | 3.22 | 0.002 | n.m. | n.m. | 5 |
| H-58 | 17/02/2017 | 2.74 | 203 | 0.1 | 93.7 | 0.07 | 5.33 | 8.5 | 0.79 | 0.01 | n.m. | n.m. | 5 |
| H-58 | 24/02/2017 | 3.44 | 146 | 0.06 | 95.4 | 0.05 | 3.87 | 6.3 | 0.61 | 0.02 | n.m. | n.m. | 5 |
| H-58 | 27/02/2017 | 3.21 | 163 | 0.08 | 94.6 | 0.06 | 4.55 | 7 | 0.7 | 0.01 | n.m. | n.m. | 5 |
| H-59 | 10/02/2017 | 1.57 | 880 | 0.03 | 88.7 | 0.29 | 6.06 | n.a. | 4.74 | 0.09 | n.m. | n.m. | 5 |
| H-59 | 17/02/2017 | 1.77 | 800 | 0.2 | 87.9 | 0.27 | 6.75 | n.a. | 4.83 | 0.01 | n.m. | n.m. | 5 |
| H-59 | 24/02/2017 | 0.88 | 1175 | 0.05 | 85.7 | 0.41 | 6.9 | n.a. | 6.67 | 0.15 | n.m. | n.m. | 5 |
| H-11 | 22/10/1987 | n.m. | n.a. | 0.07 | 95.6 | 0.57 | 3.58 | n.a. | 0.05 | 0.18 | n.m. | n.m. | 1 |
| H-16 | 14/07/1987 | n.m. | n.a. | 3.26 | 82.6 | 3.1 | 9.71 | n.a. | 1.07 | 0.3 | n.m. | n.m. | 1 |
| H-16R | 13/10/1989 | n.m. | n.a. | 2.08 | 84.4 | 1.69 | 10.53 | n.a. | 1.18 | 0.11 | n.m. | n.m. | 1 |
| H-16R | 05/04/1994 | n.m. | n.a. | 2 | 86.3 | 0.79 | 9.21 | n.a. | 0.77 | 0.94 | n.m. | n.m. | 1 |
| H-17 | 21/10/1987 | n.m. | n.a. | 0.45 | 90.1 | 2.73 | 6.35 | n.a. | 0.19 | 0.18 | n.m. | n.m. | 1 |
| H-3 | 13/04/1994 | n.m. | 300 | 0.27 | 93.5 | 0.75 | 2.75 | n.a. | 2.19 | 0.5 | 239 | 219 | 2 |
| H-9 | 14/04/1994 | n.m. | 300 | 3.37 | 85.7 | 1.4 | 7.03 | n.a. | 1.45 | 0.98 | 18 | 33.6 | 2 |
| H-11 | 14/04/1994 | n.m. | 50 | 0.43 | 96.2 | 0.21 | 2.56 | 9.5 | 0.33 | 0.23 | 195 | 36.2 | 2 |
| H-15 | 13/04/1994 | n.m. | 260 | 3.91 | 86.4 | 1.23 | 7.32 | n.a. | 0.64 | 0.53 | 121 | 34 | 2 |
| H-16 | 13/04/1994 | n.m. | 160 | 2.22 | 86.8 | 0.82 | 9.04 | n.a. | 0.76 | 0.31 | 136 | 43.8 | 2 |
| H-17 | 14/04/1994 | n.m. | 80 | 1.25 | 91.4 | 0.45 | 5.9 | 4.4 | 0.44 | 0.57 | 195 | 73.6 | 2 |
| H-28 | 14/04/1994 | n.m. | 50 | 0.68 | 95.8 | 0.27 | 2.47 | 4.1 | 0.34 | 0.4 | 224 | 32.1 | 2 |
| H-30 | 13/04/1994 | n.m. | 290 | 2.52 | 82 | 1.15 | 12.3 | n.a. | 1.26 | 0.71 | 224 | 61.3 | 2 |
| H-31 | 13/04/1994 | n.m. | 200 | 3.37 | 87.1 | 1.07 | 7.32 | n.a. | 0.8 | 0.37 | 62.2 | 20.3 | 2 |
| POZO | FECHA | Gas Total (% weight) | Ar | $CH_4$ | $CO_2$ | $H_2$ | $H_2S$ | He | $N_2$ | $NH_3$ | HCl | HF | * Reference |
| H-32 | 14/04/1994 | n.m. | 80 | 1.31 | 91.4 | 0.41 | 6.1 | 2.7 | 0.38 | 0.36 | 298 | 36.9 | 2 |
| H-33 | 13/04/1994 | n.m. | 240 | 1.75 | 86.4 | 0.91 | 9.05 | n.a. | 1.03 | 0.81 | 313 | 70.3 | 2 |
| H-23 | 02/11/1987 | 4.45 | n.a. | 0.35 | 84.5 | 0.12 | 13.64 | 3.9 | 1.18 | 0.19 | n.m. | n.m. | 5 |
| H-23 | 13/11/1987 | 4.53 | n.a. | 0.05 | 81.3 | 0.34 | 9.97 | 9.6 | 6.99 | 0.13 | n.m. | n.m. | 5 |
| H-23 | 20/01/1988 | 5.17 | n.a. | 0.32 | 90.3 | 0.11 | 7.99 | 5.6 | 1.06 | 0.19 | n.m. | n.m. | 5 |
| H-27 | 13/04/1989 | 4.67 | n.a. | 0.02 | 91.3 | 0.15 | 5.1 | n.a. | 3.03 | 0.42 | n.m. | n.m. | 5 |
| H-27 | 19/05/1989 | 6.1 | n.a. | 0 | 93.3 | 0.1 | 4.05 | n.a. | 2.34 | 0.23 | n.m. | n.m. | 5 |
| H-27 | 08/06/1989 | 6.6 | n.a. | 0.23 | 91.9 | 0.12 | 5.67 | n.a. | 1.74 | 0.32 | n.m. | n.m. | 5 |
| H-49 | 07/04/2016 | 8.46 | 508 | 0.04 | 96.2 | 0.06 | 0.55 | 15.3 | 2.95 | 0.17 | n.m. | n.m. | 5 |
| H-49 | 21/09/2016 | 8.93 | 471 | 0.02 | 94.3 | 0.05 | 1.89 | 12.4 | 3.34 | 0.33 | n.m. | n.m. | 5 |
| H-49 | 06/10/2016 | 6 | 454 | 0.02 | 94.7 | 0.05 | 1.89 | 6.1 | 3.17 | 0.13 | n.m. | n.m. | 5 |
| H-56 | 25/01/2017 | 11.8 | 39 | 0.09 | 99.5 | 0.03 | 0.07 | 3.8 | 0.27 | 0.06 | n.m. | n.m. | 5 |
| H-56 | 10/02/2017 | 18.5 | 25 | 0.08 | 99.3 | 0.02 | 0.36 | 3 | 0.21 | 0.001 | n.m. | n.m. | 5 |
| H-56 | 17/02/2017 | 13.3 | 41 | 0.09 | 99.2 | 0.03 | 0.43 | 3.7 | 0.27 | 0.02 | n.m. | n.m. | 5 |
| H-1 | 21/10/1987 | 8.72 | n.a. | 0.06 | 96.3 | 0.13 | 2.95 | n.a. | 0.23 | 0.37 | n.m. | n.m. | 1 |
| H-7 | 21/10/1987 | n.m. | n.a. | 0.04 | 92.4 | 1.25 | 5.82 | n.a. | 0.11 | 0.37 | n.m. | n.m. | 1 |
| H-8 | 22/10/1987 | n.m. | n.a. | 0.05 | 94.6 | 0.93 | 4.12 | n.a. | 0.1 | 0.24 | n.m. | n.m. | 1 |
| H-10 | 21/10/1987 | n.m. | n.a. | 0.19 | 73.9 | 3.39 | 20.6 | n.a. | 0.87 | 1.1 | n.m. | n.m. | 1 |
| H-19 | 22/10/1987 | n.m. | n.a. | 0.01 | 96.4 | 0.76 | 2.59 | n.a. | 0.12 | 0.16 | n.m. | n.m. | 1 |
| H-23 | 22/10/1987 | n.m. | n.a. | 0.1 | 77.8 | 5.69 | 15.4 | n.a. | 0.17 | 0.88 | n.m. | n.m. | 1 |
| H-1 | 14/04/1994 | n.m. | 20 | 0.16 | 98.2 | 0.12 | 1.09 | 12.8 | 0.23 | 0.2 | 416 | 57.1 | 2 |
| H-7 | 14/04/1994 | n.m. | 120 | 0.31 | 92.8 | 0.45 | 5.05 | 10.2 | 0.93 | 0.42 | 32.7 | 24.1 | 2 |
| H-8 | 14/04/1994 | n.m. | 110 | 0.44 | 94.7 | 0.37 | 3.69 | 7.2 | 0.63 | 0.21 | 209 | 54.1 | 2 |
| H-19 | 12/04/1994 | n.m. | 30 | 0.06 | 95.9 | 0.16 | 3.3 | 7.8 | 0.37 | 0.23 | 62.2 | 54.3 | 2 |
| H-20 | 12/04/1994 | n.m. | 80 | 1.9 | 89.7 | 0.59 | 7 | n.d. | 0.42 | 0.4 | 32.7 | 47.2 | 2 |
| H-34 | 12/04/1994 | n.m. | 30 | 0.48 | 96.9 | 0.2 | 1.85 | 7.5 | 0.26 | 0.27 | 3 | 58.7 | 2 |
| H-12 | 01/08/2014 | 13.2 | 15 | 0.74 | 96.6 | 0.1 | 2.43 | n.a. | 0.16 | 0.001 | n.m. | n.m. | 5 |
| H-12 | 25/03/2015 | 9.46 | 20 | 0.89 | 94.3 | 0.1 | 4.54 | n.a. | 0.22 | 0.001 | n.m. | n.m. | 5 |
| H-12 | 11/01/2017 | 10.7 | 32 | 0.51 | 96 | 0.06 | 2.8 | n.a. | 0.16 | 0.5 | n.m. | n.m. | 5 |
| H-24 | 18/05/1989 | 6.42 | n.a. | 0.88 | 96.5 | 0.08 | 1.58 | n.a. | 0.65 | 0.34 | n.m. | n.m. | 5 |
| H-41 | 21/01/2013 | 1.92 | 2174 | 0.73 | 85.7 | 0.27 | 11.74 | n.a. | 1.34 | 0.005 | n.m. | n.m. | 5 |
| H-41 | 22/01/2014 | 4.2 | 2056 | 0.4 | 91.6 | 0.15 | 6.91 | n.a. | 0.72 | 0.002 | n.m. | n.m. | 5 |
| POZO | FECHA | Gas Total (% weight) | Ar | $CH_4$ | $CO_2$ | $H_2$ | $H_2S$ | He | $N_2$ | $NH_3$ | HCl | HF | * Reference |
| H-41 | 25/01/2016 | 4.38 | 197 | 0.48 | 92.9 | 0.1 | 5.47 | n.a. | 0.36 | 0.72 | n.m. | n.m. | 5 |
| H-6 | 22/10/1987 | n.m. | n.a. | 0.25 | 88 | 2.07 | 8.28 | n.a. | 0.78 | 0.6 | n.m. | n.m. | 1 |
| H-12 | 22/10/1987 | n.m. | n.a. | 0.6 | 91.4 | 1.88 | 5.64 | n.a. | 0.16 | 0.34 | n.m. | n.m. | 1 |
| H-18 | 22/10/1987 | n.m. | n.a. | 5.72 | 86.2 | 3.19 | 4.03 | n.a. | 0.41 | 0.44 | n.m. | n.m. | 1 |
| H-6 | 14/04/1994 | n.m. | 90 | 1.7 | 91 | 0.56 | 5.9 | n.a. | 0.37 | 0.5 | 112 | 58 | 2 |
| H-12 | 14/04/1994 | n.m. | 30 | 2.7 | 92.1 | 0.66 | 4 | 0.08 | 0.28 | 0.25 | 313 | 72.5 | 2 |

n.m. – not measured; n.a. – not analysed; n.d. – not determined

| Table A7 – Chemical data for fumaroles samples collected in Los Humeros Geothermal Field (data are expressed in mmol/mol). | | | | | | | | | | |
|---|---|---|---|---|---|---|---|---|---|---|
| # | Date | T(°C) | Ar | $O_2$ | $CH_4$ | $N_2$ | $CO_2$ | $H_2S$ | $H_2$ | CO |
| LB1 | 21/03/2018 | 92.8 | 1.08 | 6.2 | 1.1 | 70 | 850 | 58.9 | 3.572 | 0.005 |
| LB1 | 24/03/2018 | 92.8 | 1.26 | 11.4 | 0.7 | 90.8 | 816 | 68.6 | 3.566 | 0.008 |
| LB2 | 24/03/2018 | 92.0 | 7.74 | 134 | 1 | 523.6 | 314 | 21.3 | 0.989 | 0.022 |
| XA1 | 24/03/2018 | 64.5 | 0.1 | 0.57 | 37.1 | 5.9 | 935 | <0.3 | 3.553 | 0.01 |

Table A8 – Stable isotopic composition of the total discharge for geothermal well of Los Humeros. R/Ra and $\delta^{13}C$-$CO_2$ are also shown.

| code | Date | $\delta^{18}O$‰ | $\delta D$‰ | R/Ra | $\delta^{13}C$-$CO_2$(‰ vPDB) | * Reference |
|---|---|---|---|---|---|---|
| H1 | 21/10/1987 | -2.7 | -65.1 | | | 1 |
| H6 | 22/10/1987 | -3.1 | -70.9 | | | 1 |
| H7 | 21/10/1987 | -3.4 | -67.2 | | | 1 |
| H8 | 22/10/1987 | -3.5 | -69 | | | 1 |
| H10 | 21/01/1987 | -5.3 | -72.4 | | | 1 |
| H11 | 22/10/1987 | -3.8 | -68.1 | | | 1 |
| H12 | 14/05/1987 | -1.2 | -60.5 | | | 1 |
| H12 | 22/10/1987 | -2.5 | -64.1 | | | 1 |
| H16 | 14/05/1987 | -4.1 | -69.9 | | | 1 |
| H16 | 27/09/1988 | -6.7 | -80.4 | | | 1 |
| H16R | 24/11/1994 | -8.22 | -84.8 | | | 1 |
| H17 | 14/05/1987 | -3.72 | -64.9 | | | 1 |
| H17 | 21/10/1987 | -4.5 | -63.3 | | | 1 |
| H17 | 28/09/1988 | -3.48 | -68.2 | | | 1 |
| H18 | 22/10/1987 | -2 | -49.4 | | | 1 |
| H19 | 22/10/1987 | -4.3 | -68.8 | | | 1 |
| H23 | 22/10/1987 | -2.5 | -66.4 | | | 1 |
| H1 | | -4.8 | -69 | | | 2 |
| H2 | | -3.8 | -70 | | | 2 |
| H3 | | -2.66 | -61.5 | | | 2 |
| H4 | | -3.7 | -65 | | | 2 |
| H29 | 10/01/1992 | 1 | -47 | | | 2 |
| H38 | | 0.96 | -48 | | | 2 |
| H03 | gen-15 | -1.86 | -62.5 | 6.35 | -5.13 | 3 |
| H06a | gen-15 | -3.3 | -66.7 | 7.62 | -3.885 | 3 |
| H07 | gen-15 | -0.08 | -57.1 | 7.32 | -3.029 | 3 |
| H12 | gen-15 | -2.97 | -64.1 | 6.95 | -5.005 | 3 |
| H15 | gen-15 | -5.02 | -66.3 | 6.96 | -2.766 | 3 |
| H17 | gen-15 | 0.26 | -47 | 6.09 | -2.482 | 3 |
| H19a | gen-15 | -3.19 | -64.8 | 7.27 | -3.09 | 3 |
| H20 | gen-15 | -3.51 | -68.2 | 7.29 | -2.236 | 3 |
| H30 | gen-15 | -4.05 | -65 | 7 | -3.862 | 3 |
| H31 | gen-15 | -3.55 | -63.6 | 7.18 | -3.846 | 3 |
| H33 | gen-15 | -4.63 | -63.6 | 6.69 | n.d. | 3 |
| H34 | gen-15 | -2.65 | -61.6 | 7.18 | -5.25 | 3 |
| H35 | gen-15 | n.d. | n.d. | 7.09 | -4.437 | 3 |
| H41 | gen-15 | n.d. | n.d. | 6.13 | -3.389 | 3 |
| H42 | gen-15 | -0.66 | -59.8 | 6.42 | n.d. | 3 |
| H44 | gen-15 | -0.66 | -51.6 | 6.64 | -2.481 | 3 |
| H45 | gen-15 | -5.1 | -67.4 | 7.22 | -2.793 | 3 |
| H48d | gen-15 | -4.38 | -69.6 | 6.8 | -3.285 | 3 |
| H49 | gen-15 | -0.8 | -52.1 | 7.28 | -3.013 | 3 |
| H-1 | 14/05/1987 | -2.71 | -77.6 | | | 4 |
| H1 | 29/09/1988 | -2.35 | -72.3 | | | 4 |
| H6 | 14/05/1987 | -2.09 | -67.8 | | | 4 |
| code | Date | $\delta^{18}O$‰ | $\delta D$‰ | R/Ra | $\delta^{13}C$-$CO_2$(‰ vPDB) | Reference |
| H6 | 29/09/1988 | -3.88 | -70.8 | | | 4 |
| H7 | 14/05/1987 | -3.18 | -66.2 | | | 4 |
| H7 | 29/09/1988 | -2.91 | -70.3 | | | 4 |
| H8 | 14/05/1987 | -2.89 | -77.5 | | | 4 |
| H8 | 28/09/1988 | -3.42 | -71.7 | | | 4 |
| H9 | 14/05/1987 | -1.47 | -62.1 | | | 4 |
| H9 | 27/09/1988 | -1.63 | -68 | | | 4 |
| H10 | 14/05/1987 | -3.56 | -66 | | | 4 |
| H10 | 29/09/1988 | -4.93 | -68 | | | 4 |
| H11 | 14/05/1987 | -2.52 | -68 | | | 4 |
| H11 | 29/09/1988 | -2.84 | -64.3 | | | 4 |
| H12 | 14/05/1987 | -1.38 | -60.1 | | | 4 |
| H12 | 29/09/1988 | -3.21 | -67.3 | | | 4 |
| H13 | 29/09/1988 | -2.2 | -71.9 | | | 4 |
| H15 | 28/09/1988 | -3.23 | -68.4 | | | 4 |
| H16 | 14/05/1987 | -4.1 | -70.4 | | | 4 |
| H16 | 27/09/1988 | -6.7 | -81.6 | | | 4 |
| H17 | 14/05/1987 | -3.72 | -64.9 | | | 4 |
| H17 | 28/09/1988 | -3.48 | -68.2 | | | 4 |
| H18 | 14/05/1987 | -1.87 | -46 | | | 4 |
| H18 | 29/09/1988 | -2.81 | -53.4 | | | 4 |
| H19 | 14/05/1987 | -2.96 | -60.4 | | | 4 |
| H20 | 28/09/1988 | -4 | -71.3 | | | 4 |
| H27 | 29/09/1988 | -3.29 | -66.2 | | | 4 |
| H-15 | 14/10/2013 | -5.69 | -65.04 | | | 5 |
| H-17 | 14/10/2013 | -5.47 | -66.86 | | | 5 |
| H-30 | 14/10/2013 | -5.84 | -67.76 | | | 5 |
| H-31 | 14/10/2013 | -5.65 | -68.79 | | | 5 |
| H-33 | 14/10/2013 | -4.43 | -63.06 | | | 5 |
| H-3 | 15/10/2013 | -2.57 | -63.97 | | | 5 |
| H-35 | 15/10/2013 | -2.8 | -61.16 | | | 5 |
| H-9 | 15/10/2013 | -3.05 | -61.88 | | | 5 |
| H-11 | 16/10/2013 | -2.95 | -64.91 | | | 5 |
| H-32 | 16/10/2013 | -2.39 | -72.18 | | | 5 |
| H-34 | 16/10/2013 | -3.15 | -65.87 | | | 5 |
| H-44 | 16/10/2013 | -3.79 | -62.08 | | | 5 |
| H-19 | 17/10/2013 | -3.55 | -63.87 | | | 5 |
| H-20 | 17/10/2013 | -4.1 | -68.06 | | | 5 |
| H-37 | 17/10/2013 | -6.04 | -72.86 | | | 5 |
| H-41 | 17/10/2013 | -4.15 | -66.09 | | | 5 |
| H-42 | 17/10/2013 | -4.18 | -65.94 | | | 5 |
| H-45 | 17/10/2013 | -5.17 | -65.78 | | | 5 |
| H-6 | 17/10/2013 | -3.59 | -66.16 | | | 5 |
| H-12 | 18/10/2013 | -4.09 | -63.09 | | | 5 |
| H-39 | 18/10/2013 | -0.48 | -61.25 | | | 5 |
| H-43 | 18/10/2013 | -0.2 | -57 | | | 5 |
| code | Date | $\delta^{18}O$‰ | $\delta D$‰ | R/Ra | $\delta^{13}C$-$CO_2$(‰ vPDB) | Reference |
| H-49 | 18/10/2013 | -2.23 | -67.07 | | | 5 |
| H-7 | 21/10/2013 | -3.78 | -66.64 | | | 5 |
| H-43 | 15/08/2014 | 2.73 | -45.8 | | | 5 |
| H-3 | 21/08/2014 | -1.8 | -63.23 | | | 5 |
| H-30 | 22/08/2014 | -5.45 | -67.12 | | | 5 |
| H-31 | 22/08/2014 | -4.17 | -63.47 | | | 5 |
| H-33 | 22/08/2014 | -3.94 | -62.19 | | | 5 |
| H-35 | 22/08/2014 | -2.29 | -60.35 | | | 5 |
| H-9 | 22/08/2014 | -1.74 | -61.3 | | | 5 |
| H-11 | 09/09/2014 | -3.17 | -65.72 | | | 5 |
| H-20 | 09/09/2014 | -4.11 | -67.56 | | | 5 |
| H-32 | 09/09/2014 | -2.42 | -67.68 | | | 5 |
| H-44 | 09/09/2014 | -3.64 | -58.98 | | | 5 |
| H-34 | 10/09/2014 | -3.2 | -64.17 | | | 5 |
| H-39 | 10/09/2014 | -2.83 | -64.9 | | | 5 |
| H-41 | 10/09/2014 | -3.44 | -66.68 | | | 5 |
| H-42 | 10/09/2014 | -3.28 | -65.71 | | | 5 |
| H-49 | 10/09/2014 | -3.61 | -66.83 | | | 5 |
| H-12 | 11/09/2014 | -3.18 | -63.8 | | | 5 |
| H-19 | 11/09/2014 | -3.22 | -65.02 | | | 5 |
| H-45 | 11/09/2014 | -4.39 | -64.51 | | | 5 |
| H-6 | 11/09/2014 | -3.4 | -66.39 | | | 5 |
| H-7 | 11/09/2014 | -3.62 | -65.38 | | | 5 |
| H-17 | 17/09/2014 | -4.51 | -65.67 | | | 5 |
| H-19 | 18/03/2015 | -3.78 | -65.63 | | | 5 |
| H-3 | 18/03/2015 | -2.3 | -62.97 | | | 5 |
| H-45 | 18/03/2015 | -4.49 | -64.96 | | | 5 |
| H-7 | 18/03/2015 | -3.99 | -65.71 | | | 5 |
| H-9 | 18/03/2015 | -2.31 | -61.89 | | | 5 |
| H-33 | 19/03/2015 | -4.08 | -62.9 | | | 5 |
| H-35 | 19/03/2015 | -3.31 | -61.51 | | | 5 |
| H-48 | 19/03/2015 | -4.19 | -67.08 | | | 5 |
| H-11 | 20/03/2015 | -3.01 | -65.57 | | | 5 |
| H-17 | 20/03/2015 | -4.97 | -66.89 | | | 5 |
| H-32 | 20/03/2015 | -3.89 | -70.81 | | | 5 |
| H-34 | 20/03/2015 | -3.08 | -64.17 | | | 5 |
| H-44 | 20/03/2015 | -3.47 | -58.32 | | | 5 |
| H-15 | 23/03/2015 | -5.41 | -65.45 | | | 5 |
| H-20 | 23/03/2015 | -4 | -67.13 | | | 5 |
| H-31 | 23/03/2015 | -5.36 | -67.52 | | | 5 |
| H-39 | 24/03/2015 | -3.26 | -67.37 | | | 5 |
| H-41 | 24/03/2015 | -4.02 | -65.91 | | | 5 |
| H-49 | 24/03/2015 | -3.39 | -66.37 | | | 5 |
| H-42 | 25/03/2015 | -3.9 | -65.7 | | | 5 |
| H-6 | 25/03/2015 | -3.88 | -65.07 | | | 5 |
| H-3 | 06-giu-16 | -1.98 | -60.1 | | | 5 |
| code | Date | $\delta^{18}O$‰ | $\delta D$‰ | R/Ra | $\delta^{13}C$-$CO_2$(‰ vPDB) | Reference |
| H-6 | 17-giu-16 | -3.4 | -63.83 | | | 5 |
| H-7 | 04-lug-16 | -3.64 | -61.43 | | | 5 |
| H-9 | 06-giu-16 | -2.09 | -58.71 | | | 5 |
| H-11 | 07-lug-16 | -2.76 | -62.63 | | | 5 |
| H-12 | 24-giu-16 | -3.6 | -59.9 | | | 5 |
| H-15 | 22-giu-16 | -4.76 | -62.2 | | | 5 |
| H-17 | 23-giu-16 | -4.63 | -61.68 | | | 5 |
| H-19 | 04-lug-16 | -3.09 | -63.58 | | | 5 |
| H-20 | 04-lug-16 | -3.55 | -67.74 | | | 5 |
| H-30 | 06-giu-16 | -4.76 | -65.11 | | | 5 |
| H-31 | 06-giu-16 | -5.36 | -65.07 | | | 5 |
| H-32 | 23-giu-16 | -3.72 | -66.44 | | | 5 |
| H-33 | 22-giu-16 | -4.45 | -61.87 | | | 5 |
| H-34 | 04-lug-16 | -2.51 | -60.06 | | | 5 |
| H-35 | 22-giu-16 | -3.02 | -63.07 | | | 5 |
| H-39 | 29-giu-16 | -2.97 | -63.6 | | | 5 |
| H-41 | 24-giu-16 | -3.59 | -66.03 | | | 5 |
| H-42 | 24-giu-16 | -3.55 | -66.6 | | | 5 |
| H-44 | 23-giu-16 | -3.13 | -54.13 | | | 5 |
| H-45 | 29-giu-16 | -4.4 | -64.22 | | | 5 |
| H-48 | 29-giu-16 | -3.78 | -65.1 | | | 5 |
| H-49 | 07-lug-16 | -1.56 | -67.8 | | | 5 |

* 1 – Arellano et al., 2003
2 – Tello et al., 2005
3 - Pinti et al., 2017
4 – Truesdell and Quijano, 1998
5 - CFE

# Chapter 3

# DEVELOPMENTS OF AUXILIARY CHEMICAL GEOTHERMOMETERS APPLIED TO THE LOS HUMEROS AND ACOCULCO HIGH-TEMPERATURE GEOTHERMAL FIELDS (MÉXICO)

## 3.1 Introduction

The knowledge of the temperature of the deep geothermal fluids, rock permeability and water reservoir capacity are three key parameters for developing deep geothermal energy. Since 1965, one of the major applications of fluid geochemistry in the exploration of the potential geothermal reservoirs involves estimation of their temperature using classical chemical, isotope and gas geothermometers on fluids collected from geothermal wells and thermal springs, such as:

- Na-K (Fournier 1979; Michard, 1979; Giggenbach, 1988), Na-K-Ca (Fournier and Truesdell, 1973), K-Mg (Giggenbach, 1988), $SiO_2$ (Fournier and Rowe, 1966; Fournier, 1977; Michard, 1979);
- $\delta^{18}O_{H2O-SO4}$ (Lloyd, 1968; Mizutani and Rafter, 1969; Kusakabe and Robinson, 1977; Sakaï, 1977; Seal *et al.*, 2000; Zeebe, 2010; Boschetti, 2013);
- $CO_2$-$CH_4$-$H_2S$-$H_2$, $CO_2$-$CH_4$-$H_2$, $CO_2$-$CH_4$, $H_2$-Ar, $CO_2$-Ar (D'Amore and Panichi, 1980; Marini, 1987; Giggenbach and Goguel, 1989; Giggenbach, 1987, 1991).

Most of the solute geothermometers are based on empirical or semi-empirical laws derived from known or unknown chemical equilibrium reactions between water and minerals occurring in the geothermal reservoirs. Unfortunately, these classical tools do not always yield concordant estimations of reservoir temperatures, even at very high temperatures, in acidic environments, for example. Discrepancies in temperature estimates may also be due to different processes occurring during the geothermal fluid ascent up to the surface and its cooling: mixing with surface cold waters or seawater, degassing, precipitation/dissolution processes, etc.

Since the early 1980s, numerical multicomponent geochemical models are also being developed for direct application to chemical geothermometry for geothermal exploration (Reed, 1982; Michard and Roeckens, 1983; Reed and Spycher, 1984; Spycher *et al.*, 2014; Peiffer *et al.*, 2014a). These models allow numerical calculations of equilibration temperature of the geothermal water with respect to a suite of reservoir minerals, and thus the estimation of the reservoir temperature. Multicomponent geothermometry is not intended to replace classical geothermometers, but rather to supplement these geothermometers, and by doing so to increase confidence in temperature estimations. However, such approach cannot be applied carelessly and without a sound conceptual understanding of the area being studied (Al and pH poorly determined, for example). For this approach, a state of full chemical equilibrium is necessary and the conditions of this equilibrium state are not always reached.

Since the early 1980s, in parallel, several auxiliary geothermometers combining a major with a trace element, like Na-Li (Fouillac and Michard, 1981; Kharaka *et al.*, 1982; Michard, 1990; Sanjuan *et al.*, 2014), Mg-Li (Kharaka and Mariner, 1989), Na-Rb, Na-Cs, K-Sr, K-Mn, K-Fe, K-F and K-W (Michard, 1990; Sanjuan *et al.*, 2016a, b; 2017), have been also developed and are available for specific types of geothermal fluids and geological environments.

BRGM aims to develop and validate this type of auxiliary chemical geothermometers and the $\delta^{18}O_{H2O-SO4}$ isotope geothermometers in order:

- to improve the geochemical methods for geothermal exploration in volcanic fields such as Los Humeros and Acoculco, with high-temperature (HT) and relatively low permeability;
- to acquire a better knowledge about the circulation of HT deep fluids and their possible interaction with more superficial waters in this type of geothermal fields, from chemical and isotopic water analyses from surface thermal springs.

In the Los Humeros field, where numerous deep wells were drilled and are presently producing, the temperature values measured at the bottom-hole and estimated using classical water and gas geothermometers, will be used to test and calibrate these auxiliary geothermometers on the fluids collected from the deep geothermal wells. Some neighbouring thermal springs will be also sampled.

In the Acoculco field, where only two deep wells were drilled (EAC-1 in 1994, at a depth of 2000 m, and EAC-2 in 2008, at a depth of 1900 m, 500 m east of EAC-1; Peiffer *et al.*, 2014b), but were not productive, these auxiliary geothermometers will be applied on fluids collected from surface thermal springs.

The temperatures estimated for the waters collected from the thermal springs during this study will be compared with those given by the classical gas and water geothermometers, with reference to the deep temperatures close to 290-330°C measured at a depth of about 2000 m in both los Humeros (Arellano *et al.*, 2003; Pinti *et al.*, 2017) and Acoculco fields (Peiffer *et al.*, 2014b). These temperatures correspond to a gradient of 14°C/100 m, three times higher than the baseline gradient measured within the Trans-Mexican Volcanic Belt (Ziagos *et al.*, 1985).

In order to be able to obtain relevant results, the BRGM activities have been planned as follows:

- a preliminary literature review relative to the geological, geophysical and geochemical data about the Los Humeros and Acoculco geothermal fields, with the collaboration of the other partners, especially the Mexican partners (CFE, for example), in order to collect the main geological information and most of the geochemical data of the fluids sampled from Los Humeros deep wells and from thermal Acoculco springs);
- the participation to a campaign of fluid sampling and on site measurements in the Los Humeros and Acoculco geothermal areas (from deep wells at Los Humeros and from thermal springs at Acoculco), with the collaboration of CNR (Matteo Lelli's team) and Mexican teams (Ruth Alfaro, CFE…);
- chemical (major and some trace species) and isotope ($\delta^{18}O_{H2O}$, $\delta^{18}O_{SO4}$, $\delta^{11}B$, $\delta^{7}Li$, $^{87}Sr/^{86}Sr$…) analyses of the waters collected during the campaign of fluid sampling, in the BRGM laboratories ;
- data interpretation, including the use of thermodynamic considerations, and main conclusions.

### 3.2 Literature review

Several interesting papers have been found during the literature review carried out by BRGM, among which the main ones are:

- Arzate *et al.* (2018), Peiffer *et al.* (2018), Carrasco-Núñez *et al.* (2018, 2017a and b), Pinti *et al.* (2017), García-Soto *et al.* (2016), Norini *et al.* (2015), Arellano Gomez *et al.* (2003, 2008, 2015), Bernard *et al.* (2011); García-Gutiérrez (2009), Barragán-Reyes *et al.* (2008, 2010), Gutiérrez-Negrín and Izquierdo-Montalvo (2010), Izquierdo *et al.* (2008, 2009), Lopez Romero (2006), Martínez-Serrano (2002), Portugal *et al*. (2002), Prol-Ledesma (1998), and Cortés *et al.* (1997) for the Los Humeros geothermal field;
- Sosa-Ceballos *et al.* (2018), Avellán *et al.* (2017), García-Palomo *et al.* (2017), Canet *et al.* (2010, 2015a, 2015b), Peiffer *et al.* (2014b, 2015), Lermo *et al.* (2009), Lopez-Hernández *et al.* (2009), Verma (2001), Lopez-Hernández and Castillo-Hernández (1997), Tello Hijonosa *et al.* (1995), Tello Hijonosa (1986, 1987, 1991), Ledezma-Guerrero (1987) for the Acoculco geothermal field.

#### 3.2.1 Los Humeros geothermal field

The main existing data of fluids from geothermal wells and neighbouring thermal springs used for this study are presented below.

Documents and Excel sheets provided by CFE in 2017 have allowed to collect geological, temperature and pressure logs from 16 wells located in the Los Humeros geothermal field (wells

H-5, H-12, H-22, H-23, H-24, H-25, H-26, H-27, H-28, H-29D, H-41, H-43, H-49, H-56, H-58, H-59). Fluid and gas geochemical data collected between 1987 and 2017 are available for only 13 of these wells (absence of data for the wells H-5, H-25 and H-26). Measurements of water stable isotopes ($\delta$D and $\delta^{18}$O) have been performed by CFE, between 2013 and 2016, on fluids from 29 wells (wells H-3, H-6, H-7, H-9, H-11, H-12, H-13R, H-15, H-17, H-19, H-20, H-29, H-30, H-31, H-32, H-33, H-34, H-35, H-37, H-38R, H-39, H-40, H-41, H-42, H-43, H-44, H-45, H-48, H-49).

Chemical data for two neighbouring thermal springs (El Tesoro and Noria Nuevo Pizarro) were also found in the tables of fluid monitoring given by CFE.

Detailed fluid geochemical data from the geothermal wells of Los Humeros field and neighbouring springs are also given by:

- Prol-Ledesma (1998) during pre- and post- exploitation of the Los Humeros geothermal field (gas and water chemical and isotopic data from deep wells, including the stable isotopes of water and $\delta^{18}$O values of dissolved sulphates);
- Arellano-Gomez *et al.* (2003) for five deep wells (H-1, H-6, H-7, H-8 and H-12), including gas and water chemical and isotopic data (water stable isotopes);
- Barragan-Reyes *et al.* (2010) for several deep wells (stable isotopes of water and gas chemical composition), and neighbouring springs (stable isotopes of water);
- Bernard *et al.* (2011) for several deep wells (water chemical and isotopic data, with boron isotopic data for 4 water samples);
- Pinti *et al.* (2017) for several deep wells (He, Ne and Ar noble gas isotopic abundances, with stable isotopes of water).

The geological and geothermal setting are presented in Chapter 1. The figure 3.2.1.1a, extracted from Pinti *et al.* (2017), and the figure 3.2.1.1b, extracted from Carrasco *et al.* (2017a), show a general view of the location of most of the Los Humeros geothermal wells.

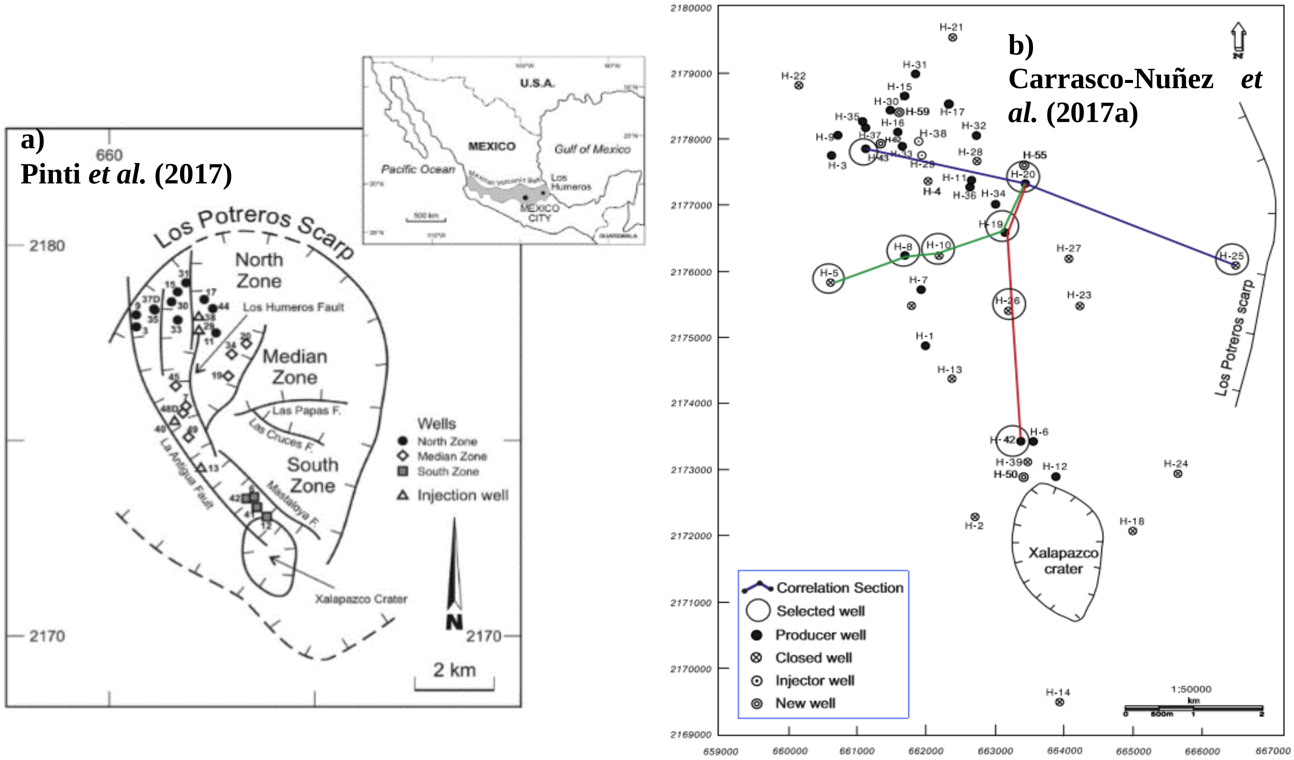


*Figure 3.2.1.1 - a) Simplified tectonic map of the central part of the Los Humeros caldera with the major faults and the position of the production and re-injection wells (from Pinti et al., 2017). b) Location of the main geothermal wells within Los Humeros geothermal field (from Carrasco et al., 2017a).*

From the geothermal reservoir consisted of medium-to low-permeability pre-caldera andesites, the wells produce biphasic fluid, with variable but high fractions of steam and limited liquid water contents, with enthalpy values over 2400 kJ/kg (Gutiérrez-Negrín and Izquierdo-Montalvo, 2010), except for some wells as H-1, which has always produced water with a low enthalpy of 1500-1700 kJ/kg. Some geothermal fluids reach 400°C in the northern production area.

### 3.2.2 Acoculco geothermal area

Geochemical data for waters sampled from 39 thermal springs located in the Acoculco geothermal area, with temperature values ranging from 13 to 49°C, have been collected in the CFE report 34-86 (Tello Hinojosa, 1986). Chemical data for 10 gas samples from the Acoculco caldera are also presented in this report. All these data have been interpreted by Tello Hijonosa (1986), and some main conclusions and recommendations were given. Some of these data were also presented and interpreted by Lopez-Hernández *et al.* (2009). Partial chemical data (pH, Na, K, $SO_4$, B) are presented for samples of drilling fluid collected from the EAC-1 exploration well in the Acoculco area, in a CFE document (Tello Hijonosa *et al.*, 1995).

Peiffer *et al.* (2014b) have reported geochemical data for waters from four Acoculco thermal springs and associated non-condensable gases (fig. 3.2.2.1). They integrated some of the previous data obtained by Tello Hijonosa (1986), interpreted all the results and drew up some main conclusions, among which the estimation of deep temperatures ranging from 243 to 353°C, using gas geothermometry ($CO_2$-Ar, $CH_4$-$CO_2$, $CO_2$ and $H_2S$). These values are in agreement with the measured well bottom hole temperatures (267 and 300°C). They might explain the intense hydrothermal alteration observed in the upper 800 m of volcanic rocks, with most abundant alteration minerals being quartz, amorphous silica, calcite, pyrite, clays (illite, smectite, kaolinite), and hematite.

The presence of a deep-water reservoir was not revealed during the EAC-1 drilling (depth of 2000 m), in 1994, in the locality of Los Azufres. However, a few permeable layers, at depths of 70 m and 300-450 m, and inflow of warm water together with significant amount of gas were observed (López-Hernández and Castillo-Hernández, 1997; López-Hernández *et al.*, 2009). The second well of 1900 m deep (EAC-2), drilled in 2008, 500 m east of EAC-1, showed a promising deep temperature of 267°C accompanied by low permeability similar to that of the EAC-1 well.

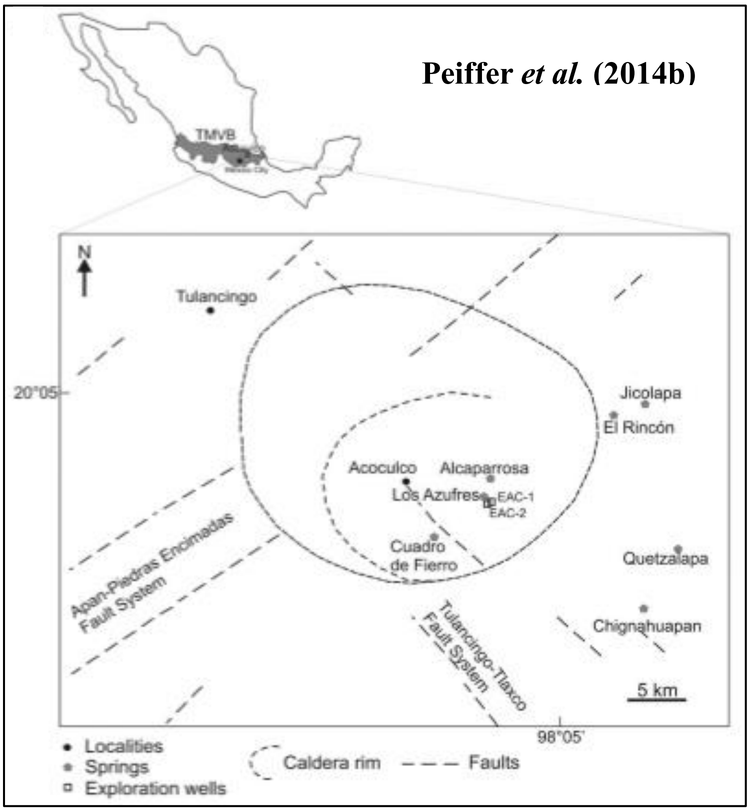


*Figure 3.2.2.1 - a) Location of the Acoculco caldera within the Trans-Mexican Volcanic Belt (TMVB) and schematic map of the Tulancingo-Acoculco caldera complex with the position of the main fault systems, thermal springs and the two exploration wells (modified in Peiffer et al., 2014b, after López-Hernández et al., 2009).*

According to Peiffer *et al.* (2014b), the high grade of alteration of the volcanic deposits induces low rock permeability and acts as a caprock probably impeding the recharge of the system by meteoric waters (López-Hernández *et al.*, 2009), and causing the absence of thermal manifestations within the caldera complex. Instead, springs with close to ambient temperatures are reported as well as hydrothermally altered grounds, cold diffuse soil degassing and bubbling pools (Polak *et al.*, 1982; Tello-Hijonosa, 1986; Bernard-Romero, 2008).

Cold degassing is probably due to conductive cooling of the deep gases on their way to the surface. Los Azufres, where EAC-1 well was drilled, and Alcaparrosa are the only two regions with noticeable active degassing ($H_2S$ smell), bubbling pools and springs with temperatures of 16-25°C (fig. 3.2.2.1). The only springs with temperature significantly above the ambient temperature are located outside the caldera towards the east and south-east at Chignahuapan (49°C, inside a thermal bath resort), Quetzalapa (30°C), Jicolapa (32°C) and El Rincón (32°C; fig. 3.2.2.1). Apart from Chignahuapan spring, all these springs are characterized by bubbling. The geological and geothermal setting are presented in Chapter 1.

### 3.2.3 Main remarks

If all the dissolved major species (Na, K, Ca, Mg, $HCO_3$, Cl, $SO_4$, $SiO_2$) and stable water isotopes ($\delta D$ and $\delta^{18}O$) were determined among most of the existing geochemical data, few trace elements (only B, Li, F, $NH_4$, Fe, Al and As) were studied. Very few data were also found for $\delta^{18}O_{SO4}$ and $\delta^{11}B$ values, and $^{87}Sr/^{86}Sr$ ratios. No value was found for $\delta^7Li$ values. The campaign of fluid sampling planned by BRGM was therefore very important and necessary to test and develop our auxiliary chemical geothermometers, integrating trace elements such as Rb, Cs, Sr, Mn, F and W, and the $\delta^{18}O_{H2O-SO4}$ geothermometer. It has also contributed to acquire new isotopic data of $\delta^{11}B$ and $\delta^7Li$ values.

The table 3.2.3.1 summarizes the existing chemical and isotopic data obtained on the scarce thermal waters of the Los Humeros and Acoculco areas.

| Thermal spring | Date | T | Cond. | pH | Na | K | Ca | Mg | $HCO_3$ | Cl | $SO_4$ | $SiO_2$ | F | B | $NH_4$ | Li | Rb | Cs | Fe | Al | TDS | δD | $\delta^{18}O$ | Reference |
|---|---|---|---|---|---|---|---|---|---|---|---|---|---|---|---|---|---|---|---|---|---|---|---|---|
| | | °C | µS/cm | | mg/l | mg/l | mg/l | mg/l | mg/l | mg/l | mg/l | mg/l | mg/l | mg/l | mg/l | mg/l | mg/l | mg/l | mg/l | mg/l | g/l | ‰ | ‰ | |
| **El Tesoro** | 06/03/2015 | 15 | 791 | 8.1 | 87.4 | 11.1 | 10.9 | 26.0 | 396 | 58.6 | 10.2 | 58.1 | | | | 0.089 | | | | | 0.7 | | | *CFE monitoring (database table)* |
| **El Tesoro** | 13/10/2015 | 14 | 774 | 7.2 | 83.7 | 11.3 | 47.3 | 23.5 | 390 | 58.6 | 5.8 | 31.9 | | | | | | | | | 0.7 | | | *CFE monitoring (database table)* |
| **El Tesoro** | 15/04/2016 | 16 | 762 | 6.6 | 82.9 | 10.2 | 42.8 | 34.1 | 380 | 49.6 | 1.8 | 55.0 | | | | 0.067 | | | | | 0.7 | | | *CFE monitoring (database table)* |
| **El Tesoro** | 17/11/2016 | 23 | 783 | 7.8 | 79.3 | 9.8 | 39.7 | 30.4 | 405 | 60.1 | 3.4 | 63.8 | | | | 0.072 | | | | | 0.7 | | | *CFE monitoring (database table)* |
| **El Tesoro** | 27/02/2017 | 15 | 791 | 8.1 | 87.4 | 11.1 | 10.9 | 26.0 | 396 | 58.6 | 10.2 | 58.1 | | | | 0.089 | | | | | 0.7 | | | *CFE monitoring (database table)* |
| **Nuevo Pizarro (Noria)** | 16/10/2015 | | 1686 | 7.3 | 303 | 26.1 | 31.4 | 18.9 | 498 | 208 | 99.0 | 21.3 | | 2.47 | | 0.378 | | | | | 1.2 | | | *CFE monitoring (database table)* |
| **Nuevo Pizarro (well)** | 25/02/2015 | 17 | 1758 | 7.3 | 360 | 1.21 | 19.4 | 1.52 | 552 | 211 | 124 | 29.5 | | 2.50 | | | | | | | 1.3 | | | *CFE monitoring (database table)* |
| **Nuevo Pizarro (well)** | 09/11/2016 | 17 | 1737 | 7.1 | 312 | 28.9 | 37.1 | 25.1 | 708 | 195 | 98.0 | 44.7 | | 3.20 | | 0.375 | | | | | 1.5 | | | *CFE monitoring (database table)* |
| **Nuevo Pizarro (well)** | 09/02/2017 | 17 | 1758 | 7.3 | 360 | 1.21 | 19.4 | 1.52 | 552 | 211 | 124 | 29.5 | | 2.50 | | | | | | | 1.3 | | | *CFE monitoring (database table)* |
| **Nuevo Pizarro (spring)** | 13/04/2016 | 17 | 1763 | 6.7 | 295 | 29.4 | 35.2 | 30.4 | 522 | 169 | 11.8 | 17.7 | | 2.30 | | 0.411 | | | | | 1.1 | | | *CFE monitoring (database table)* |
| **Baños Chignahuapan** | 21-25/04/2006 | 47.5 | | 7.0 | 87.0 | 14.0 | 196 | 26.0 | 735 | 106 | 28.0 | 19.0 | 0.7 | 1.80 | 0.5 | 0.360 | | | | | 1.2 | -70 | -10.4 | *Peiffer et al. (2014)* |
| **Baños Chignahuapan** | 02/07/1986 | 49 | 1440 | 6.5 | 95.4 | 14.4 | 173 | 30.6 | 831 | 118 | 39.0 | 24.3 | | 3.20 | 2.0 | 0.372 | < 0.1 | < 0.1 | < 0.5 | | 1.3 | -69 | -9.6 | *Tello Hijonosa (1986)* |
| **Baños Quetzalapa** | 18/06/1986 | 32 | 1942 | 5.8 | 157 | 18.6 | 193 | 47.9 | 1479 | 23.5 | 0 | 53.6 | | 0.74 | 2.0 | 0.149 | < 0.1 | < 0.1 | < 0.5 | | 2.0 | -60 | -8.7 | *Tello Hijonosa (1986)* |
| **Agua Salada** | 03/07/1986 | 21 | 2070 | 6.5 | 435 | 70.5 | 79.1 | 34.6 | 1459 | 192 | 0 | 85.0 | | 34.5 | 0.24 | 0.216 | < 0.1 | < 0.1 | 0.7 | | 2.4 | | | *Tello Hijonosa (1986)* |
| **Capulines** | 01/07/1986 | 20 | 1030 | 6.0 | 77.9 | 18.4 | 77.0 | 76.0 | 716 | 5.9 | 16.3 | 52.9 | | 0.80 | < 0,1 | 0.131 | < 0.1 | < 0.1 | < 0.5 | | 1.0 | | | *Tello Hijonosa (1986)* |
| **El Rincón** | 19/06/1986 | 32 | 878 | 5.6 | 12.9 | 12.9 | 144 | 10.3 | 500 | 9.8 | 36.9 | 64.7 | | 0.09 | 1.6 | < 0.1 | < 0.1 | < 0.1 | < 0.5 | | 0.8 | -65 | -9.3 | *Tello Hijonosa (1986)* |
| **Baños Jicolapa** | 21-25/04/2006 | 25.4 | | 6.2 | 29.0 | 15.0 | 265 | 12.0 | 894 | 7.7 | 0 | 63.0 | 0.6 | 1.00 | 0.1 | | | | | | 1.3 | -66 | -10.2 | *Peiffer et al. (2014)* |
| **Baños Jicolapa** | 03/07/1986 | 32 | 1381 | 6.5 | 31.4 | 15.6 | 230 | 17.2 | 927 | 17.6 | 0 | 66.9 | | 1.25 | 0.4 | < 0.1 | < 0.1 | < 0.1 | < 0.5 | | 1.3 | -67 | -9.5 | *Tello Hijonosa (1986)* |
| **Los Azufres** | 21-25/04/2006 | 21.4 | | 5.5 | 55.0 | 15.0 | 56.0 | 11.0 | 137 | 7.8 | 218 | 33.2 | 0.2 | 2.00 | 7.8 | | | | | | 0.5 | -72 | -10.5 | *Peiffer et al. (2014)* |
| **Los Azufres** | 25/06/1986 | 25 | 1214 | 6.0 | 124 | 28.4 | 99.8 | 29.8 | 0 | 37.2 | 2298 | 31.3 | | 167 | 94 | < 0.1 | < 0.1 | < 0.1 | < 0.5 | | 2.9 | | | *Tello Hijonosa (1986)* |
| **Los Azufres** | 25/06/1986 | 25 | 829 | 6.6 | 17.7 | 30.1 | 64.4 | 15.8 | 47.5 | 19.6 | 211 | 36.8 | | 36.6 | 86 | < 0,1 | < 0.1 | < 0.1 | 2.66 | 4.49 | 0.6 | -68 | -8.1 | *Tello Hijonosa (1986)* |
| **Los Azufres** | 25/06/1986 | 25 | 1931 | 7.0 | 332 | 36.5 | 198 | 79.4 | 1231 | 94.1 | 340 | 23.4 | | 266 | 81 | 0.159 | < 0.1 | < 0.1 | < 0.5 | 0 | 2.7 | | | *Tello Hijonosa (1986)* |
| **Cuadro de Fierro** | 20/06/1986 | 23 | 1876 | 3.4 | 42.3 | 13.6 | 145 | 87.2 | 0 | 13.7 | 1245 | 32.5 | | 1.48 | 7.6 | < 0.1 | < 0.1 | < 0.1 | 7.5 | 64 | 1.6 | -79 | -10.8 | *Tello Hijonosa (1986)* |
| **Alcaparrosa** | 29/05/2013 | 17 | | 2.4 | 15.8 | 8.5 | 9.7 | 1.3 | 0 | 2.2 | 538 | 52.0 | | | | | | | | | 0.6 | | | *Peiffer et al. (2014)* |
| **Alcaparrosa** | 21-25/04/2006 | 12.2 | | 2.4 | 11.0 | 6.7 | 10.0 | 1.6 | 0 | 8.6 | 515 | 53.0 | | | | | | | | | 0.6 | -69 | -10.7 | *Peiffer et al. (2014)* |
| **Alcaparrosa** | 24/06/1986 | 15 | 1945 | 2.2 | 13.7 | 9.48 | 36.4 | 9.2 | 0 | 13.7 | 1272 | 63.8 | | 12.6 | 9.8 | < 0.1 | < 0.1 | < 0.1 | < 0.5 | | 1.4 | -68 | -9.4 | *Tello Hijonosa (1986)* |

*Table 3.2.3.1 - Existing chemical and isotopic data of the main thermal springs discharging from the Los Humeros and Acoculco geothermal areas, with literature references.*

## 3.3 Water sampling and analytical results

### 3.3.1 Water sampling

The campaign of water sampling was carried out by BRGM, in collaboration with CFE, University of Michoacana and CNR Lelli’s team, from March 20 to 28, in the Los Humeros and Acoculco geothermal fields (fig. 3.3.1.1). Fluid samples were collected from seven geothermal wells and four thermal springs located in the Los Humeros area, from eight thermal springs located in the Acoculco area, and from three neighbouring crater lakes (lagunas), as points of surface reference. Their locations are reported in figure 3.3.1.1 and in table 3.3.1.1.


*Figure 3.3.1.1 - Location of the geothermal wells and thermal springs which were sampled during the campaign of water sampling carried out by BRGM between March 22 and 28, 2018, in the Los Humeros and Acoculco areas.*

Among the two-phase geothermal waters from Los Humeros field, very rich in steam, those which indicated the most high fractions of liquid water were selected with the valuable help of CFE (table 3.3.1.1).

Collection of the fluid samples in the field was accompanied by appropriate on-site measurements such as water temperature, conductivity, pH redox potential and alkalinity. The temperature, conductivity, pH and redox potential measurements were performed on the raw water samples, whereas alkalinity was analysed on fluid samples filtered at 0.45 µm. Absolute uncertainty concerning the pH measurements was 0.05 pH units and relative uncertainty concerning the other parameters varied from 5% to 10%, depending on the parameter and the range of measured values. All these measurements are given in table 3.3.1.1.

| Area | Sampling point | Specific enthalpy | Location | | Location (ED50 UTM North zone 14) | | | Depth | Date | T | Cond. 25°C | pH | Eh | Alk. | Alk. |
|---|---|---|---|---|---|---|---|---|---|---|---|---|---|---|---|
| | | J/g | Longitude (°E WGS84) | Latitude (°N WGS84) | X | Y | Z (m) | m | | °C | µS/cm | | mV | meq/l | mg/l $HCO_3$ |
| *Los Humeros area* | **Los Humeros H-39** | | -97.44192672 | 19.64813614 | 663433 | 2173524 | 2901 | 2890 | 22/03/2018 12:00 | 61.9 | 591 | 7.14 | -260 | 4.45 | 272 |
| | **Los Humeros Unit-11 (fluid mixing)** | | -97.44426546 | 19.64789310 | 663188 | 2173495 | 2896 | | 22/03/2018 12:50 | 52.7 | 1294 | 7.00 | -240 | 4.56 | 278 |
| | **Los Humeros H-56** | 2006 | -97.45238985 | 19.65824117 | 662325 | 2174632 | 2840 | 2380 | 22/03/2018 13:25 | 74.1 | 1196 | 7.58 | -346 | 5.68 | 347 |
| | **Los Humeros H-49** | 1640 | -97.45575398 | 19.66414467 | 661967 | 2175282 | 2824 | 2030 | 22/03/2018 13:55 | 68.0 | 1051 | 7.70 | -270 | 4.64 | 283 |
| | **Los Humeros H-9** | | -97.46771954 | 19.69284192 | 660683 | 2178448 | 2756 | 2752 | 22/03/2018 15:05 | 66.8 | 752 | 7.17 | -295 | 4.63 | 283 |
| | **Los Humeros H-32** | | -97.44843294 | 19.69107099 | 662707 | 2178270 | 2815 | 2818 | 22/03/2018 15:35 | 67.8 | 595 | 6.67 | -235 | 1.55 | 95 |
| | **Los Humeros H-55** | ≈ 2600 | -97.44178982 | 19.68610194 | 663409 | 2177726 | 2830 | | 22/03/2018 16:08 | 68.9 | 254 | 7.55 | -335 | 0.73 | 45 |
| | **El Tesoro** | | -97.25200094 | 19.73436294 | 683253 | 2183272 | 2080 | | 23/03/2018 09:30 | 22.5 | 787 | 7.49 | 220 | 6.05 | 369 |
| | **El Tesoro (in front of the first spring)** | | | | 683259 | 2183302 | 2080 | | 23/03/2018 10:00 | 21.0 | 610 | 7.50 | 240 | | |
| | **Noria Nuevo Pizarro** | | -97.45232003 | 19.49040046 | 662501 | 2156054 | 2342 | 20.18 | 23/03/2018 11:45 | 16.0 | 2090 | 8.82 | 130 | 11.21 | 684 |
| | **Pozo Hacienda San Miguel Barrientos** | | -97.57049400 | 19.50323691 | 650084 | 2157367 | 2352 | | 23/03/2018 12:45 | 18.5 | 441 | 7.81 | 210 | | |
| | **Pozo de Pochintoc** | | | | | | | 95 | 23/03/2018 13:45 | 20.2 | 660 | 7.80 | 190 | | |
| | **Virgen del Carmen** | | -97.53992885 | 19.26677171 | 653514 | 2131220 | 2364 | | 23/03/2018 15:46 | 19.1 | 2080 | 7.10 | 205 | 12.36 | 754 |
| | **Pozo de Tepeyahualco** | | -97.46732500 | 19.51728056 | 660899 | 2159015 | 2426 | 130 | 24/03/2018 10:10 | 23.8 | 4970 | 6.75 | -50 | 33.70 | 2056 |
| | **Laguna de Atexcac** | | -97.45423537 | 19.33296456 | 662456 | 2138625 | 2363 | | 24/03/2018 14:15 | 22.0 | 12640 | 8.63 | 50 | 2.05 | 125 |
| | **Laguna de Alchichica** | | -97.39758881 | 19.40821429 | 668331 | 2147009 | 2324 | | 23/03/2018 16:45 | 18.5 | 13250 | 9.07 | 106 | 41.75 | 2547 |
| | **Laguna de Quechulac** | | -97.34922053 | 19.37386715 | 673448 | 2143255 | 2342 | | 24/03/2018 16:30 | 20.4 | 894 | 8.73 | 160 | 6.75 | 412 |
| *Acoculco area* | **Los Azufres 1** | | -98.14404722 | 19.92236110 | 589656 | 2203350.946 | 2840 | | 26/03/2018 15:05 | 25.4 | 1489 | 6.41 | -355 | | |
| | **Los Azufres 2** | | -98.14442500 | 19.92255830 | 589616 | 2203372.57 | 2840 | | 26/03/2018 16:00 | 19.2 | 693 | 3.22 | -51 | | |
| | **Los Azufres 3** | | -98.14504444 | 19.92286940 | 589551 | 2203406.67 | 2840 | | 28/03/2018 09:45 | 26.6 | 1735 | 7.94 | -140 | | |
| | **Jicolapa** | | -97.99911898 | 19.98534263 | 604784 | 2210405.375 | 2230 | | 27/03/2018 09:45 | 30.7 | 1372 | 6.31 | -241 | | |
| | **El Rincon** | | -98.00717601 | 19.98889439 | 603939 | 2210793.463 | 2304 | | 27/03/2018 11:00 | 26.6 | 550 | 5.67 | 110 | | |
| | **Baños de Quetzalapa** | | -97.99399722 | 19.83767500 | 605418 | 2194065.117 | 2171 | | 27/03/2018 16:00 | 30.0 | 1964 | 6.37 | 135 | | |
| | **Baños de Chignahuapan** | | -97.98183170 | 19.87221460 | 606669 | 2197895.496 | 2190 | | 28/03/2018 07:30 | 49.0 | 1448 | 6.51 | -271 | | |

*Table 3.3.1.1 - Field data corresponding to the campaign of fluid sampling carried out by BRGM between March 22 and 28, 2018, in the Los Humeros and Acoculco geothermal areas.*

Collection and conditioning of all the water samples followed the classical procedures recommended for each of the chemical and isotopic analyses to be performed. Thus:

- for the chemical analysis of major anions and some trace elements, such as Cl, $SO_4$, Br, F, $NH_4$ and $PO_4$, the water samples were filtered at 0.45 µm and collected in 100 ml polyethylene bottles;
- for the chemical analysis of major cations, the water samples were filtered at 0.45 µm, then acidified using Suprapur $HNO_3$ and collected in 100 ml polyethylene bottles;
- in order to avoid silica precipitation, the samples of hot water for silica analysis (high contents) were collected in 50 ml polyethylene bottles and immediately diluted by a factor of 10 using Milli-Q water;
- for the chemical analysis of the other trace elements, such as B, Sr, Li, Ba, Mn, Fe, Al, Cs, Rb, Ge, As, Nd, Ag, Cd, Co, Cr, Cu, Ni, Pb and Zn, as well as for the isotopic Li and Sr analyses, the water samples were filtered at 0.2 µm, then acidified using Suprapur $HNO_3$ and collected in 50 ml polyethylene bottles;
- for the isotopic analysis of B, the water samples were filtered at 0.45 µm, then acidified using Suprapur $HNO_3$ and collected in 1 l polyethylene bottles;
- untreated fluid samples for the isotopic analysis of D and $^{18}O$ in the water and of $^{13}C$ in the carbon dioxide were collected in 100 ml and 1 l polyethylene bottles, respectively;

- for the isotopic analysis of $^{18}O$ in the dissolved sulphate, cadmium acetate was added to the water samples collected in 1 l polyethylene bottles.
-

### 3.3.2 Analytical results

All the chemical analyses for both major and trace elements in the collected water samples were done in the BRGM laboratories using standard water analysis techniques such as Ion Chromatography, Inductively Coupled Plasma-Atomic Emission Spectroscopy (ICP-AES), Inductively Coupled Plasma-Mass Spectrometry (ICP-MS), Flame Emission Spectrophotometry, TIC analysis and Colorimetry. The chemical analysis results, for which the analytical precision is better than ± 5% for the major elements and ± 10% for the trace elements, are given in tables 3.3.2.1 and 3.3.2.2. Except for Los Azufres 2 water sample (pH = 3.22), the ion balance (I. B.) values (tabl. 3) traduce a good quality of the major specie analyses.

The isotopic analyses of the water samples ($\delta D$ and $\delta^{18}O$ of the water, $\delta^{18}O$ of the dissolved sulphate, plus the $\delta^{7}Li$, $\delta^{11}B$, $^{87}Sr/^{86}Sr$) were also performed in the BRGM laboratories using Thermo Ionization Mass Spectrometry and Neptune Multi Collector ICP-MS. More details relative to the BRGM analytical procedures are given in Millot *et al.* (2011). The isotopic analysis results are given in table 3.3.2.3.

The absolute uncertainty for the analyses of $\delta D$ and $\delta^{18}O$ in the water samples was ± 0.8‰ and ± 0.1‰, respectively. The absolute uncertainty for the $\delta^{18}O$ analyses of the dissolved sulphate was ± 0.1‰. The external reproducibility of the $\delta^{7}Li$ and $\delta^{11}B$ analyses was estimated at around ± 0.5‰ and ± 0.3‰, respectively, and the in-run precision of the $^{87}Sr/^{86}Sr$ ratio was generally better than ± 10 x $10^{-6}$ ($2\sigma_m$).

All the geochemical data obtained during this study have been uploaded and stored in the GEMEX Open Access Database (OADB), as well as the required information.

| Area | Sampling point | Date | T | Cond. 25°C | pH | Eh | Na | K | Ca | Mg | Alk. | Cl | $SO_4$ | $NO_3$ | $SiO_2$ | TDS | I.B. |
|---|---|---|---|---|---|---|---|---|---|---|---|---|---|---|---|---|---|
| | | | °C | µS/cm | | mV | mg/l | mg/l | mg/l | mg/l | mg/l $HCO_3$ | mg/l | mg/l | mg/l | mg/l | g/l | % |
| *Los Humeros area* | **Los Humeros H-39** | 22/03/2018 12:00 | 61.9 | 591 | 7.14 | -260 | 119 | 23.8 | < 0.5 | < 0.5 | 268 | 46.5 | 2.3 | < 0.5 | 745 | 1.20 | 0.31 |
| | **Los Humeros Unit-11 (fluid mixing)** | 22/03/2018 12:50 | 52.7 | 1294 | 7.00 | -240 | 270 | 36.9 | 2.2 | < 0.5 | 307 | 98.8 | 227 | < 0.5 | 733 | 1.68 | 2.37 |
| | **Los Humeros H-56** | 22/03/2018 13:25 | 74.1 | 1196 | 7.58 | -346 | 244 | 38.4 | 1.0 | < 0.5 | 383 | 147 | 63.6 | < 0.5 | 931 | 1.81 | 1.31 |
| | **Los Humeros H-49** | 22/03/2018 13:55 | 68.0 | 1051 | 7.70 | -270 | 212 | 35.8 | 1.1 | < 0.5 | 305 | 129 | 86.1 | < 0.5 | 834 | 1.60 | -0.71 |
| | **Los Humeros H-9** | 22/03/2018 15:05 | 66.8 | 752 | 7.17 | -295 | 146 | 30.9 | < 0.5 | < 0.5 | 283 | 69.5 | 39.0 | 0.8 | 538 | 1.11 | 0.41 |
| | **Los Humeros H-32** | 22/03/2018 15:35 | 67.8 | 595 | 6.67 | -235 | 82.6 | 12.4 | 2.6 | < 0.5 | 95 | 86.1 | 6.3 | < 0.5 | 567 | 0.85 | -1.68 |
| | **Los Humeros H-55** | 22/03/2018 16:08 | 68.9 | 254 | 7.55 | -335 | 34.4 | 5.6 | < 0.5 | < 0.5 | 51 | 38.4 | 13.8 | < 0.5 | 155 | 0.30 | 1.51 |
| | **El Tesoro** | 23/03/2018 09:30 | 22.5 | 787 | 7.49 | 220 | 84.6 | 11.0 | 34.5 | 30.2 | 369 | 63.9 | 12.0 | 7.9 | 78.3 | 0.69 | -0.71 |
| | **Noria Nuevo Pizarro** | 23/03/2018 11:45 | 16.0 | 2090 | 8.82 | 130 | 410 | 46.3 | 17.4 | 18.0 | 684 | 240 | 115 | 43.0 | 47.9 | 1.62 | 1.47 |
| | **Virgen del Carmen** | 23/03/2018 15:46 | 19.1 | 2080 | 7.10 | 205 | 85.3 | 8.2 | 273 | 107 | 755 | 99.1 | 557 | 2.3 | 91.0 | 1.98 | -1.45 |
| | **Pozo de Tepeyahualco** | 24/03/2018 10:10 | 23.8 | 4970 | 6.75 | -50 | 659 | 30.9 | 315 | 133 | 2056 | 775 | 0.6 | < 0.5 | 91.8 | 4.06 | 0.99 |
| | **Laguna de Atexcac** | 24/03/2018 14:15 | 22.0 | 12640 | 8.63 | 50 | 2022 | 92.7 | 16.6 | 604 | 1474 | 3854 | 264 | 5.7 | 68.7 | 8.40 | 1.78 |
| | **Laguna de Alchichica** | 23/03/2018 16:45 | 18.5 | 13250 | 9.07 | 106 | 2506 | 218 | 6.8 | 431 | 2547 | 3259 | 1088 | < 0.5 | 4.0 | 10.06 | -3.78 |
| | **Laguna de Quechulac** | 24/03/2018 16:30 | 20.4 | 894 | 8.73 | 160 | 82.1 | 7.7 | 16.7 | 62.3 | 412 | 90.7 | 19.5 | 1.0 | 14.6 | 0.71 | 0.04 |
| *Acoculco area* | **Los Azufres 1** | 26/03/2018 15:05 | 25.4 | 1489 | 6.41 | -355 | 147 | 29.3 | 104 | 28.7 | 463 | 36.0 | 353 | < 0.5 | 77.4 | 1.24 | -2.87 |
| | **Los Azufres 2** | 26/03/2018 16:00 | 19.2 | 693 | 3.22 | -51 | 12.8 | 8.2 | 23.0 | 6.0 | < 10 | 0.7 | 225 | < 0.5 | 75.3 | 0.35 | -43.53 |
| | **Los Azufres 3** | 28/03/2018 09:45 | 26.6 | 1735 | 7.94 | -140 | 210 | 33.7 | 153 | 46.5 | 463 | 52.0 | 644 | < 0.5 | 56.1 | 1.66 | -2.37 |
| | **Jicolapa** | 27/03/2018 09:45 | 30.7 | 1372 | 6.31 | -241 | 31.7 | 15.1 | 278 | 13.4 | 958 | 7.6 | 4.3 | < 0.5 | 152 | 1.46 | 4.76 |
| | **El Rincon** | 27/03/2018 11:00 | 26.6 | 550 | 5.67 | 110 | 12.3 | 12.0 | 90.7 | 5.2 | 291 | 2.3 | 48.4 | < 0.5 | 140 | 0.60 | -0.22 |
| | **Baños de Quetzalapa** | 27/03/2018 16:00 | 30.0 | 1964 | 6.37 | 135 | 150 | 16.8 | 291 | 37.4 | 1436 | 16.1 | 0.8 | < 0.5 | 114 | 2.06 | 2.47 |
| | **Baños de Chignahuapan** | 28/03/2018 07:30 | 49.0 | 1448 | 6.51 | -271 | 93.0 | 14.2 | 191 | 25.9 | 756 | 115 | 26.5 | < 0.5 | 44.1 | 1.27 | -0.34 |

*Table 3.3.2.1 - Chemical composition (major species) of the geothermal and thermal waters collected during the campaign carried out by BRGM between March 22 and 28, 2018, in the Los Humeros and Acoculco geothermal areas.*

| Area | Sampling point | Date | T | $NH_4$ | $PO_4$ | F | B | Br | Sr | Ba | Mn | Li | Rb | Cs | Ge | Al | As | Fe | W | Ag | Cu | Zn | Ni | Pb | Co | Cd | U |
|---|---|---|---|---|---|---|---|---|---|---|---|---|---|---|---|---|---|---|---|---|---|---|---|---|---|---|---|
| | | | °C | mg/l | mg/l | mg/l | mg/l | µg/l | µg/l | µg/l | µg/l | µg/l | µg/l | µg/l | µg/l | µg/l | µg/l | µg/l | µg/l | µg/l | µg/l | µg/l | µg/l | µg/l | µg/l | µg/l | µg/l |
| *Los Humeros area* | **Los Humeros H-39** | 22/03/2018 12:00 | 61.9 | 0.11 | 0.67 | 13.4 | 951 | 32.0 | 1.52 | 0.71 | 7.05 | 397 | 240 | 305 | 60.1 | 4193 | 42323 | 38 | 86.5 | < 0.01 | < 0.1 | 1.96 | 0.35 | < 0.05 | < 0.05 | 0.06 | < 0.01 |
| | **Los Humeros Unit-11 (fluid mixing)** | 22/03/2018 12:50 | 52.7 | 0.15 | 0.70 | 20.6 | 1819 | 73.7 | 41.2 | 5.92 | 25.9 | 619 | 315 | 330 | 56.0 | 3310 | 21721 | 90 | 85.4 | 0.02 | < 0.1 | 0.32 | 0.65 | < 0.05 | < 0.05 | < 0.01 | < 0.01 |
| | **Los Humeros H-56** | 22/03/2018 13:25 | 74.1 | 5.51 | 0.84 | 4.2 | 256 | 90.9 | 11.0 | 1.06 | 18.7 | 871 | 392 | 705 | 47.6 | 2042 | 8077 | 110 | 84.5 | < 0.01 | 0.53 | 0.42 | 0.65 | 0.07 | < 0.05 | 0.01 | < 0.01 |
| | **Los Humeros H-49** | 22/03/2018 13:55 | 68.0 | 3.59 | 0.33 | 4.0 | 593 | 94.9 | 16.2 | 1.08 | 8.66 | 676 | 259 | 370 | 46.3 | 2362 | 3838 | 38 | 103 | < 0.01 | 0.16 | 0.46 | 0.48 | < 0.05 | < 0.05 | < 0.01 | < 0.01 |
| | **Los Humeros H-9** | 22/03/2018 15:05 | 66.8 | 5.33 | 1.15 | 7.0 | 1459 | 56.8 | 2.09 | 0.64 | 19.9 | 1182 | 178 | 122 | 8.0 | 2430 | 5E+05 | 105 | 22.9 | < 0.01 | 0.77 | 0.69 | 0.65 | < 0.05 | < 0.05 | < 0.01 | < 0.01 |
| | **Los Humeros H-32** | 22/03/2018 15:35 | 67.8 | 0.14 | 0.15 | 9.3 | 1447 | < 10 | 38.6 | 12.1 | 22.9 | 394 | 99.6 | 94.8 | 21.0 | 1925 | 54597 | 58 | 23.4 | < 0.01 | 0.20 | 0.39 | 0.70 | < 0.05 | < 0.05 | 0.06 | < 0.01 |
| | **Los Humeros H-55** | 22/03/2018 16:08 | 68.9 | 10.8 | 0.16 | 1.3 | 43.20 | 22.8 | 6.03 | 1.58 | 23.1 | 131 | 38.3 | 52.2 | 7.89 | 245 | 3379 | 22 | 9.93 | 0.10 | < 0.1 | 0.47 | 0.33 | < 0.05 | < 0.05 | 0.10 | < 0.01 |
| | **El Tesoro** | 23/03/2018 09:30 | 22.5 | < 0.05 | 0.17 | 0.4 | 1.267 | 153 | 237 | 41.6 | < 0.1 | 121 | 22.1 | < 0.5 | < 0.5 | 2.49 | 2.37 | < 20 | 0.20 | < 0.01 | < 0.1 | 0.17 | < 0.1 | < 0.05 | < 0.05 | 0.01 | 0.97 |
| | **Noria Nuevo Pizarro** | 23/03/2018 11:45 | 16.0 | < 0.05 | 14.58 | 1.5 | 2.711 | 568 | 230 | 61.1 | 1.7 | 421 | 22.6 | < 0.5 | < 0.5 | 2.60 | 32.8 | < 20 | 1.25 | < 0.01 | 2.58 | 2.31 | 2.98 | 0.08 | 0.73 | 0.33 | 2.62 |
| | **Virgen del Carmen** | 23/03/2018 15:46 | 19.1 | 0.51 | < 0.05 | 0.8 | 1.493 | 244 | 2488 | 91.3 | 132 | 108 | 13.3 | < 0.5 | < 0.5 | 1.61 | 3.05 | < 20 | < 0.05 | < 0.01 | 0.40 | 1.45 | 0.26 | < 0.05 | < 0.05 | 0.65 | 0.03 |
| | **Pozo deTepeyahualco** | 24/03/2018 10:10 | 23.8 | 0.27 | < 0.05 | 1.1 | 19.79 | 1139 | 3112 | 6110 | 311 | 1787 | 49.3 | 7.39 | < 0.5 | 4.41 | 137 | 8118 | 0.14 | 0.01 | < 0.1 | 2.24 | 1.93 | < 0.05 | 0.78 | 0.28 | 0.25 |
| | **Laguna de San Luis Atexca** | 24/03/2018 14:15 | 22.0 | 0.27 | < 0.05 | 0.5 | 65.56 | 5429 | 105 | 16.4 | 13.8 | 2667 | 104 | 21.9 | < 0.5 | 6.50 | 93.8 | < 20 | 0.32 | 0.01 | 0.31 | 0.22 | 0.76 | 0.05 | 0.07 | 0.12 | 0.17 |
| | **Laguna de Alchichica** | 23/03/2018 16:45 | 18.5 | 0.49 | < 0.05 | < 1 | 39.89 | 4822 | 31.9 | 14.2 | 5.03 | 2460 | 305 | 1.3 | < 0.5 | 7.49 | 114 | < 20 | 1.59 | 0.01 | 0.18 | 0.57 | 0.23 | < 0.05 | < 0.05 | 0.98 | 1.92 |
| | **Laguna de Quechulac** | 24/03/2018 16:30 | 20.4 | 0.11 | < 0.05 | 0.5 | 0.561 | 158 | 89.6 | 21.6 | 8.22 | 2.87 | 7.61 | < 0.5 | < 0.5 | 5.06 | 3.48 | < 20 | < 0.05 | < 0.01 | 1.33 | 0.23 | < 0.1 | < 0.05 | < 0.05 | 0.42 | 0.92 |
| *Acoculco area* | **Los Azufres 1** | 26/03/2018 15:05 | 25.4 | 14.04 | 1.13 | 0.2 | 253 | 52.7 | 1732 | 39.2 | 1219 | 38.6 | 66.8 | 2.39 | 3.99 | 40.1 | 135 | 42 | 0.45 | < 0.01 | < 0.1 | 1.12 | 0.17 | < 0.05 | < 0.05 | 0.02 | < 0.01 |
| | **Los Azufres 2** | 26/03/2018 16:00 | 19.2 | < 0.05 | < 0.05 | 0.5 | 1.444 | < 10 | 133 | 24.3 | 1160 | 6.47 | 19.3 | < 0.5 | < 0.5 | 12762 | 24.3 | 8284 | < 0.05 | < 0.01 | 0.18 | 105 | 5.81 | 0.18 | 5.31 | 0.04 | 0.01 |
| | **Los Azufres 3** | 28/03/2018 09:45 | 26.6 | 7.66 | 2.39 | 0.3 | 354 | 74.6 | 2500 | 114 | 2258 | 81.3 | 71.3 | 2.14 | 5.53 | 69.5 | 8421 | 70 | 1.09 | < 0.01 | 1.01 | 1.37 | 2.43 | 0.09 | 0.9 | 0.07 | 0.08 |
| | **Jicolapa** | 27/03/2018 09:45 | 30.7 | 0.81 | 0.08 | 0.7 | 1.915 | 20.7 | 1242 | 311 | 179 | 95.3 | 58.3 | 5.99 | 1.07 | 6.08 | 1.37 | 70 | < 0.05 | < 0.01 | 0.24 | 0.78 | 0.18 | < 0.05 | < 0.05 | 1.19 | < 0.01 |
| | **El Rincon** | 27/03/2018 11:00 | 26.6 | 0.49 | < 0.05 | 0.5 | 0.124 | 33.3 | 424 | 159 | 120 | 13.2 | 33.8 | 1.81 | < 0.5 | 6.54 | 13.3 | 2854 | < 0.05 | < 0.01 | 0.23 | 3.49 | 0.23 | < 0.05 | 0.11 | 0.08 | < 0.01 |
| | **Baños de Quetzalapa** | 27/03/2018 16:00 | 30.0 | 1.01 | < 0.05 | 0.4 | 2.240 | 44.3 | 1070 | 726 | 132 | 138 | 31.3 | 11.9 | 2.6 | 1.20 | 1.25 | < 20 | < 0.05 | < 0.01 | 0.14 | 0.23 | < 0.1 | < 0.05 | < 0.05 | 0.15 | < 0.01 |
| | **Baños de Chignahuapan** | 28/03/2018 07:30 | 49.0 | 0.57 | < 0.05 | 0.8 | 3.076 | 182 | 691 | 147 | 27.2 | 374 | 63.9 | 63.1 | 0.98 | 25.8 | 24.1 | 311 | 0.14 | < 0.01 | 0.17 | 0.89 | 0.18 | < 0.05 | < 0.05 | 0.03 | 0.05 |

*Table 3.3.2.2 - Chemical composition (minor and trace species) of the geothermal and thermal waters collected during the campaign carried out by BRGM between March 22 and 28, 2018, in the Los Humeros and Acoculco geothermal areas.*

| Area | Sampling point | Date | T | $\delta D$ | $\delta^{18}O$ | $\delta^{18}O_{SO4}$ | $\delta^7Li$ | $\delta^{11}B$ | $^{87}Sr/^{86}Sr$ |
|---|---|---|---|---|---|---|---|---|---|
| | | | °C | ‰ | ‰ | ‰ | ‰ | ‰ | |
| *Los Humeros area* | **Los Humeros H-39** | 22/03/2018 12:00 | 61.9 | -63.8 | -1.2 | 9.3 | | | |
| | **Los Humeros Unit-11 (fluid mixing)** | 22/03/2018 12:50 | 52.7 | -45.9 | 1.5 | 4.0 | | -2.50 | |
| | **Los Humeros H-56** | 22/03/2018 13:25 | 74.1 | -61.6 | -1.1 | 1.2 | 7.2 | -2.23 | 0.704310 |
| | **Los Humeros H-49** | 22/03/2018 13:55 | 68.0 | -58.3 | -0.3 | 0.9 | | -0.74 | |
| | **Los Humeros H-9** | 22/03/2018 15:05 | 66.8 | -53.1 | 1.2 | 3.4 | | | |
| | **Los Humeros H-32** | 22/03/2018 15:35 | 67.8 | -61.5 | -0.9 | 4.8 | 2.3 | -2.52 | 0.704283 |
| | **Los Humeros H-55** | 22/03/2018 16:08 | 68.9 | -51.3 | 0.5 | 5.2 | | | |
| | **El Tesoro** | 23/03/2018 09:30 | 22.5 | -79.3 | -11.1 | 3.7 | | | |
| | **Noria Nuevo Pizarro** | 23/03/2018 11:45 | 16.0 | -38.4 | -5.1 | 4.3 | | | |
| | **Virgen del Carmen** | 23/03/2018 15:46 | 19.1 | -87.2 | -11.9 | 3.4 | 12.4 | | 0.707095 |
| | **Pozo de Tepeyahualco** | 24/03/2018 10:10 | 23.8 | -73.7 | -9.4 | | 8.9 | 8.55 | 0.706862 |
| | **Laguna de Atexcac** | 24/03/2018 14:15 | 22.0 | -23.4 | 0.0 | 11.8 | 10.1 | 6.49 | 0.706864 |
| | **Laguna de Alchichica** | 23/03/2018 16:45 | 18.5 | -12.2 | 1.0 | 17.7 | | | |
| | **Laguna de Quechulac** | 24/03/2018 16:30 | 20.4 | -30.0 | -1.4 | | | | |
| *Acoculco area* | **Los Azufres 1** | 26/03/2018 15:05 | 25.4 | -69.5 | -8.1 | 4.7 | 44.8 | -4.42 | 0.705065 |
| | **Los Azufres 2** | 26/03/2018 16:00 | 19.2 | -62.1 | -8.4 | | | | 0.704778 |
| | **Los Azufres 3** | 28/03/2018 09:45 | 26.6 | -29.8 | 0.1 | 5.6 | | -5.61 | 0.705045 |
| | **Jicolapa** | 27/03/2018 09:45 | 30.7 | -67.5 | -10.0 | 5.3 | 4.9 | -6.79 | 0.707262 |
| | **El Rincon** | 27/03/2018 11:00 | 26.6 | -68.3 | -10.1 | | 5.1 | | 0.707114 |
| | **Baños de Quetzalapa** | 27/03/2018 16:00 | 30.0 | -64.2 | -9.1 | 6.5 | 5.5 | -1.20 | 0.706804 |
| | **Baños de Chignahuapan** | 28/03/2018 07:30 | 49.0 | -70.8 | -10.1 | 6.0 | 4.7 | -0.17 | 0.706272 |

*Table 3.3.2.3 - Isotopic composition of the geothermal and thermal waters collected during the campaign carried out by BRGM between March 22 and 28, 2018, in the Los Humeros and Acoculco geothermal areas.*

## 3.4 Data interpretation and discussion

### 3.4.1 Los Humeros high-temperature geothermal waters

#### *a) Chemical characteristics of the fluids*

The geothermal Na-$HCO_3$-Cl waters discharged from Los Humeros wells (fig. 3.4.1.1), completely deleted in calcium and magnesium, enriched in silica (fig. 3.4.1.2) and boron (among the highest ones in the world), with TDS and pH values ranging from 0.3 to 1.8 g/l and 6.67 to 7.58, respectively, traduce a high interaction process with the reservoir rocks, at high temperature.

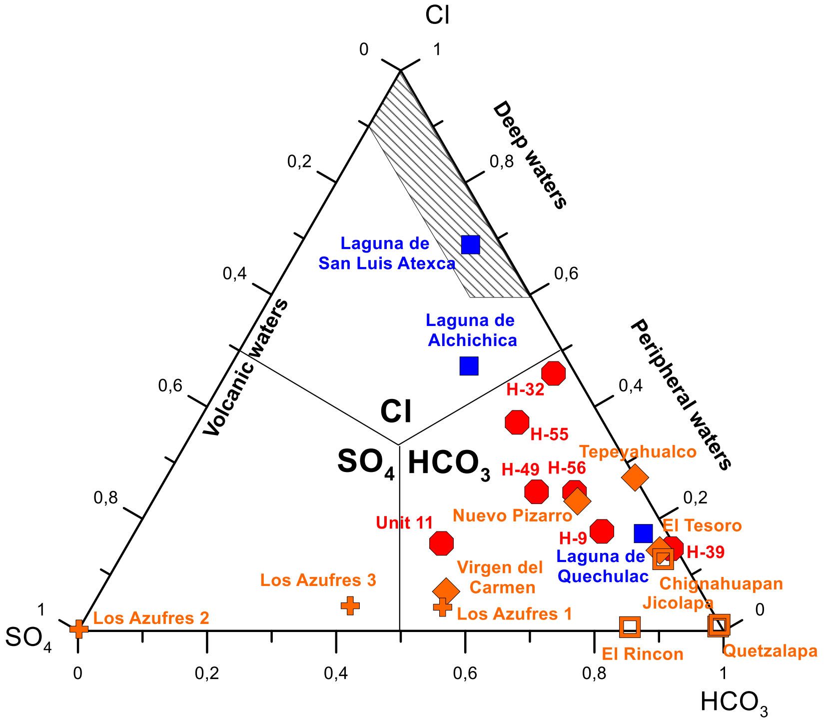


*Figure 3.4.1.1 - Position of the geothermal and thermal waters collected in the Los Humeros and Acoculco areas in the Cl-$HCO_3$-$SO_4$ ternary diagram of Giggenbach (1988).*

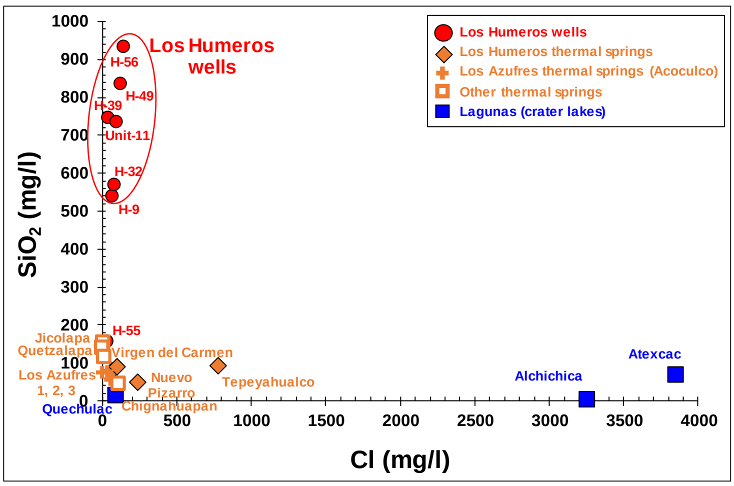


*Figure 3.4.1.2 - Diagram $SiO_2$ - Cl for the geothermal and thermal waters collected in the Los Humeros and Acoculco areas.*

***b) Water origin***

The isotopic δD and $\delta^{18}O$ values for the Los Humeros wells show a wide dispersion probably related to boiling, mixing, phase separation and condensation phenomema (fig. 3.4.1.3). The high values of $\delta^{18}O_{H2O}$ of the geothermal waters towards the right of the Global Meteoric Water Line (GMWL) are not only in concordance with high-temperature values, but also suggest a low water-rock ratio of the geothermal reservoir, when compared with the lower values observed in the Krafla geothermal field, in North-Iceland (tabl. 3.4.1.1), where the fluids are also biphasic, but the water-rock ratio is much higher. This is in agreement with a reservoir consisting of medium- to low-permeability pre-caldera andesites.

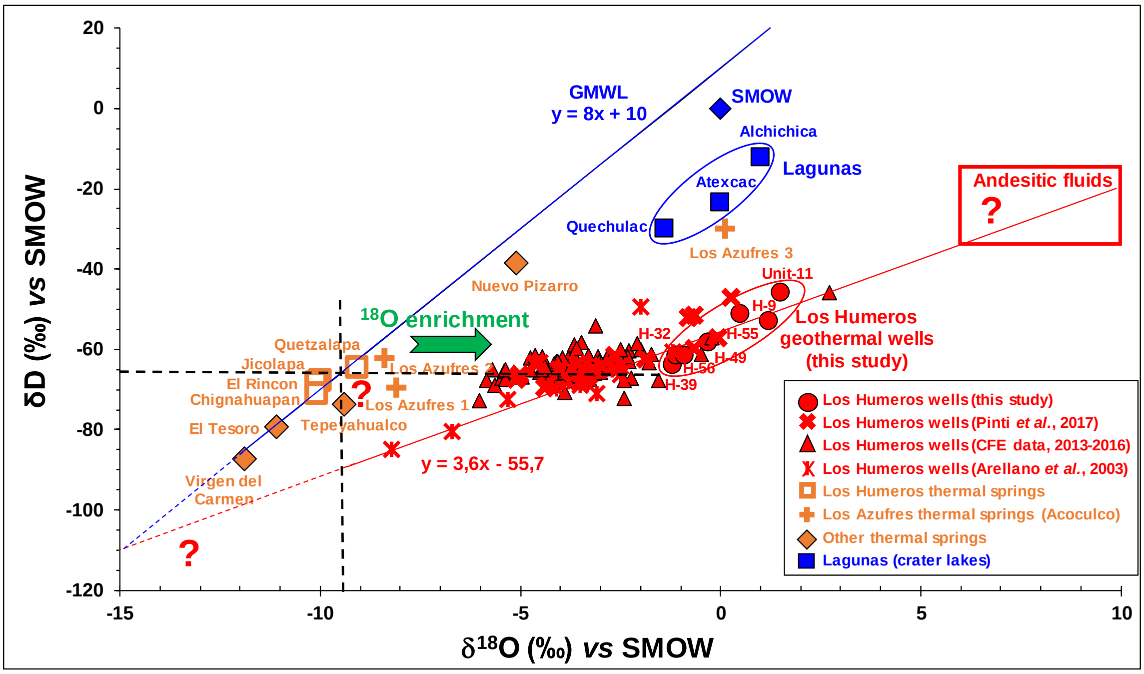


*Figure 3.4.1.3 - Diagram δD - $\delta^{18}O$ for the geothermal and thermal waters collected in the Los Humeros and Acoculco areas.*

According to Arrellano *et al.* (2003) and Barragán *et al.* (2010), the isotopic composition of the water molecule would be dominated by two main processes.

The first process would be a mixing of recharge meteoric water with a deep fluid-type andesitic water (δD ≈ -20‰ and $\delta^{18}O$ ≈ 6‰), as defined by Giggenbach (1992), leading to a positive correlation between δD and $\delta^{18}O$, with a slope close to 3.0. In this case, from the literature existing data, the intersection of the mixture line with the GMWL would result to vary from -14.5‰ to -11‰ for $\delta^{18}O$, and from -105‰ to -78.5‰ for δD (Portugal *et al.*, 2002; López-Romero, 2006; Barragán Reyes *et al.*, 2010; Bernard *et al.*, 2011). These values are lower than those measured for the meteoric waters in Los Humeros area (Oriental Basin), which are generally close to -10.7‰ for $\delta^{18}O$ and -77.3‰ for δD (Quijano *et al.*, 1981). From these values, the proportion of andesitic water was estimated to be between 25% and 50% (Portugal *et al.*, 2002; Barragán Reyes *et al.*, 2010; Bernard *et al.*, 2011).

The second process would be boiling and phase separation. At fluid temperatures higher than 220°C, $^{18}O$ is preferentially partitioned into the fluid phase, while deuterium is slightly partitioned into the vapor phase. The resulting fractionation scatters the points a few per mil perpendicular to the main mixing trend in the corresponding $\delta D$ - $\delta^{18}O$ diagram.
According to data from Verma *et al.* (1998), Arellano *et al.* (2003), Tello (2005) and Bernard (2008), the total geothermal fluid (steam + water) from Los Humeros is characterized by average values of $\delta D \approx$ -62‰ and $\delta^{18}O \approx$ -3‰.

Another assumption for the origin of the geothermal waters could be the contribution of meteoric water with a $\delta D$ value similar to that of the geothermal fluid, affected by a strong water-rock interaction process at high-temperature and low water-rock ratio, which enriches its $^{18}O$ content (up to 7-8‰). The wide dispersion observed for the isotopic values in the $\delta D$ - $\delta^{18}O$ diagram could be explained by different water-rock interaction factors and processes such as kinetic fractionation at temperatures close to boiling temperatures (Giggenbach and Stewart, 1982), with characteristic slopes of 3.0-3.5, and phase separation. In this case, the isotopic values for the meteoric water would be slightly heavier than those reported by Quijano *et al.* (1981) for the Los Humeros area, but they coincide with hydrologic studies that identify the main recharge to Los Humeros area from the Sierra Madre Oriental, with groundwater flow in a NE-SW direction (Prol-Ledesma, 1998). According to Cedillo Rodríguez (2000), recharge might also occur locally, from rainfall infiltrating the reservoir through its fault and fracture systems.

In this study, the data obtained for the water isotopic values are in the range of the previous data and it is difficult to give a preference about the different assumptions. According to the first assumption, the $\delta D$ and $\delta^{18}O$ values for the meteoric water were estimated to be close to -110‰ and -15‰, respectively (fig. 3.4.1.3). For the second assumption, these values would be rather close to -65‰ and -9.5‰, respectively (fig. 3.4.1.3). Other arguments and more information about the water recharge and origin of the Los Humeros geothermal waters would have to be probably proposed in the works carried out by other teams like CNR, within the framework of the task 4.3 of this project.

The Los Humeros geothermal waters are also characterized by high Cl/Br ratios with respect to the thermal waters (fig. 3.4.1.4), much higher than that of seawater, which could be partially explained by supply of Cl from the degassing magma chamber.

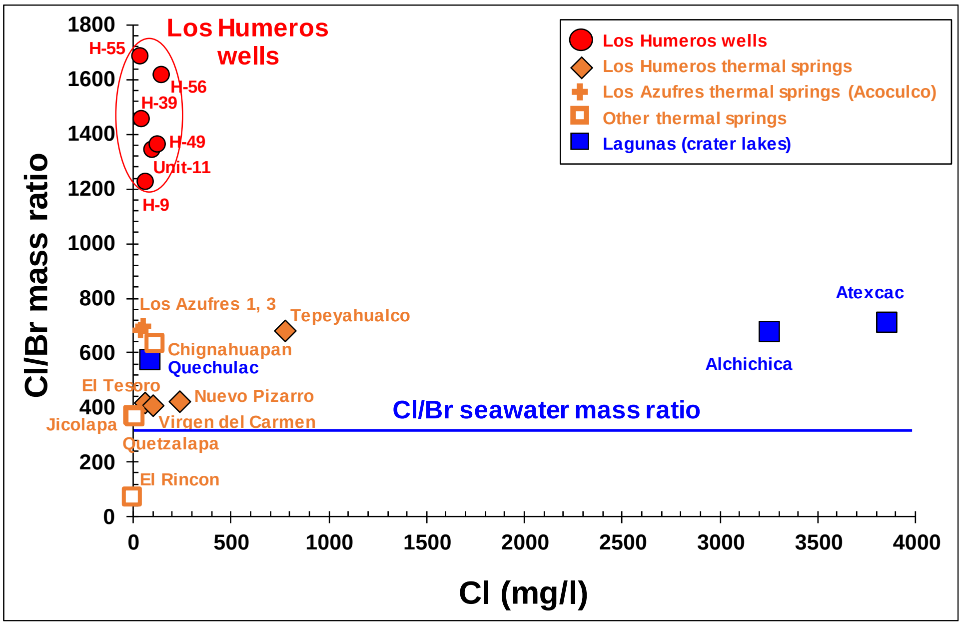


*Figure 3.4.1.4 - Diagram Cl/Br - Cl for the geothermal and thermal waters collected in the Los Humeros and Acoculco areas.*

## c) *Processes of water-rock-gas interaction*

The high boron concentrations of these geothermal waters (from 43 to 1819 mg/l; fig. 3.4.1.5) and their $\delta^{11}B$ values (-2.52 to -0.74‰; fig. 3.4.1.6) are close to those previously determined by Bernard *et al.* (2011), which range from 214 to 932 mg/l and from -1.7 to 0.3‰, respectively, and by Tello (2005) and Arellano *et al.* (2005), which vary from 118 to 3168 mg/l.

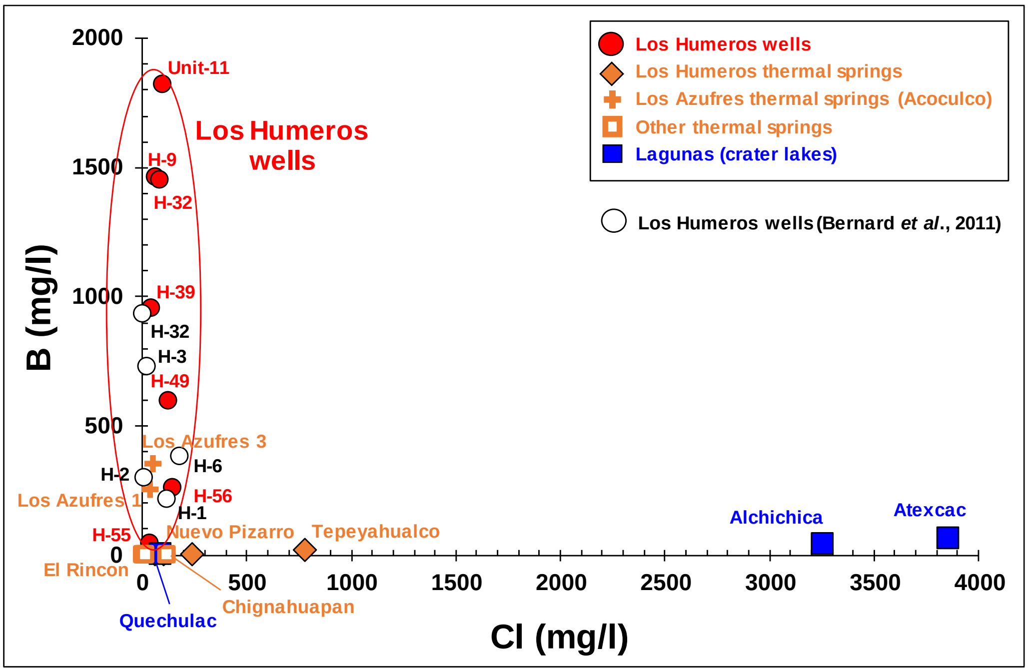


*Figure 3.4.1.5 - Diagram B - Cl for the geothermal and thermal waters collected in the Los Humeros and Acoculco areas.*

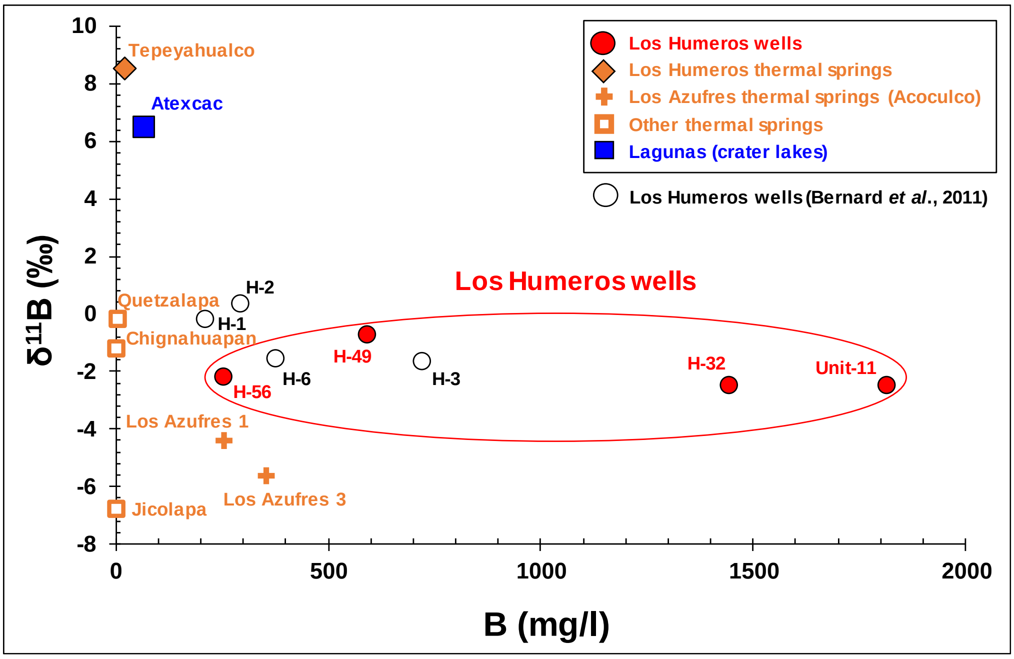


*Figure 3.4.1.6 - Diagram $\delta^{11}$B - B for the geothermal and thermal waters collected in the Los Humeros and Acoculco areas.*

High B concentrations as those observed for these geothermal waters are rare in the world (fig. 3.4.1.7). Natural hydrothermal solutions have generally B concentrations from 1 to 10 mg/l in high-temperature two-phase fluids from basaltic aquifers of Iceland such as Krafla, Nesjavellir, etc. (Arnórsson and Andrésdóttir, 1995; Aggarwal *et al.*, 2000; HITI-FP6 project, 2014).

B concentrations higher than 100 mg/l were only observed in fluids from aquifers composed of sedimentary and metamorphic rocks (Larderello, Italy; The Geysers, California; Ngahwa, New Zealand), of dacite-rhyolite volcanic rocks (Los Azufres, Mexico), and of marine carbonate and magmatic rocks, in the Yunnan-Tibet geothermal belt, in China.

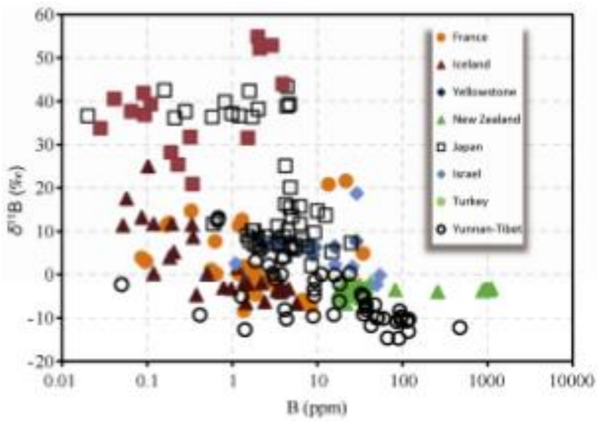


*Figure 3.4.1.7 - Diagram $\delta^{11}$B - B for worldwide geothermal waters (after Lü et al., 2014).*

In contrast, similar $\delta^{11}$B isotopic values (from -3.7 to -1.5‰) were observed in the high-temperature basaltic waters from Icelandic geothermal fields (Krafla, Nesjavellir, etc.; Aggarwal *et al.*, 2000; FP6-HITI project, 2010; tabl. 3.4.1.1) as well as in the Ngahwa

(Aggarwal *et al.*, 2003) and Lardarello (Pennisi *et al.*, 2001) geothermal fields. These values are lower for the Yunnan-Tibet thermal waters (-6.0 to -6.8‰; Lü *et al.*, 2014). Tonarini *et al.* (1998) suggest that $\delta^{11}B$ of exsolved fluids during tourmaline crystallization from pegmatites of the Elba Island could vary between -6 and -2‰ at temperatures ranging from 300 to 600°C. As a matter of fact, the $\delta^{11}B$ data related to the Tuscan magmatic Province show negligible variations. The restricted range in $\delta^{11}B$ values compared to the total concentration variations suggest that the B isotope ratios reflect differences in the $\delta^{11}B$ values of the rock rather than the results of secondary processes, such as phase separation or deposition of secondary minerals (Aggarwal *et al.*, 2000).

According to Arnórsson and Andrésdóttir (1995), the variable B and Cl concentrations and Cl/B ratios in high-temperature geothermal waters, as well as high B concentrations can be attributed to a combination of several processes. They include: i) supply of these elements from the degassing magma chamber, ii) supply from the rock with which the water interacts, and iii) phase separation in producing aquifers of wells.

Aggarwal *et al.* (2003) suggested a main source of B in Ngawha to be the greywacke wall rocks and the reason for such high B concentrations (up to 1000 mg/l) to be a lower water/rock ratio deduced from the high O isotope shift (+11‰) of deep water relative to the local meteoric water. Leeman *et al.* (2005) reported up to 240 mg/l in condensates of 300°C volcanic vapors from Vulcano, in Italy. They interpreted these values as the result of mixing of a magmatic endmember with about 70 mg/l of B and vapor derived from boiling of a modified seawater hot brine that was in contact with B-enriched Vulcano rhyolites and trachytes at low fluid/rock ratio.

The observed high B content and variable Cl concentrations in the Los Humeros geothermal waters could be the result of mixing of magmatic fluid from a deep magmatic chamber, the heat and fluid source for the system, leaching of wall rocks of the deep aquifer at a low fluid/rock ratio and phase separation process. Bernard *et al*. (2011) proposed a model based on the existence of deep acid brine to explain the B and Cl behavior in the geothermal fluids of the Los Humeros geothermal field.

| | | *Los Humeros field, Mexico (this study)* | | | | *Nesjavellir and Krafla fields, Iceland (FP6-HITI project; Sanjuan et al., 2014)* | | | | | | | | |
|---|---|---|---|---|---|---|---|---|---|---|---|---|---|---|
| **Well** | | **Unit-11 (fluid mixing)** | **H-39** | **H-49** | **H-56** | **NJ-16** | **NJ-10** | **NJ-14** | **NJ-16** | **NJ-19** | **KS-01** | **K-05** | **K-27** | **K-37** |
| **Parameters** | **Unit** | **22/03/2018** | **22/03/2018** | **22/03/2018** | **22/03/2018** | **11/06/2008** | **11/06/2008** | **11/06/2008** | **11/06/2008** | **11/06/2008** | **13/06/2008** | **13/06/2008** | **13/06/2008** | **12/06/2008** |
| **Cond. 25°C** | µS/cm | **1294** | **591** | **1051** | **1196** | **860** | **872** | **965** | **860** | **783** | **930** | **820** | **1087** | |
| **pH** | | 7.00 | 7.14 | 7.70 | 7.58 | 8.42 | 9.03 | 8.79 | 8.42 | 8.11 | 9.36 | 9.21 | 8.72 | |
| **Eh** | mV | -240 | -260 | -270 | -346 | -103 | -31 | -341 | -103 | -44 | -305 | -239 | -284 | |
| **Na** | mg/l | 270 | 119 | 212 | 244 | 145 | 157 | 161 | 145 | 126 | 175 | 180 | 206 | 268 |
| **K** | mg/l | 36.9 | 23.8 | 35.8 | 38.4 | 29.0 | 33.4 | 32.8 | 29.0 | 31.4 | 36.4 | 17.8 | 32.1 | 48.8 |
| **Ca** | mg/l | 2.2 | < 0.5 | 1.1 | 1.0 | < 0.5 | < 0.5 | < 0.5 | < 0.5 | < 0.5 | 0.34 | 8.83 | 3.13 | 1.46 |
| **Mg** | mg/l | < 0.5 | < 0.5 | < 0.5 | < 0.5 | 11.7 | < 0.5 | < 0.5 | 11.7 | < 0.5 | < 0.5 | < 0.5 | < 0.5 | < 0.5 |
| **Alk.** | mg/l $HCO_3$ | 307 | 268 | 305 | 383 | 296 | 257 | 159 | 296 | 128 | 400 | 162 | 237 | |
| **Cl** | mg/l | 98.8 | 46.5 | 129 | 147 | 69.7 | 129 | 193 | 69.7 | 162 | 76.1 | 45.0 | 39.2 | 64.7 |
| **$SO_4$** | mg/l | 227 | 2.3 | 86.1 | 63.6 | 90.5 | 81.6 | 44.0 | 90.5 | 35.9 | 40.6 | 248 | 296 | 130 |
| **$SiO_2$** | mg/l | 733 | 745 | 834 | 931 | 697 | 752 | 718 | 697 | 797 | 1001 | 361 | 538 | 1333 |
| **TDS** | g/l | **1.68** | **1.20** | **1.60** | **1.81** | **1.34** | **1.41** | **1.31** | **1.34** | **1.28** | **1.73** | **1.02** | **1.35** | **1.85** |
| **F** | mg/l | 20.6 | 13.4 | 4.0 | 4.2 | 1.25 | 1.57 | 1.11 | 1.25 | 1.13 | 1.68 | 0.89 | 0.98 | 2.72 |
| **B** | mg/l | 1819 | 951 | 593 | 256 | 1.82 | 1.52 | 1.76 | 1.82 | 3.77 | 2.68 | 0.54 | 0.56 | 2.38 |
| **Br** | µg/l | 73.7 | 32.0 | 94.9 | 90.9 | 200 | 500 | 700 | 200 | 600 | 200 | < 500 | < 500 | < 500 |
| **Sr** | µg/l | 41.2 | 1.52 | 16.2 | 11.0 | 3.0 | 2.5 | 2.3 | 3.0 | 2.0 | 2.1 | 29.3 | 15.5 | 14.1 |
| **Ba** | µg/l | 5.92 | 0.71 | 1.08 | 1.06 | 2.5 | 1.0 | 0.8 | 2.5 | 1.0 | 0.1 | 1.5 | 5.2 | 3.0 |
| **Mn** | µg/l | 25.9 | 7.05 | 8.66 | 18.7 | 0.6 | 1.0 | 0.6 | 0.6 | 0.5 | | 0.9 | 1.0 | 23.8 |
| **Li** | µg/l | 619 | 397 | 676 | 871 | 157 | 290 | 287 | 157 | 263 | 254 | 119 | 186 | 745 |
| **Rb** | µg/l | 315 | 240 | 259 | 392 | 96 | 140 | 198 | 96 | 108 | 209 | 138 | 167 | 273 |
| **Cs** | µg/l | 330 | 305 | 370 | 705 | 2.4 | 6.5 | 7.5 | 2.4 | 4.2 | 6.7 | 3.7 | 5.9 | 12.1 |
| **Ge** | µg/l | 56.0 | 60.1 | 46.3 | 47.6 | 59.8 | 60.6 | 39.6 | 59.8 | 42.7 | 39 | 34.6 | 34.2 | 49.0 |
| **As** | µg/l | 21721 | 42323 | 3838 | 8077 | 8.5 | 5.6 | 9.7 | 8.5 | 22 | 384 | 2.1 | 2.8 | 202 |
| **Zn** | µg/l | 0.32 | 1.96 | 0.46 | 0.42 | 1.1 | 0.6 | 0.8 | 1.1 | 1.1 | 0.6 | | | 4.2 |
| **Ni** | µg/l | 0.65 | 0.35 | 0.48 | 0.65 | 0.30 | 0.30 | 0.20 | 0.30 | 0.40 | 0.10 | 0.30 | 0.20 | 0.70 |
| **B/Cl** | molal ratio | 60 | 67 | 15 | 6 | 0.09 | 0.04 | 0.03 | 0.09 | 0.08 | 0.12 | 0.04 | 0.05 | 0.12 |
| **Na/K** | molal ratio | 12.5 | 8.5 | 10.1 | 10.8 | 8.5 | 8.0 | 8.4 | 8.5 | 6.8 | 8.2 | 17.2 | 10.9 | 9.3 |
| **Na/Li** | molal ratio | 132 | 90 | 95 | 84 | 279 | 163 | 170 | 279 | 145 | 208 | 458 | 334 | 108 |
| **Na/Rb** | molal ratio | 3190 | 1836 | 3047 | 2310 | 5620 | 4156 | 3029 | 5620 | 4343 | 3120 | 4860 | 4580 | 3647 |
| **Na/Cs** | molal ratio | 4735 | 2246 | 3317 | 1998 | 349560 | 139190 | 124346 | 349560 | 173665 | 151343 | 281880 | 201592 | 127947 |
| **K/Sr** | molal ratio | 2007 | 35086 | 4952 | 7822 | 21635 | 29940 | 31969 | 21635 | 35129 | 38842 | 1363 | 4642 | 7752 |
| **$\delta D$** | ‰ | -45.9 | -63.8 | -58.3 | -61.6 | -71.1 | -73.1 | -69.9 | -71.1 | -68.3 | -102.2 | | -79.9 | -58.9 |
| **$\delta^{18}O$** | ‰ | 1.5 | -1.2 | -0.3 | -1.1 | -5.4 | -5.7 | -5.8 | -5.4 | -3.9 | -6.3 | | -10.5 | -7.3 |
| **$\delta^{18}O_{SO4}$** | ‰ | 4.0 | 9.3 | 0.9 | 1.2 | -0.1 | 3.6 | | -0.1 | | | | -6.2 | -5.9 |
| **$\delta^7Li$** | ‰ | | | | 7.2 | 8.1 | 7.8 | 8.0 | 8.1 | 6.8 | 6.8 | 8.1 | 6.5 | 7.1 |
| **$\delta^{11}B$** | ‰ | -2.50 | | -0.74 | -2.23 | -2.68 | -2.19 | -3.37 | -2.68 | -2.84 | -5.45 | | -3.98 | |
| **$^{87}Sr/^{86}Sr$** | | | | | 0.704310 | 0.7036201 | 0.7034461 | 0.7035571 | 0.7036201 | 0.7035351 | 0.7034731 | 0.7032241 | 0.7032021 | |

*Table 3.4.1.1 - Comparison of water chemical and isotopic data obtained in three high-temperature (≥ 290°C) geothermal fields: Los Humeros in Mexico, and Krafla and Nesjavellir in North-Iceland.*

The low Sr concentrations and the $^{87}Sr/^{86}Sr$ ratios of these geothermal waters, ranging from 1.52 to 41.2 µg/l (fig. 3.4.1.8) and 0.704283 to 0.704310 (fig. 3.4.1.9), respectively, suggest these waters are in contact with andesite rocks in the reservoir, which is in good agreement with the well observations (Arellano *et al.*, 2003). Lower Sr isotopic values between 0.7032 and 0.7036 (FP6-HITI project, 2010) are observed for the high-temperature geothermal fluids from North-Iceland (Krafla, Nesjavellir, etc.) in contact with basalts in the reservoir (tabl. 3.4.1.1).

The high Li concentrations and the $\delta^7Li$ values of the Los Humeros geothermal waters, varying between 131 and 1182 mg/l, and between 2.3 ant 7‰ (tabl. 3.3.2.2 et 3.3.2.3), respectively, confirm that these waters interacts with volcanic rocks at high-temperatures. If the average Li concentrations are slightly higher than those observed in the high-temperature geothermal waters from the North-Iceland basaltic reservoirs (from 119 to 745 µg/l), the isotopic values are close (from 6.5 to 8.1‰; FP6-HITI project, 2014; tabl. 3.4.1.1). Note that the Cs concentrations analysed in the Los Humeros geothermal waters (from 52 to 705 µg/l) are much higher than those observed in the North-Icelandic geothermal dilute waters (from 2 to 12 µg/l) whereas the Rb concentrations are closer (FP6-HITI project, 2010; tabl. 3.4.1.1).

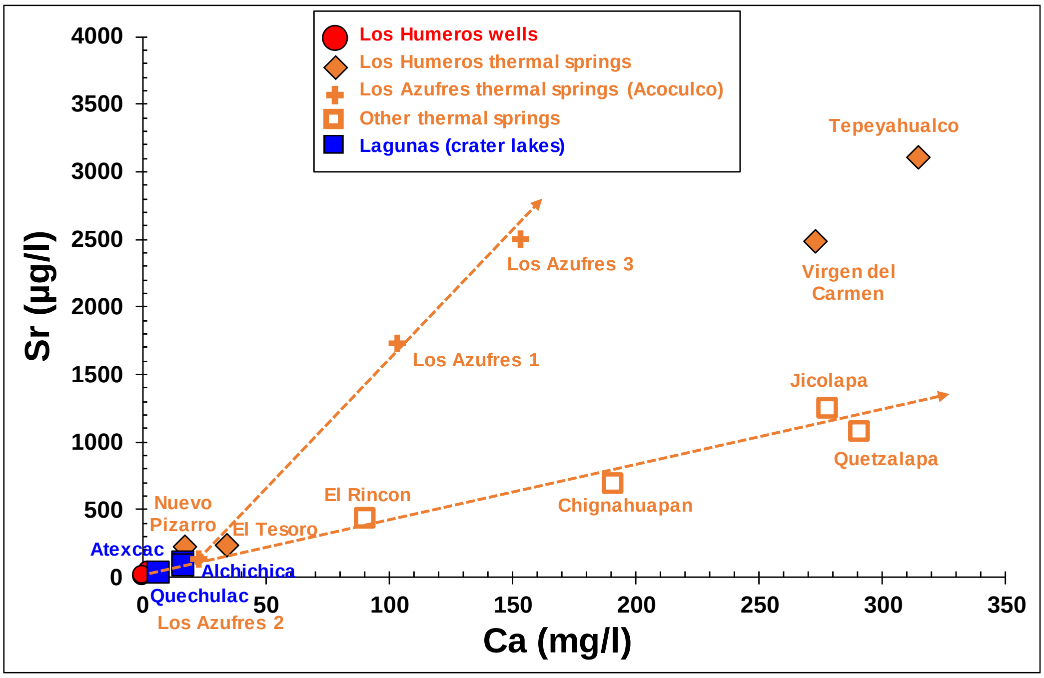


*Figure 3.4.1.8 - Diagram Sr - Ca for the geothermal and thermal waters collected in the Los Humeros and Acoculco areas.*

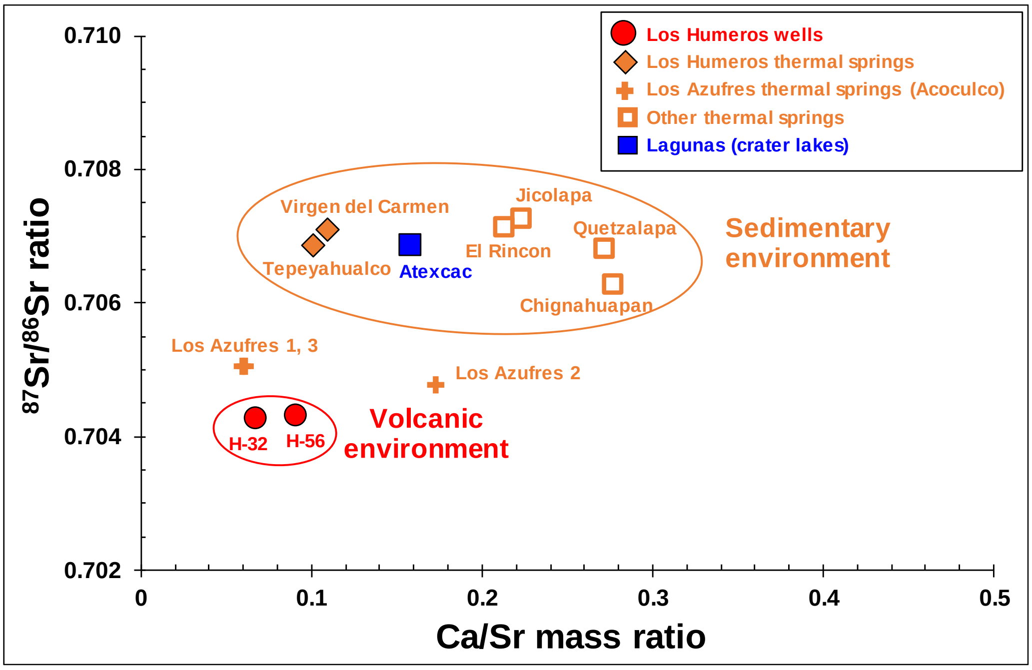


*Figure 3.4.1.9 - Diagram $^{87}Sr/^{86}Sr$ - Ca/Sr for the geothermal and thermal waters collected in the Los Humeros and Acoculco areas.*

***d) Geothermometry***

The Na-K-Mg ternary diagram from Giggenbach (1988) and the main classical geothermometers such as Silica-quartz, Na-K, Na-K-Ca and K-Ca, as well as the isotopic $\delta^{18}O_{H2O-SO4}$ geothermometric relationships established by Kusakabe and Robinson (1977) and Zeebe (2010), indicate that the full chemical equilibrium is reached for most of these waters at about 290 ± 30°C (fig. 3.4.1.10; tabl. 3.4.1.2 and 3.4.1.3). For the H-55 well, which has a very low fraction of liquid water, the temperature estimated using Silica-quartz is underestimated (163°C) because the concentration of dissolved silica is decreased by probable dilution of steam condensate. For the H-32, H-39 and H-55 water samples, the isotopic $\delta^{18}O_{H2O-SO4}$ geothermometer also gives underestimated temperature values (112 to 228°C), indicating that the isotope equilibrium conditions are not attained for these samples.

This temperature range is concordant with the presence of an upper liquid-dominated reservoir area, located in augite andesites, between 1025 and 1600 m a.s.l., with neutral pH at 290-330°C, suggested in numerous studies (Arellano *et al.*, 2003; Gutiérrez-Negrín and Izquierdo-Montalvo, 2010). The other deeper, two-phase, low-liquid saturation reservoir area, with high fractions of steam, is located in basalts and hornblende andesites, between 800 and 100 m a.s.l., with low pH fluids at temperatures of between 300 and 400°C.

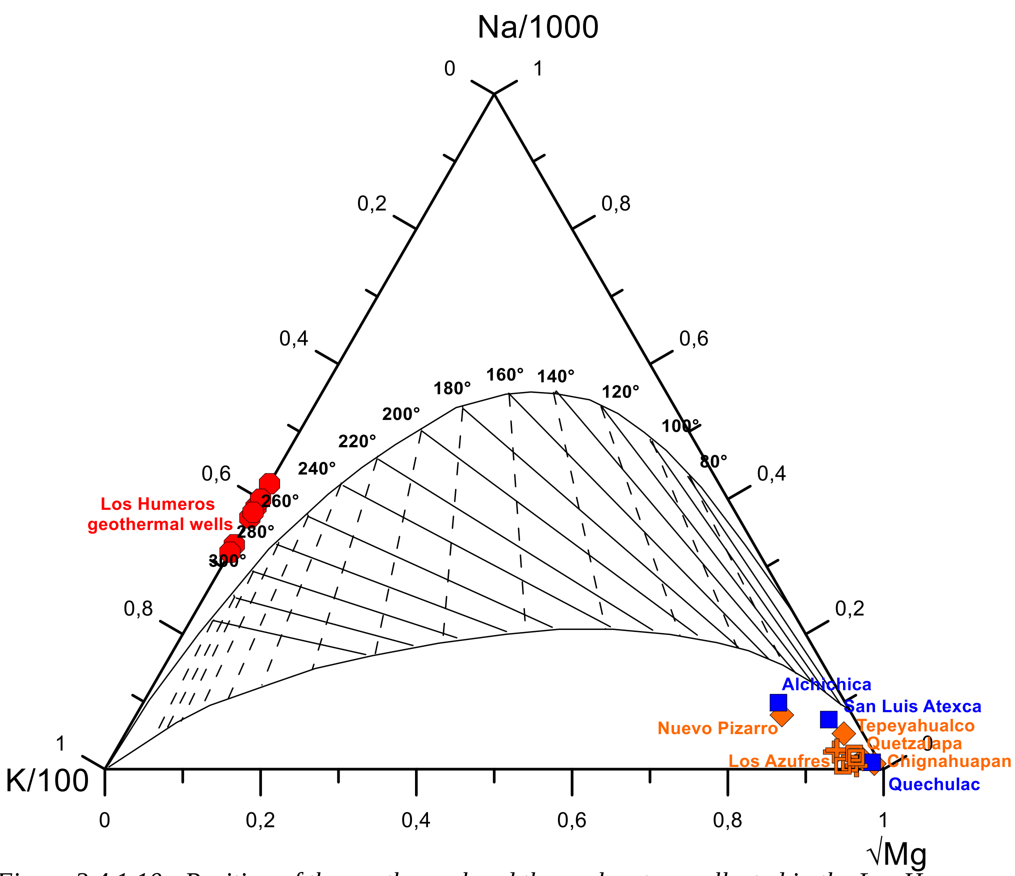


*Figure 3.4.1.10 - Position of the geothermal and thermal waters collected in the Los Humeros and Acoculco areas in the Na-K-Mg ternary diagram of Giggenbach (1988).*

| Area | Sampling point | Date | $T_{measured}$ °C | $T_{Qz}$ °C | $T_{Chalced.}$ °C | $T_{Na\text{-}K\,(1)}$ °C | $T_{Na\text{-}K\,(2)}$ °C | $T_{Na\text{-}K\,(3)}$ °C | $T_{Na\text{-}K\text{-}Ca\,(\beta=1/3)}$ °C | $T_{Na\text{-}K\text{-}Ca\,(\beta=4/3)}$ °C | $T_{Na\text{-}K\text{-}Ca\text{-}Mg}$ °C | $T_{K\text{-}Mg\,(1)}$ °C | $T_{K\text{-}Mg\,(2)}$ °C | $T_{Ca\text{-}K\,(1)}$ °C | $T_{Ca\text{-}K\,(2)}$ °C |
|---|---|---|---|---|---|---|---|---|---|---|---|---|---|---|---|
| ***Los Humeros area*** | **Los Humeros H-39** | 22/03/2018 12:00 | 61.9 | 292 | 297 | 284 | 284 | 294 | | | | | | | |
| | **Los Humeros Unit-11 (fluid mixing)** | 22/03/2018 12:50 | 52.7 | 304 | 312 | 233 | 245 | 258 | 231 | 264 | | | | 334 | 256 |
| | **Los Humeros H-56** | 22/03/2018 13:25 | 74.1 | 317 | 329 | 251 | 258 | 271 | 247 | 307 | | | | 386 | 293 |
| | **Los Humeros H-49** | 22/03/2018 13:55 | 68.0 | 320 | 334 | 260 | 266 | 278 | 248 | 292 | | | | 371 | 282 |
| | **Los Humeros H-9** | 22/03/2018 15:05 | 66.8 | 263 | 259 | 293 | 290 | 300 | | | | | | | |
| | **Los Humeros H-32** | 22/03/2018 15:35 | 67.8 | 265 | 261 | 244 | 254 | 267 | 210 | 165 | | | | 228 | 176 |
| | **Los Humeros H-55** | 22/03/2018 16:08 | 68.9 | 163 | 139 | 255 | 262 | 274 | | | | | | | |
| | ***El Tesoro (existing data)*** | *17/11/2016* | *23.0* | *114* | *83* | *221* | *235* | *250* | *172* | *80* | *13* | *54* | *23* | *131* | *99* |
| | **El Tesoro** | 23/03/2018 09:30 | 22.5 | 124 | 95 | 227 | 240 | 254 | 177 | 88 | 11 | 56 | 26 | 141 | 107 |
| | ***Nuevo Pizarro well (existing data)*** | *09/11/2016* | *17.0* | *97* | *65* | *189* | *210* | *226* | *182* | *142* | *24* | *80* | *56* | *194* | *150* |
| | **Noria Nuevo Pizarro** | 23/03/2018 11:45 | 16.0 | 100 | 68 | 210 | 227 | 242 | 206 | 196 | 30 | 97 | 77 | 257 | 198 |
| | **Virgen del Carmen** | 23/03/2018 15:46 | 19.1 | 132 | 104 | 193 | 213 | 229 | 145 | 39 | 34 | 37 | 4 | 83 | 59 |
| | **Pozo deTepeyahualco** | 24/03/2018 10:10 | 23.8 | 133 | 104 | 129 | 159 | 178 | 142 | 97 | 33 | 62 | 34 | 137 | 104 |
| ***Acoculco area*** | ***Los Azufres (existing data)*** | *21-25/04/2006* | *21.4* | *84* | *51* | *334* | *320* | *327* | *207* | *83* | *85* | *74* | *48* | *144* | *110* |
| | ***Los Azufres (existing data)*** | *25/06/1986* | *25.0* | *81* | *48* | *305* | *299* | *308* | *207* | *101* | *58* | *78* | *53* | *163* | *125* |
| | ***Los Azufres (existing data)*** | *25/06/1986* | *25.0* | *70* | *36* | *207* | *224* | *240* | *177* | *106* | *36* | *72* | *56* | *158* | *121* |
| | **Los Azufres 1** | 26/03/2018 15:05 | 25.4 | 124 | 94 | 284 | 283 | 294 | 201 | 103 | 62 | 79 | 54 | 164 | 125 |
| | **Los Azufres 3** | 28/03/2018 09:45 | 26.6 | 107 | 76 | 253 | 260 | 273 | 192 | 104 | 53 | 77 | 51 | 161 | 123 |
| | ***Jicolapa (existing data)*** | *03/07/1986* | *32.0* | *116* | *86* | *462* | *407* | *403* | *218* | *50* | *149* | *70* | *43* | *112* | *83* |
| | **Jicolapa** | 27/03/2018 09:45 | 30.7 | 162 | 137 | 452 | 400 | 397 | 213 | 46 | 172 | 72 | 46 | 107 | 79 |
| | ***El rincon (existing data)*** | *19/06/1986* | *32.0* | *114* | *84* | *702* | *545* | *521* | *250* | *45* | *170* | *72* | *45* | *114* | *85* |
| | **El Rincon** | 27/03/2018 11:00 | 26.6 | 157 | 132 | 691 | 540 | 516 | 253 | 51 | 189 | 78 | 53 | 121 | 91 |
| | ***Baños de Quetzalapa (existing data)*** | *18/06/1986* | *32.0* | *105* | *74* | *216* | *231* | *246* | *168* | *74* | *59* | *62* | *33* | *124* | *93* |
| | **Baños de Quetzalapa** | 27/03/2018 16:00 | 30.0 | 145 | 118 | 209 | 226 | 241 | 161 | 62 | 97 | 63 | 34 | 110 | 82 |
| | ***Baños de Chignahuapan (existing data)*** | *02/07/1986* | *49.0* | *71* | *37* | *245* | *254* | *267* | *173* | *64* | *80* | *62* | *33* | *115* | *86* |
| | **Baños de Chignahuapan** | 28/03/2018 07:30 | 49.0 | 96 | 64 | 247 | 255 | 268 | 172 | 61 | 96 | 63 | 35 | 112 | 83 |
| | ***Agua salada (existing data)*** | *03/07/1986* | *21.0* | *128* | *99* | *254* | *261* | *274* | *213* | *165* | *51* | *99* | *81* | *230* | *178* |
| | ***Capulines (existing data)*** | *01/07/1986* | *20.0* | *105* | *73* | *310* | *303* | *312* | *202* | *86* | *9* | *57* | *38* | *146* | *111* |

$T_{Qz}$: Fournier (1977); $T_{Chalced.}$: Michard (1979)

Recommended value

$T_{Na\text{-}K\,(1)}$: Michard (1979); $T_{Na\text{-}K\,(2)}$: Fournier (1979); $T_{Na\text{-}K\,(3)}$: Giggenbach (1988).

$T_{Na\text{-}K\text{-}Ca}$: Fournier and Truesdell (1973).

$T_{Na\text{-}K\text{-}Ca\text{-}Mg}$: Fournier and Potter (1979).

$T_{K\text{-}Mg\,(1)}$: Giggenbach (1988); $T_{K\text{-}Mg\,(2)}$: Michard (1990).

$T_{Ca\text{-}K\,(1)}$: Fournier and Truesdell (1973); $T_{Ca\text{-}K\,(2)}$: Michard (1990).

*Table 3.4.1.2 - Classical chemical geothermometers applied on waters from the Los Humeros and Los Azufres geothermal areas.*

| Area | Sampling point | Date | $T^{18}O_{H2O\text{-}SO4\,(1)}$ °C | $T^{18}O_{H2O\text{-}SO4\,(2)}$ °C | $T^{18}O_{H2O\text{-}SO4\,(3)}$ °C | $T^{18}O_{H2O\text{-}SO4\,(4)}$ °C | $T^{18}O_{H2O\text{-}BaSO4}$ °C | $T^{18}O_{H2O\text{-}CaSO4\,(1)}$ °C | $T^{18}O_{H2O\text{-}CaSO4\,(2)}$ °C |
|---|---|---|---|---|---|---|---|---|---|
| ***Los Humeros area*** | **Los Humeros H-39** | 22/03/2018 12:00 | 176 | 171 | 112 | 113 | 138 | 186 | 194 |
| | **Los Humeros Unité 11 (fluid mixing)** | 22/03/2018 12:50 | 360 | 387 | 267 | 246 | 281 | 394 | 405 |
| | **Los Humeros H-56** | 22/03/2018 13:25 | 368 | 398 | 273 | 251 | 287 | 403 | 415 |
| | **Los Humeros H-49** | 22/03/2018 13:55 | 418 | 464 | 315 | 283 | 322 | 463 | 476 |
| | **Los Humeros H-9** | 22/03/2018 15:05 | 372 | 403 | 277 | 254 | 290 | 408 | 420 |
| | **Los Humeros H-32** | 22/03/2018 15:35 | 263 | 269 | 185 | 178 | 208 | 282 | 291 |
| | **Los Humeros H-55** | 22/03/2018 16:08 | 289 | 299 | 207 | 197 | 228 | 311 | 321 |
| | **El Tesoro** | 23/03/2018 09:30 | 126 | 117 | 69 | 74 | 96 | 132 | 139 |
| | **Noria Nuevo Pizarro** | 23/03/2018 11:45 | 192 | 189 | 125 | 126 | 151 | 204 | 212 |
| | **Virgen del Carmen** | 23/03/2018 15:46 | 121 | 112 | 65 | 70 | 92 | 127 | 134 |
| | **Pozo deTepeyahualco** | 24/03/2018 10:10 | | | | | | | |
| ***Acoculco area*** | **Los Azufres 1** | 26/03/2018 15:05 | 147 | 140 | 87 | 91 | 114 | 155 | 162 |
| | **Los Azufres 3** | 28/03/2018 09:45 | 268 | 275 | 189 | 182 | 212 | 287 | 297 |
| | **Jicolapa** | 27/03/2018 09:45 | 121 | 112 | 65 | 70 | 92 | 127 | 134 |
| | **El Rincon** | 27/03/2018 11:00 | | | | | | | |
| | **Baños de Quetzalapa** | 27/03/2018 16:00 | 118 | 109 | 63 | 68 | 89 | 124 | 131 |
| | **Baños de Chignahuapan** | 28/03/2018 07:30 | 114 | 104 | 59 | 64 | 86 | 120 | 126 |

$T^{18}O_{H2O\text{-}SO4\,(1)}$: Lloyd (1968); $T^{18}O_{H2O\text{-}SO4\,(2)}$: Mizutani and Rafter (1969); $T^{18}O_{H2O\text{-}SO4\,(3)}$: Zeebe (2010); $T^{18}O_{H2O\text{-}SO4\,(4)}$: Zheng (1999).

Recommended value

$T^{18}O_{H2O\text{-}BaSO4}$: Kusakabe and Robinson (1977).

$T^{18}O_{H2O\text{-}CaSO4\,(1)}$: Chiba *et al.* (1980); $T^{18}O_{H2O\text{-}CaSO4\,(2)}$: Boschetti *et al.* (2011).

*Table 3.4.1.3 - Classical isotope geothermometers applied on waters from the Los Humeros and Los Azufres geothermal areas.*

Among the different Na-Li geothermometric relationships existing in the literature (Michard and Fouillac, 1981; Kharaka *et al.*, 1982; Michard, 1990; Sanjuan *et al.*, 2014; 2016b; 2017), only the Na-Li auxiliary geothermometer defined for North-Icelandic high-temperature geothermal dilute waters (Sanjuan *et al.*, 2014; tabl. 3.4.1.4), give concordant temperature estimations (320 ± 30°C) with those estimated using the classical Silica-quartz, Na-K and Ca-K geothermometers, and the isotopic $\delta^{18}O_{H2O\text{-}SO4}$ geothermometer, for most of the Los Humeros geothermal waters (apart H-9 and H-32 waters). The Na-Cs auxiliary geothermometer defined by Sanjuan *et al.* (2016a, b) also yields concordant temperature values (300 ± 30°C) for all the waters, and to a lesser extent, with lower estimated temperature values, and only for some waters, the Na-Rb, K-Sr and K-W auxiliary geothermometers defined by Sanjuan *et al.* (2016b). These estimations range from 227 to 255°C, 241 to 319°C, and 244 to 248°C, respectively.

| Area | Sampling point | Date | $T_{Na-Li\,(1)}$ °C | $T_{Na-Li\,(2)}$ °C | $T_{Na-Li\,(3)}$ °C | $T_{Na-Rb\,(1)}$ °C | $T_{Na-Rb\,(2)}$ °C | $T_{Na-Cs\,(1)}$ °C | $T_{Na-Cs\,(2)}$ °C | $T_{K-Sr}$ °C | $T_{K-Fe\,(1)}$ °C | $T_{K-Fe\,(2)}$ °C | $T_{KF}$ °C | $T_{KW}$ °C |
|---|---|---|---|---|---|---|---|---|---|---|---|---|---|---|
| *Los Humeros area* | Los Humeros H-39 | 22/03/2018 12:00 | 155 | 337 | 78 | 264 | 255 | 174 | 331 | 309 | 164 | 112 | 201 | 215 |
| | Los Humeros Unité 11 (fluid mixing) | 22/03/2018 12:50 | 127 | 309 | 67 | 219 | 230 | 151 | 289 | 210 | 164 | 113 | 244 | 244 |
| | Los Humeros H-56 | 22/03/2018 13:25 | 160 | 343 | 80 | 245 | 244 | 178 | 339 | 262 | 160 | 109 | 172 | 246 |
| | Los Humeros H-49 | 22/03/2018 13:55 | 151 | 334 | 77 | 223 | 232 | 162 | 309 | 241 | 193 | 143 | 167 | 248 |
| | Los Humeros H-9 | 22/03/2018 15:05 | 239 | 419 | 108 | 223 | 231 | 140 | 270 | 319 | 148 | 96 | 184 | 191 |
| | Los Humeros H-32 | 22/03/2018 15:35 | 185 | 368 | 90 | 222 | 231 | 149 | 286 | 147 | 112 | 60 | 159 | 146 |
| | Los Humeros H-55 | 22/03/2018 16:08 | 166 | 348 | 82 | 216 | 227 | 157 | 301 | 154 | 96 | 45 | 76 | 96 |
| | *El Tesoro (existing data)* | *17/11/2016* | *72* | *248* | *42* | | | | | | | | | |
| | El Tesoro | 23/03/2018 09:30 | 97 | 276 | 54 | 128 | 172 | | | 101 | 135 | 83 | 64 | 56 |
| | *Nuevo Pizarro well (existing data)* | *09/11/2016* | *87* | *265* | *49* | | | | | | | | | |
| | Noria Nuevo Pizarro | 23/03/2018 11:45 | 78 | 255 | 45 | 63 | 124 | | | 170 | 243 | 195 | 141 | 139 |
| | Virgen del Carmen | 23/03/2018 15:46 | 90 | 268 | 51 | 103 | 155 | | | 49 | 118 | 67 | 73 | |
| | Pozo deTepeyahualco | 24/03/2018 10:10 | 139 | 321 | 72 | 74 | 133 | 45 | 116 | 91 | 44 | | 118 | 82 |
| *Acoculco area* | *Los Azufres (existing data)* | *25/06/1986* | *41* | *213* | *27* | | | | | | | | | |
| | Los Azufres 1 | 26/03/2018 15:05 | 18 | 184 | 14 | 157 | 192 | 52 | 126 | 100 | 175 | 123 | 71 | 100 |
| | Los Azufres 3 | 28/03/2018 09:45 | 32 | 202 | 23 | 141 | 181 | 44 | 114 | 98 | 167 | 115 | 84 | 123 |
| | Jicolapa | 27/03/2018 09:45 | 147 | 329 | 75 | 256 | 250 | 102 | 205 | 81 | 118 | 66 | 85 | |
| | El Rincon | 27/03/2018 11:00 | 80 | 258 | 47 | 293 | 270 | 96 | 195 | 92 | 30 | | 71 | |
| | *Baños de Quetzalapa (existing data)* | *18/06/1986* | *74* | *250* | *43* | | | | | | *80* | *29* | | |
| | Baños de Quetzalapa | 27/03/2018 16:00 | 72 | 248 | 43 | 117 | 164 | 82 | 174 | 88 | 162 | 110 | 74 | |
| | *Baños de Chignahuapan (existing data)* | *02/07/1986* | *168* | *350* | *83* | | | | | | | | | |
| | Baños de Chignahuapan | 28/03/2018 07:30 | 170 | 353 | 84 | 182 | 207 | 134 | 259 | 90 | 78 | 27 | 87 | 58 |
| | *Agua salada (existing data)* | *03/07/1986* | *43* | *214* | *28* | | | | | | *140* | | | |
| | *Capulines (existing data)* | *01/07/1986* | *106* | *287* | *58* | | | | | | | | | |

$T_{Na-Li\,(1)}$: Fouillac and Michard (1981); $T_{Na-Li\,(2)}$: Sanjuan *et al.* (2014); $T_{Na-Li\,(3)}$: Sanjuan *et al.* (2017). Recommended value

$T_{Na-Rb\,(1)}$, $T_{Na-Cs\,(1)}$, $T_{K-Fe\,(1)}$, $T_{KF}$, $T_{KW}$: Michard (1990).

$T_{Na-Rb\,(2)}$, $T_{Na-Cs\,(2)}$, $T_{K-Sr}$, $T_{K-Fe\,(2)}$: Sanjuan *et al.* (2016a, b).

*Table 3.4.1.4 - Auxiliary chemical geothermometers applied on waters from the Los Humeros and Los Azufres geothermal areas.*

Thermodynamic binary diagrams representating log ($H_4SiO_4$) as a function of log (Na/K), log ($Ca/K^2$), log ($Mg/K^2$), log (Na/Li), log (Na/Cs), log (Na/Rb) and log ($K^2/Sr$) were constructed in order to illustrate these results (figs. 3.4.1.11 and 3.1.4.12).

In the log ($H_4SiO_4$) - log (Na/K) diagram (fig. 3.4.1.11), the equilibrium reaction (equation 1) at different temperatures was determined using the thermometric relationships given by Fournier (1977) for Silica-quartz and by Giggenbach (1988) for Na-K; the other equilibrium reaction (equation 2) at different temperatures was defined using the thermometric relationships given by Fournier (1977) for Silica-quartz and by Michard (1979) for Na-K.

In the log ($H_4SiO_4$) - log ($Ca/K^2$) diagram (fig. 3.4.1.11), the equilibrium reaction (equation 1) at different temperatures was determined using the thermometric relationships given by Fournier (1977) for Silica-quartz and by Michard (1990) for Ca-K; the equilibrium reaction (equation 2) at different temperatures was defined using the thermometric relationships given by Michard (1979) for Silica-chalcedony and by Michard (1990) for Ca-K.

In the log ($H_4SiO_4$) - log ($Mg/K^2$) diagram (fig. 3.4.1.11), the equilibrium reaction (equation 1) at different temperatures was determined using the thermometric relationships given by Michard (1979) for Silica-chalcedony and by Giggenbach (1988) for K-Mg; the equilibrium reaction (equation 2) at different temperatures was defined using the thermometric relationships given by Michard (1979) for Silica-chalcedony and by Michard (1990) for K-Mg.

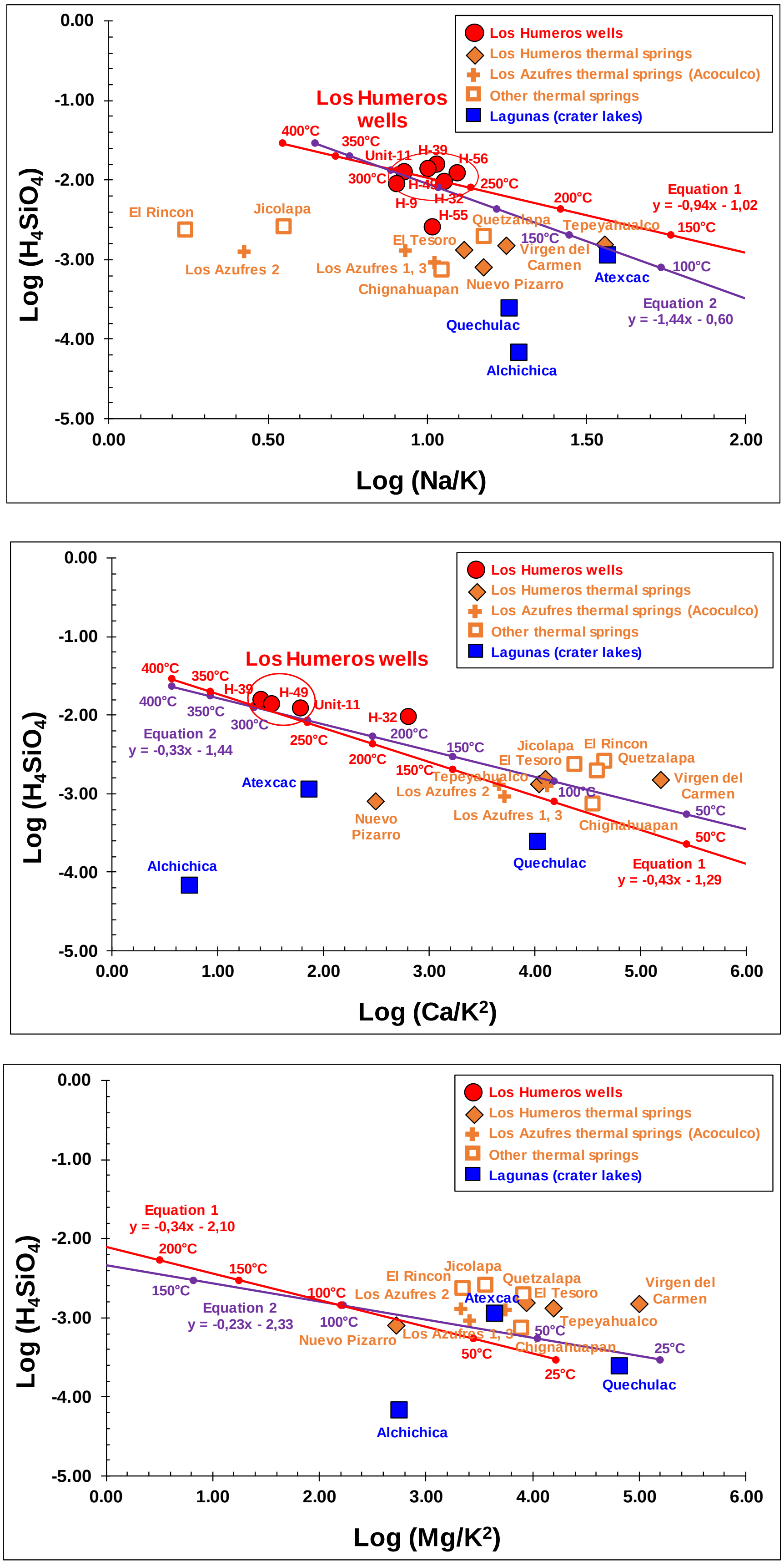


*Figure 3.4.1.11 - Diagrams log ($H_4SiO_4$) as a function of log (Na/K), log ($Ca/K^2$) and log ($Mg/K^2$) for the geothermal and thermal waters collected in the Los Humeros and Acoculco areas (all the concentrations are given in mol/l).*

In the log ($H_4SiO_4$) - log (Na/Li) diagram (fig. 3.4.1.12), the equilibrium reaction (equation 1) at different temperatures was determined using the thermometric relationships given by

Fournier (1977) for Silica-quartz and by Sanjuan *et al.* (2014) for Na-Li; the equilibrium reaction (equation 2) at different temperatures was defined using the thermometric relationships given by Michard (1979) for Silica-chacedony and by Fouillac and Michard (1981) for Na-Li.

In the log ($H_4SiO_4$) - log (Na/Cs) diagram (fig. 3.4.1.12), the equilibrium reaction (equation 1) at different temperatures was determined using the thermometric relationships given by Fournier (1977) for Silica-quartz and by Sanjuan *et al.* (2016a, b) for Na-Cs; the equilibrium reaction (equation 2) at different temperatures was defined using the thermometric relationships given by Michard (1979) for Silica-chalcedony and by Michard (1990) for Na-Cs.

In the log ($H_4SiO_4$) - log (Na/Rb) diagram (fig. 3.1.4.12), the equilibrium reaction (equation 1) at different temperatures was determined using the thermometric relationships given by Fournier (1977) for Silica-quartz and by Sanjuan *et al.* (2016a, b) for Na-Cs; the equilibrium reaction (equation 2) at different temperatures was defined using the thermometric relationships given by Fournier (1977) for Silica-chacedony and by Michard (1990) for Na-Cs.

In the log ($H_4SiO_4$) - log ($K^2$/Sr) diagram (fig. 3.1.4.12), the equilibrium reaction (equation 1) at different temperatures was determined using the thermometric relationships given by Fournier (1977) for Silica-quartz and by Sanjuan *et al.* (2016a, b) for K-Sr; the other equilibrium reaction (equation 2) at different temperatures was defined using the thermometric relationships given by Fournier (1977) for Silica-chalcedony and by Michard (1990) for K-Sr.

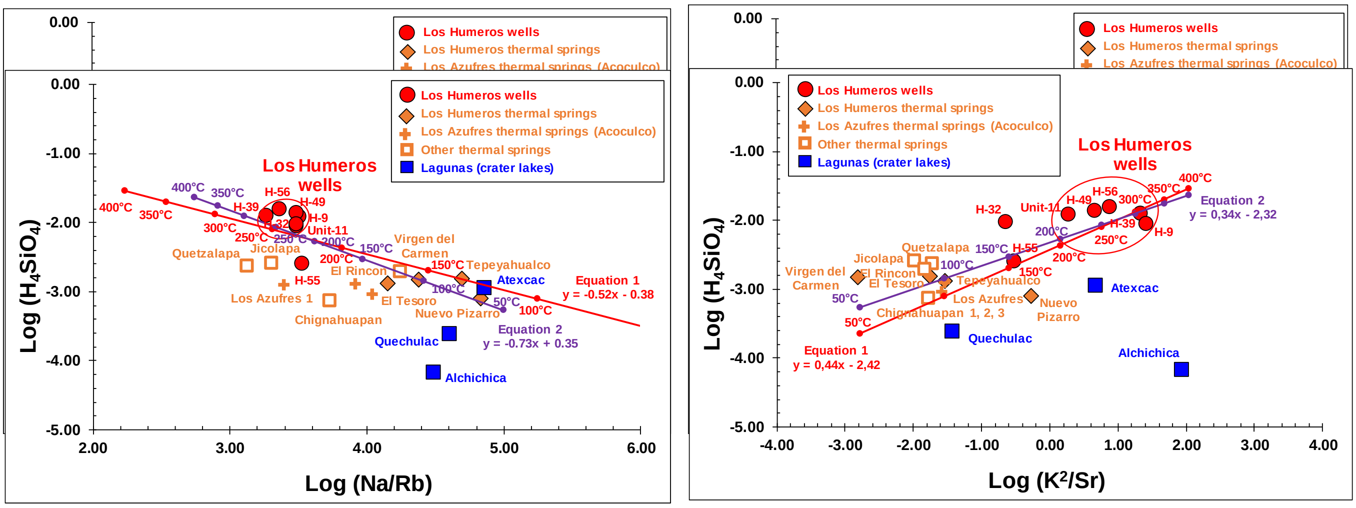


*Figure 3.1.4.12 - Diagrams log ($H_4SiO_4$) as a function of log (Na/Li), log (Na/Cs), log(Na/Rb) and log ($K^2$/Sr) for the geothermal and thermal waters collected in the Los Humeros and Acoculco areas (all the concentrations are given in mol/l).*

Other thermodynamic binary diagrams such as log (Na/Cs), log (Na/Rb), and log ($K^2$/Sr), as a function of log (Na/Li) may also illustrate these results (fig. 3.4.1.13).

In the log (Na/Cs) - log (Na/Li) diagram (fig. 3.4.1.13), the equilibrium reaction (equation 1) at different temperatures was determined using the thermometric relationships given by Sanjuan *et al.* (2014) for Na-Li and Sanjuan *et al.* (2016a, b) for Na-Cs; the other equilibrium reaction (equation 2) at different temperatures was defined using the thermometric relationships given by Fouillac and Michard (1981) for Na-Li and by Michard (1990) for Na-Cs.

In the log (Na/Rb) - log (Na/Li) diagram (fig. 3.4.1.13), the equilibrium reaction (equation 1) at different temperatures was determined using the thermometric relationships given by Sanjuan *et al.* (2014) for Na-Li and Sanjuan *et al.* (2016a, b) for Na-Rb; the other equilibrium reaction (equation 2) at different temperatures was defined using the thermometric relationships given by Fouillac and Michard (1981) for Na-Li and by Michard (1990) for Na-Rb.

In the log ($K^2$/Sr) - log Na/Li) diagram (fig. 3.4.1.13), the equilibrium reaction (equation 1) at different temperatures was determined using the thermometric relationships given by Sanjuan *et al.* (2014) for Na-Li and by Sanjuan *et al.* (2016a, b) for K-Sr; the equilibrium reaction (equation 2) at different temperatures was defined using the thermometric relationships given by Fouillac and Michard (1981) for Na-Li and by Sanjuan *et al.* (2016a, b) for K-Sr.

The geothermometric relationships used in this study are as follows (T in K):

| | | |
|---|---|---|
| Silica-quartz (Fournier, 1977): | $T = 1309 / [0.41 - \log (H_4SiO_4)]$ | |
| Silica-chalcedony (Michard, 1979): | $T = -1015 / [0.125 + \log (H_4SiO_4)]$ | |
| Na/K (Giggenbach, 1988): | $T = 1390 / [\log (Na/K) + 1.52]$ | |
| Na/K (Michard, 1979): | $T = 908 / [\log (Na/K) + 0.70]$ | |
| Ca/K (Michard, 1990): | $T = 3030 / [\log (Ca/K^2) + 3.94]$ | |
| K/Mg (Giggenbach, 1988): | $T = 4410 / [9.60 - \log (K^2/Mg)]$ | |
| K/Mg (Michard, 1990): | $T = 3000 / [5.84 - \log (K^2/Mg)]$ | |
| Na/Li (Sanjuan *et al.*, 2014): | $T = 2002 / [\log (Na/Li) + 1.322]$ | |
| Na/Li (Fouillac & Michard, 1981): | $T = 1000 / [\log (Na/Li) + 0.38]$ | (Cl < 0.3 M) |
| Na/Cs (Sanjuan *et al.*, 2016a, b): | $T = 2585 / [\log (Na/Li) + 0.923]$ | |
| Na/Cs (Michard, 1990): | $T = 2610 / [\log (Na/Cs) + 2.48]$ | |
| Na/Rb (Sanjuan *et al.*, 2016a, b): | $T = 2522 / [\log (Na/Rb) + 1.514]$ | |
| Na/Rb (Michard, 1990): | $T = 1400 / [\log (Na/Rb) - 0.66]$ | |
| K/Sr (Sanjuan *et al.*, 2016a, b): | $T = 2992 / [6.472 - \log (K^2/Sr)]$ | |
| K/Sr (Michard, 1990): | $T = 2450 / [4.44 - \log (K^2/Sr)]$ | |

*where all the specie concentrations must be expressed in mol/l.*

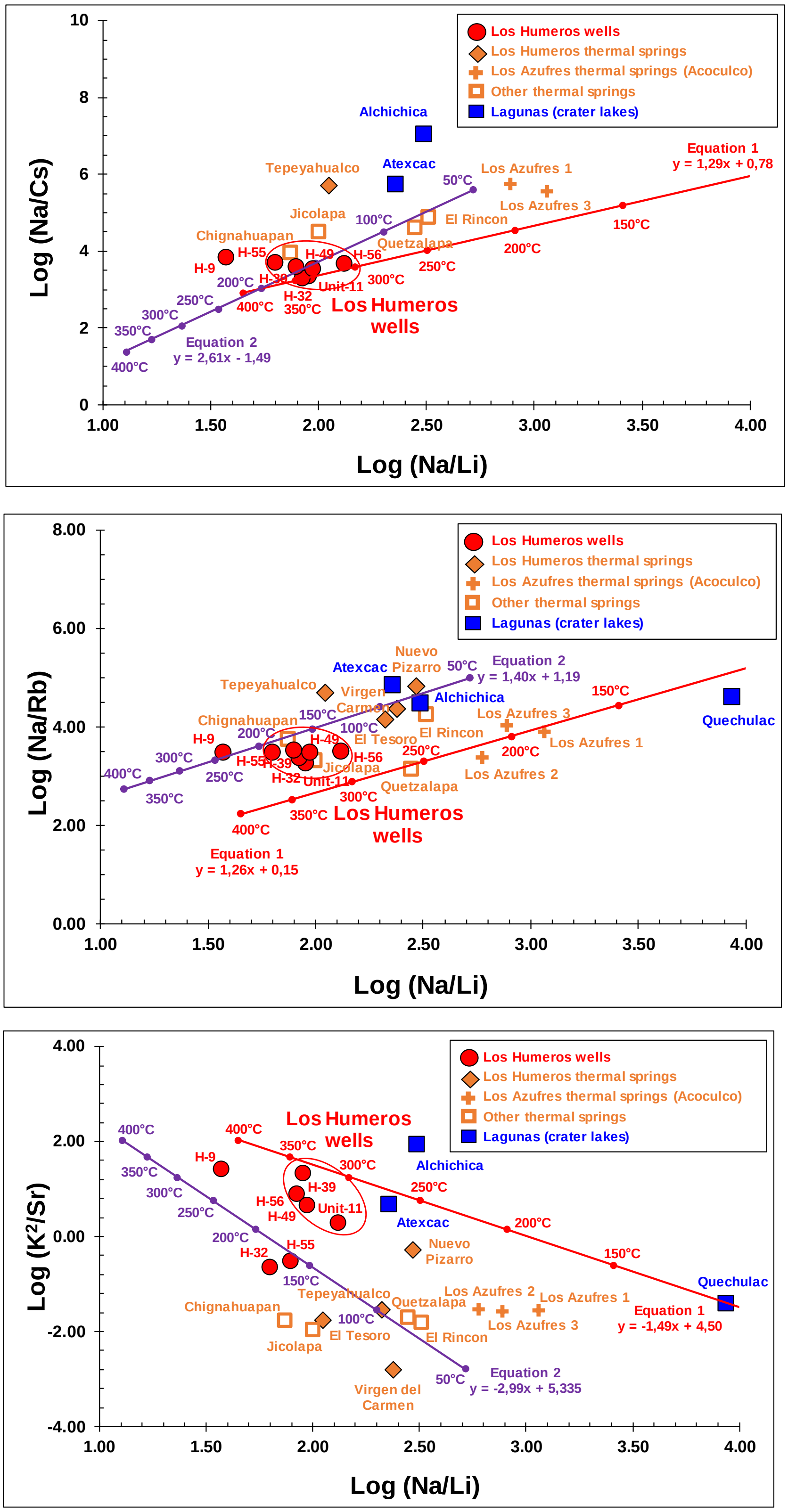

*Figure 3.4.1.13 - Diagrams log (Na/Cs), log (Na/Rb), and log ($K^2$/Sr) as a function of log (Na/Li) for the geothermal and thermal waters collected in the Los Humeros and Acoculco areas (all the concentrations are given in mol/l).*

### 3.4.2 Los Humeros and Acoculco thermal waters

#### a) *Chemical characteristics of the fluids*

The El Tesoro, Noria Nuevo Pizarro, Virgen del Carmen and Pozo de Tepeyahualco waters from the Los Humeros area, sampled during this study, Na-$HCO_3$-Cl-($SO_4$) type (fig. 3.4.1.1), have temperature, TDS and pH values ranging from 16 to 23.8°C, from 0.69 to 4.1 mg/l and from 6.75 to 8.82, respectively. The water samples collected from the Acoculco area (Los Azufres, Jicolapa, El Rincón, Quetzalapa and Chignahuapan), $HCO_3$-$SO_4$-Na-Ca and $HCO_3$-Na-Ca type (fig. 3.4.1.1), have temperature, TDS and pH values varying from 19 to 49°C, from 0.35 to 2.1 g/l and from 3.22 to 7.94, respectively. The Los Azufres 2 water, $SO_4$-Na-Ca type (fig. 3.4.1.1), which has the lowest values of pH (3.22) and TDS (0.35 g/l), is probably an acidic steam condensate.

The analytical results obtained in this study for the El Tesoro, Noria Nuevo Pizarro, Jicolapa, El Rincón, Quetzalapa and Chignahuapan thermal waters are close to those found in previous studies, when the analyses have been done (Tello Hinojosa, 1986; López-Hernández *et al.*, 2009; Peiffer *et al.*, 2014b; CFE data). For the Los Azufres thermal springs, waters like Los Azufres 3 with relatively high pH (7.94) had never been previously measured.

#### b) *Water origin*

Apart the Nuevo Pizarro, Tepeyahualco and Los Azufres waters, all the other waters show composition in $\delta D$ and $\delta^{18}O$ falling close to GMWL (fig. 3.4.1.3), which indicate a meteoric origin. The position of the Los Azufres 1 and 2 waters, at the right of GMLW suggest an enrichment in $^{18}O$ due to water-rock interaction at high-temperature and/or low water-rock ratio. That of Los Azufres 3 water could probably result from a boiling process taking into account its $\delta^{11}B$ value and its Cl content. As for the crater lake waters (lagunas), also positioned at the right of GMLW, the Nuevo Pizarro and Tepeyahualco have probably been affected by a process of water evaporation or by a mixing with an evaporated water. Given their similar values in $\delta D$, the Chignahuapan, Jicolapa, El Rincón, Los Azufres 1 thermal waters could have the same recharge area. If we consider the second assumption for the origin of the Los Humeros geothermal waters (mainly meteoric water with high water-rock interactions) and the $\delta D$ values, this area of water recharge could be also close to that of the Los Humeros geothermal waters. The relatively wide dispersion in $\delta D$ and $\delta^{18}O$ values observed for the Virgen del Carmen, El Tesoro, and Quetzalapa waters suggest that these waters have different recharge areas, probably located in the Sierra Madre Oriental.

The Cl/Br mass ratios of all these waters are much lower (from 70 to 700) than those of the Los Humeros geothermal waters (from 1200 to 1700 ; fig. 3.4.1.4). However, the higher Cl/Br values for the thermal waters are those associated with the Los Azufres 1 and 3, Chignahuapan and Tepeyahualco (600-700). The El Tesoro, Virgen del Carmen, Nuevo Pizarro and Quetchalapa waters indicate similar values of Cl/Br around 400 (fig. 3.4.1.4).

### *c) Processes of water-rock-gas interaction*

Los Azufres 1 and 3 thermal waters have B concentrations (253-354 mg/l) much higher than those analysed in the other thermal waters (from 0.12 to 20 mg/l; fig. 3.4.1.5) and specific $\delta^{11}B$ signatures (-5.61 and -4.42‰; fig. 3.4.1.6), which suggest mixing with low proportions of deep geothermal waters enriched in B (probably similar to those from the Los Humeros).
However, the relatively high B concentrations observed in most of the thermal waters and their $\delta^{11}B$ signatures could traduce very small fluxes of deep geothermal waters in these waters, especially for the Chignahuapan thermal water (B ≈ 3 mg/l), which has also a high Cl concentration (115 mg/l). López-Hernández *et al.* (2009) already mentioned that the Chignahuapan thermal water, discharged from a spring located in an area of ancient system faults (Tulancingo-Tlaxco) connecting both zones, might be the farthest SE discharge of the Acoculco hydrothermal system, constituted of a mixture of deep geothermal fluid and shallow waters. Water isotopic data do not differ from meteoric values, because important dilution with shallow meteoric water could mask the deep signature.

The high B and Cl concentrations (≈ 20 mg/l and 775 mg/l, respectively) for the Tepeyahualco water, and its specific $\delta^{11}B$ value (8.55‰), close to that of the Atexcac water (crater lake), suggest that this water is affected by a process of evaporation, like probably the Nuevo Pizarro water.

For most of the thermal waters, the Ca - $HCO_3$ diagram (fig. 3.4.2.1) shows that these waters interact with calcium carbonates and have high Ca concentrations, compared with the Los Humeros geothermal waters, which are depleted in Ca. Apart the Los Azufres thermal waters, the high Sr concentrations of the other thermal waters, compared with those of the Los Humeros geothermal waters (fig. 3.4.1.8), and their $^{86}Sr/^{87}Sr$ ratios, ranging from 0.706272 to 0.707262 (fig. 3.4.1.9), confirm that these waters are interacting with marine carbonate rocks formed during the Mesozoic period (probably the thick series of Jurassic and Cretaceous limestones, mentionned in Carrasco *et al.*, 2017a).

For Los Azufres thermal waters, the Sr concentrations are high (from 133 to 2500 µg/l), but their $^{86}Sr/^{87}Sr$ signature (from 0.704778 to 0.705065; fig. 3.4.1.9) is closer to volcanic rocks (rhyolites?). These values could also traduce a mixing process between a deep water in contact with volcanic rocks and low proportions of water interacting with sedimentary rocks.

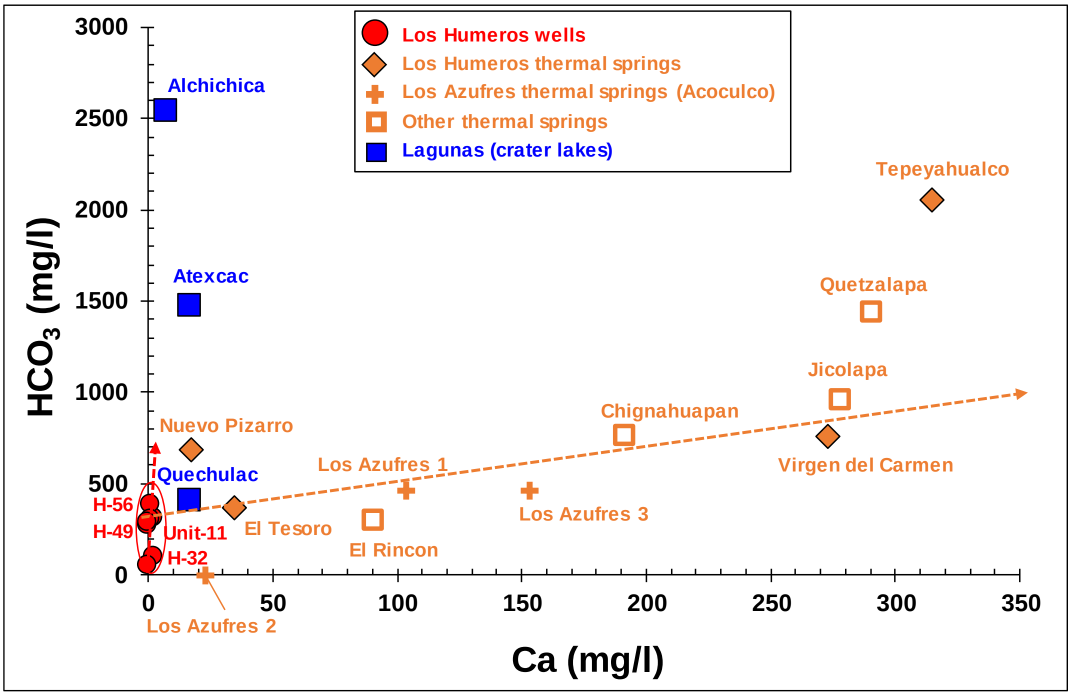


*Figure 3.4.2.1 - Diagram $HCO_3$ - Ca for the geothermal and thermal waters collected in the Los Humeros and Acoculco areas.*

## *d) Geothermometry*

The Na-K-Mg ternary plot developed by Giggenbach (1988) indicates that all the thermal waters of the Los Humeros and Acoculco areas are immature, having not reached full chemical equilibrium with the host rocks (fig. 3.4.1.10). In addition, geothermometry cannot be applied to acidic waters. However, the Na-K and Na-Li diagrams (fig. 3.4.2.2) show that the Na/K and Na/Li ratios for numerous thermal waters are close to those of the Los Humeros geothermal waters. Associated with $\delta^7$Li values ranging from 4.7 to 6.5‰ and relatively high B concentrations (especially for the Los Azufres waters), these ratios suggest that very low proportions of deep geothermal waters at about 300°C could be present in these thermal waters.

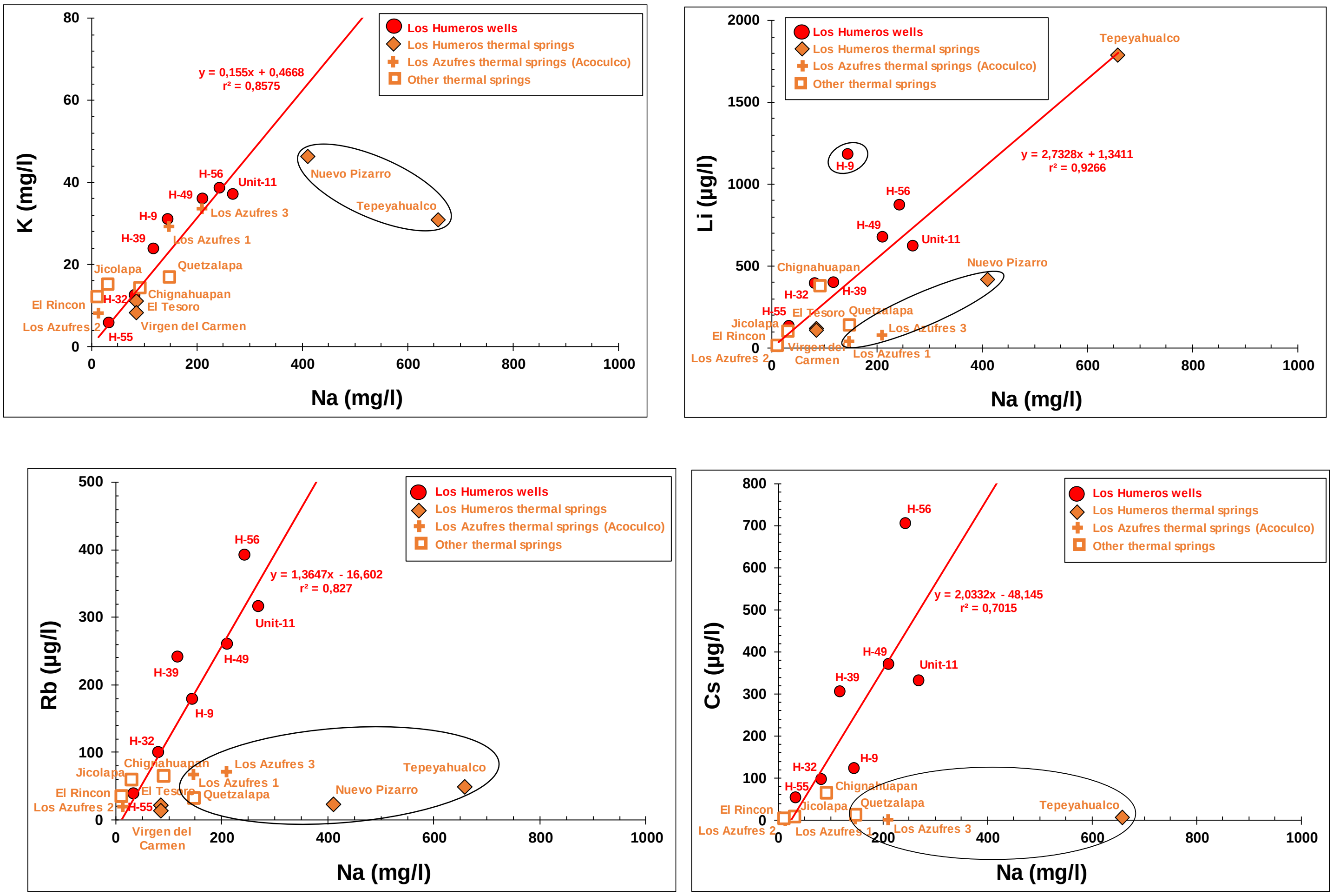


*Figure 3.4.2.2 - Diagrams K - Na, Li - Na, Rb - Na, and Cs - Na for the geothermal and thermal waters collected in the Los Humeros and Acoculco areas.*

These Na/K and Na/Li ratios, and to a lesser extent, the Na/Rb and Na/Cs ratios (fig. 3.4.2.2), could be the only witness of the presence of very small fluxes of high-temperature geothermal waters in the thermal waters, because the permeability of these areas is low, these geothermal waters are completely depleted in Ca, Mg and Sr whereas the thermal waters have relatively high concentrations in these elements, and the high silica concentrations of the geothermal waters can significantly decrease due to silica precipitation during their cooling and/or their dilution with shallow waters.

In this case, the geothermometers Na/Li and Na/K, and Na/Rb and Na/Cs sometimes, determined by Sanjuan *et al.* (2014; 2016a,b), give temperature estimations ranging from 248 to 353°C (tabl. 3.4.2.4), close to the temperature values measured in the wells and estimated using thermometric relationships.

In the Acoculco area, not only escapes of deep gases from the geothermal reservoir reach the surface (Peiffer *et al.*, 2014b), but also small fluxes of deep waters coud be able to preserve, more or less, their original Na/K and Na/Li ratios, resulting from the temperature of their deep reservoir, even after a significant mixing with cold waters, during their ascent up to the surface.

In such a context (low-permeability environment, presence of low-salinity deep waters with very low concentrations of dissolved calcium, magnesium and strontium, precipitation of dissolved silica or dilution by shallow waters during the ascent and cooling of the deep water, dissolution of marine carbonates which provides relatively high concentrations in calcium, magnesium and strontium to the thermal waters), the application of geothermometers to thermal waters in order to estimate the temperature of deep reservoir is very difficult, but the Na/K and Na/Li ratios, and sometimes the Na/Cs and Na/Rb ratios, the boron concentrations and their isotopes, as well as analyses of associated non condensable gases (Peiffer *et al.*, 2014b) may be useful tools for high-temperature geothermal exploration.

Classical geothermometers such as Silica-chalcedony, Na-K-Ca, K-Mg and Ca-K, based on the fluid equilibration with chalcedony, muscovite, clinochlore, K-felspar and calcite, which can re-equilibrate relatively fast, probably indicate subsurface temperature estimations for these thermal waters, ranging from 60 to 100°C (tabl. 3.4.1.2). The $\delta^{18}O_{H2O-SO4}$ geothermometers defined by Kusakabe and Robinson (1977), Zeng (1999) and Zeebe (2010), as well as the K-Sr and K-F auxiliary geothermometers determined by Sanjuan *et al.* (2016) and by Michard (1990), respectively, also seem to indicate concordant temperature estimations, which vary from 60 to 100°C (tabl. 3.4.1.3 and 3.4.1.4).

The relatively high concentration of dissolved silica analysed in the Atexcac water (fig. 3.4.1.2) could be explained by a thermal water input throughout the bottom of the Atexcac crater lake, according to Macek *et al.* (1994).

### 3.5. Main conclusions

The main objectives of this study were to develop and validate auxiliary chemical geothermometers such as Na-Li, Na-Cs, Na-Rb, K-Sr, … and the $\delta^{18}O_{H2O-SO4}$ isotope geothermometers in order:

- to improve the geochemical methods for geothermal exploration in volcanic fields such as Los Humeros and Acoculco, with high-temperature and relatively low permeability;
- to acquire a better knowledge about the circulation of high-temperature deep fluids and their possible interaction with more superficial waters in this type of geothermal fields, from chemical and isotopic water analyses from surface thermal springs.

In order to attain these objectives, a preliminary exhaustive literature review about the geological setting and the existing geochemical data on the geothermal and termal waters from Acoculco and the Los Humeros areas was carried by BRGM. After this review, fluid samples were collected by BRGM, between March 22 to 28, 2018, in collaboration with CFE, University of Michoacana and CNR Lelli's team, from seven geothermal wells and four thermal springs located in the Los Humeros area, from eight thermal springs located in the Acoculco area, and from three neighbouring crater lakes (lagunas), as references of surface waters. Among the two-phase geothermal waters from Los Humeros field, very rich in steam, those which indicated the most high fractions of liquid water were selected with the valuable help of CFE. The chemical (major and trace species) and isotopic analyses ($\delta D_{H2O}$ and $\delta^{18}O_{H2O}$, $\delta^{18}O_{SO4}$, $\delta^{11}B$, $\delta^{7}Li$ and $^{87}Sr/^{86}Sr$ ratios) were performed in the BRGM laboratories, and data interpretation was then carried out.

The geothermal Na-$HCO_3$-Cl waters discharged from Los Humeros wells, completely deleted in calcium and magnesium, enriched in silica and boron (among the highest ones in the world), with TDS and pH values ranging from 0.3 to 1.8 g/l and 6.67 to 7.58, respectively, traduce a high interaction process with the reservoir rocks, at high-temperature. The high values of $\delta^{18}O_{H2O}$ of these waters towards the right of of the Global Meteoric Water Line (GMWL) are not only in concordance with these high-temperature values, but also suggest a low water-rock ratio of the geothermal reservoir, when compared with the lower values observed in the Krafla geothermal field, in North-Iceland, where the fluids are also biphasic, but the water-rock ratio is much higher. This is in agreement with a reservoir consisting of medium- to low-permeability pre-caldera andesites. The volcanic nature of the reservoir rocks was confirmed by the Sr and Li isotope signatures.

The isotopic $\delta D$ and $\delta^{18}O$ for the Los Humeros wells show a wide dispersion probably related to boiling, mixing, phase separation and condensation phenomema. Two main assumptions were considered in this study:

- a mixing of recharge meteoric water with a deep fluid-type andesitic water ($\delta D \approx -20‰$ and $\delta^{18}O \approx 6‰$), as defined by Giggenbach (1992), leading to a positive correlation between $\delta D$ and $\delta^{18}O$, with a slope close to 3.0, and a proportion of andesitic water estimated to be between 25% and 50%, accompanied with processes of boiling and phase separation (Arrellano *et al.*, 2003; Barragán *et al.*, 2010);
- a contribution of meteoric water with a $\delta D$ value similar to that of the geothermal fluid (average values of $\delta D \approx -62‰$ and $\delta^{18}O \approx -3‰$ for the total geothermal fluid, steam + water, characterized by data from Verma *et al.*, 1998; Arellano *et al.*, 2003; Tello, 2005; and Bernard, 2008), affected by a strong water-rock interaction process at high-temperature and low water-rock ratio, which enriches its $^{18}O$ content (up to 7-8‰). The wide dispersion observed for the isotopic values could be explained by different water-rock interaction factors and processes such as kinetic fractionation at temperatures close to boiling temperatures (Giggenbach and Stewart, 1982), with characteristic slopes of 3.0-3.5, and phase separation.

In this study, the data obtained for the water isotopic values are in the range of the previous data and it is difficult to give a preference about the different assumptions. According to the first assumption, the $\delta D$ and $\delta^{18}O$ values for the meteoric water were estimated to be close to -110‰ and -15‰, respectively. For the second assumption, these values would be rather close to -65‰ and -9.5‰, respectively. In this last case, the isotopic values for the meteoric water would be slightly heavier than those reported by Quijano *et al.* (1981) for the Los Humeros area (Oriental Basin), close to -77.3‰ for $\delta D$ and -10.7‰ for $\delta^{18}O$, but they would coincide with hydrologic studies that identify the main recharge to Los Humeros area from the Sierra Madre Oriental, with groundwater flow in a NE-SW direction (Prol-Ledesma, 1998).

According to Arnórsson and Andrésdóttir (1995), the variable B and Cl concentrations and Cl/B ratios in high-temperature geothermal waters, as well as high B concentrations can be attributed to a combination of several processes. They include: i) supply of these elements from the degassing magma chamber, ii) supply from the rock with which the water interacts, and iii) phase separation in producing aquifers of wells. The observed high B contents and specific isotopic signatures, as well as the variable Cl concentrations in the Los Humeros geothermal waters, could be the result of mixing of magmatic fluid from a deep magmatic chamber, the heat and fluid source for the system, leaching of wall rocks of the deep aquifer at a low fluid/rock ratio and phase separation process.

The Na-K-Mg ternary diagram from Giggenbach (1988) and the main classical geothermometers such as Silica-quartz, Na-K, Na-K-Ca and K-Ca, as well as the isotopic $\delta^{18}O_{H2O-SO4}$ geothermometric relationships established by Kusakabe and Robinson (1977) and Zeebe (2010), indicate that the full chemical equilibrium is reached for most of these waters at about 290 ± 30°C. This temperature range is concordant with the presence of an upper liquid-dominated reservoir area, located in augite andesites, between 1025 and 1600 m a.s.l., with neutral pH at 290-330°C, suggested in numerous studies (Arellano *et al.*, 2003; Gutiérrez-Negrín and Izquierdo-Montalvo, 2010).

Among the different Na-Li geothermometric relationships existing in the literature (Michard and Fouillac, 1981; Kharaka *et al.*, 1982; Michard, 1990; Sanjuan *et al.*, 2014; 2017), only the Na-Li auxiliary geothermometer defined for North-Icelandic high-temperature geothermal dilute waters (Sanjuan *et al.*, 2014), give concordant temperature values (320 ± 30°C) with those estimated using the classical Silica-quartz, Na-K and Ca-K geothermometers, and the isotopic $\delta^{18}O_{H2O-SO4}$ geothermometer, for most of the Los Humeros geothermal waters (apart H-9 and H-32 waters). The Na-Cs auxiliary geothermometer defined by Sanjuan *et al.* (2016) also yields concordant temperature values (300 ± 30°C) for all the waters and to a lesser extent, with lower temperature estimations and only for some waters, the Na-Rb, K-Sr and K-W auxiliary geothermometers defined by Sanjuan *et al.* (2016). These estimations range from 227 to 255°C, 241 to 309°C, and 244 to 246°C, respectively.

Thermodynamic binary diagrams such as log ($H_4SiO_4$) as a function of log (Na/K), log ($Ca/K^2$), log ($Mg/K^2$), log (Na/Li), log (Na/Cs), log (Na/Rb) and log ($K/Sr^2$), or representing log (Na/Cs), log (Na/Rb), and log ($K^2/Sr$) as a function of log (Na/Li), were constructed in order to illustrate these results.

The El Tesoro, Noria Nuevo Pizarro, Virgen del Carmen and Pozo de Tepeyahualco waters from the Los Humeros area, sampled during this study, Na-$HCO_3$-Cl-($SO_4$) type, have temperature, TDS and pH values ranging from 16 to 23.8°C, from 0.69 to 4.1 mg/l and from 6.75 to 8.82, respectively. Those sampled from the Acoculco area (Los Azufres, Jicolapa, El Rincón, Quetzalapa and Chignahuapan), $HCO_3$-$SO_4$-Na-Ca and $HCO_3$-Na-Ca type, have temperature, TDS and pH values varying from 19 to 49°C, from 0.35 to 2.1 g/l and from 3.22 to 7.94, respectively. The Los Azufres 2 water, $SO_4$-Na-Ca type, which has the lowest values of pH (3.22) and TDS (0.35 g/l), is probably an acidic steam condensate. The Los Azufres 3 water with relatively high pH (7.94) had never been previously sampled and studied.

Apart the Nuevo Pizarro, Tepeyahualco and Los Azufres waters, all the other waters show composition in $\delta D$ and $\delta^{18}O$ falling close to GMWL, which indicates their meteoric origin. The position of the Los Azufres 1 and 2 waters, at the right of GMLW suggest an enrichment in $^{18}O$ due to water-rock interaction at high-temperature and/or low water-rock ratio. That of Los Azufres 3 water could result from a boiling process taking into account its $\delta^{11}B$ value and its Cl content. As for the crater lake waters (lagunas), also positioned at the right of GMLW, the Nuevo Pizarro and Tepeyahualco have probably been affected by a process of water evaporation or by a mixing with an evaporated water. Given their similar values in $\delta D$ and $\delta^{18}O$, the Chignahuapan, Jicolapa, El Rincón, Los Azufres 1 thermal waters (Acoculco area) could have the same recharge area. The relatively wide dispersion in δD and $\delta^{18}O$ values observed for the Virgen del Carmen, El Tesoro, and Quetzalapa waters suggest that these waters have different recharge areas, probably located in the Sierra Madre Oriental. Given the similar δD values measured in the Los Humeros geothermal waters and in the Los Azufres 1 and Chignahuapan thermal waters (Acoculco area), the meteoric water recharge area could be close for these two geothermal fields, following the selected interpretation for the origin of the Los Humeros geothermal waters.

The Cl/Br mass ratios of all these waters are much lower (from 70 to 700) than those of the Los Humeros geothermal waters (from 1200 to 1700). However, the higher Cl/Br values for the thermal waters are those associated with the Los Azufres 1 and 3, Chignahuapan and Tepeyahualco (600-700). The El Tesoro, Virgen del Carmen, Nuevo Pizarro and Quetchalapa waters indicate similar values of Cl/Br around 400.

For most of the thermal waters, the Ca-$HCO_3$ diagram shows that these waters interact with calcium carbonates and have high Ca concentrations, compared with the Los Humeros geothermal waters, which are depleted in Ca. Apart the Los Azufres thermal waters, the high Sr concentrations of the thermal waters, compared with those of the Los Humeros geothermal waters, and their $^{86}Sr/^{87}Sr$ ratios, ranging from 0.706272 to 0.707262, confirm that these waters are interacting with marine carbonate rocks formed during the Mesozoic period (probably the thick series of Jurassic and Cretaceous limestones, mentionned in Carrasco *et al.*, 2017a). For Los Azufres thermal waters, the Sr concentrations are high, but their $^{86}Sr/^{87}Sr$ signature (from 0.704778 to 0.705065) is closer to volcanic rocks (rhyolites?). These values could also traduce a mixing process between a deep end-member water in contact with volcanic rocks and low proportions of water interacting with sedimentary rocks.

The Na-K-Mg ternary plot developed by Giggenbach (1988) indicates that all the thermal waters of the Los Humeros and Acoculco areas are immature, having not reached full chemical equilibrium with the host rocks. In addition, geothermometry cannot be applied to acidic waters. However, the Na-K and Na-Li diagrams show that the Na/K and Na/Li ratios for numerous thermal waters are close to those of the Los Humeros geothermal waters. Associated with $\delta^7Li$ values ranging from 4.7 to 6.5‰ and relatively high B concentrations (especially for Los Azufres waters), these ratios suggest that very low proportions of flux of deep geothermal waters at about 300°C could be present in these thermal waters.

Indeed, these Na/K and Na/Li ratios, and to a lesser extent, the Na/Rb and Na/Cs ratios, could be the only witness of the presence of very small flux of deep high-temperature geothermal waters in the thermal waters, because the permeability of these areas is low, these geothermal waters are completely depleted in Ca, Mg and Sr whereas the thermal waters have relatively high concentrations in these elements, and the high silica concentrations of the geothermal waters can significantly decrease due to silica precipitation during their cooling and/or their dilution with shallow waters. In this case, the geothermometers Na/Li and Na/K, and Na/Rb and Na/Cs sometimes, determined by Sanjuan *et al.* (2014; 2016a,b), give temperature estimations ranging from 248 to 353°C, close to the temperature values measured in the wells and estimated using thermometric relationships.

In the Acoculco area, not only escapes of deep gases from the geothermal reservoir reach the surface (Peiffer *et al.*, 2014b), but also small fluxes of deep waters coud be able to preserve, more or less, their original Na/K and Na/Li ratios, resulting from the temperature of their deep reservoir, even after a significant mixing with cold waters, during their ascent up to the surface.

In such a context (low-permeability environment, presence of low-salinity deep waters with very low concentrations of dissolved calcium, magnesium and strontium, precipitation of dissolved silica or dilution by shallow waters during the ascent and cooling of the deep water, dissolution of marine carbonates which provides relatively high concentrations in calcium, magnesium and strontium to the thermal waters), the application of geothermometers to thermal waters in order to estimate the temperature of deep reservoir is very difficult, but the Na/K and Na/Li ratios, and sometimes the Na/Cs and Na/Rb ratios, the boron concentrations and their isotopes, as well as analyses of associated non condensable gases (Peiffer *et al.*, 2014b) may be useful tools for high-temperature geothermal exploration.

Classical geothermometers such as Silica-chalcedony, Na-K-Ca, K-Mg and Ca-K, based on the fluid equilibration with chalcedony, muscovite, clinochlore, K-felspar and calcite, which can re-equilibrate relatively fast, probably indicate subsurface temperature estimations for these thermal waters, ranging from 60 to 100°C. The $\delta^{18}O_{H2O-SO4}$ geothermometers defined by Kusakabe and Robinson (1977), Zeng (1999) and Zeebe (2010), as well as the K-Sr and K-F auxiliary geothermometers determined by Sanjuan *et al.* (2016) and by Michard (1990), respectively, also seem to indicate concordant temperature estimations, which vary from 60 to 100°C.

***Acknowledgments:*** We want to thank the CFE staff from Los Humeros and from Morelia for permission and recommandations to sample their wells in the Los Humeros geothermal field. We also are particularly grateful to Oscar López Romero from CFE for his help in collecting fluid samples in the field. We would like to express our gratitude to Rafael Alfaro from CFE for his help in collecting waters from thermal springs located in the Los Humeros area and to Ernesto Bahena Palomares, who was our driver and guide during all our field campaign. Finally, we are very grateful to Aída López Hernández, scientific coordinator of the GEMEX project, for her constant and valuable support.

## 6. Dissemination activities

BRGM participated to three GEMEX meetings, which occurred in Utretch (Netherlands), in March 2017 (F. Gal), in Akureyry (Iceland), in October 2017 (B. Sanjuan), and in Morelia (Mexico), in October 2018.

It has also contributed to a GEMEX e-News document for WP4 - Task 4.3, in 2018.

All the geochemical data obtained during this study have been uploaded and stored in the GEMEX Open Access Database (OADB), as well as the required information, by Eugenio Trumpy from CNR, responsible for maintaining this database.

## References

### *Scientific and technical literature*


Aagarwal J.K., Palmer M.R., Bullen T.D., Arnórsson S., and Ragnarsdóttir K.V. (2000) - The boron isotope systematics of Icelandic geothermal waters: 1. Meteoric water charged systems. *Geochimica et Cosmochimica Acta*, 64, n°4, 579-585.

Aagarwal J.K., Sheppard D., Mezger K., Pernicka E. (2003) - Precise and accurate determination of boron isotope ratios by multiple collector ICP-MS: Origin of boron in the Ngawha geothermal system, New Zealand. *Chemical Geology*, 199, 331-342.

Arnórsson S., Anfdrésdóttir A. (1995) - Processes controlling the distribution of boron and chlorine in natural waters in Iceland. *Geochimica et Cosmochimica Acta*, 59, n°20, 4125-4146.

Boschetti T. (2013) - Oxygen isotope equilibrium in sulfate-water systems: A revision of geothermometric applications in low-enthalpy systems. *Journal of Geochemical Exploration*, 124, 92-100.

D'Amore F. and Panichi C. (1980) - Evaluation of deep temperatures of hydrothermal systems by a new gas-geothermometer. *Geochimica et Cosmochimica Acta*, 44, 549-556.

FP6-HITI project (2010) - Geochemical data of high-temperature dilute waters sampled between 2007 and 2008, from different Icelandic geothermal areas in North-Iceland (Krafla, Namafjall, Nesjavellir). *Not published.*

Fouillac C. et Michard G. (1981) - Sodium/lithium ratio in water applied to geothermometry of geothermal reservoir. *Geothermics 10*, 55-74.

Fournier R.O. (1979) - A revised equation for the Na/K geothermometer. *Geothermal Resource Council Trans*actions, 3, 221-224.

Fournier R.O. and Rowe J.J. (1966) - Estimation of underground temperatures from the silica content of water from hot springs and wet-steam wells. *American Journal of Sciences*, 264, 685-697.

Fournier R.O. and Truesdell A.H. (1973) - An empirical Na-K-Ca geothermometer for natural waters. *Geochimica et Cosmochimica* Acta, 37, 1255-1275.

Giggenbach W.F. (1987) - Redox processes governing the chemistry of fumarolic gas discharge from White Island, New Zealand. *Applied Geochemistry*, 2, 143-161.

Giggenbach W.F. (1988) - Geothermal solute equilibria. Derivation of Na-K-Mg-Ca geoindicators. *Geochimica et Cosmochimica* Acta, 52, 2749-2765.

Giggenbach, W.F. (1991) - Chemical techniques in geothermal exploration. *In: D'Amore, F., Applications of geochemistry in geothermal reservoir development*, 119-144.

Giggenbach W.F. (1992) - Isotopic shifts in waters from geothermal and volcanic systems along convergent plate boundaries and their origin. *Earth and Planetary Science Letters*, 113, 495-510.

Giggenbach W.F. and Stewart M.K. (1982) - Processes controlling the isotopic composition of steam and water discharges from steam vents and steam-heated pools in geothermal areas. *Geothermics*, vol. 11, n°2, 71-80.

Giggenbach W.F. and Goguel R.L. (1989) - Collection and analysis of geothermal and volcanic water and gas discharges. Fourth Edition. *Report CD2401, Chemistry Division, DSIR, New Zealand*, p. 81.

Kharaka Y-K., Lico M.S. et Law-Leroy M. (1982) - Chemical geothermometers applied to formation waters, Gulf of Mexico and California basins. *AAPG Bulletin*, 66, 5, 588-595.

Kharaka Y.K. and Mariner R.H. (1989) - Chemical geothermometers and their application to formation waters from sedimentary basins. In: Naeser, N.D. and McCulloch, T.H. (eds), Thermal history of sedimentary basins: methods and case histories. *Springer-Verlad*, New York, 99-117.

Kusakabe M., Robinson B.W. (1977) - Oxygen and sulfur isotope equilibria in the system from 110 to 350°C and applications. *Geochimica et Cosmochimica Acta*, 41, 1033-1040.

Leeman W.P., Tonarini S., Pennisi M., Ferrara G. (2005) - Boron isotopic variations in fumarolic condensates and thermal waters from Vulcano Island, Italy: Implications for evolution of volcanic fluids. *Geochimica et Cosmochimica Acta*, 69, n°1, 143-163.

Lloyd, R.M. (1968) - Oxygen isotope behavior in the sulfate-water system. *J. Geophys. Res.*, 73, 6099-6110.

Lü Y.Y., Zheng M., Zhao P., Xu R. (2014) - Geochemical processes and origin of boron isotopes in geothermal water in the Yunnan-Tibet geothermal zone. *Science China*, vol. 57, n°12, 2934-2944.

Marini L. (1987) - Geochemistry of North Ghoubbat - Asal region. *Report Geotermica Italiana srl - ISERST, April 1987*, 28 p.

Michard G. (1979) - Géothermomètres chimiques. Bull. du BRGM (2ème série), Section III, n°2, 183-189.

Michard G. (1990) - Behaviour of major elements and some trace elements (Li, Rb, Cs, Sr, Fe, Mn, W, F) in deep hot waters from granitic areas. *Chemical Geology*, 89, 117-134.

Michard G., Roeckens E. (1983) - Modelling of the chemical composition of alkaline hot waters. *Geothermics*, 12, n°2/3, 161-169.

Millot R., Guerrot C., Innocent Ch., Négrel Ph., Sanjuan B. (2011) - Chemical, multi-isotopic (Li-B-Sr-U-H-O) and thermal characterization of Triassic formation waters from the Paris Basin. *Chem. Geol.*, 283, 226-241.

Mizutani Y. and Rafter T.A. (1969) - Oxygen isotopic composition of sulphates, 3. Oxygen isotopic fractionation in the bisulphate ion-water system. *New Zealand Journal of Sciences*, 12, p. 54-59.

Peiffer L., Wanner C., Spycher N., Sonnenthal E.L., Kennedy B.M., Iovenitti J. (2014a) - Optimized multicomponent vs. classical geothermometry: Insights from modeling studies at the Dixie Valley geothermal area. *Geothermics*, 51, 154-169.

Pennisi M., Magro G., Adorni-Braccesi A. (2001) - Boron and helium isotopes in geothermal fluids from Larderello (Italy). *Water-rock Interaction 2001, Cidu Ed., 2001, Swets & Zeitlinger, Lisse, ISBN 90 2651 824 2*, 899-902.

Reed M.H. (1982) - Calculation of multicomponent chemical equilibria and reaction processes in systems involving minerals, gases, and an aqueous phase. *Geochimica et Cosmochimica Acta*, 46, 513-528.

Reed M.H., Spycher N.F. (1984) - Calculation of pH and mineral equilibria in hydrothermal waters with application to geothermometry and studies of boiling and dilution. *Geochimica et Cosmochimica Acta*, 48, 1479-1492.

Sakai H. (1977) - Sulfate-water isotope thermometry applied to geothermal systems. *Geothermics*, 5, 67-74.

Sanjuan B., Millot R., Asmundsson R., Brach M., Giroud N. (2014) - Use of two new Na/Li geothermometric relationships for geothermal fluids in volcanic environments. *Chemical Geology,* 389, 60-81.

Sanjuan B., Millot R., Dezayes Ch. (2016a) - Three new auxiliary chemical geothermometers for hot brines from geothermal reservoirs. *Goldschmidt 2016 Conference Abstract, June 26 - July 1, Yokohama, Japan,* 1 p.

Sanjuan B., Gal F., Millot R., Dezayes Ch., Jirakova H., Frydrych V., Nawratil de Bono C., Martin F. (2016b) - Final report on chemical geothermometers and tracers. *Final IMAGE-D7.03 report*, 74 p.

Sanjuan B., Gal F., Millot R., Dezayes Ch., Nawratil de Bono C., Martin F. (2017) - Thônex fluid geochemistry and geothermometric aplications. *Contribution to the final IMAGE-D8.02 report, Application of exploration techniques on sedimentary and basin fields, 209 p.*, 120-147, Appendix 2.

Seal R.R.I, Alpers C.N., Rye R.O. (2000) - Stable isotope systematics of sulfate minerals. *In: Alpers C.N., Jambor J.L., Nordstrom D.K. Eds, Sulfate minerals - Crystallography: Geochemistry and Environmental significance*, 541-602.

Spycher N., Peiffer L., Sonnenthal E.L., Saldi G., Reed M.H., Kennedy B.M. (2014) - Integrated multicomponent solute geothermometry. *Geothermics*, 51, 113-123. DOI: DOI:10.1016/ j.geothermics.2013.10.012.

Zeebe E.E. (2010) - A new value for the stable oxygen isotope fractionation between dissolved sulfate ion and water. *Geochimica et Cosmochimica Acta*, 74, 818-828.

***Los Humeros geothermal system***

Arellano Gomez V.M., García A., Barragán Reyes R.M., Izquierdo G., Aragón A., Nieva D. (2003) - An updated conceptual model of the Los Humeros geotermal reservoir (México). *Journal of Volcanology and Geothermal Research*, 124, 67-88.

Arellano Gomez V.M., Torres M.A., Barragán Reyes R.M. (2005) - Thermodynamic evolution of the Los azufres, México, geothermal reservoir from 1982 to 2002. *Geothermics*, 34, 592-616.

Arellano Gomez V.M., Aragón Aguilar A., Barragán Reyes R.M., Flores Armenta M., Ramírez Montes M., Tovar Aguado R. (2008) - Análisis de datos de producción y condiciones termodinámicas del fluido de alimentación de pozos de Los Humeros, Pue. *Geotermia*, 21, n°2, 21-28.

Arellano Gomez V.M., Barragán R.M., Ramírez M., Lopez S., Paredes A., Aragón A., Tovar R. (2015) - The response to exploitation of the Los Humeros (México) geothermal reservoir. *Proceedings World Geothermal Congress 2015, Melbourne, Australia, 19-25 April 2015*, 7 p.

Arzate J., Corbo-Camargo F., Carrasco-Núñez G., Hernández J., Yutsis V. (2018) - The Los Humeros (México) geotermal field model deduced from new geophysical and geological data. *Geothermics*, 71, 200-211.

Barragán-Reyes R.M., Arellano Gomez V.M., Flores Armenta M., Tovar Aguado R. (2008) - Cambios químicos en fluidos de pozos del campo geotérmico de Los Humeros: evidencia de recarga profunda. *Geotermia*, 21, n°2, 11-20.

Barragán-Reyes R.M., Arellano Gomez V.M., Ramírez Montes M., Tovar Aguado R. (2010) - Geoquimica isotópica (d18O, dD) inicial de fluidos de pozos del campo geotérmico de Los Humeros, Pue. *Geotermia*, 23, n°1, 16-25.

Bernard R. (2008) - Isotopos de H, O, He, C and N en fluidos hidrotermales del Cinturón Volcánico Mexicano. *M.S. Thesis, Posgrado de Ciencias de la Tierra, UNAM*, 157 p.

Bernard R., Taran Y., Pennisi M., Tello E., Ramirez A. (2011) - Chloride and boron behaviour in fluids of Los Humeros geothermal field (Mexico): a model based on the existence of deep acid brine. *Applied geochemistry*, 26, 2064-2073.

Campos-Enriquez J.O, Garduño-Monroy V.H. (1987) - The shallow structure of Lod Humeros and Las Derrumbadas geothermal fields, México. *Geothermics*, 16 (5/6), 539-554.

Carrasco-Núñez G., López-Martínez M., Hernández J., Vargas V. (2017a) - Subsurface stratigraphy and its correlation with the surficial geology at Los Humeros geothermal field, eastern Trans-Mexican volcanic belt. Geothermics, 67, 1-17.

Carrasco-Núñez G., Hernández J., De León L., Dávila P., Norini G., Bernal J.P., Jicha B., Navarro M., López P. (2017b) - Geologic map of Los Humeros volcanic complex and geothermal field, eastern Trans-Mexican Volcanic Belt. *Terra Digitalis*, 1(2), 1-11.

Carrasco-Núñez G., Bernal J.P., Dávila P., Jicha B., Giordano G., Hernández J., Navarro M. (2018) - Reapraisal of Los Humeros volcanic complex by new U/Th zircon and 40Ar/39Ar dating: implications for greater geothermal potential. *Geochem.Geophys. Geosyst.*, 19. https://doi.org/10.1002/2017GC007044.

Cedillo F. (1997) - Geología del subsuelo del campo geotérmico de Los Humeros, Puebla, México. Internal report CFE, México, 30 p.

Cedillo F. (1999) - Modelo hidrogeológico de los yacimientos geotérmicos , Puebla, México. Geotermia, Revista Mexicano de Geoenergía, 15-3, 159-170.

Cedillo-Rodríguez F. (2000) - Hydrogeologic model of the geothermal reservoirs from Los Humeros , Puebla, México. *Proceedings World Geothermal Congress 2000, Kyushu - Tohoku, Japan, May 28 - June 10, 2000,* 6 p.

Cortés A., Durazo J., Farvolden R.N. (1996) - Studies of isotopic hydrology of the Basin of México and vicinity: annoted bibliography and interpretation. *Journal of Hydrology*, 198, 346-376.

Davila-Harris P., Carrasco-Núñez G. (2014) - An unusual syn-eruptive bimodal eruption: the Holocene Cuicuiltic Member at Los Humeros caldera, México. *Journal of Volcanology and Geothermal Research*, 271, 24-42.

De la Cruz V. (1983) - Estudio geológico a detalle de la zona geotérmica de Los Humeros, Pue. *Internal report 10/83, CFE*, 51 p.

Cortés A., Durazo J., Farvolden R.N. (1997) - Studies of isotopic hydrology of the basin of Mexico and vicinity: annoted bibliography and interpretation. *Journal of Hydrology*, 346-376.

Ferriz H. and Mahood G. (1984) - Eruption rates and compositional trends at Los Humeros volcanic center. Puebla, México. *J. Geophys. Res.*, 89 (B10), 8511-8524.

García-Gutiérrez A. (2009) - Estado térmico inicial del campo geotérmico de Los Humeros, Puebla, México. Geotermia, 22, n°1, 59-70.

García-Soto A.Y., Pandarinath K., Marrero-Ochoa J.E., Diaz-Gomez C. (2016) - Solute geothermometry of Cerro Prieto and Los Humeros geotermal fields, Mexico: considerations on chemical characteristics of thermal water. *Arabian Journal of Geoscience*, 9, 517, 11 p.

Gutiérrez-Negrín L.C.A., Izquierdo-Montalvo G. (2010) - Review and update of the main features of the Los Humeros geothermal field, Mexico. *Proceedings World Geothermal Congress 2010, Bali, Indonesia, 25-29 April 2010*, 7 p.

Izquierdo G., Gutiérrez-Negrín L.C.A., and Aragón A. (2009) - Considerations on the origin of acid fluids in Los Humeros geothermal field, Pue., Mexico. *GRC Transactions*, vol. 33, 59-62.

Izquierdo G., Arellano V.M., Aragón A. (2008) - Características mineralógicas y micro-termométricas del yacimiento geotérmico de Los Humeros, Pue., México. *Geotermia*, 21, n°2, 2-10.

López-Hernández A. (1995) - Estudio regional volcánico y estructural del campo geotérmico de Los Humeros, Puebla, México. *Geotermia, Revista Mexicana de Geoenergia*, 11 (1), 17-36.

López-Romero O. (2006) - Actualización del modelo geoquímico de Los Humeros, Pue., México. *Geotermia*, 19, n°1, 23-32.

Macek M., Vilaclara G., Lugo A. (1994) - Changes in protozoan assemblage structure and activity in a stratified tropical lake. *Mar. Microb. Food Webs,* 8, 235-249.

Martinez M., Fernandez R., Visquez R., Vega R., Reyes S.A. (1983) - Asimilación del método magnetotelurico para la exploración geotérmica. *Quinto informe técnico CICESE-IIE*, México.

Martínez-Serrano R.G (2002) - Chemical variations in hydrothermal minerals of the Los Humeros geotermal system, Mexico. *Geothermics*, 31, 579-612.

Norini G., Gropelli G., Sulpizio R., Carrasco-Núñez G., Davila-Harris P., Pellcioli C., Zucca F., De Franco R. (2015) - Structural analysis and thermal remote sensing of the Los Humeros volcanic complex: implication for volcano structure and geothermal exploration. *Journal of Volcanology and Geothermal Research*, 301, 221-237.

Peïfer L., Carrasco-Núñez G., Mazot A., Villanueva-Estrada R.E., Inguaggiato C., Bernard Romero R., Rocha Miller R., Hernández Rojas J. (2018). Soil degassing at the Los Humeros geothermal field (Mexico). *Journal of Volcanology and Geothermal Research*, 356, 163-174.

Pinti D.L., Castro M.C., Lopez-Hernández A., Han G., Shouakar-Stash O., Hall Ch.M., Ramírez-Montes M. (2017) - Fluid circulation and reservoir conditions of the Los Humeros Geotermal Field (LHCF), México, as revealed by a noble gas survey. *Journal of Volcanology and Geothermal Research*, 333-334, 104-115.

Portugal E., Izquiedo G., Barragan R.M., Romero B.I. (2002) - Hydrodynamic model of Los Humeros geotermal field, México, based on geochemical, mineralogical and isotopic data. *Geofísica Internacional*, 41, n°4, 415-420.

Prol-Ledesma R.M. (1998) - Pre- and post-exploration variations in hydrothermal activity in Los Humeros geothermal field, Mexico. *Journal of Volcanology and Geothermal Research*, 83, 313-333.

Quijano J.L., Latorre D.C., Payne B.R. (1981) - Algunos aspectos de la geohidrogeología isotópica de la región de Valsequillo. *Proceedings of the Interamerican Symposium on Isotope Hydrology, Colombia, 18-22 August, 1980*, 15 p.

Tello H.E. (2005) - Estado de equilibrio Soluto-Mineral y saturación de Minerales de alteración en fluidos geotérmicos de alta temperature. *Facultad de Ingeniería, UNAM, PhD Thesis*.

Verma S.P. (1983) - Magma genesis and chamber processes at Los Humeros caldera, México. Nd and Sr isotope data. *Nature*, 302, 52-55.

Verma S.P. (2000) - Geochemical evidence for a lithospheric source for magmas from Los Humeros caldera, Puebla, México. *Chemical Geology*, 164, 35-60.

Verma S.P., Tello E., Arellano V., Nieva D. (1998) - Acidic fluid in Los Humeros geothermal reservoir. A preliminary outlook. *In Proceedings 23^rd^ Workshop on Geothermal Reservoir Engineering, Stanford University, Stanford, California*, 234-239.

Yáñez García C, Casique Vázquez J. (1980) - Informe geológico del Proyecto geotérmico Los Humeros-Las Derrumbadas, Estados de Puebla y Veracruz, México. Internal CFE report (unpublished).

***Acoculco geothermal system***

Avellán D.D, Macías J.L., Layer P.W., Sosa-Ceballos G., Marti J. (2017) - Geology of the Acoculco caldera complex at the eastern Trans-Mexican Volcanic Belt (México). *Poster presentation. IAVCEI 2017, Scientific Assembly Fostering Integrative Studies of Volcanoes. Portland Oregon, USA.*

Bernard-Romero B.R. (2008) - Nuevos datos geoquímicos de yacimientos geotermales de alta temperature del cinturón vólcanico mexicano: Isótopos de helio, boro, nitrógeno y elementos traza. *(Master Thesis) Universidad Nacional Autónoma de México*, 124 p.

Canet C., Hernández-Cruz B., Jiménez-Franco A., Pi T., Peláez B., Villanueva-Estrada R.E., Alfonso P., González-Partida E., Salinas S. (2015a) - Combining ammonium mapping and short-wave infrared (SWIR) reflectance spectroscopy to constrain a model of hydrothermal alteration for the Acoculco geotermal zone, Eastern México. *Geothermics*, 53, 154-165.

Canet C., Trillaud F., Prol-Ledesma R.M., González-Hernández G., Peláez B., Hernández-Cruz B., Sánchez-Córdova M.M. (2015b) - Thermal history of the Acoculco geotermal system, Eastern Mexico: insights from numerical modeling and radiocarbon dating. *Journal of Volcanology and Geothermal Research*, 305, 56-62.

Canet C., Arana L., González-Partida E., Pi T., Prol-Ledesma R.M., Franco S.I., Villanueva-Estrada R.E., Camprubí A., Ramírez-Silva G., Lopez-Hernández A. (2010) - A statistics-based method for the short-wave infrared spectral analysis of altered rocks: an example from the Acoculco Caldera, Eastern Trans-Mexican Volcanic Belt. *Geochemical Exploration*, 105, 1-10.

García-Palomo A., Macías J.L., Jimenénez A., Tolson G., Mena M., Sánchez-Núñez J.M., Arce J.L., Layer P.W., Santoyo M.A., Lermo-Samaniego J. (2017) - NW-SE Pliocene-Quaternary extensión in the Apan-Acoculco región, Eastern Trans-Mexican Volcanic Belt. *Journal of Volcanology and Geothermal Research*. https://doi.org/10.1016/j.jvolgeores.2017.11.005.

Ledezma-Guerrero O. (1987) - Hoja Calpulalpan 14Q-h (3), con Resumen de la geología de la hoja Calpulalpan, Estados de México, Puebla, Tlaxcala e Hidalgo. Instituto de Geología, Universidad Nacional Autónoma de México, México. Quetzalapa región, soouthern México. *Rev. Mex. Cienc. Geol.*, 15, 167-180.

Lermo J., Antayhua Y., Bernal I., Venegas S., Arredondo J. (2009) - Monitoreo sísmico en la zona geotérmica de Acoculco, Pue., Mexico. *Geotermia*, 22, n°1, 40-58.

Lopez-Hernández A., Castillo-Hernández D. (1997) - Exploratory drilling at Acoculco, Puebla, Mexico: a hydrothermal system with only non-thermal manifestations. *Geothermal Resource Council Transactions*, 21, 429-433.

Lopez-Hernández A., García-Estrada G., Aguirre-Díaz G., González-Partida E., Palma-Guzmán H., Quijano-León J.L. (2009) - Hydrothermal activity in the Tulancigo-Acoculco Complex, central México: exploration studies. *Geothermics*, 38, 279-293.

Nixon G.T. (1982) - The relationship between Quaternary volcanism in central México and the seismicity and structure of subducted ocean lithosphere. *Geol. Soc. Am. Bull.*, 93, 514-523.

Peiffer L., Bernard-Romero R., Mazot M., Taran Y.A., Guevara M., Santoyo E. (2014b) - Fluid geochemistry and soil gas fluxes ($CO_2$-$CH_4$-$H_2S$) at a promissory Hot Dry Rock geotermal system: the Acoculco caldera, Mexico. *Journal of Volcanology and Geothermal Research*, 284, 122-137.

Peiffer L., Wanner Ch., Pan L. (2015) - Numerical modelling of cold magmatic $CO_2$ flux measurements for the exploration of hidden geothermal systems. *AGU publications*, *Journal of Geophysical Research: Solid Earth*, 22 p.

Polak B.G., Prasalov E.M., Kononov V.I., Verkovsky A.B., González A., Templos L.A., Espíndola J.M., Arellano J.M., Manon A. (1982) - Isotopic composition and concentration of inert gases in Mexican hydrothermal systems. *Geofis. Int.*, 21, 193-227.

Sosa-Ceballos G., Macías J.L., Avellán D.R., Salazar-Hermenegildo N., Boijseauneau-López M.E., Pérez-Orozco J.D. (2018) - The Acoculco caldera complex magmas: Genesis, evolution and relation with the Acoculco geothermal system. *Journal of Volcanology and Geothermal Research*, 358, 288-306.

Tello Hijonosa E. (1986) - Geoquímica de la zona geotérmica de la caldera de Acoculco, Puebla. Informe 34-86, Departamento de exploración, Comisión Federal de Electricidad, 14 p + anexos.

Tello Hijonosa E. (1987) - Composición química e isotópica del agua de los manantiales de la zona geotérmica de Acoculco, Puebla. Informe 23/87, Departamento de exploración, CFE-GPG.

Tello Hijonosa E. (1991) - Química de los fluidos hidrotermales de la zona geotérmica de la Caldera de Acoculco. *Geotermia*, 7, n°2, 201-230.

Tello Hijonosa E., Ruiz Aceves L., Velázquez N. (1995) - Geoquímica de lodos de perforación del pozo EA-1, Acoculco, Puebla. Informe GQ-AC-012/95, Comisión Federal de Electricidad, 4 p + anexos.

Verma P. (2001) - Geochemical evidence for a lithospheric source for magmas from Acoculco Caldera, Eastern Mexican Volcanic Belt. International Geology review, 43, 31-51.

Ziagos J.P., Blackwell D.D., Mooser F. (1985) - Heat flow and the thermal effects of subduction in Southern México. *Journal of Geophysical Research*, 90, 5410-5420.

# Chapter 4

## DIFFUSE DEGASSING

### 4.1 Methods and sampling approach

In total three soil gas surveys were conducted at the Los Humeros Geothermal Field. The first survey in 2017 (5 weeks) concentrated on the measurement of $CO_2$ efflux covering an area 4x6km. $CO_2$ efflux was selected as a scouting parameter to identify areas of interest for future planned surveys. A regular spaced sampling grid (25 x 200 m) was defined. Closely spaced measurements (25 m) were performed along sampling profiles oriented perpendicular to the main fault strike to ensure that small variations in soil gas emissions can be detected. By means of the accumulation chamber method, $CO_2$ efflux can be measured in-situ in a very short time (60s-120s). This allows maximum flexibility during the survey and when necessary further sampling sites could easily be added for a better delineation of areas characterized by increased gas emissions. $\delta^{13}C\text{-}CO_2$ samples were collected from selected sites and analyzed at the laboratory for compound-specific isotope analysis at the German Research Center for Geoscience (GFZ) in Potsdam with a Delta V Plus gas chromatograph coupled to an isotopic ratio mass spectrometer. Samples were collected from the major geothermal production field in areas with low, intermediate and high $CO_2$ effluxes to identify the origin of $CO_2$ emissions. No $CO_2$ efflux measurements were performed within the village to avoid artificial effects (Fig. 4.1).

During the second survey in 2018 (5 weeks) we focused on a smaller core region, which was identified as a result of the $CO_2$ efflux scouting survey. The campaign in 2018 concentrated on the radiometric measurement of Radon ($^{222}Rn$) and Thoron ($^{220}Rn$) activity concentrations. Due to the long measuring time of $^{222}Rn$ (15 min) the point distance had to be increased by 25 m. Nevertheless, the sampling campaign followed the same grid as of 2017. Soil temperatures were measured in 50 cm depth with a GMH 285-BNC thermocouple. Furthermore, helium samples were taken from active degassing sites to determine the $^3He/^4He$ ratios, which are normalized to the air ratio ($R/R_A$). The isotopic signature of helium yields important information about the origin and history of a fluid sample. The samples were analyzed in the noble gas laboratory of the GFZ with a Helix SFT mass spectrometer. Please see table 4.1 for a summary of all investigated parameters.

| Parameters | Size of study area [km] | Grid spacing [m] | No of samples | Analysis/ Sampling procedure | Sampling time [min] |
|---|---|---|---|---|---|
| **$CO_2$ efflux** | 6 x 4 | 25 x 200 | 2823 | In-situ, on surface | 1-2 |
| **$\delta^{13}C$-$CO_2$** | Selected sites | Single points | 44 | Lab, 1m below surface (b.s.) | 10 |
| **$^{222}Rn$** | 5.8 x 2.4 | 50 x 200 | 883 | In-situ, 1m b.s. | 15 |
| **$^{220}Rn$** | 5.8 x 2.4 | 50 x 200 | 867 | In-situ, 1m b.s. | 15 |
| **$T_s$** | 5.8 x 2.4 | 50/100 x 200 | 858 | In-situ, 50 cm b.s. | 10 |
| **$^3He/^4He$** | Selected sites | Single points | 6 | Lab, Variable depth (max. 30 cm b.s) | 10 |

Table 4.1 Summary of measured parameters

### 4.2 Determination of $CO_2$ efflux

Herein, all measurements of diffuse $CO_2$ emission rates were performed according to the accumulation chamber method described in detail by Chiodini et al. (1998). The measurement of $CO_2$ efflux allows an efficient real time analysis, without any necessary ground installation of sampling devices. Two portable diffuse flux meter (developed by West Systems Ltd.) have been used for analyses of $CO_2$ efflux. The instrument is equipped with a LICOR LI-820 single path, dual wavelength, nondispersive infrared (NDIR) carbon dioxide analyzer (West Systems Ltd., 2002). All measurements were performed with the accumulation chamber type A due to its higher sensitivity to lower fluxes (Jolie et al., 2012).

### 4.3 Determination of alpha radiation

The radiometric measurement of Radon and Thoron activity concentration in soil gas was performed with two RTM2200 monitors (developed by SARAD Ltd.) for portable and stationary applications. The RTM 2200 is an active instrument that allows in-situ data reading in the field. The gaseous isotopes $^{222}Rn$ (Radon) and $^{220}Rn$ (Thoron) have been studied simultaneously. The measurement enables to determine their short living radon daughter products $^{218}Po$ in fast mode, measuring 15 min at each sampling site. For the preparation of the sampling site a metal probe was inserted approximately 1 m into the ground. The soil gas was pumped from 1 m below the surface at a constant flow rate through a tube to the RTM2200 gas analyzer.

### 4.4 Mobile open path laser and soil gas survey

The BGS survey consisted of wide area mobile traverses of areas of interest using $CO_2$ laser detection, combined with point measurements, typically in a grid formation, for soil gas, gas flux and temperature, and selected gas samples collected for laboratory analysis.

Mobile laser surveys were carried out on foot to measure near ground atmospheric $CO_2$ concentrations over five discrete pre-selected areas (designated areas 1 to 5 in Fig. 4.7) between 20th February and 1st March 2018. The survey areas were selected on the basis of earlier $CO_2$

flux surveys performed project partners at GFZ (Section 4.1), or information from the UAV team or the site operator, CFE. The surveys consisted of a hand-held lightweight aluminium frame-mounted open path $CO_2$ laser combined with a back-mounted GasFinder 2 $CO_2$ laser unit (Boreal Laser Inc.), 2 x 6V battery pack and differential GPS (Trimble Inc.,). Lines were walked at an average speed of 4.0 km/h with a parallel line spacing of 10 m – 15 m. Data were recorded at a frequency of 1 Hz and, using proprietary GasMap® software, were displayed in real time on a dedicated Panasonic ToughBook.® Location data were recorded simultaneously via a Trimble® GPS.

Soil gas and flux measurements were carried out as a series of linear traverses across areas surveyed by the mobile laser, with 25 m point spacing intervals and a parallel line spacing of 100 m. Point measurements of $CO_2$ and $CH_4$ flux were made at the soil surface using a non-invasive closed-loop accumulation chamber method (West Systems flux meter equipped with Li-COR® model LI820 infra-red analysers). Point measurements of soil gas ($CH_4$, $CO_2$, $O_2$, $H_2S$, $H_2$, and a residual approximately equated to $N_2$) were made at the same locations by driving a narrow diameter hollow steel push probe 0.5-1 m into the ground. Soil gases were determined directly from the push probe using field instruments (Geotechnical Instruments GA5000® gas analyser and Huberg Laser One® methane detector). Temperature measurements were also taken at these same locations using a Hanna HI-93510® thermistor thermometer fitted with a custom-built long reach (c.50 cm) temperature probe.

For selected sampling points, primarily governed by a change in the characteristics of the *in situ* soil gas, flux or temperature measurements, gas samples were also collected for the determination stable isotopes of carbon in $CO_2$. Sample gas was flushed into a non-sterile 50 ml luer slip syringe via a two-way Omnifit® stopcock fitted to the push probe. The sample (c.24 ml) was then transferred to evacuated 12 ml glass Exetainer® vials with a septum screw cap using a non-sterile hypodermic needle. The samples were transported to the UK by air for laboratory determination of stable isotopes of carbon in $CO_2$ by continuous flow isotope ratio mass spectrometry.

### 4.5 Results

Within the following chapter we refer to specific areas by using capital letters A-E (Fig. 4.6) or, for the BGS survey, numerical references 1-5 (Fig. 4.7). $CO_2$ efflux values range from non-detectable (detection limit is 0.03 ppm/s) in the northwestern part of the geothermal field up to 838 g $m^{-2}d^{-1}$ in the southwest of Los Humeros village (Area E). Furthermore, there is a clear correlation between elevated $CO_2$ emissions (> 33 g $m^{-2}$ $d^{-1}$) and areas with known geothermal surface activity however, degassing was also observed in areas without obvious surface activity. This applies to all areas from A to E (Fig. 4.6). Active degassing sites are very prominent almost all along the Los Humeros fault, particularly on its fractured footwall and within its fault scarp. Surface alteration is a typical feature along the northern part of the Los Humeros fault, which coincides with increased degassing rates (Fig.4.2).

Similar spatial variations can be identified for Radon activity concentration, which ranges from 110 Bq $m^{-3}$ up to 100,730 Bq $m^{-3}$. The highest value was determined in Area C, which is ~100 m north of the Los Humeros village. The overall trend of $^{222}Rn$ correlates with $CO_2$ efflux, but elevated $^{222}Rn$ values have been measured across a larger area (Fig.4.4).

The maximum soil temperature of 91.3 °C was measured in Area C, in the southern section of the Loma Blanca fault. Even though surface temperatures show a less prominent spatial pattern they do correlate with $^{222}Rn$ and $CO_2$ (Fig. 4.5).

$\delta^{13}C$-$CO_2$ isotopic compositions range from -19.1 to -1.2. The more negative values correspond to biogenic sources (mostly C4 plants like maize), the less negative values originate from a deeper source. As seen in figure 4.3, almost all sites which are characterized by elevated degassing rates (> 33 g $m^{-2}d^{-1}$ ), show a hydrothermal or mixed $\delta^{13}C$-$CO_2$ isotopic composition, except for one sample which is possibly contaminated by air (Fig. 4.3).

All results for helium isotopic ratios $^3He/^4He$ are illustrated in figure 4.5. Four samples show a clear trend towards mantle derived helium, whereas the other two have been sampled at locations where a saturation of atmospheric $CO_2$ must have been present in the first 50 cm below the surface.

| Parameters | Min | Max | Mean |
|---|---|---|---|
| **$CO_2$ efflux [g $m^{-2}d^{-1}$]** | 0 | 839 | 8.5 |
| **$^{222}Rn$ [Bq $m^{-3}$]** | 110 | 100,730 | 3,610 |
| **$^{220}Rn$ [Bq $m^{-3}$]** | 135 | 35,063 | 3,835 |
| **$T_s$ [°C]** | 5.9 | 91.3 | 17.5 |
| **$^3He/^4He$ [$R/R_a$]** | 2.31 | 4.88 | 3.4 |
| **$\delta^{13}C$-$CO_2$ [δ ‰ vs. VPBD]** | -19.2 | -1.2 | |

Table4.2 Minima, maxima and mean values of measured parameters

| Population | Fraction [%] | Mean efflux [g m$^{-2}$ d$^{-1}$] | Interval [g m$^{-2}$ d$^{-1}$] |
|---|---|---|---|
| **Anomalous** | 1.9 | 139.8 | 47.8 - 839 |
| **Mixture** | 0.9 | 40.5 | 33.3 – 47.8 |
| **Background** | 97.2 | 6 | 0.1 – 33.3 |

Table 4.3 Statistical parameters for $CO_2$ efflux

| Population | Fraction [%] | Mean concentration [Bq m$^{-3}$] | Interval [Bq m$^{-3}$] |
|---|---|---|---|
| **Anomalous** | 1.6 | 35,024.4 | 22,218 – 100,727 |
| **Mixture** | 0.3 | 18,143.6 | 15,724 – 22,218 |
| **Background** | 98.1 | 3,030.7 | 110 – 15,724 |

Table 4.4 Statistical parameters for $^{222}$Rn activity concentrations

Spatial plots of the mobile laser traverses, along with point measurement data collected during this fieldwork, were generated in ArcGIS® and projected onto a georeferenced satellite imagery base map, alongside data collected by other GEMex project partners where appropriate (e.g. in Fig. 4.13). Laser data are presented as raw concentrations of volume % $CO_2$ as an illustration in Figs. 4.8 and 4.9, but primarily they are presented as absolute differences in adjacent 5 point averaged data values since this did not result in any appreciable loss of detail. The 5 point average differences were used in attempting to identify small but significant changes in background $CO_2$ concentrations over relatively short time periods.

Data from the mobile laser surveys are plotted and viewed together with point measurements of soil gas and flux for each of the five survey areas to determine whether any relationships between datasets could be identified (Figs. 4.8 to 4.12). The spatial distribution of stable isotopes of carbon ($\delta^{13}C$-$CO_2$) across areas 1 to 5 are shown in Fig. 4.18.

## 4.6 Discussion

Welded ignimbrite deposits that act as a low-permeability barrier (Gutiérrez-Negrín and Izquierdo-Montalvo, 2010) as well as hydrothermal alteration within the fault zones cause heterogeneous gas emissions along mapped faults. The presence of very high degassing areas ($CO_2$ efflux > 300 g m$^{-2}$d$^{-1}$) at the surface can only be explained by convection along permeable faults/ fractures. There is a potential structural link between Area C and Area E, which is supported by the results of Radon measurements. The Los Humeros fault might be much more complex in the subsurface than expected. Its horse tailing structure could possibly evolve around Area E (Fig. 4.6), which could have an effect on structural permeability. Another theory is that there is a single structure connecting Area E towards Area C and continuing to La Cuesta Fault. The area SE of Los Humeros village, where the general fault strike changes from NNE-SSW to E-W appears as an area of increased gas emissions (Fig. 4.2). This is due to the change in soil cover (from unconsolidated soils to humus with pine forest). The overall spread in $\delta^{13}C$-$CO_2$ values shows different sources of $CO_2$ due to biological processes (-30 to -10‰), contamination with atmospheric $CO_2$ in the upper soil portion (-8 ‰), magmatic source (-8 to -5‰ MORB type gases), and sedimentary or hydrothermal $CO_2$ (-5 to 2.73 ‰). Limestone samples from the basement taken by González-Partida et al. (1993) show a $\delta^{13}C$-$CO_2$ composition ranging from 0.32 to −0.8 ‰. Portugal et al. (1994) sampled geothermal fluids from wells, which show $\delta^{13}C$-$CO_2$ composition ranging from −4.5 to −6.6 ‰.

All samples taken from areas with increased gas emissions have less negative $\delta^{13}C$-$CO_2$ values, coinciding with sampled geothermal fluids from Portugal et al. (1994) and indicating a deep origin. Interestingly, some of the very low $CO_2$ effluxes, which have been assigned to the background population (from 14 g $m^{-2}d^{-1}$ and higher), still show magmatic/hydrothermal $\delta^{13}C$-$CO_2$ signatures. Elevated $^3He/^4He$ ratios (> 3) indicate a mantle contribution. By carbon isotopic analysis of $CO_2$ and helium isotopic analysis $^3He/^4He$ it is indicated that faults and fractures in the subsurface have a link to the deep geothermal reservoir and favor the upflow of hydrothermal fluids. This can also be seen by the observed thermal anomalies at the surface. Results from all three measured parameters indicate that the most permeable zone in the Los Humeros geothermal field is located in Area E (SW) and extends towards the north (Area A) and northeast (Area B, C, and D). Our results suggest that the combination of various soil gas measurements is a useful approach to indicate major structural discontinuities in the subsurface that act as migration pathways of hydrothermal fluids. Furthermore, we would like to point out that a strategic sampling network plays a major role not only to identify but also determine the geometry and distribution of permeable volcano-tectonic structures.

The objective of the BGS soil gas campaign was to provide more detail within areas of interest emerging from the May 2017 campaign, rather than attempt to duplicate those measurements. Nonetheless, around 30% of flux sample points used during the current survey fell on the existing $CO_2$ flux survey lines, and measurements of $CO_2$ flux taken in February 2018 are compared in Fig. 4.13 with $CO_2$ flux taken as part of the May 2017 scoping exercise. Given the elapsed time between surveys and the accuracy constraints of the field GPS systems, none can realistically be considered field duplicates and comparisons between data from the two surveys are, at this stage, confined to a visual comparison on an area by area basis. Even so, despite the time elapsed and limited overlap, the datasets for this region of the Los Humeros both indicate coincident areas of relatively high $CO_2$ flux. The circled points in Figs. 4.14 and 4.15 highlight areas where the datasets show coincident elevated soil gas $CO_2$ and $CO_2$ flux. The green points represent flux data collected during the May 2017 campaign. The areas outlined display elevated concentrations in both datasets, falling within an approximate distance of 5 m from each other. These areas warrant further investigation, e.g. a closer examination of this data in view of other available survey data.

The Los Humeros campaign was one of the first field deployments of the lightweight hand held open path laser prototyped by BGS. The laser unit and battery pack are mounted on a rigid frame backpack, with a rugged laptop providing the user interface with real time displays of $CO_2$ concentration and GPS position. This configuration provides greatly improved mobility across terrain that is difficult to survey even in all terrain/off-road vehicles. The trade-off is in the sensitivity that can be achieved. Nonetheless, a number of hot spots were identified as highly elevated $CO_2$ concentrations measured during the mobile laser surveys, principally in areas 1 and 3. These were confirmed by point measurements of soil gas and gas fluxes (Figs. 4.8 to 4.12). Particularly the hot spot at Area 3 (Fig. 4.16) was previously unrecorded, having been missed by all previous grid-based surveys.

The previously unrecorded area of high $CO_2$ concentration detected by the mobile laser system is shown in more detail in Fig. 4.16, where the mobile laser $CO_2$ data are shown as 5-point average differences. The absolute mobile laser $CO_2$ concentrations (the raw data) are shown in Fig. 4.17 for comparison. As can be seen, the anomalously high concentrations identified in the absolute data are preserved in the 5-point averaged difference data. The mobile laser $CO_2$ data are also confirmed by a number of point measurements of $CO_2$ in soil gas and $CO_2$ flux. The anomaly was initially identified whilst traversing the gravel track in area 3 with the mobile laser. The extent of the anomalous zone was then better defined to extend along a length of approximately 18 m, oriented linearly NW – SE.

The mobile laser data show the extent and orientation of the high $CO_2$ anomaly, with $CO_2$ concentrations significantly above the atmospheric background. A static laser log also detected elevated $CO_2$, with peak values >1000 mg $kg^{-1}$. Soil gas and flux measurements made adjacent to the static laser log were also indicative of very anomalously high $CO_2$, with 20.7% $CO_2$ in soil gas at 0.90 m depth and a $CO_2$ flux of 1464 g $m^{-2}$ $day^{-1}$ (Fig.4.17). Slight discrepancies in the locations of the soil gas and flux points is likely to be due to the accuracy of the GPS units used.

The extremely localised nature of observed anomalies i.e. the very rapid change from anomalously high concentrations to background over distances of a few meters or less, was evident from both the soil gas/flux traverses and the mobile laser surveys. This may imply that the transport of free gas through soil is discrete and could be evidence of distinct degassing pathways, as opposed to diffuse $CO_2$ gas dispersing though a contiguous layer of soil or overburden cover. Taking a wide area open path laser approach and combining with 5 point average absolute difference is appropriate, even helpful, in being potentially able to link soil gas anomalies to underlying faults, but there is a risk, even with a parallel line spacing of 10 m, the mobile laser could fail to detect extremely discrete areas of elevated $CO_2$ concentration. Even so, the identification and subsequent quantification of this previously unrecorded anomaly demonstrates the versatility and screening potential of the lightweight open path laser. Where $CO_2$ flux is more diffuse, it may be more appropriate to consider absolute $CO_2$ concentrations over the absolute differences.

Finally, the spatial distribution of stable isotopes of carbon ($\delta^{13}C$-$CO_2$) across the BGS survey areas 1 to 5 is shown in Fig. 4.18. The distribution is consistent with the findings of the May 2017 survey and a deep geogenic origin of $CO_2$ ($\delta^{13}C$-$CO_2$ > -15‰). This is most apparent in areas 1, 3 and 4 (i.e. Areas A and E of the May 2017 survey, NW and S of Los Humeros village), compared with isotope ratios more typical of biogenic $CO_2$ ($\delta^{13}C$-$CO_2$ < -15‰) in area 5 to the south east of the BGS survey area (Area D), and a mixed distribution in area 2 (Area B) where the 2014 vent is found.

**Acknowledgements**

We would like to thank all Mexican and German students who where part of our field campaigns and without them this extensive field surveys would not have been possible. We acknowledge the Comision Federal de Electricidad (CFE) for kindly providing support and advice and for granting access to their geothermal fields. We thank the entire GEMex team with scientists from Mexico and Europe.

**References**

Chiodini, G., Cioni, R., Guidi, M., Raco, B., & Marini, L. (1998). Soil CO2 flux measurements in volcanic and geothermal areas. *Applied Geochemistry*, *13*(5), 543–552. https://doi.org/10.1016/S0883-2927(97)00076-0

Gutiérrez-Negrín, L.C. & Izquierdo-Montalvo, G., 2010. Review and update of the main features of the Los Humeros geothermal field, Mexico. Proccedings World Geothermal Congress, Bali, Indonesia, April 2010.

González-Partida, E., Barragán, R.M., Arellano, V.M., 1993. Las especies carbónicas del fluido geotérmico de Los Humeros, Puebla, México. Geotermia 9, 205–218.

Jolie, E., Klinkmueller, M., & Moeck, I. (2012). Diffuse Degassing Measurements as a Geochemical Exploration Tool A Case Study From the Brady's Geothermal System (Nevada, USA). *GRC Transactions*, *36*, 685–688.

Portugal, E., Verma, M.P., Barragán, R.M.,Mañón, A., 1994. Geoquímica isotópica de 13C, D,y 18O de fluidos del sistema geotérmico Los Humeros Puebla (México). Geofis. Int. 33, 607–618.

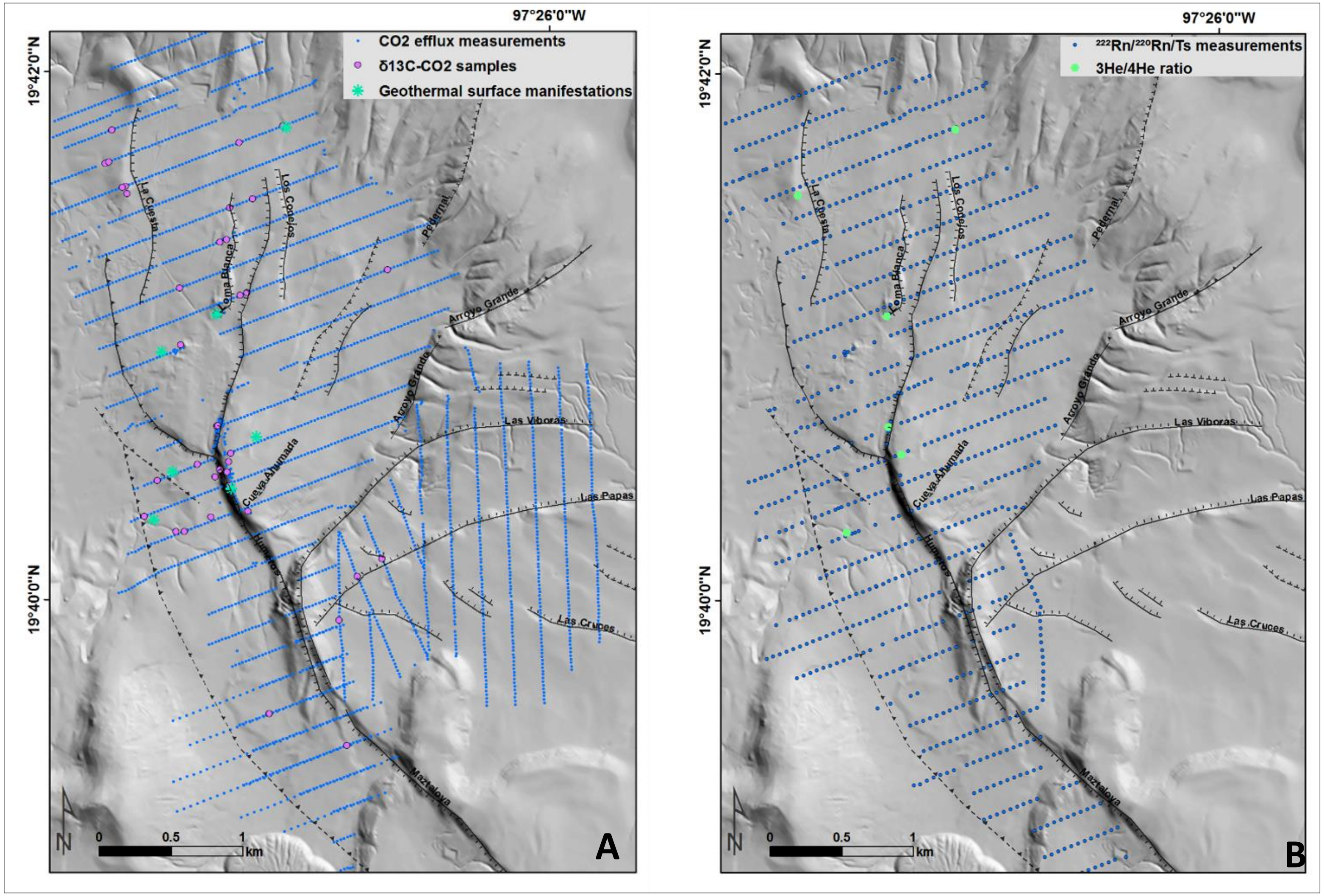


Figure 4.1 Survey design A: $CO_2$ efflux measurements (blue points), $\delta^{13}C$-$CO_2$ samples (purple points) and natural geothermal surface manifestations (green stars; steaming/hot ground, argillic alteration) and B: $^{222}Rn$ (Radon), $^{220}Rn$ (Thoron) and $T_s$ (soil temperatures) (blue points) and helium samples (green points). Black solid lines show mapped fault traces. Black dashed lines are inferred faults.

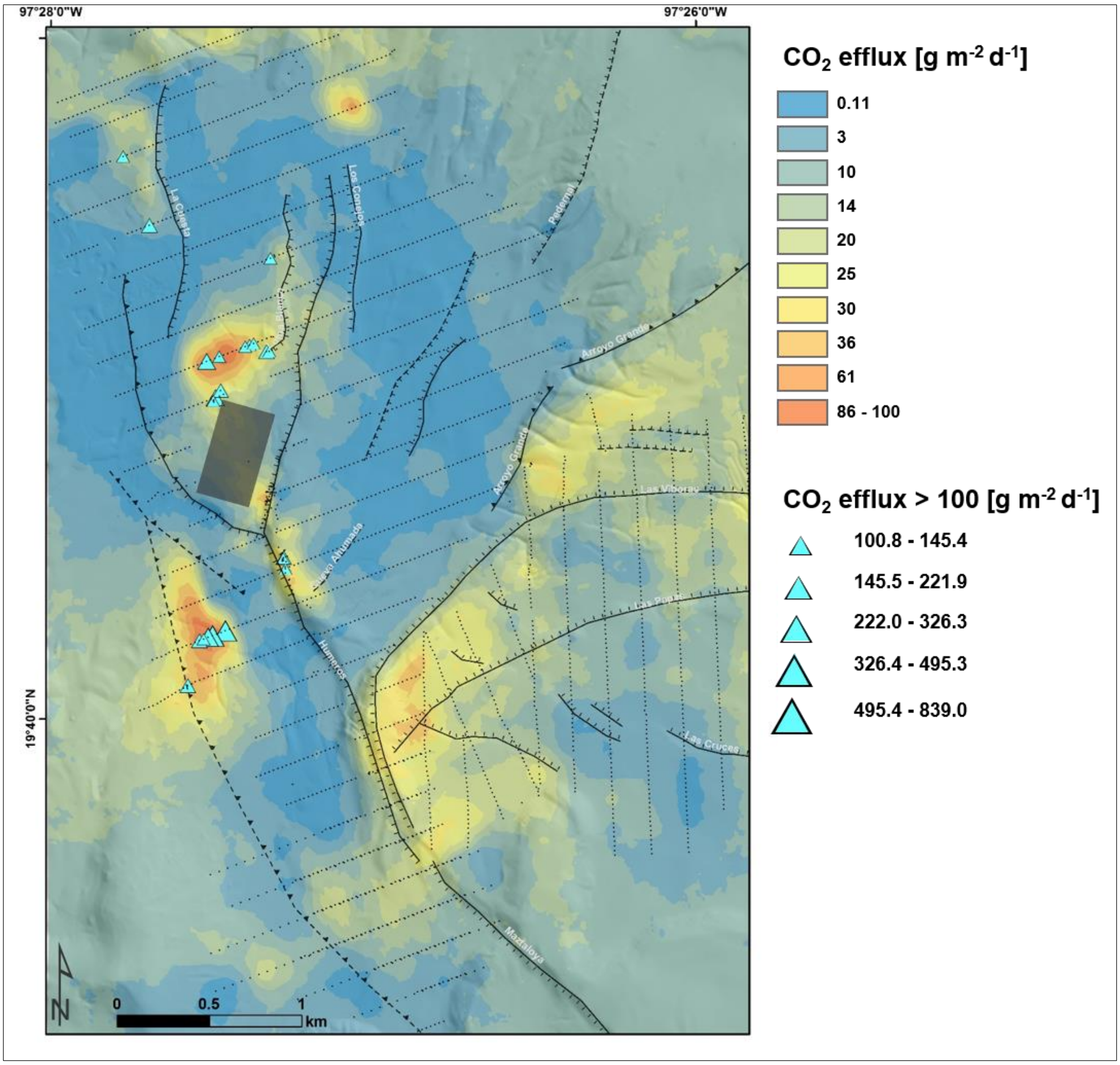


Figure 4.2 Interpolation map of $CO_2$ efflux excluding values > 100 g m$^{-2}$d$^{-1}$. Values above > 100 g m$^{-2}$d$^{-1}$ are shown as graduated triangles in turquoise. Small black dots represent sampling locations. Dark grey rectangle shows the Los Humeros village.

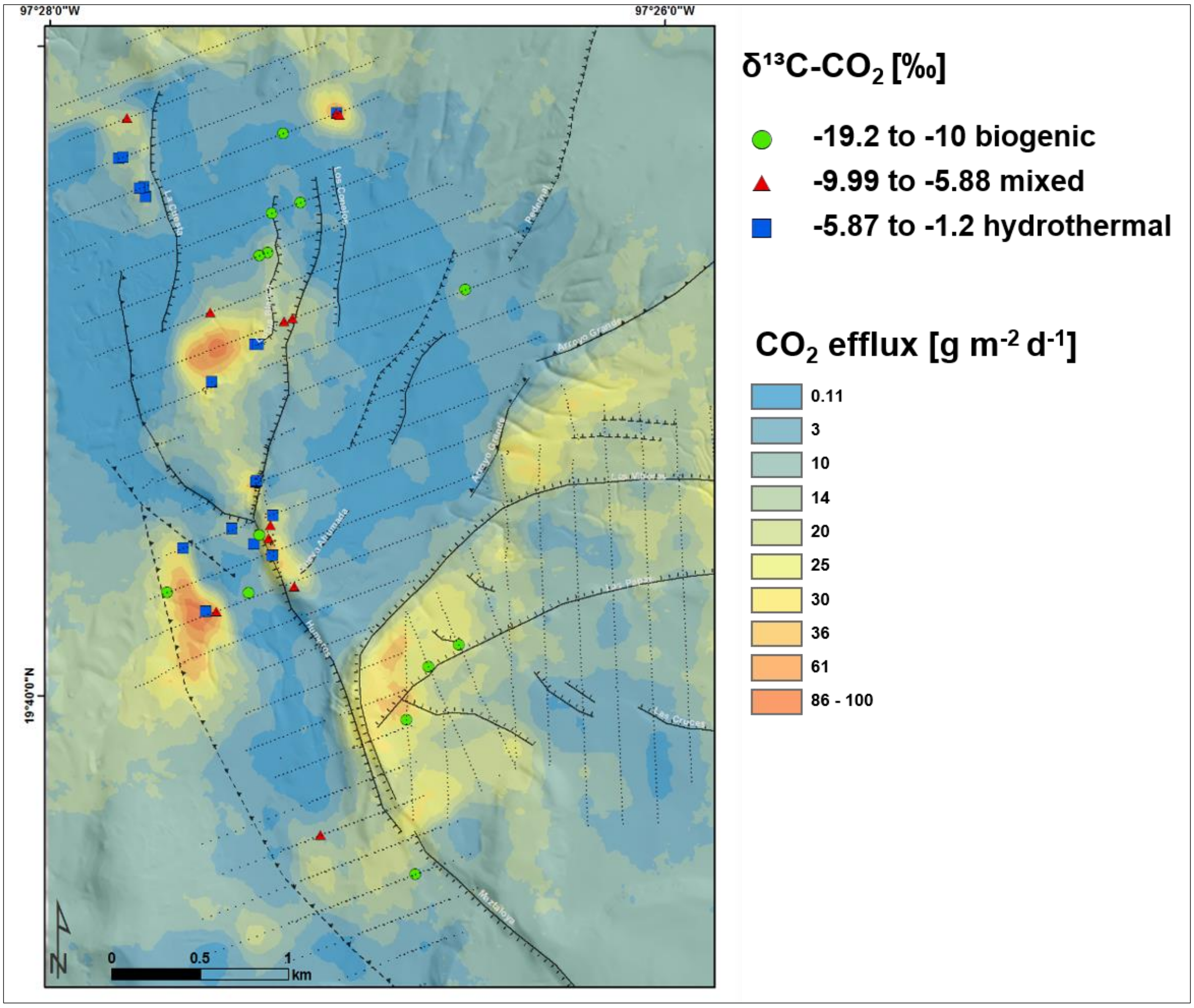


Figure 4.3 Overview of the distribution of $\delta^{13}C$-$CO_2$ samples and their isotopic signature.

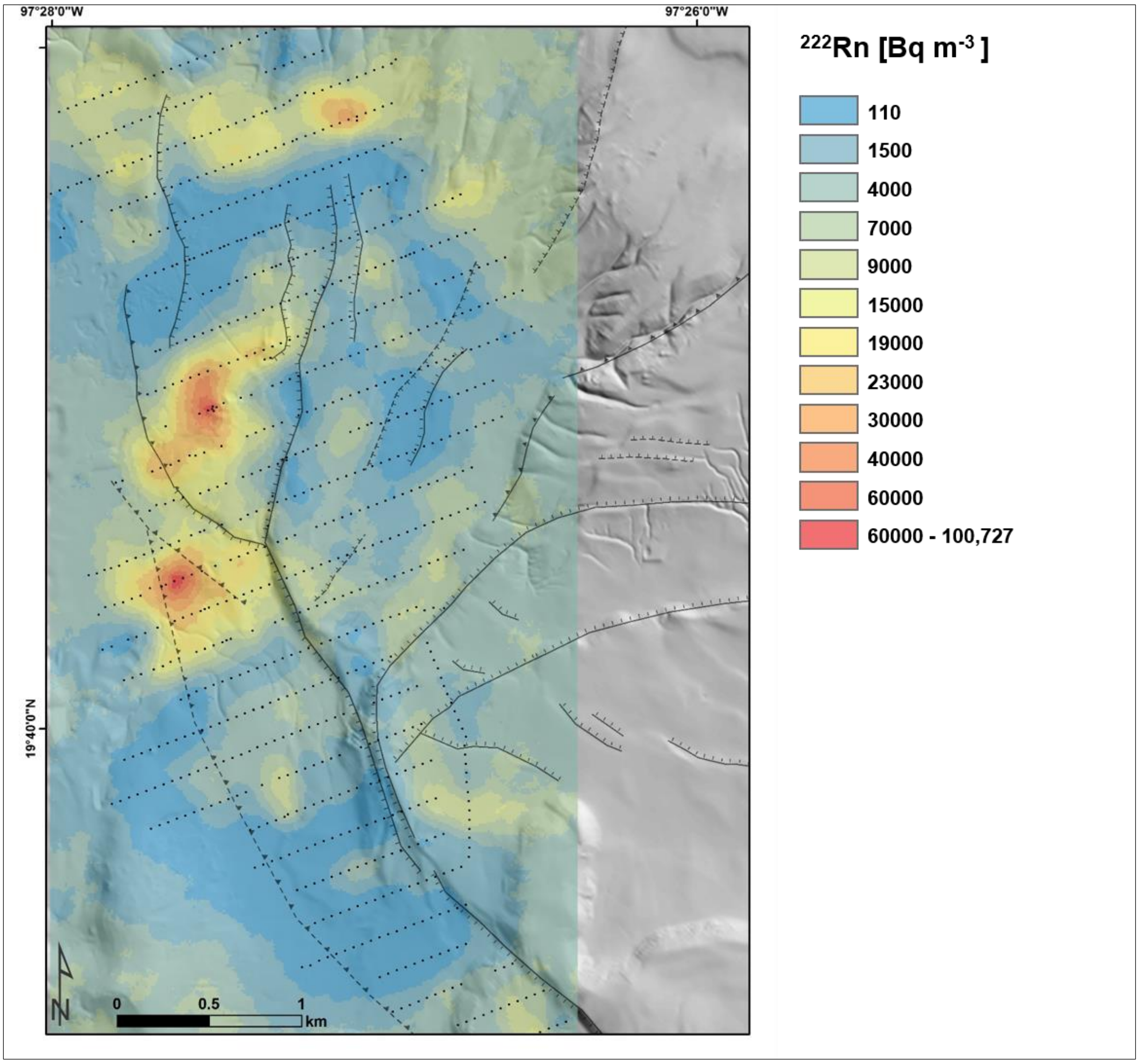


Figure 4.4 Interpolation map of Radon. Small block dots illustrate sampling sites.

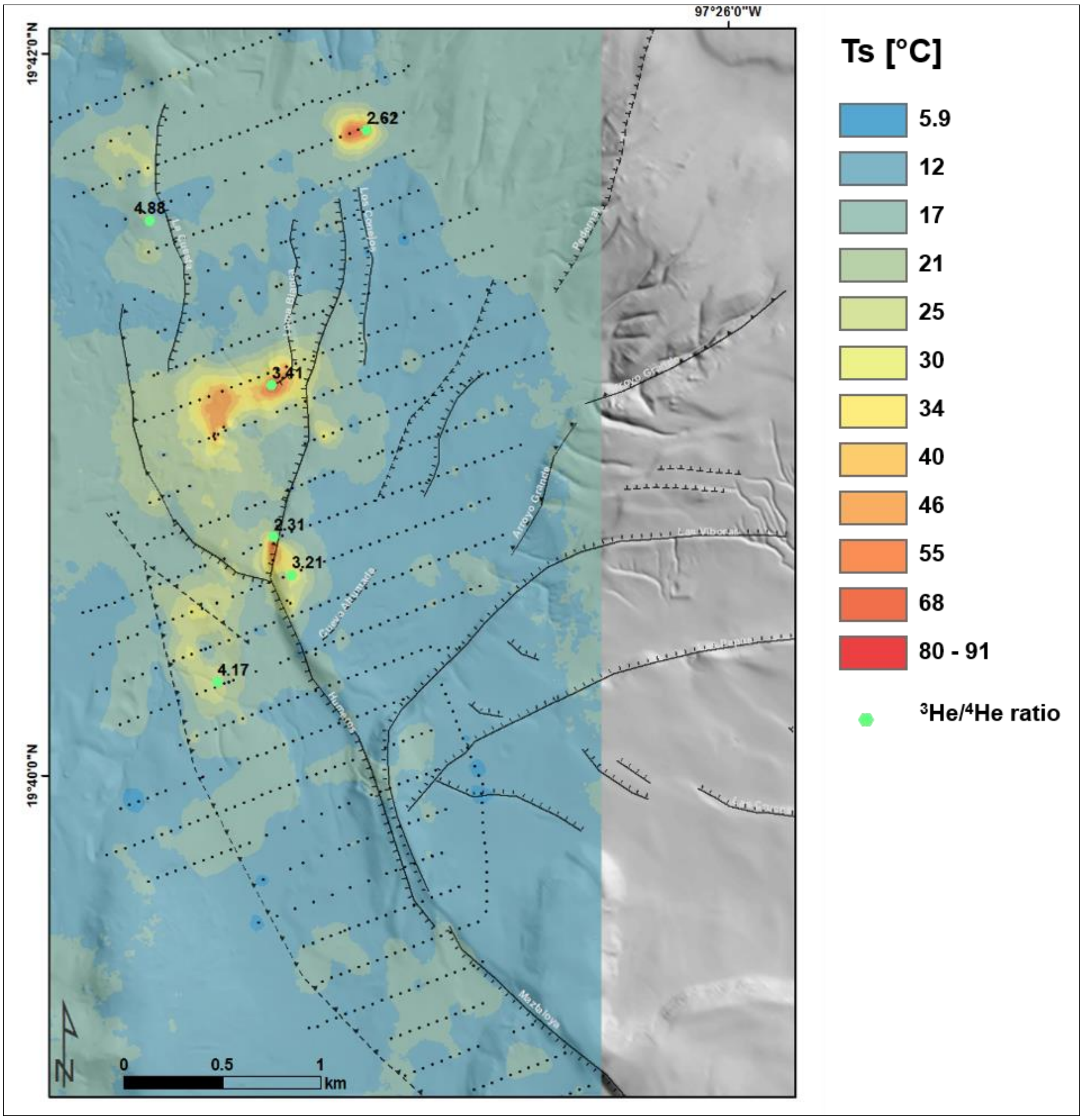


Figure 4.5 Interpolation map of soil temperatures together with sampling sites of soil temperatures (black points). The green dots illustrate $^3He/^4He$ ratios.

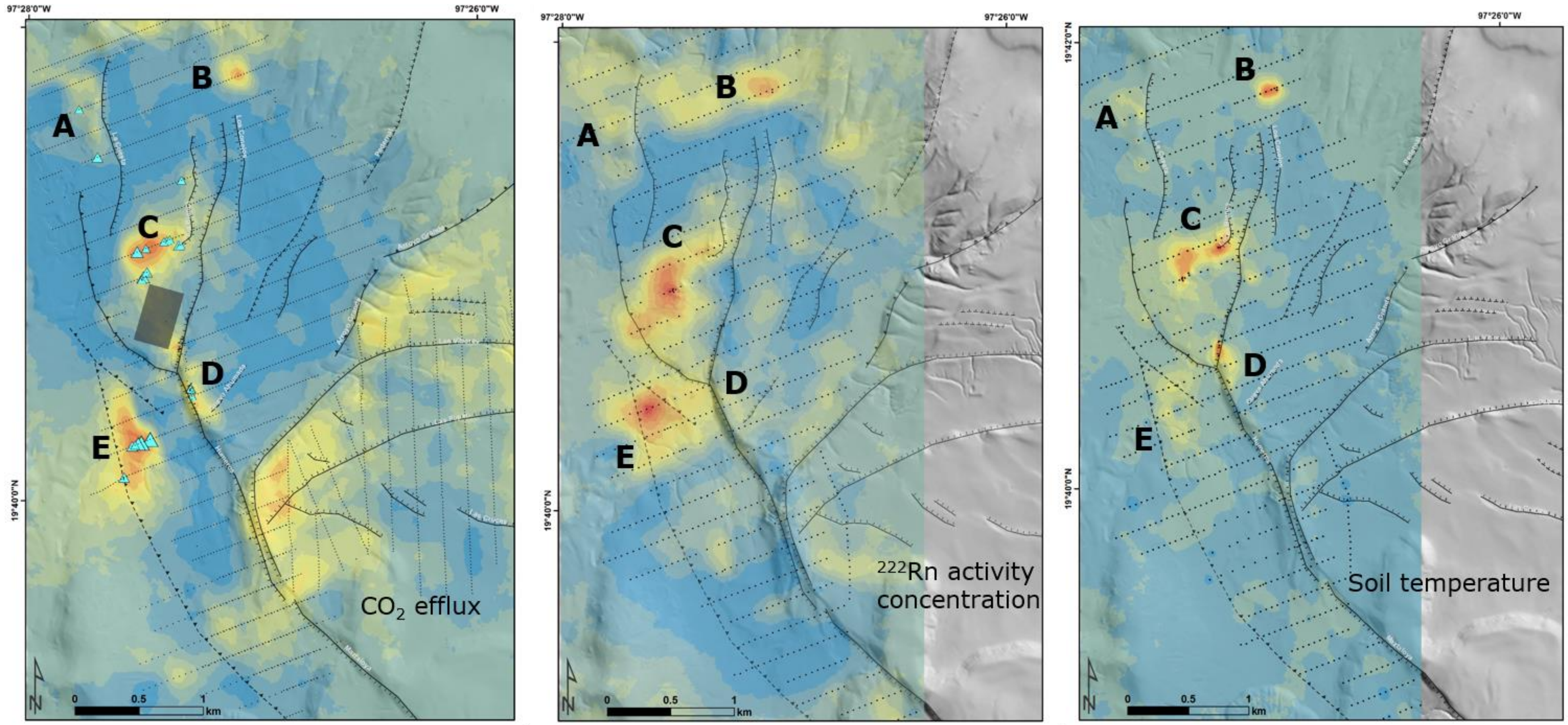


Figure 4.6 Comparison of all three parameters. Bold capital letters indicate areas of interest described in the text. Dark-grey square illustrates Los Humeros village.

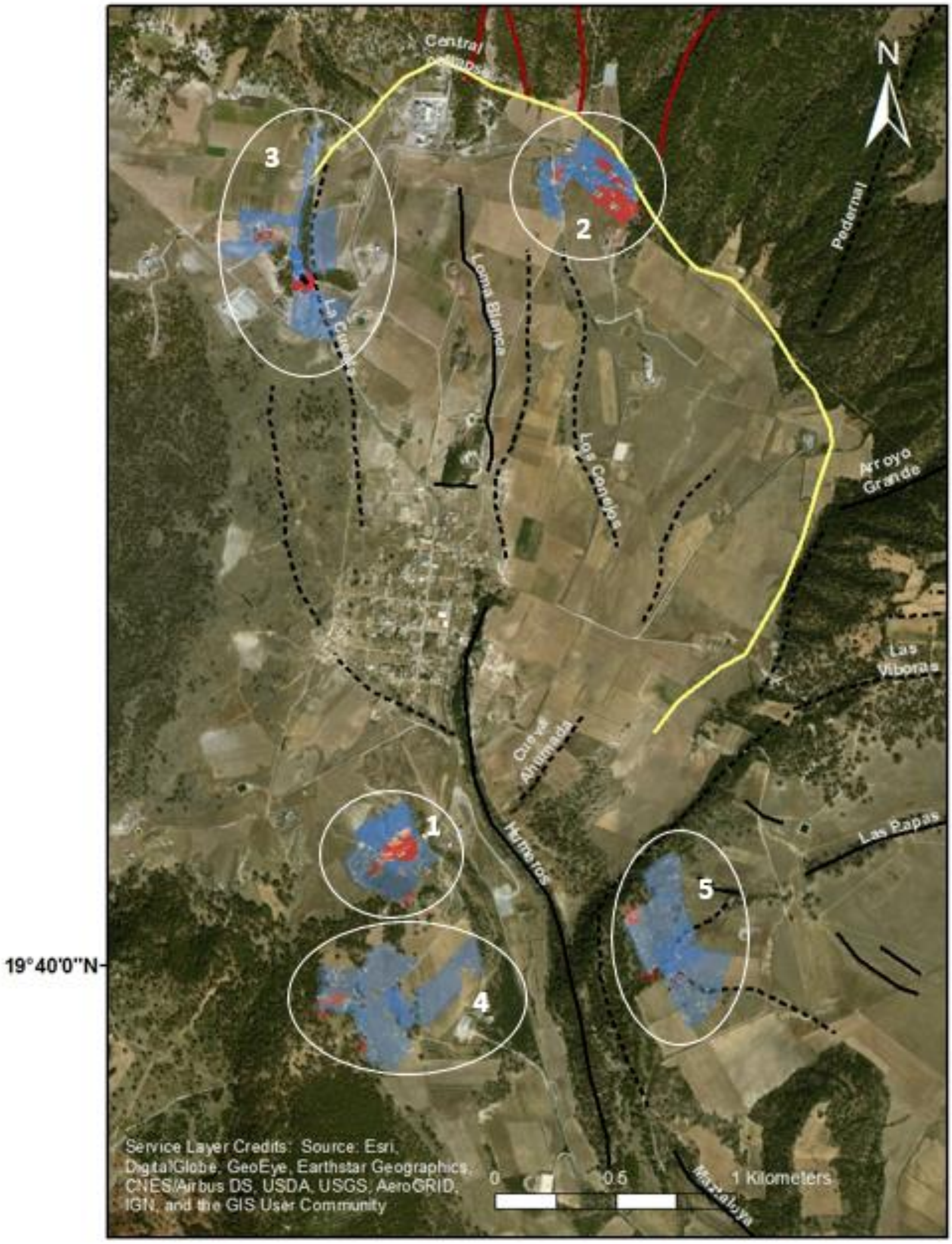


Figure 4.7 BGS soil gas survey areas 1 to 5.

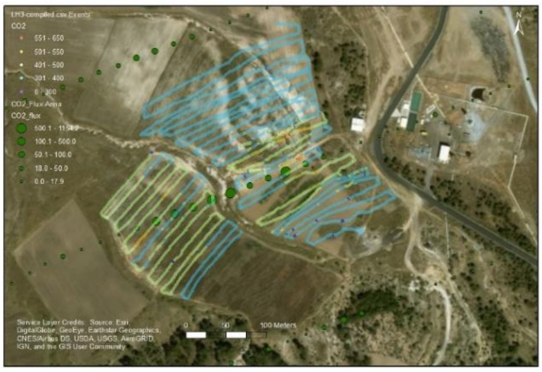

**Mobile laser survey, raw data, $CO_2$ ppm**

**Mobile laser survey, absolute difference**

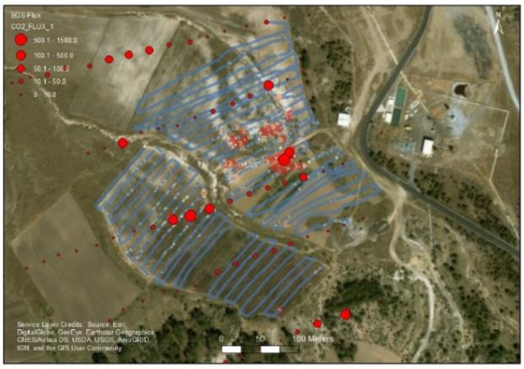

**$CO_2$ flux, g m$^{-2}$ day$^{-1}$**

**$CH_4$ flux, g m$^{-2}$ day$^{-1}$**

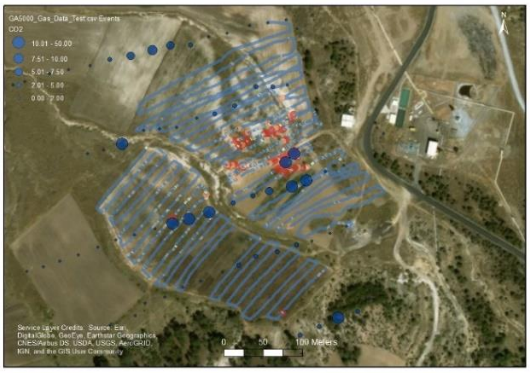

**Soil gas $CO_2$, volume %**

**Soil gas $CH_4$, volume ppm**

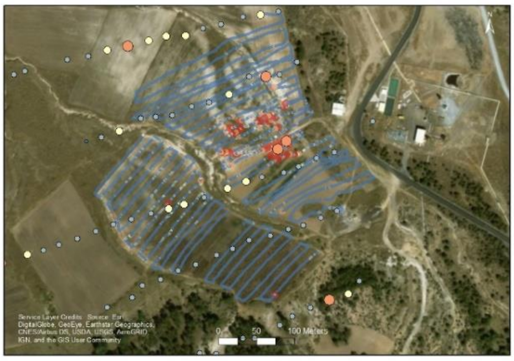

**Temperature, °C**

Figure 4.8. Area 1, upper panels: $CO_2$ laser survey, raw data with $CO_2$ flux data from GFZ survey as green transect points (left); absolute differences in adjacent 5 point averaged data, with $CO_2$ flux data from GFZ survey as green transect points (right). Centre panels: $CO_2$ (left) and $CH_4$ (right) flux. Lower panels: $CO_2$ (left) and $CH_4$ (right) in soil gas, and temperature.

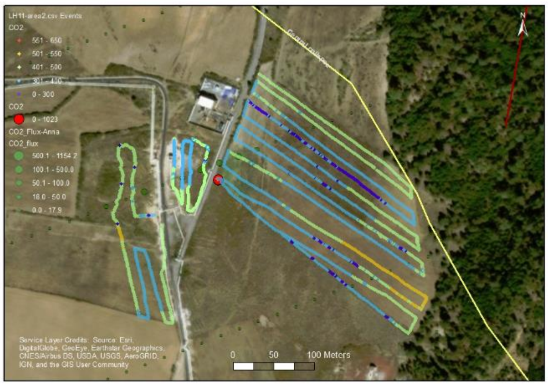

**Mobile laser survey, raw data, $CO_2$ ppm**

**Mobile laser survey, absolute difference**

**$CO_2$ flux, g $m^{-2}$ $day^{-1}$**

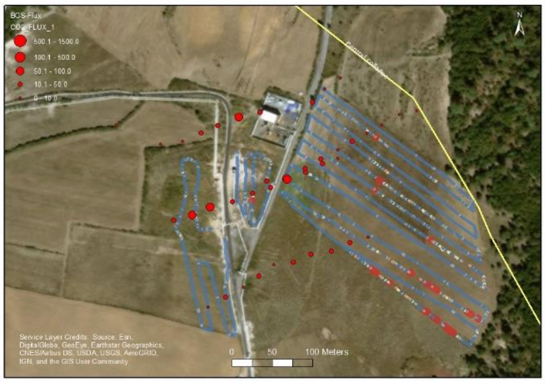

**$CH_4$ flux, g $m^{-2}$ $day^{-1}$**

**Soil gas $CO_2$, volume %**

**Soil gas $CH_4$, volume ppm**

**Temperature, °C**

Figure 4.9. Area 2, upper panels: $CO_2$ laser survey, raw data with $CO_2$ flux data from GFZ survey as green transect points (left); absolute differences in adjacent 5 point averaged data, with $CO_2$ flux data from GFZ survey as green transect points (right); single red point shows location of the 2014 vent. Centre panels: $CO_2$ (left) and $CH_4$ (right) flux. Lower panels: $CO_2$ (left) and $CH_4$ (right) in soil gas, and temperature (°C).

**Mobile laser survey, absolute difference**

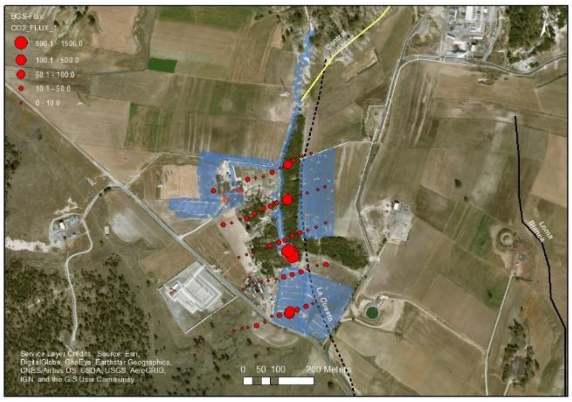

**$CO_2$ flux, g $m^{-2}$ $day^{-1}$**

**$CH_4$ flux, g $m^{-2}$ $day^{-1}$**

**Soil gas $CO_2$, volume %**

**Soil gas $CH_4$, volume ppm**

Figure 4.10. Area 3, upper panels: $CO_2$ laser survey, absolute differences in adjacent 5 point averaged data, with $CO_2$ flux data from GFZ survey as green transect points (left) and $CO_2$ flux (right). Centre panels: $CH_4$ flux (left) and $CO_2$ in soil gas (right). Lower panel: $CH_4$ in soil gas.

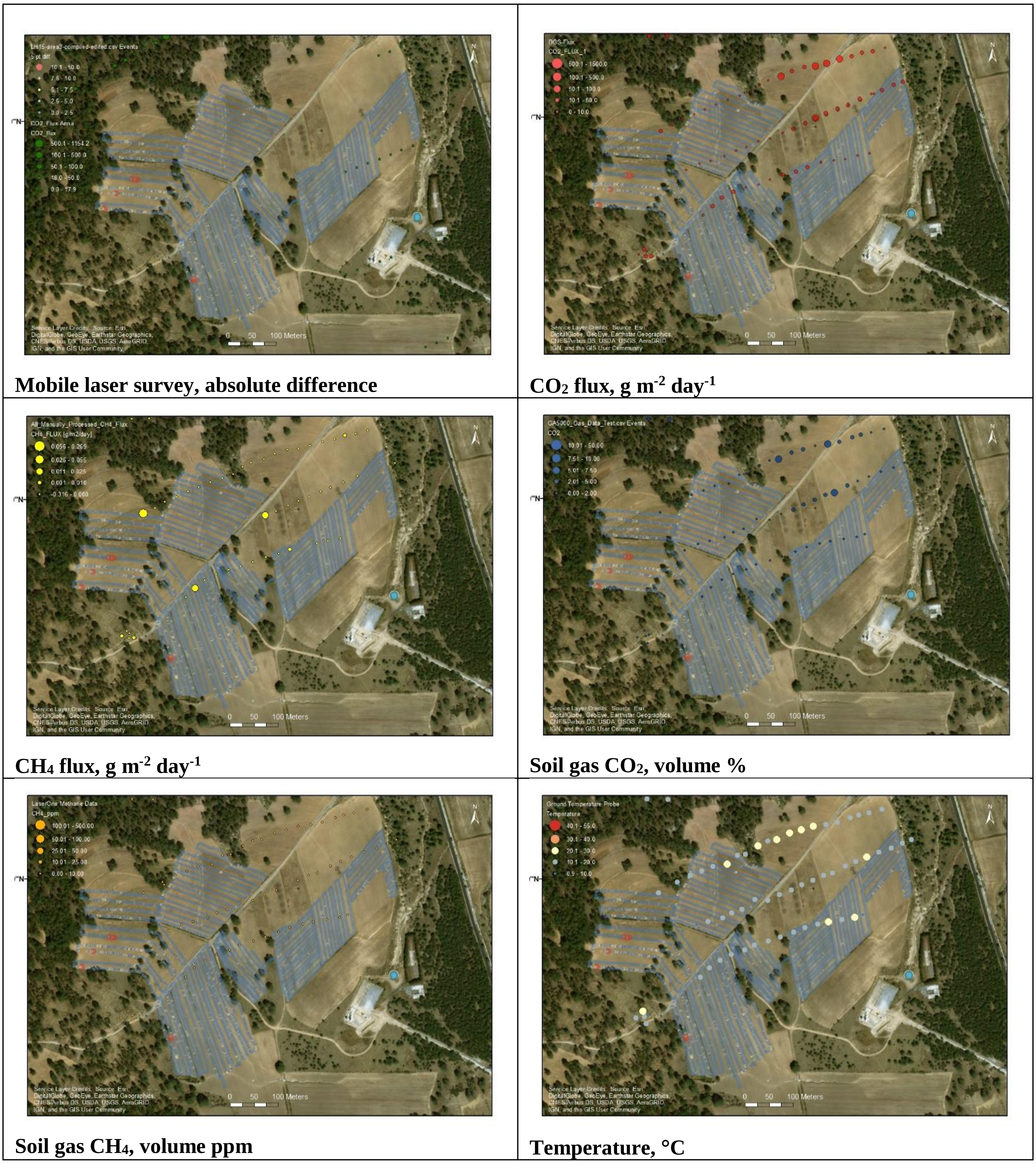

**Mobile laser survey, absolute difference**

**$CO_2$ flux, g m$^{-2}$ day$^{-1}$**

**$CH_4$ flux, g m$^{-2}$ day$^{-1}$**

**Soil gas $CO_2$, volume %**

**Soil gas $CH_4$, volume ppm**

**Temperature, °C**

Figure 4.11. Area 4, upper panels: $CO_2$ laser survey, absolute differences in adjacent 5 point averaged data, with $CO_2$ flux data from GFZ survey as green transect points (left) and $CO_2$ flux (right). Centre panels: $CH_4$ flux (left) and $CO_2$ in soil gas (right). Lower panels: $CH_4$ in soil gas (left) and temperature (right).

**Mobile laser survey, absolute difference**

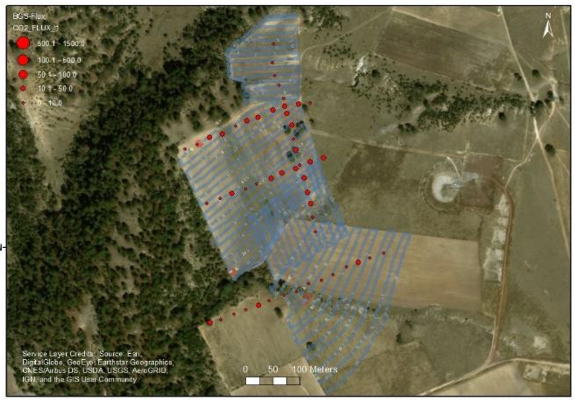

**$CO_2$ flux, g m$^{-2}$ day$^{-1}$**

**$CH_4$ flux, g m$^{-2}$ day$^{-1}$**

**Soil gas $CO_2$, volume %**

**Soil gas $CH_4$, volume ppm**

**Temperature, °C**

Figure 4.12 Area 5, upper panels: $CO_2$ laser survey, absolute differences in adjacent 5 point averaged data, with $CO_2$ flux data from GFZ survey as green transect points (left) and $CO_2$ flux (right). Centre panels: $CH_4$ flux (left) and $CO_2$ in soil gas (right). Lower panels: $CH_4$ in soil gas (left), and temperature (right).

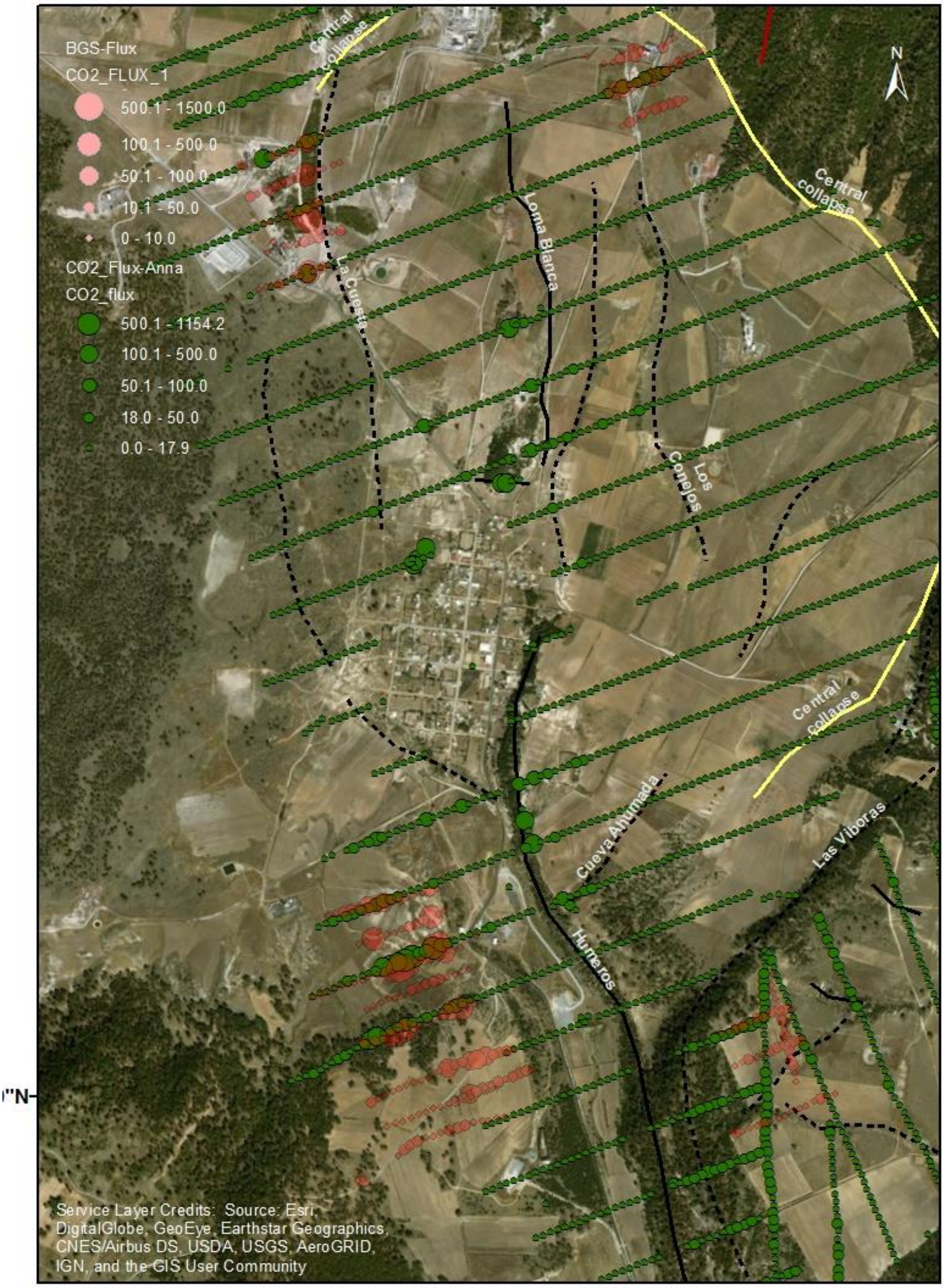


Figure 4.13. Transect selection for BGS point measurements ($CO_2$ flux shown) based on $CO_2$ flux data from GFZ.

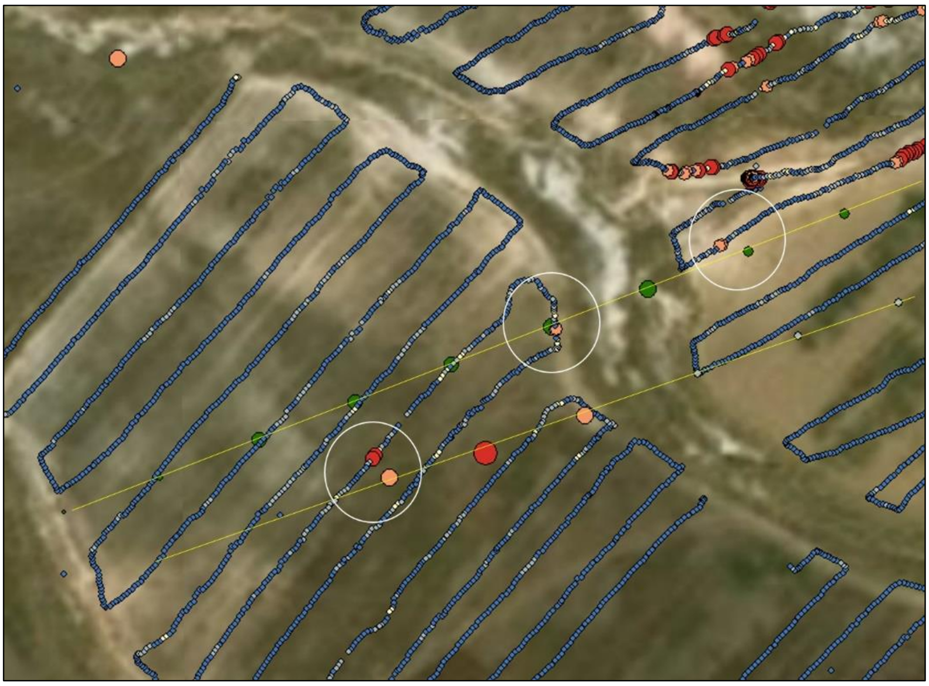

Figure 4.14. Mobile laser 5-point absolute difference and $CO_2$ flux data for Area 1

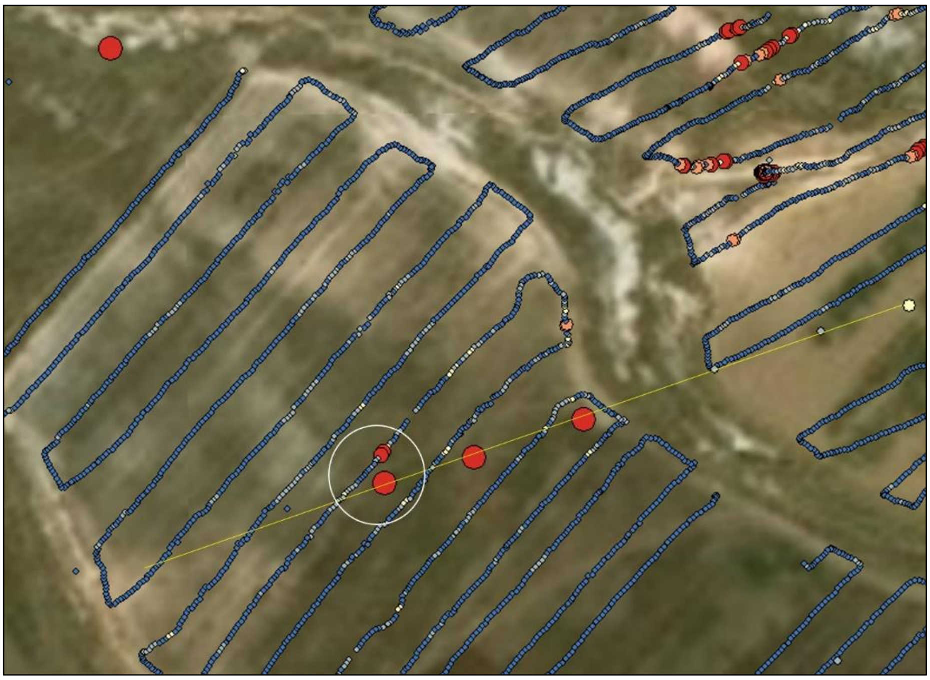

Figure 4.15. Mobile laser 5-point absolute difference and $CO_2$ soil gas data for Area 1

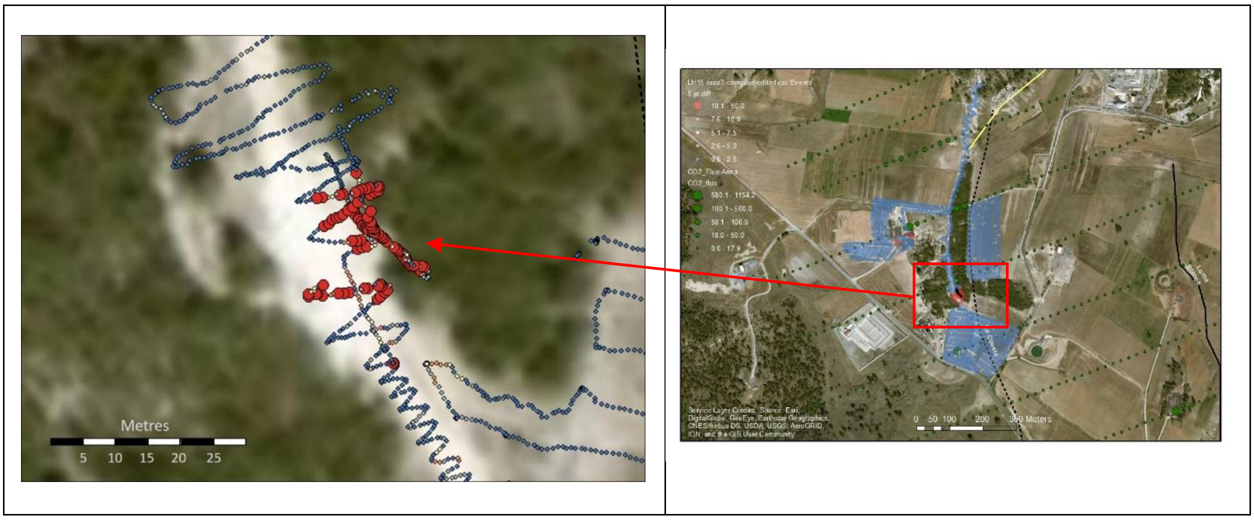


Figure 4.16. Previously unrecorded area of high $CO_2$ concentration detected by the mobile laser system (5-point average differences, left), subsequently confirmed by both soil gas measurements and $CO_2$ flux, in Area 3.

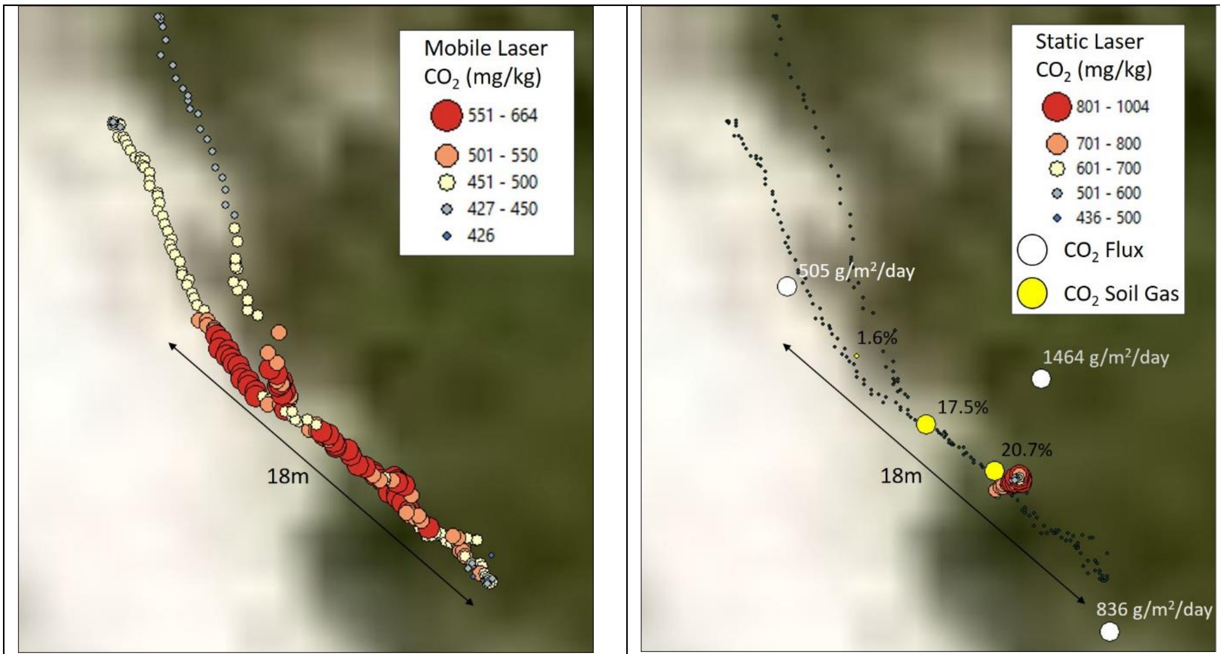


| Mobile laser absolute $CO_2$ concentrations | Static laser absolute $CO_2$ concentrations with gas and flux |
|---|---|

Figure 4.17. Previously unrecorded area of high $CO_2$ concentration detected by the mobile laser system (absolute $CO_2$ concentrations, left), subsequently confirmed by both soil gas measurements and $CO_2$ flux, in Area 3.

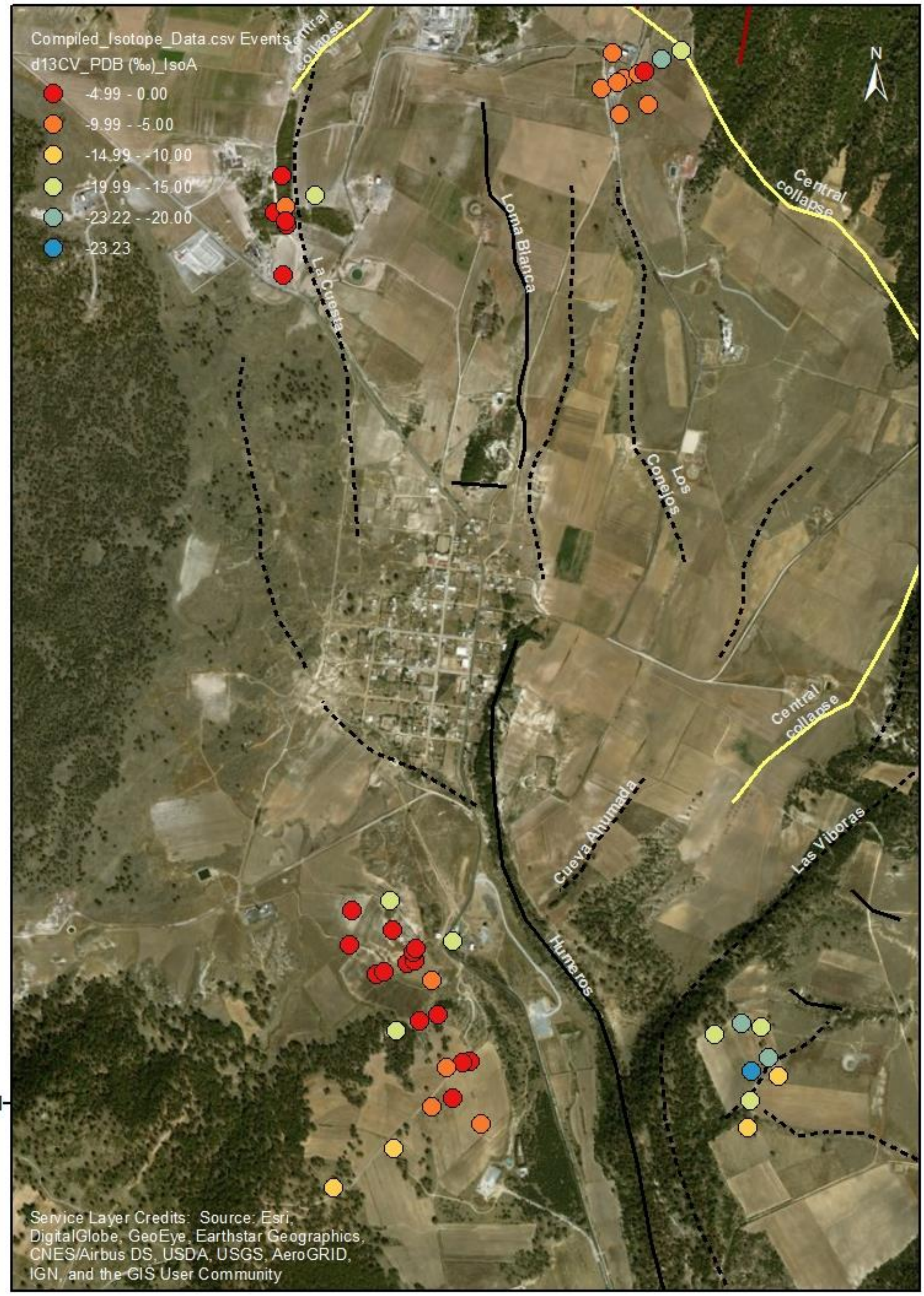


Figure 4.18. [13]C isotope ratios in soil gas $CO_2$ survey areas 1-5.

# Chapter 5

# LABORATORY EXPERIMENTS FOR THE STUDY OF FLUID/ROCK INTERACTION PROCESSES AT HIGH-TEMPERATURE

## 5.1 Introduction

### 5.1.1 Aim of the experiments

Several fluid-rock interaction experiments at different temperatures (T) and pressure (P) have been carried out within Task 4.3 to constrain the physical-chemical processes occurring in the upper reservoir of the geothermal field of Los Humeros (Mexico). Lab experiments interested only this geothermal field (and disregarded Acoculco), since the starting materials (rocks and fluids) could not be made available in the allotted timeframe. Purpose of the experiments is to enhance understanding of the chemical and mineralogical changes occurring in both rocks and fluids as a result of the fluid-rock inter-reactions at medium to relatively high-temperature (200-300°C). The results will be compared with various evidences (e.g. rock alteration, fluid chemistry…) observed in nature, to better model the geothermal field itself and to constraint the P-T conditions of alteration of the reservoir rocks.

### 5.1.2 Geothermal reservoirs in Los Humeros

Los Humeros Geothermal Field (LHGF) has two productive reservoirs:

i) *Shallow reservoir*. It is formed by pre-caldera pliocenic andesites of the Teziutlan Formation. The existing wells encounter its top at depth from 1650 to 2328 m above sea level (e.g. Giordano et al. 2017; ground level is around 2800 – 2900 m above sea level). This Formation has a 1200 m mean thickness and outcrops beyond the caldera rim, about 10 km NW from Los Humeros (e.g. (Carrasco-Núñez et al., 2017). The characteristic mafic mineral is augite in the shallower horizons and hornblende in the deeper ones (Elders et al., 2014). A liquid-dominant geothermal horizon is exploited between 1025 and 1600 m above sea level, at T =280 -330 °C (Arellano et al., 2003).

ii) *Deep reservoir*. It is formed by Mesozoic limestones. Wells encounter its top at 250-1340 m above sea level (Giordano et al., 2017). Fluids are exploited between 800 and 100 m above sea level, at T ranging from 300 to 400 °C (Arellano et al., 2003). This reservoir is separated from the shallower one by a vitreous tuff layer (Arellano et al., 2003).

Evidence gained from well cuttings indicate that both reservoirs are hydrothermally altered.

Main alteration minerals occurring in the shallow reservoir are chlorite, epidote, quartz, calcite, smectite, kaolinite, illite, anhydrite, amphibole, garnet, wairakite, montmorillonite, leucoxene and pyrite (Martínez-Serrano, 2002; Pulido, 2008; Elders et al., 2014; Norini et al., 2015; Giordano et al., 2017) and they are similar to those found in Acoculco geothermal area (López-Hernández et al., 2009; García-Vallés et al., 2015; Canet et al., 2015). Total percentage of alteration minerals can be up to 25-50 wt% (Pulido, 2008).

Typical alteration products of the deep reservoir are skarns with grossular + wollastonite + diopside paragenesis (Martinez Serrano, 2002; Giordano et al., 2017).

Fluids from geothermal wells are sodium- chloride to bicarbonate-sulfated type, have high B contents (>2000 ppm), $SiO_2$ variable (100-1400 ppm) and are characterized by high ammonia and arsenic contents (Elders et al., 2014). Fluids in wells are characterized by non-condensable gas/steam ratios (in mol) from 0.002 to 0.042; $CO_2$ is the principal component of non-condensable gas (74 -96 mol%), the other component being $H_2$ (2.5-20 mol%), $CH_4$, $N_2$ and $NH_3$ (Arellano et al., 2003).

## 5.2. Methodology

### 5.2.1 Choice of starting materials and their characterization

#### 5.2.1.1 Solids

We performed fluid rock interaction experiments to simulate reactions occurring in the shallow reservoir. Concurrently, water-rock interaction experiments at conditions of the deep reservoir of the Super-Hot-Geothermal-System (SHGS) of Los Humeros have been planned within Task 6.1.

For our experiments we selected two andesites of Teziutlan lava, thought to be representative of the shallowest portion of the andesitic reservoir. These rock samples (**RUGG04** and **RUGG09**) were collected by G. Norini (CNR), during geological and structural surveys, in an area where the same rocks of the geothermal reservoir crop out. The coordinates of the sampling site are: longitude -97.1685400000 (UTM easting 691998.73), latitude 19.66255900000 (UTM northing 2175173.50). The rocks are aphanitic, holocrystalline, porphyric with plagioclase phenocrystals up to 5 mm.

Whole rock analyses are reported in Table 5.1 and classification diagram (Total Alkali Silica, Le Bas et al., 1986) is shown in Figure 5.1. Rugg04 andesite is more primitive than Rugg09 sample, mainly due to the presence of olivine crystals (see below).

| Rock | **RUGG04** | **RUGG09** |
|---|---|---|
| *Contents in wt%* | | |
| $SiO_2$ | 55.93 | 61.26 |
| $Al_2O_3$ | 15.52 | 16.68 |
| $Fe_2O_3(T)$ | 7.89 | 5.16 |
| MnO | 0.13 | 0.111 |
| MgO | 4.21 | 2.94 |
| CaO | 7.16 | 6.02 |
| $Na_2O$ | 3.54 | 3.4 |
| $K_2O$ | 2.17 | 2.17 |
| $TiO_2$ | 1.279 | 0.59 |
| $P_2O_5$ | 0.33 | 0.11 |
| LOI | 1.59 | 1.82 |
| Total | 99.75 | 100.3 |
| *Contents in ppm:* | | |
| Sc | 22 | 14 |
| Be | 2 | 1 |
| V | 178 | 122 |
| Ba | 508 | 389 |
| Sr | 456 | 484 |
| Y | 26 | 18 |
| Zr | 260 | 141 |
| Cr | 110 | 40 |
| Co | 22 | 15 |
| Ni | < 20 | 20 |
| Cu | 40 | 30 |
| Zn | 90 | 70 |
| Ga | 19 | 20 |
| Ge | 1 | 1 |
| As | < 5 | < 5 |
| Rb | 59 | 60 |
| Nb | 13 | 4 |
| Mo | < 2 | 3 |
| Ag | 0.6 | < 0.5 |
| In | < 0.2 | < 0.2 |
| Sn | 1 | < 1 |
| Sb | < 0.5 | < 0.5 |
| Cs | 1.4 | 3.3 |
| La | 31.6 | 15.5 |
| Ce | 66.9 | 33.8 |
| Pr | 8.24 | 4.39 |
| Nd | 32.9 | 17.5 |
| Sm | 7.1 | 4.1 |
| Eu | 1.88 | 1.12 |
| Gd | 5.8 | 3.5 |
| Tb | 0.9 | 0.6 |
| Dy | 5.4 | 3.7 |
| Ho | 1 | 0.7 |
| Er | 2.8 | 2 |
| Tm | 0.42 | 0.3 |
| Yb | 2.6 | 2.1 |
| Lu | 0.37 | 0.31 |
| Hf | 5.8 | 3.6 |
| Ta | 1 | 0.4 |
| W | 2 | 1 |
| Tl | 0.2 | 0.2 |
| Pb | 10 | 8 |
| Bi | < 0.4 | < 0.4 |
| Th | 9.4 | 4.1 |
| U | 2.7 | 1.6 |

Table 5.1: Whole rock analyses of rocks selected for experiments. LOI= loss on ignition.
Analyses performed by ICP (Actalabs, Canada).

X-ray diffraction spectra only show peaks attributable to plagioclases and clinopyroxenes (Figure 5.2). Spectra were acquired to allow direct comparison between starting material spectra and experimental products ones (also characterized through XRD).

Electron microprobe analyses of **RUGG04** rock (Table 5.2) have shown the presence of plagioclase (labradorite, andesine and oligoclase) together with K-feldspar, clinopyroxenes (augite), orthopyroxene (enstatite), olivine (forsterite 56-65 mol%), oxides (ilmenite-hematite and magnetite-ulvospinel solid solutions), apatite, quartz and rare Fe and Mn rich carbonates (?) around some voids. The presence of clinopyroxenes and the absence of hornblende suggest that the sample can be a proxy of the shallower portion of the andesitic reservoir (e.g. Carrasco-Núñez et al., 2017).

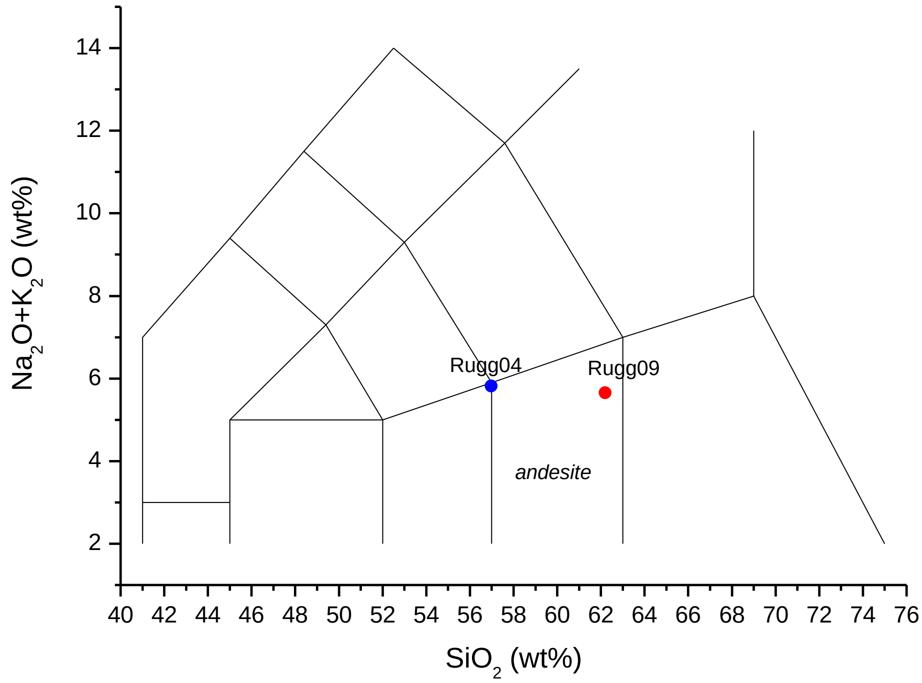


Figure 5.1: Selected rocks for experiments in Total Alkali Silica classification diagram (Le Bas et al., 1986).

**RUGG09** sample shown the presence of plagioclase (labradorite, andesine and oligoclase), clinopyroxene (augite), Fe-Ca-Mn-Mg carbonates, quartz, ilmenite, apatite, glass and rare sulphides (Table 5.3). The sample had been selected presuming the presence of amphibole in its paragenesis but electron microprobe analysis failed to reveal this phase. The major presence of carbonate respect to the previous sample denote RUGG09 was greatly exposed to fluid circulation and deuteric alteration.

All rock samples were grinded in an agate mill and the obtained powders sieved. The 50-150 µm granulometric size interval was selected for the fluid-rock interaction experiments.

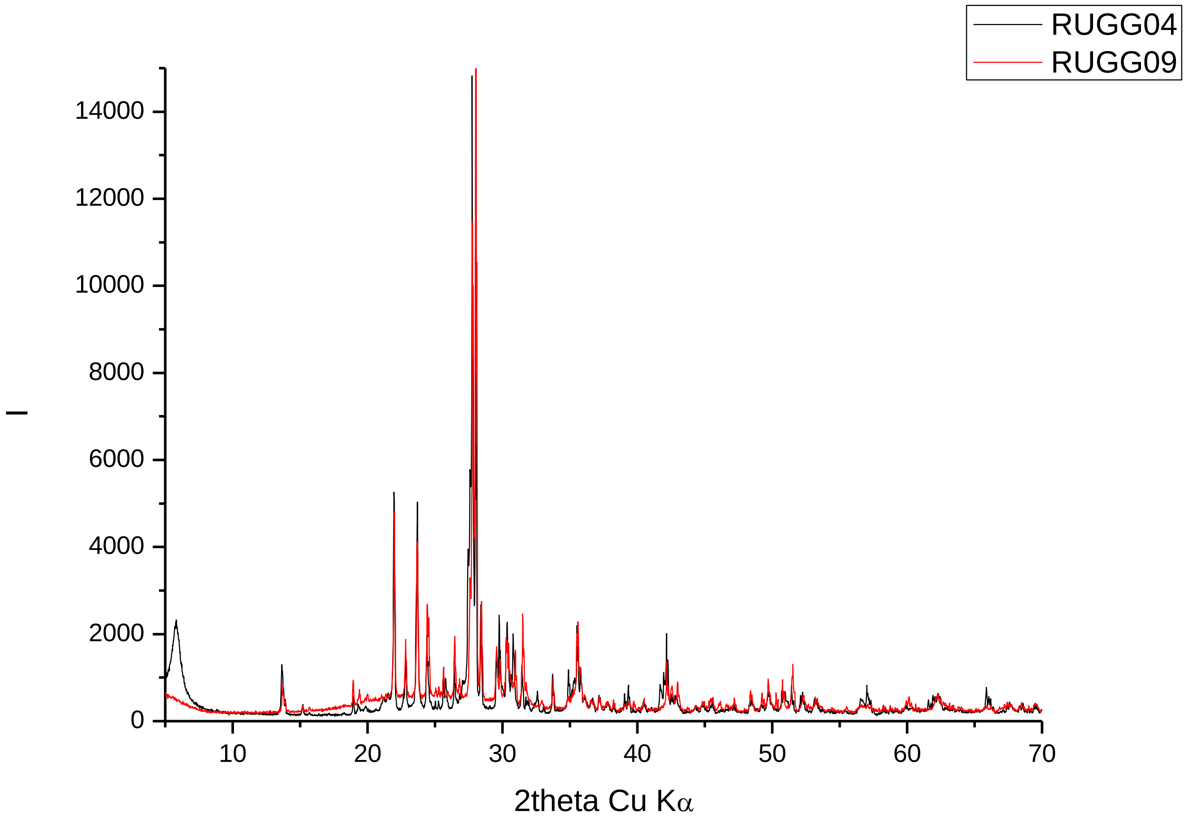


Figure 5.2: XRD spectra of selected rocks. Spectra were acquired at Centro di Servizi di Cristallografia Strutturale (C.R.I.S.T.) UNIFI through a Cu anticathode diffractometer.

| Sample | Rugg04 | Rugg04 | Rugg04 | Rugg04 | Rugg04 | Rugg04 | Rugg04 | Rugg04 | Rugg04 | Rugg04 |
|---|---|---|---|---|---|---|---|---|---|---|
| Label | 1 | 12 | 26 | 28 | 33 | 34 | 39 | 42 | 44 | 45 |
| Phase | cpx | cpx | cpx | cpx | cpx | cpx | cpx | cpx | cpx | cpx |
| SiO2 | 50.96 | 51.18 | 50.38 | 50.02 | 50.29 | 49.49 | 50.43 | 51.64 | 50.52 | 47.78 |
| TiO2 | 0.73 | 1.01 | 1.06 | 1.05 | 0.88 | 1.01 | 0.71 | 0.83 | 0.79 | 1.37 |
| Al2O3 | 2.02 | 1.65 | 1.82 | 1.77 | 2.13 | 2.20 | 1.16 | 1.61 | 1.85 | 2.94 |
| Cr2O3 | 0.17 | 0.03 | 0.02 | 0.00 | 0.08 | 0.18 | 0.06 | 0.04 | 0.00 | 0.16 |
| FeO | 9.71 | 10.45 | 10.93 | 11.07 | 10.75 | 10.93 | 13.72 | 11.32 | 12.05 | 11.46 |
| MnO | 0.22 | 0.30 | 0.28 | 0.40 | 0.48 | 0.32 | 0.47 | 0.39 | 0.40 | 0.34 |
| MgO | 15.07 | 15.02 | 15.32 | 14.75 | 14.79 | 14.70 | 14.64 | 15.14 | 15.12 | 14.21 |
| CaO | 18.02 | 18.47 | 17.95 | 18.08 | 18.15 | 17.63 | 15.61 | 18.01 | 16.84 | 17.16 |
| Na2O | 0.31 | 0.16 | 0.25 | 0.18 | 0.43 | 0.27 | 0.25 | 0.37 | 0.41 | 0.36 |
| K2O | 0.03 | 0.02 | 0.00 | 0.04 | 0.00 | 0.00 | 0.03 | 0.02 | 0.00 | 0.01 |
| Sum | 97.24 | 98.30 | 98.01 | 97.37 | 97.98 | 96.73 | 97.07 | 99.36 | 97.96 | 95.81 |
| *Cations per 6 O. Fe2+ and Fe3+ based on charge balance.* | | | | | | | | | | |
| Si | 1.947 | 1.942 | 1.914 | 1.920 | 1.911 | 1.908 | 1.953 | 1.938 | 1.923 | 1.863 |
| IVAl | 0.053 | 0.058 | 0.086 | 0.080 | 0.089 | 0.092 | 0.047 | 0.062 | 0.077 | 0.135 |
| Fe3+ | 0.000 | 0.000 | 0.000 | 0.000 | 0.000 | 0.000 | 0.000 | 0.000 | 0.000 | 0.002 |
| Sum | 2.000 | 2.000 | 2.000 | 2.000 | 2.000 | 2.000 | 2.000 | 2.000 | 2.000 | 2.000 |
| VIAl | 0.037 | 0.016 | -0.004 | 0.000 | 0.006 | 0.008 | 0.006 | 0.009 | 0.006 | 0.000 |
| Fe 3+ | 0.000 | 0.000 | 0.048 | 0.033 | 0.062 | 0.040 | 0.016 | 0.031 | 0.056 | 0.078 |
| Ti | 0.021 | 0.029 | 0.030 | 0.030 | 0.025 | 0.029 | 0.021 | 0.023 | 0.023 | 0.040 |
| Mg | 0.858 | 0.850 | 0.868 | 0.844 | 0.838 | 0.845 | 0.846 | 0.847 | 0.858 | 0.826 |
| Cr | 0.005 | 0.001 | 0.001 | 0.000 | 0.002 | 0.006 | 0.002 | 0.001 | 0.000 | 0.005 |
| Fe2+ | 0.078 | 0.104 | 0.058 | 0.092 | 0.066 | 0.072 | 0.110 | 0.088 | 0.058 | 0.050 |
| Sum | 1.000 | 1.000 | 1.000 | 1.000 | 1.000 | 1.000 | 1.000 | 1.000 | 1.000 | 1.000 |
| Na | 0.023 | 0.012 | 0.019 | 0.013 | 0.032 | 0.020 | 0.018 | 0.027 | 0.030 | 0.027 |
| Mn | 0.007 | 0.010 | 0.009 | 0.013 | 0.015 | 0.010 | 0.015 | 0.012 | 0.013 | 0.011 |
| Ca | 0.737 | 0.751 | 0.731 | 0.743 | 0.739 | 0.728 | 0.648 | 0.724 | 0.687 | 0.717 |
| Fe2+ | 0.232 | 0.228 | 0.242 | 0.230 | 0.214 | 0.241 | 0.319 | 0.237 | 0.271 | 0.244 |
| Mg | 0.000 | 0.000 | 0.000 | 0.000 | 0.000 | 0.000 | 0.000 | 0.000 | 0.000 | 0.000 |
| Sum | 1.000 | 1.000 | 1.000 | 1.000 | 1.000 | 1.000 | 1.000 | 1.000 | 1.000 | 1.000 |
| Sum catio | 4.000 | 4.000 | 4.000 | 4.000 | 4.000 | 4.000 | 4.000 | 4.000 | 4.000 | 4.000 |
| *End-members (mol%)* | | | | | | | | | | |
| Wo | 38.5 | 38.6 | 37.4 | 38.0 | 38.2 | 37.6 | 33.2 | 37.3 | 35.4 | 37.2 |
| En | 44.9 | 43.8 | 44.4 | 43.2 | 43.3 | 43.6 | 43.3 | 43.7 | 44.2 | 42.8 |
| Fs | 16.6 | 17.6 | 18.2 | 18.9 | 18.5 | 18.8 | 23.6 | 19.0 | 20.4 | 20.0 |
| Mg # | 73.4 | 71.9 | 74.4 | 72.4 | 75.0 | 73.0 | 66.4 | 72.3 | 72.3 | 73.8 |
| FeO | 9.71 | 10.45 | 9.41 | 10.04 | 8.81 | 9.70 | 13.22 | 10.33 | 10.30 | 9.01 |
| Fe2O3 | 0.00 | 0.00 | 1.68 | 1.15 | 2.16 | 1.37 | 0.55 | 1.10 | 1.94 | 2.73 |

| | Rugg04 | Rugg04 | Rugg04 | Rugg04 | Rugg04 |
|---|---|---|---|---|---|
| | 2 | 11 | 17 | 36 | 37 |
| | ol | ol | ol | ol | ol |
| SiO2 | 35.46 | 34.00 | 36.09 | 35.68 | 34.66 |
| TiO2 | 0.00 | 0.07 | 0.00 | 0.05 | 0.03 |
| Al2O3 | 0.02 | 0.04 | 0.00 | 0.02 | 0.14 |
| Cr2O3 | 0.01 | 0.00 | 0.05 | 0.04 | 0.00 |
| FeO | 36.20 | 40.45 | 30.33 | 35.16 | 36.87 |
| MnO | 0.54 | 0.75 | 0.71 | 0.59 | 0.64 |
| MgO | 27.89 | 24.10 | 31.05 | 27.82 | 26.39 |
| CaO | 0.26 | 0.19 | 0.36 | 0.25 | 0.20 |
| Na2O | 0.16 | 0.02 | 0.00 | 0.12 | 0.00 |
| K2O | 0.00 | 0.02 | 0.04 | 0.02 | 0.00 |
| Sum | 100.53 | 99.62 | 98.62 | 99.76 | 98.93 |
| *Numbers of ions on the basis of 4 oxygens.* | | | | | |
| Si | 0.988 | 0.981 | 0.997 | 0.998 | 0.988 |
| Fe | 0.844 | 0.977 | 0.701 | 0.823 | 0.880 |
| Mn | 0.013 | 0.018 | 0.017 | 0.014 | 0.016 |
| Mg | 1.159 | 1.037 | 1.279 | 1.160 | 1.122 |
| Ca | 0.008 | 0.006 | 0.011 | 0.008 | 0.006 |
| Sum | 2.024 | 2.038 | 2.007 | 2.004 | 2.024 |
| *End-members (mol%)* | | | | | |
| Fo | 57.9 | 51.5 | 64.6 | 58.5 | 56.1 |
| Fa | 42.1 | 48.5 | 35.4 | 41.5 | 43.9 |

| | Rugg04 | Rugg04 | Rugg04 | Rugg04 | Rugg04 | Rugg04 |
|---|---|---|---|---|---|---|
| | 3 | 4 | 14 | 15 | 40 | 41 |
| | ox | ox | ox | ox | ox | ox |
| SiO2 | 0.00 | 0.04 | 0.06 | 0.19 | 0.07 | 0.87 |
| TiO2 | 47.91 | 14.74 | 47.38 | 12.49 | 27.34 | 16.39 |
| Al2O3 | 0.16 | 1.41 | 0.28 | 2.35 | 1.13 | 11.38 |
| Cr2O3 | 0.12 | 0.42 | 0.10 | 0.06 | 0.12 | 0.18 |
| FeO | 47.77 | 76.94 | 48.97 | 78.94 | 66.39 | 64.31 |
| MnO | 0.52 | 0.43 | 0.69 | 0.47 | 0.54 | 0.35 |
| MgO | 2.01 | 0.96 | 1.47 | 0.63 | 0.56 | 0.27 |
| CaO | 0.04 | 0.10 | 0.02 | 0.10 | 0.14 | 0.31 |
| Na2O | 0.00 | 0.00 | 0.06 | 0.00 | 0.00 | 0.00 |
| K2O | 0.03 | 0.03 | 0.01 | 0.03 | 0.06 | 0.02 |
| Sum | 98.55 | 95.06 | 99.02 | 95.25 | 96.36 | 94.10 |
| *Cations per 3 O (**4 O in bold**). Fe2+ and Fe3+ based on charge balance.* | | | | | | |
| *(Ilmenite-hematite s.s., magnetite-ulvospinel in bold )* | | | | | | |
| Si | 0.000 | **0.001** | 0.002 | **0.007** | 0.002 | 0.021 |
| Al | 0.005 | **0.063** | 0.008 | **0.104** | 0.034 | 0.328 |
| K | 0.001 | **0.001** | 0.000 | **0.001** | 0.002 | 0.001 |
| Ti | 0.903 | **0.419** | 0.891 | **0.353** | 0.520 | 0.302 |
| Mg | 0.075 | **0.054** | 0.055 | **0.035** | 0.021 | 0.010 |
| Cr | 0.002 | **0.013** | 0.002 | **0.002** | 0.002 | 0.004 |
| Na | 0.000 | **0.000** | 0.003 | **0.000** | 0.000 | 0.000 |
| Mn | 0.011 | **0.014** | 0.015 | **0.015** | 0.012 | 0.007 |
| Ca | 0.001 | **0.004** | 0.001 | **0.004** | 0.004 | 0.008 |
| Fe3+ | 0.188 | **1.086** | 0.208 | **1.176** | 0.923 | 1.022 |
| Fe2+ | 0.814 | **1.346** | 0.817 | **1.303** | 0.481 | 0.297 |
| Sum | 2.000 | **3.000** | 2.000 | **3.000** | 2.000 | 2.000 |
| FeO | 38.85 | **42.61** | 39.06 | **41.52** | 22.76 | 14.48 |
| Fe2O3 | 9.91 | **38.15** | 11.02 | **41.59** | 48.48 | 55.38 |
| FeO* | 47.77 | **76.93** | 48.97 | **78.94** | 66.39 | 64.31 |
| Sum | 99.54 | **98.88** | 100.13 | **99.42** | 101.22 | 99.65 |

| | Rugg04 | Rugg04 | Rugg04 | Rugg04 | Rugg04 | Rugg04 | Rugg04 | Rugg04 | Rugg04 |
|---|---|---|---|---|---|---|---|---|---|
| | 5 | 6 | 10 | 22 | 25 | 35 | 43 | 47 | 48 |
| | feld | feld | feld | feld | feld | feld | feld | feld | feld |
| SiO2 | 61.50 | 56.18 | 53.55 | 57.18 | 54.76 | 65.83 | 54.08 | 59.38 | 57.91 |
| TiO2 | 0.13 | 0.07 | 0.10 | 0.07 | 0.11 | 0.16 | 0.01 | 0.11 | 0.07 |
| Al2O3 | 22.78 | 26.09 | 27.47 | 24.74 | 26.21 | 18.87 | 27.35 | 28.02 | 27.17 |
| Cr2O3 | 0.00 | 0.00 | 0.00 | 0.00 | 0.00 | 0.01 | 0.00 | 0.00 | 0.00 |
| FeO | 1.40 | 1.04 | 0.53 | 0.56 | 0.91 | 0.37 | 0.61 | 0.62 | 0.88 |
| MnO | 0.00 | 0.00 | 0.00 | 0.01 | 0.00 | 0.00 | 0.00 | 0.00 | 0.00 |
| MgO | 0.26 | 0.13 | 0.06 | 0.13 | 0.04 | 0.06 | 0.10 | 0.11 | 0.09 |
| CaO | 5.08 | 9.26 | 10.74 | 8.18 | 9.50 | 1.28 | 9.88 | 9.20 | 9.37 |
| Na2O | 7.12 | 5.64 | 4.68 | 6.27 | 5.89 | 5.64 | 5.38 | 5.92 | 5.81 |
| K2O | 1.45 | 0.46 | 0.57 | 0.76 | 0.53 | 6.72 | 0.57 | 0.68 | 0.49 |
| Sum | 99.71 | 98.86 | 97.71 | 97.91 | 97.97 | 98.93 | 97.98 | 104.04 | 101.79 |
| *Cations per 8 O:* | | | | | | | | | |
| Si | 2.759 | 2.562 | 2.480 | 2.627 | 2.529 | 2.982 | 2.494 | 2.567 | 2.560 |
| Al | 1.205 | 1.402 | 1.499 | 1.340 | 1.426 | 1.007 | 1.487 | 1.427 | 1.416 |
| Fe | 0.058 | 0.044 | 0.023 | 0.024 | 0.039 | 0.015 | 0.026 | 0.025 | 0.036 |
| Sum | 4.022 | 4.007 | 4.002 | 3.991 | 3.995 | 4.005 | 4.008 | 4.018 | 4.012 |
| Ca | 0.244 | 0.452 | 0.533 | 0.403 | 0.470 | 0.062 | 0.488 | 0.426 | 0.444 |
| Na | 0.620 | 0.498 | 0.420 | 0.558 | 0.527 | 0.496 | 0.481 | 0.496 | 0.498 |
| K | 0.083 | 0.027 | 0.034 | 0.045 | 0.032 | 0.388 | 0.034 | 0.038 | 0.027 |
| Sum | 0.947 | 0.977 | 0.987 | 1.006 | 1.029 | 0.946 | 1.003 | 0.960 | 0.969 |
| Sum catio | 4.969 | 4.985 | 4.989 | 4.996 | 5.023 | 4.951 | 5.010 | 4.978 | 4.982 |
| *End-members (mol%)* | | | | | | | | | |
| An | 25.8 | 46.3 | 54.0 | 40.0 | 45.7 | 6.6 | 48.7 | 44.4 | 45.8 |
| Ab | 65.5 | 51.0 | 42.6 | 55.5 | 51.2 | 52.4 | 48.0 | 51.7 | 51.4 |
| Or | 8.8 | 2.7 | 3.4 | 4.4 | 3.1 | 41.0 | 3.4 | 3.9 | 2.8 |
| | *oligoclase* | *andesine* | *labradorite* | *andesine* | *andesine* | *K-feldspar* | *andesine* | *andesine* | *andesine* |

| Sample | Rugg04 | Rugg04 | Rugg04 | Rugg04 | Rugg04 | Rugg04 | Rugg04 |
|---|---|---|---|---|---|---|---|
| Label | 8 | 9 | 20 | 21 | 23 | 24 | 29 |
| Phase | opx | opx | opx | opx | opx | opx | opx |
| SiO2 | 47.29 | 51.15 | 47.61 | 52.83 | 45.90 | 51.66 | 52.28 |
| TiO2 | 0.09 | 0.11 | 0.02 | 0.40 | 0.06 | 0.57 | 0.41 |
| Al2O3 | 4.89 | 6.26 | 4.61 | 0.87 | 5.73 | 0.57 | 0.83 |
| Cr2O3 | 0.00 | 0.00 | 0.00 | 0.01 | 0.01 | 0.00 | 0.00 |
| FeO | 24.47 | 23.90 | 21.91 | 19.52 | 23.07 | 22.00 | 19.83 |
| MnO | 0.27 | 0.27 | 0.34 | 0.61 | 0.27 | 0.58 | 0.59 |
| MgO | 11.07 | 14.89 | 13.65 | 23.08 | 13.35 | 18.97 | 23.48 |
| CaO | 1.81 | 1.72 | 1.26 | 1.96 | 2.10 | 5.27 | 1.84 |
| Na2O | 0.30 | 0.17 | 0.36 | 0.05 | 0.23 | 0.08 | 0.06 |
| K2O | 0.13 | 0.09 | 0.13 | 0.05 | 0.23 | 0.05 | 0.00 |
| Sum | 90.30 | 98.55 | 89.88 | 99.37 | 90.95 | 99.76 | 99.32 |
| *Cations per 6 O. Fe2+ and Fe3+ based on charge balance.* | | | | | | | |
| Si | 2.037 | 1.982 | 2.024 | 1.963 | 1.936 | 1.954 | 1.941 |
| IVAl | 0.000 | 0.018 | 0.000 | 0.037 | 0.064 | 0.025 | 0.036 |
| Fe3+ | 0.000 | 0.000 | 0.000 | 0.000 | 0.000 | 0.021 | 0.023 |
| Sum | 2.037 | 2.000 | 2.024 | 2.000 | 2.000 | 2.000 | 2.000 |
| VIAl | 0.248 | 0.268 | 0.231 | 0.001 | 0.220 | 0.000 | 0.000 |
| Fe 3+ | 0.000 | 0.000 | 0.000 | 0.017 | 0.000 | 0.020 | 0.041 |
| Ti | 0.003 | 0.003 | 0.001 | 0.011 | 0.002 | 0.016 | 0.011 |
| Mg | 0.711 | 0.729 | 0.768 | 0.970 | 0.777 | 0.964 | 0.948 |
| Cr | 0.000 | 0.000 | 0.000 | 0.000 | 0.000 | 0.000 | 0.000 |
| Fe2+ | 0.038 | 0.000 | 0.000 | 0.000 | 0.000 | 0.000 | 0.000 |
| Sum | 1.000 | 1.000 | 1.000 | 1.000 | 1.000 | 1.000 | 1.000 |
| Na | 0.025 | 0.013 | 0.029 | 0.004 | 0.019 | 0.006 | 0.004 |
| Mn | 0.010 | 0.009 | 0.012 | 0.019 | 0.010 | 0.019 | 0.019 |
| Ca | 0.084 | 0.071 | 0.057 | 0.078 | 0.095 | 0.214 | 0.073 |
| Fe2+ | 0.845 | 0.775 | 0.780 | 0.590 | 0.814 | 0.656 | 0.553 |
| Mg | 0.000 | 0.132 | 0.097 | 0.309 | 0.063 | 0.106 | 0.352 |
| Sum | 0.963 | 1.000 | 0.976 | 1.000 | 1.000 | 1.000 | 1.000 |
| Sum catio | 4.000 | 4.000 | 4.000 | 4.000 | 4.000 | 4.000 | 4.000 |
| *End-members (mol%)* | | | | | | | |
| Wo | 5.0 | 4.2 | 3.4 | 3.9 | 5.4 | 10.7 | 3.6 |
| En | 42.1 | 50.1 | 50.5 | 64.5 | 47.8 | 53.5 | 64.7 |
| Fs | 52.9 | 45.7 | 46.2 | 31.6 | 46.8 | 35.8 | 31.6 |
| Mg # | 44.6 | 52.6 | 52.6 | 68.4 | 50.8 | 62.0 | 70.2 |
| FeO | 24.5 | 23.9 | 21.9 | 19.0 | 23.1 | 20.7 | 17.8 |
| Fe2O3 | 0.0 | 0.0 | 0.0 | 0.6 | 0.0 | 1.4 | 2.3 |

| | Rugg04 | Rugg04 |
|---|---|---|
| | 18 | 19 |
| | carb | carb |
| SiO2 | 0.00 | 0.00 |
| TiO2 | 0.00 | 0.02 |
| Al2O3 | 0.01 | 0.05 |
| Cr2O3 | 0.00 | 0.06 |
| FeO | 1.11 | 1.41 |
| MnO | 10.22 | 10.82 |
| MgO | 1.16 | 1.13 |
| CaO | 48.63 | 48.89 |
| Na2O | 0.08 | 0.00 |
| K2O | 0.01 | 0.00 |
| Sum | 61.21 | 62.39 |

Table 5.2: Electron microprobe analyses of Rugg04 sample. Analyses acquired through a Jeol JXA-8600 (beam at 15 kV and 10 nA) at CNR-IGG, Firenze.

| Sample | Rugg09 | Rugg09 | Rugg09 | Rugg09 |
|---|---|---|---|---|
| Label | 1 | 9 | 23 | 35 |
| Phase | carb | carb | carb | carb |
| SiO2 | 0.57 | 0.32 | 0.00 | 0.02 |
| TiO2 | 0.00 | 0.06 | 0.07 | 0.00 |
| Al2O3 | 0.09 | 0.05 | 0.06 | 0.17 |
| Cr2O3 | 0.10 | 0.00 | 0.05 | 0.01 |
| FeO | 47.34 | 48.97 | 47.11 | 50.22 |
| MnO | 1.93 | 1.92 | 3.19 | 6.52 |
| MgO | 4.68 | 4.07 | 0.89 | 1.81 |
| CaO | 4.42 | 4.56 | 8.51 | 1.95 |
| Na2O | 0.18 | 0.31 | 0.11 | 0.35 |
| K2O | 0.06 | 0.00 | 0.00 | 0.00 |
| Sum | 59.38 | 60.25 | 59.98 | 61.06 |
| | | | | |
| SiO2 | 0.57 | 0.32 | 0 | 0.02 |
| FeCO3 | 76.33 | 78.97 | 75.97 | 80.99 |
| MnCO3 | 3.13 | 3.1 | 5.17 | 10.57 |
| MgCO3 | 9.78 | 8.52 | 1.85 | 3.78 |
| CaCO3 | 7.17 | 7.15 | 14.83 | 2.33 |
| Na2Ca*2 | 2.94 | 4.92 | 1.76 | 5.64 |
| K2Ca*2 | 0.81 | 0 | 0 | 0.06 |
| Sum Ox% | 100.73 | 102.97 | 99.58 | 103.38 |
| | | | | |
| Si | 0.011 | 0.006 | 0 | 0 |
| Fe2+ | 0.729 | 0.752 | 0.748 | 0.797 |
| Mn2+ | 0.03 | 0.03 | 0.051 | 0.105 |
| Mg | 0.128 | 0.112 | 0.025 | 0.051 |
| Ca | 0.087 | 0.09 | 0.173 | 0.04 |
| Na | 0.007 | 0.011 | 0.004 | 0.013 |
| K | 0.002 | 0 | 0 | 0 |
| Sum Cat# | 0.993 | 1 | 1.002 | 1.006 |
| | | | | |
| Buetschild | 0.2 | 0.0 | 0.0 | 0.0 |
| Eitelite | 0.7 | 1.1 | 0.4 | 1.3 |
| Rhodochr | 3.0 | 3.0 | 5.1 | 10.5 |
| Magnesite | 12.8 | 11.2 | 2.5 | 5.1 |
| Siderite | 72.9 | 75.2 | 74.8 | 79.7 |
| Calcite | 7.9 | 7.9 | 16.9 | 2.7 |

| Sample | Rugg09 | Rugg09 | Rugg09 |
|---|---|---|---|
| Label | 2 | 3 | 13 |
| Phase | clay? | clay? | clay? |
| SiO2 | 79.82 | 75.22 | 80.74 |
| TiO2 | 0.06 | 0.10 | 0.18 |
| Al2O3 | 3.87 | 5.77 | 5.11 |
| Cr2O3 | 0.00 | 0.00 | 0.00 |
| FeO | 3.06 | 3.90 | 5.08 |
| MnO | 0.03 | 0.04 | 0.00 |
| MgO | 1.32 | 1.48 | 0.84 |
| CaO | 1.25 | 1.78 | 1.39 |
| Na2O | 0.04 | 0.20 | 0.13 |
| K2O | 0.21 | 0.25 | 0.38 |
| Sum | 89.64 | 88.73 | 93.86 |

| Sample | Rugg09 | Rugg09 | Rugg09 | Rugg09 | Rugg09 |
|---|---|---|---|---|---|
| Label | 4 | 6 | 18 | 21 | 34 |
| Phase | feld | feld | feld | feld | feld |
| | | | | | ? |
| SiO2 | 50.14 | 56.55 | 52.65 | 49.55 | 62.73 |
| TiO2 | 0.03 | 0.00 | 0.00 | 0.00 | 0.25 |
| Al2O3 | 30.69 | 28.23 | 30.66 | 28.20 | 22.96 |
| Cr2O3 | 0.00 | 0.00 | 0.03 | 0.03 | 0.00 |
| FeO | 0.61 | 0.94 | 0.68 | 3.26 | 0.77 |
| MnO | 0.04 | 0.00 | 0.00 | 0.20 | 0.00 |
| MgO | 0.09 | 0.04 | 0.03 | 0.41 | 0.09 |
| CaO | 14.16 | 10.43 | 13.02 | 12.01 | 6.15 |
| Na2O | 3.53 | 6.33 | 4.93 | 4.57 | 7.48 |
| K2O | 0.09 | 0.37 | 0.13 | 0.23 | 1.16 |
| Sum | 99.39 | 102.89 | 102.12 | 98.46 | 101.59 |
| | | | | | |
| *Cations per 8 O:* | | | | | |
| Si | 2.306 | 2.489 | 2.351 | 2.325 | 2.764 |
| Al | 1.664 | 1.465 | 1.613 | 1.560 | 1.192 |
| Fe | 0.026 | 0.039 | 0.028 | 0.142 | 0.032 |
| sumT | 3.995 | 3.993 | 3.993 | 4.027 | 3.987 |
| | | | | | |
| Ca | 0.698 | 0.492 | 0.623 | 0.604 | 0.290 |
| Na | 0.315 | 0.540 | 0.426 | 0.415 | 0.639 |
| K | 0.005 | 0.021 | 0.008 | 0.014 | 0.065 |
| sum | 1.018 | 1.053 | 1.057 | 1.033 | 0.994 |
| | | | | | |
| sum catio | 5.014 | 5.045 | 5.049 | 5.060 | 4.981 |
| | | | | | |
| *End-members (mol%)* | | | | | |
| An | 68.5 | 46.7 | 58.9 | 58.5 | 29.2 |
| Ab | 30.9 | 51.3 | 40.3 | 40.2 | 64.3 |
| Or | 0.5 | 2.0 | 0.7 | 1.3 | 6.6 |
| | | | | | |
| | *labradorite* | *andesine* | *labradorite* | *labradorite* | *oligoclase* |

| Sample | Rugg09 | Rugg09 | Rugg09 |
|---|---|---|---|
| Label | 5 | 22 | 31 |
| Phase | glass | glass | glass |
| SiO2 | 74.07 | 75.13 | 72.34 |
| TiO2 | 0.89 | 0.81 | 0.62 |
| Al2O3 | 11.27 | 12.10 | 15.87 |
| Cr2O3 | 0.00 | 0.01 | 0.00 |
| FeO | 1.62 | 1.50 | 1.63 |
| MnO | 0.00 | 0.04 | 0.02 |
| MgO | 0.10 | 0.09 | 0.08 |
| CaO | 0.58 | 0.45 | 2.11 |
| Na2O | 0.99 | 2.06 | 4.69 |
| K2O | 5.30 | 5.50 | 3.71 |
| Sum | 94.82 | 97.70 | 101.09 |
| | | *There is Cl* | |

| Sample | Rugg09 | Rugg09 | Rugg09 | Rugg09 | Rugg09 |
|---|---|---|---|---|---|
| Label | 8 | 10 | 11 | 30 | 33 |
| Phase | cpx | cpx | cpx | cpx | cpx |
| SiO2 | 53.49 | 53.06 | 52.07 | 53.31 | 53.47 |
| TiO2 | 0.20 | 0.29 | 0.55 | 0.49 | 0.56 |
| Al2O3 | 1.62 | 2.40 | 3.06 | 1.94 | 1.72 |
| Cr2O3 | 0.20 | 0.09 | 0.06 | 0.00 | 0.03 |
| FeO | 5.30 | 6.42 | 8.66 | 10.73 | 9.72 |
| MnO | 0.05 | 0.14 | 0.16 | 0.18 | 0.25 |
| MgO | 17.69 | 17.15 | 15.85 | 15.12 | 15.55 |
| CaO | 21.12 | 20.94 | 20.30 | 19.43 | 20.35 |
| Na2O | 0.12 | 0.20 | 0.51 | 0.56 | 0.32 |
| K2O | 0.00 | 0.00 | 0.02 | 0.06 | 0.00 |
| Sum | 99.78 | 100.69 | 101.24 | 101.82 | 101.99 |
| | | | | | |
| *Cations per 6 O. Fe2+ and Fe3+ based on charge balance.* | | | | | |
| Si | 1.955 | 1.928 | 1.895 | 1.947 | 1.946 |
| IVAl | 0.045 | 0.072 | 0.105 | 0.053 | 0.054 |
| Fe3+ | 0.000 | 0.000 | 0.000 | 0.000 | 0.000 |
| Sum | 2.000 | 2.000 | 2.000 | 2.000 | 2.000 |
| | | | | | |
| VIAl | 0.025 | 0.031 | 0.027 | 0.030 | 0.020 |
| Fe 3+ | 0.012 | 0.035 | 0.082 | 0.036 | 0.026 |
| Ti | 0.005 | 0.008 | 0.015 | 0.013 | 0.015 |
| Mg | 0.952 | 0.923 | 0.860 | 0.823 | 0.844 |
| Cr | 0.006 | 0.003 | 0.002 | 0.000 | 0.001 |
| Fe2+ | 0.000 | 0.000 | 0.014 | 0.097 | 0.094 |
| Sum | 1.000 | 1.000 | 1.000 | 1.000 | 1.000 |
| | | | | | |
| Na | 0.009 | 0.014 | 0.036 | 0.039 | 0.023 |
| Mn | 0.001 | 0.004 | 0.005 | 0.006 | 0.008 |
| Ca | 0.827 | 0.815 | 0.792 | 0.760 | 0.793 |
| Fe2+ | 0.151 | 0.160 | 0.167 | 0.195 | 0.176 |
| Mg | 0.012 | 0.007 | 0.000 | 0.000 | 0.000 |
| Sum | 1.000 | 1.000 | 1.000 | 1.000 | 1.000 |
| | | | | | |
| Sum catio | 4.000 | 4.000 | 4.000 | 4.000 | 4.000 |
| | | | | | |
| *End-members (mol%)* | | | | | |
| Wo | 42.3 | 41.9 | 41.2 | 39.6 | 40.9 |
| En | 49.3 | 47.8 | 44.8 | 42.9 | 43.5 |
| Fs | 8.4 | 10.3 | 14.0 | 17.4 | 15.7 |
| | | | | | |
| Mg # | 86.5 | 85.3 | 82.6 | 73.8 | 75.7 |
| FeO | 4.9 | 5.3 | 6.0 | 9.6 | 8.9 |
| Fe2O3 | 0.4 | 1.3 | 3.0 | 1.3 | 0.9 |

| Sample | Rugg09 | Rugg09 |
|---|---|---|
| Label | 25 | 29 |
| Phase | opx | opx |
| SiO2 | 55.69 | 56.80 |
| TiO2 | 0.29 | 0.20 |
| Al2O3 | 1.68 | 0.71 |
| Cr2O3 | 0.00 | 0.00 |
| FeO | 16.56 | 16.10 |
| MnO | 0.44 | 0.40 |
| MgO | 27.73 | 27.95 |
| CaO | 1.40 | 1.64 |
| Na2O | 0.08 | 0.04 |
| K2O | 0.00 | 0.02 |
| Sum | 103.87 | 103.87 |
| | | |
| *Cations per 6 O. Fe2+ and Fe3+ based on charge balance.* | | |
| Si | 1.935 | 1.974 |
| IVAl | 0.065 | 0.026 |
| Fe3+ | 0.000 | 0.000 |
| Sum | 2.000 | 2.000 |
| | | |
| VIAl | 0.003 | 0.003 |
| Fe 3+ | 0.052 | 0.016 |
| Ti | 0.008 | 0.005 |
| Mg | 0.936 | 0.976 |
| Cr | 0.000 | 0.000 |
| Fe2+ | 0.000 | 0.000 |
| Sum | 1.000 | 1.000 |
| | | |
| Na | 0.006 | 0.003 |
| Mn | 0.013 | 0.012 |
| Ca | 0.052 | 0.061 |
| Fe2+ | 0.429 | 0.452 |
| Mg | 0.500 | 0.472 |
| Sum | 1.000 | 1.000 |
| | | |
| Sum catio | 4.000 | 4.000 |
| | | |
| *End-members (mol%)* | | |
| Wo | 2.6 | 3.1 |
| En | 72.4 | 72.8 |
| Fs | 24.9 | 24.1 |
| | | |
| Mg # | 77.0 | 76.2 |
| FeO | 14.8 | 15.5 |
| Fe2O3 | 2.0 | 0.6 |

| Sample | Rugg09 | Rugg09 |
|---|---|---|
| Label | 24 | 36 |
| Phase | quartz | quartz |
| SiO2 | 101.99 | 101.36 |
| TiO2 | 0.07 | 0.05 |
| Al2O3 | 1.13 | 1.03 |
| Cr2O3 | 0.00 | 0.00 |
| FeO | 0.81 | 0.48 |
| MnO | 0.00 | 0.05 |
| MgO | 0.02 | 0.02 |
| CaO | 0.04 | 0.05 |
| Na2O | 0.88 | 0.42 |
| K2O | 0.00 | 0.03 |
| Sum | 104.94 | 103.52 |

| Sample | Rugg09 | Rugg09 |
|---|---|---|
| Label | 26 | 32 |
| Phase | ilm | ilm |
| SiO2 | 1.38 | 1.68 |
| TiO2 | 19.54 | 14.55 |
| Al2O3 | 1.75 | 3.32 |
| Cr2O3 | 0.12 | 0.28 |
| FeO | 67.87 | 70.66 |
| MnO | 0.32 | 0.26 |
| MgO | 1.08 | 1.81 |
| CaO | 0.10 | 0.13 |
| Na2O | 0.02 | 0.33 |
| K2O | 0.03 | 0.03 |
| Sum | 92.22 | 93.04 |
| | | |
| *Cations per 3 O. Fe2+ and Fe3+ based on charge balance.* | | |
| *(Ilmenite-hematite s.s.)* | | |
| Si | 0.036 | 0.042 |
| Al | 0.054 | 0.098 |
| K | 0.001 | 0.001 |
| Ti | 0.381 | 0.275 |
| Mg | 0.042 | 0.068 |
| Cr | 0.003 | 0.006 |
| Na | 0.001 | 0.016 |
| Mn | 0.007 | 0.006 |
| Ca | 0.003 | 0.003 |
| Fe3+ | 1.112 | 1.279 |
| Fe2+ | 0.361 | 0.206 |
| Sum | 2.000 | 2.000 |
| | | |
| FeO | 16.64 | 9.82 |
| Fe2O3 | 56.93 | 67.61 |
| FeO* | 67.87 | 70.65 |
| | | |
| Sum | 97.92 | 99.81 |

Table 5.3: Electron microprobe analyses of Rugg09 sample. Analyses acquired through a Jeol JXA-8600 (beam at 15 kV and 10 nA) at CNR-IGG, Firenze.

### 5.2.1.2 Liquids

The fluid selected for the experiments (**LH35**) comes from a cold spring in the area of the Cofre de Perote, which is the highest volcano in the Eastern area of Los Humeros geothermal field, and it is mainly composed by andesites and trachyandesites (Carrasco-Núñez et al., 2017). The fluid was sampled by M. Lelli at 3020 meters above the sea level in the site with latitude UTM easting 689961 and northing 2160999 coordinates. The fluid is bicarbonate-rich and it has low conductivity (~84 µS*cm$^{-1}$), indicating a very low mineralization. It is thus assumed that fluid with such composition infiltrate in the volcanic rocks of Cofre de Perote and interact with the andesitic rocks of the reservoir. In many cases, before starting the experiments an aliquot of this water was put in a bubbler under nitrogen flow for ~ 1 day in order to strip air from it in an effort to prevent oxidation of any Fe(II) released from minerals, which could trigger Fe(III) oxide precipitation over their surfaces.

With the refinement of the geochemical modelling of LHGF it has been hypothesized that recharge of the geothermal field is mainly west-driven. As a consequence, a liquid (**LH3**) was sampled from a well at UTM easting 647263 and northing 2165018 coordinates and it was utilized in an experiment. Analyses show that this liquid has a greater total dissolved solids respect to LH35 (Table 5.4). In particular, $Ca^{2+}$, $Na^{+}$, $HCO_3^{-}$ and $NO_3^{-}$, $SO_4^{2-}$ are more abundant in LH3 than in LH35, as a consequence of fluid interaction with carbonatic rocks during percolation in geothermal reservoir.

### 5.2.1.3 Gas

Geothermal fluids contain gas whose main components are $CO_2$ (predominant), $H_2S$, $H_2$, $N_2$, Cl, F (e.g. Arellano et al, 2003). These gases can be responsible of the formation of low pH fluids induced by the exploitation of geothermal fluids. In fact, in their way to the surface they can react with aqueous fluids, producing aqueous corrosive species (Gutiérrez-Negrín & Izquierdo-Montalvo, 2010). It is thus crucial to take into account the role of gas in the experiments and we choose to impose a $CO_2$ overpressure. Data from gas stripped from fluids in the wells (Arellano et al., 2003) indicate that 5 bar $CO_2$ overpressure is a realistic value. We therefore decided to apply this overpressure after stripping out air from the micro-reactor and before starting to increase T.

| Sample | LH35 | LH3 |
|---|---|---|
| Type | Cold Spring | Well |
| X (m) | 689961 | 647263 |
| Y (m) | 2160999 | 2165018 |
| Alt. (m.a.s.l.) | 3020 | 2416 |
| Depth (m) | - | 95 |
| T (°C) | 11.9 | 20.2 |
| pH | 6.44 | 7.8 |
| O2 diss. (mg/L) | 6.6 | - |
| E.C. (μS/cm) | 84.1 | 610 |
| *Analyses in mg/l:* | | |
| Cl | 1.56 | 31.7 |
| B | <0.05 | 0.03 |
| HCO3 | 54.29 | 138 |
| SO4 | 3.8 | 26 |
| Na | 7.02 | 39.3 |
| K | 4.06 | 5.2 |
| Ca | 7.16 | 78.5 |
| Mg | 3.53 | 9.07 |
| F | <0.1 | 0.27 |
| NO3 | 3.25 | 183 |
| *Analyses in meq/l:* | | |
| $HCO_3^-$ | 0.89 | 2.26 |
| $F^-$ | 0.00 | 0.00 |
| $Cl^-$ | 0.04 | 0.89 |
| $NO_3^-$ | 0.05 | 2.95 |
| $SO_4^{2-}$ | 0.08 | 0.54 |
| $Ca^{2+}$ | 0.36 | 3.92 |
| $Mg^{2+}$ | 0.29 | 0.75 |
| $Na^+$ | 0.31 | 1.71 |
| $K^+$ | 0.1038 | 0.1330 |
| Sum cations | 1.06 | 6.51 |
| Sum anions | 1.07 | 6.65 |
| Eror | -0.40% | -1.09% |

Table 5.4: Analyses of fluids utilized in the experiments. Fluids were sampled and analyzed by M. Lelli.

### 5.2.2 The micro-reactor and P-T conditions

Fluid-rock interaction experiments were performed in a T316 stainless steel micro-reactor (Parr Instrument Company, Mod. 5500, Figure 5.3). The instrument has a 25 ml capacity and it is equipped with a magnetic drive that allows the solid and the fluid to be mixed continuously. Furthermore, a gas inlet valve permits to charge gas into the vessel while gas and liquid sampling valves allows fluids to be sampled during the experiment (*in situ* sampling). The vessel is rated for a maximum working pressure of 200 bar. The maximum operating temperature is dependent upon the seal selected; if PTFE gasket are used, as in our case, it can reach 350 °C. The micro-reactor can be filled up to 2/3 of the volume, higher degrees of filling can produce over-pressures, which can potentially produce failure of the experiment. It was then decided to let react **1 g of rock with 16 ml of liquid**. The solid/liquid ratio (~0.0625 in wt%) was low in order to maximize reactions in solid phases.

Following considerations in the previous paragraph, in most of the experiments we applied **$CO_2$ overpressure (5 bar)** after stripping out air from the micro-reactor and before starting to increase T.

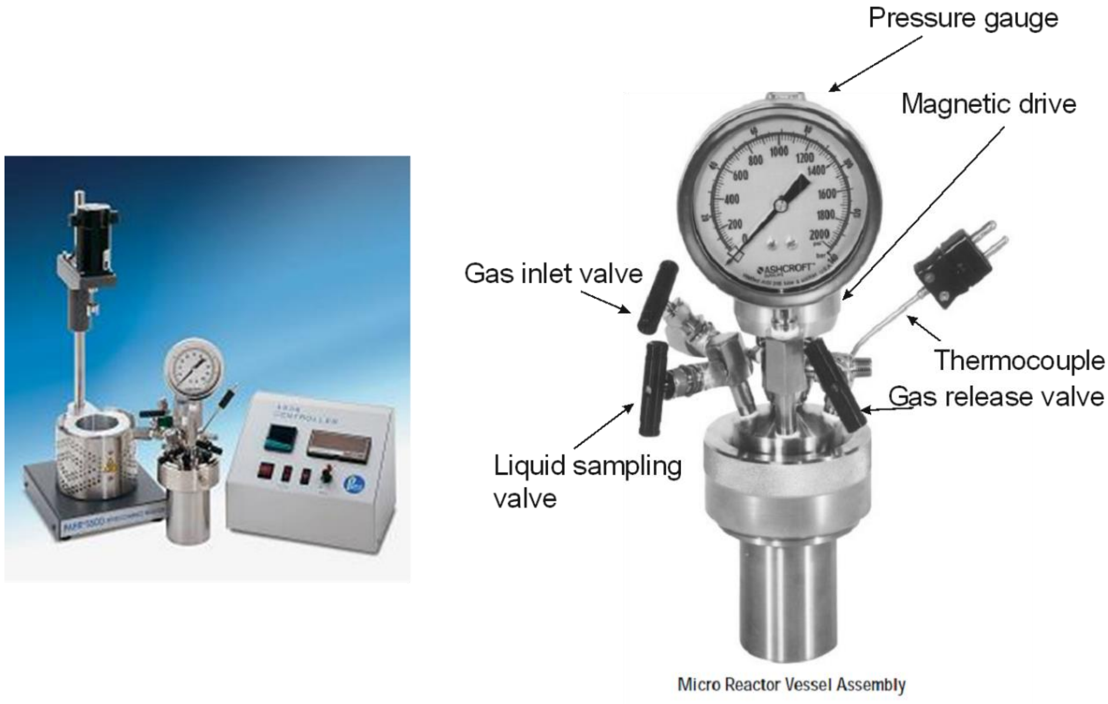


Figure 5.3: Image of the Mod. 5500 Parr micro-reactor used in the experiments (left). Enlargement of the reactor showing valves, magnetic drive and pressure gauge (right).

Three experiments were planned at the following T: **200**, **250** and **300 °C**. Considering the liquid + vapor curve of the water, related pressure values should be ~16, 40 and 86 bar (Wagner & Pruss, 1995). Nevertheless, $CO_2$ overpressure must be taken into account, even if some of this gas is being dissolved in the liquid phase. Actual recorded values were 20 (at 200 °C), 44 (250 °C) and 88 (300 °C) bar. Actual run duration of experiments varied from 191 to 379 hours. Before ending each experiment liquid was sampled *in situ* through the liquid valve. Care was taken to keep the collecting flask as cool as possible in order to minimize steam loss.

Nonetheless, a variable amount of 35-75 wt% of the charged liquid (16 ml) was consistently lost during sampling. After liquid sampling the micro-reactor was cooled, switching off the electric power and ventilating it. After ~ 2 hours, the vessel attained near-room T and solid could be removed and collected. Encrustations usually formed on the micro-reactor walls and they had to be mechanically removed with a spatula; after that, the vessel was washed with a dilute HCl solution in an ultrasonic bath.

### 5.2.3 Analyses of experimental products

Sampled liquids were filtered (filter with pore size= 0,45 µm) and analyzed through liquid chromatography utilizing Metrohm 761 Compact IC and Metrohm 861 Advanced Compact IC instruments at Dipartimento di Scienze della Terra, Università degli Studi di Firenze. The analyzed species were $Cl^-$, $HCO_3^-$, $SO_4^{2-}$, $F^-$, $Br^-$, $NO_3^-$, $NH_4^+$, $Na^+$, $K^+$, $Ca^{2+}$, $Mg^{2+}$, $Sr^{2+}$ and $Li^+$. In few cases, solids entrapped in filters were recovered and analyzed through SEM (see below). Solids run products were characterized by XRD on a Philips PW 1050/37 powder diffractometer, operating with a Cu anode, a graphite monochromator and with a PANalytical X'Pert PRO data acquiring system (Dipartimento di Scienze della Terra, Università degli Studi di Firenze). Spectra were also acquired at Centro di Cristallografia Strutturale (CRIST) of the University of Firenze (Bruker New D8 Da Vinci instrument, Theta-Theta goniometer, CuKα radiation, 40kV x 40mA conditions, 2Θ from 5° to 70°, step scan 0.020°, time per step 57.6 s) in order to get spectra with reduced noise background. In some cases, solid products were mounted on stubs for observation in a Scanning Electron Microscope (SEM) ZEISS EVO MA15 equipped with EDS microanalyses OXFORD INCA 250 (MEMA, Centro di Servizi di Microscopia Elettronica e Microanalisi - Università degli Studi di Firenze). Microanalyses results are only qualitative since samples were not embedded in epoxy resin and polished, but they were simply put on a carbon adhesive stub and C coated for microscope observation.

## 5.3 Results

Experimental details are reported in Table 5.5. Summing up, we arbitrarily chose to fix solid/liquid ratio and we varied the following parameters:

- Solid (Rugg04, Rugg09);
- Liquid (LH35, LH3);
- T (200, 250, 300°C);
- $P_{CO2}$ at the beginning of the experiment (0, 5 bar)
- De-airing procedure with $N_2$ flow before starting the experiment (yes, no)
- Run duration (from 191 to 379 hours).

Results are reported in the following paragraphs, considering the solid used in the experiments.

| Experiment | 139 | 142 | 154 | 168 | 143 | 147 | 146 | 167 | 149 |
|---|---|---|---|---|---|---|---|---|---|
| Solid (type) | Rugg04 | Rugg04 | Rugg04 | Rugg04 | Rugg04 | Rugg09 | Rugg09 | Rugg09 | Rugg09 |
| Fluid (type) | LH35 | LH35 | LH35 | LH3 | LH35 | LH35 | LH35 | LH35 | LH35 |
| T (°C) | 200 | 250 | 250 | 250 | 300 | 200 | 250 | 250 | 300 |
| Initial PCO2 | 5 | 5 | 0 | 5 | 5 | 5 | 5 | 0 | 5 |
| De-air | YES | YES | YES | YES | YES | YES | YES | NO | YES |
| P (bar) | 20 | 44 | 41 | 41 | 88 | 21 | 38 | 41 | 90 |
| Duration (h) | 262 | 263 | 379 | 263 | 191 | 239 | 307 | 308 | 258 |

Table 5.5: Details of fluid-rock stirred experiments. In all the experiments 1 g of solid and 16 ml of fluid were utilized.

### 5.3.1 Experiments using the more primitive andesite (Rugg04)

At the end of the experiments extensive encrustations around micro-reactor walls were often observed. They are whitish – ochre in color (Figure 3.4) and their mechanical removal proved to be tricky.


Figure 5.4: Images of the whitish –ochre encrustations on the walls and at the bottom of the micro-reactor. The internal diameter is about 2.5 cm. The images refer to Experiment 142.

XRD spectra of run products are reported in Figure 5.5. In this Figure, spectrum of encrustation formed in Experiment 139 (T=200 °C) is also reported. Unfortunately, starting material have numerous peaks, attributable mainly to plagioclases; this makes difficult the detection of new phases possibly formed during experiments. Nevertheless, some new peaks not existing in the starting material can be evidenced (Figure 5.5). They are attributed to quartz ($SiO_2$), boehmite ($AlO(OH)$), possibly kaolinite ($Al_2Si_2O_5(OH)_4$) (or phillipsite, see below) and calcite ($CaCO_3$). Quartz is particularly abundant in the encrustations grown on reactor walls. The finding of quartz and boehmite occurs in the whole range of the investigated temperatures, even if peaks intensities for these phases are higher for experimental products obtained at 200°C (Figure 5.5). The presence of kaolinite could be revealed by the presence of its most intense peak at ~12.5° 2θ CuKα. This phase can be stable up to 260-270 °C under P conditions such as those of the experiments (Hurst & Kunkle, 1985), even if its stability is lowered at T< 250 °C in presence of quartz (Matsuda et al., 1992). Alternatively, this peak could be attributed to phillipsite ($(Ca,K,Na)_{1-2}(Si,Al)_8O_{16}\bullet 6H_2O$), a common zeolite found in volcanic rocks. This phase has three intense peaks, two of them at ~12.4° CuKα, and the other at ~27.8° CuKα which could be masked by the most intense peaks pertaining to plagioclases. Anyway, it should be remembered that, as a rule of the thumb, powder XRD can evidence the presence of phases more abundant than ~5 wt%; thus, this technique cannot reveal the presence of newly formed phases if they are present in small amounts among the experimental products.

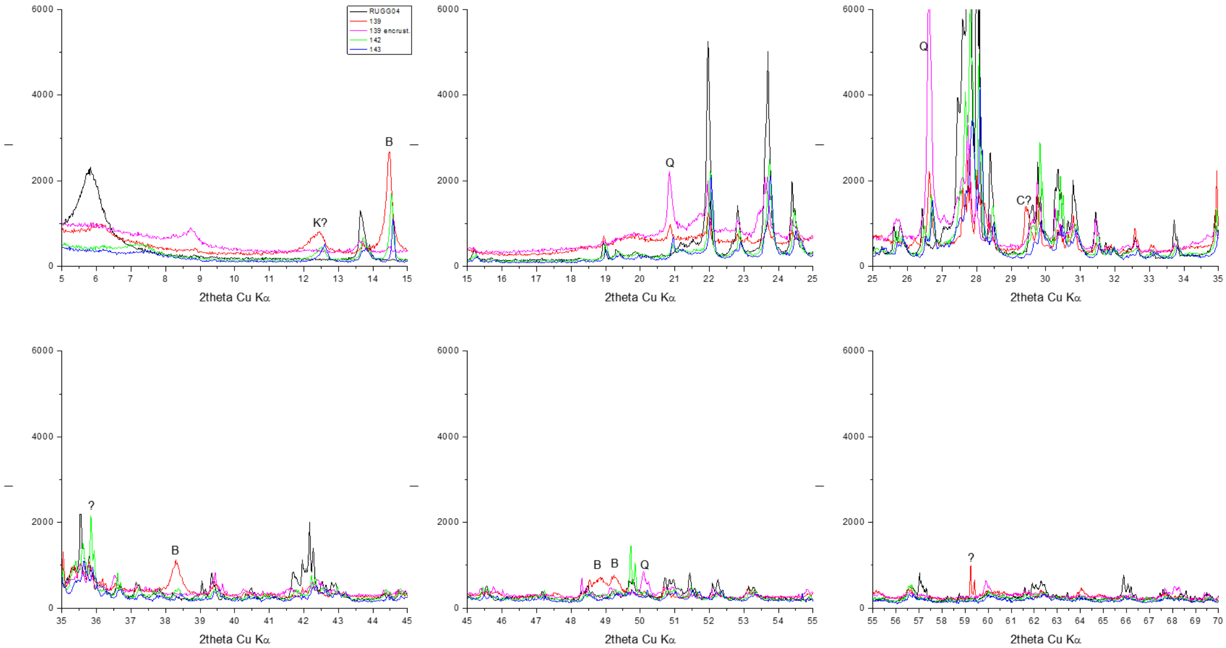


Figure 5.5: XRD spectra of **Rugg04** starting material and experimental products of experiments 139 (**200°C**), 142 (**250°C**), 143 (**300°C**). For sake of clarity spectrum the spectrum relative of the encrustation (encrust.) is reported only for experiment 139. Peaks attributed to K (=kaolinite), Q (=quartz), B (=boehmite), C (= calcite) are shown.

SEM observations and microanalyses (albeit qualitative), besides highlighting the presence of quartz crusts, allowed to evidence the presence of an Al-rich phase, compatible with boehmite and a Si, Al, K, Fe, Mg –bearing phase, compatible with illite, not evidenced by XRD, probably because of its paucity in experimental products, (Figure 5.6).

Quartz, boehmite and possibly kaolinite (or phillipsite?) are found also in the experiment run without charging the reactor with an initial $P_{CO2}$ (Figure 5.7). Moreover, SEM observations on encrustations of experiment 154 evidenced the presence of tiny Na-Si rich crystals on the quartzitic matrix (Figure 5.6d).

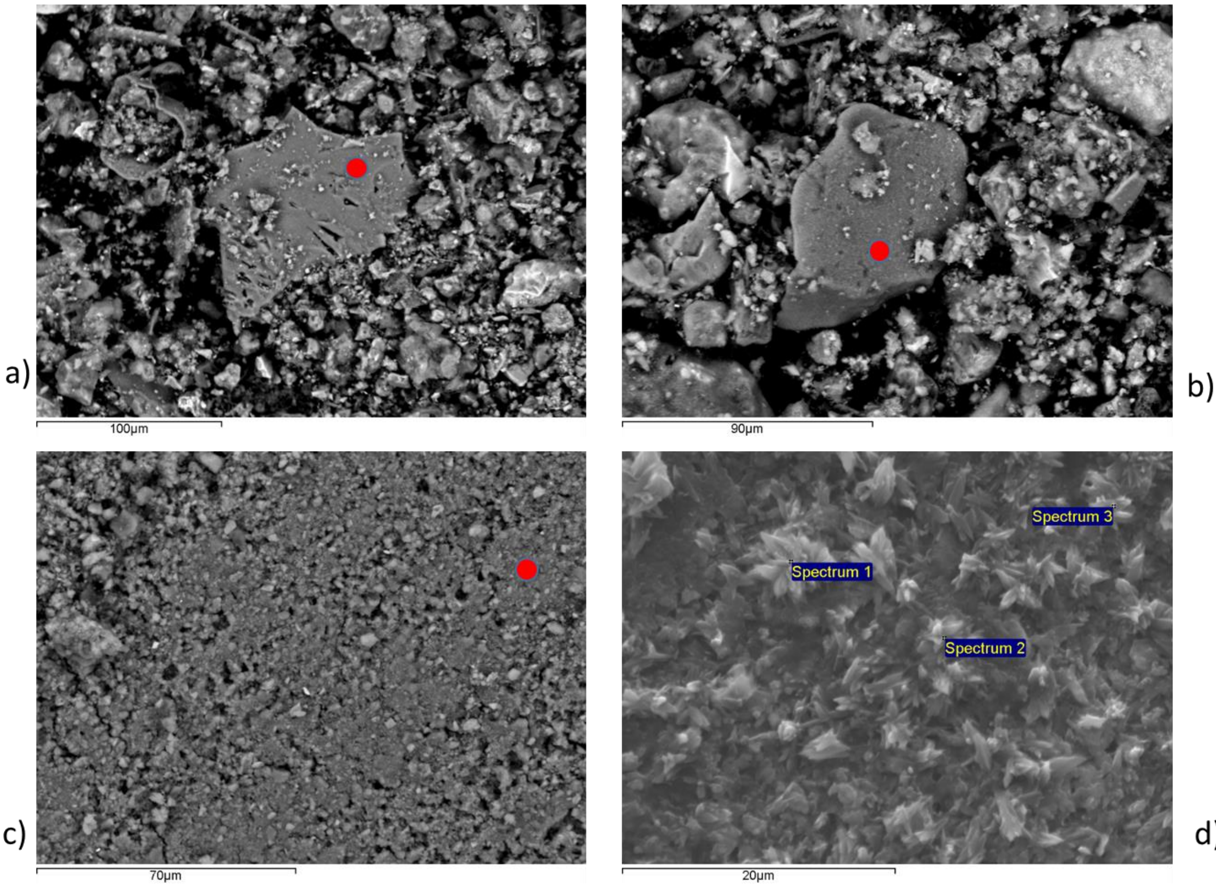


Figure 5.6: BSE images of representative area of experimental products. Red dots indicate: a) Angular quartz fragment (exp. 139), b) Al-rich (Al2O3~73 wt%) rounded phase (boehmite?, exp.139), c) Al-Si-K-rich phase (SiO2~66 wt%, Al2O3~15wt%, K2O~10 wt%, FeO~3-5 wt%, MgO~1 wt% illite?, exp. 139), d) solids in crusts of exp. 154. Phases indicated by labels are Na2O (40-58 wt%) and SiO2 (31-44 wt%)-rich.

XRD spectrum of experimental product obtained in run performed with LH3 fluid sample confirm the presence of peaks attributable to quartz and, possibly, to wairakite ($CaAl_2Si_4O_{12}$•$2H_2O$) beside the lack of boehmite's peaks (Figure 5.8). In fact, the two most intense peaks of wairakite (at 2theta of 26.11° and 15.95° for Cu Kalpha) are clearly visible in the XRD spectrum of products of experiment 168 (Figure 5.8), the less intense peaks being likely hidden by the numerous plagioclase peaks.

Analyses of fluids sampled in situ just before ending the experiments are reported in Table 5.6. $HCO_3^-$ is the most abundant anion and $NH_4$ is almost always the most abundant cation. Nevertheless, values associated to this analyte should be treated with caution since a $NH_4$ contamination was found to occur during sampling. Some "blank" experiments at 200°C with only deionised water still resulted to yield a fluid with $NH_4$ contamination (1-4.5 mg/l). We presume contamination should come from reactor's walls but efforts to reduce it as much as possible by means of iterated "washing runs" failed. It has to be considered that $NH_4$ caused by $NO_3$ reduction could contribute only by ~ 1.3 mg/l. It should be highlighted the low cations contents of elements such as Na and Ca, potentially released by plagioclase dissolution of the starting material. Anyway, beside the critical issues in the sampling procedure (see paragraph

5.2.2), phases precipitation occurred during sampling since $Na_2O$-$Al_2O_3$-rich solid phases were found in the filters used to inject sampled fluids into chromatograph (Figure 3.9).

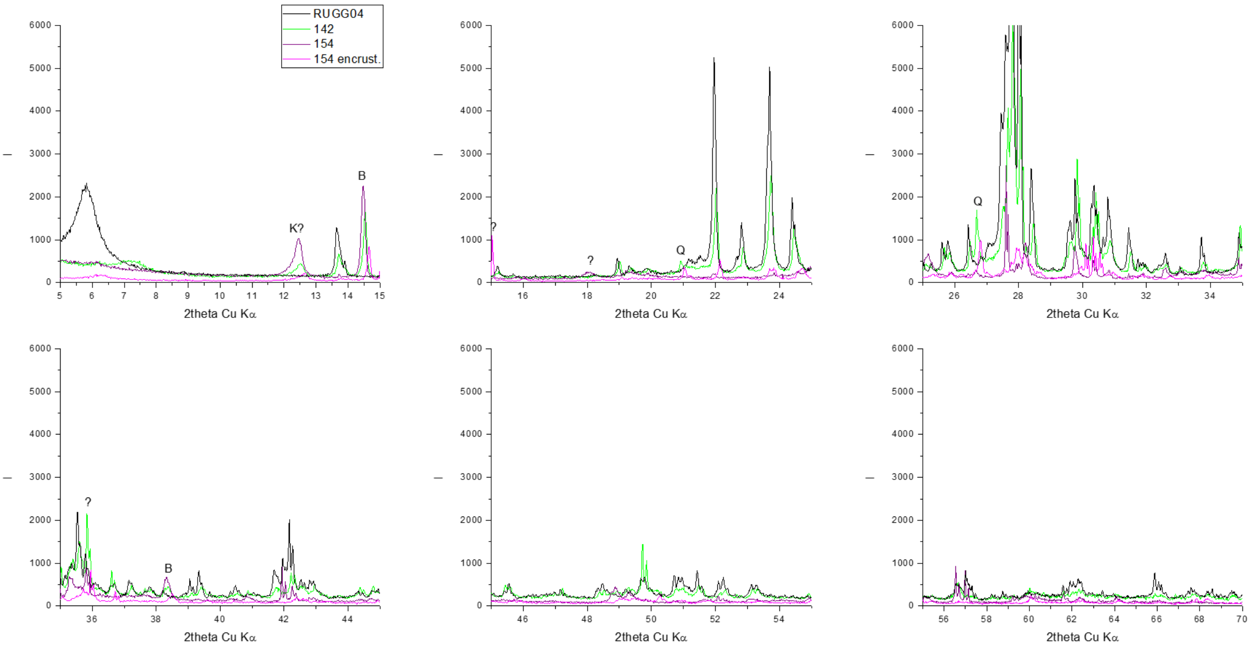


Figure 5.7: XRD spectra of **Rugg04** starting material and experimental products of run 142 (**250°C, with initial PCO2=5 bar**), 154 (**250°C, initial $P_{CO2}$=0**). Meaning of the letters as in Figure 3.5.

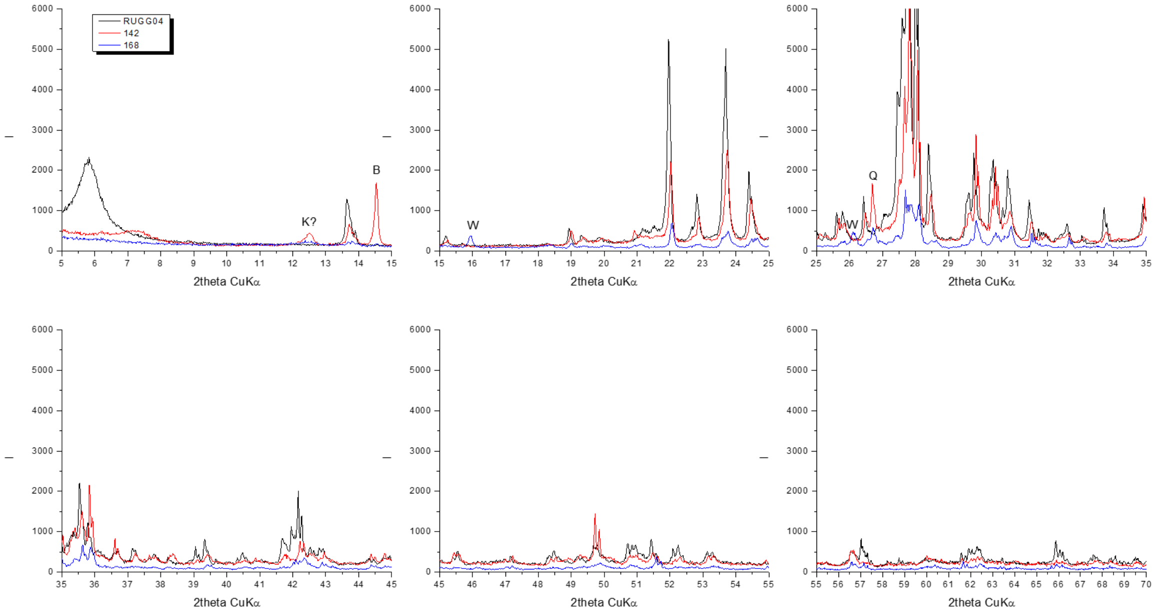


Figure 5.8: XRD spectra of **Rugg04** starting material and experimental products of run 142 (**250°C, liquid=LH35**), 154 (**250°C, liquid= LH3**). Meaning of the letters as in Figure 3.5, W= wairakite.

| Experiment | LH35 | 139 | 142 | 154 | 168 | 143 | 147 | 146 | 167 | 149 |
|---|---|---|---|---|---|---|---|---|---|---|
| Rock | | | | Rugg04 | | | | Rugg09 | | |
| T(°C) | | **200** | **250** | **250** | **250** | **300** | **200** | **250** | **250** | **300** |
| Contents (mg/l): | | | | | | | | | | |
| Cl | 1.95 | 1.75 | 1.7 | 1.99 | 4.7 | 1.4 | 1.00 | | 0.6 | 1.60 |
| NH4 | 0.05 | 16.5 | 7.3 | 6.3 | 39.0 | 5.9 | 25 | 16 | 8.1 | 16 |
| HCO3 | 65 | 384.3 | 80 | 366 | 165 | 326 | 132 | | 61 | 61 |
| SO4 | 4.80 | 4.06 | 8.7 | 3.34 | 3.2 | 3.3 | 2.20 | | 1.7 | 2.90 |
| Na | 7.5 | 4.94 | 6.2 | 1.4 | 4.0 | 1.6 | 2.3 | 1.8 | 3.2 | 1.4 |
| K | 4.3 | 1.99 | 3.1 | 0.7 | 1.5 | 0.8 | 1.2 | 3.3 | 1.5 | 0.7 |
| Ca | 8.7 | 9.04 | 10 | 7.7 | 8.4 | 13 | 2.7 | 12 | 2.9 | 5.2 |
| Mg | 4.00 | 0.25 | 1.6 | 0.33 | 1.60 | 0.4 | 0.26 | 14 | 0.29 | 0.38 |
| F | 0.32 | 0.61 | 0.33 | | | | 0.80 | | | |
| Br | | | 0.01 | 0.008 | | | | | | 0.007 |
| NO3 | 4.50 | 0.35 | 0.6 | 0.80 | 0.57 | 0.1 | 0.26 | | 0.01 | 0.67 |
| Li | | | | | | | 0.013 | | | |
| Sum cations (meq/l) | 1.20 | 1.65 | 1.40 | 0.84 | 2.93 | 1.12 | 1.67 | | 0.80 | 1.26 |
| Sum anions (meq/l) | 1.31 | 6.47 | 1.57 | 6.14 | 2.91 | 5.45 | 2.28 | | 1.05 | 1.12 |
| Error (%) | -4.34 | -59.30 | -5.52 | -75.83 | 0.26 | -65.98 | -15.39 | | -13.90 | 5.93 |

Table 5.6: Analyses of fluids sampled in situ, just before ending the experiment. In Experiment 146 fluid was sampled in a flask in which an acidified solution was added to analyze cations only. Note that a NH4 contamination occurs during sampling, since this analyte was found to be in the 1 cidifibly, range, even in de-ionized water experiments run without solid at T=200°C.

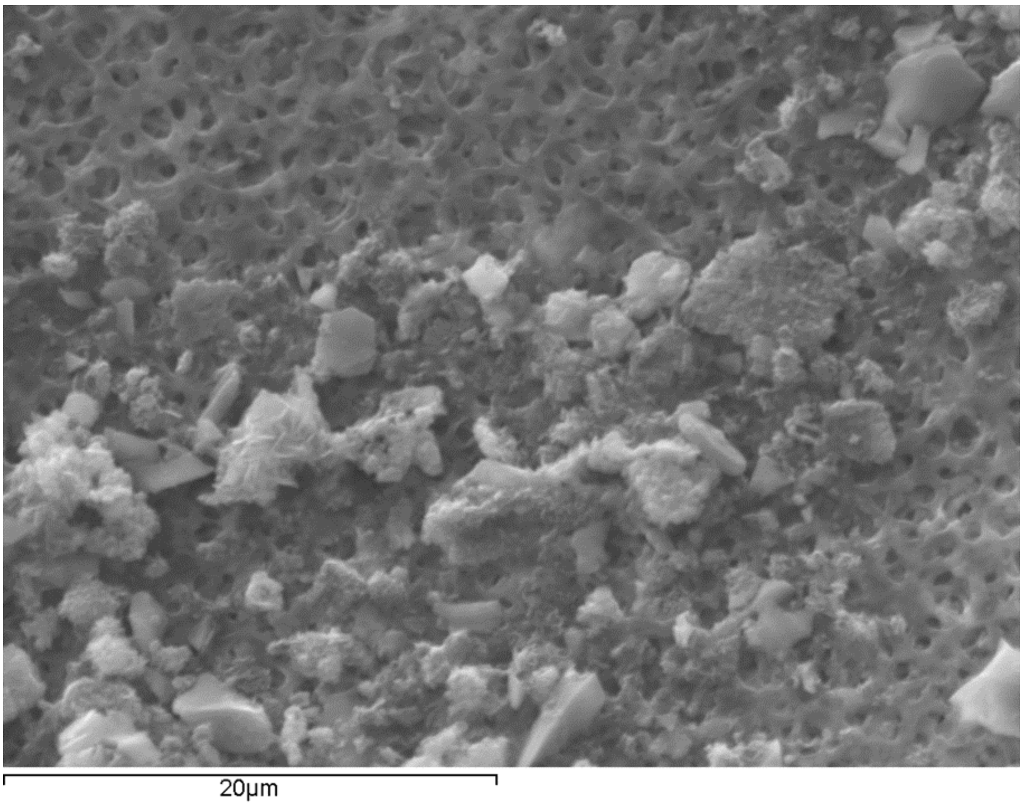


Figure 5.9: SE image of solids entrapped in filters utilized to inject liquid into LC. Qualitative EDS analyses on the red points gave Na2O= 67-70wt%, Al2O3=20-22 wt%, SiO2= 2-4 wt%, K2O= 3-10 wt%). The image refers to Experiment 147, but similar products were found in filters relative to runs performed using Rugg04 andesite.

### 5.3.2 Experiments using less primitive andesite (Rugg09)

XRD spectra show the crystallization of quartz and boehmite during these experiments (Figure 3.10). Furthermore, a peak attributable to kaolinite or phillipsite (at Cu Kα 2θ ~ 12.5°) suggests the presence of this phase among experimental products, as in experiments run with Rugg04 starting material. In addition, magnesite ($MgCO_3$) is possibly detected in run executed at 250 °C, since the most intense peak of this phase is clearly visible at ~ Cu Kα 2θ ~ 32.6°. Similar results were found also for the experiment run without imposing an initial $P_{CO2}$ (Figure 5.10). Encrustations stuck in reactor's walls are mainly formed by quartz, since peaks of this phase are the most intense in correspondent XRD spectra (Figure 5.11). SEM investigation lead to results similar to those obtained for experiments run using Rugg04 andesite. More detailed SEM-EDS investigations on encrustations formed in experiment 167 evidenced the presence of a Si-Na-rich phase with a mammillary appearance and bundles of Na-rich tiny crystals (Figure 5.12). The former resemble zeolites but the absence of Al in EDS analyses suggest they are not. Tiny crystals could be natrite ($Na_2CO_3$) and their acicular aspect (Figure 5.12) suggests they crystallised during experiment termination.

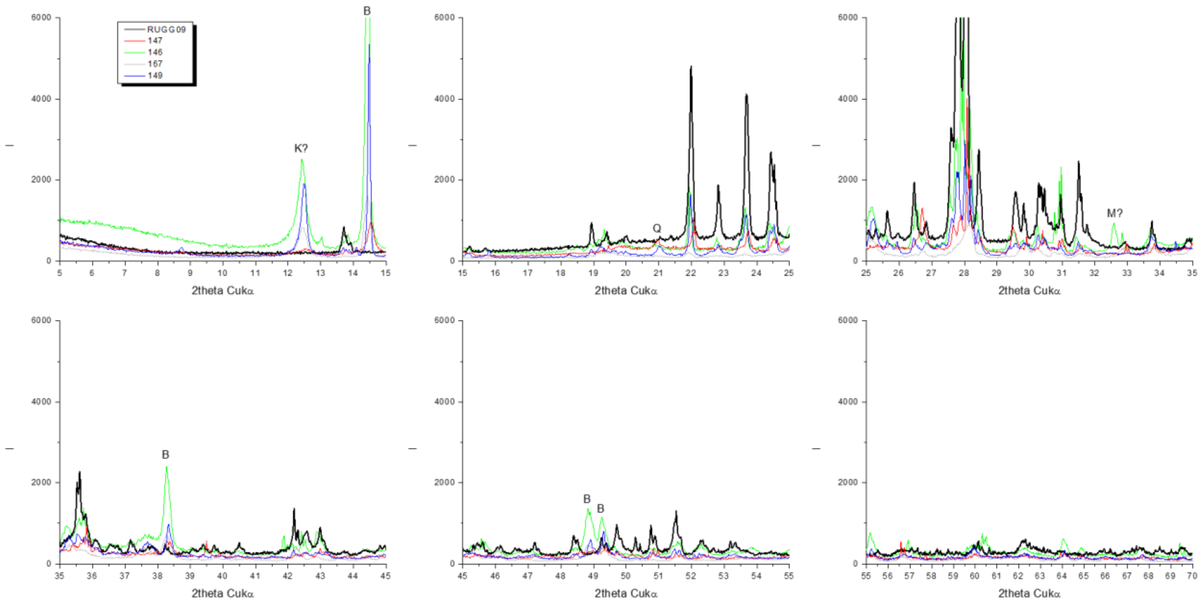


Figure 5.10: XRD spectra of **Rugg09** starting material and experimental products of experiments 147 (**200°C**), 146 (**250°C**), 167 (**250°C, initial PCO2=0)**, 149 (**300°C**). Peaks attributed to K? (=kaolinite), Q (=quartz), B (=boehmite), M? (= magnesite) are shown.

Solids filtered from liquid before injection to chromatograph resulted to have $SiO_2$= 17-26 wt%, $Al_2O_3$= 47-68 wt%, FeO= 7-15 wt%, MgO= 3-4 wt%, $K_2O$~ 1 wt% (EDS analyses, Figure 5.13). The analyses do not identify a single mineralogical phase, but they possibly represent "cumulative" analyses, comprising neo-formed Al-rich phases, such as boehmite.

Analyses of sampled liquids are not quite different from analyses just reported for other experiments (Table 5.6), the main cations being $HCO_3^-$ and $NH_4^+$.

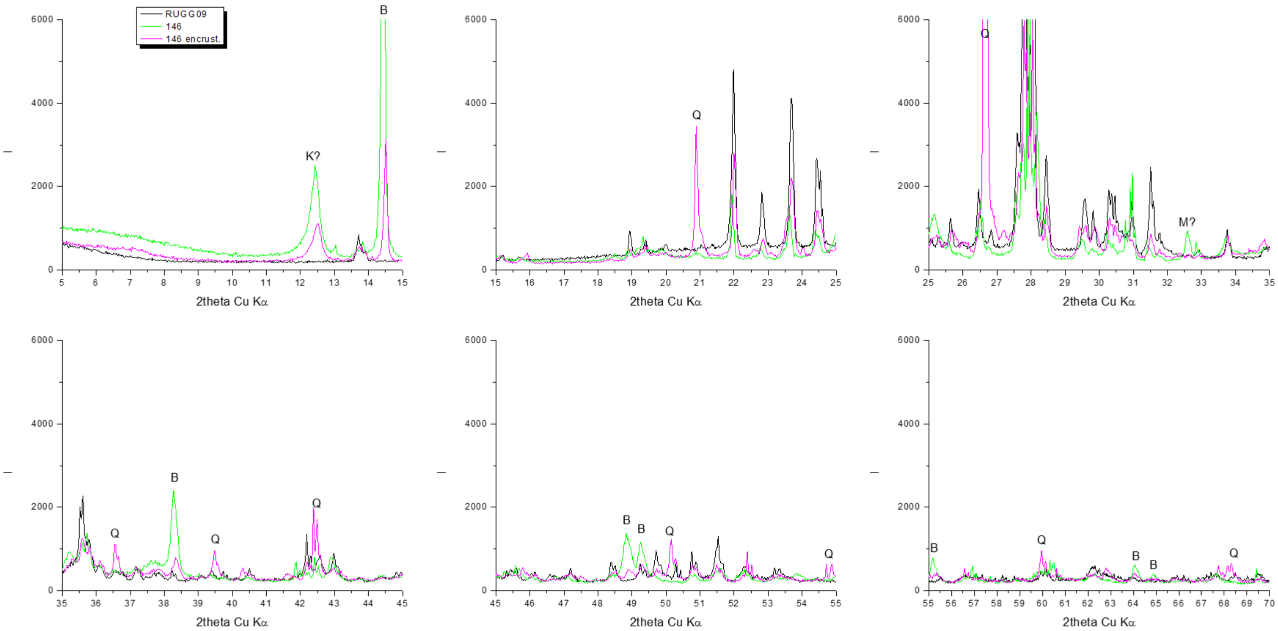


Figure 5.11: XRD spectra of **Rugg09** starting material and experimental products of experiments 146 (**250°C**) and **encrustations** formed. Meaning of the letters as in Figure 3.10.

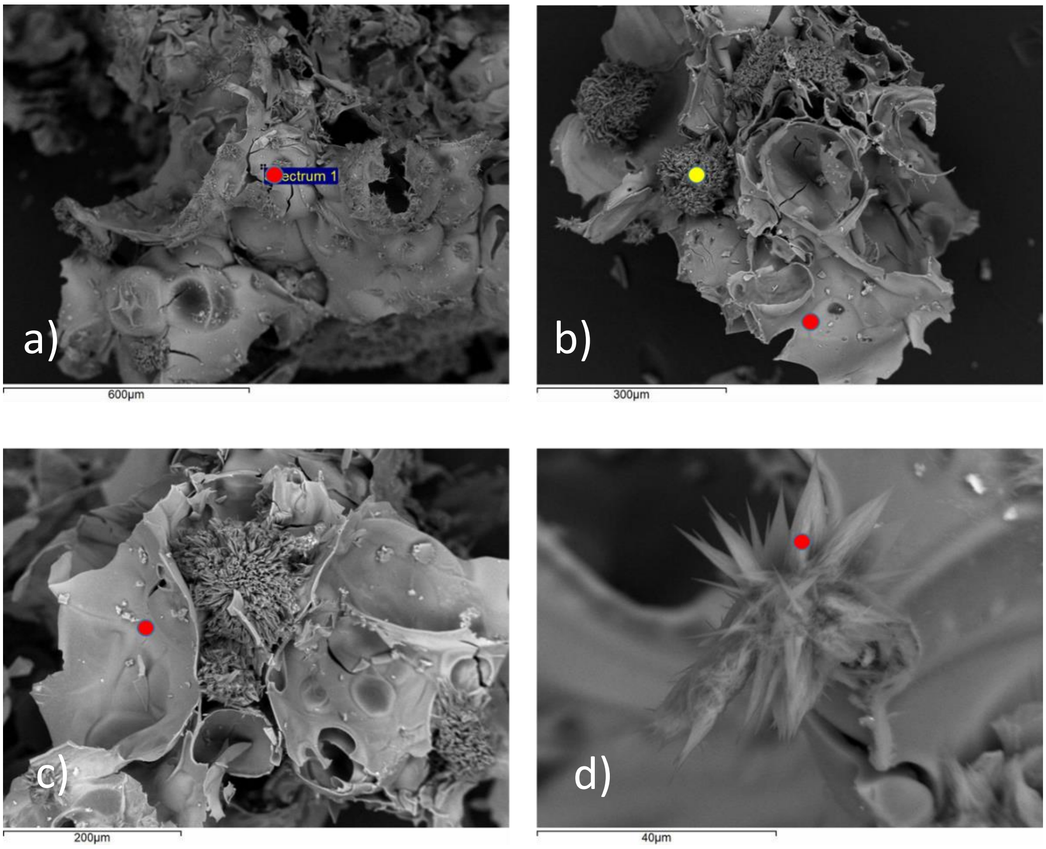


Figure 5.12: BSE images of encrustations formed in Experiment 167. Colored points indicate points analyzed through ED Rounded appearance hints to zeolite but analyses show Al absence. Bundles of tiny crystals are Na-rich (natrite?..).
a) $SiO_2$= 77 wt%, $Na_2O$= 19 wt%, $K_2O$= 4 wt%, b) red point: $SiO_2$= 58 wt%, $Na_2O$= 35 wt%, $K_2O$= 7 wt%, yellow point: $SiO_2$= 2 wt%, $Na_2O$= 97wt%, c) $SiO_2$= 74 wt%, $Na_2O$= 22 wt%, $K_2O$= 4 wt%,
d) $SiO_2$= 43 wt%, $Na_2O$= 55 wt%, $K_2O$= 2 wt%.

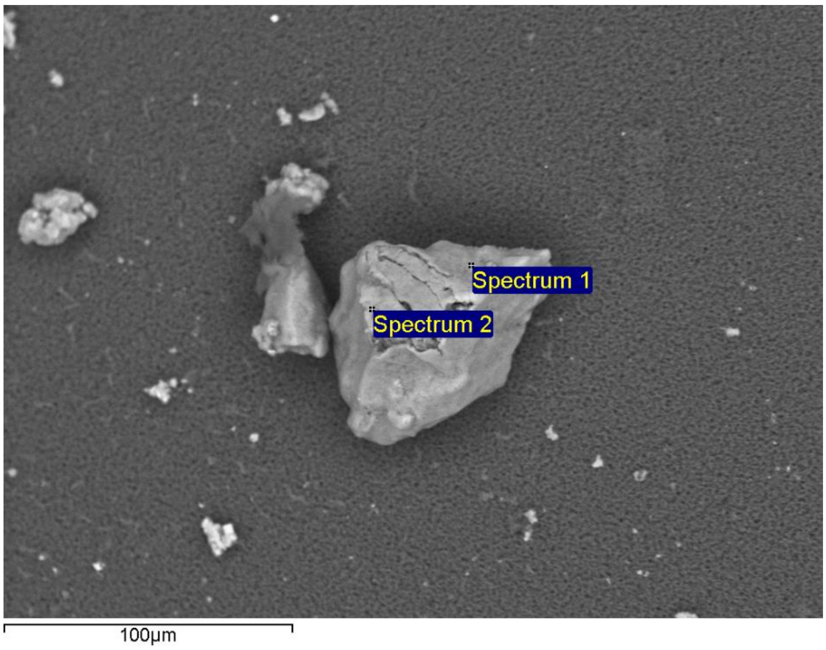


Figure 5.13: BSE image of solids trapped in the filter used to inject liquid sample in the chromatograph (Experiment 149). EDS spectra in the 2 points give $SiO_2$ ~ 26 wt%, $Al_2O_3$= 58 wt%, FeO= 10 wt%, MgO= 4 wt% and $K_2O$~ 1 wt%.

## 5.4. Discussion

Experimental products showed extensive change respect to the rocks used as solid starting materials. Encrustations forming all around the micro-reactor walls are the most apparent and intense alteration products and they are mainly composed by quartz. Additionally, XRD spectra and SEM observation revealed the presence of diffuse boehmite, most likely a result of plagioclase dissolution. Besides quartz, XRD and/or SEM observation suggested the presence of kaolinite? (or phillipsite?) and sporadic carbonates such as magnesite and calcite in runs in which $CO_2$ was used as pressurizing gas. Other minor Al-Si-(Na)-rich neo-formed phases were individuated either among powdered material recovered at the end of experiments and in encrustations and in filters used to inject sampled liquid into the chromatograph.

In general, the main alteration process revealed in experiments is silicification. This process is commonly observed in geothermal fields in which may occur in different styles (e.g. Lagat, 2009). One common and important style is the replacement of the rock with microcrystalline quartz (chalcedony). This process could be facilitated and enhanced by rock's porosity. Another common style is the formation of fractures in a network, or "stockworks", which are filled with quartz (Lagat, 2009).

In Los Humeros geothermal field hydrothermal alteration transformed primary minerals in secondary minerals such as those reported in paragraph 5.1.2. The formation of secondary minerals depends upon different parameters such as temperature, pressure, fluid composition, permeability, initial composition of the rock and duration of hydrothermal activity. Samples from deep (~2 km) drill holes in Los Humeros geothermal field often are intensively silicified with zones constituted almost entirely of microcrystalline quartz (e.g. Elders et al., 2014). Quartz was also found as altered phase in cuttings from more superficial (800-1200 m) depths (Pulido, 2008). Furthermore, Martínez-Serrano, (2002) reported that quartz revenue is common in the three hydrothermal zones of the geothermal field (shallow argillitic, propylitic and skarn) and it is very abundant at depths of <900 m.

In geothermal area quartz can be a common product of both low sulfidation and high sulfidation alteration (Boden, 2016). Quartz produced in experiments is a product of the first alteration type, since reactant fluids have near-neutral-pH. Under these conditions quartz content of the rock can increase making it less permeable. On the contrary, in high sulfidation alteration the presence of low pH (<3) fluids would leave a silica residue (referred to as vuggy quartz) with good porosity, thus favoring fluid circulation (Boden, 2016). In Los Humeros reservoir rocks contain hydrothermal alteration minerals typical of those produced by neutral or alkaline fluids, even if local alteration with acidic fluids is sometimes observed, especially in the lower hornblende-containing andesites (Elders et al., 2014; Tello et al., 2000: Rodriguez, 2000, see paragraph 5.1.2). As a consequence, quartz formation could have played a dual role either decreasing or enhancing rock porosity.

The finding of quartz and Al-rich phases such as boehmite in all experiments reveal they mainly formed by reaction interesting plagioclases in andesites. Plagioclases can dissolve incongruently according to the following reaction:

$$Na_xCa_{(1-x)}Al_{(2-x)}Si_{(2+x)}O_8 + 4(2-x)H^+ = xNa^+ + (1-x)Ca^{2+} + (2-x)Al^{3+} +(2+x)SiO_2 + 2(2-x)\ H_2O$$

where x=mol fraction of albite in plagioclase (x=1, pure albite; x=0, pure anorthite).
The reaction usually led to kaolinite ($Al_2Si_2O_5(OH)_4$) crystallization in conditions where natural weathering and diagenetic processes occur at the Earth's surface.
At ambient T, dissolution rates of plagioclases are a function of pH, with values decrease with increasing pH at acidic conditions but rise with increasing pH at alkaline conditions (U-shaped behavior, (Gudbrandsson et al., 2014). Furthermore, only at acidic conditions, dissolution rates increase with anorthite contents (Gudbrandsson et al., 2014). At higher T (200-300°C), plagioclases dissolution was investigated under hydrothermal conditions in the presence of aqueous solutions and supercritical $CO_2$ by (Hangx & Spiers, 2009). The experiments, finalized to investigate $CO_2$ mineral trapping, were performed in similar conditions and settings of our experiments, albeit starting with plagioclases (albite or anorthite) as starting materials. They mainly got precipitation of boehmite, kaolinite and a phyllo-silicate phase (smectite or illite) and little or no carbonate formations. They suggest that reaction controlling plagioclase dissolution may have occurred to a limit extent. As in our experimental products, the finding of boehmite as a main phase is intriguing, since this phase is not commonly found in geological contexts in which plagioclases alter. Nevertheless, boehmite crystallization is reported to be a common secondary phases generated by plagioclase dissolution under moderately acidic conditions even at 200-300 °C (Murakami et al., 1998; Tsuzuki & Suzuki, 1980). This phase could be considered as a precursor of kaolinite formation, whose precipitation rates are relatively slow compared with plagioclase dissolution rates (Gudbrandsson, 2014). The paucity of carbonates among our experimental products is not surprising since the crystallization of these phases is hindered by a sort of “kinetic barrier” due to the fact that their nucleation would have to be heterogeneous (Hangx & Spiers, 2009).
Experiments show that alteration occur also when $CO_2$ is not used as pressurizing gas. The presence of this gas is therefore not a prerequisite in order to explain the alteration paragenesis mineralogy found in experiments and, in a broader context, even in Los Humeros geothermal area.
Another evidence of the experiments is the absence of propylitic alteration, i.e. formation of new minerals (e.g. chlorite, actinolite, epidote) formed by the decomposition of Fe-Mg minerals, such as micas, amphiboles and pyroxenes. Temperatures of the experiments are rather favorable to the development of propylitic alteration (Figure 5.14). This process, although commonly observed in low sulfidation alteration (and present in Los Humeros geothermal reservoir) could have not be happened in experiments due to kinetic factors (duration of experiments short?) or to the

relatively low abundance of pyroxenes and the lack of amphiboles in the rock used for the experiments. As an alternative hypothesis, propylitic alteration could have developed but gone undetected by the investigations performed, due to instrumental and/or analytical constraints (i.e. powder XRD phases < 5 wt%).

It is noteworthy the wairakite appearance among alteration products in the experiment in which west-driven infiltrating fluid was taken into account. This fluid interacted with carbonatic rocks before entering into the reservoir and its high Ca contents allowed the crystallization of wairakite as the aluminosilicate phase, instead of boehmite. Wairakite is a common alteration product in LHGF at 200-300 °C (e.g. Martínez-Serrano, 2002) and is expected to develop in such geological scenario (Figure 5.14). Its crystallization, in solid solution with analcime ($NaAlSi_4O_{12}$•$2H_2O$) is possible in the 200-350 °C range, as a consequence of reaction of an anorthite rich plagioclase with quartz and fluid (Galbarczyk-Gasiorowska & Slaby, 2001).

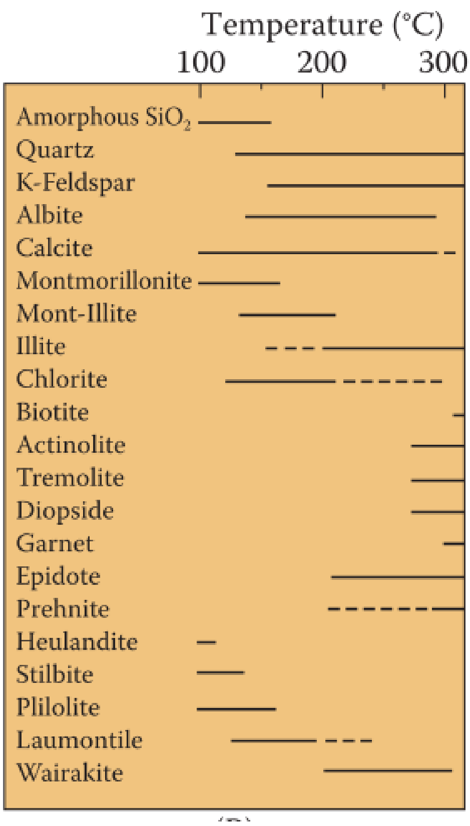


Figure 5.14: Chart showing temperature stability ranges of common alteration minerals (from Boden, 2016).

### 5.5. Conclusions

Fluid –rock interaction experiments run at 200-300 °C considering Los Humeros andesitic reservoir and fluids flowing through it, indicate silicification as the most important alteration process. Labradorite, andesine and oligoclase plagioclases in andesites are the principally involved phases in such process leading also to the development of Al-rich phases such boehmite.

The use of $CO_2$ as pressurizing gas in experiments has the only result of bringing sporadic crystallization of carbonates but do not particularly increase the extent of alteration of rocks used in experiments. Plagioclase dissolution should have caused Ca, Na-rich phase precipitation, as wairakite, phillipsite or other unidentified phases; however, the analytical methods used were not able to establish with any certainty the presence of phillipsite, nor to establish if other minor phases formed during alteration. In particular, wairakite crystallization during the experiment in which high salinity (Ca-rich) water was used suggests that in LHGF high mineralized waters likely reacted with andesitic reservoir. This phase is commonly found among alteration products in LHGF and its finding in such experimental products could corroborate the hypothesis that infiltrating waters extensively reacted with crossed rocks before reaching the reservoir. Finally, the widespread formation of quartz encrustations following hydrothermal alteration could provoke a porosity decrease of andesitic reservoir, especially under conditions in which reactant fluids have near-neutral pH.

**Acknowledgements**

*G. Norini and M. Lelli are acknowledged to have provided rock and liquid samples, respectively. J. Cabassi and F. Capecchiacci performed liquid chromatography analyses, L. Chiarantini and M-Ulivi are acknowledged for SEM investigations, L. Chelazzi (CRIST-Unifi) and E. Pecchioni (DST-Unifi), for assistance during XRD analyses. The authors wish to thank C. Rochelle, O. Vaselli, S. Caporali and G. Morelli for helpful discussions. This project has received funding from the European Union's Horizon 2020 research and innovation program under grant agreement No. 727550.*

## 5.6. References

Arellano, V. M., García, A., Barragán, R. M., Izquierdo, G., Aragón, A., & Nieva, D. (2003). An updated conceptual model of the Los Humeros geothermal reservoir (Mexico). *Journal of Volcanology and Geothermal Research*, *124*(1–2), 67–88. http://doi.org/10.1016/S0377-0273(03)00045-3

Boden. (2016). 10. Geothermal Systems and Mineral Deposits.

Canet, C., Trillaud, F., Prol-Ledesma, R. M., González-Hernández, G., Peláez, B., Hernández-Cruz, B., & Sánchez-Córdova, M. M. (2015). Thermal history of the Acoculco geothermal system, eastern Mexico: Insights from numerical modeling and radiocarbon dating. *Journal of Volcanology and Geothermal Research*, *305*, 56–62. http://doi.org/10.1016/j.jvolgeores.2015.09.019

Carrasco-Núñez, G., López-Martínez, M., Hernández, J., & Vargas, V. (2017). Subsurface stratigraphy and its correlation with the surficial geology at Los Humeros geothermal field, eastern Trans-Mexican Volcanic Belt. *Geothermics*, *67*, 1–17. http://doi.org/10.1016/j.geothermics.2017.01.001

Elders, W. A., Izquierdo, G. M., Arag, A. A., Tovar, R. A., & Flores, M. A. (2014). Significance of deep zones of intense bleaching and silicification in the Los Humeros high-temperature geothermal field, Mexico: Evidence of the effects of acid alteration. *Transactions - Geothermal Resources Council*, *38*, 497–502. Retrieved from http://www.scopus.com/inward/record.url?eid=2-s2.0-84937884462&partnerID=tZOtx3y1

Galbarczyk-Gasiorowska, L., & Slaby, E. (2001). Experimental investigation of the reaction : An-rich plagioclase + quartz+ fluid = analcime-wairakite ss. *Acta Geologica Polonica*, *51*(2), 155–162.

García-Vallés, M., Pi, T., Alfonso, P., Canet, C., Martínez, S., Jiménez-Franco, A., … Hernández-Cruz, B. (2015). Kaolin from Acoculco (Puebla, Mexico) as raw material: Mineralogical and thermal characterization. *Clay Minerals*, *50*(3), 405–416. http://doi.org/10.1180/claymin.2015.050.3.12

Giordano, G., Calzolari, G., & Lucci, F. (2017). Regional structural and tectonic synthesis of the Acoculco and Los Humeros Geothermal fields.

Gudbrandsson, S. (2014). Experimental weathering rates of aluminium-silicates Snorri Gudbrandsson To cite this version : HAL Id : tel-00933440.

Gudbrandsson, S., Wolff-Boenisch, D., Gislason, S. R., & Oelkers, E. H. (2014). Experimental determination of plagioclase dissolution rates as a function of its composition and pH at 22°C. *Geochimica et Cosmochimica Acta*, *139*, 154–172. http://doi.org/10.1016/j.gca.2014.04.028

Gutiérrez-Negrín, L. C. ., & Izquierdo-Montalvo, G. (2010). Review and Update of the Main Features of the Los Humeros Geothermal Field , Mexico OS HUMEROS. In *Proceedings World Geothermal Congress* (pp. 25–29).

Hangx, S. J. T., & Spiers, C. J. (2009). Reaction of plagioclase feldspars with CO2under hydrothermal conditions. *Chemical Geology*, *265*(1–2), 88–98. http://doi.org/10.1016/j.chemgeo.2008.12.005

Hurst, V. J., & Kunkle, A. C. (1985). Dehydroxylation, Rehydroxylation, and Stability of Kaolinite. *Clays and Clay Minerals*, *33*(1), 1–14. http://doi.org/10.1346/CCMN.1985.0330101

Lagat, J. (2009). Hydrothermal Alteration Mineralogy in Geothermal Fields With Hydrothermal Alteration Mineralogy in Geothermal Fields With Case Examples From Olkaria Domes Geothermal Field , Kenya.

Le BAS, M. J., Maitre, R. W. Le, Streckeisen, A., Zanettin, B., & Rocks, I. S. on the S. of I. (1986). A chemical classification of volcanic rocks based on the total alkali-silica diagram. *Journal of Petrology*, *27*(3), 745–750.

López-Hernández, A., García-Estrada, G., Aguirre-Díaz, G., González-Partida, E., Palma-Guzmán, H., & Quijano-León, J. L. (2009). Hydrothermal activity in the Tulancingo-Acoculco Caldera Complex, central Mexico: Exploratory studies. *Geothermics*, *38*(3), 279–293. http://doi.org/10.1016/j.geothermics.2009.05.001

Martínez-Serrano, R. G. (2002). Chemical variations in hydrothermal minerals of the Los Humeros geothermal system, Mexico. *Geothermics*, *31*(5), 579–612. http://doi.org/10.1016/S0375-6505(02)00015-9

Matsuda, T., Kurosaki, M., & Henmi, K. (1992). Equilibrium between kaolinite and pyrophyllite. *Clay Science*, *8*, 297–308.

Murakami, T., Kogure, T., Kadohara, H., & Ohnuki, T. (1998). Formation of secondary minerals and its effect on anorthite dissolution. *American Mineralogist*, *83*(11–12), 1209–1219. http://doi.org/10.2138/am-1998-11-1209

Norini, G., Groppelli, G., Sulpizio, R., Carrasco-Núñez, G., Dávila-Harris, P., Pellicioli, C., … De Franco, R. (2015). Structural analysis and thermal remote sensing of the Los Humeros Volcanic Complex: Implications for volcano structure and geothermal exploration. *Journal of Volcanology and Geothermal Research*, *301*, 221–237. http://doi.org/10.1016/j.jvolgeores.2015.05.014

Pulido, C. D. L. (2008). *Borehole Geophysics and Geology of Well H-43 , Los Humeros Geothermal Field , Puebla , México*. *Geothermal Training Programme*.

Rodrguez, F. C. (2000). Hydrogeologic model of the geothermal reservoir from Los Humeros, Puebla, Mexico. *Geothermal Resources Council Transactions*, *24*, 381–409. http://doi.org/10.1080/09640560701402075

Tello, E. H., Verma, M. P., & Tovar, R. A. (2000). Origin Of Acidity In The Los Humeros , México , Geothermal Reservoir. *World Geothermal Congress*, 2959–2967.

Tsuzuki, Y., & Suzuki, K. (1980). Experimental study of the alteration process of labradorite in acid hydrothermal solutions. *Geochimica et Cosmochimica Acta*, *44*(5). http://doi.org/10.1016/0016-7037(80)90157-X

Wagner, W., Pruss, A. (2002). The IAPWS formulation 1995 for the thermodynamic properties of ordinary water substance for general and scientific use. J. *Phys. Chem. Ref. Data, 31(2), 387-535.*

# Chapter 6

# GEOCHEMICAL MODELING
# Well fluids geochemical data analysis and modeling

## 6.1. Introduction

The aim of the present work is to define the origin of chemicals present in the fluids of Los Humeros geothermal field, providing an insight on recharge input and contribution of eventual deep component.

The fluid analysis from geothermal wells were provided by CFE, and consist of time series of different time-span from many wells within Los Humeros geothermal field. After inspection of the data, we have a total of 38 wells with suitable data. In a well specific data investigation, we have selected the "first" complete analysis available (in some cases gas analysis have different data from water analysis) as representative of the starting composition of the well. In fact, in the time series we can observe large fluctuation of composition over time, due to the recharge and other different contribution to the produced fluid, but this may jeopardize the true source. For this reason, we choose to use only the first data available for each well, that in theory are not very perturbed from other contribution.

The data are then recomputed to have a total composition in moles / Kg of water, including the non condensable gas and here reported in table 1.

Geochemical data in this format could be used in a consistent way for both statistical analysis and geochemical modeling.

| Well | Coordinate_X | Coordinate_Y | H+ | Cl | B | HCO3 | SiO2 | SO4 | Na | K | Li | Ca | Mg | As | Fe | Ar | CH4 | CO2 | H2 | H2S | He | N2 | NH3 |
|---|---|---|---|---|---|---|---|---|---|---|---|---|---|---|---|---|---|---|---|---|---|---|---|
| H-1V | 661906 | 2175060 | 6.31E-09 | 3.09E-03 | 2.08E-02 | 0.00E+00 | 1.24E-02 | 6.59E-04 | 1.30E-02 | 1.16E-03 | 2.59E-04 | 2.25E-05 | 0.00E+00 | 0.00E+00 | 0.00E+00 | - | - | - | - | - | - | - | - |
| H-2 | 662646 | 2172440 | 5.01E-09 | 1.13E-03 | 3.05E-04 | 4.40E-03 | 7.59E-04 | 1.92E-04 | 6.52E-05 | 3.07E-05 | 0.00E+00 | 7.49E-06 | 0.00E+00 | 0.00E+00 | 0.00E+00 | - | - | - | - | - | - | - | - |
| H-3D | 660622 | 2177900 | 1.58E-08 | 6.91E-04 | 6.36E-02 | 3.02E-03 | 1.11E-02 | 1.89E-03 | 1.57E-02 | 1.20E-03 | 9.22E-05 | 3.74E-05 | 1.23E-06 | 1.20E-05 | 0.00E+00 | - | - | - | - | - | - | - | - |
| H-6-V | 663508 | 2173550 | 1.00E-08 | 9.56E-03 | 3.52E-02 | 6.59E-04 | 1.97E-02 | 6.45E-05 | 1.23E-02 | 1.18E-03 | 0.00E+00 | 2.87E-05 | 8.23E-06 | 0.00E+00 | 0.00E+00 | - | - | - | - | - | - | - | - |
| H-7-V | 661838 | 2175870 | 6.31E-09 | 3.95E-03 | 5.89E-02 | 7.20E-04 | 1.27E-02 | 3.57E-04 | 9.57E-03 | 1.01E-03 | 1.01E-04 | 2.74E-05 | 0.00E+00 | 0.00E+00 | 0.00E+00 | - | - | - | - | - | - | - | - |
| H-8-V | 661582 | 2176390 | 5.01E-09 | 3.20E-03 | 4.96E-02 | 2.40E-03 | 2.13E-02 | 4.51E-04 | 1.66E-02 | 1.41E-03 | 8.65E-05 | 2.00E-05 | 0.00E+00 | 0.00E+00 | 0.00E+00 | - | - | - | - | - | - | - | - |
| H-9-V | 660618 | 2178220 | 5.01E-07 | 3.37E-03 | 4.28E-01 | 1.35E-02 | 2.23E-02 | 0.00E+00 | 1.77E-02 | 1.99E-03 | 1.30E-04 | 9.98E-05 | 1.23E-05 | 0.00E+00 | 0.00E+00 | - | - | - | - | - | - | - | - |
| H-10-V | 662081 | 2176380 | 7.94E-07 | 7.62E-05 | 3.05E-01 | 1.52E-03 | 1.70E-03 | 2.19E-05 | 0.00E+00 | 0.00E+00 | 0.00E+00 | 3.74E-05 | 0.00E+00 | 0.00E+00 | 0.00E+00 | - | - | - | - | - | - | - | - |
| H-11-D | 662574 | 2177440 | 3.98E-05 | 3.40E-02 | 1.12E-01 | 7.05E-05 | 2.01E-02 | 9.89E-05 | 7.57E-03 | 7.37E-04 | 0.00E+00 | 8.73E-05 | 0.00E+00 | 0.00E+00 | 0.00E+00 | - | - | - | - | - | - | - | - |
| H-12 | 663803 | 2173050 | 1.58E-07 | 4.29E-04 | 2.13E-01 | 4.87E-04 | 9.70E-03 | 3.36E-04 | 6.70E-03 | 5.75E-04 | 9.37E-05 | 1.09E-04 | 5.35E-06 | 2.56E-04 | 0.00E+00 | - | - | - | - | - | - | - | - |
| H-13-D | 662244 | 2177410 | 5.01E-09 | 1.04E-02 | 2.59E-02 | 7.61E-04 | 1.08E-02 | 5.96E-04 | 1.62E-02 | 1.51E-03 | 2.13E-04 | 0.00E+00 | 1.23E-06 | 0.00E+00 | 0.00E+00 | - | - | - | - | - | - | - | - |
| H-14-V | 663832 | 2169630 | 3.16E-09 | 2.05E-03 | 1.52E-02 | 1.84E-02 | 1.14E-02 | 2.56E-04 | 1.66E-02 | 4.35E-04 | 4.18E-05 | 2.69E-04 | 2.18E-05 | 2.00E-05 | 0.00E+00 | - | - | - | - | - | - | - | - |
| H-15 | 661638 | 2178800 | 3.16E-09 | 5.36E-04 | 2.00E-02 | 5.87E-04 | 1.64E-02 | 1.21E-04 | 5.78E-03 | 6.47E-04 | 1.01E-04 | 3.74E-06 | 3.70E-06 | 3.34E-05 | 0.00E+00 | 0.00E+00 | 2.17E-02 | 6.38E-01 | 1.41E-02 | 8.56E-02 | 0.00E+00 | 1.11E-02 | 0.00E+00 |
| H-16 | 661557 | 2178250 | 3.16E-10 | 2.68E-04 | 2.39E-02 | 9.25E-04 | 6.43E-03 | 2.26E-03 | 3.29E-02 | 7.19E-04 | 2.31E-04 | 5.99E-06 | 3.70E-06 | 4.00E-05 | 0.00E+00 | 1.39E-04 | 6.58E-03 | 3.48E-01 | 3.51E-03 | 5.02E-02 | 0.00E+00 | 5.06E-03 | 8.12E-04 |
| H-17 | 662298 | 2178610 | 3.98E-08 | 5.36E-04 | 3.56E-02 | 6.25E-04 | 1.43E-02 | 1.86E-04 | 3.78E-03 | 4.19E-04 | 4.61E-05 | 3.49E-06 | 3.70E-06 | 1.68E-04 | 0.00E+00 | 4.67E-04 | 4.21E-03 | 4.12E-01 | 2.13E-03 | 5.28E-02 | 0.00E+00 | 4.01E-03 | 4.49E-04 |
| H-18-V | 664916 | 2172080 | 7.94E-09 | 3.64E-03 | 1.39E-02 | 6.67E-03 | 1.66E-04 | 2.19E-04 | 4.87E-03 | 3.32E-04 | 1.15E-04 | 1.50E-05 | 1.65E-06 | 0.00E+00 | 0.00E+00 | - | - | - | - | - | - | - | - |
| H-19 | 662881 | 2176640 | 1.26E-07 | 1.61E-03 | 1.94E-01 | 1.72E-03 | 1.11E-02 | 1.12E-04 | 6.61E-03 | 6.47E-04 | 1.18E-04 | 2.02E-04 | 8.64E-06 | 2.94E-04 | 0.00E+00 | 2.55E-04 | 5.61E-09 | 6.43E-01 | 2.08E-03 | 4.25E-02 | 0.00E+00 | 4.61E-03 | 6.52E-03 |
| H-20-V | 663330 | 2177490 | 1.58E-07 | 9.36E-03 | 6.13E-02 | 3.44E-05 | 1.28E-02 | 1.77E-05 | 4.78E-03 | 4.35E-04 | 6.48E-05 | 3.49E-04 | 2.06E-06 | 0.00E+00 | 0.00E+00 | - | - | - | - | - | - | - | - |
| H-22 | 660055 | 2178850 | 2.00E-09 | 9.73E-04 | 7.21E-03 | 7.27E-03 | 1.46E-02 | 2.31E-04 | 1.35E-02 | 8.44E-04 | 1.30E-04 | 6.49E-05 | 8.23E-06 | 0.00E+00 | 0.00E+00 | - | - | - | - | - | - | - | - |
| H-23 | 664184 | 2175460 | 2.00E-06 | 2.10E-02 | 1.20E-02 | 1.64E-05 | 2.59E-03 | 1.22E-03 | 2.02E-02 | 7.26E-04 | 1.30E-04 | 3.78E-04 | 6.17E-06 | 0.00E+00 | 0.00E+00 | 0.00E+00 | 9.80E-03 | 8.55E-01 | 2.62E-02 | 1.78E-01 | 4.34E-05 | 1.88E-02 | 5.04E-03 |
| H-24 | 665497 | 2172940 | 0.00E+00 | 1.19E-02 | 5.38E-03 | 6.66E-03 | 2.26E-04 | 2.97E-03 | 2.00E-03 | 2.30E-05 | 1.08E-04 | 1.25E-06 | 0.00E+00 | 2.08E-02 | 0.00E+00 | 0.00E+00 | 3.52E-02 | 1.41E+00 | 2.40E-02 | 2.98E-02 | 0.00E+00 | 1.49E-02 | 1.27E-02 |
| H-27 | 663986 | 2176290 | 3.98E-08 | 7.12E-03 | 1.77E-02 | 1.69E-04 | 3.08E-04 | 1.09E-04 | 3.26E-03 | 1.53E-04 | 2.88E-05 | 2.12E-05 | 1.65E-06 | 0.00E+00 | 0.00E+00 | 0.00E+00 | 5.30E-04 | 9.69E-01 | 3.35E-02 | 6.99E-02 | 0.00E+00 | 5.05E-02 | 1.14E-02 |
| H-28 | 662601 | 2177740 | 1.86E-09 | 1.02E-04 | 7.28E-03 | 2.62E-03 | 8.66E-03 | 8.51E-04 | 8.95E-03 | 4.35E-04 | 1.55E-04 | 6.41E-06 | 4.94E-06 | 0.00E+00 | 0.00E+00 | 1.57E-04 | 4.45E-03 | 1.01E+00 | 6.23E-03 | 1.99E-02 | 0.00E+00 | 1.41E-03 | 5.78E-04 |
| H-30-V | 661488 | 2178550 | 5.01E-06 | 1.41E-02 | 5.52E-01 | 4.26E-03 | 2.54E-03 | 7.29E-05 | 4.87E-03 | 3.68E-04 | 3.31E-05 | 9.98E-06 | 1.65E-06 | 0.00E+00 | 0.00E+00 | - | - | - | - | - | - | - | - |
| H-31-V | 661832 | 2179040 | 1.58E-08 | 2.76E-04 | 5.23E-02 | 5.25E-05 | 1.24E-02 | 3.33E-05 | 6.70E-03 | 7.83E-04 | 7.20E-05 | 3.74E-06 | 2.06E-06 | 0.00E+00 | 0.00E+00 | - | - | - | - | - | - | - | - |
| H-32-V | 662631 | 2178040 | 6.31E-08 | 3.07E-03 | 4.04E-02 | 1.07E-04 | 9.83E-03 | 1.27E-04 | 3.70E-03 | 6.14E-04 | 2.88E-05 | 4.99E-06 | 2.06E-06 | 0.00E+00 | 0.00E+00 | - | - | - | - | - | - | - | - |
| H-33-V | 661534 | 2177990 | 7.94E-08 | 7.35E-03 | 1.48E-01 | 2.84E-04 | 1.22E-02 | 2.04E-04 | 1.13E-02 | 1.02E-03 | 7.78E-05 | 6.11E-05 | 2.47E-06 | 0.00E+00 | 0.00E+00 | - | - | - | - | - | - | - | - |
| H-34-D | 662965 | 2177210 | 1.00E-08 | 1.12E-03 | 3.32E-02 | 2.16E-03 | 7.20E-03 | 2.92E-04 | 7.83E-03 | 5.93E-04 | 1.05E-04 | 1.57E-05 | 8.23E-07 | 4.00E-05 | 0.00E+00 | - | - | - | - | - | - | - | - |
| H-37-D | 661074 | 2178350 | 5.01E-09 | 1.21E-04 | 1.37E-01 | 1.77E-03 | 1.00E-02 | 2.29E-03 | 2.20E-02 | 1.51E-03 | 6.77E-05 | 7.73E-05 | 0.00E+00 | 1.56E-05 | 0.00E+00 | - | - | - | - | - | - | - | - |
| H-38-V | 661897 | 2178160 | 2.00E-07 | 4.51E-05 | 3.24E-03 | 4.07E-04 | 1.75E-04 | 1.04E-06 | 4.35E-06 | 2.56E-06 | 1.44E-06 | 2.50E-06 | 0.00E+00 | 2.48E-04 | 0.00E+00 | - | - | - | - | - | - | - | - |
| H-39 | 663365 | 2173290 | 5.01E-07 | 8.97E-04 | 2.71E-01 | 9.49E-04 | 8.80E-03 | 6.35E-04 | 6.96E-03 | 5.52E-04 | 8.36E-05 | 1.40E-04 | 9.88E-06 | 4.07E-04 | 0.00E+00 | 4.41E-04 | 3.64E-03 | 7.82E-01 | 1.25E-02 | 3.22E-02 | 9.46E-05 | 1.92E-02 | 1.01E-03 |
| H-40-D | 661754 | 2175710 | 3.98E-09 | 5.59E-03 | 1.35E-02 | 2.25E-02 | 1.59E-02 | 3.31E-03 | 2.25E-02 | 2.33E-03 | 1.14E-04 | 2.40E-04 | 1.93E-05 | 9.61E-05 | 0.00E+00 | - | - | - | - | - | - | - | - |
| H-41 | 663570 | 2173280 | 0.00E+00 | 2.80E-02 | 2.42E-03 | 3.44E-03 | 2.21E-04 | 8.61E-04 | 2.28E-04 | 6.69E-06 | 9.13E-05 | 3.34E-06 | 7.02E-05 | 1.83E-02 | 0.00E+00 | 2.16E-04 | 1.30E-02 | 9.24E-01 | 2.11E-02 | 7.03E-02 | 0.00E+00 | 5.57E-03 | 1.85E-02 |
| H-43 | 661175 | 2178040 | 1.48E-06 | 1.27E-04 | 3.16E-03 | 2.44E-04 | 2.16E-04 | 8.01E-05 | 1.35E-05 | 6.91E-06 | 0.00E+00 | 4.99E-06 | 0.00E+00 | 9.00E-05 | 0.00E+00 | 5.05E-03 | 2.69E-02 | 2.24E+00 | 1.75E-01 | 2.28E-01 | 0.00E+00 | 4.21E-01 | 1.19E-04 |
| H-49 | 661866 | 2175000 | 4.27E-09 | 4.62E-03 | 1.90E-02 | 3.64E-04 | 1.61E-02 | 6.91E-04 | 1.08E-02 | 1.03E-03 | 1.12E-04 | 5.66E-05 | 4.94E-06 | 0.00E+00 | 0.00E+00 | 1.83E-04 | 1.59E-02 | 7.40E-04 | 7.60E-02 | 7.98E-04 | 1.58E+00 | 3.88E-02 | 4.08E-03 |
| H-56 | 662238 | 2174380 | 2.09E-08 | 6.25E-03 | 6.50E-02 | 4.29E-03 | 2.06E-02 | 8.98E-04 | 1.20E-02 | 1.13E-03 | 1.15E-04 | 7.56E-05 | 1.89E-05 | 0.00E+00 | 8.95E-06 | 9.32E-05 | 8.70E-03 | 3.59E+00 | 2.90E-02 | 8.26E-02 | 1.21E-04 | 2.37E-02 | 1.49E-02 |
| H-58 | 662555 | 2177460 | 0.00E+00 | 1.03E-01 | 6.22E-03 | 8.42E-04 | 4.83E-04 | 3.61E-04 | 7.35E-05 | 2.66E-06 | 2.94E-03 | 2.86E-05 | 2.67E-03 | 5.24E-02 | 0.00E+00 | 1.26E-04 | 1.31E-03 | 7.45E-01 | 8.66E-03 | 3.91E-02 | 5.38E-05 | 7.46E-03 | 3.89E-04 |
| H-59 | 661574 | 2178240 | 9.12E-08 | 5.02E-03 | 2.30E-01 | 4.84E-03 | 6.57E-03 | 1.14E-03 | 1.44E-02 | 1.42E-03 | 1.44E-05 | 1.35E-03 | 1.11E-03 | 0.00E+00 | 1.50E-03 | 6.36E-04 | 1.34E-03 | 1.75E-01 | 4.04E-02 | 8.02E-02 | 0.00E+00 | 4.74E-02 | 5.36E-03 |

**Table 1** – CFE data from Los Humeros well fluids expressed in moles/Kg of water

### 6.2. Principal Component Analysis (PCA)

In this section, the focus is on describing the results of the classical and robust version of principal component analysis (PCA) for the geochemical data. These methods are applied to all variables with reasonable data quality of the data set. For 38 observations, i.e. 38 well fluid compositions, the concentrations of chemical species have been investigated.

The aim of principal component analysis is to find the relationships between the fluid composition and to characterize the chemical-spatial behavior. Since the data consist of different groups, a robust analysis will focus on the homogeneous data extracted so far.

Classical principal component analysis can be driven mainly by the *outlying groups*, and thus the focus is less on the homogeneous majority.

Principal component analysis (PCA) is a statistical procedure that uses an orthogonal transformation to convert a set of observations of possibly correlated variables (entities each of which takes on various numerical values) into a set of values of linearly uncorrelated variables called principal components. If there are n with p variables, then the number of distinct principal components is $\min(n-1, p)$. This transformation is defined in such a way that the first principal component has the largest possible variance (that is, accounts for as much of the variability in the data as possible), and each succeeding component in turn has the highest variance possible under the constraint that it is orthogonal to the preceding components. The resulting vectors (each being a linear combination of the variables and containing n observations) are an uncorrelated orthogonal basis set. PCA is sensitive to the relative scaling of the original variables; to avoid this, the data are elaborated subtracting the average value for each variable and then dividing by it, to obtain a scaled working matrix with zero average. Some difficulty may arise while correlating the results of PCA investigation with the real data, but for this second step we looked for meaningful variables that have similar spatial distribution to PCA components and hence we can safely attribute the physical meaning to the results of the statistical analysis. In our investigation, out of the resulting 21 components, the 1$^{st}$ one explain 86.24% data variability, 2$^{nd}$ one 10.40% data variability and 3$^{rd}$ one 2.40% and the others are negligible; our complex dataset could be explained by using only 3 component that are described here below.

### 6.2.1 PCA 1st component, water-rock interaction

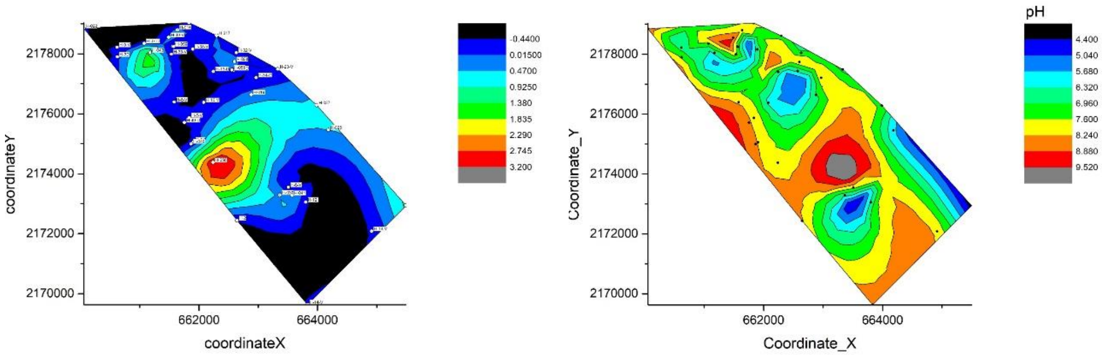


**Figure 1** PCA 1st component score distribution, left, and pH distribution, right. Coordinates are in meters.

The first component pf PCA analysis is closely related to pH, and according to Tello et al., 2000, the Los Humeros geothermal reservoir is in an unbalanced state having only a partial water-rock chemical equilibrium. The magmatic components in the geothermal fluids are not neutralized by the reaction with feldespars and micas, with high concentrations of HCl and HF detected in the steam phase. The oxidation of sulphur species and the $CO_2$ content may have a secondary role in the acidity. As a consequence, the PCA 1st first component is related to water-rock interaction driven by acidity, and include CO2(g), SiO2, Fe, Ca, Cl, Li, Mg, As, H2S, N2(g), H2(g). This component have also some relationship with the 3rd component, that is represented by Boron.

The variability in the Los Humeros reservoir, can be explained by 2 fluids types. Low mineralized waters form part of a liquid-dominated, bicarbonate reservoir at a depth from 1330 to 1755 m b.s.l., here represented by PCA 2nd component, characterized by a smaller range and lower concentrations of As. In contrast, deeper wells produce a two-phase fluid with maximum As concentrations of 162 mg/l.

Main hydrothermal zones are formed by chlorite, epidote, quartz, calcite, and low proportions of leucoxene and pyrite, as well as clays, biotite, zeolite, anhydrite, garnet, diopside and wollastonite (Izquierdo et al. 2000). However, no As minerals have been recognized, and having here classified Cloride (Bernard et al., 2011) as part of a deep fluid source undergoing to strong water-rock interaction and fractionation processes we can gues that As have a similar fate.

### 6.2.2 PCA 2nd component, recharge

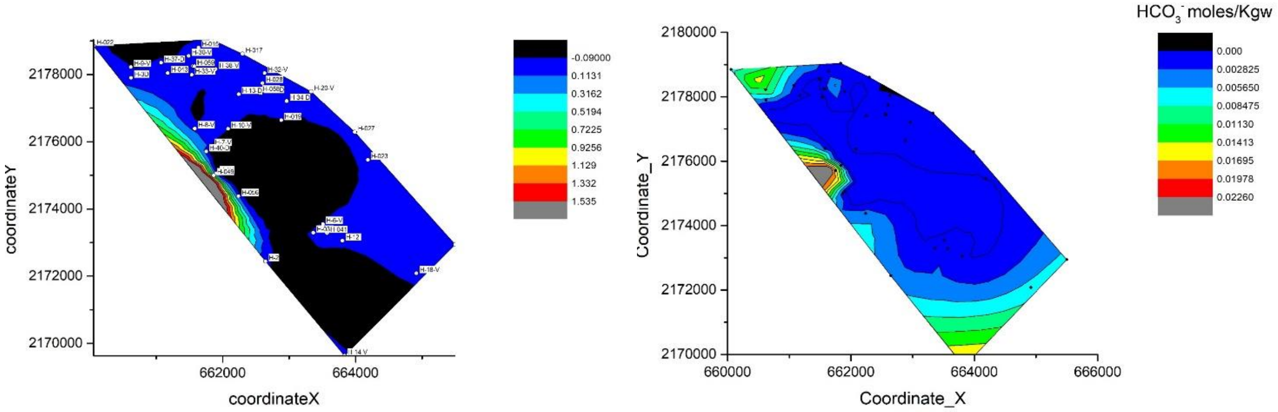


**Figure 2** PCA 1st component score distribution, left, and pH distribution, right. Coordinates are in meters.

The second component pf PCA analysis is closely related to bicarbonates, as shown in figure 2. The composition of this second component is made by mainly HCO3-, SO4-2, Na, K, Ar and it is clearly related to regional recharge mechanism, being significatively different in composition and salinity with respect to the rest of the system. The presence of low mineralized waters that form part of a liquid-dominated, bicarbonate reservoir at a depth from 1330 to 1755 m b.s.l., could be related to the regional recharge that seem to have its main contribution from western / North-western section of the geothermal system.

### 6.2.3 PCA 3rd component

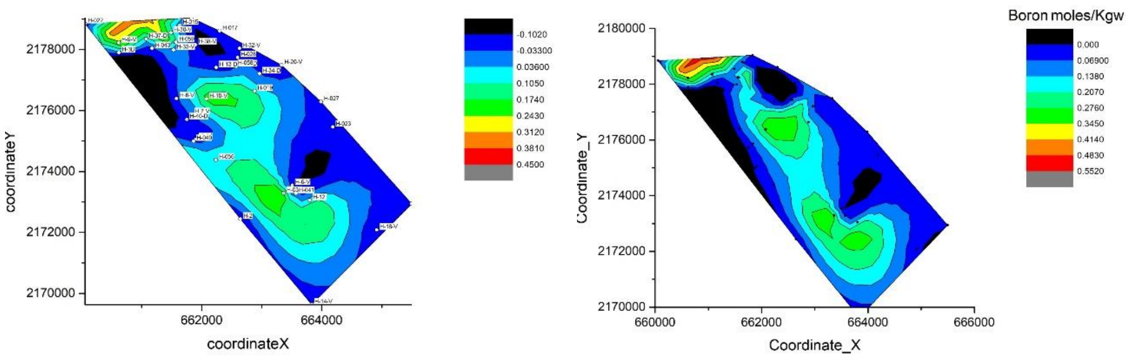


**Figure 3** PCA 3rd component score distribution, left, and boron concentration in fluid in moles/ Kg of water, right. Coordinates are in meters.

The third component pf PCA analysis is closely related to Boron as shown in figure 3. According to Bernard et al., 2011, Isotopic composition of B (-0.8 ± 1.6‰) suggests its magmatic origin, though sedimentary origin cannot be ruled out.

The absence of correlation they found, and here confirmed as low as -0.0772 correlation coefficient, between B and Cl concentrations may be interpreted by invoking at least two reasons, (1) different sources of Cl and B in Los Humeros fluids and (2) different behavior of H3BO3 and Cl at phase separation (boiling).

To explain the unusual behavior of Cl and B in well fluids of Los Humeros aBernard et al., 2011, proposed a model which invokes the existence of a deep acid brine boiling at a temperature of about 350 °C producing H3BO3 and HCl-bearing vapor that condenses and neutralizes at an upper level where it is tapped by wells. In our current analysis, the correlation coefficient of Boron with pH reach 0.6967 but the difference is clear while looking at the spatial distribution of 1$^{st}$ and 3$^{rd}$ PCA component as well as pH and Boron (figure 1 and 3) that although the spatial distribution is similar, the area of 1$^{st}$ and 3$^{rd}$ PCA component are neighboring and only slightly overlapping. This is due to the low reactivity of Boron, in contrast to the 1$^{st}$ PCA component that is the most representative of water-rock interaction, and even though the source at depth is the same the path while uprising is very different.

### 6.3. Geochemical modeling of well fluids data as function of temperature

#### 6.3.1 Introduction

The dataset obtained from CFE data, selecting the "first fluid" composition, is the base data here used as reference for the geochemical modeling, being less to no affected by any disturbance that will come during the geothermal system management. Using chemical analyses and 25° pH measurements of quenched high-temperature waters, we calculate in situ pH and distribution of aqueous species at high temperature; data in table 1 are referred to total fluids, reconstructed from available data, on wich we can compute the concentration change due to phase segregation at the different process stage. It is here noteworthy to point out that NCG gas solubility will change both in well and reservoir, but steam phase separation is a process mostly related to well production, being the reservoir at its initial state mainly in liquid condition with possible 2 phase (and maybe steam) zones only at depth, in the northern sector. In the present work we will compute the activities of aqueous ions in a given water at high temperature, which are used to calculate an ion activity product (Q) for each minerals. The value of log(Q/K) for each mineral, where K is the equilibrium constant, provides a measure of proximity of the aqueous solution to equilibrium with the mineral. By plotting log Q/K vs. T for natural waters, it is possible to determine: a) whether the water was in equilibrium with a host rock mineral assemblage, b) probable minerals in the equilibrium assemblage and c) the temperature of equilibrium. In cases where the fluid departs from equilibrium with a host rock assemblage, it is possible to determine whether this may result from boiling or dilution, and an estimate of amount of lost gas or diluting water can be determined.

Moreover, in the present models saturated minerals are allowed to precipitate thus providing an insight on the current most likely secondary phases among the one known in Los Humeros and to evidence the presence of possible scaling minerals. The well fluid composition here selected are a subset of all the analysis available, and are the ones that could be constrained by phase separation effect that account for boiling and $CO_2$ solubility. Moreover, some key elements are completely missing like Aluminium, and other relevant are rarely measured, like Iron. To partially ought to this inconvenient, a small amount (1E-7moles/Kgw) of $Al^{+3}$ is added to the fluid composition. The reservoir steady state model providing the thermodynamic and steam/liquid saturation conditions in the reservoir is from WP 6. The temperature runs are all uniforms and cover a temperature range 160-350 °C, to include all the temperature from shallow to deep feed zones.

The code used for the following computation is chim-xpt (Reed et al., 2012). CHIM-XPT and its ancestors were developed for modeling the geochemistry of hydrothermal processes, it applies to any problem that involves calculating states of equilibrium or partial equilibrium in gas-solid-aqueous systems and it is able to deal with boiling and phase separation problems up to high temperature (up to 600°C). The thermodynamic database here used is computed with Supcrt (Johnson et al., 1992), with only some modification, addition of aqueous H4SiO4 from Stefánsson, A. (2001), for improved silicate mineral log Ks at low T and all minerals from Holland and Powell (2011).

### 6.3.2 well H-15

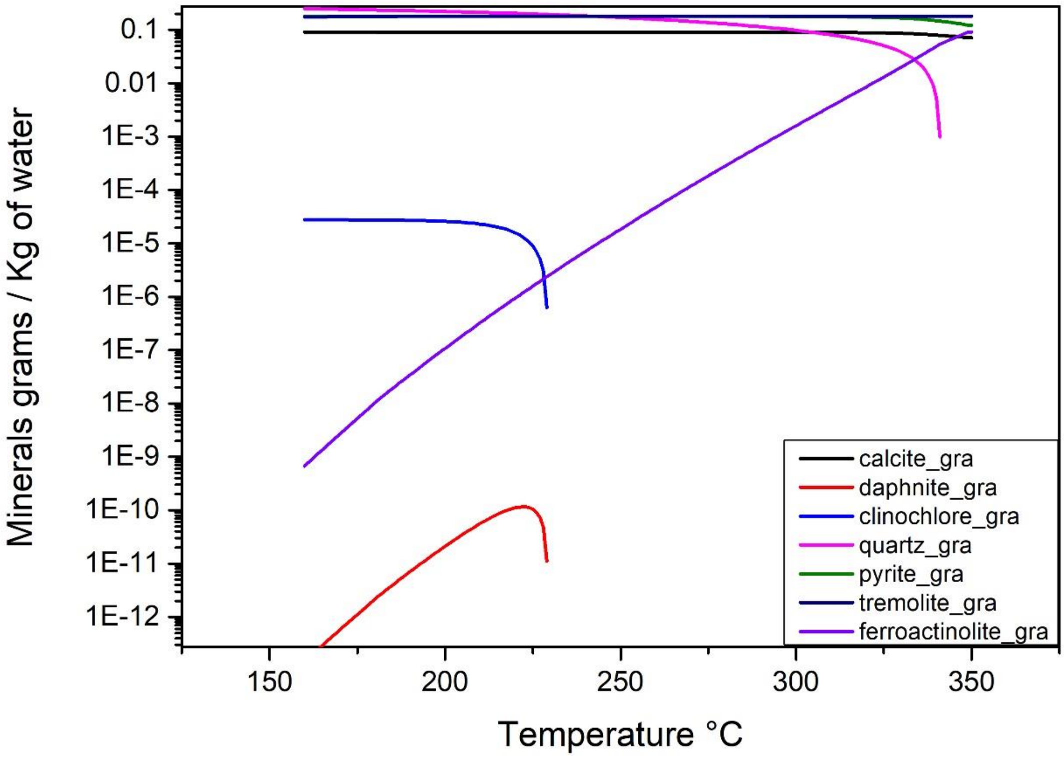


In well H-15 are encountered some of the most common secondary minerals, like chlorite and daphnite as part of the argillification process of andesites. The abundances of these phases are not too reliable due to our add af Aluminium, needed to include these minerals in the model. The main secondary minerals resulting from our model are calcite, pyrite and quartz, that are common secondary phases at Los Humeros both in the reservoir rocks and as scaling minerals in wells. Tremolite result always present, and it is a methamorphic amphibole pertaining to the original rock, like ferroactinolite, that at lower temperature and in presence of $CO_2$ tend to decompose in to talc/clay, calcite and quartz.

### 6.3.3 well H-16

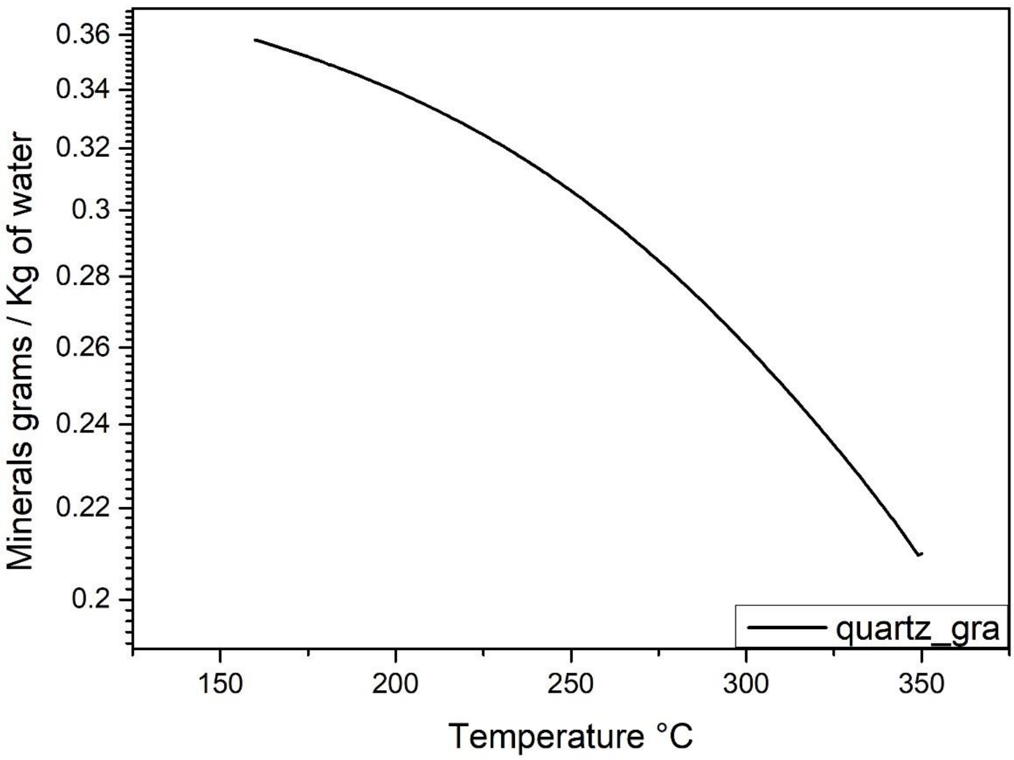


In well H-16 unfortunately we cannot compare directly with the mineral assemblage published by Gutierrez Negrin et al., 1990, since they found as main scaling minerals Iron sulphides, Iron oxides and quartz, but in the chemical analysis Iron is missing, thus we results with only quartz precipitation.

### 6.3.4 well H-17

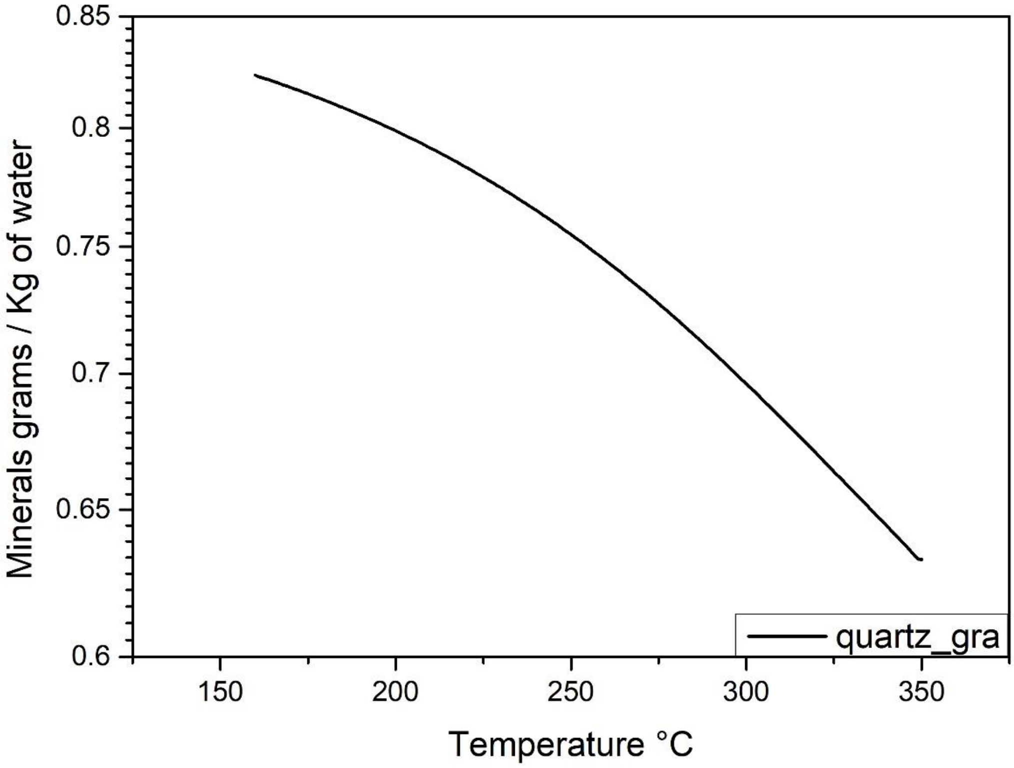


In well H-17 we have only quartz as secondary phase; this is a common occurrence in case of missing analysis of Iron.

### 6.3.5 well H-19

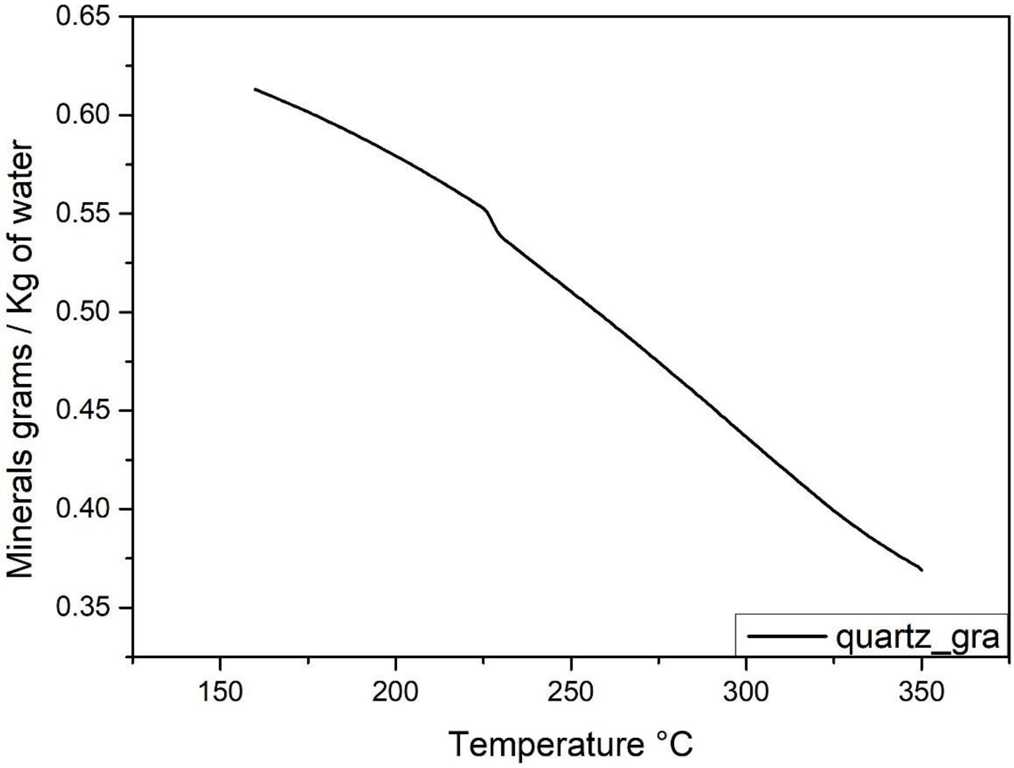


In well H-19 we have only quartz as secondary phase; this is a common occurrence in case of missing analysis of Iron.

### 6.3.6 well H-22

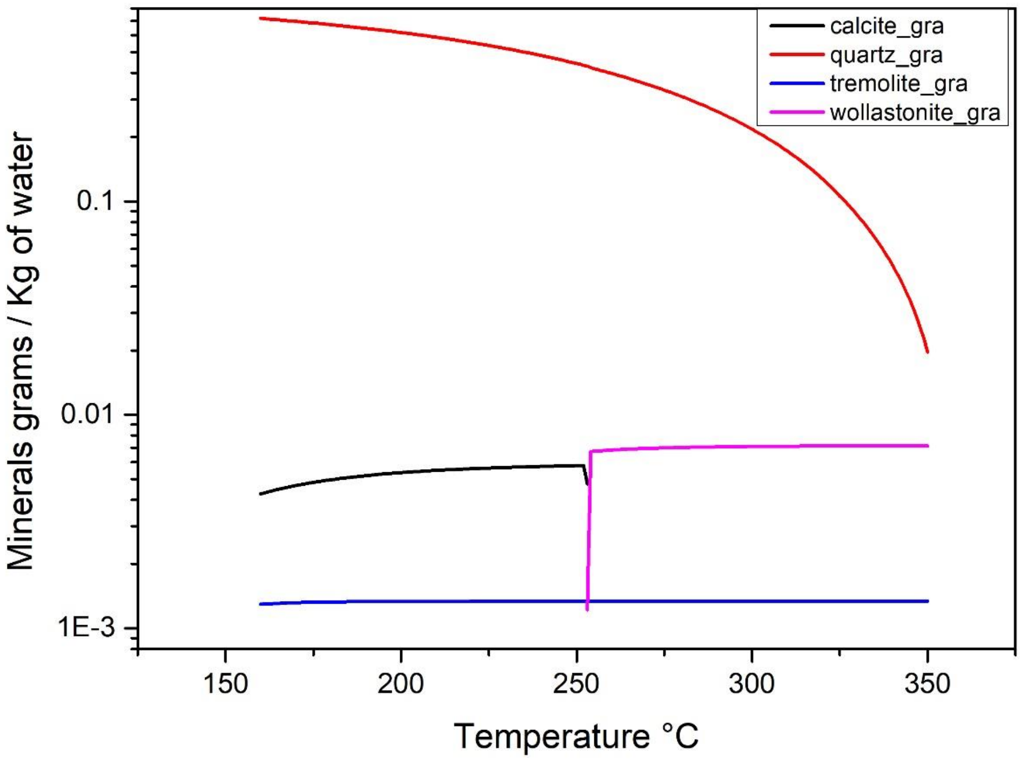


In well H-22 we have quartz as secondary phase, tremolite pertaining to the original rock and an interesting example of change from wollastonite to calcite, being the former pertaining to the skarn/hydrothermal alteration at high temperature and the latter a secondary mineral likely to act as potential scaling mineral.

### 6.3.7 well H-23

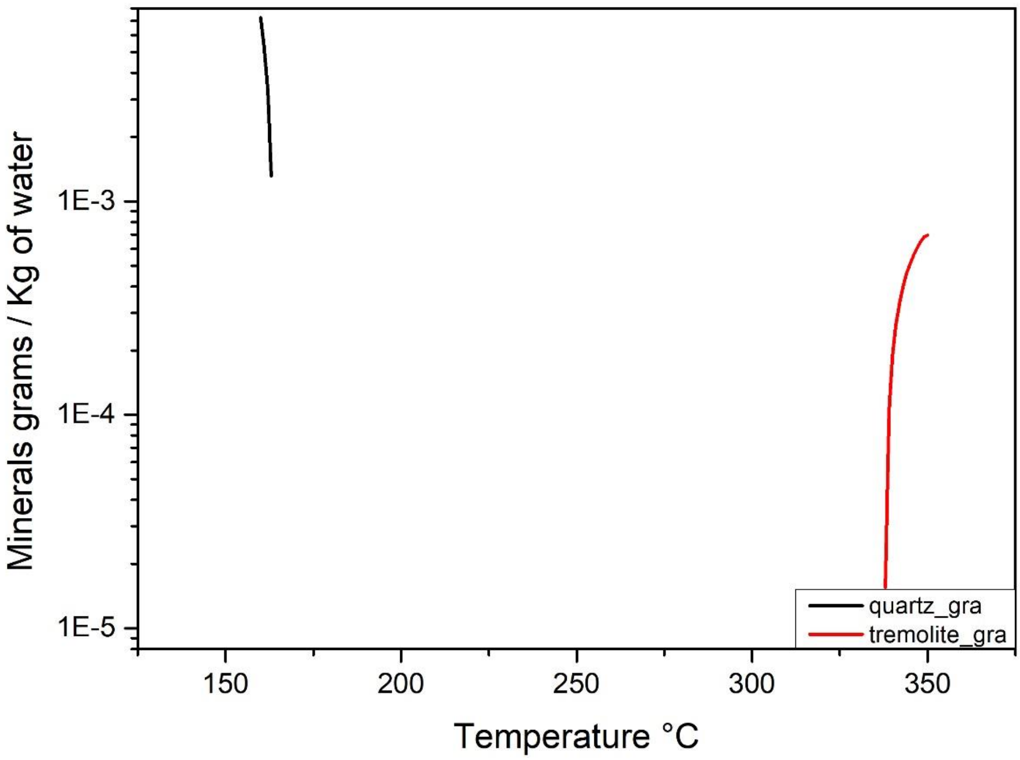


In well H-23 we have only quartz at very low temperature and tremolite at very high temperature, both temperature out of range for shallow and deep feed zones.

### 6.3.8 well H-28

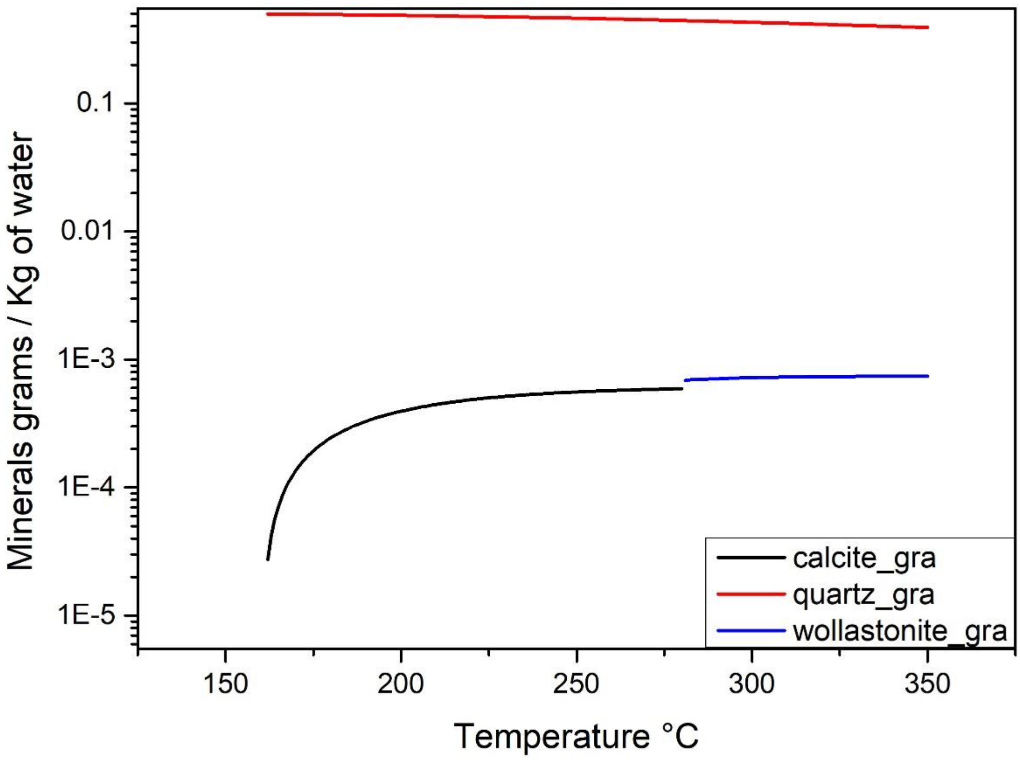


In well H-28 we have quartz as secondary phase, and another interesting example of change from wollastonite to calcite, being the former pertaining to the skarn/hydrothermal alteration at high temperature and the latter a secondary mineral likely to act as potential scaling mineral.

### 6.3.9 well H-49

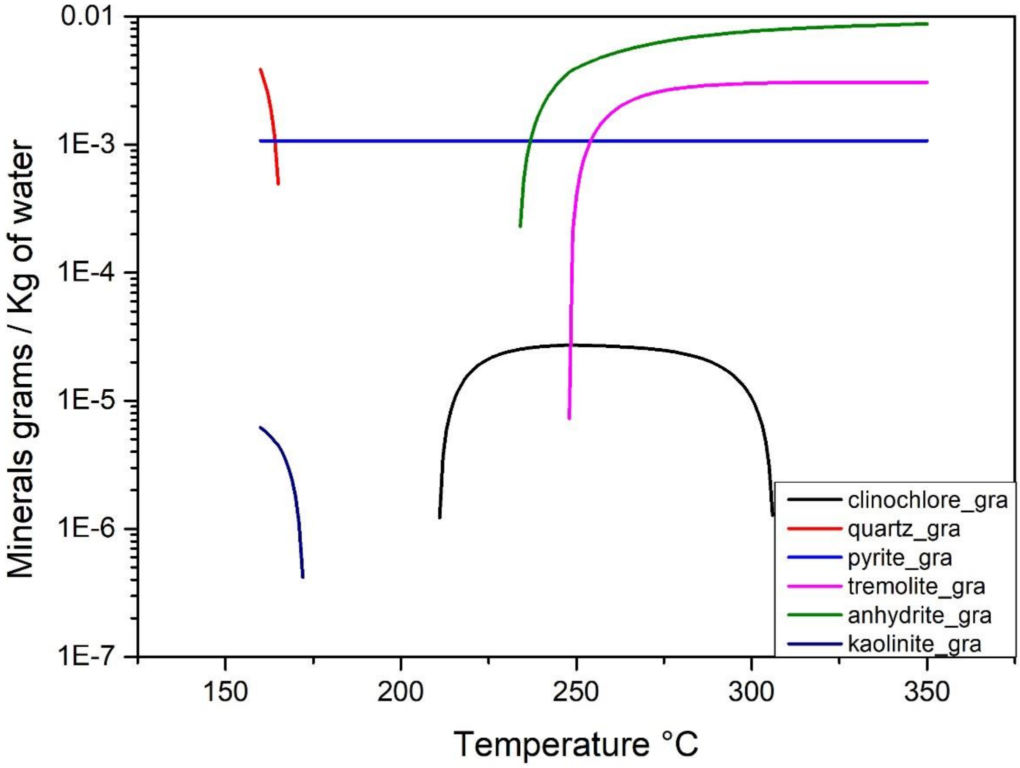


In well H-49 we have a possible low temperature alteration producing quartz ad kaolinite. The presence of chlorite is at 220-310°C, around the disappearance of tremolite, and we found a sulphate phase made of anhydrite at high temperature (>240°C).

**6.3.10 well H-56**

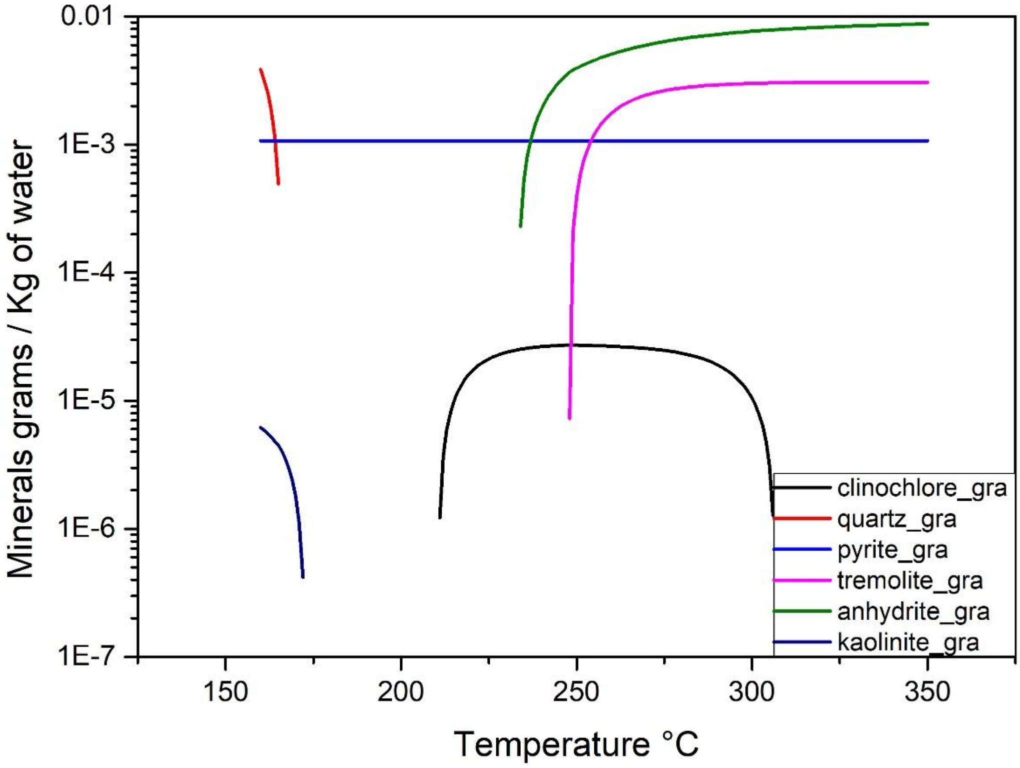


In well H-56 we have a possible low temperature alteration producing quartz ad kaolinite. The presence of chlorite is at 220-310°C, around the disappearance of tremolite, and we found a sulphate phase made of anhydrite at high temperature (>240°C), similar to well H-49.

**6.3.11 well H-59**

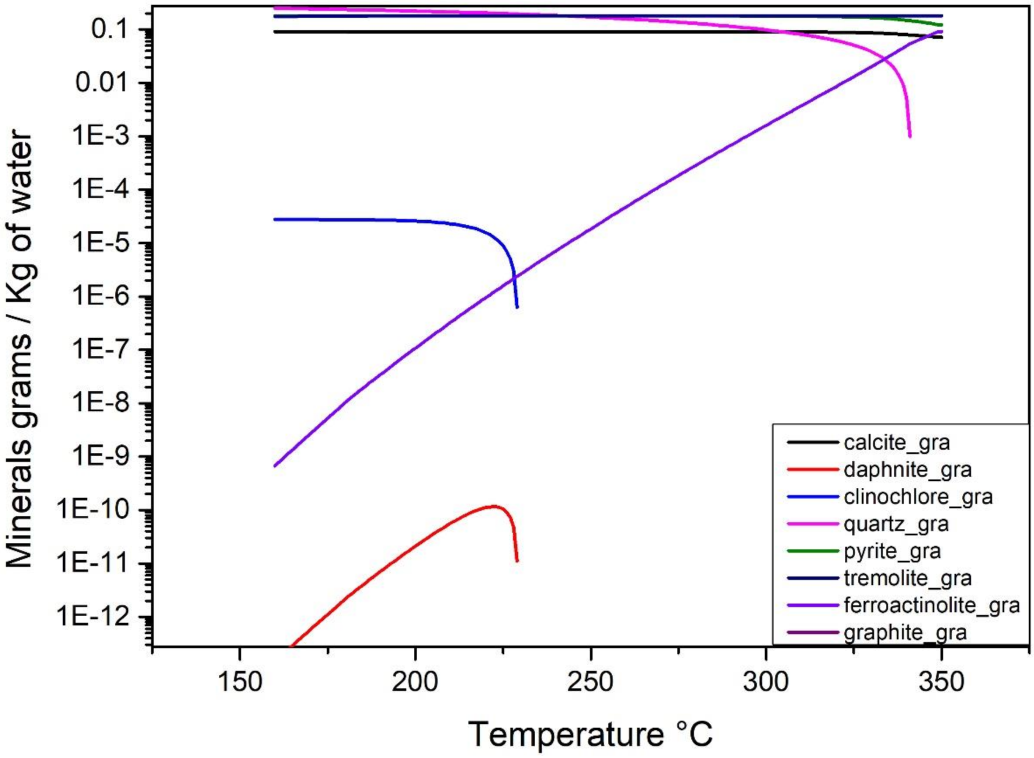


In well H-59 are encountered some of the most common secondary minerals, like chlorite and daphnite as part of the argillification process of andesites. The abundances of these phases are not too reliable due to our add af Aluminium, needed to include these minerals in the model. The main secondary minerals resulting from our model are calcite, pyrite and quartz, that are common secondary phases at Los Humeros both in the reservoir rocks and as scaling minerals in wells. Tremolite result always present, and it is a methamorphic amphibole pertaining to the original rock, like ferroactinolite, that at lower temperature and in presence of $CO_2$ tend to decompose in to talc/clay, calcite and quartz. These results are very similar to well H-15.

### 6.3.12 Simultaneous equilibria

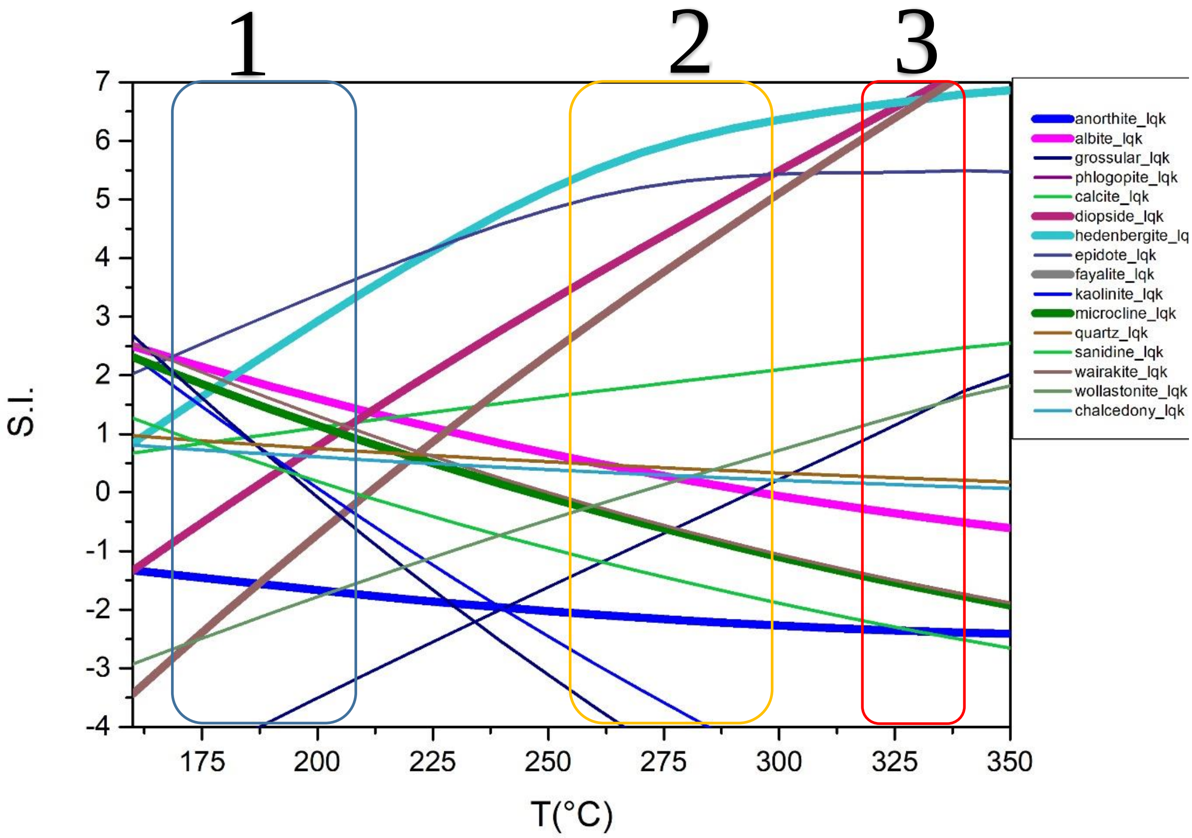


We used the fluid sample from well H-59 sampled 16/8/2016 as representative fluid sample at depth, since it is a sample with the best score on PCA 1st component, and added 1e-7 moles/Kgw of $Al^{+3}$, to investigate the Saturation Index (S.I.) vs temperature following the approach described in Reed and Spycher 1984. In this approach, S.I. line crossing represent the equilibrium among two or more minerals at crossing point. Ideally, the crossing happen at S.I. = 0, but due to many possible interferences and our guessing of $Al^{+3}$ concentration this may happen at different values of S.I. In the figure, primary minerals are evidenced by bold lines and are Anorthite – Albite, Diopside-Hedenbrgite (Pyroxene), Augite, K-feldspar, Olivine (Fayalite-Forsterite) in Basaltic andesites. In this computation, anorthite is always not stable, mainly due to the pH that is nearly neutral to slightly acidic, while anorthite would require an alkaline environment.

In this diagram we are able to find 3 different zones with important simultaneous equilibria.

The zone number 1, at temperature ranging 170-210°C is related to low temperature equilibrium, in wich the final phases of alteration like quartz, chalcedony and kaolinite become the most stable. In our opinion, this process is related to self-sealing mechanism above the shallow feed zone.

The zone number 2, at temperature ranging 255-300°C, is characterized by the appearing of high temperature metamorphic minerals like wollastonite, epidote and the disappearance of albite and microcline to form quartz/chalcedony; this particular facies of thermos-methamorphism in the hydrothermal system could be responsible for the separation between shallow and deep feed zone, due to the formation of hydrothermal minerals in the small fractures that are responsible for the low permeability of the feed zones.

The zone number 3, at temperature ranging 320-340°C, have the simultaneous equilibrium of hedenbergite, forsterite and albite pointing out the starting condition for the hydrothermal alteration.

### 6.4. Conclusion

In the investigation of the possible mineral phases and their behavior as function of temperature, including the finding of Prol-Ledesma and Browne 1989 and Martinez-Serrano 2002, we can summarize the behavior as due to assemblage of primary minerals:

Anorthite – Albite, Diopside-Hedenbrgite (Pyroxene), Augite, K-feldspar, Olivine (Fayalite-Forsterite) in Basaltic andesites

The possible hydrothermal/methamorphic high temperature secondary minerals are:

Tremolite – Actinolite (amphibole), Daphnite/Chlorite, Quartz, Calcite, Kaolinite, Illite – Montmorillonite – Muscovite, Epidote, Pyrite, Wairakite, K-feldspar, Diopside-Hedenbrgite (Pyroxene), Biotite, Garnet

Due to water-rock interaction (including $CO_2$ and the acidic fluids), in particular at low temperature, a group of secondary minerals with scaling potential could be defined as:

Pyrrhotite, Pyrite, Quartz – Chalcedony, Calcite, Anhidrite-Bassanite-Gypsum

In this assemblage, pyrite is more common than pyrrhotite in spite of the high temperature, due the $H_2S$ fugacity, while iron oxides are expected to appear in case of very low Sulphur concentration. These findings are also consistent with Gutierrez Negrin et al., 1990, that found scaling in well H-16 made up of Iron sulphides and oxides, amorphous silics, quartz, chalcedony, anhydrite and gypsum with some carbonatetes.

Moreover, the simultaneous equilibria method show that on top of the shallow feed zone a permeability reduction is expected due to self-sealing made by quartz/chalcedony, kaolinite and possible calcite minerals.

The main hydrothermal alteration start at a temperature intermediate between shallow and deep feed zones, and could be responsible for the partial separation of the two feed zone inside a single low permeability reservoir.

## References


Bernard R., Taran Y., Pennisi M.;. Tello E., Ramirez A., "Chloride and Boron behavior in fluids of Los Humeros geothermal field (Mexico):A model based on the existence of deep acid brine", Applied Geochemistry 26 (2011) 2064–2073

J. Bundschuh, M.A. Armienta, P. Birkle, P. Bhattacharya, J. Matschullat & A.B. Mukherjee, "Geogenic Arsenic in Groundwater of Latin AmericaChapter: The abundance of natural arsenic in deep thermal fluids of geothermal and petroleum reservoirs in Mexico", CRC PressEditors, 2009

Gutierrez Negrin L.C.A., Guerra J.C.V., "Corrosion and scaling in the well H-16 of the Los Humeros Geothermal Field", Geothermal Resources Council Transactions, Vol. 14, Part 11, August 1990

Holland T.J.B., Powell R.,"An improved and extended internally consistent thermodynamic dataset for phases of petrological interest, involving a new equation of state for solids", J. Metamorph. Geol., 29 (2011), pp. 333-383

Johnson J.W., Oelkers E.H.,† Helgeson H.C. "SUPCRT92: A software package for calculating the standard molal thermodynamic properties of minerals, gases, aqueous species, and reactions from 1 to 5000 bar and 0 to 1000°C", Computers & Geosciences, Volume 18, Issue 7, August 1992, Pages 899-947

Martinez-Serrano R.G., "Chemical variations in hydrothermal minerals of the Los Humeros geothermal system", Mexico, Geothermics 31 (2002) 579–612

Prol-Ledesma R.M. and Browne P.R.L., "Hydrothermal alteration and fluid inclusion geothermometry of Los Humeros Geothermal Field, Mexico", Geothermics, Vol. 18, No. 5/6, pp. 677-690, 1989.

Reed M., Spycher N., "Calculation of pH and mineral equilibria in hydrothermal waters with application to geothermometry and studies of boiling and dilution", Geochimica et Cosmochimica Acta, Volume 48, Issue 7, p. 1479-1492

Reed M.H., Spycher, N.F., Palandri J., "CHIM-XPT: A Program for Computing Reaction Processes in Aqueous-Mineral-Gas Systems", 2012

Stefánsson A., "Dissolution of primary minerals of basalt in natural waters: I. Calculation of mineral solubilities from 0 °C to 350 °C", Chem. Geol., 172 (3) (2001), pp. 225-250

Tello E., Mahendra H, Verma P, Tovar R. A., "Origin of acidity in the Los Humeros, Mexico, Geothermal Reservoir", Proceedings World Geothermal Congress 2000, pp 1-9

# Chapter 7

# HIGH TEMPERATURE TRACERS

## 7.1 Introduction

Organic compounds like naphthalene and pyrene sulfonates have been applied successfully as water tracers in geothermal reservoirs, and some of these compounds have been reported to be thermally stable up to 350°C at reservoir conditions [1, 2]. It has, however, been a demand for development of water tracers that are stable at even higher temperatures for tracer applications in geothermal reservoirs. Many inorganic ions have a higher thermal stability than organic anions applied as tracers in geothermal reservoirs, and it was thought that the possibility of applying inorganic anions as tracers should be investigated further. Cobalt hexacyanate [$Co(CN)_6^{3-}$] has been applied by IFE as an inter-well water tracer for petroleum reservoirs previously using the radioactive isotope $^{60}Co$. The tracer was found to be less stable at temperatures above 100°C, and the anionic complex is therefore not regarded as a suitable tracer for geothermal reservoirs. The task of this project was to test out the suitability of other anionic metal complexes as water tracers for geothermal reservoirs by testing their thermal stability and flooding properties, and measure their natural occurrence in geothermal fluids. One advantage when analysing metal ions in water is the high detectability that can be achieved using advanced analytical instrumentations like inductively coupled plasma mass spectrometry (ICP-MS) or neutron activation analysis. The idea of using such metal containing anions as tracers for geothermal reservoirs and other fields of tracer research has led to a patent application. In order to prevent any release of information that can create problems for the patent application process, the seven compounds tested are not at this stage revealed, but are indicated with a letter from A to G.

## 7.2 Methodology, Data Analysis and Discussion

### 7.2.1 Static Thermal Stability Tests

Seven tracer candidates were first tested for thermal stability in closed quarts vials at temperatures from 150 to 250°C. The tracer concentration for each component was about 500 ng/ml (ppb), and the test solution contained 4% NaCl. The oxygen in the vials was replaced by argon before the vials were heated in an autoclave. The autoclave chamber was pressurized with $N_2$ to a pressure corresponding to the inside vapour pressure of the water in the vials at the actual temperature. This was done to reduce the risk of vial breakage. The solutions were analysed by ICP-MS after one week at temperatures 150, 200 and 250°C. The measured recoveries were as shown in Figure 1.

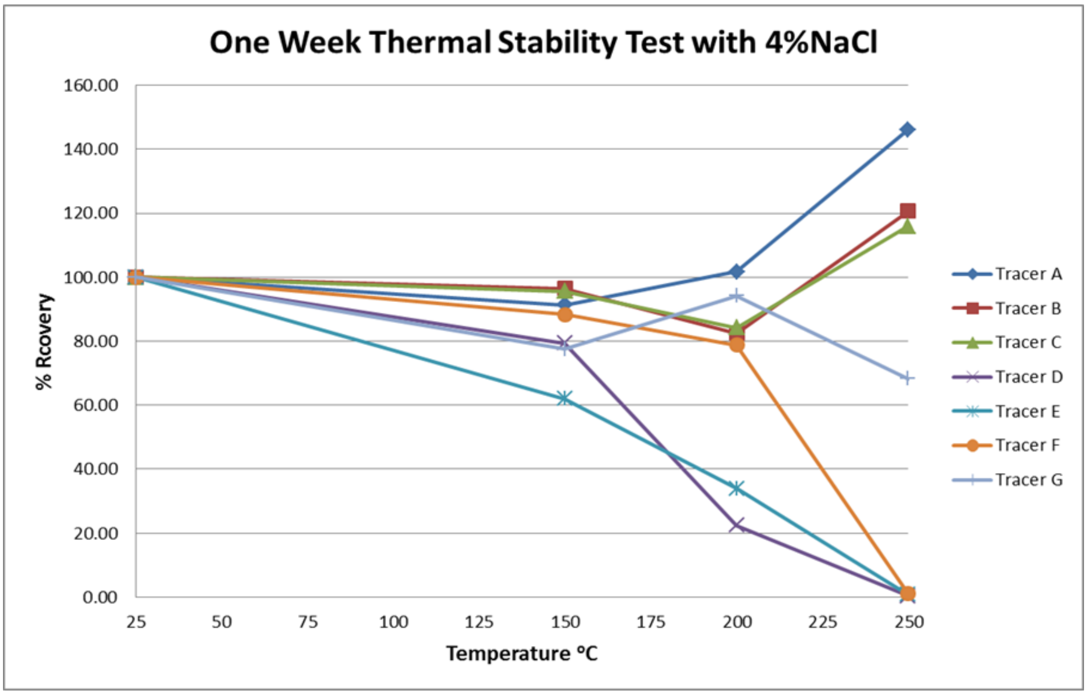


Figure 7.1. Plot showing recoveries of 7 different tracer candidates at 150, 200 and 250°C

The results indicate that the tracer candidates A, B, C and G were reasonably stable at the temperatures applied, while the candidates D, E and F had a lower thermal stability. The increased recoveries of Tracer A, B and C at 250oC was due to contamination from the quarts vials since it was observed that some of the quarts had started to dissolve from the inside walls at the highest temperature and that the contamination was coming from impurities in the quarts. This contamination was corrected for in later experiments by increasing the tracer concentration and by including blank samples and correcting for the concentration found in the blank samples.

The same test was also performed with crushed basalt rock material present in the vials. Plots of the recoveries are shown in Figure 2.

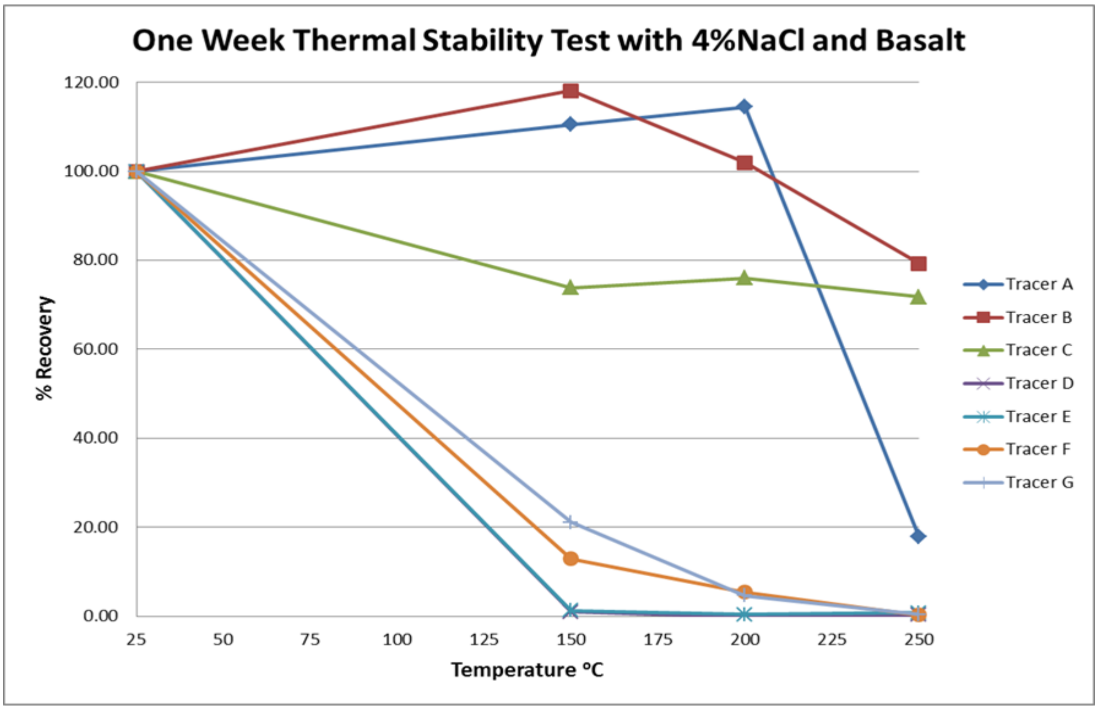


Figure 7.2. Plot showing recoveries of 7 different tracer candidates at 150, 200 and 250°C with basalt rock material present in the vials

When basalt was present in the vials, the best recoveries were obtained for Tracer B and C. The recovery for Tracer A was high up to 200°C, but at 250°C the recovery was much lower. For the other three candidates the recoveries were markedly lower when basalt was present at temperatures 150, 200 and 250°C, indicating that the tracers were either adsorbed on or transferred to other less soluble compounds in contact with the Basalt rock particles. Vials stored at 25°C for one week were not included in the experiment, and the point of 100% at 25°C was only included in the diagram as a reference for no degradation or adsorption.

### 7.2.2 Development of HPLC-ICP-MS method and thermal stability tests at higher temperatures

#### 7.2.2.1 Ion exchange HPLC method

Metals can be present in water solutions in the form of different species and hyphenated techniques have been applied for separation of the species prior to detection by for instance ICP-MS [3, 4, and 5]. A high performance liquid chromatographic (HPLC) method based on ion exchange chromatography was developed that was combined with ICP-MS, and this method was applied for analysis of Tracer A, B and C. In Figure 3 overlaid response curves from HPLC-ICP-MS analysis of standard solutions of Tracer A and B are shown. With this chromatography method the two tracers could be separated from other species of the metal elements that might be present in the sample.

The column applied was Allsep AS-2, 100x4.6mm (Alltech part No. 51219), and the eluent consisted of 0.1M $NH_4CO_3$ solution in water at a flow rate of 0.8 ml/min.

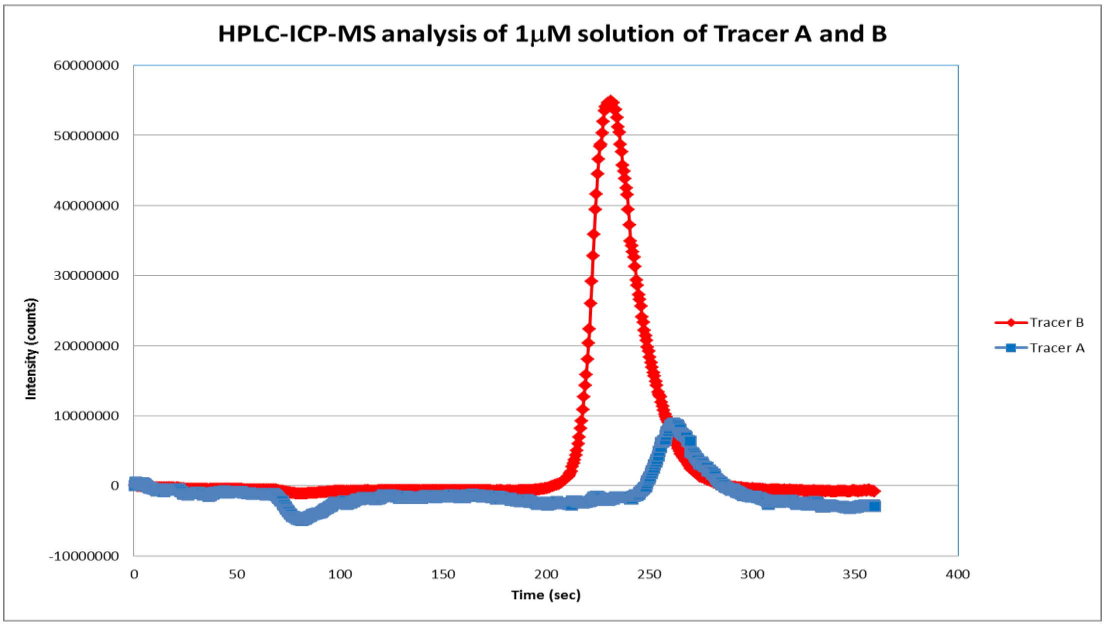


Figure 7.3. Plot of intensity response versus time from HPLC-ICP-MS analysis of standard solutions of Tracer A and B

Tracer C would not elute from the same column as used for Tracer A and B within reasonable time. Therefore a different shorter column was applied for Tracer C. In Figure 4 is shown chromatogram from HPLC-ICP-MS analysis of a standard solution of 10 ng/l (ppb) of Tracer C using an AG-9 50x4mm column (Dionex part No.043186). The Eluent applied was 0.2M $NH_4CO_3$ at a flow rate of 1 ml/min.

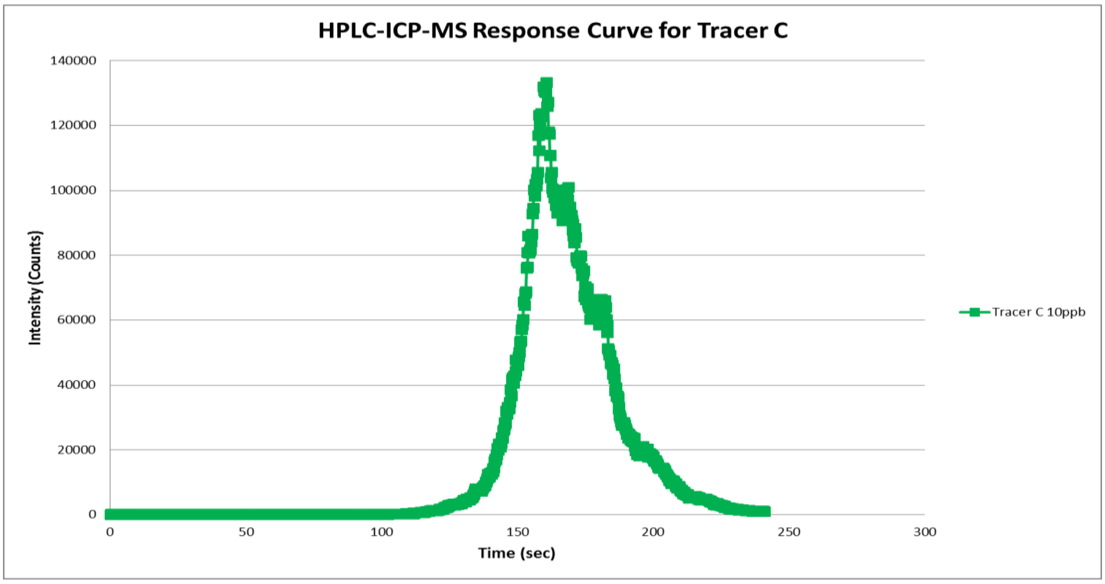


Figure 7.4. Plot of intensity response versus time from HPLC-ICP-MS analysis of standard solutions of Tracer C

#### 7.2.2.2 Ion pair reverse phase chromatography method

There is a limitation to what sort of eluent the ICP-MS instrument can tolerate in terms of salt concentration and content of organic solvents. High salt concentrations may result in clogging of the nebulizer or the MS inlet orifice, and when the content of organic solvents like methanol exceeds 20%, a layer of carbon particles may build up in the torch. Different ion pair counter ions were tested for reverse phase chromatography of the tracer candidates, and during the method development stage UV detection was applied. Tracer A and B was also available as tetra thio compounds instead of the original oxygen complex, and one task was to test such sulphur compounds as alternative or additional tracers to Tracer A and B. It was therefore important to develop a chromatographic method that could separate the oxygen and sulphur containing anions of the same metal. The sulphur containing candidates could not be analysed by the ion exchange chromatography method because the anions were too strongly retained. Analysis of Tracer A, B and C and the sulphur containing version of Tracer B by ion pair reverse chromatography with UV detection is shown in Figure 5. The column was a 2 x 50mm $C_{18}$ reverse phase column and the eluent consisted of 5 mM tetraethylammonium chloride and 30 mM ammoniumacetate at a flow-rate of 0.3 ml/min.

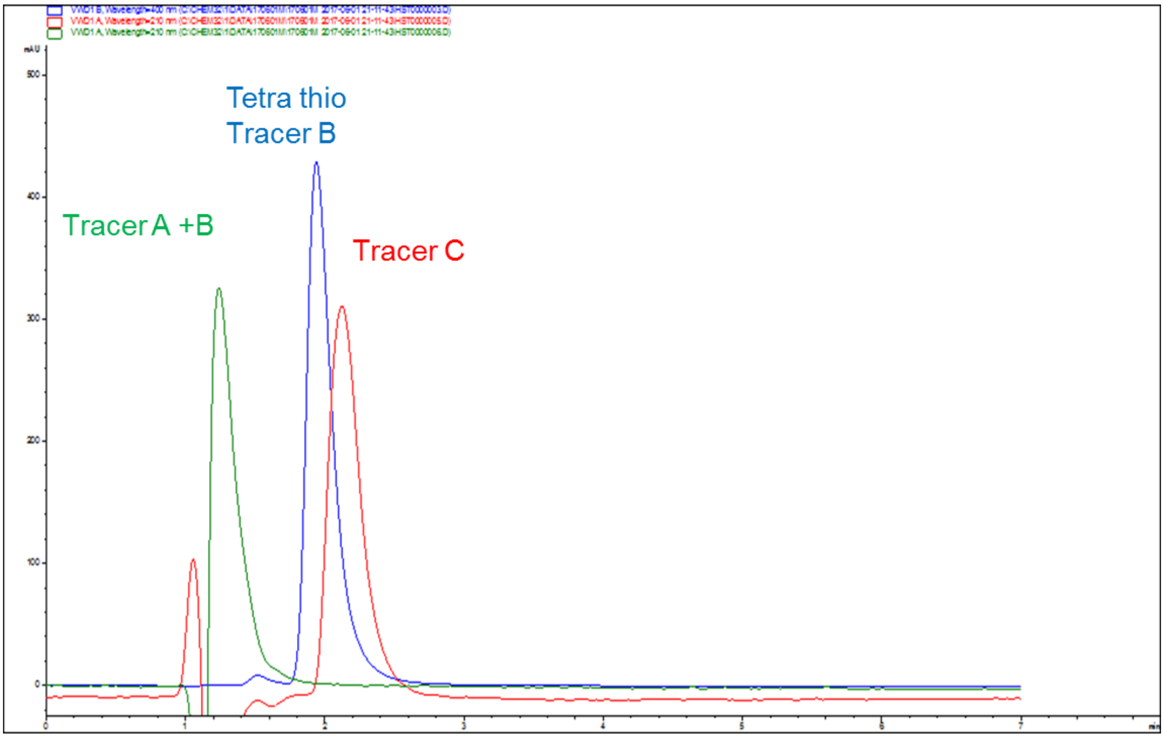


Figure 7.5. Reverse phase ion pair chromatography separation of tracer candidates using a 50mm long $C_{18}$ column

When using a longer column, a better separation between the oxygen and sulphur containing version of Tracer B was achieved as shown in Figure 6.

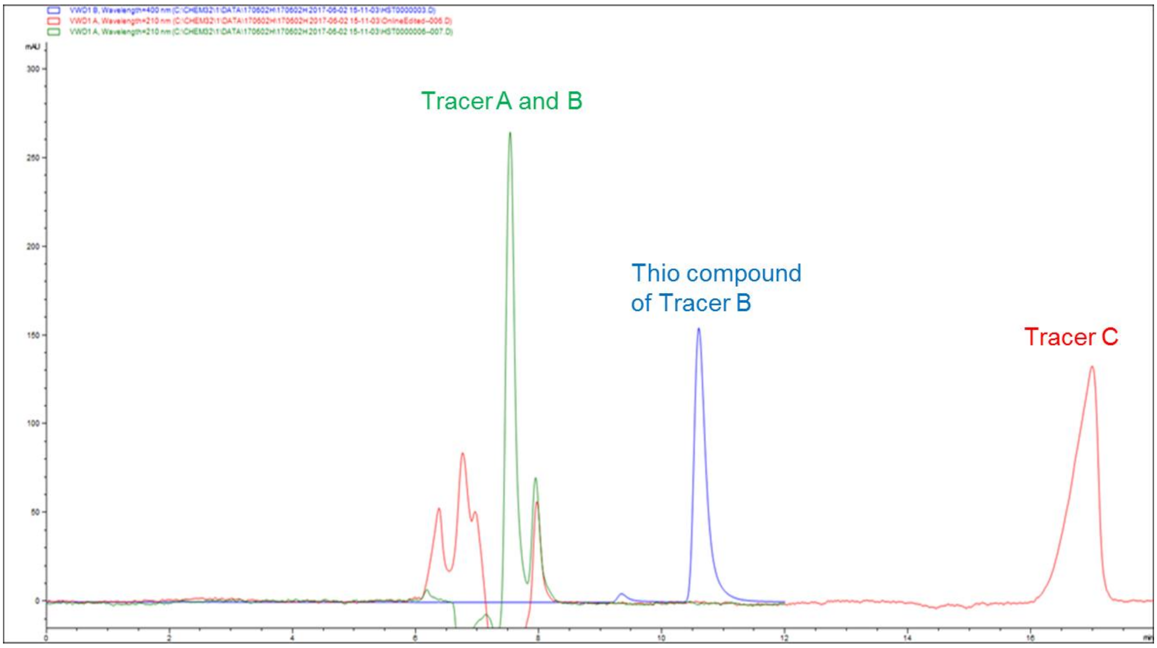


Figure 7.6. Reverse phase ion pair chromatography separation of tracer candidates using a 250mm long $C_{18}$ column

The sulphur containing version of Tracer A was found not to be stable in 4% NaCl-solution even at ambient temperature. The sulphur containing version of Tracer B was tested for thermal stability at 200$^{o}$C, and the results are showed graphically in Figure 7.

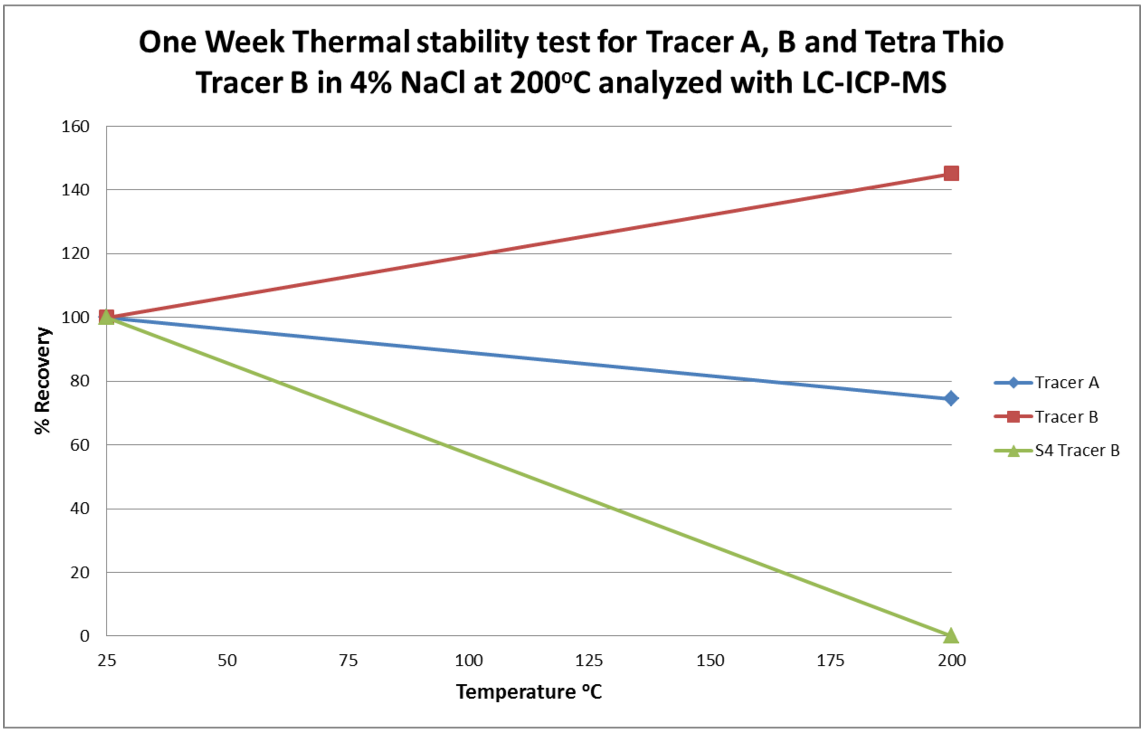


Figure 7.7. Graphical presentation of recovery of Tracer A and B and the sulphur containing version of Tracer B for one week thermal stability test at 200$^{o}$C

After one week at 200$^{o}$C the sulphur containing compound could no longer be detected in the test solutions. The concentration of Tracer B had increased considerably compared to the amount originally added to the test solutions. It was therefore concluded that the sulphur containing compound had been converted into the oxygen containing compound of Tracer B. The recovery of Tracer A was found to be near 80% in this experiment. The sulphur containing type of Tracer A was not included in the test solution. Since the sulphur containing compounds showed a lower thermal stability than the corresponding oxygen compounds, it was decided not to test the sulphur containing compounds any further.

#### 7.2.2.3 Thermal Stability Tests of Tracer A, B and C at higher temperatures

The tracer candidates A, B and C were tested for thermal stability at temperatures up to 350°C in 4% NaCl solution. The test solutions were analyzed using ICP-MS only (not HPLC-ICP-MS), so that only the concentration of the metal element itself was recorded. The results that are shown graphically in Figure 8 indicate that the three metal elements were almost completely recovered up to 350°C under these conditions.

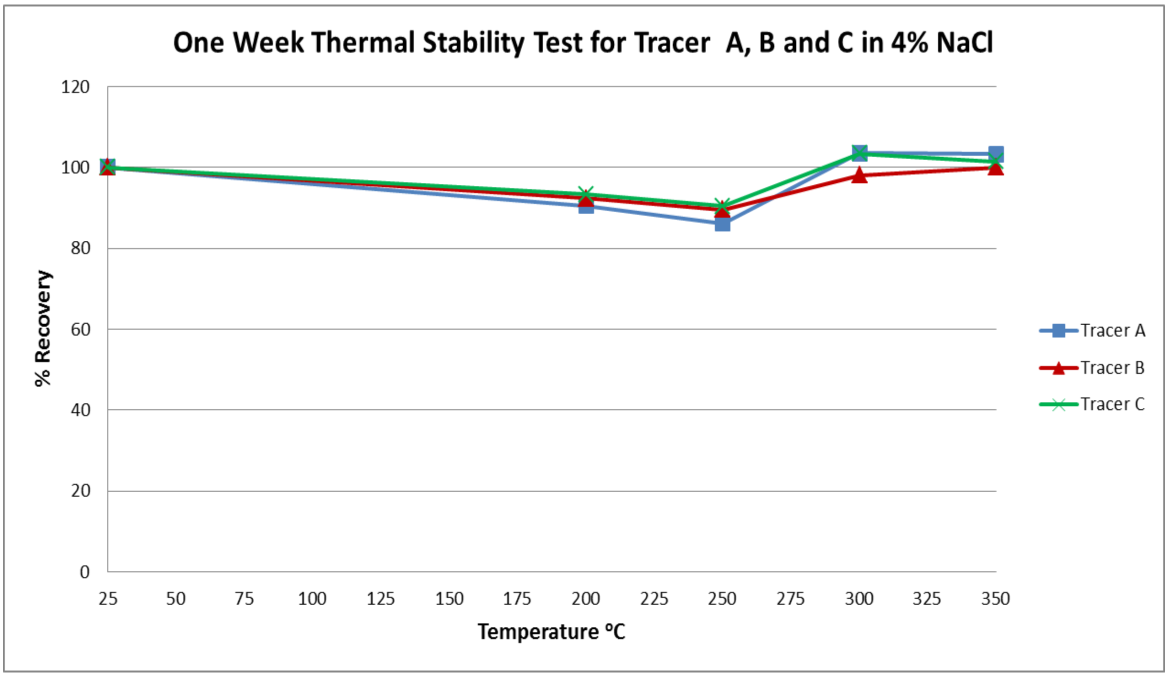


Figure 7.8. Plot showing recovery of Tracer A, B and C after one week thermal stability test in 4% NaCl at temperatures up to 350°C

The stability was also tested with Basalt rock particles in the test vials, and the results obtained are plotted in Figure 9.

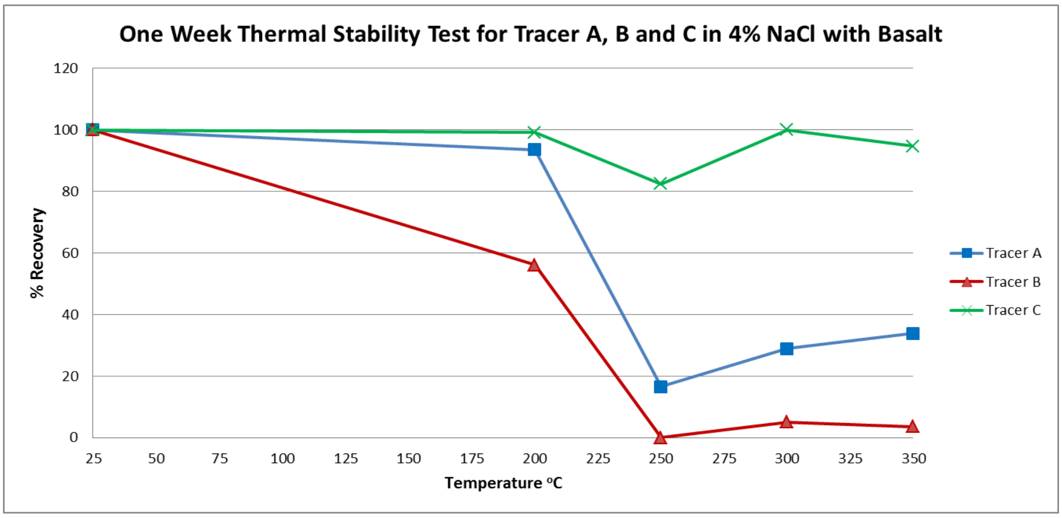


Figure 7.9. Plot showing recovery of Tracer A, B and C after one week thermal stability test in 4% NaCl with Basalt rock in the vials at temperatures up to 350°C

The recovery of the metal element from Tracer C was near 100% at temperatures up to 350°C. For Tracer A the recovery of the metal element was almost 100% up to 200°C, while for Tracer B the recovery was reduced already at 200°C and was near nil at higher temperatures. The Basalt rock applied must contain some sulphide minerals since $H_2S$ could be smelled from the vials when the Basalt containing vials were opened after exposure to high temperatures. The reason for the reduced recovery of Tracer A and B at high temperatures may therefore be due to formation of insoluble metal element sulphides.

### 7.2.2.4 LC-ICP-MS of thermal stability test solutions

The solutions from the thermal stability tests were also analyzed using the HPLC-ICP-MS method shown in Figure 5. A chromatogram from analysis of Tracer C  is shown in Figure10.

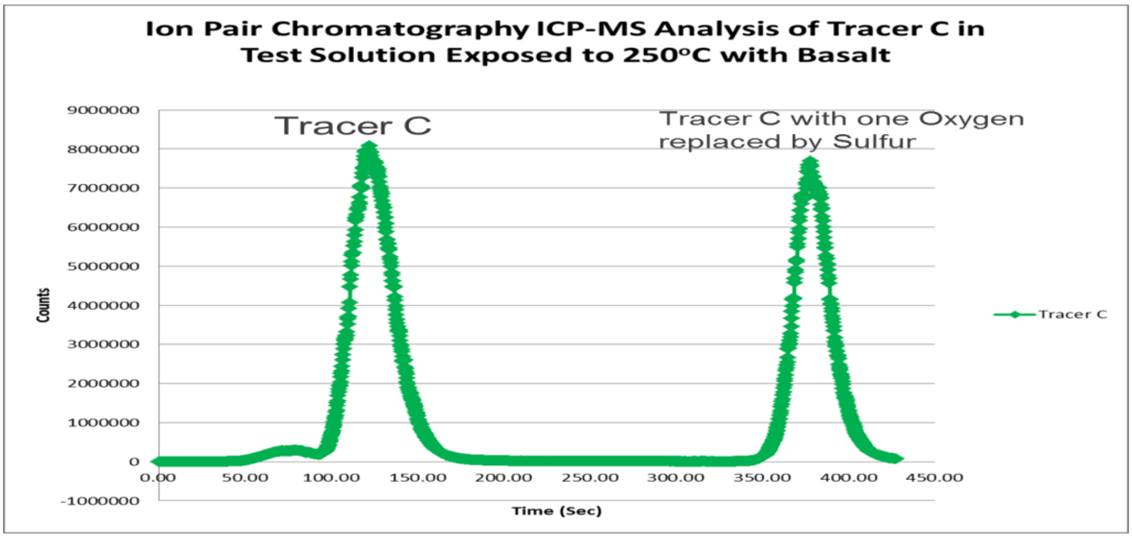


Figure 7.10. Chromatogram from HPLC-ICP-MS analysis of Tracer C in test solution with Basalt rock at 250°C

The first peak in the chromatogram at about 2 minutes had the same retention time as a standard solution of Tracer C. After about 6 minutes another peak eluted that contained the same metal element as Tracer C, but could not be the same component due to different retention. By analyzing the test solution using liquid chromatography mass spectrometry (LC-MS) it was found that the second peak consisted of a compound identical to Tracer C, but with one oxygen atom replaced by sulfur. This compound must be water soluble and was not adsorbed by the Basalt rock since when the test solution was analyzed by ICP-MS and only the total concentration of the metal element was recorded, almost 100% of the element was recovered. Therefore, as long as the tracer was measured as the total concentration of the metal, the tracer could still function at high temperatures even though it was partly converted to a sulfur containing compound.

### 7.2.3 Flooding Experiments

The first flooding experiment was performed using a 3.8x7.9cm Berea sandstone core. Tracer A, B, C and G were injected, and $Co(CN)_6^{3-}$ was also included for comparison. The temperature was set at 70°C and the mobile phase was 0.7M NaCl solution. The elution curves for the tracers are shown in Figure 11.

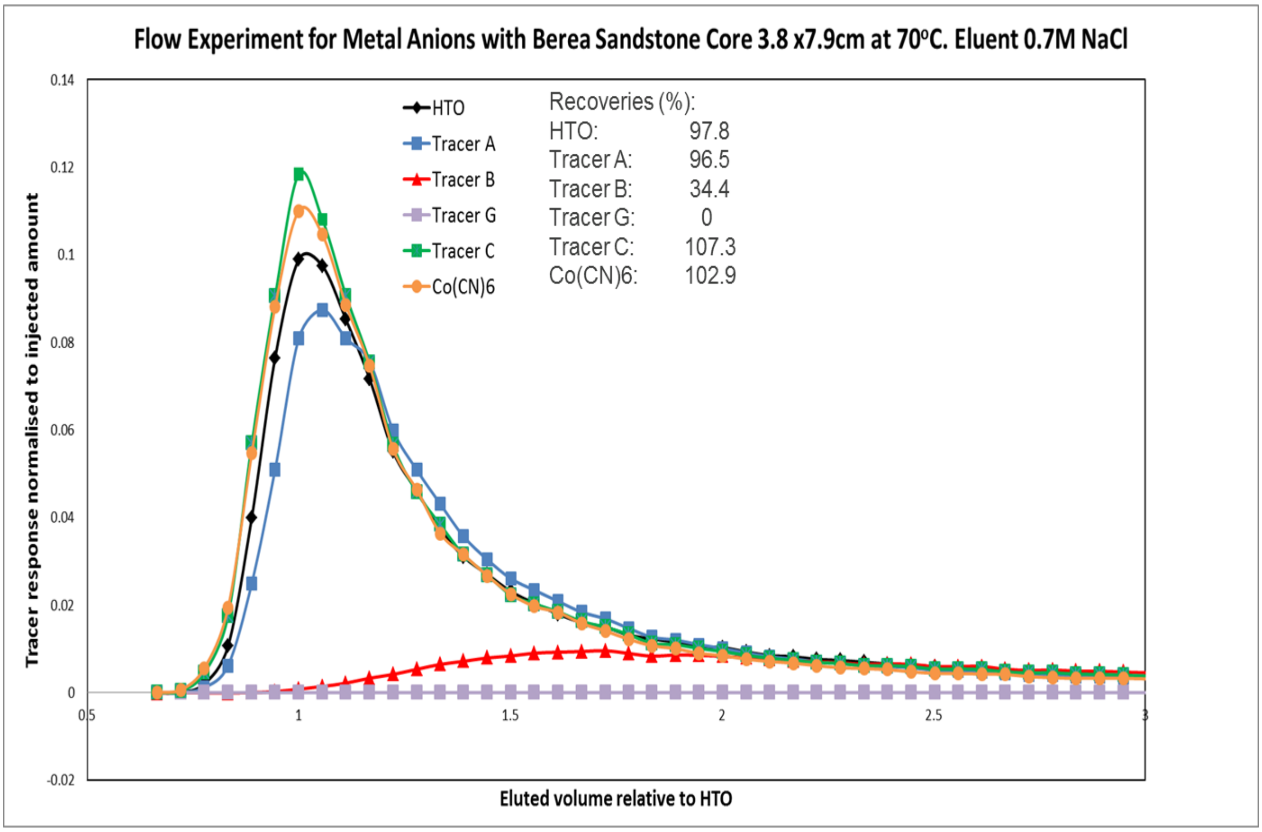


Figure 7.11. Plot of elution curves for tracer candidates on a Berea sandstone core at 70°C

Tracer C and $Co(CN)_6^{3-}$ were eluted in about the same elution volume as the ideal water tracer tritiated water (HTO), while Tracer A was slightly retained. Tracer B was much more strongly retained and only 34.3% was recovered. No response was seen from Tracer G.

The next flooding experiments were performed using a setup as shown in Figure 12.

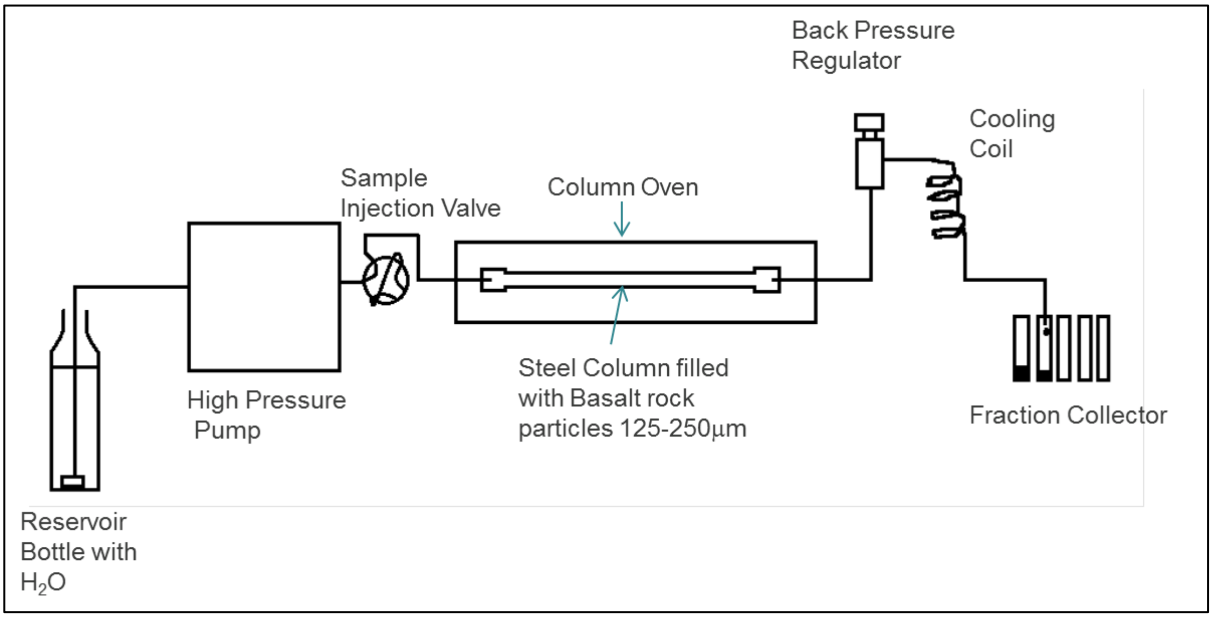


Figure 7.12. Schematic illustration of flooding experiment setup

A 42cm long steel column with internal diameter 8mm was packed with Basalt rock with particle size from 125 to 250 μm. Deionized water was pumped at a flow rate of 50μl/min using a high pressure pump. The column was installed in an oven that could be set at temperatures from ambient up to 400°C, and the back pressure was adjusted using a back pressure regulator. The water was cooled by air in a cooling coil before collected in vials using a fraction collector. The samples were injected through a 6-port injection valve with a loop of 50μl internal volume. The fraction collector was set to shift to the next vial after 5 minutes so that 250μl was collected in each vial. The vials were covered with a plastic film to reduce evaporation of water from the vials during the experiment, and the vials were capped after the experiment was finished to avoid evaporation. The first experiment with the Basalt packed column was for testing flooding properties of Tracer D, E and F. $Co(CN)_6^{3-}$ and HTO were also included for comparison. The collected fractions were analysed by radio nuclear analysis for HTO and by ICP-MS for the metal element content from Tracer D, E and F. None of the three tracer candidates D, E and F were recovered from the column within the time frame of the experiment, only $Co(CN)_6^{3-}$ and HTO. The response curves are plotted in Figure 13.

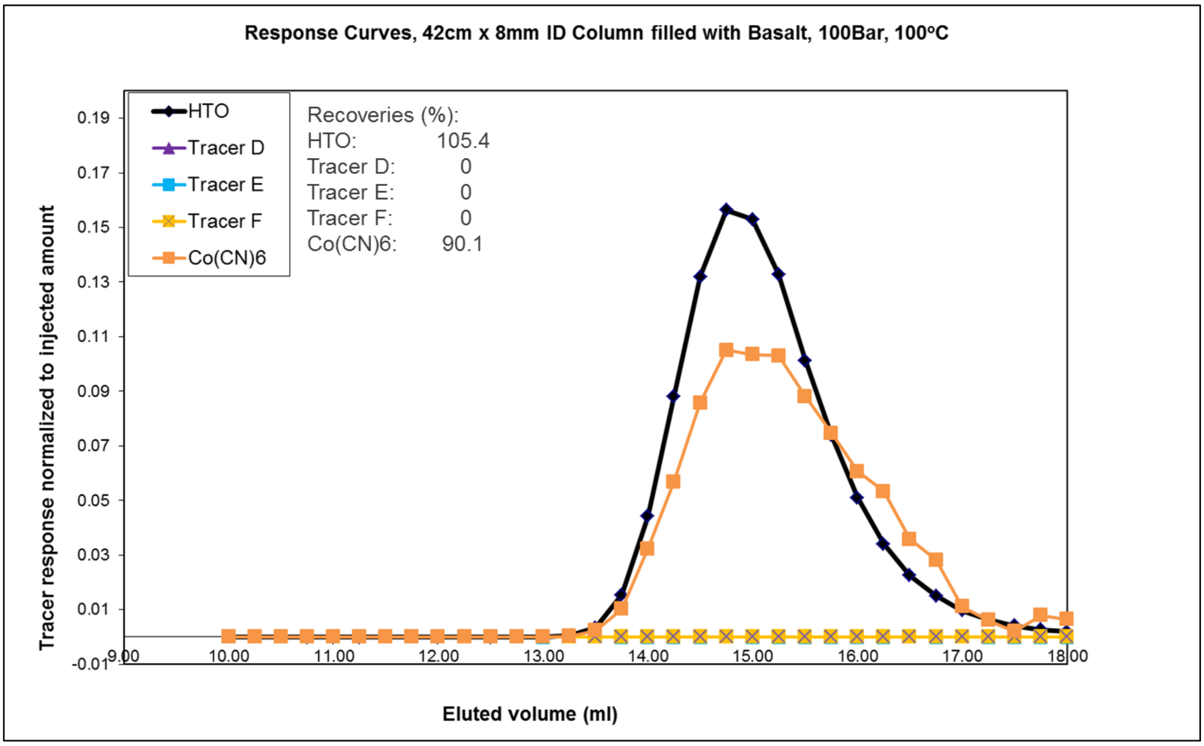


Figure 7.13. Response curves for the metal elements from Tracer D, E, F and $Co(CN)_6^{3-}$ as a function of eluted volume compared to ideal tracer HTO in a flooding experiment with Basalt rock at 100ºC and 100bar back pressure

The next experiments were performed for Tracer A, B and C at 250, 300 and 375ºC and at back pressures of 100, 200 and 240 bars respectively. HTO was added to each sample before injection as a reference water tracer. The collected fractions were analysed by radio nuclear analysis for HTO and by ICP-MS for the metal element content from Tracer A, B and C.

The response curves for HTO and the metal elements from the tracer candidates are plotted in Figures 14, 15 and 16.

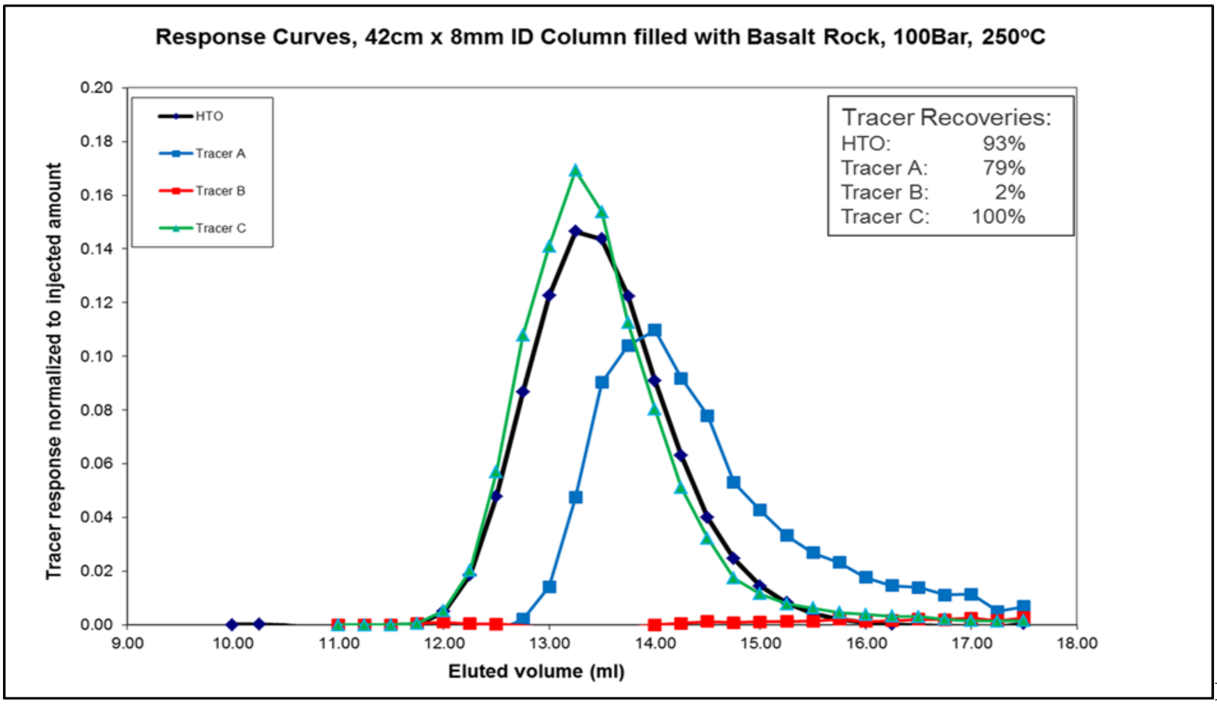


Figure 7.14. Response curves for the metal elements from Tracer A, B and C as a function of eluted volume compared to ideal tracer HTO in a flooding experiment with Basalt rock at 250ºC and 100bar back pressure

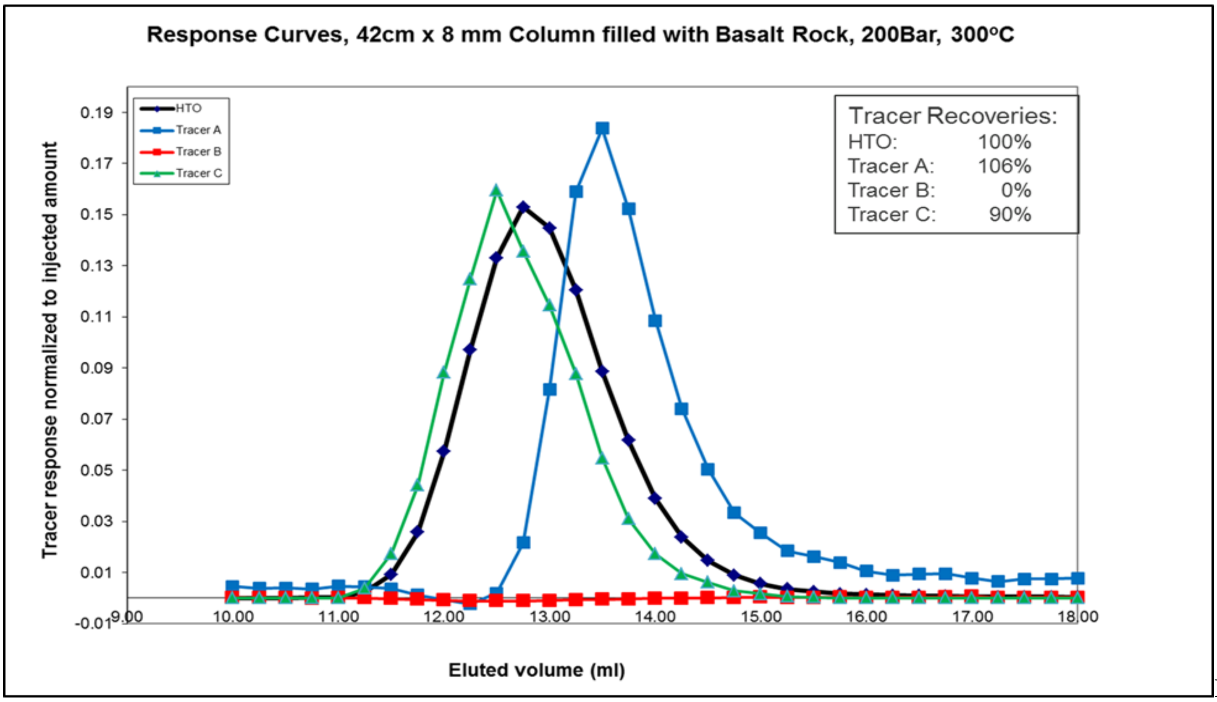


Figure 7.15. Response curves for the metal elements from Tracer A, B and C as a function of eluted volume compared to ideal tracer HTO in a flooding experiment with Basalt rock at 300ºC and 200bar back pressure

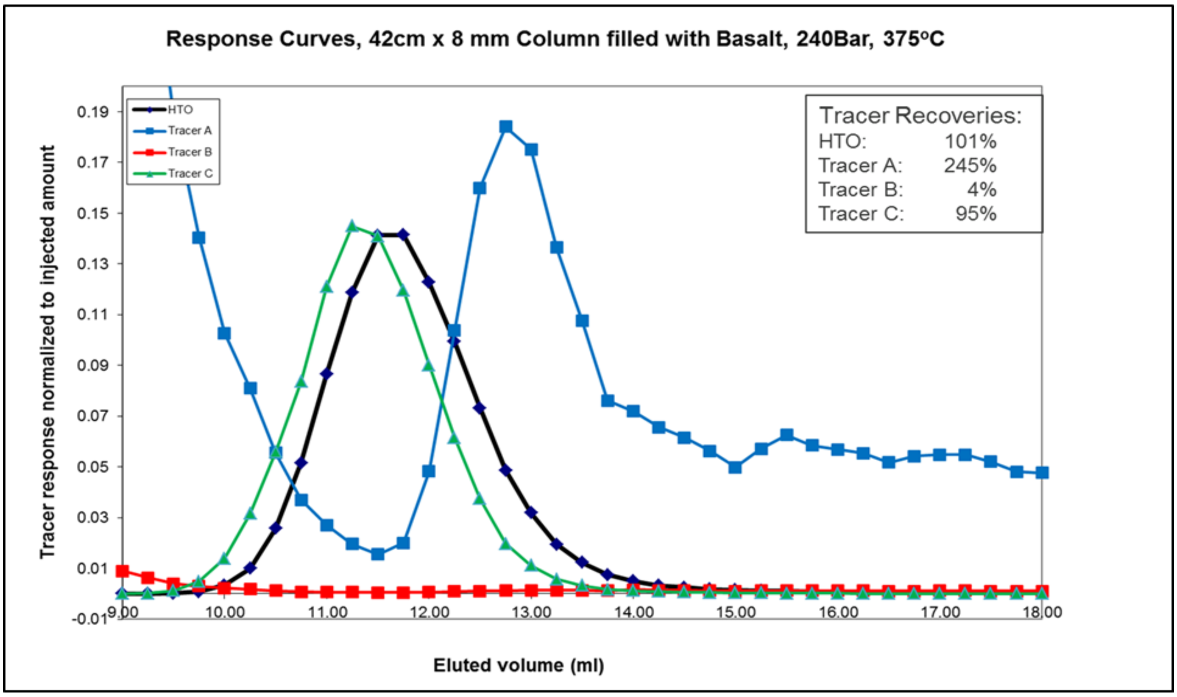


Figure 7.16. Response curves for the metal elements from Tracer A, B and C as a function of eluted volume compared to ideal tracer HTO in a flooding experiment with Basalt rock at 375°C and 240bar back pressure

At 250°C Tracer C and HTO were eluted in nearly the same volume and the recovery of Tracer C based on metal element concentration was calculated to 100%. The slightly lower recovery for HTO may be due to evaporation of HTO during the experiment. The slightly faster elution of Tracer C compared to HTO can be explained by ion exclusion effects. Tracer A was delayed in comparison with the ideal tracer HTO and the recovery was calculated to 79%. This result indicate that Tracer A was retained due to adsorption and that the tracer may have been partly converted to some other insoluble compound. Tracer B was almost completely adsorbed or converted into some other insoluble compound in the column. At 300°C the HTO and Tracer C were eluted faster and the ion exclusion effect was a bit more pronounced. The recoveries for HTO and Tracer C were 100 and 90% respectively. Also at this temperature Tracer A was delayed compared to HTO, but the recovery in this experiment was higher. It was observed also during the static experiments that the Basalt rock contained some mineral that could release Tracer A at high temperature, and it is anticipated that this was the reason for the higher recovery of Tracer A. Tracer B was not recovered in this experiment also. At 375°C which is just above supercritical conditions, HTO and Tracer C were eluted even faster from the column. The calculated pore volume of the column was reduced from 62.8% to 55.7% when the temperature was raised from 250 to 375°C. This corresponds well with the water expansion due to increased temperature from the first to the third experiment, and this is therefore regarded as the main reason for the decreased elution volume for HTO and Tracer C at higher temperatures. The reason for the more enhanced difference in elution speed for Tracer C compared to HTO is unclear. The reason for the high recovery of Tracer A must be that some of the same compound was released from the Basalt when heated. When the column was heated from 300 to 375°C before the tracer was injected, some Tracer A was released from the Basalt and eluted earlier than the peak at about 13ml that derived from the injection of Tracer A. Also at 375$^oC$ Tracer B was not recovered.

### 7.2.4 Pre-concentration method for Tracer C

Produced water from geothermal reservoirs may contain high concentrations of sodium chloride or other dissolved minerals, and high salt solutions cannot be analysed by ICP-MS directly. This type of water samples will have to be diluted or may have to go through a clean-up procedure to remove most of the dissolved salts. For some metal elements detection limits down to 10 pg/ml (ppt) can be achieved when the element is present in pure water, but for instance when sea water or produced water from petroleum fields are to be analysed, a dilution by a factor of 100 or more may be necessary, resulting in higher detection limits. In order to achieve a low detection limit for the tracers and thereby reduce the necessary amount needed for well injection, development of a clean-up or pre-concentration method is required. For Tracer C a special clean-up procedure was developed. The method is based on application of an organic cation for formation of a lipophilic compound with the metal complex anion of Tracer C, and the organic compound can be trapped on a lipophilic resin so that inorganic ions can be removed. With this method a detection limit of about 10 ppt should be obtainable.

## 7.3 Conclusions

Of the seven tracer candidates tested for static thermal stability up to 250$^oC$, three were regarded as sufficiently stable to qualify for further stability and flooding property tests. The three candidates (Tracer A, B and C) were tested further for thermal stability in closed quarts vials in 4% NaCl solution and with oxygen removed and exchanged by argon. The vials were tested at temperatures up to 350$^oC$, with and without Basalt rock particles present in the vials for a duration of one week. When Basalt was not present, the recoveries of Tracer A, B and C were near 100% for all the three candidates. When Basalt was present, the recoveries of Tracer A and B were considerably reduced, while the recovery for Tracer C remained unchanged. Flooding experiments were performed at temperatures up to 375$^oC$ using a column filled with Basalt rock particles. The Tracer B was not recovered in the flooding experiments. Tracer A was slightly retained while Tracer C was eluted in nearly the same volume as the ideal tracer tritiated water. Tracer A was leaking from the Basalt rock particles in the column when it was heated to 300$^oC$ or above. Tracer A will therefore be less suitable in this type of rock, but may perhaps be suitable in others. Tracer B is not regarded as suitable due to adsorption. It was observed that Tracer C was partly transformed to another compound containing Sulphur when heated above 250$^oC$ with Basalt present in the vials. The Sulphur compound of Tracer C was not retained during the flooding experiment, resulting in near 100% recovery when the measurement was based on analysis of the metal element and not of any of the species of the metal element.

Of the seven compounds tested, one tracer candidate (Tracer C) showed satisfactory properties as geothermal tracer and is expected to be suitable at temperatures up to at least 375°C. Further testing of Tracer C in field experiments is therefore recommended.

**References**

/1/ Rose, P.E., Benoir, W.R. and Adams, C. *Tracer Testing at Dixie Valley, Nevada, Using Pyrene Tetrasulfonate, Amino G, and Fluorescein.* Geothermal Resource Council Transactions 22, 583-587, 1998

/2/ Rose, P.E., Benoir, W.R. and Kilbourn, P.M. *The application of the polyaromatic sulfonates as tracers in geothermal reservoirs*. Geothermics 30 (2001), 617-640

/3/ Uden, P.C. *Modern trends in the speciation of selenium hyphenated techniques*. Anal Bioanal Chem (2002) 373, 422-431

/4/Wille, A., Czyborra, S., Kleimann, J. *Hyphenated techniques as modern detection systems in ion chromatography*. Metrohm AG, Application note 8.000.6005EN

/5/ http://www.speciation.net/Public/Document/2007/06/21/2914.html

# PART 2– ACOCULCO GEOTHERMAL SYSTEM

## Chapter 1
## STATE OF THE ART ON ACOCULCO GEOTHERMAL SYSTEM BEFORE GeMex

### 1.2 Geological and geothermal setting

The Acoculco Caldera (~18 km in diameter) is located at the eastern portion of the Trans-Mexican Volcanic Belt (TMVB), at the intersection of NE–SW Tenochtitlan-Apan, NW–SE Taxco-San Miguel de Allende, and E–W Chapala-Tula fault systems and on the NE–SW Rosario-Acoculco horst (García-Palomo et al., 2017). It lies within the structure of the older Tulancingo Caldera (~32 km in diameter, activity between 3.0 and 2.7 Ma; López-Hernández et al., 2009). The caldera is associated with 1.7–0.24 Ma eruptive events, the last of which generated the Acoculco andesitic ignimbrite and resulted in the caldera collapse (López-Hernández et al., 2009; Calcagno et al., 2018). Post-calderic eruptive events, resulting in scoria cones and basaltic lava flows, lasted until 0.06 Ma (Sosa-Ceballos et al., 2018). The Acoculco Caldera basement, from base to top, is formed by granite, Jurassic sandstones, Cretaceous calcarenites, limestones and marbles of the Sierra Madre Oriental, the Zacatlan-Chignahuapan basalt plateau and pre-calderic domes and lavas (10–3 Ma) (Campos-Enríquez et al., 2003; López-Hernández et al., 2009; Canet et al., 2015a; Calcagno et al., 2018; Avellán et al., 2018). The granitic intrusion, associated with at least four magma bodies at depths of 1 to > 2 km (Calcagno et al., 2018), has a presumed Late Cretaceous age since it produced a metamorphic aureole of marbles and skarns within the Cretaceous limestones (Sosa-Ceballos et al., 2018), suggesting temperatures above 350 °C (López-Hernández et al., 2009). Late-stage intrusions are represented by aplite dikes, cutting the skarn but not the overlying volcanic rocks (López-Hernández et al., 2009). Some preliminary studies performed by the National Mexican Power Company (Comisión Federal de Electricidad, CFE), identified Acoculco Caldera as a potential candidate for Enhanced Geothermal Systems (EGS) technology. Following this indication, the basement was regarded as a possible location for a geothermal reservoir (Hot Dry Rock Geothermal System, HDR), also considering that the overlying volcanites associated with the caldera are intensely hydrothermalized (López-Hernández et al., 2009; Pulido et al., 2010; Peiffer et al., 2014, 2015; Garcia-Valles et al., 2015; Canet et al., 2015b). DC Schlumberger surveys (Palma, 1987) and geochemical characterization of some local spring fluids (Tello-Hinojosa, 1986, 1987) provided the location of the first exploration borehole (i.e. EAC-1 well, drilled in 1995) in the Los Azufres area, where cold bubbling pools and extensive areas of argillic alteration are present (López-Hernández et al., 2009). Downhole measurements, analyses of samples and temperature logs (> 300 °C at ~2000 m depth) are reported in Tello-Hinojosa (1994), Palma (1995), García-Estrada (1995), Gama et al. (1995) and López-Hernandez and Castillo-Hernandez (1997). Despite the high geothermal gradient (three times the average for TMVB), a pure conductive heat transfer regime resulted from the downhole temperature profiles (López-Hernández et al., 2009; Canet et al., 2015a). Permeable zones with warm water and significant amount of gas were intercepted at shallow depth, nevertheless a deep water reservoir was not found (López-Hernández and Castillo-Hernández, 1997; López-Hernandez et al., 2009). Another well (EAC-2), distant from EAC-1 ~500 m to the NE, was drilled in 2008 (Viggiano-Guerra et al., 2011) and the active gas bubbling area of Alcaparrosa was also proposed for a possible future drilling of the EAC-3 well. Based on samples extracted from EAC-1 and EAC-2, Canet et al. (2010) identified two major zones of alteration in the subsurface rocks, i.e. a shallow one extending to 500-600 m depth with ammonium-argillic alteration of the volcanic rocks indicating temperatures > 200 °C, and a deeper one down to ~1000 m depth with an alteration assemblage of epidote–calcite–chlorite suggesting temperatures of ~240 °C. At greater depth, a calc-silicate paragenesis with wollastonite, garnet and diopside in marbles and skarns suggests temperatures above 350 °C (López-Hernández et al., 2009). Surficial rocks are characterized by a widespread silicic alteration, whilst advanced argillic alteration occurs principally near the gas manifestations of Los Azufres and Alcaparrosa (Canet et al., 2015a, 2015b).The composition of cold gas samples at Los Azufres and Alcaparrosa is dominated by $CO_2$, followed by $H_2S$. Accordingly, the waters discharging in these areas are acidic and $SO_4$-rich due to dissolution of $H_2S$ (and subsequent oxidation to $H_2SO_4$ at shallow levels) and are strongly different from the calcium-bicarbonate thermal waters discharged outside the Acoculco Caldera (e.g. Chignahuapan at SE) and the sodium-bicarbonate waters at the N periphery of the caldera and near Los Azufres (López-Hernández et al., 2009).

Although the AGF is considered since many years as a potential site for EGS technology, the possible occurrence of hot fluids at depth close the central sector of the Acoculco Caldera is still debates. Also, the identification of the origin and kinematic of regional and local faults/fracture systems represent another open question. Even if various geochemical studies were performed in the AGF for physico-chemical characterization of known natural manifestations, before the GeMex project no detailed investigation regarding the identification of source areas and description of fluid flow-path were never been performed. It is well known that rainfall is high in the Tulancingo-Acoculco area. At high altitude the average annual precipitation is about 1000 mm, whereas in the surrounding plains is about 600 mm (Lopez-Hernandez, 2009). Therefore, Acoculco's surrounding areas could represent the infiltration system. These represent two of the main topics of the investigation performed in Acoculco in the framework of the Task 4.3.

# Chapter 2

## WATER AND GAS GEOCHEMISTRY

### 2.1 Introduction

The AGF was studied in the framework of the task 4.3 with the same goals and approach used for Los Humeros. Regarding the locations of possible cold springs and wells located around AGF, before GeMex no large database was present. However, thanks to the collaboration and support with Mexican partners (Cicese Ensenada, UMSNH, University of Guanajuato, CFE) it was possible to obtained a suitable distribution of sampling points and measurements. Sampling trip was performed in January 25$^{th}$-February 06$^{th}$ 2018, in which 45 water and 3 dry gas samples were collected, and 418 measurements of $CO_2$ diffused from soils were carried out.

### 2.2 Waters: Sampling, field measurements and laboratory analyses

Water samples from 45 thermal and cold discharges, located inside and outside the Acoculco Caldera (Fig. 2.1), and free gas samples from three bubbling pools (one at Los Azufres and two at Alcaparrosa) were collected. Sampling and in-situ measurements (temperature, electrical conductivity, pH, total alkalinity, flow rate and dissolved oxygen) of cold and thermal waters from springs and wells were performed by portable devices. Sampled fluids were analysed in the IGG laboratories in Pisa and Florence (Italy). Collected samples were also analysed in laboratories of the CICESE (Ensenada). Three non-filtered and three filtered (0.45 μm) and acidified (two with ultrapure HCl and one with ultrapure $HNO_3$, respectively) water samples were collected in polyethylene bottles for the analysis of anions, isotopes of water ($\delta D\text{-}H_2O$ and $\delta^{18}O\text{-}H_2O$), $SiO_2$, cations, $NH_4$ and trace species, respectively. Total alkalinity was measured directly in the field and then checked in the lab by acidimetric titration (AT) with 0.01 N HCl using a Metrohm 794 automatic titration unit. The analytical error for AT analysis was ≤5%. The main anions ($Cl^-$, $SO_4^{2-}$, $NO_3^-$, $Br^-$, and $F^-$) and cations ($Na^+$, $K^+$, $Ca^{2+}$, $Mg^{2+}$) were analyzed by ion chromatography (IC) using Metrohm 761 and Metrohm 861 chromatographs, respectively. Instruments performance are the same as for fluids analyses of Los Humeros.

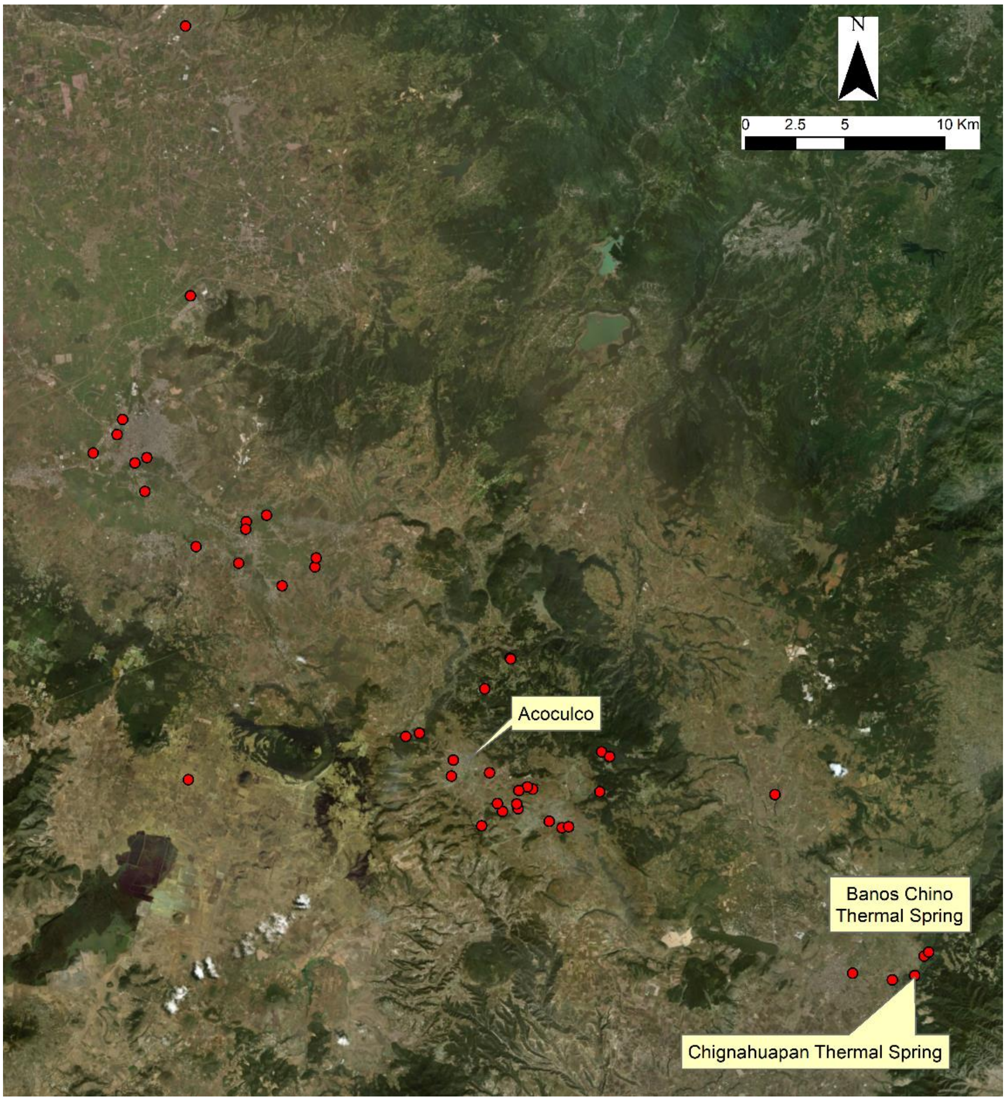

Figure 2.1 – Location of water samples from thermal and cold discharges of the Acoculco campaign.

### 2.2.1 Hydrogeochemical classification and binary plots

As regards the water samples, temperature and pH, chemical composition (main and trace solutes, in mg/L), TDS (total dissolved solids, in mg/L) and δD-$H_2O$ and $\delta^{18}O$-$H_2O$ (‰ V-SMOW) values are listed in Table A1-A (-A stands for Acoculco). Outlet temperatures ranging from 7.5 to 48.3 °C, while pH and TDS values varied respectively from 2.08 and 8.64 and between 94 and 1602 mg/L (see figure 2.2.1). Springs in Alcaparrosa and Los Azufres are clearly affected by dissolution of $H_2S$ and subsequent oxidation to $H_2SO_4$, which decrease pH values. During the sampling trip, smell of $H_2S$ was reported also close to other cold springs (AC-25, AC-47 and AC-48). $H_2S$ source is located within the Acoculco Caldera (López-Hernández et al., 2009; Peiffer et al., 2014) and its presence is ascertained by the chemical analysis of the sampled gases (Table A3-A).

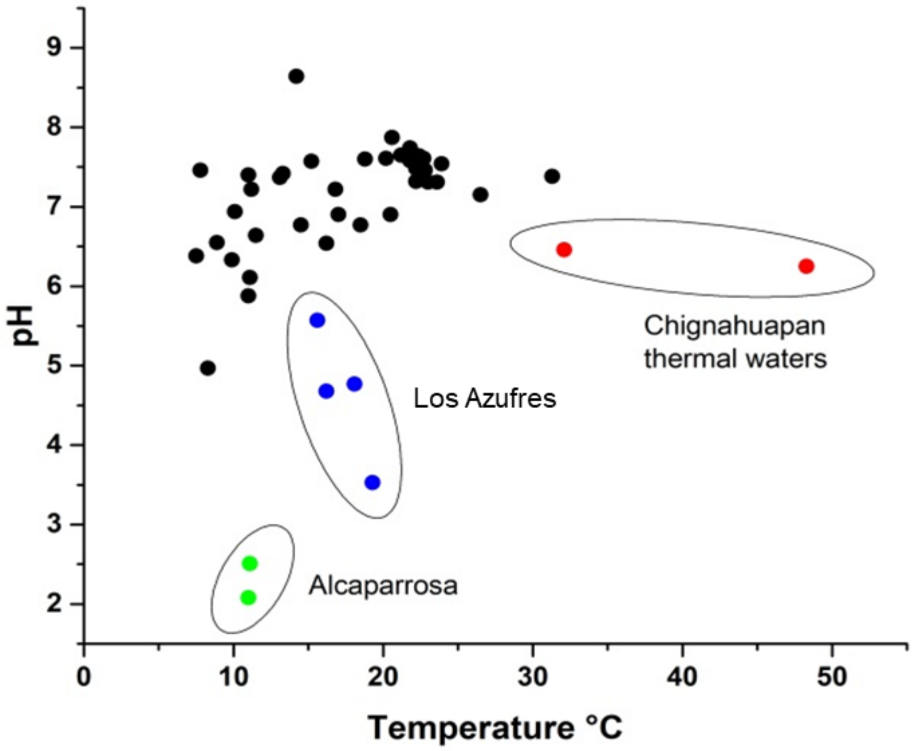

Figure 2.2.1 - Binary plot Temperature vs. pH of water samples of the Acoculco campaign. Samples from Los Azufres, Alcaparrosa and Chignahuapan are also highlighted in blue, green and red, respectively.

As for Los Humeros, the hydrogeochemical classification was performed using the LL-diagrams (Langelier-Ludwig, 1942). Variable compositions from $Ca^{2+}$–$SO_4^{2-}$ or $Na^+$–$SO_4^{2-}$ (acid or near-acid waters from the Acoculco Caldera, e.g. Los Azufres and Alcaparrosa) to $Ca^{2+}$–$HCO_3^-$ or $Na^+$–$HCO_3^-$ (especially from outside the caldera, e.g. Chignahuapan) were observed (Figs. 2.2.2-2.2.4). Moving away from the caldera, the waters tend to lose this contribution and the compositions become near-neutral calcium-sodium-bicarbonate, also due to the solubility difference between $H_2S$ and $CO_2$, with the latter more able to migrate towards the periphery of the system (Peiffer et al., 2014). The chemistry of the $Na^+$-$HCO_3^-$ waters is due to water-rock interaction processes involving Na-silicates of the volcanic rocks of the study area. On the other hand, most of the $Ca^{2+}$-$HCO_3^-$ samples (e.g. those from the Tulancingo area) are originated from meteoric water interacting with carbonates, which extensively outcrop around the AGF (e.g. in the Sierra Madre Oriental).

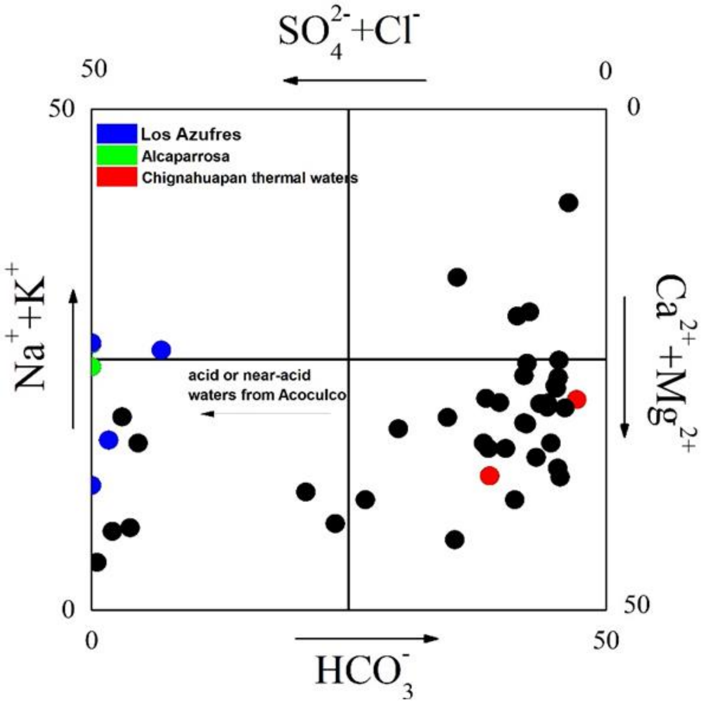


Figure 2.2.2 – $LL_{HCO3}$ diagram for collected waters in AGF.

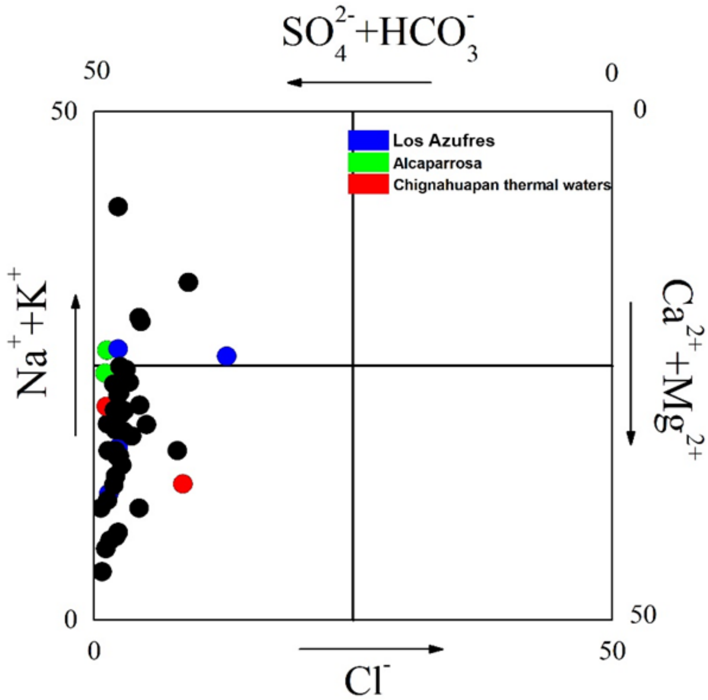


Figure 2.2.3 – $LL_{CL}$ diagram for collected waters in AGF

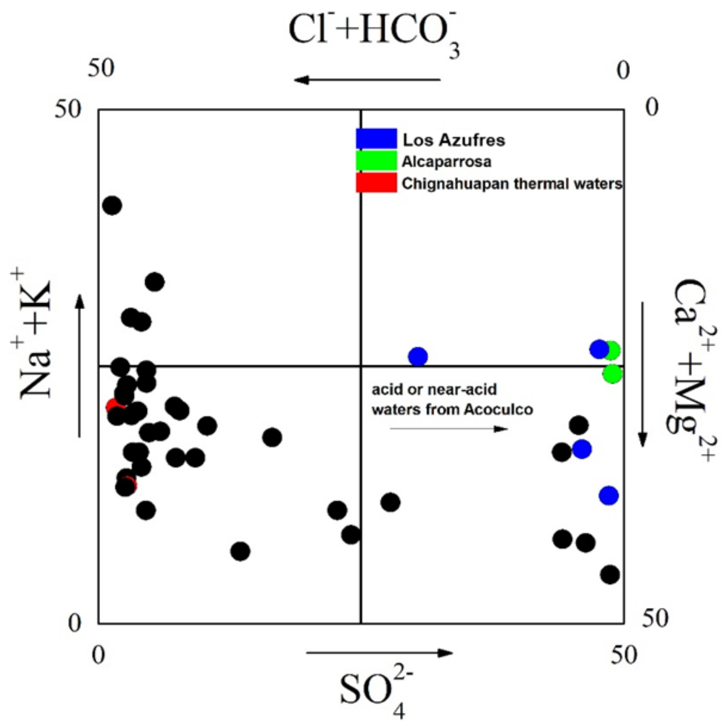


Figure 2.2.4 – $LL_{SO4}$ diagram for collected waters in AGF.

From the correlation plot $HCO_3$ vs $Cl+SO_4$ (figure 2.2.5 left) and Na vs K+Ca+Mg (figure 2.2.5 right), for collected thermal waters it is evident that $HCO_3$ and (Na+Ca), respectively are the most abundant anions and cations. Water from springs in Alcaparrosa and Los Azufres show high $SO_4$ concentration due to $H_2S$ dissolution and its oxidation to $H_2SO_4$. Same feature characterizes also three cold springs samples (AC25, AC47 and AC48), where smell of $H_2S$ was recognized during sampling activities.

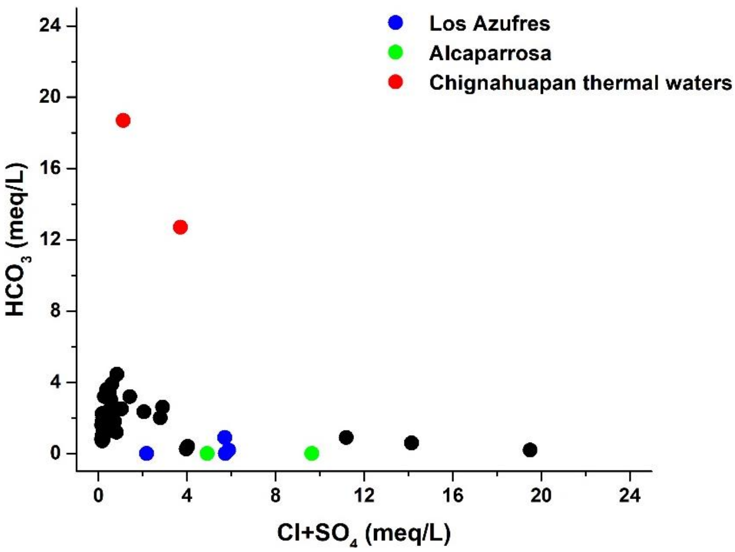


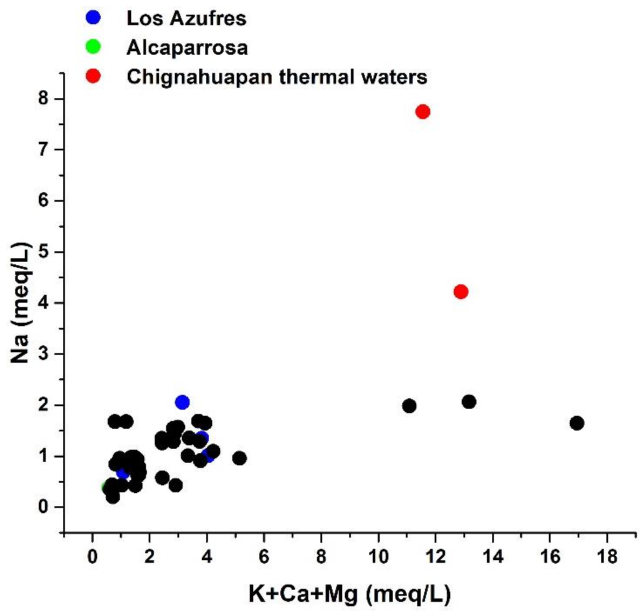


Figure 2.2.5 – Correlation plot $HCO_3$ vs Cl+$SO_4$ (left) and Na vs K+Ca+Mg (right) for collected water samples in AGF.

The acid samples AC-05, AC-06 and AC-07 from Los Azufres are also characterized by the highest contents of B and $NH_4^+$, testifying an input of hydrothermal fluids and dissolution of rocks/sediments at the surface close to the discharge points (see figure 2.2.5 left). The calcium-bicarbonate waters from Chignahuapan showed some features typical for hydrothermal fluids: i) relatively high TDS values; ii) relatively high temperature; iii) high $NH_4^+$, B and $Li^+$ concentrations (Table 2, Fig. 2.2.5 right). The relatively high concentrations of $HCO_3^-$ in Chignahuapan waters are likely controlled by $CO_2$ dissolution. Water from cold springs and wells are characterized by lower values of B and Li.

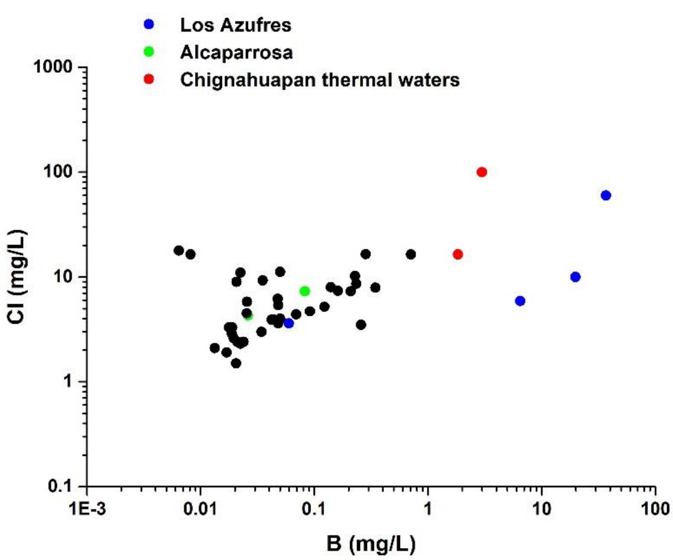


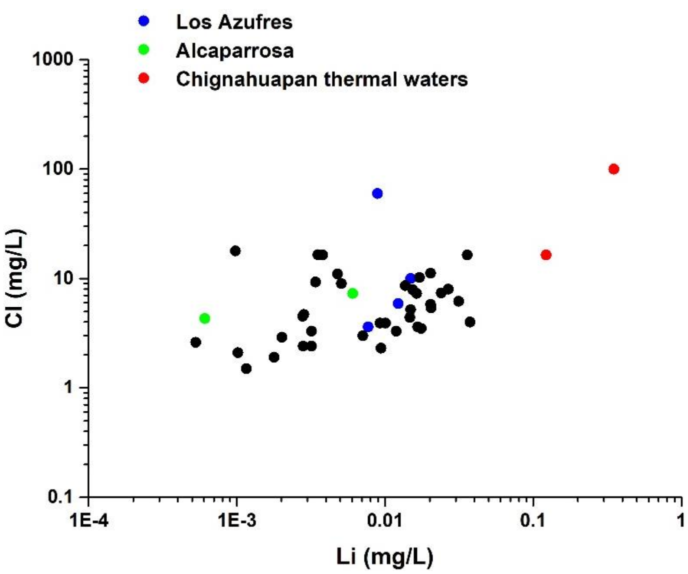


Figure 2.2.6 – Correlation plot B vs Cl (left) and Li vs Cl (right) for collected samples in the AGF.

### 2.2.2 Dissolved carbon dioxide

Taking into account the very low flux of $CO_2$ diffused from soil (see paragraph 2.4) and the goal of the task 4.3 regarding the identification of faults/fracture at local scale, which can be used by deep gases as vertical permeability, the dissolved $CO_2$ was calculated for waters collected in the AGF. The same approach for LHGF was used (Solveq numerical code, with soltherm98 database - Spycher N, Reed M.H., 1998). The results are shown in table A3_A (in appendix). Values for $P_{CO2}$ are generally less than 0.1 bar, a typical value for decomposition of organic matter and/or soil respiration. In thermal waters of Chignahuapan and Banos Chino higher values commonly found in hydrothermal systems were calculated (respectively 0.28 and 0.24 bars). Water samples located in the central sector of the Acoculco caldera (AC06, AC07, AC12, AC13, AC18, AC19 and AC25) are characterized by medium values. It could be interpreted, at least in part, as the results of CO2-rich gas rising from depth and interacting with circulating water at shallow levels (e.g. AC6 and AC7 are close to drilled boreholes EAC1 and EAC2). The geographical distribution of the dissolved $CO_2$ does not evidence any correlation with faults/fractures alignments.

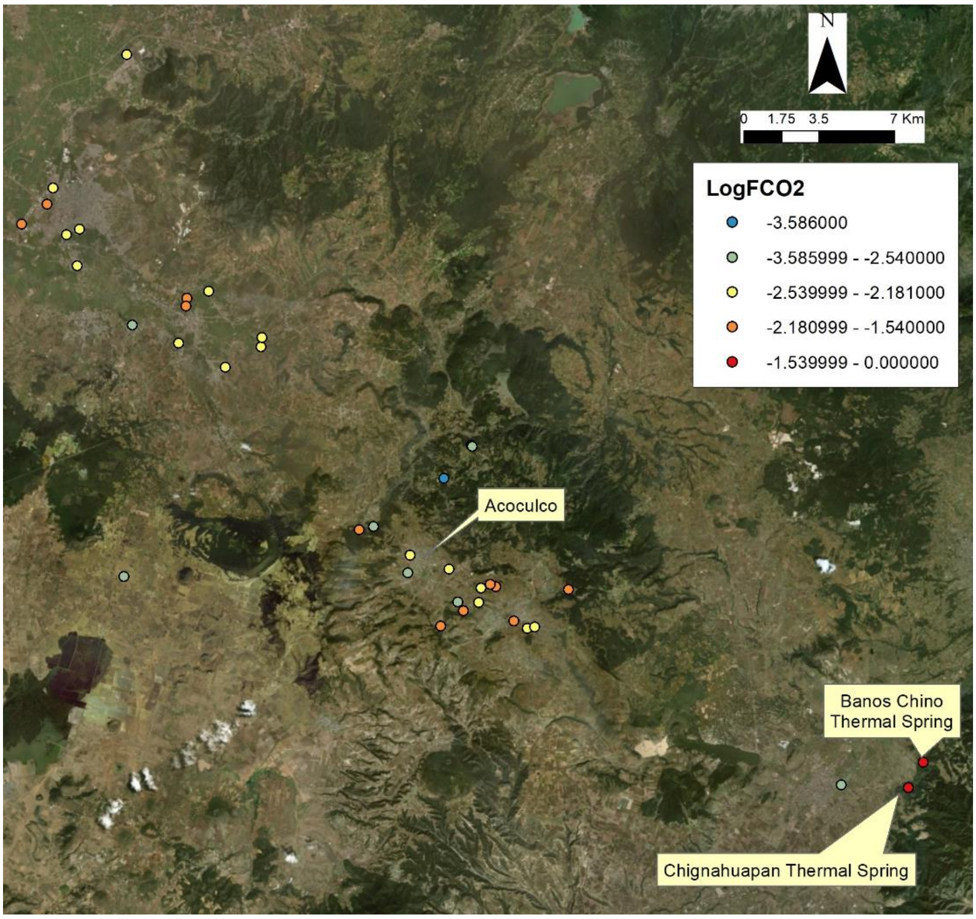


Figure 2.2.7 – Map of dissolved $P_{CO2}$ calculated for collected waters in AGF. Data are expressed as $LogCO_2$-fugacities.

### 2.2.3 Stable isotopes of water

The $\delta^2H$ and $\delta^{18}O$ values of $H_2O$ for the water samples collected in the AGF and its surrounding are shown in the correlation diagram of Figure 2.2.8, together with the worldwide meteoric water line (WMWL - $\delta^2H = 8\cdot\delta^{18}O+10$, Craig, 1961). As for reference, a meteoric water line (MWL) defined by Perez Quezadas et al. (2015) is also reported, even if it was defined using precipitation samples collected along a transect from the Port of Veracruz to Cofre de Perote. Therefore, it represent a local meteoric water line for the upwind Sierra Madre Oriental area and it is not specific for Acoculco area.

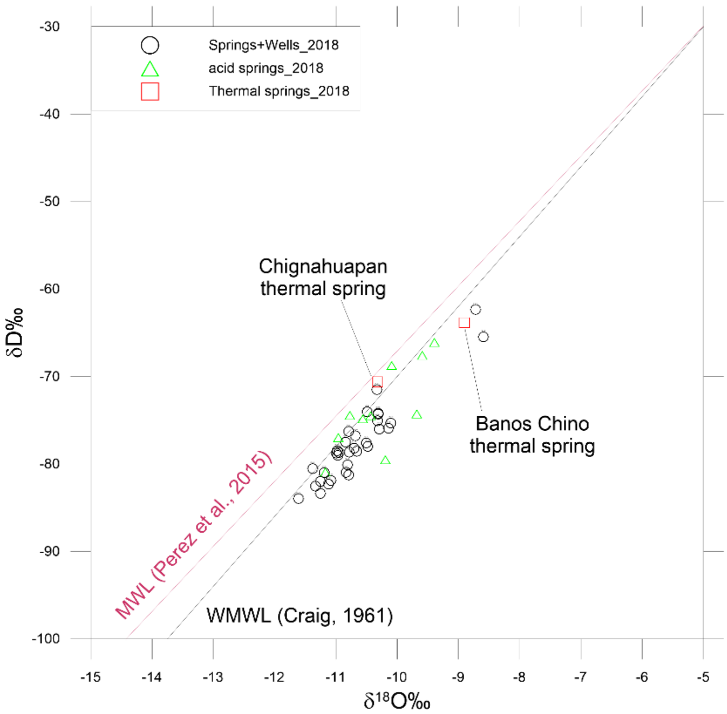


Figure 2.2.8 - Correlation diagram of $\delta^2H$-$H_2O$ vs. $\delta^{18}O$-$H_2O$ for the water samples collected in the AGF and its surroundings. The World Meteoric Water Line (WMWL – Craig, 1961) and Meteoric Water Line (MWL) by Perez et al. (2015) are also shown.

All samples plot preferentially along the WMWL, even if some of them are shifted to the right. This scatter of isotope values could be due to i) occurrence of evaporation processes, ii) water-rock interaction processes at the surface, combined or not with interaction with deep $CO_2$ (Chiodini et al., 2000). In fact, various samples are characterized by low pH values (evidenced in the figure 2.2.8 as acid springs) and presence of $CO_2$-rich gases at the discharge points. For what concerns the thermal waters sampled during this work, they plot close to the WMWL and are, therefore, of meteoric origin. The thermal spring of Banos Chino is the isotopically heavies water collected during this work and probably reflects a less altitude of infiltration. On the other hand, Banos Chino is characterized by a lower altitude for the discharge (2050 m.a.s.l.). Just two cold springs (AC20 and AC48) have the same isotopic signature, but they are probably affected by other processes: during the field trip a smell of $H_2S$ was reported and one of this (AC20) was collected during rain event.

In general, mean values of $\delta^2H$ and $\delta^{18}O$ for cold water collected in the AGF (excluding the acid waters) are similar to those for LHGF and this feature points out to the regionalization of the meteoric component.

## 2.3 Natural gas emissions

### 2.3.1 Sampling and laboratory measurements

Free gases at Los Azufres and Alcaparrosa were sampled using a plastic funnel up-side-down positioned above the bubbling sites and connected through a silicon tube to a pre-evacuated glass bottle equipped with a thorion valve (Vaselli et al., 2006) or to 40 mL gas vials equipped with a rubber septum instead of the glass bottle. The gas fraction ($CO_2$, $H_2S$, $N_2$, Ar, $O_2$ and $CH_4$) was analyzed by gas chromatography (GC) using a Shimadzu 15A instrument equipped with a Thermal Conductivity Detector (TCD). Argon and $O_2$ were separately analyzed using a Thermo Focus gas chromatograph equipped with a 30 m long capillary molecular sieve column and a TCD. Methane was determined by using a Shimadzu 14A gas chromatograph equipped with a Flame Ionization Detector (FID) and a 10 m long stainless-steel column packed with Chromosorb PAW 80/100 mesh coated with 23% SP 1700 (Vaselli et al. 2006). The analytical error for the GC analysis was ≤10%. The carbon isotopes in $CO_2$ (expressed as $\delta^{13}C\text{-}CO_2$ ‰ vs. V-PDB) were determined by using a Finnigan Delta Plus mass spectrometer (MS), after extracting and purifying $CO_2$ by using liquid $N_2$ and $N_2$-trichloroethylene cryogenic traps (Evans et al. 1998; Vaselli et al. 2006). Internal (Carrara and S. Vincenzo marbles) and international (NB18 and NBS19) standards were used for estimating the external precision. Analytical uncertainty and reproducibility were ±0.05‰ and ±0.1‰, respectively. The carbon isotopes in $CH_4$ (expressed as δ13C-CH4 ‰ vs. V-PDB) were measured by Cavity Ring-Down Spectroscopy (CRDS) using a Picarro G2201-i Analyzer. The errors of the CRDS analysis was <1 ‰. In order to avoid interferences, the instrument inlet line was equipped with (i) a Drierite trap and (ii) a copper trap for the removal of water vapor and $H_2S$, respectively. According to the operative ranges of the Picarro G2201-i instrument (up to 500 ppm), gas samples were diluted using a $N_2$-$O_2$-Ar gas mixture. The locations of the collected samples are shown in the map of figure 2.3.1, whereas the chemical and isotopic data are included in table A4_A (in appendix).

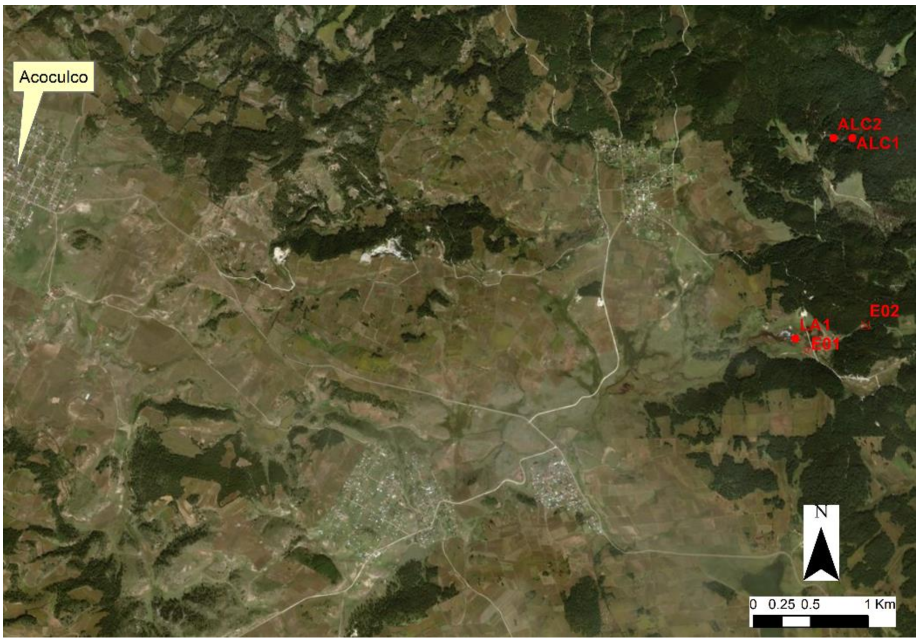


Figure 2.3.1 – Location map of dry gas samples collected from natural manifestation in AGF. Drilled boreholes EAC1 and EAC2 are also shown.

### 2.3.2 Chemical classification

For Alcaparrosa samples (ALC1 and ALC2), the $N_2/Ar$ ratios are higher than that of atmospheric air ($N_2/Ar$ = 83.5 – figure 2.3.2 left). Dry gas sample of Los Azufres plots along the line mantle-air, suggesting dilution processes with air of a deep component. In fact all gas samples show the $N_2/Ar$ ratios higher than that of water saturated air ($N_2/Ar$ = 38), possible indicating a deep fluids input. Los Azufres shows a different $N_2/CH_4$ ratio compared to Alcaparrosa samples, probably reflecting different redox conditions. This finding seems to be confirmed by the $\delta^{13}C-CH_4$ values, which are more negative than that for Alcaparrosa. However, all $\delta^{13}C-CH_4$ values are consistent with those typically related to thermogenic processes involving pre-existing organic matter (e.g. Schoell, 1980, 1988; Whiticar et al., 1986; Whiticar, 1999), thus $CH_4$ probably originated at reducing hydrothermal conditions. The $\delta^{13}C-CO_2$ values (Table 3) of the free gas samples are significantly less negative than those typically produced by biogenic processes ($\delta^{13}C-CO_2 \leq -20$ ‰ vs. V-PDB; e.g. O'Leary, 1988; Hoefs, 2009) and are consistent with the isotopic value measured by Peiffer et al. (2014) and in the range of gases from mantle degassing (from −9 to −2 ‰ vs. V-PDB; e.g. Javoy et al., 1982; Rollinson, 1993; Hoefs, 2009).

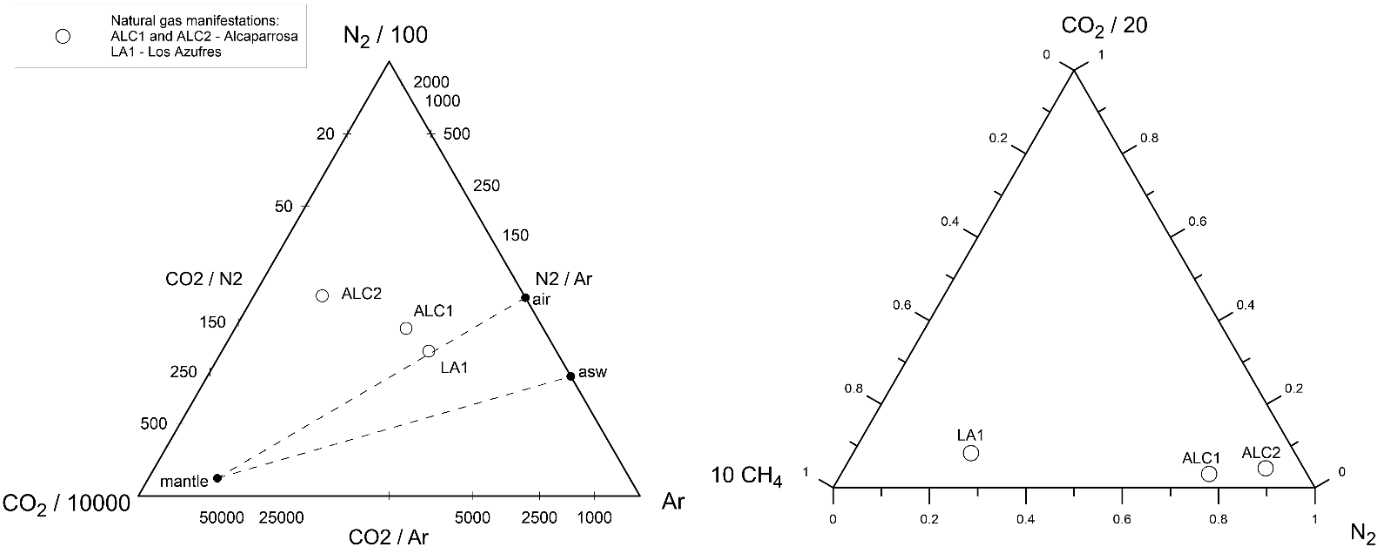


Figure 2.3.2 – Triangular plots $CO_2$-Ar-$N_2$ (left) and $CH_4$-$N_2$-$CO_2$ (right) for dry gas samples collected in AGF.

# Chapter 3
# Diffuse degassing
## 3.1 Field measurements

Before the field trip, some areas of interest in which to perform diffuse degassing measurement were selected according to the indication coming from geologists involved in the project. Among all the areas affected by tectonic features, one corresponding to the rectangle A1 (Fig. 3.1) was targeted for soil diffuse $CO_2$ degassing. In addition, another three areas (Los Azufres, Alcaparrosa and "Lagunilla") characterized by gas emission or argillic alteration of the soil were also investigated (Fig. 3.1). However, once in the field, the grid of the measurement points was adapted to the local conditions (i.e. presence of swamp, mud pools, vegetation, villages). The $\phi CO_2$ values were measured at 418 sites within the Acoculco Caldera using the Accumulation Chamber (AC) method (e.g. Chiodini et al., 1996, 1998, 2001; Gerlach et al., 2001; Cardellini et al., 2003). All measurements performed in the field are included in the table A5_A (in appendix).

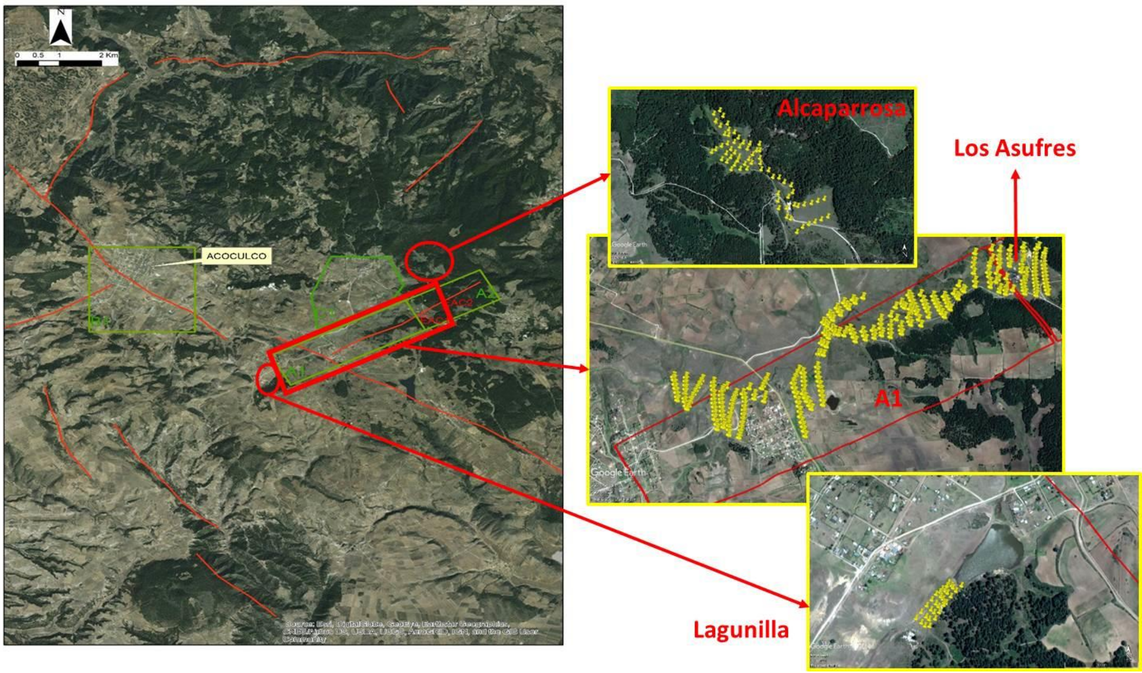


Figure 3.1 – The 418 sites of $\phi CO_2$ measurement within the Acoculco Caldera.

The instrumental apparatus used for the AC measurements consisted of: 1) a metal cylindrical vase (the chamber) with a basal area of 200 cm$^2$ and an inner volume of 3060 cm$^3$, 2) an Infra-Red (IR) spectrophotometer (Licor® Li-820). A low-flow pump (20 mL s$^{-1}$) conveyed the gas from the chamber positioned above the soil to the IR that provided continuous $CO_2$ measurements (up to 20,000 ppm), with an accuracy of 4%. The soil gas was re-injected into the chamber to minimize the disturbance effects due to changes of barometric conditions. The $\phi CO_2$ values were computed on the basis of the measured $CO_2$ concentrations over time ($dC_{CO2}\ dt^{-1}$), using a palmtop computer connected with the IR through an analog-digital (AD) converter and equipped with a software, according to the following equation:

$$(1)\ \phi CO_2 = cf \times dC_{CO2}\ dt^{-1}$$

The instrumentation was calibrated by using an induced flux in the laboratory and calculating the appropriate conversion factor (cf) between the native unit ppm/sec to the user unit (i.e. mol $m^{-2}$ $day^{-1}$). The cf factor was computed as the slope of the linear best-fit line of $\phi CO_2$ vs. $dC_{CO2}\ dt^{-1}$. Finally, $CO_2$ flux was obtained as mol $m^{-2}$ $day^{-1}$ as a function of temperature and atmospheric pressure, which were measured in the field during the measurements.

### 3.2 Results and discussion

The $\phi CO_2$ values range from 0.12 to 48.9 g $m^{-2}$ $day^{-1}$, whereas the average, median and standard deviation values were 12.6, 11.8 and 7.4 g $m^{-2}$ $day^{-1}$, respectively. The air temperature and pressure values varied from 1.5 to 20 °C and from 721 to 735 mbar, respectively.

To estimate the total amount of the released $CO_2$ fluxes, the measured data were processed using a classical graphical-statistical method (Sinclair, 1974, 1991). Through this approach, and not considering the highest flux outliers, six main flux populations were found within the area that includes the central polygon A1 and Los Azufres. Flux measurements in each previous areas have a normal distribution. This polymodal distribution is very likely due to the various types of soil encountered within the area, from the soft and marshy soil to the rocky substrate. Consequently, the database was divided into 6 classes and it was plotted together with the traces of the main known regional faults/fractures (Fig. 3.2). This map shows a general scatter of $CO_2$ flux values with no appreciable differences, crossing the main faults/fractures alignment. Just in the south-west side, in which the two main faults/fractures systems meet, a group of higher values seems to be localized. However, also in this area, $CO_2$ fluxes are very low and the presence of the village could affect some of the measurements.

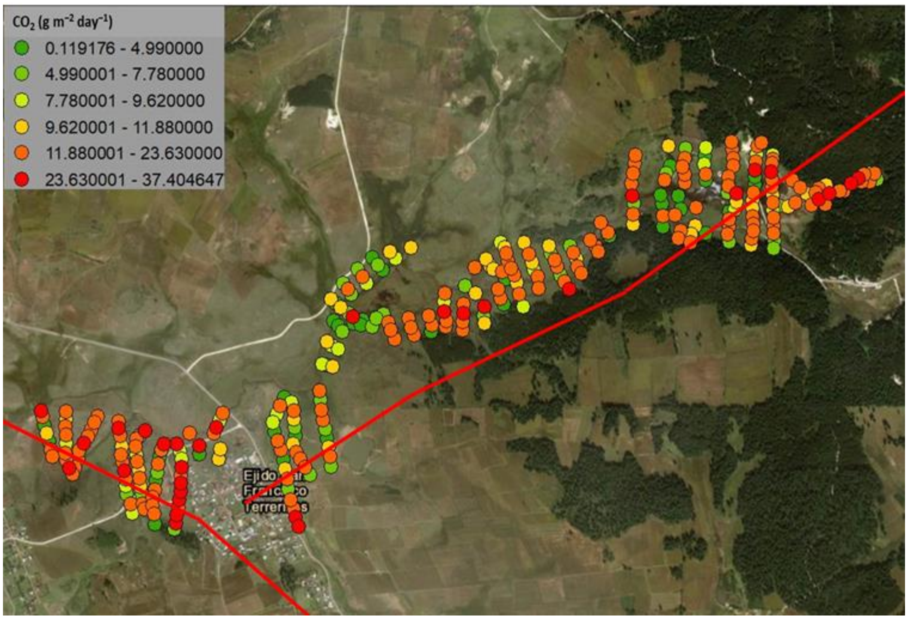


Figure 3.2 – Dot-map of the $CO_2$ flux values for the polygon A1 and Los Azufres areas. Traces of main regional faults/fractures are also reported.

Regarding the Alcaparrosa and “Lagunilla” areas, excluding outliers, the data distribution was normal. Thus, 3 classes of values were sufficient to represent the dot-maps (Fig. 3.3).

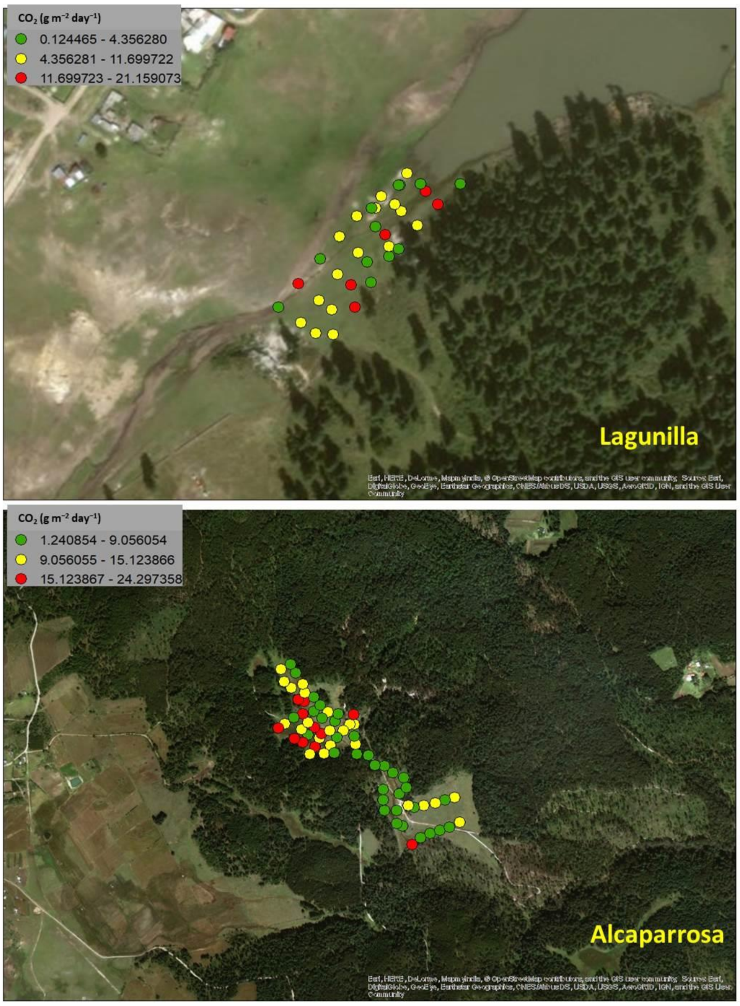


Figure 3.3 – Dot-maps of the $CO_2$ flux values for Alcaparrosa and “Lagunilla” areas.

Summing up, the $\phi CO_2$ results indicate that:

- $CO_2$ flux anomalies depending on preferential tectonic lines were not clearly observed;
- low $CO_2$ fluxes were measured (ranging between 0.12 and 48.9 g $m^{-2}$ $day^{-1}$), implying that most data were associated with soil respiration and reflecting low permeability conditions, at least at shallow levels.

The causes of these low flux values are likely due to the presence of large areas characterized by swamp and to the climate conditions during the survey, favoring a mostly water-saturated soil. However, similar measurements performed during the dry season gave the same indications (Peiffer et al., 2014).

According to the Sichel's t estimator (David, 1977), the total diffuse $CO_2$ outputs at the area of central polygon A1-Los Azufres, Alcaparrosa and "Lagunilla" were estimated in ~27, 2.3 and 0.1 t $day^{-1}$, respectively.

### 3.3 Conclusions

Sampling campaigns was performed in AGF in January 25$^{th}$-February 06$^{th}$ 2018, in which 45 water and 3 dry gas samples were collected, and 418 measurements of $CO_2$ diffused from soils were carried out. Sampling trip was performed in collaboration with CICESE (Ensenada), Guanajuato University and Michoacán University (UMSNH). Particular attention was focused on the selection of "target" areas in which to perform sampling of cold springs, providing information regarding the origin of fluids.

Chemical characterization of samples collected from cold springs and wells suggest an interaction between meteoric water and different rock types. The chemistry of the $Na^+$-$HCO_3^-$ waters is due to water-rock interaction processes involving Na-silicates of the volcanic rocks of the study area. Most of the $Ca^{2+}$-$HCO_3^-$ samples (e.g. those from the Tulancingo area) are originated from meteoric water interacting with carbonates, which extensively outcrop around the AGF (e.g. in the Sierra Madre Oriental). Acid waters enriched in $SO_4$ are originated by dissolution of deep $H_2S$, followed by the oxidation to $H_2SO_4$ at surface levels: in fact, this kind of springs are located close to or at the discharge point of natural gas manifestations (Los Azufres and Alcaparrosa sites). Dissolved $CO_2$ calculated in collected water samples doesn't show correlations with main alignments of regional faults/fractures. Just in Chignahuapan and Banos Chino thermal waters the dissolved $CO_2$ shows higher values, but anyway in the typical range of variation for hydrothermal systems.

For what concern the stable isotopic composition, cold waters from springs and wells follow the WMWL, even if some of them are shifted on the right. This scatter of isotope values could be due to i) occurrence of evaporation processes, ii) water-rock interaction processes at the surface, combined or not with interaction with deep $CO_2$. In fact, various samples are characterized by low pH values and presence of $CO_2$-rich gases at the discharge points. Mean values of $\delta^2H$ and $\delta^{18}O$ for cold water collected in the AGF (excluding the acid waters) are similar to those for LHGF and this feature point out to the regionalization of the meteoric component. Natural gas emissions sampled at Los Azufres and Alcaparrosa sites represent a mixing between deep component and surface one. Dry gas sample of Los Azufres suggest dilution processes with air of a deep component. In general, all gas samples show the $N_2/Ar$ ratios higher than that of water saturated air ($N_2/Ar = 38$), possible indicating a deep fluids input. Measurements of $CO_2$ flux diffused from the soil show low values, typically associated to soil respiration. In general, no clear correlation between geographical distribution of higher values of $CO_2$ fluxes and main regional faults/fractures alignments were evidenced. Just close to natural gas emission $CO_2$ fluxes reach higher values.

**Acknowledgements**
We want to thank the CFE staffs from Los Humeros and from Morelia for their collaboration, effort and helpful discussions before and during field trips. Finally, we are very grateful to Aída López Hernández, scientific coordinator of the GEMEX project, for her support during all phases of scientific activities.

**References**

Avellán, D.R., Macías, J.L., Layer, P.W., Cisneros, G., Sánchez-Núñez, J.M., Gómez-Vasconcelos, Pola, A., Sosa-Ceballos, G., García-Tenorio, F., Reyes-Agustín, G., Osorio-Ocampo, S., García-Sánchez, L., Mendiola, F., Marti, J., López-Loera, H., and Benowitz, J.: Geology of the Late Pliocene – Pleistocene Acoculco caldera complex, eastern Trans-Mexican Volcanic Belt (México). J. Maps, https://doi.org/10.1080/17445647.2018.153107, 2018.

Calcagno, P., Evanno, G., Trumpy, E., Gutiérrez-Negrín, L.C., Macías, J.L., Carrasco-Núñez, G., and Liotta, D.: Preliminary 3-D geological models of Los Humeros and Acoculco geothermal fields (Mexico) – H2020 GEMex Project. Adv. Geosci., 45, 321-333, https://doi.org/10.5194/adgeo-45-321-2018, 2018.

Campos-Enríquez, J.O., Alatriste-Vilchis, D.R., Huizar-Álvarez, R., Marines-Campos, R., Alatorre-Zamora, M.A.: Subsurface structure of the Tecocomulco subbasin (northeastern Mexico basin), and its relationship to regional tectonics. Geofis. Int., 42, 3–24, 2003.

Canet, C., Arana, L., González-Partida, E., Pi, T., Prol-Ledesma, R.M., Franco, S.I., Villanueva-Estrada, R.E., Camprubí, A., Ramírez-Silva, G., and López-Hernández, A.: A statistics-based method for the short-wave infrared spectral analysis of altered rocks: an example from the Acoculco Caldera, Eastern Trans-Mexican Volcanic Belt. J. Geochem. Explor., 105, 1–10, 2010.

Canet, C., Trillaud, F., Prol-Ledesma, R.M., González-Hernández, G., Peláez, B., Hernández-Cruz, B., and Sánchez-Córdova, M.M.: Thermal history of the Acoculco geothermal system, eastern México: insights from numerical modeling and radiocarbon dating. J. Volcanol. Geotherm. Res., 305, 56–62, 2015a.

Canet, C., Hernández-Cruz, B., Jiménez-Franco, A., Pi, T., Peláez, B., Villanueva-Estrada, R.E., Alfonso, P., González-Partida, E., and Salinas, S.: Combining ammonium mapping and short-wave infrared (SWIR) reflectance spectroscopy to constrain a model of hydrothermal alteration for the Acoculco geothermal zone, Eastern Mexico. Geothermics, 53, 154–165, 2015b.

Cardellini, C., Chiodini, G., Frondini, G.: Application of stochastic simulation to $CO_2$ flux from soil: mapping and quantification of gas release. J. Geophys. Res. 108, 2425, doi:10.1029/2002JB002165, 2003.

Chiodini, G., Frondini, F., Raco, B.: Diffuse emission of $CO_2$ from the Fossa crater, Vulcano Island. Bull. Volcanol. 58, 41–50, 1996.

Chiodini, G., Cioni, R., Guidi, M., Raco, B., Marini, L.: Soil $CO_2$ flux measurements in volcanic and geothermal areas. Appl. Geochem. 13, 543–552, 1998.

Chiodini G., Allard P., Caliro S., Parello F.: $^{18}O$ exchange between steam and carbon dioxide in volcanic and hydrothermal gases: Implications for the source of water. Geochimica et Cosmochimica Acta, Vol.64(14), 2479-2488, 2000.

Chiodini, G., Frondini, F., Cardellini, C., Granieri, D., Marini, L., Ventura, G.: $CO_2$ degassing and energy release at Solfatara volcano, Campi Flegrei, Italy. J. Geophys. Res. 106, 16213–16221, doi:10.1029/2001JB000246, 2001.

Craig, H.: Isotopic variations in meteoric waters. Science, 133, 1702–1703, 1961.

David, M.: Geostatistical Ore Reserve Estimation. Elsevier Sci., New York, 1977.

Gama, V.R., Martínez, E.I., Cedillo, R.F.: Informe geológico del pozo EAC-1. CFE-GPG internal report RG/HU/02/95, 26 p, 1995.

García-Estrada, G.H.: Comentarios sobre el modelo gravimétrico en Acoculco, Puebla. CFE-GPG internal report GF-AC-009/95, 10 p, 1995.

García-Palomo, A., Macías, J.L., Jiménez, A., Tolson, G., Mena, M., Sánchez-Núñez, J.M., Arce, J.L., Layer, P.W. Santoyo, M.A., and Lermo-Samaniego, J.: NW-SE Pliocene-Quaternary extension in the Apan-Acoculco region, eastern Trans-Mexican Volcanic Belt. J. Volcanol. Geoth. Res., 349, 240–255, 2017.

Garcia-Valles, M., Pi, T., Alfonso, P., Canet, C., Martínez, S., Jiménez-Franco, A., Tarrago, M., and Hernández-Cruz, B.: Kaolin from Acoculco (Puebla, Mexico) as raw material: Mineralogical and thermal characterization. Clay Miner., 50, 405–416, 2015.

Gerlach, T.M., Doukas, M.P., McGee, K.A., Klesser, R.: Soil efflux and total emission rates of magmatic $CO_2$ at the Horseshoe Lake tree kill, Mammoth Mountain California, 1995–1999. Chem. Geol. 177, 85–99, 2001.

Guevara, M., Santoyo, E., Perez-Zarate, D., and Almirudis, E.: Diffuse $CO_2$ Degassing to Study Blind Geothermal Systems: The Acoculco, Puebla (Mexico) Case Study. World Academy of Science, Engineering and Technology, 11(3), 641 – 645, 2017.

Hoefs, J.: Stable isotope geochemistry, 6th edn. Springer, Berlin, p. 288, 2009.

Javoy, M., Pineau, F., Allegre, C.J.: Carbon geodynamic cycle. Nature, 300 (5888), 171–173, 1982.

Langelier, W.F., and Ludwig, H.F.: Graphical methods for indicating the mineral character of natural waters. Journal (American Water Works Association), 34(3), 335-352, 1942.

López-Hernandez, A., and Castillo-Hernandez, D.: Exploratory Drilling at Acoculco, Puebla, México: A Hydrothermal System With Only Nonthermal Manifestations, (No. CONF-971048). Geothermal Resources Council Transactions 21, Davis, CA (United States), 1997.

López-Hernández, A., García-Estrada, G., Aguirre-Díaz, G., González-Partida, E., Palma-Guzmán, H., and Quijano-León, J.L.: Hydrothermal activity in the Tulancingo–Acoculco Caldera Complex, central Mexico: Exploratory studies. Geothermics, 38, 279–293, 2009.

O'Leary, M.H.: Carbon isotopes in photosynthesis. BioScience, 38, 328-336, 1988.

Pulido, C.L., Armenta, M.F., and Silva, G.R.: Characterization of the Acoculco Geothermal Zone as a HDR System. GRC Transactions, 34, 369–372, 2010.

Palma, G.S.H.: Estudio geoeléctrico en la zona geotérmica de La Alcaparrosa-Los Azufres (Acoculco), Puebla, Interpretación cualitativa. CFE-GPG internal report 16/87, 12 p., 1987.

Palma, G.S.H.: Análisis geoeléctrico para la ubicación de pozos exploratorios en el área geotérmica de Acoculco, Puebla. CFE-GPG internal report GF-AC-021/95, 21 p, 1995.

Peiffer, L., Bernard-Romero, R., Mazot, A., Taran, Y.A., Guevara, M., and Santoyo, E.: Fluid geochemistry and soil gas fluxes ($CO_2$–$CH_4$–$H_2S$) at a promissory Hot Dry Rock Geothermal System: The Acoculco caldera, Mexico. J. Volcanol. Geoth. Res., 284, 122–137, 2014.

Peiffer, L., Wanner, C., and Pan, L.: Numerical modeling of cold magmatic $CO_2$ flux measurements for the exploration of hidden geothermal systems. J. Geophys. Res.-Sol. Ea., 120, 6856–6877, https://doi.org/10.1002/2015JB012258, 2015.

Pérez Quezadas, J., Cortés Silva, A., Inguaggiato, S., del Rocío Salas Ortega, M., Cervantes Pérez, J., Michael Heilweil, V.: Meteoric isotopic gradient on the windward side of the Sierra Madre Oriental area, Veracruz – Mexico. Geofísica Internacional, 54(3), 267-276, 2015.

Rollinson, H.: Using Geochemical Data. Longman, London, UK, p. 352, 1993.

Schoell, M.: The hydrogen and carbon isotopic composition of methane from natural gases of various origins. Geochim. Cosmochim. Acta, 44, 649–661, 1980.

Schoell, M.: Multiple origins of methane in the Earth. Chem. Geol., 71, 1–10, 1988.

Sinclair, A.J.: Selection of thresholds in geochemical data using probability graphs. J. Geochem. Expl., 3, 129-149, 1974.

Sinclair, A.J.: A fundamental approach to threshold estimation in exploration geochemistry: probability plots revisited. J. Geochem. Expl., 41, 1-22, 1991.

Sosa-Ceballos, G., Macías, J.L., Avellán, D.R., Salazar-Hermenegildo, N., and Boijseauneau-López, M.E.: The Acoculco Caldera Complex magmas: genesis, evolution and relation with the Acoculco geothermal system. J. Volcanol. Geoth. Res., 358, 288–306, 2018.

Spycher N, Reed M.H. (1998). SOLVEQ: A Computer Program for Computing Aqueous Mineral Gas Equilibria. Department of Geological Sciences, University of Oregon, Eugene, OR., 28 pp.

Tello-Hinojosa, E.: Geoquímica de la zona geotérmica de la caldera de Acoculco, Puebla. CFE-GPG internal report 34/86, 15 p, 1986.

Tello-Hinojosa, E.: Composición química e isotópica del agua de los manantiales de Acoculco, Puebla. CFE-GPG internal report 23/87, 7 p, 1987.

Tello-Hinojosa, E.: Química de los fluidos hidrotermales de la zona geotérmica de la caldera de Acoculco, Puebla. CFE-GPG internal report GQ-013-94, 14 p, 1994.

Vaselli, O., Tassi, F., Montegrossi, G., Capaccioni, B., Giannini, L.: Sampling and analysis of volcanic gases. Acta Volcanologica 18, 65–76, 2006.

Viggiano-Guerra, J.C., Flores-Armenta, M., and Ramírez-Silva, G.R.: Evolución del sistema geotérmico de Acoculco, Pue., México: un estudio con base en estudios petrográficos del pozo EAC-2 y en otras consideraciones. Geotermia 24 (1), 14–24, 2011.

Whiticar, M.J., Faber, E., Schoell, M.: Biogenic methane formation in marine and freshwater environments: $CO_2$ reduction vs. acetate fermentation — isotopic evidence. Geochim. Cosmochim. Acta, 50, 693–709, 1986.

Whiticar, M.J.: Carbon and hydrogen isotope systematic of bacterial formation and oxidation of methane. Chem. Geol., 161, 291–314, 1999.

# APPENDIX

Table A1_A - Main physico-chemical parameters measured in the field for collected water samples (Acoculco). Total alkalinity was determined on the field by acid-base titration. DO stands for Dissolved Oxygen.

| ID | Station | Date, hour | Type | X(m) | Y(m) | Altitude (masl) | Depth (m) | Flow (L/min) | Temp. (°C) | pH | Cond. (μS/cm) | DO (mg/L) |
|---|---|---|---|---|---|---|---|---|---|---|---|---|
| AC-01 | Auditorio Chignahuapan | 25/01/18, 10:07 | cold spring | 604318 | 2193645 | 2261 | - | 28.2 | 17.3 | 6.95 | 287 | 7.08 |
| AC-02 | El Ameyal | 25/01/18, 11:39 | cold spring | 605912 | 2194837 | 2216 | - | 4.8 | 15.6 | 7.93 | 236 | 7.46 |
| AC-03 | Rio Zacatlan | 25/01/18, 11:50 | river | 605912 | 2194837 | 2216 | - | 51000 | 18.7 | 8.81 | 1094 | 7.78 |
| AC-04 | Baño Chino | 25/01/18, 12:37 | hot spring | 606132 | 2195045 | 2050 | - | 48 | 32.1 | 6.46 | 1590 | 1.09 |
| AC-05 | Pozo 1 CFE | 27/01/18, 10:51 | cold spring | 589590 | 2203103 | 2850 | - | - | 16.2 | 4.68 | 543.4 | 3.23 |
| AC-06 | Pozo 1 CFE | 27/01/18, 11:22 | cold spring | 589590 | 2203103 | 2850 | - | - | 18.1 | 4.77 | 553 | 4.62 |
| AC-07 | Pozo 1 CFE | 27/01/18, 12:15 | cold spring | 589590 | 2203103 | 2850 | - | 0.3 | 15.6 | 5.57 | 522.7 | 2.61 |
| AC-08 | Alcaparrosa | 27/01/18, 15:05 | cold spring | 589676 | 2205110 | 2828 | - | - | 11 | 2.08 | 3579 | 2.95 |
| AC-09 | Alcaparrosa | 27/01/18, 15:56 | cold spring | 590088 | 2204870 | 2844 | - | 3 | 11.1 | 2.6 | 24.2 | 3.29 |
| AC-10 | Pozo 1 CFE | 27/01/18, 17:04 | cold spring | 598406 | 2202965 | 2842 | - | 24.66 | 19.3 | 3.53 | 764 | 3.86 |
| AC-11 | Presilla | 28/01/18, 09:44 | cold spring | 587682 | 2201300 | 2870 | - | 10.8 | 15.2 | 7.57 | 355.3 | 6.81 |
| AC-12 | Rabanillo | 28/01/18, 10:19 | cold spring | 587041 | 2201626 | 2900 | - | 4.8 | 11.5 | 6.64 | 152.9 | 6.89 |
| AC-13 | La Agüitongo | 28/01/18, 11:13 | cold spring | 586209 | 2203240 | 2826 | - | 7.8 | 10.1 | 6.94 | 336.2 | 4.95 |
| AC-14 | La Agüitongo | 28/01/18, 12:57 | cold spring | 585951 | 2203344 | 2813 | - | 19.6 | 14.5 | 6.77 | 494.2 | 6.23 |
| AC-15 | Sn. Francisco Terrerillos | 29/01/18, 11:20 | cold spring | 588020 | 2201347 | 2854 | - | 2.52 | 11 | 7.4 | 463.2 | 6.78 |
| AC-16 | El Cristo | 29/01/18, 11:21 | cold spring | 585471 | 22022522 | 2758 | - | 3 | 9.9 | 6.33 | 553.6 | 6.71 |
| AC-17 | El Cristo | 29/01/18, 13:45 | cold spring | 585404 | 2202493 | 2803 | - | 18.6 | 11 | 5.88 | 434.8 | 6.22 |
| AC-18 | Ejido Sn. Jose Corral Blanco | 29/01/18, 12:49 | cold spring | 584688 | 2202116 | 2791 | - | - | 7.5 | 6.38 | 127.6 | 5.16 |
| AC-19 | El Cazadero | 29/01/18, 13:50 | cold spring | 583645 | 2201395 | 2790 | - | 3.92 | 11.2 | 7.22 | 396.8 | 2.57 |
| AC-20 | Rancho del Encanto | 29/01/18, 15:30 | cold spring | 584441 | 2202511 | 2770 | - | 480 | 7.8 | 7.46 | 173.7 | 8.2 |
| AC-21 | Baño Chino | 30/01/18, 9:45 | hot spring | 606132 | 2195045 | 2050 | - | - | 32.1 | 6.46 | 1590 | 1.09 |
| AC-22 | Agua del Aire | 30/01/18, 15:45 | cold spring | 584037 | 2204055 | 2802 | - | - | 8.9 | 6.55 | 100.4 | 4.39 |
| AC-23 | Acoculco | 30/01/18, 16:12 | cold spring | 582213 | 2204701 | 2768 | - | 4.44 | 13.1 | 7.37 | 248.2 | 3.43 |
| AC-24 | Pozo del Agua de Oro | 30/01/18, 16:45 | well | 582116 | 2203887 | 2760 | 140 |  | 22.4 | 7.64 | 645 | 2.44 |
| AC-25 | Tlahuitongo | 30/01/18, 17:21 | cold spring | 585510 | 2203167 | 2814 | - | 3.75 | 8.3 | 4.97 | 1660 | 5.91 |
| AC-26 | Balneario Agua Termal | 31/01/18, 10:55 | hot spring | 605437 | 2193867 | 2304 | - | - | 48.3 | 6.25 | 1566 | 0.16 |
| AC-27 | Laguna Chignahuapan | 31/01/18, 12:03 | cold spring | 602307 | 2193987 | 2267 | - | - | 18.8 | 7.6 | 351.1 | 6.91 |
| AC-28 | Ventoquipa | 01/02/18, 13:55 | cold spring | 569268 | 2215428 | 2228 | - | 17940 | 20.6 | 7.87 | 347.6 | 6.85 |
| AC-29 | Ventoquipa | 01/02/18, 14:12 | cold spring | 569268 | 2215428 | 2228 | - | 1440 | 20.2 | 7.61 | 163.6 | 6.83 |
| AC-30 | Tezoquipa-Almoloya | 01/02/18, 15:21 | cold spring | 571417 | 2214594 | 2221 | - | 1080 | 22.2 | 7.32 | 238.8 | 3.5 |
| AC-31 | Laguna Hueyapan | 01/02/18, 16:04 | cold spring | 575256 | 2214418 | 2258 | - | 750 | 23.9 | 7.54 | 464.7 | 5.59 |
| AC-32 | Pozo Valle Verde | 02/02/18, 10.45 | well | 564095 | 2220138 | 2172 | 300 | 360 | 23.6 | 7.31 | 683.5 | 4.66 |
| AC-33 | Pozo Prepa 2 | 02/02/18, 11:30 | well | 566193 | 2219643 | 2170 | 300 | ? | 21.8 | 7.58 | 392.5 | 5.31 |
| AC-34 | Pozo Moises Rivera | 02/02/18, 12:00 | well | 566692 | 2218203 | 2166 | 239 | 900 | 21.2 | 7.65 | 490.5 | 5.23 |
| ID | Station | Date, hour | Type | X(m) | Y(m) | Altitude (masl) | Depth (m) | Flow (L/min) | Temp. (°C) | pH | Cond. (μS/cm) | DO (mg/L) |
| AC-35 | Pozo 18 de marzo | 02/02/18, 12:20 | well | 566797 | 2219901 | 2197 | 103 | 1800 | 22.8 | 7.46 | 359 | 5.76 |
| AC-36 | Pozo Caracolitos | 02/02/18, 13:06 | well | 565295 | 2221068 | 2152 | 300 | 3600 | 23 | 7.31 | 389.5 | 5.67 |
| AC-37 | Pozo Peni | 02/02/18, 13:55 | well | 565574 | 2221823 | 2157 | 120 | 3600 | 22.7 | 7.61 | 943.1 | 6.39 |
| AC-38 | Pozo Napateco | 02/02/18, 14:27 | well | 568990 | 2228040 | 2151 | 170 | 1800 | 26.5 | 7.15 | 331.9 | 5.69 |
| AC-39 | La Soledad | 02/02/18, 15:30 | cold spring | 580514 | 2206046 | 2805 | - | - | 16.8 | 7.22 | 373 | 8.21 |
| AC-40 | El Tepeyac | 03/02/18, 14:20 | cold spring | 571799 | 2216682 | 2245 | - | - | 18.5 | 6.77 | 929.8 | 4.99 |
| AC-41 | Pozo Santa María | 03/02/18, 15:02 | well | 572820 | 2217004 | 2240 | n.k. | - | 31.3 | 7.38 | 463.9 | 1.71 |
| AC-42 | Ojito de Agua | 03/02/18, 16:43 | cold spring | 573595 | 2213459 | 2284 | - |  | 22.2 | 7.48 | 342.2 | 6.3 |
| AC-43 | Laguna Hueyapan | 03/02/18, 17:36 | cold spring | 575310 | 2214861 | 2267 | - | 80 | 20.5 | 6.9 | 369.7 | 3.56 |
| AC-44 | Tlacomulco | 03/02/18, 18:11 | well | 571763 | 2216309 | 2258 | n.k. |  | 17 | 6.9 | 520.7 | 1.87 |
| AC-45 | Los Laureles | 04/02/18, 13:50 | cold spring | 579830 | 2205884 | 2808 | - | 25 | 16.2 | 6.54 | 81.5 | 6.39 |
| AC-46 | Huiztongo | 04/02/18, 15:09 | river | 583797 | 2208283 | 2489 | - | 390 | 14.2 | 8.64 | 430.8 | 7.74 |
| AC-47 | Las Tires | 04/02/18, 16:25 | cold spring | 585072 | 2209822 | 2637 | - | 3.3 | 11.1 | 6.11 | 1113 | 3.39 |
| AC-48 | Las Tires | 04/02/18, 17:04 | cold spring | 585105 | 2209776 | 2588 | - | - | 13.3 | 7.42 | 989.5 | 7.22 |
| AC-49 | Coatzetzengo | 05/02/18, 16:00 | well |  |  | 2790 | n.k. |  | 22.7 | 7.39 | 580.6 | 5.66 |
| AC-50 | Coatzetzengo | 05/02/18, 17:38 | well | 568878 | 2203713 | 2623 | n.k. |  | 21.8 | 7.74 | 180.4 | 5.71 |
| AC-51 | Col. Ignacio Zaragoza | 06/02/18, 15:40 | well | 568738 | 2241603 | 2181 | 200 | 2160 | 19.5 | 7.86 | 167.2 | 5.14 |

n.k. – not known

Table A2_A – Concentration of chemical species determined in collected water samples (Acoculco). Data are expressed in mg/L. Stable isotopic composition of Deuterium and 18-oxygen are also included (data are referred to the V-SMOW).

| ID | $HCO_3^-$ | $F^-$ | $Cl^-$ | $Br^-$ | $NO_3^-$ | $SO_4^{2-}$ | $PO_4^{3-}$ | $Ca^{2+}$ | $Mg^{2+}$ | $Na^+$ | $K^+$ | $NH_4^+$ | $Li^+$ | B | $SiO_2$ | δD‰ | $\delta^{18}O$‰ |
|---|---|---|---|---|---|---|---|---|---|---|---|---|---|---|---|---|---|
| AC-05 | - | 1.1 | 5.9 | n.d. | 0.14 | 267 | n.d. | 58 | 11.7 | 23.3 | 10.2 | 2.2 | 0.012 | 6.5 | 73 | -66.1 | -9.4 |
| AC-06 | 12 | 1.1 | 10 | 0.08 | 0.28 | 269 | n.d. | 47 | 13 | 31 | 16 | 2.2 | 0.015 | 20 | 76 | -67.6 | -9.6 |
| AC-07 | 55 | 0.42 | 60 | n.d. | 3.4 | 193 | n.d. | 37.7 | 10 | 48.3 | 25.6 | 5.7 | 0.009 | 37 | 84 | -74.8 | -10.6 |
| AC-08 | - | 0.52 | 7.3 | n.d. | 0.13 | 453 | n.d. | 7.6 | 2.1 | 9.7 | 3.9 | 0.51 | 0.006 | 0.08 | 96 | -68.7 | -10.1 |
| AC-09 | - | 0.37 | 1.5 | 0.05 | 0.1 | 230 | n.d. | 6.9 | 1.2 | 8.7 | 4.8 | 0.59 | 0.001 | 0.03 | 97 | -74.5 | -10.8 |
| AC-10 | - | 0.64 | 3.6 | 0.03 | 0.21 | 99 | n.d. | 11.7 | 2.9 | 15.8 | 9.9 | 0.32 | 0.008 | 0.06 | 88 | -77 | -11 |
| AC-11 | 153 | 0.46 | 9.3 | 0.09 | 4.4 | 13 | n.d. | 28.5 | 11.3 | 13.2 | 3.6 | 0.11 | 0.003 | 0.04 | 56 | -82.5 | -11.3 |
| AC-12 | 73 | 0.31 | 2.4 | 0.06 | 0.19 | 14 | n.d. | 11.8 | 4.8 | 9.9 | 1.5 | 0.14 | 0.003 | 0.02 | 42 | -78.2 | -10.7 |
| AC-13 | 153 | 0.32 | 2.9 | 0.06 | 0.32 | 46 | n.d. | 32.3 | 15.3 | 9.8 | 1.7 | 0.1 | 0.002 | 0.02 | 47 | -82.3 | -11.1 |
| AC-14 | 122 | 0.37 | 4.5 | 0.09 | 5.3 | 128 | n.d. | 48.5 | 20 | 25.2 | 6.2 | 0.11 | 0.003 | 0.03 | 70 | -81.3 | -10.8 |
| AC-15 | 159 | 0.33 | 9 | 0.11 | 4.5 | 127 | n.d. | 58 | 26.2 | 22 | 3.7 | 0.02 | 0.005 | 0.02 | 68 | -82 | -11.3 |
| AC-16 | 24 | 0.51 | 4.4 | 0.07 | 0.05 | 188 | n.d. | 43 | 12.4 | 31.2 | 8.7 | 0.13 | 0.015 | 0.07 | 93 | -74.3 | -9.7 |
| AC-17 | 15 | 0.52 | 3.9 | 0.02 | 0.26 | 185 | n.d. | 34.1 | 11.5 | 33.2 | 8.4 | 0.14 | 0.009 | 0.04 | 107 | -79.5 | -10.2 |
| AC-18 | 49 | 0.3 | 1.9 | 0.04 | 0.01 | 7.5 | n.d. | 8.5 | 2.8 | 8.6 | 3.5 | 0.09 | 0.002 | 0.02 | 54 | -83.4 | -11.3 |
| AC-19 | 220 | 0.45 | 5.8 | 0.04 | 0.06 | 10 | n.d. | 32.5 | 18.2 | 23.2 | 8.8 | <0.01 | 0.02 | 0.03 | 83 | -81 | -10.8 |
| AC-20 | 79 | 0.41 | 4.7 | 0.01 | 0.03 | 4.5 | n.d. | 8.5 | 3 | 19.3 | 5.8 | 0.1 | 0.003 | 0.09 | 20 | -65.5 | -8.6 |
| AC-21 | 1141 | 1.8 | 16 | 0.09 | 0.04 | 32 | n.d. | 148 | 46.2 | 178 | 14.7 | 0.72 | 0.12 | 1.8 | 22 | -63.9 | -8.9 |
| AC-22 | 43 | 0.2 | 1.5 | 0.03 | 1.3 | 6.2 | n.d. | 7.5 | 3 | 4.7 | 3.6 | 0.08 | 0.001 | 0.02 | 33 | -75.9 | -10.1 |
| AC-23 | 127 | 0.52 | 3.3 | 0.03 | 2.3 | 8.5 | 0.22 | 16.6 | 7.1 | 18.2 | 8 | 0.09 | 0.012 | 0.02 | 81 | -81 | -11.2 |
| AC-24 | 137 | 0.76 | 4 | 0.02 | 0.03 | 3 | n.d. | 6.3 | 1.8 | 38.6 | 12.8 | 0.6 | 0.038 | 0.05 | 81 | -76.8 | -10.7 |
| AC-25 | 12 | 1.8 | 11 | 0.13 | 9.9 | 921 | n.d. | 242 | 57.5 | 37.8 | 5.3 | n.d. | 0.02 | 0.05 | 78 | -80.9 | -11.2 |
| AC-26 | 775 | 1.6 | 100 | 0.34 | 0.55 | 43 | n.d. | 203 | 29 | 97 | 14.6 | 0.8 | 0.35 | 3 | 1.9 | -70.6 | -10.3 |
| AC-27 | 98 | 0.3 | 2.4 | 0.02 | 3.2 | 4.3 | n.d. | 13.8 | 8.8 | 9.7 | 3.5 | 0.14 | 0.003 | 0.02 | 49 | -71.5 | -10.3 |
| AC-28 | 90 | 0.46 | 11 | 0.03 | 9.6 | 7.2 | n.d. | 12 | 11 | 14.5 | 4.8 | 0.05 | 0.005 | 0.02 | 66 | -78.7 | -11 |
| AC-29 | 120 | 0.4 | 3.3 | 0.03 | 8.8 | 6.9 | 0.16 | 11.8 | 10.7 | 14.1 | 4.7 | 0.14 | 0.003 | 0.02 | 67 | -79 | -11 |
| AC-30 | 122 | 0.49 | 3.9 | 0.06 | 4.1 | 5.2 | 0.16 | 14 | 8.4 | 21.6 | 7.2 | 0.11 | 0.01 | 0.04 | 60 | -78.7 | -10.8 |
| AC-31 | 116 | 0.62 | 3.5 | 0.04 | 2.6 | 5 | n.d. | 13.3 | 6.1 | 17.8 | 5.9 | 0.1 | 0.018 | 0.26 | 60 | -81.9 | -11.1 |
| AC-32 | 195 | 0.52 | 5.4 | 0.04 | 2 | 5.9 | 0.24 | 18.6 | 15.5 | 29 | 9.1 | 0.1 | 0.021 | 0.05 | 69 | -74.1 | -10.5 |
| AC-33 | 185 | 0.74 | 7.3 | 0.09 | 10 | 17 | n.d. | 30.5 | 12.9 | 29.5 | 9.6 | 0.06 | 0.016 | 0.21 | 53 | -78 | -10.5 |
| AC-34 | 238 | 0.54 | 8.6 | 0.05 | 17 | 18 | n.d. | 44.3 | 15.7 | 29.6 | 9.8 | 0.09 | 0.014 | 0.23 | 57 | -77.6 | -10.5 |
| AC-35 | 153 | 0.9 | 10 | 0.08 | 20 | 23 | n.d. | 25.1 | 11.3 | 31.1 | 9.7 | 0.06 | 0.017 | 0.23 | 57 | -78.5 | -10.7 |
| AC-36 | 207 | 0.69 | 8 | 0.09 | 6.2 | 13 | n.d. | 27.7 | 14.5 | 35.5 | 10 | 0.04 | 0.027 | 0.14 | 64 | -76 | -10.3 |
| AC-37 | 220 | 0.6 | 7.4 | 0.08 | 6.6 | 12 | n.d. | 28 | 16 | 36.1 | 10.7 | 0.09 | 0.024 | 0.16 | 42 | -74.3 | -10.3 |
| AC-38 | 98 | 1.1 | 6.2 | 0.06 | 4.2 | 7.6 | n.d. | 10.7 | 3.1 | 22 | 6.5 | 0.08 | 0.031 | 0.05 | 62 | -80.5 | -11.4 |
| AC-39 | 61 | 0.4 | 2.6 | 0.04 | 1.5 | 5.2 | n.d. | 7.7 | 2.3 | 10.1 | 4.6 | 0.12 | 0.001 | 0.02 | 74 | -78.5 | -11 |
| AC-40 | 271 | 0.72 | 7.9 | 0.1 | 16 | 30 | 0.5 | 41.3 | 16 | 38.8 | 12.7 | 0.04 | 0.015 | 0.34 | 66 | -74.2 | -10.3 |
| AC-41 | 110 | 1.4 | 16 | 0.08 | 0.5 | 13 | n.d. | 11.6 | 4.6 | 38.5 | 8.7 | 0.08 | 0.036 | 0.71 | 75 | -77.5 | -10.8 |
| AC-42 | 112 | 0.77 | 3.6 | 0.04 | 4.7 | 4 | 0.4 | 13.3 | 6.1 | 22.5 | 7.2 | 0.02 | 0.017 | 0.05 | 64 | -78.7 | -11 |
| AC-43 | 73 | 0.5 | 5.2 | 0.03 | 9.8 | 32 | 1 | 17.4 | 7.5 | 15.7 | 6.3 | 0.12 | 0.015 | 0.12 | 17 | -76.3 | -10.8 |
| AC-44 | 195 | 0.63 | 17 | 0.06 | 22 | 46 | 6.5 | 43.8 | 15.3 | 37.9 | 19.5 | 0.06 | 0.004 | 0.28 | 20 | -75.1 | -10.3 |
| AC-45 | 49 | 0.23 | 2.3 | 0.02 | 1.5 | 4.2 | 0.11 | 6.7 | 2.2 | 8.1 | 3.9 | 0.06 | 0.009 | 0.02 | 16 | -84 | -11.6 |
| AC-46 | 143 | 0.42 | 2.1 | 0.02 | 0.42 | 96 | 0.46 | 53 | 12.3 | 21 | 4.8 | 0.1 | 0.001 | 0.01 | 54 | -75.3 | -10.1 |
| AC-47 | 37 | 0.69 | 16 | 0.15 | 0.7 | 657 | 1.6 | 192 | 39.6 | 47.4 | 13.2 | 0.09 | 0.004 | 0.01 | 26 | -74.5 | -10.4 |
| AC-48 | 55 | 0.54 | 18 | 0.18 | 0.68 | 513 | n.d. | 165 | 32.6 | 45.6 | 6.7 | 0.12 | 0.001 | 0.01 | 29 | -62.3 | -8.7 |
| AC-50 | 122 | 0.75 | 3 | 0.06 | 6.6 | 5.8 | 0.15 | 13.4 | 7.8 | 22.6 | 6 | 0.14 | 0.007 | 0.03 | 21 | -80.1 | -10.8 |

n.d. – not determined

Table A3_A – Dissolved $CO_2$ calculated for collected waters in AGF

| Code | $P_{CO2}$(bars) | $CO_{2(aq)}$ (mmol/L) | logFCO2 |
|---|---|---|---|
| AC-11 | 0.003313 | 0.1586 | -2.482 |
| AC-12 | 0.008668 | 0.4603 | -2.065 |
| AC-13 | 0.01074 | 0.5936 | -1.972 |
| AC-14 | 0.01213 | 0.5918 | -1.919 |
| AC-15 | 0.004509 | 0.2429 | -2.348 |
| AC-16 | 0.003928 | 0.2184 | -2.408 |
| AC-18 | 0.007416 | 0.4425 | -2.133 |
| AC-19 | 0.009228 | 0.4942 | -2.037 |
| AC-20 | 0.002 | 0.1183 | -2.702 |
| AC-21 | 0.2369 | 7.39 | -0.6274 |
| AC-22 | 0.005516 | 0.3159 | -2.261 |
| AC-23 | 0.004128 | 0.2095 | -2.387 |
| AC-24 | 0.002887 | 0.1141 | -2.542 |
| AC-26 | 0.2825 | 6.248 | -0.5508 |
| AC-27 | 0.002132 | 0.09257 | -2.674 |
| AC-28 | 0.001102 | 0.04562 | -2.96 |
| AC-29 | 0.002597 | 0.1087 | -2.588 |
| AC-30 | 0.005047 | 0.2005 | -2.299 |
| AC-31 | 0.0031 | 0.1179 | -2.511 |
| AC-32 | 0.0083 | 0.3182 | -2.083 |
| AC-33 | 0.004281 | 0.1719 | -2.371 |
| AC-34 | 0.004627 | 0.1886 | -2.337 |
| AC-35 | 0.004678 | 0.183 | -2.332 |
| AC-36 | 0.008669 | 0.3375 | -2.064 |
| AC-37 | 0.004817 | 0.189 | -2.319 |
| AC-38 | 0.006183 | 0.2205 | -2.211 |
| AC-39 | 0.002901 | 0.1329 | -2.54 |
| AC-40 | 0.029 | 1.269 | -1.54 |
| AC-41 | 0.004629 | 0.1472 | -2.337 |
| AC-42 | 0.003316 | 0.1317 | -2.482 |
| AC-43 | 0.006634 | 0.2755 | -2.181 |
| AC-44 | 0.01627 | 0.7414 | -1.791 |
| AC-45 | 0.007357 | 0.3427 | -2.136 |
| AC-46 | 0.000261 | 0.01285 | -3.586 |
| AC-47 | 0.007374 | 0.3959 | -2.135 |
| AC-48 | 0.001473 | 0.0743 | -2.834 |
| AC-50 | 0.00203 | 0.08148 | -2.695 |
| AC-05 | | | |
| AC-06 | 0.004409 | 0.195 | -2.358 |
| AC-07 | 0.01653 | 0.7822 | -1.784 |
| AC-08 | | | |
| AC-09 | | | |
| AC-10 | | | |
| AC-17 | 0.003603 | 0.1941 | -2.446 |
| AC-25 | 0.003255 | 0.1895 | -2.49 |

Table A4_A – Chemical and isotope data for collected gas from natural manifestations in AGF. Data for $CO_2$, $H_2S$, $N_2$, Ar, $O_2$ and $CH_4$ are expressed in % v/v. $\delta^{13}C\text{-}CO_2$ and $\delta^{13}C\text{-}CH_4$ are expressed in ‰ and are referred to v-PDB

| ID | DATE | TYPE | $CO_2$ | $H_2S$ | $N_2$ | Ar | $O_2$ | $CH_4$ | $\delta^{13}C\text{-}CO_2$ | $\delta^{13}C\text{-}CH_4$ |
|---|---|---|---|---|---|---|---|---|---|---|
| ALC1 | 30/01/2018 | free gas | 97.2 | 0.13 | 0.78 | 0.011 | 0.009 | 1.83 | -4.1 | -33.8 |
| ALC2 | 30/01/2018 | free gas | 91.5 | 0.69 | 2.71 | 0.031 | 0.007 | 5.1 | -4.1 | -34 |
| LA1 | 28/01/2018 | free gas | 98.9 | 0.29 | 0.61 | 0.008 | 0.005 | 0.18 | -4.5 | -40.5 |

Table A5_A – Temperature and $CO_2$ flux measurements performed in AGF. Data on air temperature and pressure are also included.

| ID | Date | X(m) | Y(m) | $T_{air}$ (°C) | $P_{air}$ (mbar) | $CO_2$ Flux (g $m^{-2}$ $day^{-1}$) |
|---|---|---|---|---|---|---|
| 1 | 27/01/2018 | 589777 | 2202915 | 19 | 723 | 5.66 |
| 2 | 27/01/2018 | 589780 | 2202945 | 19 | 723 | 5.31 |
| 3 | 27/01/2018 | 589777 | 2202977 | 19 | 723 | 15.45 |
| 4 | 27/01/2018 | 589775 | 2203008 | 19 | 723 | 13.09 |
| 5 | 27/01/2018 | 589774 | 2203041 | 19 | 723 | 16.15 |
| 6 | 27/01/2018 | 589773 | 2203073 | 19.5 | 723 | 7.89 |
| 7 | 27/01/2018 | 589771 | 2203104 | 19.5 | 723 | 14.01 |
| 8 | 27/01/2018 | 589771 | 2203134 | 19.5 | 723 | 10.24 |
| 9 | 27/01/2018 | 589769 | 2203169 | 19.5 | 723 | 16.6 |
| 10 | 27/01/2018 | 589767 | 2203199 | 20 | 723 | 19.62 |
| 11 | 27/01/2018 | 589764 | 2203232 | 20 | 723 | 29.26 |
| 12 | 27/01/2018 | 589767 | 2203265 | 20 | 722 | 19.95 |
| 13 | 27/01/2018 | 589770 | 2203281 | 20 | 722 | 16.78 |
| 14 | 27/01/2018 | 589772 | 2203301 | 19 | 722 | 9.54 |
| 15 | 27/01/2018 | 589723 | 2203351 | 19 | 722 | 22.37 |
| 16 | 27/01/2018 | 589706 | 2203336 | 19 | 722 | 18.37 |
| 17 | 27/01/2018 | 589702 | 2203304 | 19 | 722 | 9.54 |
| 18 | 27/01/2018 | 589698 | 2203271 | 19.5 | 722 | 14.93 |
| 19 | 27/01/2018 | 589695 | 2203239 | 19.5 | 722 | 34.21 |
| 20 | 27/01/2018 | 589695 | 2203210 | 19.5 | 722 | 3.76 |
| 21 | 27/01/2018 | 589694 | 2203178 | 19.5 | 722 | 3.53 |
| 22 | 27/01/2018 | 589689 | 2203146 | 19.5 | 722 | 13.99 |
| 23 | 27/01/2018 | 589687 | 2203112 | 18.5 | 723 | 11.1 |
| 24 | 27/01/2018 | 589687 | 2203078 | 18.5 | 723 | 11.22 |
| 25 | 27/01/2018 | 589687 | 2203045 | 18.5 | 723 | 12.17 |
| 26 | 27/01/2018 | 589689 | 2203015 | 18.5 | 723 | 12.17 |
| 27 | 27/01/2018 | 589689 | 2202985 | 17 | 723 | 23.27 |
| 28 | 27/01/2018 | 589683 | 2202954 | 17 | 723 | 19.23 |
| 29 | 27/01/2018 | 589679 | 2202928 | 17 | 723 | 10.69 |
| 30 | 27/01/2018 | 589586 | 2202942 | 17.5 | 723 | 7.23 |
| 31 | 27/01/2018 | 589580 | 2202971 | 17.5 | 723 | 16.71 |
| 32 | 27/01/2018 | 589586 | 2203002 | 17.5 | 723 | 14.34 |
| 33 | 27/01/2018 | 589585 | 2203033 | 16.5 | 722 | 22.09 |
| 34 | 27/01/2018 | 589587 | 2203064 | 16.5 | 722 | 3.21 |
| 35 | 27/01/2018 | 589608 | 2203077 | 16.5 | 722 | 9.62 |
| 36 | 27/01/2018 | 589615 | 2203106 | 16.5 | 722 | 11.88 |
| 37 | 27/01/2018 | 589617 | 2203140 | 16.5 | 722 | 23.63 |
| 38 | 27/01/2018 | 589578 | 2203143 | 16.5 | 722 | 6.41 |
| 39 | 27/01/2018 | 589581 | 2203171 | 15 | 722 | 17.19 |
| 40 | 27/01/2018 | 589582 | 2203209 | 15 | 722 | 16.71 |
| 41 | 27/01/2018 | 589602 | 2203253 | 15 | 722 | 16 |
| 42 | 27/01/2018 | 589602 | 2203286 | 15 | 722 | 14.68 |
| 43 | 27/01/2018 | 589599 | 2203322 | 15 | 722 | 14.09 |
| 44 | 27/01/2018 | 589595 | 2203352 | 15 | 722 | 15.52 |
| 45 | 27/01/2018 | 589485 | 2203330 | 15.5 | 722 | 8.58 |
| 46 | 27/01/2018 | 589480 | 2203296 | 15.5 | 722 | 0.12 |
| 47 | 27/01/2018 | 589478 | 2203260 | 15.5 | 722 | 9.53 |
| 48 | 27/01/2018 | 589484 | 2203218 | 15.5 | 722 | 18 |
| 49 | 27/01/2018 | 589483 | 2203195 | 15.5 | 722 | 3.58 |
| 50 | 27/01/2018 | 589393 | 2203183 | 15.5 | 722 | 14.54 |
| 51 | 27/01/2018 | 589393 | 2203219 | 16 | 723 | 16.92 |
| 52 | 27/01/2018 | 589385 | 2203251 | 16 | 723 | 17.04 |
| 53 | 27/01/2018 | 589394 | 2203283 | 16 | 723 | 16.08 |

| ID | Date | X(m) | Y(m) | T (°C) | P (mbar) | $CO_2$ Flux (g $m^{-2}$ $day^{-1}$) |
|---|---|---|---|---|---|---|
| 54 | 27/01/2018 | 589397 | 2203325 | 16 | 723 | 7.74 |
| 55 | 27/01/2018 | 589326 | 2203334 | 16 | 723 | 11.08 |
| 56 | 27/01/2018 | 589331 | 2203252 | 17.5 | 723 | 2.13 |
| 57 | 27/01/2018 | 589316 | 2203222 | 17.5 | 723 | 5.93 |
| 58 | 27/01/2018 | 589309 | 2203195 | 17.5 | 723 | 23.11 |
| 59 | 27/01/2018 | 589168 | 2203181 | 17.5 | 723 | 16.59 |
| 60 | 27/01/2018 | 589174 | 2203221 | 16.5 | 722 | 20.9 |
| 61 | 27/01/2018 | 589180 | 2203261 | 16.5 | 722 | 12.71 |
| 62 | 27/01/2018 | 589182 | 2203298 | 16.5 | 722 | 16.03 |
| 63 | 27/01/2018 | 589171 | 2203127 | 16.5 | 722 | 36.46 |
| 64 | 27/01/2018 | 589173 | 2203010 | 16.5 | 722 | 10.69 |
| 65 | 27/01/2018 | 589175 | 2203054 | 16.5 | 722 | 22.57 |
| 66 | 27/01/2018 | 589176 | 2203096 | 16.5 | 722 | 5.94 |
| 67 | 27/01/2018 | 589292 | 2203134 | 16.5 | 722 | 4.99 |
| 68 | 27/01/2018 | 589299 | 2203097 | 15.5 | 721 | 4.76 |
| 69 | 27/01/2018 | 589301 | 2203045 | 15.5 | 721 | 12.97 |
| 70 | 27/01/2018 | 589301 | 2203003 | 15.5 | 721 | 1.19 |
| 71 | 27/01/2018 | 589369 | 2202955 | 15.5 | 721 | 14.04 |
| 72 | 27/01/2018 | 589380 | 2202985 | 15.5 | 721 | 12.26 |
| 73 | 27/01/2018 | 589354 | 2203050 | 15.5 | 721 | 13.69 |
| 74 | 27/01/2018 | 589377 | 2203074 | 15.5 | 721 | 3.81 |
| 75 | 27/01/2018 | 589367 | 2203129 | 15.5 | 721 | 3.57 |
| 76 | 27/01/2018 | 589445 | 2203082 | 14 | 721 | 15.91 |
| 77 | 27/01/2018 | 589439 | 2203005 | 14 | 721 | 9.93 |
| 78 | 27/01/2018 | 589423 | 2202972 | 14 | 721 | 11.25 |
| 79 | 27/01/2018 | 589420 | 2202937 | 14 | 721 | 19.86 |
| 80 | 27/01/2018 | 589487 | 2202975 | 14 | 721 | 1.2 |
| 81 | 28/01/2018 | 589076 | 2202964 | 9 | 721 | 1.22 |
| 82 | 28/01/2018 | 589068 | 2202978 | 9 | 735 | 12.54 |
| 83 | 28/01/2018 | 589015 | 2202918 | 9 | 725 | 13.47 |
| 84 | 28/01/2018 | 589025 | 2202899 | 9 | 725 | 15.3 |
| 85 | 28/01/2018 | 589036 | 2203018 | 9 | 725 | 15.79 |
| 86 | 28/01/2018 | 588991 | 2202946 | 9 | 725 | 16.77 |
| 87 | 28/01/2018 | 588906 | 2202920 | 9 | 725 | 7.22 |
| 88 | 28/01/2018 | 588920 | 2202892 | 9 | 725 | 13.71 |
| 89 | 28/01/2018 | 588933 | 2202865 | 9 | 725 | 11.63 |
| 90 | 28/01/2018 | 588866 | 2202802 | 9 | 725 | 7.71 |
| 91 | 28/01/2018 | 588851 | 2202833 | 9 | 725 | 13.96 |
| 92 | 28/01/2018 | 588839 | 2202861 | 9 | 725 | 14.57 |
| 93 | 28/01/2018 | 588824 | 2202888 | 9 | 724 | 7.34 |
| 94 | 28/01/2018 | 588815 | 2202922 | 10 | 724 | 9.75 |
| 95 | 28/01/2018 | 588710 | 2202935 | 10 | 724 | 10.96 |
| 96 | 28/01/2018 | 588729 | 2202886 | 10 | 724 | 21.32 |
| 97 | 28/01/2018 | 588743 | 2202853 | 10 | 724 | 10.36 |
| 98 | 28/01/2018 | 588752 | 2202823 | 10 | 724 | 8.89 |
| 99 | 28/01/2018 | 588767 | 2202793 | 10 | 724 | 13.77 |
| 100 | 28/01/2018 | 588679 | 2202770 | 10 | 724 | 11.33 |
| 101 | 28/01/2018 | 588668 | 2202798 | 10 | 724 | 11.94 |
| 102 | 28/01/2018 | 588654 | 2202826 | 10 | 724 | 18.64 |
| 103 | 28/01/2018 | 588641 | 2202856 | 10 | 724 | 16.32 |
| 104 | 28/01/2018 | 588631 | 2202887 | 10 | 724 | 18.03 |
| 105 | 28/01/2018 | 588625 | 2202911 | 10 | 724 | 9.99 |
| 106 | 28/01/2018 | 588607 | 2202934 | 10 | 724 | 8.53 |
| 107 | 28/01/2018 | 588545 | 2202864 | 10 | 724 | 10.6 |
| 108 | 28/01/2018 | 588499 | 2202829 | 10 | 724 | 13.16 |
| 109 | 28/01/2018 | 588562 | 2202835 | 10 | 724 | 9.75 |
| 110 | 28/01/2018 | 588577 | 2202823 | 10 | 724 | 11.09 |

| ID | Date | X(m) | Y(m) | T (°C) | P (mbar) | $CO_2$ Flux (g $m^{-2}$ $day^{-1}$) |
|---|---|---|---|---|---|---|
| 111 | 28/01/2018 | 588615 | 2202814 | 10 | 724 | 15.96 |
| 112 | 28/01/2018 | 588628 | 2202783 | 10 | 724 | 2.8 |
| 113 | 28/01/2018 | 588600 | 2202740 | 10 | 724 | 16.81 |
| 114 | 28/01/2018 | 588610 | 2202704 | 9.5 | 724 | 15.5 |
| 115 | 28/01/2018 | 588623 | 2202678 | 9.5 | 724 | 3.42 |
| 116 | 28/01/2018 | 588707 | 2202670 | 9.5 | 724 | 8.54 |
| 117 | 28/01/2018 | 588690 | 2202722 | 9.5 | 724 | 21.97 |
| 118 | 28/01/2018 | 588773 | 2202744 | 9.5 | 724 | 14.89 |
| 119 | 28/01/2018 | 588883 | 2202773 | 9.5 | 724 | 23.19 |
| 120 | 28/01/2018 | 588904 | 2202742 | 9.5 | 724 | 30.51 |
| 121 | 28/01/2018 | 588955 | 2202807 | 9.5 | 724 | 13.42 |
| 122 | 28/01/2018 | 588937 | 2202834 | 9.5 | 724 | 12.57 |
| 123 | 28/01/2018 | 588456 | 2202755 | 10 | 724 | 4.99 |
| 124 | 28/01/2018 | 588371 | 2202724 | 10 | 724 | 13.64 |
| 125 | 28/01/2018 | 588367 | 2202687 | 10 | 724 | 9.14 |
| 126 | 28/01/2018 | 588367 | 2202648 | 10 | 724 | 23.63 |
| 127 | 28/01/2018 | 588377 | 2202608 | 10 | 724 | 21.32 |
| 128 | 28/01/2018 | 588376 | 2202586 | 10 | 724 | 17.3 |
| 129 | 28/01/2018 | 588448 | 2202571 | 10 | 724 | 13.89 |
| 130 | 28/01/2018 | 588448 | 2202605 | 10 | 724 | 15.11 |
| 131 | 28/01/2018 | 588449 | 2202640 | 10 | 724 | 25.22 |
| 132 | 28/01/2018 | 588452 | 2202678 | 10 | 724 | 16.93 |
| 133 | 28/01/2018 | 588539 | 2202668 | 8 | 724 | 26.75 |
| 134 | 28/01/2018 | 588536 | 2202629 | 8 | 724 | 6.5 |
| 135 | 28/01/2018 | 588542 | 2202598 | 8 | 724 | 10.06 |
| 136 | 28/01/2018 | 588503 | 2202724 | 8 | 724 | 10.43 |
| 137 | 28/01/2018 | 588302 | 2202629 | 8 | 724 | 19.26 |
| 138 | 28/01/2018 | 588317 | 2202593 | 8 | 724 | 12.64 |
| 139 | 28/01/2018 | 588313 | 2202563 | 10 | 724 | 4.87 |
| 140 | 28/01/2018 | 588241 | 2202549 | 10 | 724 | 14.86 |
| 141 | 28/01/2018 | 588228 | 2202581 | 10 | 724 | 19.25 |
| 142 | 28/01/2018 | 588215 | 2202619 | 10 | 724 | 15.47 |
| 143 | 28/01/2018 | 588108 | 2202636 | 10 | 724 | 6.09 |
| 144 | 28/01/2018 | 588128 | 2202602 | 10 | 724 | 12.55 |
| 145 | 28/01/2018 | 588141 | 2202569 | 10 | 724 | 14.62 |
| 146 | 28/01/2018 | 588157 | 2202533 | 10 | 724 | 12.67 |
| 147 | 29/01/2018 | 586050 | 2201009 | 4 | 725 | 9.97 |
| 148 | 29/01/2018 | 586066 | 2201030 | 4 | 725 | 14.71 |
| 149 | 29/01/2018 | 586078 | 2201049 | 4 | 725 | 1.74 |
| 150 | 29/01/2018 | 586091 | 2201069 | 4 | 725 | 1 |
| 151 | 29/01/2018 | 586091 | 2201077 | 4 | 725 | 5.48 |
| 152 | 29/01/2018 | 586098 | 2201075 | 4 | 725 | 3.99 |
| 153 | 29/01/2018 | 586112 | 2201093 | 4 | 725 | 6.48 |
| 154 | 29/01/2018 | 586127 | 2201109 | 4 | 725 | 18.2 |
| 155 | 29/01/2018 | 586144 | 2201125 | 4 | 725 | 3.86 |
| 156 | 29/01/2018 | 586118 | 2201119 | 4 | 725 | 17.57 |
| 157 | 29/01/2018 | 586100 | 2201104 | 4 | 725 | 8.85 |
| 158 | 29/01/2018 | 586088 | 2201086 | 4 | 724 | 13.94 |
| 159 | 29/01/2018 | 586075 | 2201065 | 4 | 724 | 1.87 |
| 160 | 29/01/2018 | 586063 | 2201047 | 4 | 724 | 21.16 |
| 161 | 29/01/2018 | 586049 | 2201028 | 4 | 724 | 5.6 |
| 162 | 29/01/2018 | 586037 | 2201010 | 4 | 724 | 11.7 |
| 163 | 29/01/2018 | 586026 | 2201018 | 4 | 724 | 6.47 |
| 164 | 29/01/2018 | 586039 | 2201035 | 4 | 724 | 6.6 |
| 165 | 29/01/2018 | 586053 | 2201055 | 4 | 724 | 9.83 |
| 166 | 29/01/2018 | 586068 | 2201072 | 4 | 724 | 6.1 |
| 167 | 29/01/2018 | 586081 | 2201092 | 4 | 724 | 0.5 |

| ID | Date | X(m) | Y(m) | T (°C) | P (mbar) | $CO_2$ Flux (g $m^{-2}$ $day^{-1}$) |
|---|---|---|---|---|---|---|
| 168 | 29/01/2018 | 586081 | 2201106 | 4 | 724 | 5.85 |
| 169 | 29/01/2018 | 586078 | 2201106 | 4 | 724 | 0.12 |
| 170 | 29/01/2018 | 586095 | 2201109 | 4 | 724 | 7.34 |
| 171 | 29/01/2018 | 586114 | 2201125 | 4 | 724 | 4.23 |
| 172 | 29/01/2018 | 586104 | 2201133 | 4 | 724 | 7.84 |
| 173 | 29/01/2018 | 586099 | 2201124 | 4 | 724 | 1 |
| 174 | 29/01/2018 | 586098 | 2201124 | 4 | 724 | 1.87 |
| 175 | 29/01/2018 | 586085 | 2201115 | 4 | 724 | 10.46 |
| 176 | 29/01/2018 | 586067 | 2201100 | 4 | 724 | 9.83 |
| 177 | 29/01/2018 | 586054 | 2201084 | 4 | 724 | 5.6 |
| 178 | 29/01/2018 | 586040 | 2201067 | 4 | 724 | 4.36 |
| 179 | 29/01/2018 | 586024 | 2201048 | 4 | 724 | 16.43 |
| 180 | 29/01/2018 | 586009 | 2201030 | 4 | 724 | 3.36 |
| 181 | 29/01/2018 | 587998 | 2202819 | 4 | 726 | 6.99 |
| 182 | 29/01/2018 | 588017 | 2202790 | 4 | 726 | 13.1 |
| 183 | 29/01/2018 | 588035 | 2202762 | 4 | 726 | 9.11 |
| 184 | 29/01/2018 | 588104 | 2202817 | 4 | 726 | 4.87 |
| 185 | 29/01/2018 | 588082 | 2202839 | 4 | 726 | 5.49 |
| 186 | 29/01/2018 | 588059 | 2202867 | 4 | 726 | 1.75 |
| 187 | 29/01/2018 | 588136 | 2202893 | 4 | 726 | 10.86 |
| 188 | 29/01/2018 | 588159 | 2202867 | 4 | 726 | 8.74 |
| 189 | 29/01/2018 | 588224 | 2202910 | 4 | 726 | 11.23 |
| 190 | 29/01/2018 | 587969 | 2202717 | 4 | 726 | 6.37 |
| 191 | 29/01/2018 | 587956 | 2202739 | 4 | 726 | 14.85 |
| 192 | 29/01/2018 | 587936 | 2202762 | 4 | 726 | 4.99 |
| 193 | 29/01/2018 | 587885 | 2202697 | 4 | 726 | 10.36 |
| 194 | 29/01/2018 | 587903 | 2202679 | 4 | 726 | 2.5 |
| 195 | 29/01/2018 | 587924 | 2202660 | 4 | 726 | 11.86 |
| 196 | 29/01/2018 | 587895 | 2202607 | 4 | 726 | 2 |
| 197 | 29/01/2018 | 587914 | 2202587 | 4 | 726 | 3.62 |
| 198 | 29/01/2018 | 587933 | 2202563 | 4 | 726 | 5.12 |
| 199 | 29/01/2018 | 587979 | 2202625 | 4 | 726 | 29.45 |
| 200 | 29/01/2018 | 587959 | 2202639 | 4 | 726 | 7.49 |
| 201 | 29/01/2018 | 588020 | 2202609 | 4 | 726 | 2.25 |
| 202 | 29/01/2018 | 588012 | 2202591 | 4 | 726 | 2.25 |
| 203 | 29/01/2018 | 588062 | 2202585 | 4 | 726 | 5.37 |
| 204 | 29/01/2018 | 588076 | 2202619 | 4 | 726 | 6.37 |
| 205 | 29/01/2018 | 587980 | 2202597 | 4 | 726 | 0.12 |
| 206 | 29/01/2018 | 587915 | 2202489 | 4 | 726 | 9.49 |
| 207 | 29/01/2018 | 587888 | 2202505 | 4 | 726 | 8.36 |
| 208 | 29/01/2018 | 587867 | 2202519 | 4 | 726 | 9.98 |
| 209 | 29/01/2018 | 587846 | 2202426 | 4 | 726 | 7.86 |
| 210 | 29/01/2018 | 587864 | 2202426 | 4 | 726 | 1.75 |
| 211 | 29/01/2018 | 587892 | 2202419 | 4 | 726 | 11.11 |
| 212 | 30/01/2018 | 589952 | 2204293 | 3 | 729 | 17.61 |
| 213 | 30/01/2018 | 589985 | 2204321 | 3 | 729 | 7.55 |
| 214 | 30/01/2018 | 590020 | 2204336 | 3 | 729 | 8.8 |
| 215 | 30/01/2018 | 590056 | 2204349 | 3 | 729 | 9.06 |
| 216 | 30/01/2018 | 590092 | 2204362 | 4 | 729 | 4.26 |
| 217 | 30/01/2018 | 590130 | 2204379 | 4 | 729 | 15.04 |
| 218 | 30/01/2018 | 590110 | 2204476 | 4 | 729 | 11.03 |
| 219 | 30/01/2018 | 590074 | 2204464 | 5 | 729 | 2.37 |
| 220 | 30/01/2018 | 590038 | 2204452 | 5 | 729 | 9.49 |
| 221 | 30/01/2018 | 589996 | 2204444 | 5 | 729 | 14.24 |
| 222 | 30/01/2018 | 589960 | 2204436 | 6 | 729 | 3.86 |
| 223 | 30/01/2018 | 589917 | 2204365 | 6 | 727 | 7.45 |
| 224 | 30/01/2018 | 589895 | 2204375 | 7 | 727 | 7.42 |

| ID | Date | X(m) | Y(m) | T (°C) | P (mbar) | $CO_2$ Flux (g $m^{-2}$ $day^{-1}$) |
|---|---|---|---|---|---|---|
| 225 | 30/01/2018 | 589895 | 2204424 | 7 | 727 | 7.91 |
| 226 | 30/01/2018 | 589939 | 2204442 | 7 | 727 | 12.74 |
| 227 | 30/01/2018 | 589845 | 2204505 | 7 | 727 | 4.95 |
| 228 | 30/01/2018 | 589845 | 2204464 | 7 | 727 | 5.93 |
| 229 | 30/01/2018 | 589849 | 2204423 | 6 | 727 | 1.24 |
| 230 | 30/01/2018 | 589904 | 2204488 | 5 | 727 | 6.72 |
| 231 | 30/01/2018 | 589930 | 2204513 | 5 | 727 | 8.22 |
| 232 | 30/01/2018 | 589921 | 2204551 | 5 | 727 | 7.85 |
| 233 | 30/01/2018 | 589880 | 2204568 | 5 | 727 | 7.47 |
| 234 | 30/01/2018 | 589850 | 2204594 | 5 | 727 | 5.23 |
| 235 | 30/01/2018 | 589814 | 2204597 | 5 | 727 | 7.47 |
| 236 | 30/01/2018 | 589789 | 2204635 | 5 | 727 | 8.47 |
| 237 | 30/01/2018 | 589746 | 2204640 | 5 | 727 | 5.48 |
| 238 | 30/01/2018 | 589741 | 2204676 | 5 | 727 | 11.83 |
| 239 | 30/01/2018 | 589737 | 2204707 | 5 | 727 | 6.23 |
| 240 | 30/01/2018 | 589737 | 2204753 | 5 | 727 | 11.46 |
| 241 | 30/01/2018 | 589734 | 2204791 | 8 | 727 | 19.1 |
| 242 | 30/01/2018 | 589718 | 2204753 | 8 | 727 | 12.07 |
| 243 | 30/01/2018 | 589695 | 2204730 | 8 | 727 | 10.72 |
| 244 | 30/01/2018 | 589672 | 2204702 | 8 | 727 | 4.93 |
| 245 | 30/01/2018 | 589649 | 2204672 | 8 | 727 | 10.84 |
| 246 | 30/01/2018 | 589624 | 2204642 | 8 | 727 | 10.97 |
| 247 | 30/01/2018 | 589663 | 2204644 | 8 | 727 | 8.38 |
| 248 | 30/01/2018 | 589590 | 2204667 | 8 | 727 | 21.68 |
| 249 | 30/01/2018 | 589572 | 2204639 | 5.5 | 727 | 10.94 |
| 250 | 30/01/2018 | 589606 | 2204699 | 5.5 | 727 | 13.3 |
| 251 | 30/01/2018 | 589614 | 2204717 | 5.5 | 727 | 19.27 |
| 252 | 30/01/2018 | 589588 | 2204740 | 5.5 | 727 | 16.53 |
| 253 | 30/01/2018 | 589565 | 2204711 | 5.5 | 727 | 7.46 |
| 254 | 30/01/2018 | 589544 | 2204684 | 5.5 | 727 | 17.65 |
| 255 | 30/01/2018 | 589514 | 2204697 | 5.5 | 727 | 15.91 |
| 256 | 30/01/2018 | 589539 | 2204733 | 5.5 | 727 | 12.18 |
| 257 | 30/01/2018 | 589565 | 2204759 | 5.5 | 727 | 11.81 |
| 258 | 30/01/2018 | 589544 | 2204792 | 5.5 | 727 | 18.89 |
| 259 | 30/01/2018 | 589511 | 2204777 | 5.5 | 727 | 7.83 |
| 260 | 30/01/2018 | 589477 | 2204755 | 5.5 | 727 | 9.57 |
| 261 | 30/01/2018 | 589455 | 2204738 | 5.5 | 727 | 16.53 |
| 262 | 30/01/2018 | 589645 | 2204729 | 5.5 | 725 | 14.63 |
| 263 | 30/01/2018 | 589663 | 2204764 | 5.5 | 725 | 6.57 |
| 264 | 30/01/2018 | 589677 | 2204793 | 5.5 | 725 | 6.69 |
| 265 | 30/01/2018 | 589638 | 2204799 | 5.5 | 725 | 11.16 |
| 266 | 30/01/2018 | 589617 | 2204775 | 5.5 | 725 | 8.68 |
| 267 | 30/01/2018 | 589584 | 2204801 | 5.5 | 725 | 7.81 |
| 268 | 30/01/2018 | 589608 | 2204827 | 5.5 | 725 | 3.6 |
| 269 | 30/01/2018 | 589585 | 2204857 | 5.5 | 725 | 8.68 |
| 270 | 30/01/2018 | 589550 | 2204841 | 5.5 | 725 | 19.96 |
| 271 | 30/01/2018 | 589527 | 2204846 | 5.5 | 725 | 24.3 |
| 272 | 30/01/2018 | 589551 | 2204872 | 5.5 | 725 | 12.27 |
| 273 | 30/01/2018 | 589543 | 2204906 | 5.5 | 725 | 10.04 |
| 274 | 30/01/2018 | 589501 | 2204892 | 5.5 | 725 | 15.12 |
| 275 | 30/01/2018 | 589475 | 2204916 | 5 | 725 | 12.79 |
| 276 | 30/01/2018 | 589517 | 2204950 | 5 | 725 | 6.95 |
| 277 | 30/01/2018 | 589498 | 2204981 | 5 | 725 | 7.58 |
| 278 | 30/01/2018 | 589462 | 2204962 | 5 | 725 | 11.67 |
| 279 | 30/01/2018 | 587749 | 2201757 | 4 | 724 | 27.13 |
| 280 | 30/01/2018 | 587736 | 2201796 | 4 | 724 | 26.26 |
| 281 | 30/01/2018 | 587728 | 2201831 | 4 | 724 | 15.68 |

| ID | Date | X(m) | Y(m) | T (°C) | P (mbar) | $CO_2$ Flux (g $m^{-2}$ $day^{-1}$) |
|---|---|---|---|---|---|---|
| 282 | 30/01/2018 | 587716 | 2201866 | 4 | 724 | 23.15 |
| 283 | 30/01/2018 | 587703 | 2201911 | 4 | 724 | 6.47 |
| 284 | 30/01/2018 | 587700 | 2201953 | 4 | 724 | 14.56 |
| 285 | 30/01/2018 | 587691 | 2201995 | 4 | 724 | 11.7 |
| 286 | 30/01/2018 | 587684 | 2202031 | 4 | 724 | 1.49 |
| 287 | 30/01/2018 | 587672 | 2202074 | 4 | 724 | 11.95 |
| 288 | 30/01/2018 | 587657 | 2202110 | 4 | 724 | 15.56 |
| 289 | 30/01/2018 | 587646 | 2202147 | 4 | 724 | 4.11 |
| 290 | 30/01/2018 | 587639 | 2202185 | 4 | 724 | 8.46 |
| 291 | 30/01/2018 | 587654 | 2202220 | 2 | 724 | 8.27 |
| 292 | 30/01/2018 | 587667 | 2202254 | 2 | 724 | 19.06 |
| 293 | 30/01/2018 | 587685 | 2202289 | 2 | 724 | 4.39 |
| 294 | 30/01/2018 | 587717 | 2202269 | 2 | 724 | 8.27 |
| 295 | 30/01/2018 | 587727 | 2202234 | 2 | 724 | 15.04 |
| 296 | 30/01/2018 | 587727 | 2202200 | 2 | 724 | 10.66 |
| 297 | 30/01/2018 | 587732 | 2202166 | 2 | 724 | 5.64 |
| 298 | 30/01/2018 | 587733 | 2202130 | 2 | 724 | 2.63 |
| 299 | 30/01/2018 | 587723 | 2202097 | 2 | 724 | 9.65 |
| 300 | 30/01/2018 | 587738 | 2202064 | 2 | 724 | 12.41 |
| 301 | 30/01/2018 | 587757 | 2202035 | 2 | 724 | 12.54 |
| 302 | 30/01/2018 | 587777 | 2202000 | 2 | 724 | 13.04 |
| 303 | 30/01/2018 | 587796 | 2201972 | 2 | 724 | 7.77 |
| 304 | 30/01/2018 | 587888 | 2202006 | 2 | 724 | 7.77 |
| 305 | 30/01/2018 | 587883 | 2202045 | 2 | 724 | 12.54 |
| 306 | 30/01/2018 | 587876 | 2202085 | 2 | 724 | 10.41 |
| 307 | 30/01/2018 | 587870 | 2202121 | 2 | 724 | 4.01 |
| 308 | 30/01/2018 | 587861 | 2202161 | 2 | 724 | 6.9 |
| 309 | 30/01/2018 | 587851 | 2202199 | 2 | 724 | 15.8 |
| 310 | 30/01/2018 | 587843 | 2202238 | 2 | 724 | 21.56 |
| 311 | 30/01/2018 | 587842 | 2202281 | 1.5 | 724 | 5.9 |
| 312 | 30/01/2018 | 587838 | 2202318 | 1.5 | 724 | 15.07 |
| 313 | 30/01/2018 | 587424 | 2202224 | 19.5 | 726 | 12.17 |
| 314 | 01/01/2018 | 587411 | 2202191 | 19.5 | 726 | 8.27 |
| 315 | 01/01/2018 | 587397 | 2202163 | 19.5 | 726 | 34.28 |
| 316 | 01/01/2018 | 587384 | 2202141 | 19.5 | 726 | 14.77 |
| 317 | 01/01/2018 | 587282 | 2202141 | 19.5 | 726 | 15.84 |
| 318 | 01/01/2018 | 587324 | 2202087 | 19.5 | 726 | 29.55 |
| 319 | 01/01/2018 | 587325 | 2202055 | 17.5 | 726 | 1.19 |
| 320 | 01/01/2018 | 587407 | 2202035 | 17.5 | 726 | 9.64 |
| 321 | 01/01/2018 | 587414 | 2202075 | 17.5 | 726 | 9.64 |
| 322 | 01/01/2018 | 587228 | 2202095 | 17.5 | 726 | 24.04 |
| 323 | 01/01/2018 | 587242 | 2202064 | 17.5 | 726 | 7.85 |
| 324 | 01/01/2018 | 587248 | 2202032 | 17.5 | 726 | 8.33 |
| 325 | 01/01/2018 | 587248 | 2201998 | 17.5 | 729 | 37.4 |
| 326 | 01/01/2018 | 587245 | 2201963 | 17.5 | 729 | 16.85 |
| 327 | 01/01/2018 | 587244 | 2201932 | 17.5 | 729 | 35.49 |
| 328 | 01/01/2018 | 587244 | 2201900 | 17.5 | 729 | 34.66 |
| 329 | 01/01/2018 | 587237 | 2201866 | 17.5 | 729 | 31.79 |
| 330 | 01/01/2018 | 587234 | 2201833 | 17.5 | 729 | 22.71 |
| 331 | 01/01/2018 | 587228 | 2201802 | 17.5 | 729 | 31.19 |
| 332 | 01/01/2018 | 587224 | 2201768 | 17.5 | 729 | 30.47 |
| 333 | 01/01/2018 | 587218 | 2201743 | 17.5 | 729 | 5.26 |
| 334 | 01/01/2018 | 587136 | 2201764 | 17.5 | 729 | 2.39 |
| 335 | 01/01/2018 | 587132 | 2201805 | 17.5 | 729 | 20.67 |
| 336 | 01/01/2018 | 587123 | 2201840 | 17.5 | 729 | 19.96 |
| 337 | 01/01/2018 | 587125 | 2201873 | 17.5 | 729 | 14.7 |
| 338 | 01/01/2018 | 587135 | 2201904 | 17.5 | 729 | 12.67 |

| | | | | | | |
|---|---|---|---|---|---|---|
| 339 | 01/01/2018 | 587139 | 2201942 | 17.5 | 729 | 1.2 |
| 340 | 01/01/2018 | 587144 | 2201978 | 17.5 | 729 | 5.98 |
| 341 | 01/01/2018 | 587147 | 2202013 | 17.5 | 729 | 15.18 |
| 342 | 01/01/2018 | 587154 | 2202042 | 17.5 | 729 | 4.06 |
| 343 | 01/01/2018 | 587162 | 2202069 | 19 | 729 | 19.14 |
| 344 | 01/01/2018 | 587171 | 2202094 | 19 | 729 | 31.62 |
| 345 | 01/01/2018 | 587093 | 2202149 | 19 | 729 | 24.13 |
| 346 | 01/01/2018 | 587068 | 2202128 | 19 | 729 | 12.01 |
| 347 | 01/01/2018 | 587055 | 2202115 | 19 | 729 | 14.15 |
| 348 | 01/01/2018 | 587051 | 2202082 | 19 | 729 | 17.95 |
| 349 | 01/01/2018 | 587055 | 2202049 | 19 | 729 | 9.51 |
| 350 | 01/01/2018 | 587058 | 2202021 | 19 | 723 | 20.87 |
| 351 | 01/01/2018 | 587063 | 2201988 | 19 | 723 | 10.14 |
| 352 | 01/01/2018 | 587067 | 2201953 | 19 | 723 | 16.63 |
| 353 | 01/01/2018 | 587072 | 2201919 | 19 | 723 | 11.08 |
| 354 | 01/01/2018 | 587078 | 2201888 | 19 | 723 | 7.07 |
| 355 | 01/01/2018 | 587083 | 2201848 | 19 | 723 | 13.91 |
| 356 | 01/01/2018 | 587088 | 2201825 | 19 | 723 | 19.81 |
| 357 | 01/01/2018 | 587039 | 2201808 | 19 | 723 | 7.78 |
| 358 | 01/01/2018 | 587031 | 2201847 | 19 | 723 | 12.38 |
| 359 | 01/01/2018 | 587014 | 2201887 | 19 | 723 | 6.72 |
| 360 | 01/01/2018 | 587011 | 2201921 | 19 | 723 | 8.73 |
| 361 | 01/01/2018 | 587009 | 2201950 | 19 | 723 | 14.39 |
| 362 | 01/01/2018 | 587001 | 2201985 | 19 | 723 | 24.29 |
| 363 | 01/01/2018 | 586994 | 2202017 | 20 | 723 | 19.39 |
| 364 | 01/01/2018 | 586990 | 2202050 | 20 | 723 | 22.8 |
| 365 | 01/01/2018 | 586991 | 2202085 | 20 | 723 | 9.64 |
| 366 | 01/01/2018 | 586983 | 2202127 | 20 | 723 | 19.39 |
| 367 | 01/01/2018 | 586979 | 2202159 | 20 | 723 | 32.67 |
| 368 | 01/01/2018 | 586979 | 2202188 | 20 | 723 | 14.92 |
| 369 | 01/01/2018 | 586888 | 2202207 | 19 | 726 | 15.51 |
| 370 | 01/01/2018 | 586874 | 2202182 | 19 | 726 | 18.94 |
| 371 | 01/01/2018 | 586859 | 2202153 | 19 | 725 | 16.55 |
| 372 | 01/01/2018 | 586845 | 2202125 | 19 | 725 | 16.55 |
| 373 | 01/01/2018 | 586828 | 2202096 | 19 | 725 | 25.07 |
| 374 | 01/01/2018 | 586810 | 2202064 | 19 | 725 | 20.93 |
| 375 | 01/01/2018 | 586804 | 2202031 | 19 | 726 | 13.5 |
| 376 | 01/01/2018 | 586792 | 2201997 | 19 | 726 | 16.22 |
| 377 | 01/01/2018 | 586780 | 2201970 | 19 | 726 | 17.76 |
| 378 | 01/01/2018 | 586766 | 2201994 | 19 | 726 | 32.32 |
| 379 | 01/01/2018 | 586754 | 2202028 | 19 | 726 | 17.4 |
| 380 | 01/01/2018 | 586693 | 2202040 | 19 | 726 | 16.22 |
| 381 | 01/01/2018 | 586688 | 2202068 | 19 | 726 | 12.67 |
| 382 | 01/01/2018 | 586680 | 2202103 | 19 | 726 | 4.74 |
| 383 | 01/01/2018 | 586670 | 2202137 | 19 | 726 | 11.6 |
| 384 | 01/01/2018 | 586661 | 2202171 | 19 | 726 | 2.6 |
| 385 | 01/01/2018 | 586654 | 2202207 | 17.5 | 726 | 19.99 |
| 386 | 01/01/2018 | 586647 | 2202231 | 17.5 | 726 | 24.64 |
| 387 | 01/01/2018 | 586753 | 2202228 | 17.5 | 726 | 12.38 |
| 388 | 01/01/2018 | 586753 | 2202196 | 17.5 | 726 | 10 |
| 389 | 01/01/2018 | 586751 | 2202165 | 16 | 725 | 12.66 |
| 390 | 01/01/2018 | 586754 | 2202131 | 16 | 726 | 15.55 |
| 391 | 01/01/2018 | 586754 | 2202097 | 16 | 726 | 9.21 |
| 392 | 01/01/2018 | 586749 | 2202055 | 16 | 726 | 21.05 |
| 393 | 02/02/2018 | 589796 | 2203091 | 13.5 | 728 | 6.53 |
| 394 | 02/02/2018 | 589837 | 2203088 | 13.5 | 728 | 10.29 |
| 395 | 02/02/2018 | 589869 | 2203104 | 13.5 | 728 | 13.92 |

| ID | Date | X(m) | Y(m) | T (°C) | P (mbar) | $CO_2$ Flux (g $m^{-2}$ $day^{-1}$) |
|---|---|---|---|---|---|---|
| 396 | 02/02/2018 | 589938 | 2203096 | 13.5 | 728 | 20.57 |
| 397 | 02/02/2018 | 589970 | 2203118 | 13.5 | 727 | 25.38 |
| 398 | 02/02/2018 | 589995 | 2203098 | 13.5 | 727 | 21.75 |
| 399 | 02/02/2018 | 590012 | 2203142 | 13.5 | 727 | 27.91 |
| 400 | 02/02/2018 | 589953 | 2203146 | 13.5 | 727 | 16.8 |
| 401 | 02/02/2018 | 589918 | 2203144 | 13.5 | 727 | 10.15 |
| 402 | 02/02/2018 | 589890 | 2203165 | 13.5 | 727 | 14.5 |
| 403 | 02/02/2018 | 589853 | 2203197 | 13.5 | 727 | 13.29 |
| 404 | 02/02/2018 | 589970 | 2203164 | 13.5 | 726 | 15.93 |
| 405 | 02/02/2018 | 590000 | 2203176 | 13.5 | 726 | 9.65 |
| 406 | 02/02/2018 | 590039 | 2203144 | 13.5 | 726 | 48.87 |
| 407 | 02/02/2018 | 590060 | 2203153 | 13.5 | 726 | 21.96 |
| 408 | 02/02/2018 | 590074 | 2203153 | 13.5 | 726 | 15.69 |
| 409 | 02/02/2018 | 590106 | 2203183 | 13.5 | 726 | 26.55 |
| 410 | 02/02/2018 | 590138 | 2203204 | 13.5 | 726 | 25.1 |
| 411 | 02/02/2018 | 590151 | 2203192 | 13.5 | 726 | 14.48 |
| 412 | 02/02/2018 | 590185 | 2203191 | 13.5 | 729 | 12.12 |
| 413 | 02/02/2018 | 590217 | 2203202 | 11.5 | 729 | 5.12 |
| 414 | 02/02/2018 | 590205 | 2203226 | 11.5 | 726 | 12.15 |
| 415 | 02/02/2018 | 590187 | 2203227 | 11.5 | 726 | 9.36 |
| 416 | 02/02/2018 | 590188 | 2203217 | 11.5 | 726 | 1.22 |
| 417 | 02/02/2018 | 590163 | 2203221 | 11.5 | 726 | 21.39 |
| 418 | 02/02/2018 | 590149 | 2203200 | 11.5 | 726 | 5.1 |